BULLETIN OF THE 18TH MEETING

JANAF-ARPA-NASA

SOLID PROPELLANT GROUP

X62 10211

X6210253

[redacted]

BULLETIN OF THE 18TH MEETING

JANAF-ARPA-NASA SOLID PROPELLANT GROUP

JUNE 5-7, 1962

Pittsburgh-Hilton Hotel
PITTSBURGH, PENNSYLVANIA

Volume III

THE SOLID PROPELLANT INFORMATION AGENCY

THE JOHNS HOPKINS UNIVERSITY
APPLIED PHYSICS LABORATORY
8621 Georgia Ave. Silver Spring, Md.

Operating under Contract NOrd 7386 with the
Bureau of Naval Weapons, Department of the Navy

[redacted]

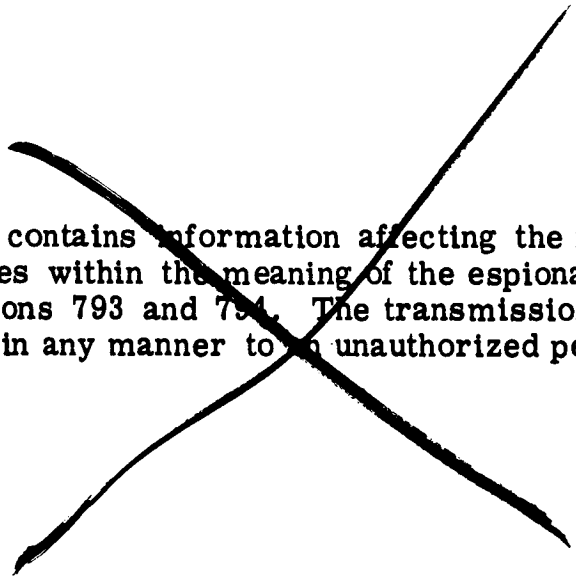

This document contains information affecting the national defense of the United States within the meaning of the espionage laws, Title 18, U. S. C., sections 793 and 794. The transmission or the revelation of its contents in any manner to an unauthorized person is prohibited by law.

Foreword

Each year since 1946 the U.S. Government offices concerned with solid rocket propulsion have held classified Solid Propellant Group meetings. These meetings promote the free and direct exchange of scientific and technical information among working level scientists and engineers. Attendance is by invitation of the sponsors to organizations actively engaged in solid propellant and rocket motor research and development.

The sponsors of the meeting are: Department of the Army, Office, Chief of Ordnance; Department of the Navy, Bureau of Naval Weapons; Department of the Air Force, 6593d Test Group, Space Systems Division; the Advanced Research Projects Agency; and the National Aeronautics and Space Administration. Host for this year's meeting is the Bureau of Naval Weapons. The Solid Propellant Information Agency assists in planning and conducting the meeting and publishes the proceedings.

This volume is one of several preprinted before the meeting so that participants can study the technical presentations in advance, establishing a firm ground for discussion. Together with an Addendum (to be published after the meeting), they constitute the record of the eighteenth meeting.

Table of Contents

VOLUME I

Rocket Motor Design (Cont'd.)

Rocket Motor Cases 275

VOLUME II

Research Propellants 1

Research Propellants (Cont'd.)

Development and Production Propellants 255

Development and Production Propellants (Cont'd.)

VOLUME III

Miscellaneous Papers 1

Nozzles and Thrust Vector Control 107

Rocket Motor Materials

PAPERS NOT PREPRINTED

The following papers could not be published within the Preprint deadline for Volumes I to III. It is expected that they will be published in the Addendum (Volume IV of this Bulletin) in the Summer of 1962.

Space Vehicle Boosters

LARGE SOLID ROCKET DEVELOPMENT, D. F. Sprenger, Aerojet-General Corp., Sacramento

SOLID ROCKET MOTORS FOR SPACE BOOSTERS--PROGRESS IN DEVELOPMENT, G. R. Makepeace, Lockheed Propulsion Co.

THE DEVELOPMENT OF LARGE SOLID PROPELLANT ROCKET MOTORS, B. R. Adelman, W. C. Phillips, United Technology Corp.

Rocket Motor Cases

SANDWICH ROCKET MOTOR CASE, F. L. Rish, E. H. Baker, R. W. Spencer, North American Aviation, Inc., Space and Information Systems Div.

APPLICATION OF AUSFORM PROCESSING TO SHEAR SPUN ROCKET MOTOR CASES, R. P. Sernka, E. L. Harmon, Aeronutronic, Div. of Ford Motor Co.

[redacted]

Development and Production Propellants

Nozzles and Thrust Vector Control

Rocket Motor Materials

[redacted]

Author Index

Listed below are the authors of technical papers published in Volumes I, II and III of this Bulletin. A complete author index will appear in the Addendum (Volume IV).

Organization Source Index

Listed below are the organizations submitting technical papers published in Volumes I, II, and III of this Bulletin. A complete organization source index will appear in the Addendum (Volume IV).

MISCELLANEOUS PAPERS

Chairman

Mr. Gerald Makepeace
Lockheed Propulsion Company

[redacted]

RADAR ATTENUATION IN SOLID PROPELLANT ROCKET EXHAUSTS*

H. F. Calcote and H. Silla
AeroChem Research Laboratories, Inc.
a subsidiary of Pfaudler Permutit Inc.
Princeton, New Jersey

SUMMARY

The absorption, reflection, and refraction of electromagnetic waves in rocket exhausts is due to the presence of free electrons. These may be produced by thermal or chemi-ionization in the rocket chamber or when afterburning occurs in the exhaust. No single explanation suffices for all situations and the problem is complicated by the interrelationship of a multitude of factors. Nevertheless, by the application of electromagnetic theory, thermodynamics, chemical kinetics and fluid dynamics, quantitative predictions are possible. These are mostly limited by our lack of detailed knowledge of reaction kinetics and insufficient information on propellants, e.g., the concentration of alkali metal impurities. After summarizing rocket motor experience, our present state of knowledge is outlined in a coherent framework which should be a guide for future efforts.

INTRODUCTION

The problem of radar communication with rocket systems, particularly solid propellant rockets, is becoming of increasing concern. Attenuation, reflection, refraction, and even the phase-shift of the electromagnetic wave as it passes through the rocket exhaust, is caused by the free electrons in the gas. This is precisely the same phenomena which one experiences with radio waves in the ionosphere and the attenuation encountered when vehicles re-enter the atmosphere. The general principles of the electromagnetic theory are known, but a detailed application of the phenomena to rocket exhausts is incomplete, principally because of the lack of elementary reaction-rate data. This is not to say that unexplainable and unanticipated phenomena have not been and will not be observed, but it seems safe to say that the main causes and explanations are, at least in principal, available.

In spite of this, popular opinion would lead one to conclude that the whole phenomena of radar attenuation and electron formation in flames is shrouded in mystery. In this paper we will summarize some of the specific experiences with rockets in terms of actual practice. Next, we will outline the electromagnetic theory and discuss the various sources of electrons in the rocket exhaust, with some detail as to the mechanisms of electron production and removal.

It will be the intent of this paper to assume that we understand the phenomena and to construct a framework upon which to view it in the future. Much effort and work will be involved in completing the skeleton presented here. This will have to be done by careful analysis of rocket experience and correlation of this information with data from the laboratory. It should

*Supported by the Navy Dept., Bureau of Weapons, Contract NOw-62-0540-c with technical direction by Charles Blank, whose suggestions in preparing this manuscript are gratefully acknowledged. Assistance of R. Revolinski, A. Schell, and F. Kuehner is also acknowledged.

[redacted] Preceding page blank

become clear, as the picture unfolds, as to what specific data should be obtained. The picture presented herein will not be so complete as we would like, because of the limitation in time for preparing this summary and the difficulty in collecting and correlating all of the information. Additional references have been included in each section which are not mentioned in the text. These references are included to give the interested reader a more complete background on the problem.

ROCKET EXPERIENCE

An attempt has been made to summarize the most recent information on attenuation of electromagnetic signals in rocket exhausts. However, because of the short time that was available to compile this report, it is possible that some valuable rocket experience has been omitted. In addition, some information contained in secret reports has been omitted, and no attempt has been made to include the experience obtained with liquid propellant motors. Much of the information contained in this summary is fragmentary because the original reports were fragmentary. For example, data on signal frequency, chamber temperature, chamber pressure, propellant composition, etc. was often missing.

Polaris

To date, (Dec. 19, 1961) negligible attenuation with the Polaris A-1 and A-2 (two stage surface-to-surface rocket) first stages has been observed in flight.[1] However, the antennas are located sufficiently forward on the missile so that RF is not propagated through the first stage exhaust stream.

Signals on all communication links were lost during a portion of powered flight on the first A2X flights.[2,3] The problem was avoided by relocating the ground antennas to avoid the exhaust plume. Fig. 1 shows the importance of antenna location. However, this is not a practical operational solution to the problem since antennas are fixed to the submarine or ship. Fig. 2 shows a plot of the received signal strength against flight time.

Balwanz[3] measured the ionization of the A1X and A2X Polaris propellants in the laboratory and found greater ionization from the A2X propellant, although both propellants contained 30 ppm of sodium. No mention was made of potassium in the report although, as we shall see, potassium is the major impurity in ammonium perchlorate. He suggested that the differences could be attributed to differences in the combustion temperature:

Propellant Designation	ANP-2655AF	DDP-70
Rocket Model	A1X	A2X
Ammonium Perchlorate	69.75	20%
Aluminum	7.75	21
Polyurethane	22.42	-
Copper Chromite	.08	-
Nitrocellulose-Nitroglycerin	-	48
Combustion Temperature, ^{o}K	2745	3765

Some preliminary data on attenuation of 24.15 KMC (K-band) and 9.33 KMC (X-band) was made by Barnes[4] of Stanford Research Institute on static firings of the Polaris first and second stage engines. He estimated an

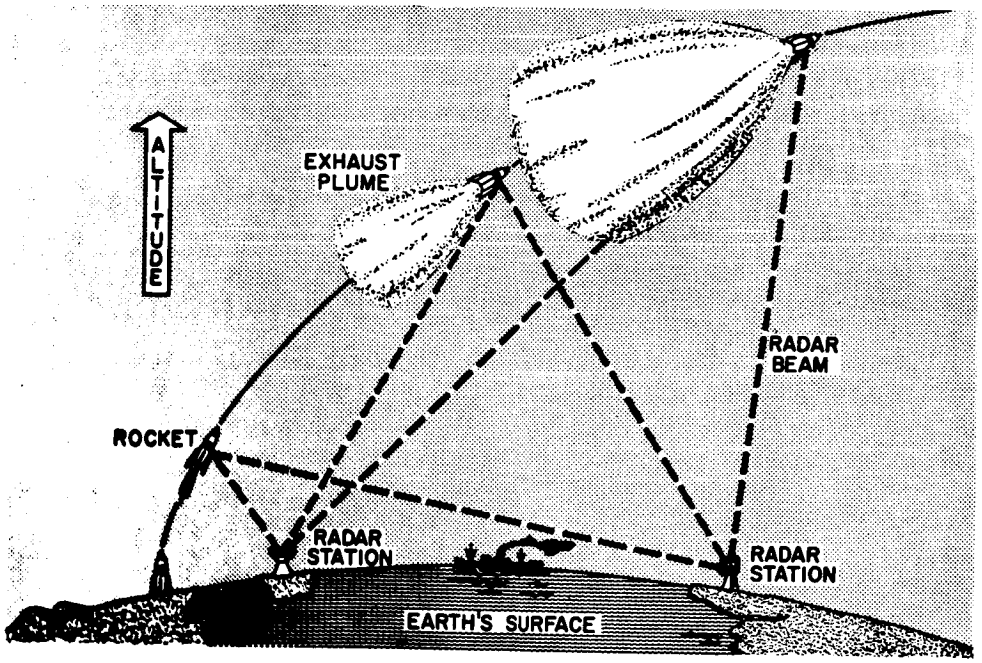

FIG. 1 EFFECT OF ALTITUDE AND DISTANCE ON RADAR BEAM TRAMSMISSION THROUGH THE EXHAUST PLUME

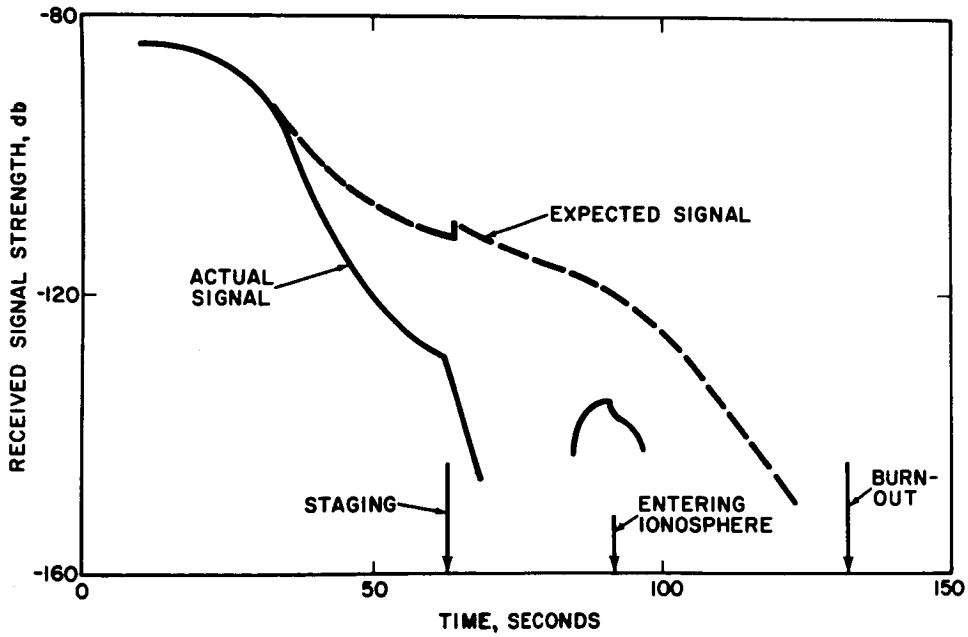

FIG. 2 RECEIVED SIGNAL STRENGTH FROM AN EARLY A2X POLARIS FLIGHT

Poehler Ref. 2

electron density of 3×10^{10} for the Polaris first stage engine. Only one measurement was made for the second-stage motor at the K-band. Some difficulties were encountered with the second stage firing, so that only an estimated average of 3.1 db attenuation could be measured.

Minuteman

Barnes[4] has also made measurements on several static test firings of the Minuteman (a three stage surface-to-surface missile) second and third stage motors, using 24.15 KMC (K-band) and 9.33 KMC (X-band). He measured an electron density of 7 to 15×10^{10} electrons/cc in the third stage motor and 3×10^{10} electrons/cc in the second stage motor, which is comparable to the Polaris first stage. All the propellants contained from 17-19% aluminum. Barnes concluded that the level of ionization can be fairly well accounted for by sodium and potassium contaminants.

The University of Utah[5] has been continuing at Hercules, Utah, the measurements initiated by Stanford, using Stanford equipment. In static measurements, on a modified very hot double base propellant (CYH) containing about 20% aluminum, they found about 55 db attenuation for X-band and about 40 db attenuation for K-band. This corresponds to an electron concentration of about 10^{11} electrons/cc.

An estimate of 1.8×10^{10} electrons/cc in the Minuteman exhaust[6] was obtained for the CYH propellant at the exit plane of an 18.9 expansion ratio nozzle. The estimate was made considering the ionization of potassium, sodium, aluminum, and the attachment of electrons to chlorine. The electron concentration is small compared to the degree of ionization because of electron attachment to Cl and OH. The concentrations of potassium and sodium in the propellant used for the analysis was 800 ppm and 150 ppm, respectively. The results of the first Minuteman flight (401) indicated much less signal attenuation than anticipated from the above analysis.

Brown[5] is convinced that attenuation is due to aluminum oxide particles. They have caught some aluminum oxide particles and found them highly contaminated with Ca and K. The calcium may come from a Buna-N rubber liner which has 1760 ppm Ca, 1600 ppm Na and 700 ppm K.

Terrier

The operational version of the Terrier 3B Sustainer uses a complex double-base non-aluminized propellant. The sustainer operates from 3-30 seconds after launch, and attenuation due to afterburning is experienced at 20,000 to 30,000 ft. This is not duplicated on the ground.[7] As a means of reducing afterburning as much as 5% potassium sulphate, a well known gun-flash inhibitor, has been added to the sustainer propellant. This has been a partial cure, but, of course, it also reduces performance. Very short flame bursts, about 1/100th of a second, are observed with a 1 to 1 correspondence between flame bursts and radar attenuation during the last 10 seconds of flight, i.e., 20-30 seconds after launch. Thus, for this missile there is a very definite correlation between attenuation and flame bursts. It is rare to find flame bursts above 30,000 ft., and they seem more prevelant at lower altitudes.

[redacted]

Both Terrier and the Talos Ramjet are radar-guided beam-riders and operate from 0 to about 100,000 ft. altitude. There has never been any difficulty with the Talos Ramjet or any other hydrocarbon ramjet where the exhaust is oxygen rich because of excess air, so no afterburning is experienced.[6] The exhaust temperatures are also very low. A large number of attempts, mechanical for example, using resonant rods, variation in propellant shape, etc. have been made to alter the afterburning problem.[6] All have failed. An explanation of the afterburning ignition has been proposed, based on the missile picking up an electrostatic charge and then a spark igniting the exhaust. Static firings on the ground in fact demonstrated that the missile picks up a charge of several thousand volts. W. Berl[8] reports that this explanation is no longer considered adequate.

Berl has proposed a theory based on the observation that in Mesa burning propellants a loose film of non-attached carbon forms on the surface during stable burning, but during unstable burning the surface is clean. Berl proposes that the surface is shaken through the missile structure from aerodynamic noise. This throws carbonized material into the exhaust which has been associated with an increase in attenuation.

A new propellant for the Terrier 3BA is under development at Atlantic Research.[6] This is a composite end-burning propellant with silver alloy wires to increase propellant loading. The chamber pressure will be 800 to 1,000 psi. No attenuation has been observed while the propellant is burning, that is, for about 38 seconds. However, for 15-20 seconds after the cessation of thrust production, the rubber-like insulation material around the propellant continues to smoulder and produce a tail flame with severe attenuation. Quantities of soot were expelled during smouldering.

Potassium bromide, potassium bitartrate, and molybdenum trioxide were tried by ABL[9] as afterburning surpressors in the Terrier, but none were found to be more effective than potassium sulfate. Some additional additive work has been done in connection with the Terrier program at Convair.[10,11] They have successfully eliminated a major portion of the afterburning flame on full scale test rocket motors. Their additives were injected from a series of nozzles externally mounted around the tail pipe. They emphasized that the quencher must be tailored to the system. In some cases it was found that adding as much as 10% K_2SO_4 to the propellant was ineffective in eliminating afterburning, whereas in other systems just a few percent was effective. For the Tartar missile iodine was selected as the most effective quencher and diiodmethane, CH_2I_2, as the best carrier.

Sparrow

This is an eight inch diameter air-to-air missile which uses a propellant containing 16-18% aluminum with a specific impulse of 246 seconds.[7,12] Fifteen to twenty db attenuation has been experienced. However, when the aluminum was reduced to less than 5%, the radar attenuation was reduced to less than 3 db. The chamber temperature originally, 5500°F, dropped only by 400 or 500°F. It was noted, however, that in reducing the aluminum content, the ammonium perchlorate concentration was increased, which increased the combustion efficiency. Silver[7] indicated they thought ionization from the combustion chamber flame, which continued burning outside the nozzle, was responsible for ionization in this case and that afterburning did not occur.

[redacted]

[redacted]

Scout

The Scout Vehicle (NASA)[13,14] employs a double-base propellant with about 3% aluminum. At an altitude of 150,000 to 250,000 ft., and frequencies of 220 to 240 megacycles, a 40 db loss was experienced at about 25° aspect angle. They correlated the instantaneous (within 1/100 second) recovery of the signal with the firing of auxiliary "pitch" and "yaw" auxiliary jets powered by hydrogen peroxide. The signal attenuation then built up in about 0.3 second. The "roll control" jet did not produce signal recovery. There is more propellant, however, in the pitch and yaw auxiliary jets. The products of the hydrogen peroxide rockets are water and oxygen. About 3½ pounds/second of exhaust products are put in the stream; the main exhaust from the rocket is about 70 times this mass flow. They have considered the following possible causes of ionization and explanation of recovery:

1. Ionosphere electrons - because difficulty occurs at 197,000 ft., approximate beginning of D region.

2. Antenna pattern - which is altered by the exhaust plume. In laboratory experiments a magnetic field of approximately 1,000 gauss eliminated a 6 db attenuation through the solid propellant exhaust. This is consistent with theoretical predictions on the effect of magnetic fields around antennas.[15,16]

3. Afterburning - Simulation tests (only to 150,000 ft. altitude) in the laboratory failed, and new experiments are planned for higher simulated altitudes.

4. Separated aerodynamic flow field - because the exhaust expansion acts as a solid body. Experiments are planned with flow separation sensors on vehicles scheduled for flight in mid 1962.

5. Local phenomena - A camera on a vehicle will be used to photograph the exhaust plume, which at an altitude of 200,000 ft. is approximately 80 ft. in diameter. They assume that the ionized gases from the exhaust plume may be pulled up around the vehicle, and the hydrogen peroxide rocket makes a small hole in this plume through which the radar signal penetrates.

Because of the rapid response to the auxiliary rocket, attenuation is not due to the exhaust but due to the front surface of the exhaust plume. They assume the water from the propellant blankets the plume surface and that water vapor increases the ion recombination rate.

RADAR ATTENUATION THEORY

When radar waves, i.e., electromagnetic waves, propagate through an ionized gas such as exists in the exhaust of solid propellant rockets, they may be attenuated, refracted, reflected, or experience a phase shift. A number of detailed theoretical analysis are available and the principles involved are well known[1-5] We will contend ourselves with outlining some of the essential features of the problem of attenuation, and presenting a numerical example.

[redacted]

As an electromagnetic wave traverses a conducting medium or plasma, it will be attenuated according to

$$E = E_o e^{-\alpha x} \qquad (1)$$

where

E_o = electric field strength on entering the medium
E^o = electric field strength after traversing the distance x through the plasma
α = attenuation factor or absorption coefficient

The absorption process can be pictured as one in which electrons are accelerated by the electric field and lose energy to the gas via collisions with the gas molecules. Thus, as an electric field travels through an ionized medium, it will cause the electrons to move in the field direction. If the electrons were free and did not suffer collisions, they would reradiate their energy as a non-loaded antenna and the electric field would continue to move through the medium without energy loss. However, when an electron collides with a molecule of the gas, kinetic energy of the electron is transferred to kinetic energy of the molecules, resulting in a loss of energy from the wave. In addition to the simple transfer of kinetic energy of translation to the molecules, the electron may cause the molecule to rotate or vibrate more than that due to the temperature environment. Under sufficiently intense electric fields, the electron may receive sufficient energy to excite the gas molecules to an electronic energy level. All of these energy transfer processes remove energy from the propagating electromagnetic wave without returning it, so the wave is attenuated with respect to its energy content.

Although any exhaust gas is made up of equal numbers of electrons (including negative ions) and positive ions only electrons are considered in the energy absorption process, because the positive ions are relatively much heavier than the electrons and are thus essentially unmoved by the electric field. The potassium ion (K^+) is, for example, 7.2×10^4 times heavier than an electron.

From this discussion it can be seen that the attenuation of radar waves traversing an ionized rocket exhaust would be expected to depend upon the number or frequency of collisions of electrons with gas molecules and the quantity of energy transferred on each collision. These quantities can be related to the collision cross-section, which is the effective area of a molecule which the electron "sees". Since the traveling electric component of the electromagnetic wave can be pictured as continually reversing its direction with the wave frequency, and thus the direction in which it exerts a force on the electrons, a relationship can be obtained between the attenuation and the relative radar and electron collision frequency. Thus, when the electromagnetic frequency is small with respect to the collision frequency, the electric conductivity of the gas is the same as the dc value; but when the electromagnetic wave frequency is large, the conductivity depends on the frequency. Since the electrons are absorbing energy, the attenuation depends upon their concentration. These factors all enter into the problem in a rather complicated way, and the manner of interpreting the phenomena has varied greatly, at least mathematically, from author to author. Nevertheless, the same principles have been involved and most of the

differences are semantic. We will present the equations necessary to show the relationship of the above parameters and to calculate radar attenuation in rocket exhausts from molecular parameters, such as electron number density and collision cross-sections. Rigor will be sacrificed to minimize and simplify the number of equations with the intent of conveying a feel for the problem to the uninitiated.

Attenuation is measured in decibels, db, which is defined as ten times the logarithm of the power ratio P/P_o. Thus, when an electromagnetic wave of power P_o enters an ionized medium and is reduced after traveling a distance x to 1/10 the original power, it is said to have suffered a -10 db attenuation. From this definition and Eq. (1), we have

$$\text{attenuation in db} = 10 \log \frac{P}{P_o} = 20 \log \frac{E}{E_o} = -\frac{20}{2.303} \alpha x$$

$$\text{db} = -8.68 \alpha x \tag{2}$$

To better see the meaning of α we observe that the electric and magnetic components of a plane electromagnetic wave are described by

$$E = E_o e^{j\omega t - \gamma x}$$
$$H = H_o e^{j\omega t - \gamma x} \tag{3}$$

which represents a wave varying periodically in time with the frequency $\nu = (\omega/2\pi)$ and advancing in the x direction through space with a complex propagation factor

$$\gamma = \alpha + j\beta \tag{4}$$

where α is the attenuation factor of Eq. (2) and β is the phase factor of the wave. The phase factor determines the distance, or wave length λ, that a wave must travel to experience a total phase shift of 2π radians, so the wave length is $\lambda = (2\pi/\beta)$ and the phase velocity is ω/β, which may exceed the velocity of light.

By means of Maxwell's equations, it can be shown that in the important case where $\omega_p/\omega \ll 1$, i.e., the plasma frequency is less than the frequency of the propagating wave (ω_p will be defined subsequently)

$$\alpha = \frac{2\pi \sigma_r}{c} \tag{5}$$

with c = velocity of light; 3×10^{10} cm/sec.

The phase factor can be shown to be[2]

$$\beta = \frac{1}{c}[\omega - \sigma_i]^{\frac{1}{2}}$$

where σ_r and σ_i are the real part and the imaginary part, respectively, of the complex conductivity. This conductivity now has to be related to the fundamental properties of the medium.

The motion of an electron in the electric field is described by the equation

$$m_e \frac{dv}{dt} + m_e \nu v = e E \tag{6}$$

where v is the velocity of the electron, m_e the mass of the electron, and ν the electron collision frequency which is assumed independent of velocity. We will observe subsequently the velocity dependence of the collision frequency but for this analysis that can be safely neglected. The solution of Eq. (6) is

$$v = \frac{e}{m_e} \frac{E_o \, e^{j\omega t}}{j\omega + \nu} \tag{7}$$

The recognition that the current density, J, electron concentration, n_e, and conductivity, σ, are related by

$$J = n_e e v = \sigma E \tag{8}$$

allows the solution for electrical conductivity

$$\sigma = \sigma_r + j\sigma_i = \frac{ne^2}{m_e} \frac{\nu + j\omega}{\nu^2 + \omega^2} \tag{9}$$

The plasma frequency, i.e., the frequency at which the electrons will execute simple harmonic motion about their equilibrium position due to an electron produced space charge restoring force is

$$\omega_p^2 = \frac{4\pi ne^2}{m_e} \tag{10}$$

It is convenient to rewrite Eq. (9) with the plasma frequency

$$4\pi \sigma = \frac{\omega_p^2 \nu}{\nu^2 + \omega^2} + j \frac{\omega_p^2 \omega}{\nu^2 + \omega^2} \tag{11}$$

The real part of this equation is that required to calculate the radar attenuation factor, α, in Eq. (5)*

$$4\pi \sigma_r = \frac{\omega_p^2 \nu}{\nu^2 + \omega^2} \quad \text{statmhos/cm} \tag{12}$$

It is observed in Eqs. (11) and (12) that the conductivity depends, as expected, on the concentration of electrons, the collision frequency of electrons with the gas, ν, and a relationship between the collision frequency and the frequency of the applied field, ω. Thus, as the applied field is increased beyond the collision frequency, a phenomena frequently observed in

*When $\nu^2 > \omega^2$, Eq. (12) reduces to the dc conductivity

$$\sigma_{dc} = 0.626 \frac{e^2}{m_e kT} \cdot \frac{1}{Q} \cdot \frac{n_e}{n_o}$$

which differs from that presented by Sherman[6] only in the numerical coefficient, 0.626 instead of 0.532.

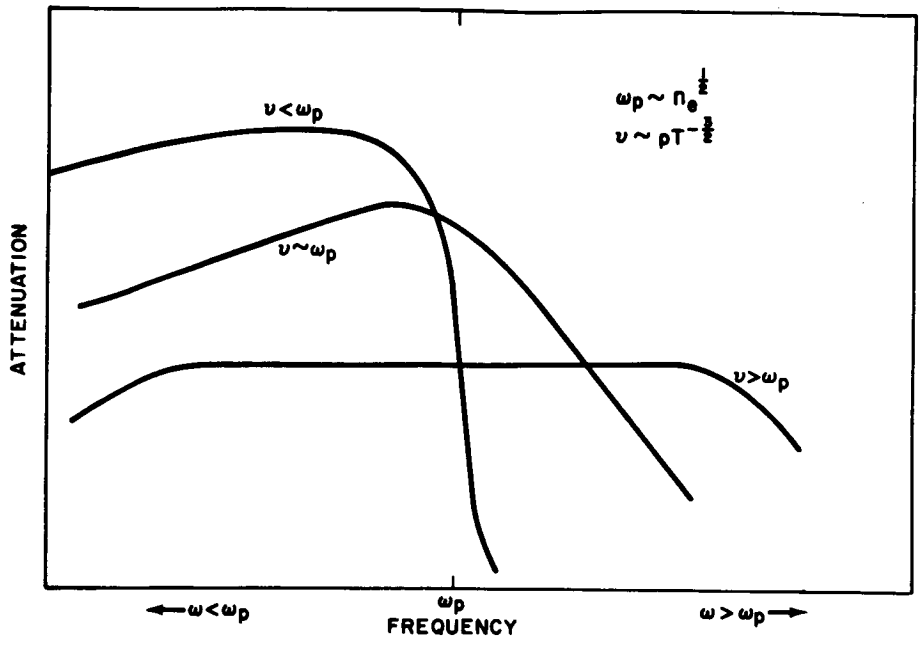

FIG. 3 INFLUENCE OF RADAR FREQUENCY, COLLISION FREQUENCY AND PLASMA FREQUENCY ON ATTENUATION

time dependent systems is observed called dispersion; the conductivity suddenly is reduced with increasing electromagnetic frequency. Thus, one of the possible solutions to a radar attenuation problem is to increase the signal frequency. This, of course, is done when reasonable, but other complications arise which greatly limits this as a standard "fix". For example, at the higher frequencies it becomes more difficult to effectively produce electric power and molecular absorption becomes important.

Eq. (12) indicates the rather complex manner by which the attenuation (Eqs. 2 and 5) depends upon the radar frequency, collision frequency and electron density via the plasma frequency, ω_p. A better demonstration of this is shown in Fig. 3, which is obtained from a more exact mathematical representation. For detailed curves, see Balwanz.[7] Since the collision frequency as well as the electron density are dependent upon the pressure and temperature, and thus the altitude, as well as the chemistry of the system, this shows why an understanding of details is required. The problem, however, is by no means hopeless because, as we will see, we already have an understanding of the rudiments.

In order to predict the radar attenuation, the electron concentration and collision frequency are all that is required at a given radar frequency. The estimation of the electron concentration is the subject of laboratory studies of rates of ion (and electron) formation and removable, or when equilibrium pertains, the electron concentration can be obtained by a straightforward thermodynamic equilibrium calculation.

The collision frequency, ν, is related to the collision cross-section, Q_e by

$$\nu = \frac{v_e}{\lambda_e} = \sqrt{\frac{8k\,T_e}{\pi m_e}} \sum_s n_s\, Q_{es} \qquad (13)$$

where

v_e = electron velocity
T_e = electron temperature
λ_e = electron mean free path
n_s = number density for the s species with which the electrons collide
Q_{es} = electron collision cross-section with the s species.

Since the collision cross-sections for electrons with exhaust products are not well known in the low energy range of interest, an average value is frequently used. Eq. (13) then becomes, in terms of the total particle density, n_o

$$\nu = \sqrt{\frac{8k}{\pi m_e}} \cdot \sqrt{T_e} \cdot n_o\, \bar{Q}_e \qquad (14)$$

Because of the large dipole of water vapor and its usual large concentration in exhaust gases, Altshuler[6] has shown that its collision cross-section normally dominates all others and may be expressed by

$$Q_e\, v_e^2 = 5.9 \text{ cgs units}$$

$$\text{or} \quad Q_e = 5.9 \left(\frac{\pi m}{8k}\right) \frac{1}{T_e} = \frac{1.5 \times 10^{-11}}{T_e} \qquad (15)$$

Collision cross-sections frequently show large variations with electron energies. With solid propellants of the ammonium perchlorate type, large concentrations of HCl will also be present in the exhaust. This has an electron collision cross-section of about 5.5×10^{-15} cm^2 over the temperature range of interest in rocket exhausts. This is comparable to that for water which is, according to Eq. (15)

Temperature	Q_e (H_2O)
1,000°K	15×10^{-15} cm^2
2,000	7.7
3,000	5.1
4,000	3.9

Other cross-sections are the order of 20% of these, so can probably be neglected for most rocket exhausts - the overall calculation is probably not that good.

The electron temperature is required in both Eq. (14) and (15) and may differ from the gas temperature. This is to be expected when electrons are

being produced by chemi-ionization reactions at the point of interest. Langmuir probe studies in laboratory flames show electron temperatures several thousands of degrees greater than the flame temperatures and these temperatures persist downstream from the reaction zone for a longer time than would be predicted by electron temperature relaxation theories. This situation needs clarification - until then, the flame temperature will probably have to be used.

To more clearly convey some idea of the numerical magnitude of attenuation due to electrons, the curves in Fig. 4 have been prepared with reasonable assumptions covering ranges of possible interest. The electron concentration is presented in mole fraction of electron, n_e/n_o, where n_o is the total number of molecules in the gas phase and is given by

$$n_o = 2.687 \cdot 10^{19} \cdot \frac{273}{T} \cdot \frac{p}{1} \text{ molecules/cc}$$

with p in atmospheres and T in ^oK. The curves were generated by use of Eqs. (2), (5), (10), (12) and (14). When $\omega_p/\omega > 1$ the detailed curves prepared by Balwanz[7] were used instead of Eqs. (2), (5) and (12). These detailed curves are in a very usable form and are recommended to anyone desirous of making attenuation calculations. In computing the collision frequency, ν, by Eq. (14), an average electron collision cross-section $\bar{Q}_e$ of 6×10^{-15} cm^2 was assumed at $T_e = 2{,}000^oK$. The following pressures with their equivalent neutral number density (at $2{,}000^oK$) and equivalent altitude (ARDC model)[10] were chosen

Pressure, Atm.	n_o (at $2{,}000^oK$)	Altitude, Ft.
1.0	3.67×10^{18}	0
0.1	3.67×10^{17}	53,000
0.01	3.67×10^{16}	100,000
0.001	3.67×10^{15}	160,000

The following frequencies corresponding to the indicated radar bands and wave lengths were chosen

Frequency KMC	Band Designation	Frequency Range KMC	Wave Length cm
1	L	0.39 - 1.55	77 - 20
5	S	1.55 - 5.20	20 - 5.8
	C	3.90 - 6.20	11.8 - 7.3
10	X	5.20 - 10.9	5.8 - 2.5
	K	10.9 - 36.0	2.5 - 0.8
	Q	36 - 46	0.8 - 0.6
50	V	46 - 56	0.6 - 0.5

SOURCES OF ELECTRONS

There are several possible sources of electrons from solid propellant rockets. These sources are illustrated in Fig. 5. First consider the solid propellant in the combustion chamber itself. Here both the temperature and pressure level are quite high so that reaction rates will be fast. There are two potential sources of ions in the rocket chamber. First, because of the high temperature level, thermal ionization of low ionization potential

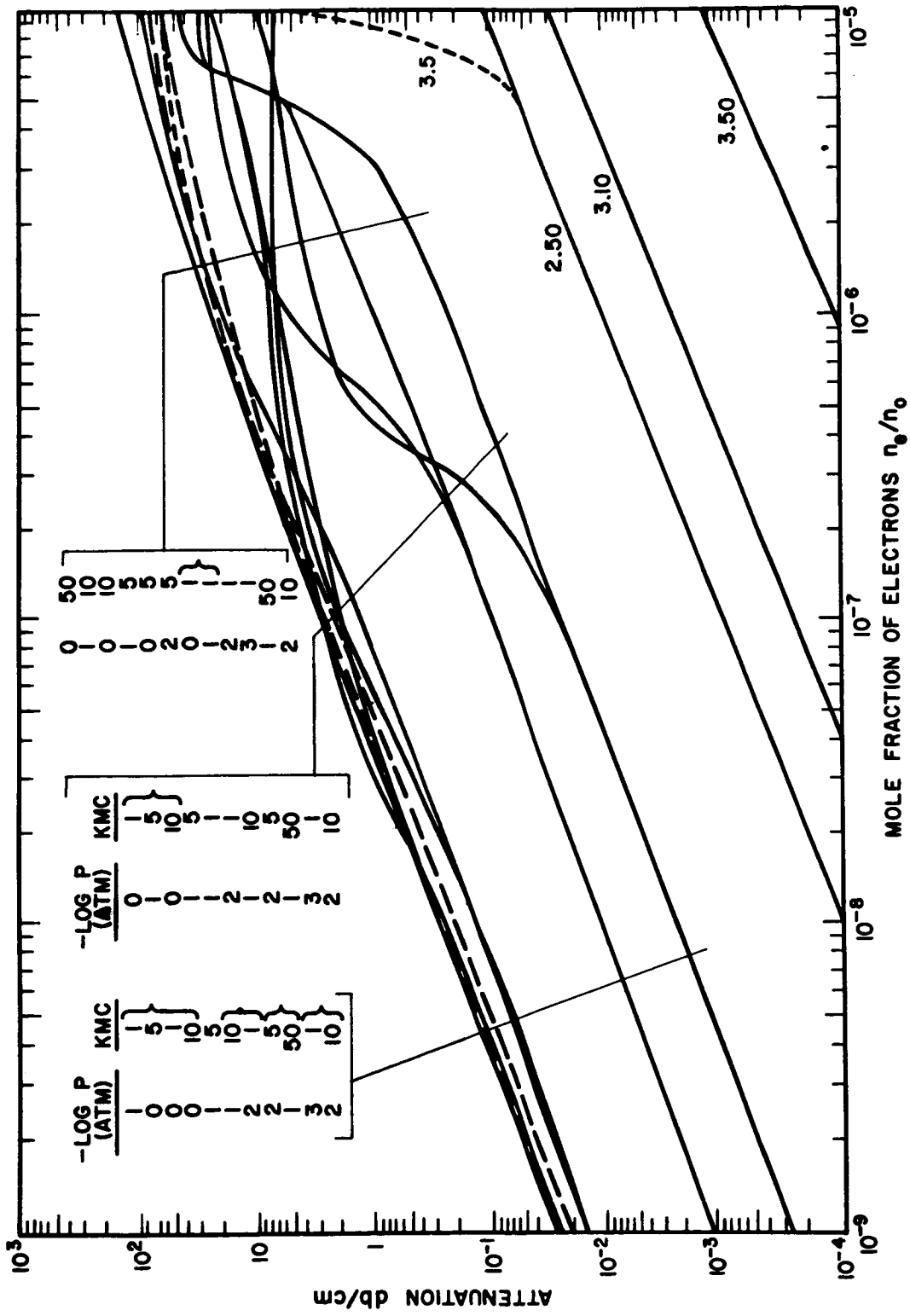

FIG. 4 ATTENUATION AS A FUNCTION OF ELECTRON MOLE FRACTION FREQUENCY AND PRESSURE

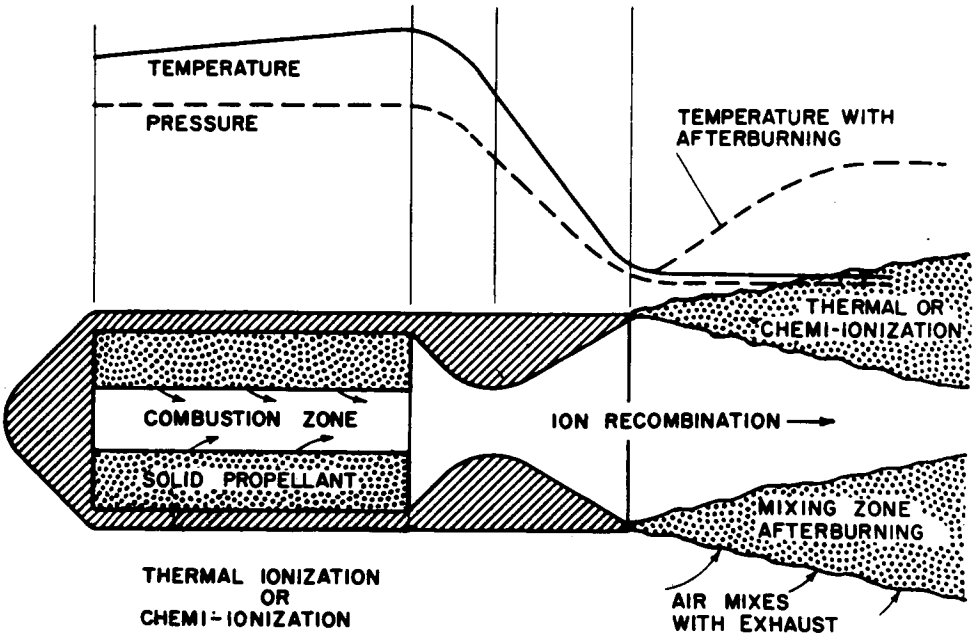

FIG. 5 ELECTRON SOURCES IN SOLID PROPELLANT ROCKETS

substances such as potassium, sodium, aluminum, and nitric oxide may occur. These substances may be part of the solid propellant or impurities in the propellant. For example, ammonium perchlorate commercial grade has about 400 ppm of potassium and about 40 ppm of sodium, while atomized aluminum powder may contain about 500 ppm potassium and about 20 ppm sodium. (See Table II in next section). As will be seen in the next section, these quantities of material are sufficient to produce thermal ionization at the high temperatures of rocket propellants. Were these sources not present, it is also possible that ions could be produced by chemi-ionization. This would be expected particularly when hydrocarbons are present to react with oxygen. However, no evidence has yet been obtained for chemi-ionization in solid propellants, and at these temperatures it seems quite likely that thermal ionization will mask any chemi-ionization. Some examples of electron concentrations in solid propellant strands burned in a burning-rate bomb are presented in Fig. 6. These concentrations were calculated from conductivity measurements between small wires emersed in the solid propellant flame (AeroChem Data). However, until better information is obtained, we must hold open the possibility of chemi-ionization. Even in the presence of low ionization potential alkali metals, chemi-ionization could produce ions above the thermal level by charge exchange reactions such as

$$H_3O^+ + Na \rightarrow H_2O + H + Na^+$$

It should be noted that enhancement of ionization in alkali-containing flames has been observed[1,2,3], Fig. 7. This enhancement may also occur at the pressure of the rocket chamber.

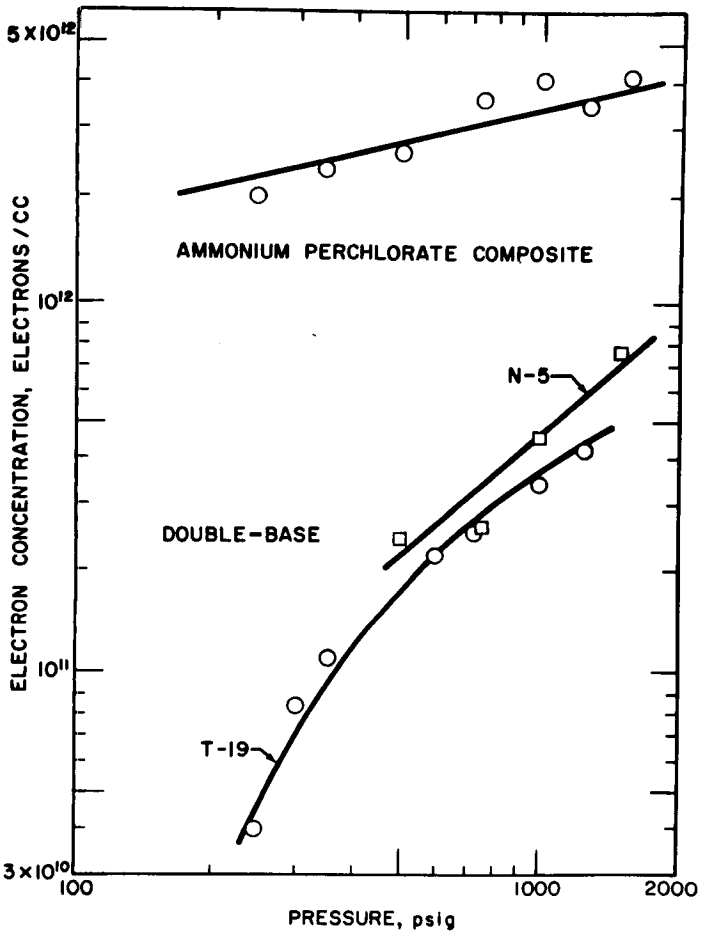

FIG. 6 ELECTRON CONCENTRATIONS IN TYPICAL SOLID PROPELLANT FLAMES

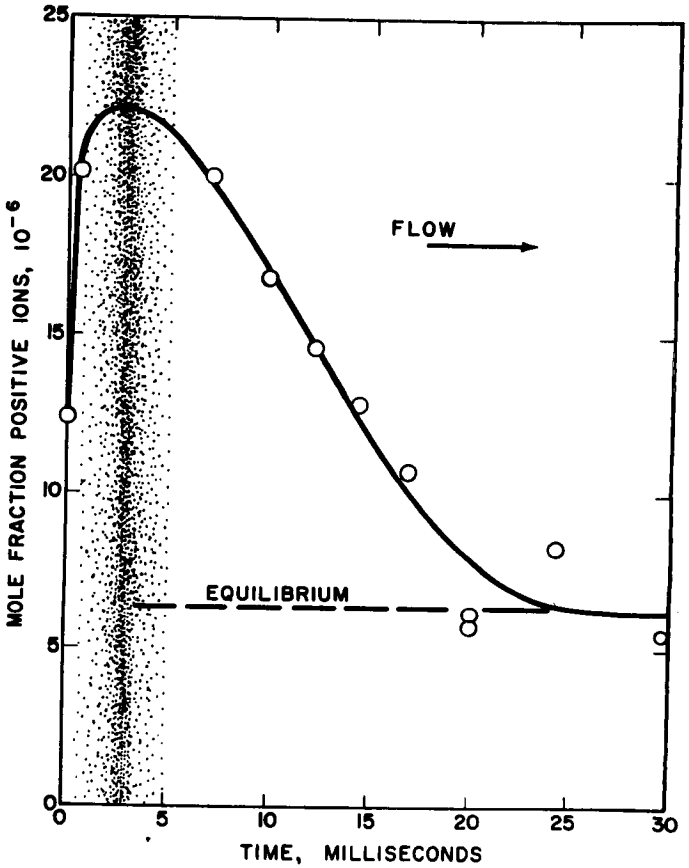

FIG. 7 NON-EQUILIBRIUM IONIZATION IN A POTASSIUM CONTAINING FLAME

Propane - Air at 0.093 atm. with 2×10^{14} atoms/cc Potassium added

Calcote Ref. 3

The ionization thus produced in the rocket chamber will decay as the combustion gases are exhausted from the combustion chamber through the rocket nozzle. The temperature and the pressure will drop as the gases expand in the nozzle. During this process the ions produced in the chamber will be lost by recombination. Recombination of alkali metal ions is slower than recombination of chemi-ion ions. This will be discussed in detail in a subsequent section. It should be noted here, however, that with fluid dynamic theories which are quite adequate for expansion of gases in the nozzle, and with a knowledge of the variation of ion recombination coefficients with temperature and pressure, one should be able to predict the variation in ion concentration as the gases are expanded. Electron attachment can also reduce the electron concentration during expansion, and a knowledge of attachment coefficients would permit a prediction of the extent of electron decay expected due to this source. The same problems associated with frozen equilibrium of the combustion products will prevail for these calculations and can be treated in the same fashion as in determining where frozen flow occurs in the nozzle. This will also be discussed in more detail in a subsequent section.

The gases, after leaving the rocket motor, may mix with the outer atmosphere. Should such mixing produce a combination of temperature, pressure, and composition appropriate to thermal ignition, afterburning will be obtained. This afterburning will increase the temperature so that again it is possible to thermally ionize any impurities which may have been in the rocket chamber. Such impurities may also arise from the case or any lining material in the nozzle. Again, the possibility of chemi-ionization should also be considered. It may even be more important here because the gas temperatures due to afterburning may be considerably lower than those in the rocket chamber. The possibility that shock diamonds formed in the exhaust gas will produce ionization has also been considered[4,5], as well as the possibility of solar ionization of excited products[3,6,7] and the reflection from solid particles.[7] The high relative velocity of the exhaust gases with respect to ambient gases may also increase the temperature - this will be considered subsequently.

Ionization in rocket exhausts may come from a number of sources, and it is thus difficult to generalize and compare observations from one rocket firing to another when the conditions vary greatly. A detailed understanding of the basic processes involved, such as thermal ionization, chemi-ionization, ion recombination, ignition, and afterburning will go far toward allowing one to predict when difficulties will be experienced. Solid particles such as carbon produced in rich flames due to degradation of the case material, as well as solid particles such as aluminum oxide produced in the combustion of aluminized propellants, also offer a possible source of ionization; these too will be discussed in more detail.

THERMAL IONIZATION

If one were faced with the problem of determining the source of ionization for the first time, thermal ionization would be the first step in the process. Indeed, the earliest advocates of a chemi-ionization mechanism in hydrocarbon-oxygen flames had to first prove that the source of ionization was not the result of ionization of intermediates, e.g., free radicals or impurities such as potassium or sodium, having a low ionization potential.

Ionization of Gases

A rough idea of the ionization to be expected from substances appearing in solid propellant flames can be gained by a comparison of the ionization potentials, V_i, of possible components of the flame, Table I.

TABLE I. IONIZATION POTENTIALS, eV

Substance	V_i	V_i/R^a
Cs	3.89	45,200
K	4.34	50,300
Na	5.14	59,600
Ca	6.11	70,900
Al	5.98	69,400
Al_2O	7.7	89,000
NO	9.25	110,000

[a] V_i/R has dimensions of T ^oK

If it is certain that the source of ionization is thermal then the calculation of the electron concentration is in principle a simple matter by using Saha's equation, which expresses the concentrations of the ion, electron, and neutral species in equilibrium.

$$A \rightleftarrows A^+ + e$$

Saha's equation for a singly ionized substance is obtained by simplifying the equilibrium constant partition function ratio and is usually used as

$$\log K_n = \log \frac{n_+ n_e}{n_o} = \log G + 15.38 + 1.5 \log T - \frac{5040\, V_i}{T}, \text{ where}$$

K_n = equilibrium constant

n_e, n_+, n_o = the number density of electrons, ions, and neutral species respectively

$G = \frac{g_+ g_e}{g_o}$ = the statistical weight of ions, electrons, and neutral species respectively.

For the alkali metals such as sodium and potassium, $g_e = 2$, $g_+ = 1$, and $g_o = 2$; therefore, $G = 1$. For the alkaline earth metals such as calcium and barium, $g_e = 2$, $g_+ = 2$, and $g_o = 1$; therefore, $G = 4$. The Saha equation in the above form considers only equilibrium between the ground state and ionization and neglects other excited states, so that a more exact calculation may give a smaller degree of ionization.[3] Thus, for a specific liquid propellant motor, the ionization of NO at 3400^{o}K and 500 psi, the above method gives 3.6×10^{-9} mole fraction electrons, and the exact method gives 2.6×10^{-9} mole fraction electrons.

The appearance of at least trace quantities of potassium and sodium appearing as impurities in most materials can be accepted without question. As an example of this, analyses of some propellant ingredients and rocket

TABLE II

ANALYSIS OF PROPELLANT INGREDIENTS FOR SODIUM AND POTASSIUM

(parts per million)

Ingredients[1]		Na	K
Aluminum:	dynamite grade	10	1
	Metals Distintegrating Co., spherical	29	180
	Alcoa 123[2]	0	490
	Alcoa 123[3]	<5	<30
Ammonium perchlorate:	commercial	80	420
	"	42	380
	reagent	12	14
Nitrocellulose:	Parlin Plant	50	0
	Olin Ball	147	440
Triacetin		0	0
Resorcinol		28	1
2 Nitrodiphenylamine (NDPA)		0	0
Nitroglycerin		16	17
Buna-N:	insulator	600	50
	liner also 1760 ppm Ca[4]	1600	700
DDP propellant:	base-grain process	29	100
	slurry-cast process	100	160

[1] From Ref. 17 except where indicated

[2] Private communication from Paul Molmud Space Technology Laboratories, Aug. 8, 1961

[3] From the Aluminum Company of America November 7, 1961

[4] Private communication from Billings Brown, Hercules Powder, Magna, Utah, February 8, 1962

materials have been accumulated from various sources and shown in Table II.

Using Saha's equation and a reasonable range of potassium and sodium concentrations in ppm by weight (assuming an average gas molecular weight of 25) that can be expected in ammonium perchlorate propellants, the electron concentrations were calculated for three different pressures (1000 psi, 1 atm, .001 atm) and plotted against temperature in Figs. 8, 9, and 10. The curves were constructed by considering the equilibrium only between alkali metal atoms and electrons. No account has been taken of the equilibrium of the potassium and sodium atoms with their oxides or salts which would reduce the electron concentration, nor was the attachment of electrons to form chloride ions or hydroxyl ions considered in this computation.

The question has been raised as to why potassium sulfate, which is used as an additive in propellants in order to prevent afterburning, does not ionize appreciably. Certainly the potassium will ionize appreciably when the gas temperature is high enough. However, the potassium sulfate prevents afterburning and thus prevents the formation of high temperatures.

Because of the low ionization potential of cesium, quantities as low as 1 ppm could cause appreciable ionization. In connection with the Minuteman program[4], there was some concern about the presence of small quantities of cesium in ammonium perchlorate. It was found, however, that cesium is not present in any detectable amount in the ammonium perchlorate obtained from the Henderson Plant of American Potash and Chemical Corporation; therefore, no problem is anticipated from cesium.

Nitric oxide also was considered as a source of ionization in the Minuteman.[4] An equilibrium calculation showed that the electron concentration produced from the ionization of nitric oxide in the exhaust would be only one percent of that produced from the sodium impurity.

Considerable attenuation is encountered when aluminum is added to propellants to increase rocket performance. We may expect aluminum to increase the ionization in rocket exhausts in several ways. One way may be the direct result of the increase in combustion temperature associated with the large quantities of aluminum. Consequently, the exhaust temperature will increase, and therefore the electron concentration will increase by thermal ionization of potassium and sodium present in the propellant. As an illustration of the magnitude of this effect, DDP-70 propellant which contains 29% aluminum has an equilibrium exhaust temperature of 2088°K.[5] Using Fig. 9 and a potassium content of as small as 10 ppm in the propellant, the electron concentration in the exhaust will be 4.2×10^{11} electrons/cc. The trend in solid propellant rockets appears to be toward hotter propellants. Examples of this are the above DDP-70 propellant which has a combustion temperature of 3279°K (1000 psi) and CYH propellant which has a combustion temperature of 3660°K (300 psi). In the above example, afterburning was neglected. Ignition of the exhaust gases will become easier as a result of the hotter exhausts which would augment the problem.

Still another possible source of trouble with aluminized propellants is the thermal ionization of gaseous aluminum and its oxides. The thermal ionization of aluminum oxide molecules should be clearly distinguished from the thermal ionization of small aluminum oxide particles, which will be discussed

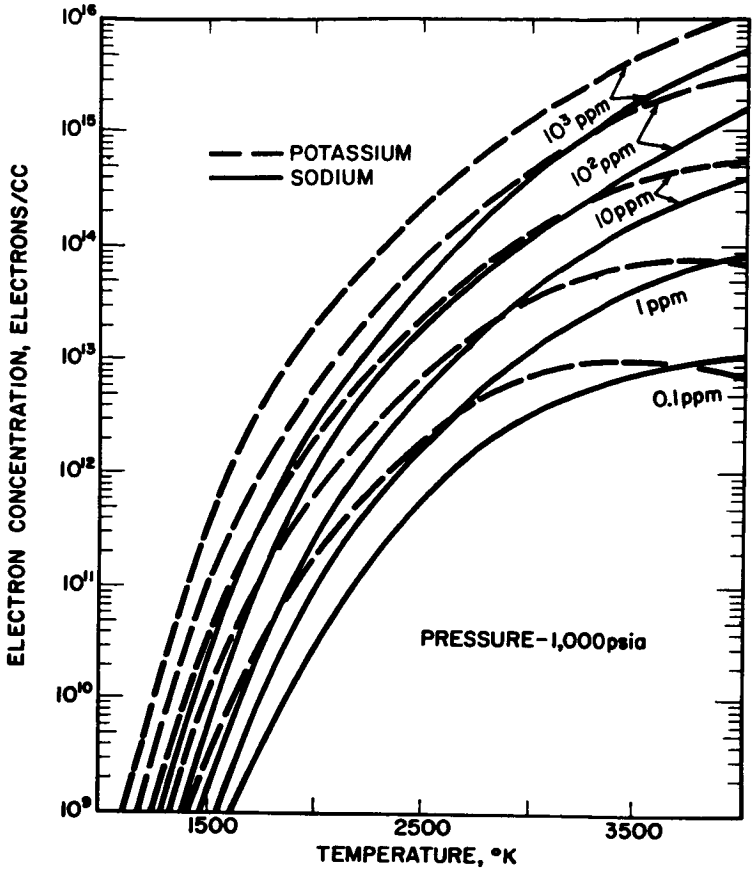

FIG. 8 EQUILIBRIUM ELECTRON CONCENTRATIONS AT 1,000 PSIA

Potassium and Sodium Concentrations in ppm by Weight

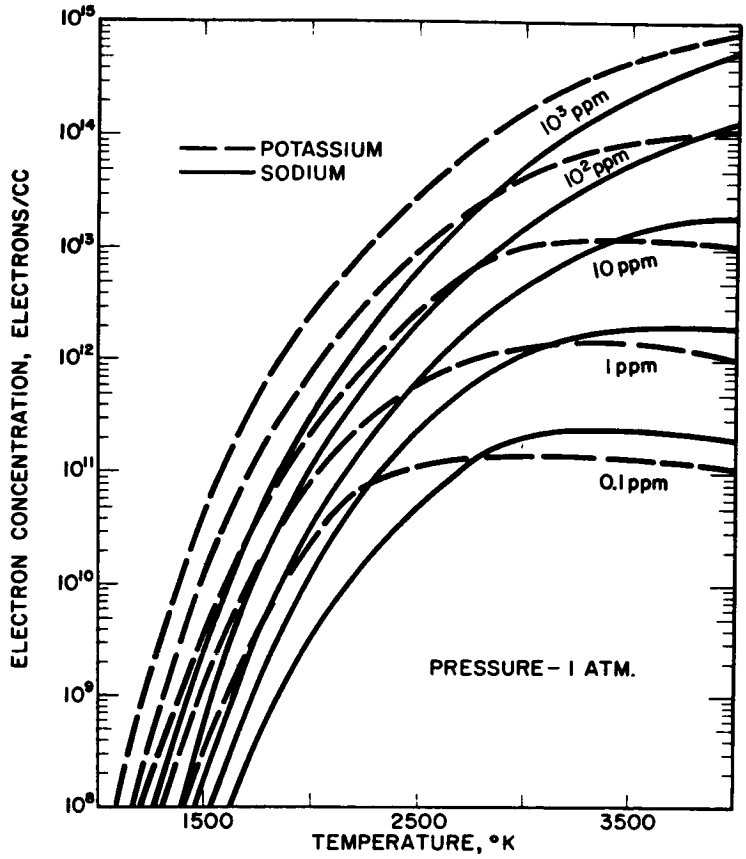

FIG. 9 EQUILIBRIUM ELECTRON CONCENTRATIONS AT 1 ATM.

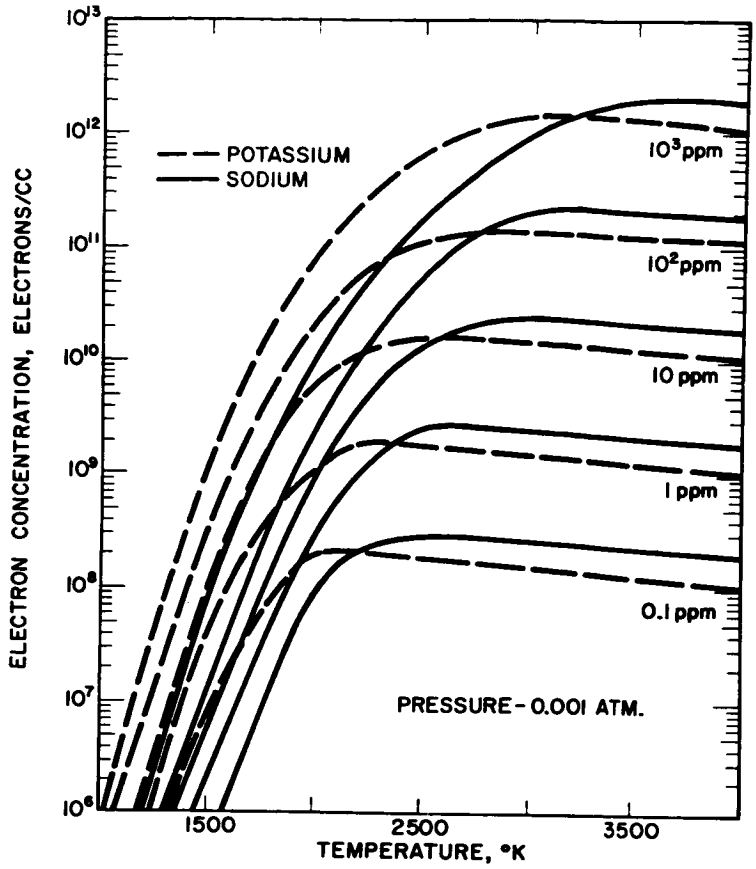

FIG. 10 EQUILIBRIUM ELECTRON CONCENTRATIONS AT 0.001 atm.

in a subsequent section. The ionization potential of aluminum is comparable to calcium (Table I). The ionization of aluminum was considered in a recent Minuteman report.[6] The first results of a machine calculation indicated that aluminum is as important as potassium in giving free electrons in the chamber (Table III). However, at one atmosphere the aluminum contributes only about 6×10^{-3} as many electrons as potassium. This, of course, assumes equilibrium - if the aluminum does not burn completely, it may make a larger contribution.

The ionization potentials of the aluminum oxides are unknown with the exception of Al_2O, which has an ionization potential of 7.7 eV. An estimate of the ionization potentials of the other aluminum oxides can be obtained by comparison with the ionization potentials of adjacent groups in the periodic table, which shows that the ionization potential of the other aluminum oxides will not differ greatly from that of Al_2O.

Attachment

When substances are present with large electron affinities, these may remove electrons by attachment. The electron affinities for some such species are summarized in Table IV. The importance of attachment is shown in Table III. Because of the large electron affinity of chlorine and the large quantities of chlorine in the exhaust, an estimate of electron attachment to chlorine atoms has been made to show when it might be important, Fig. 11. Attachment of electrons to hydroxyl radicals is also significant as Table III shows, but it was not considered in preparing Fig. 11. Only two equilibria

TABLE III

THERMAL IONIZATION IN PROPELLANT TYPES DDP 70 AND CYH

(Concentrations in moles per 100/gm)

From Ref. 6

SPECIE	DDP 70			CYH		
	20.3 atm 3638°K	1.0 atm 2730°K	0.3 atm 2390°K	20.4 atm 3662°K	1 atm 2722°K	0.3 atm 2367°K
Al^+	5.23×10^{-4}	1.00×10^{-6}	1.14×10^{-8}	5.15×10^{-4}	5.1×10^{-7}	3.7×10^{-9}
K^+	2.75×10^{-4}	1.6×10^{-4}	6.98×10^{-5}	3.00×10^{-4}	1.7×10^{-4}	6.84×10^{-5}
OH^-	4.72×10^{-4}	5.09×10^{-5}	1.50×10^{-5}	---	---	---
Cl^-	3.20×10^{-4}	1.09×10^{-4}	5.45×10^{-5}	2.11×10^{-4}	8.77×10^{-5}	4.39×10^{-5}
e^-	6.23×10^{-6}	8.03×10^{-7}	2.13×10^{-7}	7.98×10^{-6}	1.16×10^{-6}	2.93×10^{-7}
Al^o	8.47×10^{-3}	1.30×10^{-4}	6.06×10^{-6}	9.1×10^{-3}	9.9×10^{-5}	3.59×10^{-6}
K^o	2.34×10^{-5}	1.86×10^{-5}	1.26×10^{-5}	2.9×10^{-5}	2.99×10^{-5}	2.07×10^{-5}
OH^o	4.47×10^{-2}	7.08×10^{-3}	2.0×10^{-3}	5.07×10^{-4}	8.24×10^{-5}	2.4×10^{-5}
Cl^o	2.72×10^{-2}	1.32×10^{-2}	6.15×10^{-3}	---	---	---
Mols Gas	3.2075	3.0458	3.0113	3.2839	3.1195	3.0838
Mols Al	0.3664	0.3929	0.3944	0.3451	0.3662	0.3668
TOTAL	3.5739	3.4414	3.4057	3.6290	3.4857	3.4516

Inputs:		
Aluminum	21.3 wt. %	19.8 wt. %
Potassium	0.015	.015
Sodium	0.015	.015
Ammonium Perchlorate	20.47	10.8

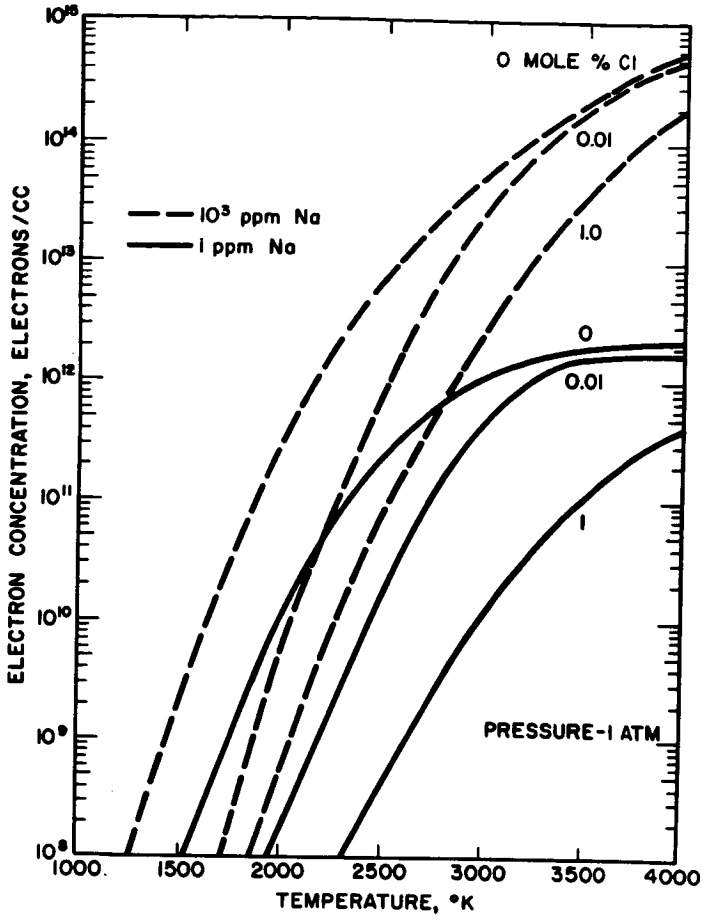

FIG. 11 REDUCTION OF ELECTRON CONCENTRATION BY ATTACHMENT TO CHLORINE ATOMS

were considered

$$Na \rightleftarrows Na^+ + e^-$$

$$Cl + e^- \rightleftarrows Cl^-$$

and the chlorine atom concentration was considered constant for 1 and 0.01 mole % over the temperature range. To consider all the required equilibria, of course, is a complex calculation. The reduction of the electron concentration as a result of equilibrium attachment can be appreciable, as seen in Fig. 11 and Table III. As will be pointed out in a subsequent section, attachment rates may be slow so equilibrium may not be attained; thus, the actual electron concentration will lie between the attachment and non-attachment calculations.

TABLE IV. ELECTRON AFFINITIES, eV

O_2	0.9[7]
OH	2.2[7]
CN	3.6[7]
Cl	3.7[8]
Br	3.5[8]

Solid Particles

The possibility that solid particles might be responsible for ion formation in flames has for a long time been an attractive hypothesis for many

people who would explain ionization in hydrocarbon flames by small carbon particles. Mass spectrometric studies have conclusively eliminated this explanation[1,9,10] and, in fact, it is most likely that the mechanism of ion formation in hydrocarbon flames explains the formation in some instances of carbonaceous particles.[9] Nevertheless, under conditions when large concentrations of carbon particles exist at high temperatures, thermal ionization of these particles to produce electrons can be expected. The exhaust of many solid propellant rockets, particularly those containing metals, are frequently rich in solid particles such as Al_2O_3, and these also must be considered as possible sources of thermal electrons.

The energy required to remove an electron from a solid, i.e., the work function, is low compared to the energy required to ionize an atom or molecule which makes solid particles attractive electron sources. However, many atoms or molecules are required to produce a particle which in turn can usually be responsible for only a few electrons per particle. Einbinder[11] and F. Smith[12] have developed theoretical expressions for the thermal production of electrons from solid particles in terms of the size of particles, the temperature, the number density of particles and the work function of the substance. Because the particles are small, an effective correction to the work function is required to account for the electrical capacitance of the particle, which will make removal of an electron more difficult. The work function of small solid particles has yet to be determined experimentally.

As a rational approach to the problem, we have assumed three widely different percentages of total molecules in the gas tied up as solid particles; i.e., we have assumed that of the total molecules present at the temperature-pressure conditions, a given percentage is tied up as a solid particle. This method of presentation avoids the possible error of choosing a particle size and number density which is unrealistic with respect to the total gas composition. Thus, for example, in an ammonium perchlorate-polyester resin propellant of 80-20% by weight, the mole percent carbon atoms in the atomic make-up of the products is 14%. This is available to produce not only carbon particles but carbon dioxide and carbon monoxide which are present (at equilibrium, no carbon particles are anticipated) to the extent of 9 and 22 mole percent, respectively. Any carbon in the form of particles must come at the expense of these two products, and the oxygen which would have been attached to the carbon must be accounted for. For aluminized propellants, Hogland and Saarlas[13] state that as much as 20-40% by weight of exhaust gases can be solid Al_2O_3 particles of about 2-4 microns diameter. Other estimates of particle size are 1-2 microns.[14] There may, however, be many fines which are not reported because the major interest in solid particles has been chiefly in terms of velocity and temperature lag in nozzle flow, and for this purpose the large particles are of most concern.

The volume occupied by each carbon atom is 8.84×10^{-24} cc for a density of 2.25 gm/cc for graphite (amorphous carbon has a density of 1.8 to 2.1 gm/cc). Then the number density of solid particles in the gas is

$$a = \left(\frac{3}{4\pi}\right) 8.84 \times 10^{-24} \left(\frac{n_{cg}}{r^3}\right)$$

where n_{cg} is the hypothetical number density of carbon atoms in the form of particles, and r is the particle radius. The calculation proceeds according to Smith[12] by calculating a saturation electron density near the bulk solid,

n_s, and then correcting this for the capacitance effect to the real electron density in the gas phase, n_e. The saturation density is given by

$$n_s = 2\left(\frac{2\pi m_e k}{h^2}\right)^{3/2} T^{3/2}\, e^{-\Phi/kT}$$

where

m_e = electron mass = 9.11×10^{-28} gm
k = Boltzman constant = 1.38×10^{-16} erg/degree
h = Planck's constant = 6.63×10^{-27} erg/sec
Φ = work function, ergs (1 eV = 1.60×10^{-12} ergs)

The work function for carbon has been taken as 4.35 eV. It should be noted that the work function is very sensitive to surface contaminates as well as bulk composition. The carbon particles found in flames are known to contain rather large concentrations of hydrogen, so before this treatment can be accepted with any level of confidence, measurements of work function will have to be made of carbon particles actually experienced in propellant combustion. F. Smith[15] has deduced a work function for Al_2O_3 particles of 6.1 eV from measurements of electron concentrations in an oxy-acetylene flame made by Pearson.[16]

The rather complex equation required to complete the calculation has been plotted by Smith as n_e/n_s as a function of W, and this graph is reproduced here as Fig. 12. The function W can be written as

$$W = \left(\frac{4\pi k}{e^2}\right) \frac{arT}{n_s}$$

where e = charge on electron = 4.80×10^{-10} esu (cgs-units). In writing W, the solid particles have been assumed to be spherical and their capacitance substituted as $C = 4\pi\varepsilon r$. If other particle shapes are of interest their capacity may be substituted.

This procedure has been used to generate the curves in Figs. 13, 14, and 15, which may be used to estimate the electron density due to carbon particles when a portion of exhaust is in the form of carbon particles and the particle sizes are available.

Similar curves could be produced for Al_2O_3 particles. If the work function is 6.1 eV[15], the electron concentration will be less than for carbon. If, for example, we assume 33% by weight of Al_2O_3 in the exhaust, a particle radius of 1 micron, a temperature of 2,000°K and a pressure of 1.0 atm, the electron number density would be about 10^5 per cc. For the same weight percent carbon at the same radius and assuming a work function of 4.35 eV, the electron concentration would be 4×10^9 per cc.

CHEMI-IONIZATION

In chemi-ionization, the energy of an elementary exothermic chemical reaction leaves one of the products in an ionized state

$$A + B \rightarrow C + D^+ + e^-$$

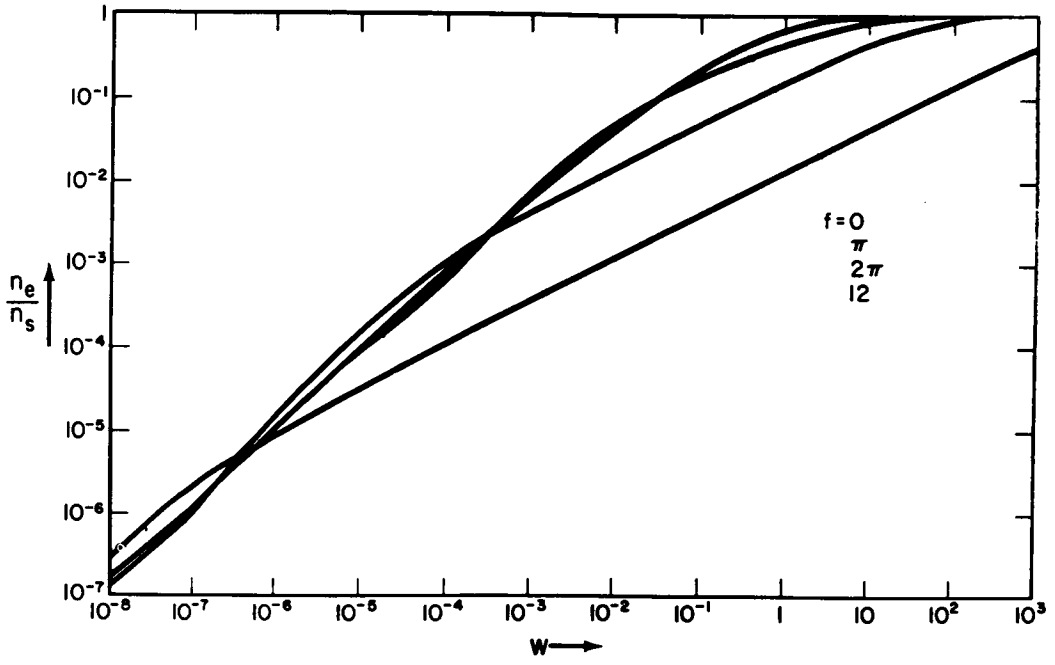

FIG. 12 DEPENDENCE OF ELECTRON DENSITY ON PARTICLE SIZE

F. Smith Ref. 12

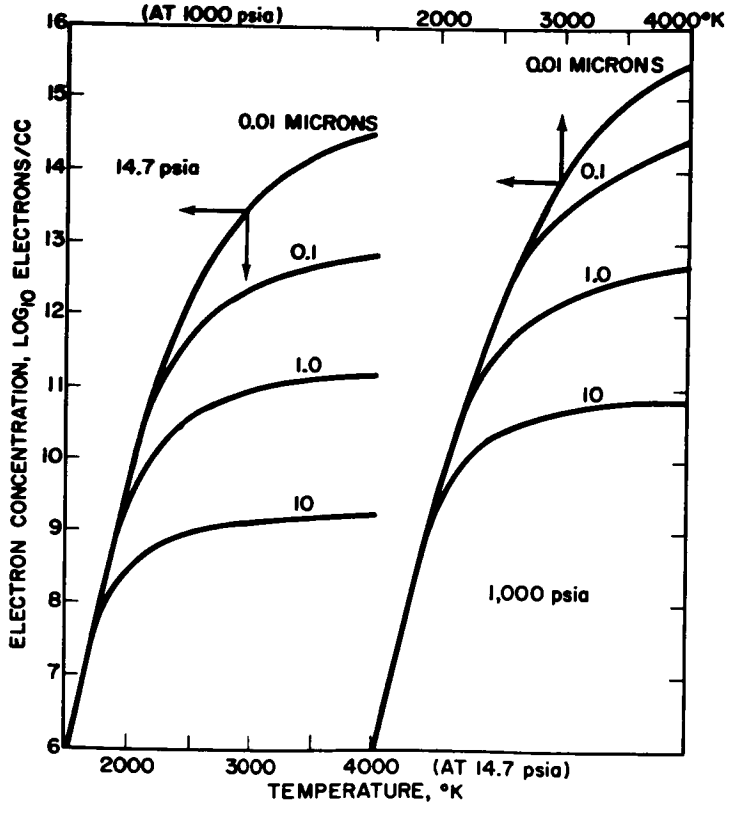

FIG. 13
THERMAL IONIZATION OF
CARBON PARTICLES

50% of Total Molecules
in Form of Particles

It has been demonstrated[1] that chemi-ionization is the principal cause of the large excess of ions in hydrocarbon-air or hydrocarbon-oxygen flames. The significance of this mechanism can be readily appreciated when it is realized that the ion concentration in some low temperature hydrocarbon air flames may exceed that which one would predict by thermal equilibrium, i.e., treating the products of combustion including radicals by means of Saha's equation by as much as 10^{12}. Contrary to somewhat popular belief, the process of chemi-ionization does not refer to a mysterious process. It describes simply the reaction of two reactive species where a major part of the energy of reaction goes into ionizing one of the products. Reactions in which vibrational energy of one of the products is concentrated in one degree of freedom are not uncommon. A rather large number of possible candidates have been considered for the specific ion-producing reaction. Although a number of these may actually participate, the reaction

$$CH + O \rightarrow CHO^+ + e^-$$

has been considered most probable.[2,3] The increase in attenuation experienced when entering the ionosphere, where oxygen is dissociated (see Fig. 2), may be due to the above reaction or to more intense afterburning by oxygen atoms.

From the measurements of maximum ion concentrations in hydrocarbon-air flames and the rate of ion recombination, the rate of ion production has been deduced as about 3×10^{13} ions/cc/sec. From studies of ionization flame detectors used in gas chromatography, it has been demonstrated[4] that ionization in hydrocarbon type molecules with air is very nearly linearly dependent upon the concentration of hydrocarbon from extremely low values of the order of 10^{-9} mole fraction to .01. It has also been demonstrated that the ion concentration is directly proportional to the number of carbon atoms in the hydrocarbon molecule with a somewhat smaller ion yield for carbon atoms which are already partially oxidized. From this data, as well as data on low pressure flames, it is estimated that an electron is produced for every million carbon atoms in the molecules which are burned.

Thus, if one knew the concentration of hydrocarbon fragments in a rocket exhaust, the number of ions produced from these fragments in afterburning could be predicted. It is not safe, however, to use the thermodynamic estimate of the hydrocarbon fragment concentration, so that the quantitative difficulty here hinges upon knowing either the concentration of hydrocarbon fragments or the concentration of CH radicals and oxygen atoms in the exhaust in order to predict the rate of chemi-ionization. Although we may understand the process we are not much better off, because we are ignorant of these concentrations. This represents a fundamental problem in general combustion chemistry.

The dominant ion in hydrocarbon-air flames has been shown by mass spectrometric studies[5,6,7] from several mm Hg to 1 atm to be the hydroxonium ion H_3O^+. This ion is produced from the CHO^+ ion above by an ion molecule charge exchange reaction in which the proton is transferred from the CHO^+ ion to the water molecule

$$CHO^+ + H_2O \rightarrow CO + H_3O^+$$

The rate constant for this reaction has been estimated[2] to be about 1×10^{-8} cc/molecule sec. Many other ions are produced in hydrocarbon-air flames, some of which can be rather simply explained, while others, to date, remain

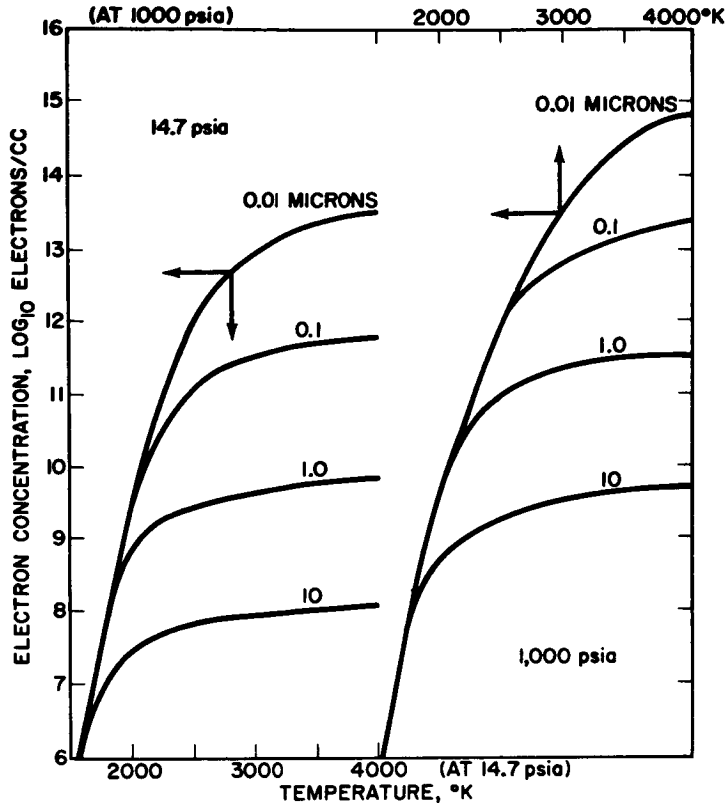

FIG. 14
THERMAL IONIZATION OF
CARBON PARTICLES

5% of Total Molecules
in Form of Particles

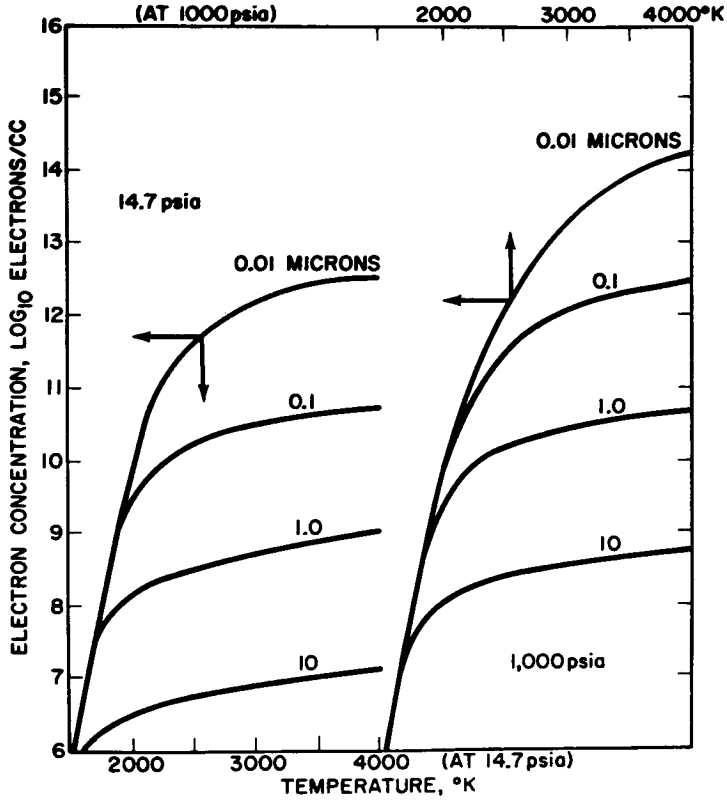

FIG. 15
THERMAL IONIZATION OF
CARBON PARTICLES

0.5% of Total Molecules
in Form of Particles

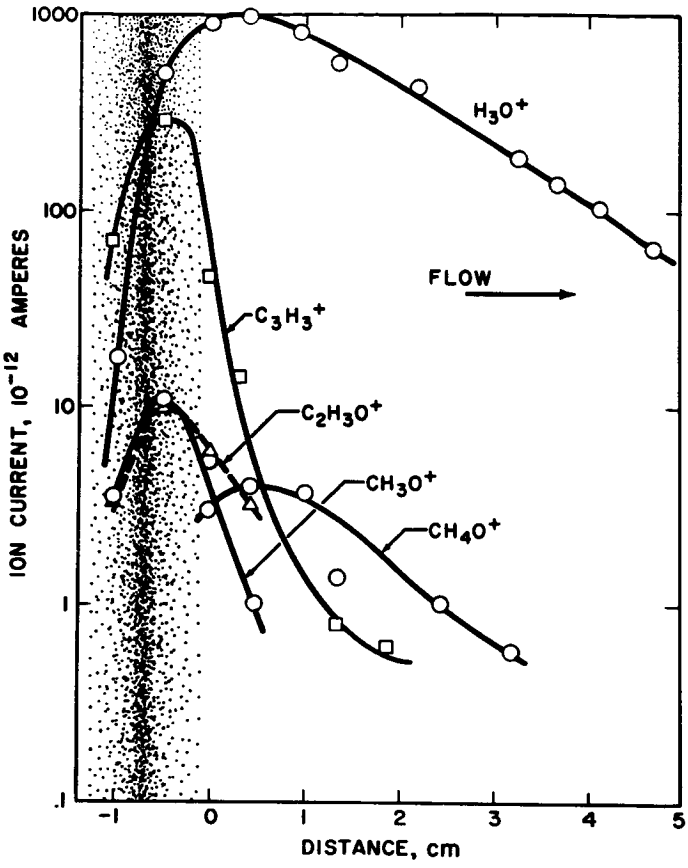

FIG. 16 ION PROFILES IN LEAN ACETYLENE-OXYGEN FLAME AT 3.3×10^{-3} ATMOSPHERES

Calcote and Reuter Ref. 5

a mystery. In rich flames with an excess of hydrocarbon radicals present, the formation of hydrocarbon ions occurs by the process

$$C_n H_{m-1} + H_3O^+ \rightarrow C_n H_m^+ + H_2O$$

Build-up reactions of hydrocarbon ions are generally exothermic with very small activation energies, so once a hydrocarbon ion or ion radical is produced we are on our way to larger ions via

$$R^+ + R \rightarrow RR^+$$

In low pressure hydrocarbon-oxygen flames, ion profiles typical of those presented in Fig. 16 have been obtained.

The importance of the mechanism of chemi-ionization is not limited to hydrocarbon-air flames because when small concentrations of alkali metals are added to hydrocarbon-air flames at low temperatures, the concentration of alkali metal ion can exceed the hydrocarbon-ion concentration, probably by charge exchange

$$H_3O^+ + Na \rightarrow Na^+ + H_2O + H$$

In these reactions the concentration of ions due to the alkali metal may actually exceed the equilibrium ionization concentration for the alkali metal[8,9] (see Fig. 7). The large effect which additives can have on the ion concentration is further evidence of some of the complexities of the multitude of reactions involved in a flame. Therefore, we might summarize by saying that

[redacted]

although a frame of reference exists to explain the phenomena of chemi-ionization and rather adequate explanations are available in some situations, the details in many cases have yet to be worked out; and the significance of this phenomena on ionization in rocket exhausts has yet to be completely defined.

ELECTRON LOSS MECHANISMS

Electron loss mechanisms are important because, coupled with the rates of ion formation, they determine the steady state electron concentration, and under some conditions, they will be the rate limiting step. Thus, when chemi-ions are produced either in the rocket chamber or in afterburning, the electron loss mechanism will determine the electron concentration as a function of time after production, which can be related to position in the rocket nozzle and in the expanding exhaust plume. For thermal ionization, the electron loss processes will determine the position in the nozzle at which the electron concentration is essentially frozen.

The important electron loss mechanisms are[1,2]: 1. Electron attachment, 2. Recombination (dissociative or three-body) and 3. Ambipolar diffusion. These will each be discussed as will the electron decay during nozzle expansion.

Electron Attachment

Electrons may be removed by attachment to atoms or molecules. As we have already noted, attenuation is due to electrons and not ions, so production of a relatively heavy negative ion by attachment effectively reduces the attenuation. Should the electron then become detached further downstream, possibly by photodetachment, attachment would in effect have reduced the electron density but increased the size of the exhaust plume. It seems, however, more likely that the fate of the negative ion would be to recombine with a positive ion and remove the electron completely. The equilibrium degree of electron attachment may be calculated by Saha's equation as described in the section on thermal ionization. However, the actual rate of attachment, i.e., the rate at which equilibrium is approached may become important.

Three processes for attachment are generally recognized, and these are distinguished by the manner in which the electron attachment energy is dissipated. These are ("A" represents a molecule or atom with an electron affinity)

1. Radiation:
$$A + e^- \rightarrow A + h\nu$$
2. Three body:
$$A + e^- + M \rightarrow A + M \text{ (excess energy)}$$
3. Resonance transfer to an excited electronic or vibrational state:
$$A + e^- \rightarrow A^*$$

The rate of the process is frequently described by an attachment coefficient, β (cc/electron-sec) defined by the equation

$$\frac{dn_e}{dt} = \beta\, n_e\, n_o$$

[redacted]

where n_o is the concentration of molecules attaching electrons. The attachment coefficient is related to the average electron velocity by

$$\beta = \bar{v}_e Q_a$$

where Q_a is the attachment cross-section. Another term, the attachment probability, h, is frequently used. This is the number of attachments per collision and relates the attachment cross-section, Q_a, to the kinetic theory electron cross-section Q_e by

$$Q_a = h Q_e$$

All three terms in this relationship are functions of electron temperature.

Electron attachment processes are apparently slow compared to other flame processes. Typical values are $Q_a = 10^{-22}$ cm^2 and $h = 10^{-7}$. Yet they may play an important part when large concentrations of halogen are present; see Table IV and Fig. 11. Experimental studies of attachment rates for chlorine containing flames are a must.

Measurements of attachment to form, presumably, OH^-, in hydrocarbon-air flames have been made by Williams[3,4] who finds $h = 2 \times 10^{-8}$. Knewstubb and Sugden found very little OH^- with a mass spectrometer[5] in hydrogen flames, while our Langmuir probe studies would indicate large concentrations of negative ions.

The capture of electrons by small particles has also been considered[6] and has been proposed as a means of removing free electrons.[7]

Electron Recombination

Two processes of electron recombination may be important in flames, again identified by the means of dissipating the energy of recombination. The important processes in a flame are

1. Three body:

$$A^+ + e^- + M \rightarrow A + M \quad \text{or}$$
$$A^+ + B^- + M \rightarrow A + B + M$$

2. Dissociative recombination:

$$AB^+ + e^- \rightarrow A + B$$

The recombination coefficient, α, is defined by

$$\frac{dn_\pm}{dt} = \alpha\, n_+\, n_e \text{ or } \alpha\, n_+\, n_-$$

Although this is a reaction rate law the α differs from the chemists rate constant, k, in that α may depend on the concentration and thus pressure. Because electrical neutrality must be preserved, the electron or negative ion concentration is usually equated to the positive ion concentration and the expression written $\alpha\, n_+^2$. For dissociative recombination, α is independent of pressure; and for three-body recombination it is dependent on the first power of pressure. The half life, i.e. the time it takes the ion

concentration to decay to one-half its original value is

$$\tau_{\frac{1}{2}} = \frac{1}{\alpha\, n_+}$$

The three-body process would be expected for alkali metal ions, and such coefficients are in the range of 10^{-11} to 10^{-9} cc/sec, dependent upon whether the negative species is an electron or ion. For dissociative recombination a value of $\sim 10^{-7}$ cc/sec is expected.

Recently measured values[8] for sodium and potassium in a 1 atm propane-air flame at 1970°K are $\alpha \sim 0.4 \times 10^{-9}$ and 3×10^{-9} cc/sec respectively. Earlier measurements of Knewstubb and Sugden[9] were interpreted to give $\alpha \sim 5 \times 10^{-9}$ cc/sec for the reaction

$$A^+ + OH^- \rightarrow A + OH$$

where A^+ is an alkali metal ion. Padley and Sugden[10] measured $\alpha = 3 \times 10^{-9}$ cc/sec for lead ions. It is interesting that a calculation according to Thompson's three-body theory[2] at 2,000°K and 1 atm gives for sodium and potassium $\alpha = 3 \times 10^{-11}$ and 2×10^{-11} with electrons, and 4×10^{-9} and 3×10^{-9} with OH^- ions.

The recombination coefficient for the normal flame ion decay has been measured over a pressure range of 0.04 atm to 1.0 atm for propane-air flames and is found to be 2×10^{-7} cc/sec and independent of pressure.[11] This value has been confirmed in hydrogen-air flames.[12] Because the dominate ion in both flames is H_3O^+, this is probably the recombination coefficient for the reaction[9]

$$H_3O^+ + e^- \rightarrow H_2O + H \text{ or } OH + 2H$$

although the negative species may be OH^-.[13] The temperature dependence has not been established. Bate's theory[1,2] would predict a temperature dependence of $T^{-1/2}$ to $T^{-3/2}$.

Ambipolar Diffusion

Diffusive loss of electrons will become more important as the altitude is increased and will be greater for smaller diameter exhaust jets than for larger jet diameters. When electrons diffuse out of the jet, they will pull the positive ions along because of the electrostatic potential created by charge separation. This is called ambipolar diffusion. The ambipolar diffusion coefficient is given by[2,14]

$$D_a = \frac{D_+ \mu_e + D_e \mu_+}{\mu_+ + \mu_e}$$

where the D's are diffusion coefficients and the μ's are mobilities.

The relaxation time, i.e. the time for the electron concentration to decay to 1/e of its original value is

$$\tau_D = \frac{\Lambda^2}{D_a}$$

where Λ is a characteristic dimension. For a long cylindrical exhaust jet of radius R

$$\Lambda = \frac{R}{2.4}$$

The rate of electron decay is given by

$$\frac{dn_e}{dt} = \frac{D_a}{\Lambda^2} n_e = - \frac{n_e}{\tau_D}$$

The ambipolar diffusion coefficient can be estimated[2] in flames where H_3O^+ dominates by

$$D_a \sim 100 \left(\frac{1}{p}\right)\left(\frac{T}{273}\right)^{3/2} \text{ cm}^2/\text{sec}$$

where p is the pressure in mm Hg and T is the temperature in ^oK. There is a need for better measurements of D_a in flames over a larger range of conditions and for flames including potassium, sodium and aluminum ions.

A simple calculation shows that for an exhaust temperature of 1000^{o}K at an altitude of about 160,000 ft. and an exhaust jet diameter of 10 ft., electron diffusion loss would become important in about 5 seconds.

Additives

Additives may be effective in two ways. They may prevent the ignition of the exhaust gases, and thus afterburning, or they may alter the electron concentration in a combustion flame. Inhibition of combustion will be discussed in the section on afterburning; changes in electron concentration by additives in burning flames will be discussed here. Very small concentrations of additives can produce large changes in electron concentration. See, for example, Fig. 17 and 18. This data was obtained with a Langmuir probe at fixed voltages. In this experiment the additive was added in small concentrations (0.2 mole percent of total fuel-air mixture) to a lean hydrocarbon-air flame at 0.043 atmospheres total pressure. This flame was chosen for screening studies because there is apparently no difference in performance between a hydrocarbon-air flame and a hydrogen-carbon monoxide-hydrocarbon (small concentration) - air flame used to simulate afterburning. The results will ultimately be examined in flames more equivalent to afterburning compositions, including the presence of chlorine.

The effect of additives is complex. In all cases where a decrease in electron concentration has been observed, the positive ion concentration has been increased. Because electrical neutrality must be preserved, this means that large concentrations of negative ions must be produced. Iron pentacarbonyl ($Fe(CO)_5$) has a profound effect on decreasing the electron concentrations when added in concentrations of about 0.1 mole percent; but in much smaller concentrations, ~ 0.01 mole percent, it increased the electron concentration by almost a factor of two and the positive ion concentration by about three times. The additives which we find cause changes in electron concentrations have also been observed to have a profound effect in reducing the burning velocity.[15] In our additive studies we frequently observe extinguishment of the flame by the addition of small concentrations of additive. The possibility thus exists of completely inhibiting afterburning (see a subsequent section and the discussion on the Terrier).

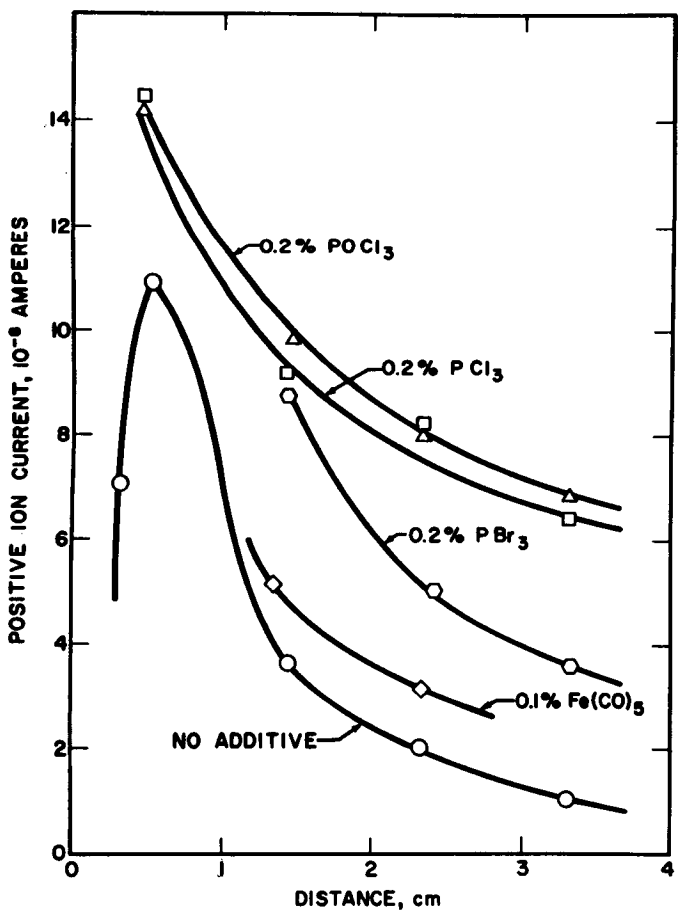

FIG. 17 EFFECT OF ADDITIVES
ON POSITIVE ION CONCENTRATION

Lean Propane-Air Flame
At 0.043 atm.

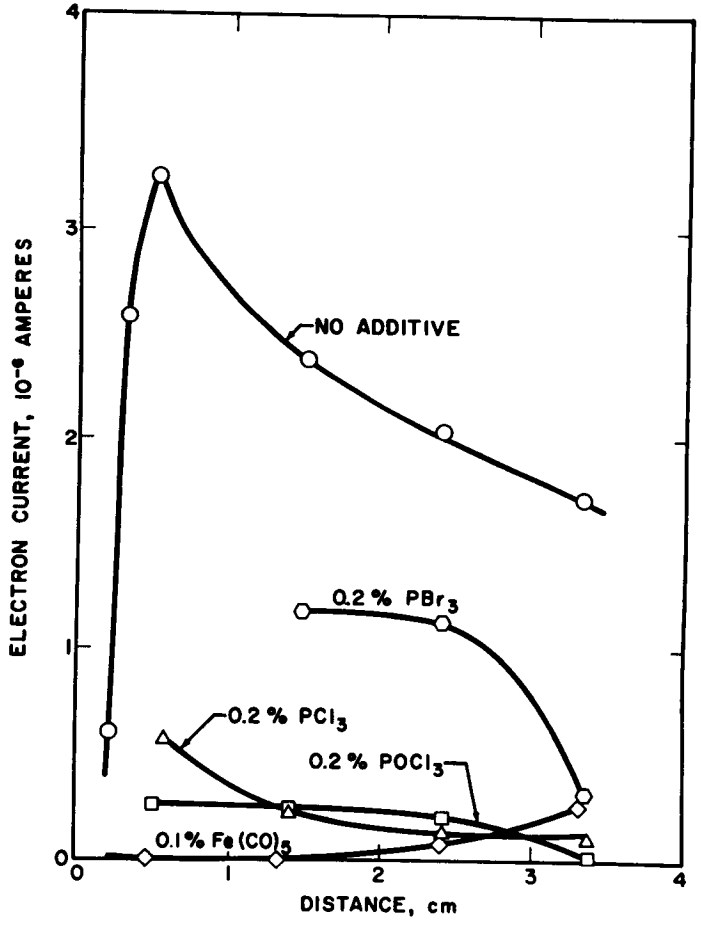

FIG. 18 EFFECT OF ADDITIVES
ON ELECTRON CONCENTRATION

Lean Propane-Air Flame
At 0.043 atm.

There are several conceivable mechanisms by which additives might affect electron concentrations. The most obvious is that of attachment

$$e^- + X \rightleftarrows X^-$$

where X must have a large electron affinity. Some typical attachment coefficients are given in Table IV. Chlorine is a good potential attacher and will be a natural product from the combustion of ammonium perchlorate propellants. Since the concentration of electrons is a function of the rate of formation and removal, any alteration of either of these processes will change the electron concentration. For example, if the rate of recombination of the negative ion with the positive ion is less than the rate of recombination of the electron with the positive ion, the addition of a substance which attaches electrons would cause the positive ion concentration to increase, while the electron concentration was decreased as in Figs. 17 and 18. Halogens have also been found to increase the electron concentration when added to alkali laden flames.[16]

Another mechanism by which the additive could play a role is in increasing or decreasing the rate of ion formation by altering the concentration of ion precursor, e.g., CH or O. This must be the situation when the additive either increases or decreases both the positive ion and the electron concentration. The details will be available from mass spectrometer studies and we will then be in a better position to recommend specific additives to solve specific attenuation problems. It is premature to seriously consider using $Fe(CO)_5$, for example, in the rocket exhaust to solve the attenuation problem.

Nozzle Expansion

High electron concentrations produced in the rocket chamber will be reduced as the thrust producing gases are expanded through the nozzle. This expansion causes a reduction in pressure which itself reduces the electron number density, assuming the mole fraction to remain constant.

If the electron production process is chemi-ionization, the source of ionization ceases as the combustion ceases so the electrons will recombine with positive ions as the gases expand through the nozzle. It should then be possible to use the laboratory measured rate constants of recombination, along with their temperature and pressure dependence, to calculate the decay of electron concentration with known temperature-pressure relations for the nozzle expansion process. So long as the combustion gases are in frozen equilibrium, this would offer no great difficulty. The process for a shifting equilibrium expansion would offer only the difficulty of calculating shifting equilibrium nozzle flow. To make an accurate calculation of the gas condition, the various reaction rates involved in approaching equilibrium must be known.

When ionization in the chamber is thermal, e.g., due to sodium or potassium impurities, the same problems are involved as in usual nozzle flow. Again, the extent to which the reaction rates maintain equilibrium expansion must be known to do an exact calculation. Such calculations are possible, but are long and tedious. As an approximation to actual conditions, the chamber gases may be considered to be frozen and to expand isentropically through the nozzle. The degree of ionization can be assumed to maintain an

equilibrium value until some point where the rates of recombination are too slow to keep up with the change in temperature and pressure due to expansion, and at this point, the electron mole fraction may be considered as frozen. This point can be estimated by use of a parameter which is the ratio of a characteristic flow time to a characteristic life time for the electrons.

A local characteristic flow time τ_{flow} may be defined

$$\tau_{flow} = \left[\frac{d}{dt}(\ln n_e)\right]^{-1} = \left(\frac{u}{n_e} \cdot \frac{dn_e}{dx}\right)^{-1}$$

where

u = local axial gas velocity
x = axial distance in nozzle
n_e = local electron concentration (electrons/cc)

Similarly, a useful characteristic lifetime for electrons is given by the local half life for recombination

$$\tau_{recomb} = \frac{1}{\alpha_r n_e}$$

There will be some point in the nozzle at which $\tau_{flow} \simeq \tau_{recomb}$, beyond which the electron mole fraction is likely to remain nearly frozen. Since upstream of this point the local electron concentration n_e can be approximated by its equilibrium value $n_{e,eq}$, the freeze will occur approximately where

$$\frac{\tau_{flow}}{\tau_{recomb}} \sim \frac{\alpha_r n_{e,eq}}{u \frac{d}{dx}(\ln n_{e,eq})} \sim 1$$

The location of the freeze point can be determined more rigorously than this however,[17,18,19,20] and its position can alternately be correlated with a rate parameter C_r closely related to the left hand side of the above equation, but which is usually known a priori; i.e.

$$C_r \equiv \left(\frac{D_t}{c^*}\right) \alpha_{r,c} n_{e,c}$$

where

D_t = nozzle throat diameter
c^* = characteristic propellant velocity

and the electron half life $(\alpha_r n_e)^{-1}$ is evaluated in the chamber. Thus, in what follows, an approximate but rather general method is outlined for predicting the electron concentration in the exhaust from conditions in the chamber.[19] The treatment will be outlined for the case of thermal ionization in the chamber - it could just as well be done when chemi-ionization dominates.

By considering isentropic flow through the nozzle and the maintenance of equilibrium ionization at every point with the combustion products acting simply as a carrier gas, i.e. constant $\gamma (\gamma = c_p/c_v)$, the normalized (with respect to the chamber) electron concentration decay curves in Fig. 19 can

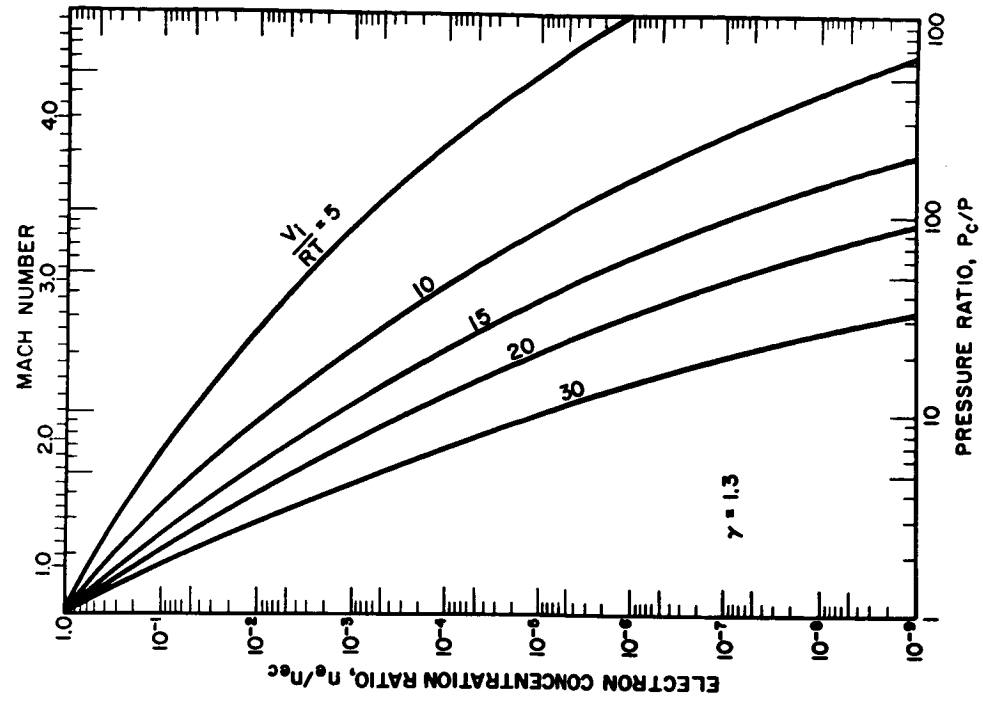

FIG. 20 ELECTRON DECAY DURING NOZZLE EXPANSION, γ = 1.3
15° Expansion Angle

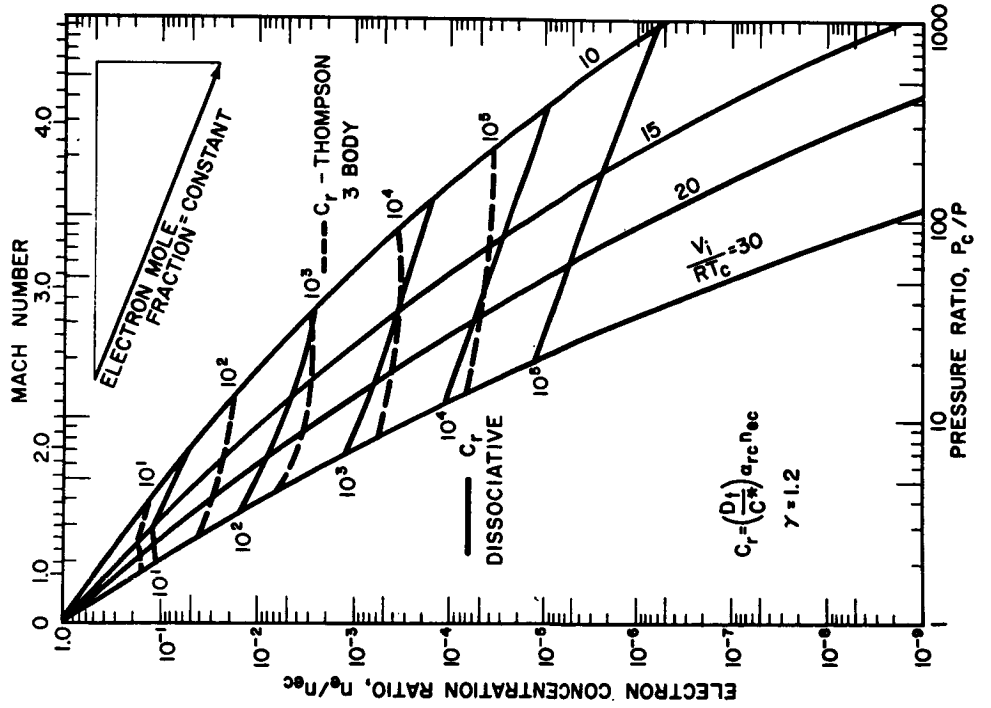

FIG. 19 ELECTRON DECAY DURING NOZZLE EXPANSION, γ = 1.2
15° Expansion Angle

be drawn. The equilibrium constant enters into this calculation via the ionization potential, V_i, which through Saha's equation is all that is required to determine the equilibrium constant variation with temperature and pressure. The curves are thus presented for several values of the nondimensional parameter $V_i/(RT_c)$, where R is the universal gas constant and T_c the chamber temperature. For the substances of interest the pertinent values are given in Table I.

Contours of constant recombination parameter, C_r, have been superimposed on the graphs of electron concentration ratio vs pressure ratio, or Mach number, for two different ion recombination mechanisms. These mechanisms enter only as the temperature and pressure dependence of the recombination coefficient. For the Thompson three-body process this has been taken as

$$\alpha_r \propto T^{-7/2}\ p^1$$

and for the dissociative recombination process this has been taken as

$$\alpha_r \propto T^{3/2}\ p^0$$

Note that this graph has been prepared for a specific heat ratio of $\gamma = 1.2$ and a conical expansion section nozzle with a divergence half angle of 15°, and the radius of curvature at the throat equal to the throat diameter. Fig. 20 has been prepared for $\gamma = 1.3$ but does not include chemical kinetic information (i.e., freeze point locations).

In using the curves shown in Fig. 19 to determine the electron concentration at the exit plane, i.e. at a given p_c/p (p_c is the chamber pressure) from the electron concentration in the rocket chamber, one proceeds along the appropriate equilibrium curve to the value of C_r computed from the values in the chamber. This gives the pressure ratio at which the electron concentration is effectively frozen. Thereafter, the change in electron concentration with further change in pressure ratio is obtained by drawing a line parallel to the hypotenuse of the indicated triangle. The ratio of electron concentration in the exhaust to that in the chamber is then read off at the appropriate pressure ratio. The pressure ratio for a given nozzle area ratio can be found from standard curves, e.g., Fig. 3-7 in Sutton.[21] Needless to say, this treatment is only applicable for one-dimensional isentropic expansions - at the position in the nozzle where over expansion occurs, other considerations must be brought to bear.

The above method also assumes that the transition region between equilibrium and frozen flow is small enough to disregard, so that local ionization equilibrium and frozen flow solutions can be abruptly patched together. More exact solutions are possible, but do not differ greatly[19], so unless the carrier gas taken into account the additional accuracy hardly seems worthwhile.

EXHAUST PLUME AND AFTERBURNING

The exhaust gases expand in a manner dependent upon the altitude (Fig. 21). At very high altitudes a large plume will be formed. For example, for the Scout vehicle, which was discussed earlier, the exhaust diameter was estimated to be 80 feet at an altitude of 200,000 feet. At somewhat lower altitudes the exhaust will be smaller, and shock phenomena will play a role.

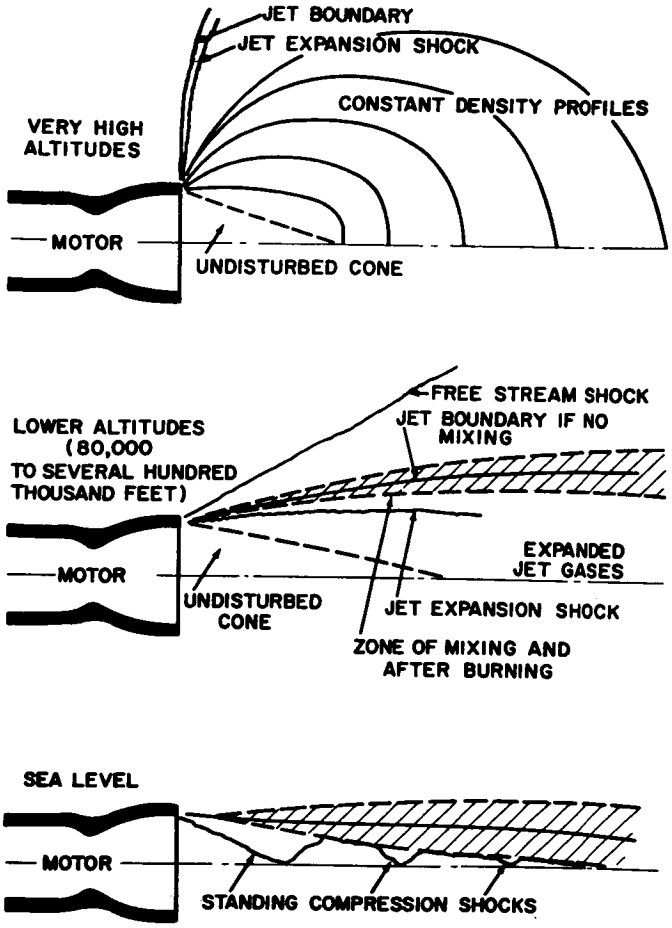

FIG. 21 ROCKET EXHAUSTS AT VARYING ALTITUDES

Boynton Ref. 6

The expansion into a vacuum has been treated by Molmud,[1] while others have been concerned about the mixing of the exhaust gases with the ambient atmosphere, ignition and afterburning.[2,3] A group at Thiokol, Reaction Motors Division,[4] are experimentally studying the mixing of hot combustible gases with the ambient atmosphere and auto-ignition of these gases to produce the equivalent of ignition of an afterburning flame. They are also studying the effects of various additives in preventing afterburning.[5]

The overall problem of the exhaust plume and afterburning involves the expansion of gases, formation of shocks, and mixing of the exhaust gases with air followed by ignition.

When afterburning is absent, a knowledge of the fluid dynamics relating to the pressure-temperature history of any pocket of gas with the time it leaves the rocket chamber, combined with a knowledge of the rates and mechanisms of electron decay (i.e. attachment, recombination and ambipolar diffusion) should lead to an estimate of the electron distribution in space. With this information, it should be possible to calculate radar attenuation, reflection and refraction.

The more important phenomena of afterburning seems to dominate in the case of solid propellants with fuel-rich exhausts. Here, we can anticipate an understanding of the problem when we can find from fluid dynamics the degree of mixing; the composition, temperature and pressure profiles in the exhaust; and the duration of these profiles for any set of conditions. This information should be related to what we know about ignition phenomena in the laboratory - ignition energies, ignition limits and auto-ignition.

In considering auto-ignition, which is expected to be the most important process, the duration of a given composition-temperature-pressure condition will be of great importance. Several major problems unfortunately arise. For example, in the laboratory, vessel walls act as heat sinks and free radical chain quenchers and even initiators, while in the exhaust no walls exist. A detailed understanding of the laboratory situation should, however, permit the extrapolation to be made. Another major difference is the composition of the exhaust gases which differs from the laboratory system in complexity - we are now dealing with not only a complex mixture but one which may contain atoms and radicals which will make ignition easier. At high altitudes of the order of 300,000 or more feet where oxygen is dissociated, the oxygen atoms present can accelerate the ignition process when mixed with the combustion gases. It is then not surprising that afterburning is observed both at relatively low altitudes of say 20,000 feet, where the combination of the partial pressure of oxygen molecules and diffusion and mixing rates result in favorable ignition conditions, and at about 300,000 feet where oxygen atoms again make ignition a probable process.

Some work of Boynton and Neu[6] gives an insight into the problem and the nature of afterburning temperatures involved. They assume the following exhaust composition (the fuel was $C_{10}H_{20}$)

Species	Mole Fraction
H_2O	32.2
CO	36.2
H_2	13.1
CO_2	11.8
H	2.9
OH	2.9
O	0.44
O_2	0.43

a chamber pressure of 500 psi. The temperature of the exhaust and ambient air are plotted in Fig. 22. A calculation of the exhaust jet temperature as a function of altitude and air entrainment ratio is plotted in Fig. 23. The air entrainment ratio, R, is the weight ratio of entrained air to exhaust gases. In calculating these curves the jet enthalpy includes: enthalpy of the exhaust gases, enthalpy of the air, and a term containing the square of the velocity difference between air and exhaust. They comment that this last term is important both at low altitudes and very high altitudes. This may account for as much as a 1,000°K temperature rise, e.g., with a velocity difference of 8,000 feet/sec and an air entrainment ratio of 1.0 the velocity term amounts to about 750°K.

The possibility and actual experience in preventing afterburning by chemical additives has already been mentioned. There seems to be considerable

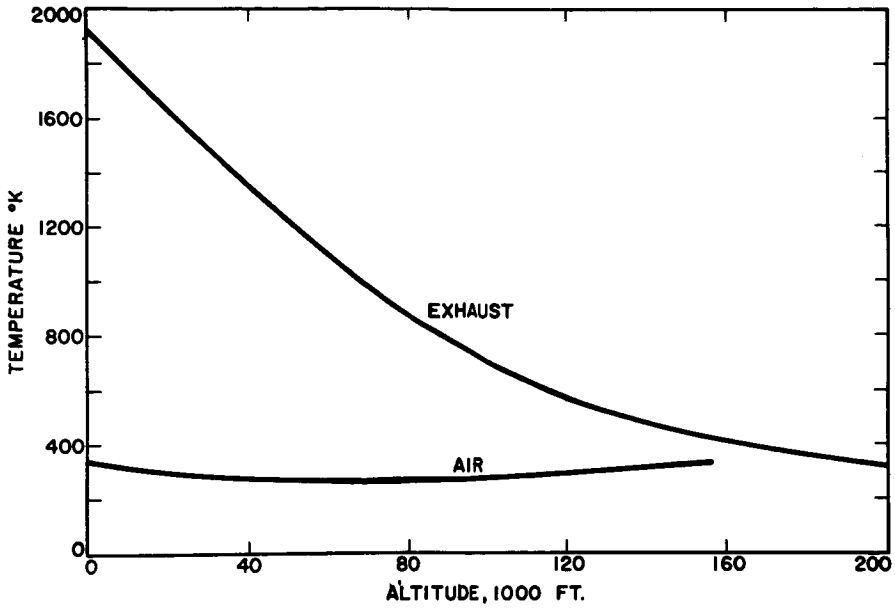

FIG. 22 TEMPERATURE OF AIR AND EXPANDED EXHAUST GASES AT FUNCTIONS OF ALTITUDE

Boynton and Neu Ref. 6

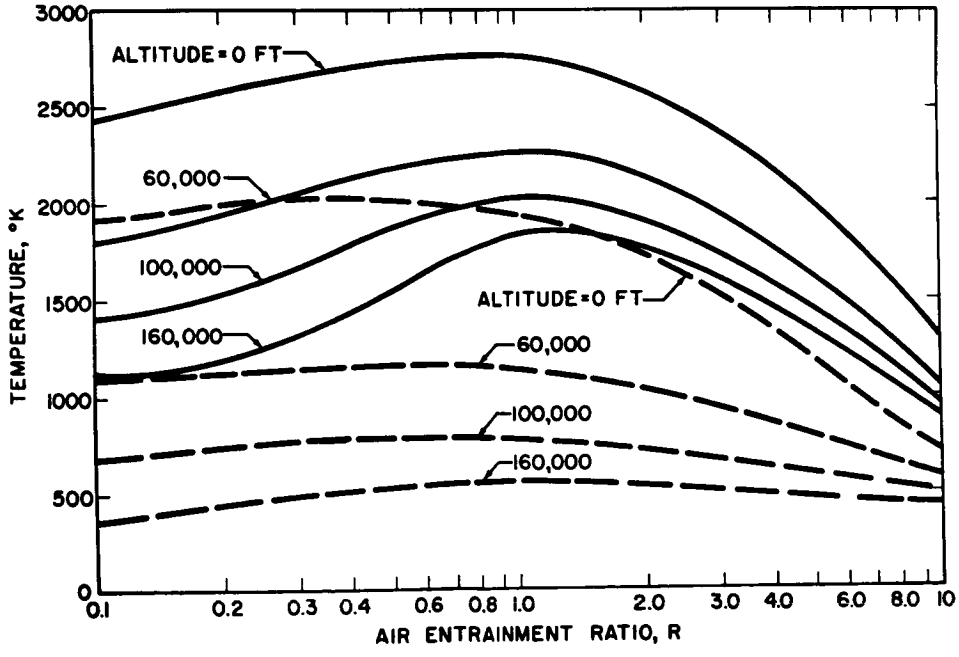

FIG. 23 TEMPERATURE OF EXHAUST WITH AND WITHOUT AFTERBURNING

Boynton and Neu Ref. 6

hope in this approach, especially in view of the success of Lask-Wagner[7] in reducing burning velocities with extremely small concentrations of additives. They, for example, reduced the flame velocity of stoichiometric n-hexane-air mixtures by 30% with the following additive concentrations

Additive	Vol. %
N_2	8
Cl_2	3.3
CCl_4	1.38
Br_2	0.7
$POCl_3$	0.19
$Fe(CO)_5$	0.072
CrO_2Cl_2	0.024

A review of the problem of ionization in afterburning in rocket exhausts with recommendations for a research program is in its second year at Stanford Research[7] for the Ballistic Systems Division of AFSC under general supervision of the Space Technology Laboratories.

REFERENCES

Rocket Experience

[1] Albrecht, G.H., Conference at the Naval Research Laboratory, to discuss TYPHON MR RadarAttenuation and Radar Attenuation in general, Applied Physics Laboratory, Johns Hopkins University, TLM-361, Dec. 1961. (CONF.)

[2] Poehler, H.A., "The A2X Attenuation Problem", Space Technology Report GM PTM 3262, AFMTC, MT60-10836, Dec. 1960. (CONF.)

[3] Balwanz, W.W., "The Plasmas of Missile Flight - Analysis of Polaris A2X Signal Absorption", U. S. Naval Research Laboratory, NRL Report 5636, July 1961. (CONF.)

[4] Barnes, C., Jr., "Study of Radar Beam Attenuation in Rocket Exhaust Gases, Part I: Microwave Measurements in Rocket Exhaust Gases", Stanford Research Institute, AFBMD-TR-61-39, Feb. 1961. (CONF.)

[5] Brown, B., (Private Communication), Hercules Powder Co., Magna, Utah, Feb. 8, 1962. (CONF.)

[6] Minuteman Program Quarterly Progress Report, Hercules Powder Co., Chemical Propulsion Div., MCS-62, Dec. 1960. (CONF.)

[7] Silver, I., Solid Propellant Exhaust Flame Attenuation Conference , Forrestal Research Center, Princeton, N.J., Jan. 11, 1962. (CONF.)

[8] Berl, W., Solid Propellant Exhaust Flame Attenuation Conference , Forrestal Research Center, Princeton, N.J., Jan. 11, 1962. (CONF.)

[9] Fuller, W.H., "Factors Affecting Secondary Burning in Double-Base Rocket Motors and a Summary of the Investigations of Secondary Burning Associated with the Terrier Missile", Allegany Ballistics Laboratory, Hercules Powder Co., June 1960. (CONF.)

[10] Abrams, M.C., "Chemical Quenching of Missile Exhaust Afterburning", Proceedings of Conference on Ions in Flames, (Eds., P. Molmud and J. H. Gardner) Stanford Research Institute, p. 197, GM-60-0000-13732, May 1960. (SECRET)

[11] Miller, D.G. and Abrams, M.C., "The Extinguishing of Rocket Motor Afterburning", Western States Section of the Combustion Institute, Palo Alto, Calif., April 1960.

[12] Keeling, J.W., "EX-5-MOD O Solid Propellant Rocket Motor", Quarterly Progress Report, Rocketdyne, R-4100-1, Aug. 1961. (CONF.)

[13] Nelson, C., Solid Propellant Exhaust Flame Attenuation Conference, Forrestal Research Center, Princeton, N.J., Jan. 11, 1962. (CONF.)

[14] Sims, T.E. and Jones, R.F., "Rocket Exhaust Effects on Radio Frequency Propagation from a Scout Vehicle and Signal Recovery During the Injection of Decomposed Hydrogen Peroxide", NASA TM X-529, Feb. 1961. (CONF.)

[15] Hodara, H., "The Use of Magnetic Fields in the Elimination of the Re-Entry Radio Blackout", Proc. Inst. Radio Engrs., 49, 1825 (1961).

[16] Hodara, H. and Cohn, G.I., "Radiation Characteristics of Long Narrow Slot Antennas in Lossy Anisotropic Plasmas", 17th Annual NEC, p. 622, Chicago, Ill., Oct. 1961.

[17] Kerridge, L.A., "Attenuation and Amplitude Modulation of a 3 CM Radio Signal by the Exhaust Jet of Interim Albatross, Staghound and Wolfhound Solid Propellant Motors", Rocket Propulsion Establishment Technical Note No. 196, Nov. 1960. (SECRET)

[18] Fuller, W.H., Sutphin, W.R., Pelton, J.M., Hixon, J.F., "Rocket Motor X234 Terrier Sustainer Summary Report Development and Flame Elimination Studies", Allegany Ballistics Laboratory, Hercules Powder Co., ABL/X-51, Jan. 1960. (CONF.)

[19] Breitengross, R.A., "A Review of Rocket Motor Afterburning Phenomena and Chemical Suppression", U.S. Naval Ordnance Test Station, Propulsion Development Dept., IDP 1454, Dec. 1961. (CONF.)

Radar Attenuation

[1] Stratton, J.A., Electromagnetic Theory, McGraw-Hill, N.Y., 1941.

[2] Altshuler, S., Moe, M.M., and Molmud, P., "The Electromagnetics of the Rocket Exhaust", Space Technology Report GM-TM-0165-00397, June 1958 (CONF.)

[3] Margenau, H., "Conduction and Dispersion of Ionized Gases at High Frequencies", Phys. Rev., 69, 508 (1946)

[4] Epstein, M., "Some Aspects of a Nonlinear Electrical Conductivity on Propagation of Electromagnetic Waves", Second Symposium on Engineering Aspects of MHD, University of Pennsylvania, March 1961.

[5] Taylor, L.S., "Microwave Reflection and Absorption by a Non-Uniform Plasma Sheath", Second Symposium on Engineering Aspects of MHD, University of Pennsylvania, March 1961.

[6] Sherman, A., "Calculation of Electrical Conductivity of Ionized Gases", ARS Journal, 30, 559 (1960).

[7] Balwanz, W.W., "Interaction Between Electromagnetic Waves and Flames, Part VI: Theoretical Plots of Absorption, Phase Shift, and Reflection", U.S. Naval Research Laboratory, NRL Report 5388, Sept. 1959.

[8] Altshuler, S., "Theory of Low-Energy Electron Scattering by Polar Molecules", Phys. Rev., 107, 114 (1957).

[9] Massey, H.S.W. and Burhop, E.H.S., Electronic and Ionic Impact Phenomena, Clarendon Press, Oxford, p. 206, 1956.

[10] Minzner, R.A. and Ripley, W.S., "The ARDC Model Atmosphere 1956", Air Force Cambridge Research Center TN-56-204, 1956.

[11] Hunziker, R.R., "Propagation of Strong Electromagnetic Waves in Weakly Ionized Rocket Exhausts", Sixth Symposium on Ballistic Missile and Aerospace Technology, University of Southern California, Aug. 1961.

[12] August, G., "Coulomb Collisions in Strong RF Electric Fields", Electronics Research Laboratory, University of California, Scientific Report No. 15, AFCRL 1103, Aug. 1961.

[13] Molmud, P., "The Nonlinear Propagation of Strong Electromagnetic Waves Through Weakly Ionized Media", Space Technology Laboratories, TM-59-0000-00397, Oct. 1959.

[14] Bulewicz, E.M. and Padley, P.J., "Asymmetry of Cyclotron Resonance Lines in the Reaction Zones of Low-Pressure Acetylene and Cyanogen Flames", J. Chem. Phys., 35, 1590 (1961).

Sources of Ionization

[1] Rice, W.E., King, I.R., Calcote, H.F., and Leicht, J.V., "Ionization Probes in Rocket Exhausts", Experiment, Inc. TP-118, Nov. 1957.

[2] Padley, P.J., Page, F.M. and Sugden, T.M., "Effect of Halogens on the Ionization in Alkali-Laden Hydrogen and Acetylene Flames, Part I: The Theory of Steady State Ionization in Flames", Trans. Faraday Soc., 57, 1552 (1961).

[3] Calcote, H.F., "Ions in Flames", Final Report, AeroChem TP-24, AFBMD-TR-61-54, ASTIA AD 258 229, Dec. 1960.

[4] Balwanz, W.W., "Ionization in Rocket Exhausts - A Survey", U.S. Naval Research Laboratory, NRL Report 5193, Aug. 1958. (CONF.)

[5] Smith, F.T., "Ionization in Afterburning Rocket Exhausts", Stanford Research Institute Quarterly Report No. 2, TN BSD-TR-61-26, Aug. 1961.

[6] Discussions with P. Molmud, S. Altshuler, and J. Gardner, Space Technology Laboratories, 1959.

[7] Project Firefly 1960, Geophysics Research Directorate, AFCRL 256, March 1961. Vol. I, Mass Transport, Spectrophotometry, Release Chemical Physics Vol. II, Release Chemical Physics, RF Backscatter Studies, RF Forward Scatter Studies; Vol. III, Missile Trail Mechanisms.

Thermal Ionization

[1] Calcote, H.F., "Mechanisms for the Formation of Ions in Flames", Combustion and Flame, I, 385 (1957).

[2] See Reference 3 in section on Sources of Ionization.

[3] Rosner, D.E., "Calculation of Equilibria in Thermally Ionized Gaseous Mixtures: The Saha Equation", AeroChem TM-11, Sept. 1958.

[4] Minuteman Program Quarterly Progress Report, Hercules Powder Co., Chemical Propulsion Division, MCS-73, May 1961. (CONF.)

[5] Geene, R.W., "Solid Bipropellant as a Technique to High Energy Propellant Development", Bulletin of the 17th Meeting JANAF-ARPA-NASA Solid Propellant Group, Vol. II, p. 203, May 1961. (CONF.)

[6] Minuteman Program Quarterly Progress Report, Hercules Powder Co., Chemical Propulsion Division, MCS-82, Oct. 1961. (CONF.)

[7] Branscomb, L.M., Advances in Electronics and Electron Physics, Vol. IX, p. 66, Academic Press, N.Y., 1957.

[8] Cubicciotti, D., "Lattice Energies of the Alkali Halides and the Electron Affinities of the Halogens", J. Chem. Phys., 31, 1646 (1959).

[9] Knewstubb, P.F. and Sugden, T.M., "Mass Spectrometry of the Ions Present in Hydrocarbon Flames", Seventh Symposium (International) on Combustion, p. 247, Butterworth's Scientific Publications, London, 1959.

[10] Deckers, J. and Van Tiggelen, A., "Ion Identification in Flames", Seventh Symposium (International) On Combustion, p. 254, Butterworth's Scientific Publications, London, 1959.

[11] Einbinder, H., "Generalized Equations for the Ionization of Solid Particles", J. Chem. Phys., 26, 948 (1957).

[12] Smith, F.T., "On the Ionization of Solid Particles", J. Chem. Phys., 28, 746 (1958).

[13] Hogland, S. and Saarlas, M., "Expansion Nozzles for Gas-Particle Flow", Bulletin of the 17th Meeting JANAF-ARPA-NASA Solid Propellant Group, Vol. III, p. 5, May 1961.

[14] McCarty, K., Personal Communication on Al_2O_3 Particle Size in Rocket Exhausts, Allegany Ballistics Laboratory, Hercules Powder Co., Feb. 1962 (CONF.)

[15] Gatz, C.R., Rosser, W.A., and Smith, F.T., "Study of Radar Beam Attenuation in Rocket Exhaust Gases, Part II: The Chemistry of Ionization in Rocket Exhausts", Stanford Research Institute Technical Report AFBMD-TR-61-39, SRI Project No. SU-2643, Feb. 1961.

[16] Pearson, M., "Electron Density in Aluminum Oxide Contaminated Flames", Am. Phys. Soc., Summer Meeting, Hawaii, Aug. 1959. see also, Karp, I.L., Larsen, O.W. and Pearson, M., "Electromagnetic Wave Propagation Through Minuteman Solid Propellant Exhaust Gases", Boeing Airplane Co., D2-7297, June 1961. (SECRET)

[17] Minuteman Program Quarterly Progress Report, Hercules Powder Co., Chemical Propulsion Division, MCS-78, July 1961. (CONF.)

[18] Mullaney, G.J., Kydd, P.H. and Dibelius, N.R., "Electrical Conductivity in Flame Gases with Large Concentrations of Potassium", J. Appl. Phys., 32, 668 (1961).

[19] Hord, R.A. and Pennington, J.B., "Temperature and Composition of a Plasma Obtained by Seeding a Cyanogen-Oxygen Flame with Cesium", NASA TN D-380, May 1960.

[20] Gay, N.R., Agnew, J.T., Witzell, O.W. and Karabell, C.E., "Thermo-Chemical Equilibrium in Hydrocarbon-Oxygen Reactions Involving Polyatomic Forms of Carbon", Combustion and Flame, 5, 257 (1961).

[21] Brogan, T.R., Kantrowitz, A.R., Rosa, R.J. and Stekly, Z.J.J., "Progress in MHD Power Generation", Second Symposium on the Engineering Aspects of Magnetohydrodynamics, University of Pennsylvania, Phila., Pa., March 1961.

[22] Huber, P.W., "Experiments with Plasmas Produced by Alkali-Metal-Seeded Cyanogen-Oxygen Flames for Study of Electromagnetic Wave Propagation at the Langley Research Center", Symposium on the Plasma Sheath - Its Effect on Communication and Detection, Air Force Cambridge Research Center, Boston, Mass., Dec. 1959.

[23] Nichol, J., Siminski, V. and Wolfhard, H.G., "Ionization in Rocket Flames", Thiokol Chemical Corp., Reaction Motors Division, Denville, N.J., AFOSR-TN-60-285

[24] Smith, F.T., "Ionization in Flames: The Role of Complex Hydrocarbons and the Ionization of Mixtures", SRI TP-1, Stanford Research Institute, May 1957.

[25] Arshinov, A.A. and Musin, A.K., "Thermal Emission of Electrons from Carbon Particles", Dokl. Akad. Nauk SSSR, 118, 461 (1958).

[26] Dimmock, T.H. and Kineyko, W.R., "Electrical Properties of Ionized Flames, I. Study of Flame Ionization", Thiokol Chemical Corp., Reaction Motors Division, AFOSR-825, Aug. 1961.

[27] Huber, P.W. and Gooderum, P.B., "Experiments with Plasmas Produced by Potassium-Seeded Cyanogen Oxygen Flames for Study of Radio Transmission at Simulated Re-entry Vehicle Plasma Conditions", NASA TN D-627, Jan. 1961.

Chemi-Ionization

[1] See Reference 1 in section on Thermal Ionization.

[2] Calcote, H.F., "Ion Production and Recombination in Flames", Eighth Symposium (International) on Combustion, In Press, Williams and Wilkins Co. Baltimore, Md.

[3] Bulewicz, E.M. and Padley, P.J., "Suggested Origin of Anomalous Line-Reversal Temperature in the Reaction Zone of Hydrocarbon Flames", Combustion and Flame, 5, 331 (1961).

[4] Sternberg, J.C., Gallaway, W.S., and Jones, T.L., "The Mechanism of Response of Flame Ionization Detectors", Pittsburg Conference on Analytical Chemistry and Applied Spectroscopy, Feb. 1961.

[5] Calcote, H.F. and Reuter, J.L., "Mass Spectrometric Study of Ion Profiles in Low Pressure Flames", ISA Fall Conference, Los Angeles, Calif., Preprint No. 69-LA-61, Sept. 1961.

[6] Knewstubb, P.F. and Sugden, T.M., "Mass Spectrometry of the Ions Present in Hydrocarbon Flames", Seventh Symposium (International) on Combustion, p. 247, Butterworth's Scientific Publications, London, 1959.

[7] Deckers, J. and Van Tiggelen, A., "Ion Identification in Flames", Seventh Symposium (International) on Combustion, p. 254, Butterworth's Scientific Publications, London, 1959.

[8] See Reference 3 in section on Sources of Ionization.

[9] Mullaney, G.J. and Dibelius, N.R., "Electrical Conductivity of Flames Seeded with Large Concentration of Sodium, Barium and Strontium", Bull. Am. Phys. Soc., 117, 157 (1962).

[10] "Study Group on Missile Launch Phenomenology", Stanford Research Institute, SRI Control 1.266, Jan. 1962.

Electron Loss Mechanisms

[1] Massey, H.S.W. and Burhop, E.H.S., Electronic and Ionic Impact Phenomena, Oxford University Press, London, 1956.

[2] Calcote, H.F., "Relaxation Processes in a Plasma", Dynamics of Conducting Gases, Proceedings of the Third Biennial Gas Dynamics Symposium, p. 36, Northwestern University Press, Ill., March 1960.

[3] Williams, H., "The Predominant Process of Electron Decay in the Mantle of an Acetylene-Air Flame", Seventh Symposium on Combustion, Butterworth's Scientific Publications, London, 1959.

[4] Williams, H., "Further Studies on the Decay of Free Electrons in the Mantle on an Acetylene-Air Flame", Eighth Symposium (International) on Combustion, Aug. 1960. (In Press, Williams and Wilkins Co., Baltimore, Md.)

[5] Knewstubb, P.F. and Sugden, T.M., "Mass Spectrometrometric Studies of Ionization in Flames, I: The Spectrometer and Its Application to Ionization in Hydrogen Flames", Proc. Royal Soc., 255, 520 (1960).

[6] Gatz, C.R., Rosser, W.A., and Smith, F.T., "Study of Radar Beam Attenuation in Rocket Exhaust Gases, Part 2: The Chemistry of Ionization in Rocket Exhausts", Stanford Research Institute Final Report, Technical Report AFBMD-TR-61-39, Feb. 1961.

[7] Rosen, G., "A Method for the Removal of Free Electrons in a Plasma", Martin Marietta Corp. (Personal Communication), Feb. 8, 1962. (CONF.)

[8] King, I.R., "Recombination Rates of Alkali Metal Ions", J. Chem. Phys., 36, 553 (1962).

[9] Knewstubb, P.F. and Sugden, T.M., "Observations on the Kinetics of Ionization of Alkali Metals in Flame Gases", Trans. Faraday Soc., 54, 372 (1958).

[10] Padley, P.J. and Sugden, T.M., "Some Observations on the Production and Recombination of Ions and Electrons from Metallic Additives in Hydrogen and Hydrocarbon Flames", Eighth Symposium (International) on Combustion, Aug. 1960 (In Press, Williams and Wilkins Co., Baltimore, Md.)

[11] Calcote, H.F., "Ion Production and Recombination in Flames", Eighth Symposium (International) on Combustion, Aug. 1960. (In Press, Williams and Wilkins Co., Baltimore, Md.)

[12] Bascombe, K., Jenkins, D., Schiff, H.I. and Sugden, T.M., "The Production of NH_4^+ and NO^+ Ions in Flames", Mass Spectrometry Conference, p. 28, Chicago, Ill., June 1961.

[13] King, I.R., "Recombination of Ions in Flames", Texaco Experiment Inc., Richmond, Va., TP-174A, EXP 278, AFOSR 596, Dec. 1961.

[14] Loeb, L.B., Basic Processes of Gaseous Electronics, University of California Press, Berkeley and Los Angeles, Calif., 1955.

[15] Lask, G. and Wagner, H.G., "Influence of Additives on the Propagation of Laminar Flames", Eighth Symposium (International) on Combustion, Aug. 1960. (In Press, Williams and Wilkins Co., Baltimore, Md.)

[16] See Reference 2 in section on Sources of Ionization.

[17] Smith, F.T., "On the Analysis of Recombination in an Expanding Gas Stream", Seventh Symposium (International) on Combustion, p. 93, Butterworth's Scientific Publications, London, 1959.

[18] Eschenroeder, A.Q., "Ionization Nonequilibrium in Expanding Flows", ARS Journal, 32, 196 (1962).

[19] Rosner, D.E., "Magnetogasdynamic Thrust Vectoring of Rocket Motors, Including the Effects of Finite Electron-Ion Recombination Kinetics", AeroChem TN-41, Feb. 1962.

[20] Rosner, D.E., "Rapid Estimation of Electrical Conductivity and Electron Number Density at the Exit Section of Rocket Nozzles", AeroChem TP-41, Feb. 1962.

[21] Sutton, G.P., Rocket Propulsion Elements, John Wiley and Sons, Inc., N.Y., 1956.

Exhaust Plume and Afterburning

[1] Molmud, P., "The Expansion of a Rarified Gas into a Vacuum", Space Technology Laboratories, Inc., Los Angeles, Calif., 6M47.3-55, Nov. 1958. Revised July 1959.

[2] Vasiliu, J., "Determination of Temperature, Velocity and Concentration Profiles in the Mixing Layer Between a Rocket Exhaust Jet and the Surrounding Supersonic Air Stream", Convair, Astronautics Division, General Dynamics, ERR-AN-005 Applied Research, March 1960.

[3] Project Firefly, Missile Trial Mechanisms, AFCRL 256, March 1961. (SECRET)

[4] "The Investigation of Re-Ignition and Afterburning in Exhaust Gases", Report RMD 2043-L-5, Thiokol Chemical Corp., Reaction Motors Division, Denville, N.J., March 1961. (CONF.)

[5] "Afterburning of Rocket Exhausts", Report RMD 2157 L-3, Thiokol Chemical Corp., Reaction Motors Division, Dec. 1961.

[6] Boynton, F.P. and Neu, J.T., "Rocket Plume Radiance V: Calculation of Adiabatic Flame Temperatures of Afterburning Rocket Exhaust", Convair, Astronautics Division, General Dynamics Corp., ERR-AN-011 Applied Research, May 1960.

[7] See Reference 15 in section on Electron Loss Mechanisms.

[8] Smith, F.T. and Gatz, C.R., "Ionization in Afterburning Rocket Exhausts", Stanford Research Institute Final Report, BSD-TR-61-76, Nov. 1961.

[redacted]

MICRO-MOTOR EVALUATION OF SPECIFIC IMPULSE

by

L. M. Brown & B. L. Cockrell

Rohm & Haas Company
Redstone Arsenal Research Division
Huntsville, Alabama

ABSTRACT

The evaluation of novel solid propellant systems by using only small quantities of ingredients is of considerable interest to the solid propellant industry. This paper reviews current work using small rocket motors containing 50 grams or less of propellant for evaluation purposes.

A micro-motor evaluation system requiring 10 to 30 grams of propellant per motor has been designed, fabricated, and evaluated by this Division. This system for measuring specific impulse uses the best evaluation techniques available and considers every phase of the design and measurement problems.

The motor design, measurement techniques, and reproducibility are discussed together with the results obtained with a number of high energy aluminized composite double-base plastisol propellants which are compared with larger motor firings. Methods for predicting large motor impulses from micro-motor firings are outlined in detail.

These micro-motors have been used to evaluate the specific impulses of a series of high energy NF-propellants of current interest to this Division. Results of these evaluations are given together with predicted values for larger motors. The latter are compared with results of firings of NF-propellants in larger motors (100 grams).

The micro-motor hardware is being redesigned to allow remote casting and firing of propellants of all viscosities.

The work presented shows that precise, reproducible, predictable, usable data can be obtained with very small quantities of propellant; and that ballistic characterization of the specific impulse of a novel propellant can be carried out with less than two pounds of propellant.

[redacted]

INTRODUCTION

Over the past several years there has been a general trend in propellant research toward the use of smaller motors for ballistic evaluation purposes. Many factors have contributed to this including (a) a large number of new contractors in the field of propellant research, most of whom which have an upper restriction on propellant quantity or propellant size, (b) increasing toxicity and/or sensitivity of new formulations, and (c) limited availability or excessive costs of novel propellant ingredients. These factors make ballistic evaluation of propellants in small motors either highly desirable or mandatory and have caused many groups, both old and new to the field, to reevaluate their ideas concerning motor size and ballistic measurements. The old clichés of "the larger the motor the higher the impulse" and "no meaningful specific impulse can be obtained from a test motor having less the x pounds of propellant" are being replaced in some circles by "one ten gram motor will tell us all we need to know." As is usually the case, neither extreme position is right; and neither can be substantiated by unbiased experiments.

The purpose of this paper is to review briefly the current work being done in the field of ballistic testing of very small quantities of propellant with added emphasis on work underway at Esso Research and to discuss in detail the development and application of micro-motors currently in use by Rohm & Haas Company.

Although many facilities are now using motors containing one pound or less of propellant for ballistic evaluation, this review of current work is limited to that using 50 grams or less per motor firing.

Most organizations who are using very small quantities of propellant are using end burning charges for getting initial information on the combustion properties of new formulations in order to answer questions such as: Does it burn smoothly? Can we ignite it? What are its P-K and P-r relationships? Currently using this technique are Elkton Division of Thiokol (1)[1], American Cyanimid (2), Dow Chemical Company (3), Minnesota Mining and Manufacturing Company (4), and Esso Research Company (5). Many others probably also use this approach, but have not reported the results.

[1]Numbers in parenthesis refer to references at the end of the paper.

Of the above facilities only 3M and Esso measure specific impulse from these small end-burning motors. In addition, Dow Chemical has a small ballistic pendulum which uses five grams of granulated propellant, but no mention of this device is made in their recent reports. Aerojet General Corp. (6, 7) is developing a 50-gram test motor having a star shaped grain and which is fired on a small inertia wheel of the JPL type. United Technology Corp. is reported to have a ten-gram motor with which heat loss is measured by a calorimetric technique. No reference to this has been found in the classified literature available.

Studies[1] at Esso Research & Engineering Company (5) as part of an integrated ARPA program under Army Ordnance Contract DA-30-069-ORD-2487 have led to the development of new small test motors designed for maximum flexibility in handling experimental high energy formulations. These motors utilize an end-burning charge, 1.625 inch in diameter, and contain from 10 to 50 grams of propellant. Successful firings have been made with cartridge loaded grains and with grains formed directly in the motor by casting or by pressing. Uncured slurries were also fired successfully. When specific impulse is measured in these motors and is corrected for some known perturbations as well as the usual standard corrections, combustion efficiencies of about 94% are normally obtained.

Although several different propellant types and compositions have been evaluated in this motor, most of the motor evaluation used Rohm & Haas plastisol Composition 137 containing 2% aluminum. Only this work will be summarized here.

Recognizing that heat losses can be a major cause of efficiency loss in small motors, Esso Research has designed their motor with phenolic-asbestos insulation[2]. They have also designed a similar motor using an internal burning cylindrical charge for which they have only limited data. These designs are shown in Figure 1a and 1b respectively. Although limited data show somewhat higher efficiencies for the internal burning cylinder for one composition, no rounds of Composition 137 have been fired in this configuration.

---

[1]The Esso work reported here is taken from a summary sent to the authors by Mr. John Reed and is included at the request of the Papers Committee of this meeting.

[2]"Rocketon" – a product of the Haveg Corporation.

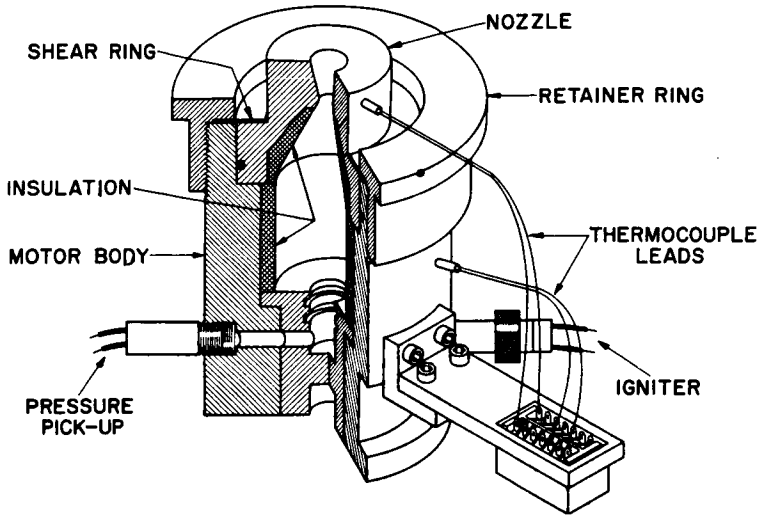

A – Hollow Grain

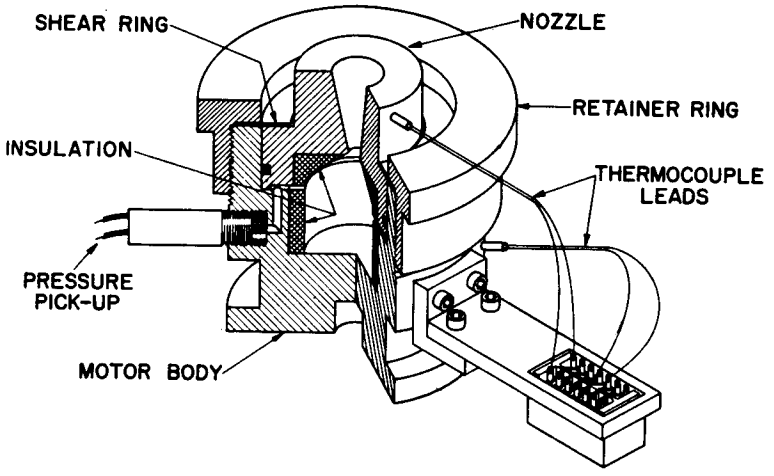

B – End-Burning Grain

Figure 1 – Motor Designs of Esso Research

The only motor fired repeatedly was the end burning motor with R&H 137 formulation. In eleven firings of this formulation a standard deviation of σ = 1.2% was obtained at an average corrected efficiency of 94.4% of theoretical. Small corrections were made in reporting the measured specific impulse to account for insulator loss, propellant weight loss, igniter, and heat loss. The usual corrections to 1000 psi, optimum expansion and zero degree half angle were applied. Table I shows the average corrections for the eleven firings of Composition 137.

TABLE I

ESSO RESULTS

Average Firing Efficiency Corrections
for Eleven Rohm & Haas 137
End-Burning Motors ("Unimproved" Nozzles)

Insulator	-1.0%
Propellant, Wt. Loss	+0.3
Igniter	-2.3
Heat Loss	+1.6
0° Exit Angle	+1.6
Net Correction	-0.2%

The insulator loss correction of -1.0% is obtained from a total insulator loss of 1.8% on the assumption that the lost insulation burns to equilibrium with the propellant. The propellant weight loss correction is obtained from the fact that vertical firings are made such that weight loss results in lower measured thrust. The validity of the igniter impulse correction was checked by observing that the corrected firing efficiency was independent of the amount of igniter used between 0.5 g and 3.0 g although the igniter loss correction itself varied from 1.5 to 4.1%. The heat loss correction was made by subtracting the heat gain of the nozzle and motor body, as determined from thermocouple measurements, from the propellant enthalpy available in the combustion chamber. Finally, the correction to 0° exit angle corresponds to a 13° half angle.

Although the above summary of the Esso work shows that specific impulse measurements can be made with small end burning charges, certain critical comments about this technique are still in order. The principal difficulty in intrepreting the Esso work comes from the correction procedures for insulation losses and igniter weight. While the results using these corrections may be reasonably precise, they may be very inaccurate.

For comparison let us consider results with the .75C.50-1.5 micromotor containing approximately 10 grams of propellant for Composition 163 (containing 1% aluminum) which is similar to Composition 137 (2% Al) used

by Esso. Ten rounds gave an average F^0_{1000} of 234.1 (with a standard deviation of 0.5%) which is 97% of the calculated specific impulse. These motors, as will be seen below, contain no insulation and the results have no heat loss correction included although 0.25% is subtracted for an igniter correction.

The second difficulty with the Esso approach to date is that no consideration is made for two phase flow effects. This effect is of the same order of magnitude as the heat loss effects for propellants containing large amounts of Al_2O_3 in the exhaust products. For this reason it cannot be ignored for most propellants of current interest.

The development of micro-motors and associated techniques[1] began at this Division when we sought an answer to the question "What are the best results obtainable from a ten-gram motor under the most ideal conditions with well characterized propellants?" Since that time considerable effort has been expended in this regard using the best approaches available (8), which had proven superior with the evaulation of larger test motors. In the remainder of this paper the results of two years of intensive effort are presented which show that if proper care is taken, reliable, reproducible, meaningful data can be obtained with these micro-motors, and that in their present state of development they are useable with certain types of novel propellants.

In this paper we will discuss the experimental techniques, results with plastisol double base propellant, comparisons with larger motor firings and a way of predicting large motor results from micro-motor data. Finally, results from a number of novel propellant compositions are given together with future plans to further develop the technique so that it may be applied to a wider variety of novel systems.

EXPERIMENTAL TECHNIQUES

The original micro-motor developed by this Division was designed as a scale of the standard 6C5-11.4 motor which has been used for propellant evaluation purposes for several years. The resulting scaled motor which would contain a nominal ten grams of propellant is the 0.75C.5-1.5 micro-motor. Currently motor lengths of 1.5, 2.5 and 3.5 inches are in use. These micro-motors are fabricated from 0.75-inch I. D. seamless mild steel high-pressure tubing having a nominal wall thickness of 1/8 inch. The propellant charge has a 0.50-inch I. D. cylindrical perforation, and is trimmed back 1/16-inch from the ends of the case. Nominal charge weights vary from 10 grams

[1]This work has been carried out under Army Contract No. DA-01-021 ORD-11878 and more recently under ARPA Order No. 21-61, Army Contract No. DA-01-021 ORD-11909.

for the .75C.50-1.5 to 25 grams for the .75C.50-3.5. Photographs of the motors and casting fixtures are shown in Figure 2. Fabrication details have been reported previously (9).

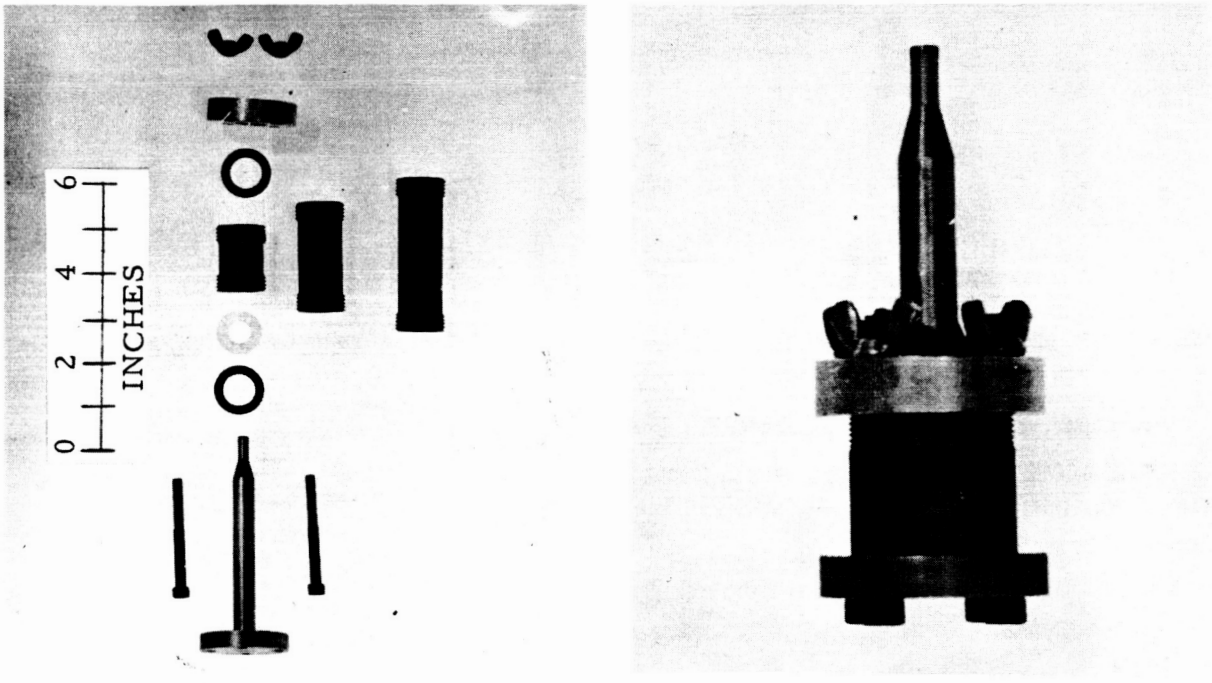

Figure 2 – Micro-Motor Cases and Casting Fixtures

Micro-motors are fired vertically in a head-down position. Positive thrust alignment is provided by close-tolerance mating of machined surfaces between the thrust gauge, pressure gauge, motor case, and nozzle. Photographs of the static test assembly are shown in Figure 3.

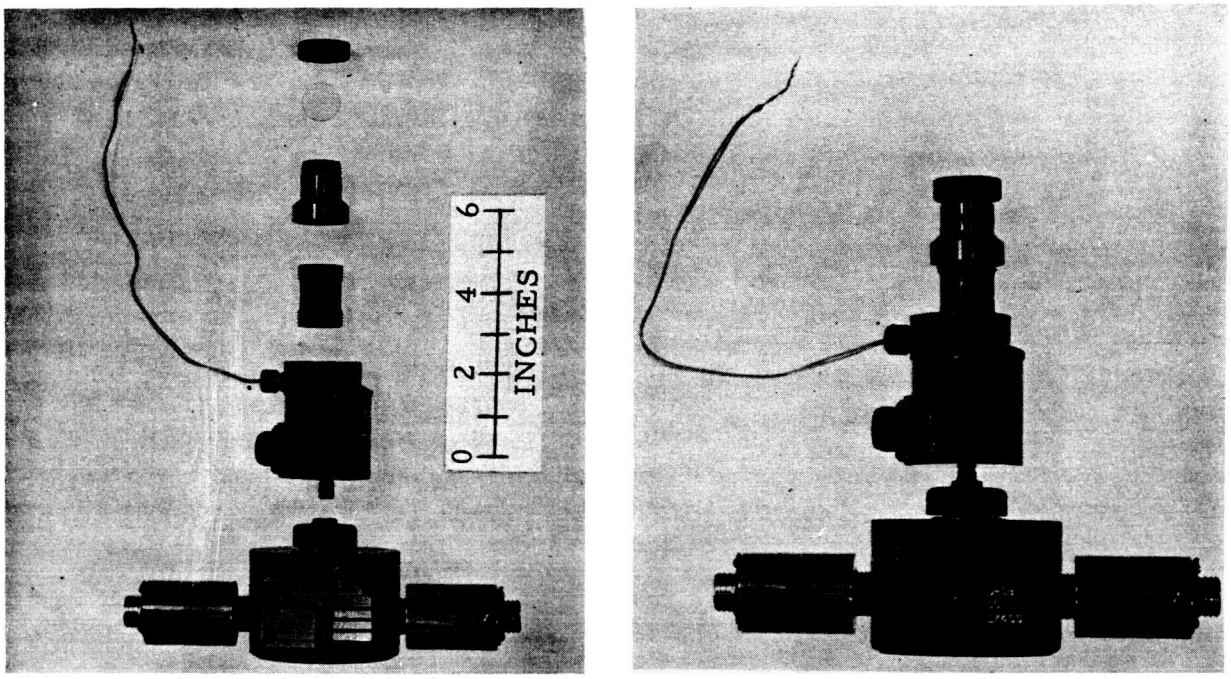

Figure 3 – Micro-Motor Static Test Assembly

Detailed descriptions of the data acquisition instrumentation system and data reduction procedures for micro-motors have been reported previously (9). The best available evaluation techniques (8) are used to acquire, reduce, and interpret micro-motor ballistic data. A prime requisite for acceptable ballistic data is the use of extreme care in the determination of such physically measured quantities as web thickness, nozzle throat and exit diameter, and charge weight. Due to the small magnitude of these quantities, allowable tolerances on measurements are inherently very small and difficult to maintain.

One other area which must be rigidly controlled is that of ignition. It has been reported previously (8) that corrected specific impulse for the micro-motor is markedly dependent upon ignition delay time and weight of igniter material. Long ignition delay times invariably result in low values of specific impulse, due to propellant cook-off and increased heat losses. On the other hand, too high a specific impulse will be obtained if a relatively large weight of igniter material is used and no correction for igniter contribution is applied. Since igniter correction techniques are at best questionable, it has been the policy of this Division to choose igniters

which weigh no more than one-half percent of the charge weight and to make no igniter correction. This correction, if made, would approximately cancel an opposite correction for loss in weight of the motor on firing.

The present micro-motor ignition system, which has gradually evolved as a result of tests of many different types of ignition systems, utilizes a single M1-A1 squib mounted at the head-end of the motor, and a 0.030-inch thick cellulose acetate disc closure retained at the nozzle exit. The weight of combustible material for the M1-A1 squib is about 50 milligrams, which is one-half percent of the nominal charge weight of the .75C.50-1.5 micro-motor. For .75C.50-2.5 and .75C.50-3.5 motors, additional RIP igniter powder is added to make the total weight of RIP plus squib charge add up to one-half percent of the charge weight. Ignition delay times have been reduced to 10-20 msec with this system.

Typical pressure-time and thrust-time traces for the .75C.50-1.5 micro-motor are shown in Figure 4. The traces are smooth and the end of burning is sharp indicating no perturbation in the burning due to the small size.

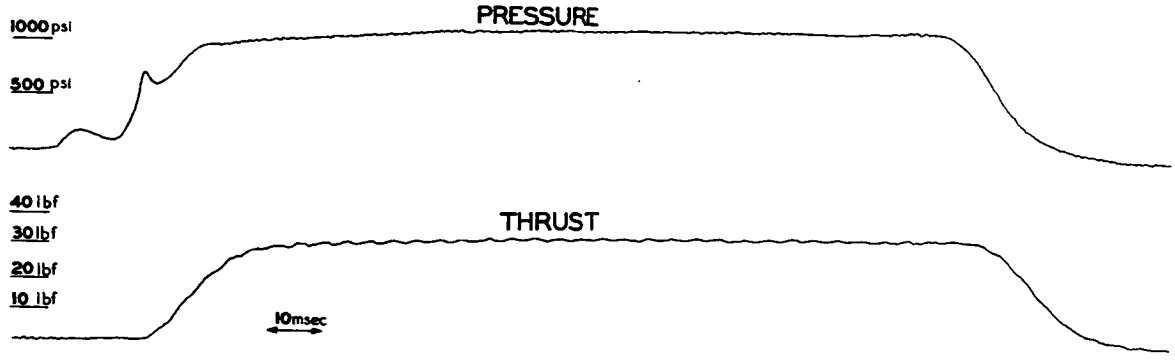

Figure 4: Typical Pressure and Thrust Traces Obtained from Micro-motor Firings.

RELIABILITY, PRECISION AND REPRODUCIBILITY

The reliability of the micro-motor has proven to be phenomenal. A total of approximately 850 micro-motors have been fired to date, at least 110 of which contained novel, high energy propellant formulations having relatively unknown sensitivity characteristics and which had never been previously fired in any static test motor. Out of all these rounds, not a single blow-up or burn-through has occurred. The most serious malfunction experienced was the loss of a portion of the carbon nozzle insert on one round, and it is suspected that a fault in the carbon was responsible for that malfunction. Also, one pressure gauge and one thrust gauge were damaged internally due to over-ranging, caused by a severe over-pressurization of one round. Both malfunctions occurred with experimental compositions.

The precision of specific impulse measurements for micro-motors can be excellent when all variables are properly and rigidly controlled. To illustrate this, the specific impulse results from three ten-motor groups of .75C.50-3.5 motors containing 112cb propellant are shown in Table II.

TABLE II

Specific Impulse Data from .75C.50-3.5 Micro-Motors

Group No.	Group Size	Average F^0_{1000}	1σ (absolute)	1σ (per cent)
1	10	241.0	1.0	0.4
2	10	241.3	0.9	0.4
3	10	240.0	0.4	0.2

The differences in average specific impulse for the three groups probably reflect batch-to-batch propellant variation, since the groups were cast on different days. Even so, the precision of individual groups as reflected in the quoted standard deviation (1σ) values is very good. For the sake of comparison, the standard Rohm & Haas 6C5-11.4 impulse test motor has a standard deviation (1σ) of about 0.25 per cent.

It must be emphasized that the precision level demonstrated in Table II is difficult to achieve. A minute change in some obscure variable is capable of causing the data to scatter so badly it becomes unusable, or even of causing the motors to misfire completely. Meticulous attention to small details is a strict necessity, but precise, reproducible, predictable, usable data can be obtained.

SCALING CONSIDERATIONS

It is a well-known fact that corrected specific impulse[1] of a metal-containing solid propellant varies with motor size and geometry. The prevalent opinion throughout the industry seems to be that specific impulse is a function of charge weight, and that heavier charges will automatically yield higher values of specific impulse than lighter charges. It has been demonstrated conclusively that this is not the case; that in fact propellant specific impulse is primarily dependent upon motor and charge configuration and propellant burning rate, rather than upon charge weight (10). Figure 5 taken from results of specific impulse scaling studies (10) will serve to prove the point. The highest specific impulse measured in a 2C1.5 motor (14.6 inches long) was 246.7, for a charge weight of approximately one pound. On the other hand, a specific impulse of only 245.7 was measured for the 9C7.5-17.1 motor which contained about twenty pounds of propellant.

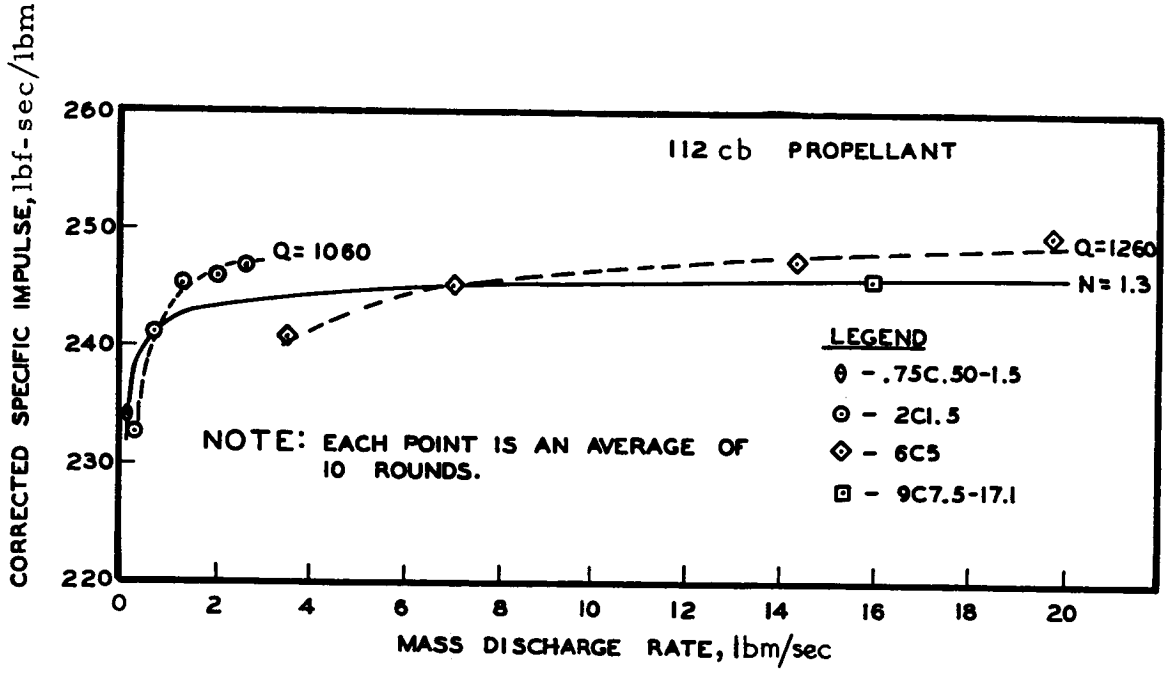

Figure 5 – Corrected Specific Impulse Versus Mass Discharge Rate for Motors Containing Composition 112 Propellant.

[1]Corrected specific impulse is defined as measured impulse corrected to 1000 psig average action time chamber pressure, optimum nozzle expansion ratio for 14.7 psia ambient pressure, and zero degree nozzle divergence angle.

[redacted]

Since propellants evaluated in micro-motors may ultimately be used in large motors, and since comparisons with performance of currently developed propellant in large motors is desirable, it is necessary to have some knowledge of the relationship between the micro-motor specific impulse and the expected large motor specific impulse. Theoretically, the corrected specific impulse of a motor-propellant system is dependent upon the following factors: (a) the available combustion energy of the propellant, (b) the amount of energy lost from the propellant gases in the form of heat transfer to the motor components, (c) the degree of kinetic and thermal equilibrium attained between the gaseous and condensed phases of the combustion products during the nozzling process, (d) combustion efficiency, or the relative completeness of combustion achieved in the motor chamber, and (e) dissociation and recombination of product gases. Items (b) through (e) can be expected to vary with motor size and configuration, and these variations are responsible for the oft-observed interaction of motor size with specific impulse.

A recent experimental investigation of the specific impulse scaling effect (10) by this Division, in which a series of motors were fired containing Rohm & Haas plastisol propellant Composition 112 and ranging in size from the .75C.50-1.5 micro-motor to a 9C7.5-17.1 motor (containing approximately 20 lbm. of propellant), has revealed that good correlations of specific impulse data can be made by assuming that specific impulse variations are due only to items (b) and (c) above, i.e., heat loss and two-phase flow effects. An example of the precision of the correlation is shown in Figure 5 which presents specific impulse data obtained for all motor sizes tested in connection with the specific impulse scaling investigation. The N = 1.3 curve is a theoretical curve generated from two-phase flow theory (11, 12) for an assumed condensed phase particle diameter of 1.3 microns, which should describe the specific impulse variation for linearly scaled motors (.75C.50-1.5, 2C1-5.4, 6C5-11.4, and 9C7.5-17.1). The q = 1260 and q = 1060 are theoretical curves generated from heat loss considerations for assumed heat flux values of 1260 Btu/sec-ft^2 and 1060 Btu/sec-ft^2, to describe the specific impulse variation for various lengths of 6C5 and 2C1.5 motors, respectively. It can be seen that the actual data fit the theoretical curves almost perfectly.

The procedure outlined in Reference (10) and illustrated in Figure 5 provides a method for prediction of expected large motor specific impulse from micro-motor specific impulse data, provided that suitable values of effective condensed phase particle diameter (N) and effective heat flux (q) are used.

[redacted]

It should be stressed at this point that the use of the micro-motor as a screening tool (i. e., firing a propellant in the micro-motor and comparing its specific impulse with the specific impulse of a "reference" propellant fired in the micro-motor) is to be discouraged. Biased results will almost certainly be obtained unless the two propellants being compared have similar heat loss and two-phase flow properties. Flame temperatures, burning rates, and percentages of condensible products in the exhaust must be about equal for the propellants before any significance can be read into comparative specific impulses. Figure 6 illustrates how erroneous conclusions could be drawn by simply comparing micro-motor specific impulses. For 112 propellant (15% Al), a specific impulse of 234.1 was measured in the micro-motor. For 168 propellant (22% Al), a specific impulse of 226.4 was measured in the micro-motor. A simple comparison indicates that 112 is superior to 168 by about 8 impulse points. However, by applying two-phase flow theory and generating theoretical curves (labeled N = 1.3 on Figure 6) which pass through the micro-motor points, it becomes apparent that for larger linearly scaled motors having an $\dot{m}$ of about 36 lbm/sec, identical values of specific impulse should be measured for either composition. For values of $\dot{m}$ higher than 36 lbm/sec (a range which is probably representative of the end-application of the propellant), Composition 168 should have a slightly higher specific impulse than Composition 112. Application of an arbitrary screening procedure with micro-motors would have resulted in the elimination of a better propellant than the "reference" 112 propellant, since the propellants did not have similar two-phase flow properties.

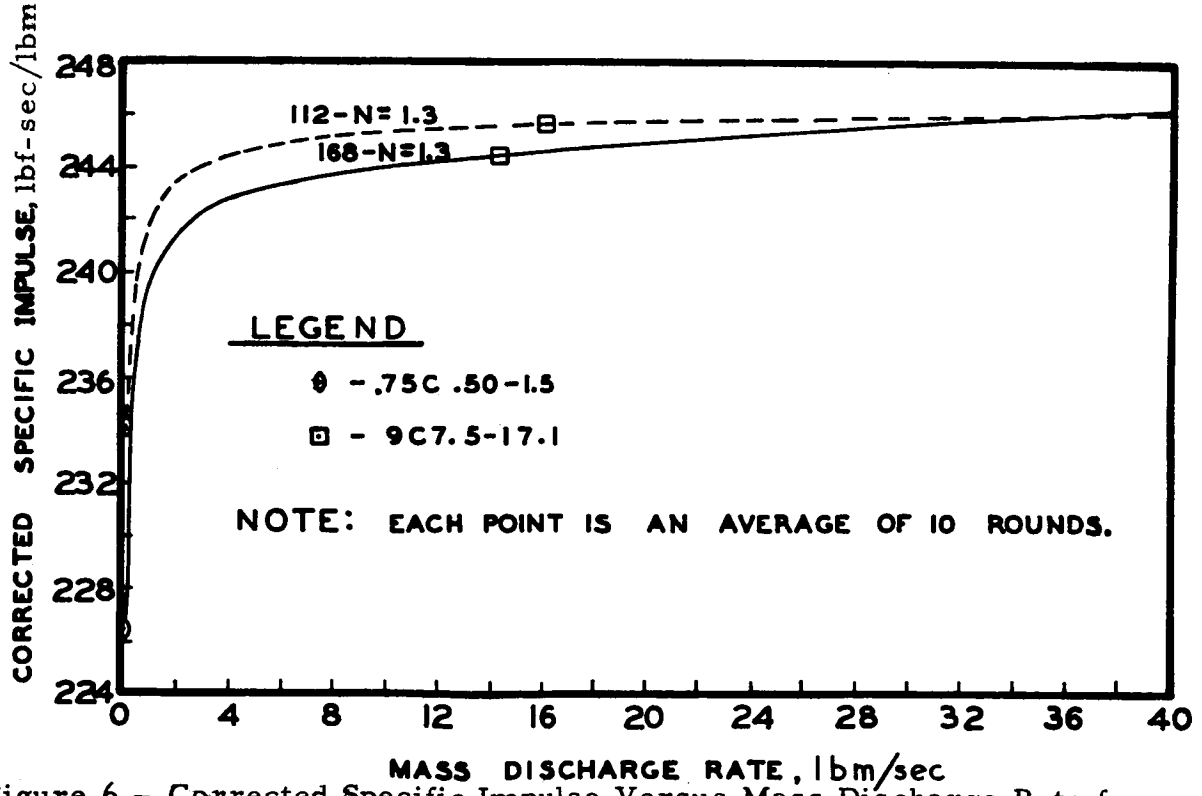

Figure 6 – Corrected Specific Impulse Versus Mass Discharge Rate for Motors Containing Compositions 112 and 168 propellants.

PREDICTION OF LARGE MOTOR SPECIFIC IMPULSE

The specific impulse equation (10, 13, 14) may be written as

$$F^0_{1000} = \sqrt{(I^0_{HL})^2 - \frac{2J\eta Q}{g_o m}} = \sqrt{(I^0_{HL})^2 - \frac{2J\eta q}{g_o}\left(\frac{tA}{m}\right)} \qquad (1)$$

where F^0_{1000} = actual measured specific impulse for a rocket motor, corrected to standard conditions, lbf-sec/lbm

I^0_{HL} = corrected specific impulse which could have been measured for the case of zero heat loss, lbf-sec/lbm

J = energy conversion factor, 778.16 ft-lbf/Btu

g_o = mass conversion factor, 32.174 ft-lbm/lbf-sec^2

η = thermal efficiency, $1 - \frac{Te}{Tc}$

Q = total heat loss from combustion products to motor hardware, Btu

q = heat flux from combustion products to motor hardware, Btu/sec-ft^2

t = motor burning time, sec

A = area of motor hardware exposed to combustion products, ft^2

m = propellant charge weight, lbm

Te = static temperature at nozzle exit, °K

Tc = chamber temperature, °K

The negative term under the radical in Eq. 1 represents the energy lost in the form of heat transfer to the motor chamber and nozzle.

The equation relating specific impulse to velocity lag of the condensed phase (11, 12) is

$$\frac{F^0_{1000}}{I^0_{VL}} = \frac{I^0_{HL}}{I^{00}} = 1 - x\Delta \qquad (2)$$

where I^0_{VL} = corrected specific impulse which could have been measured for the case of no velocity lag of the condensed phase, lbf-sec/lbm

I^{00} = corrected specific impulse which could have been measured for the case of no velocity lag and zero heat loss, lbf-sec/lbm

$x = \frac{m_s}{m_s + m_g}$

$\Delta = \frac{V_g - V_s}{V_g}$

m_s = mass flow rate of condensed combustion products, lbm/sec

m_g = mass flow rate of gaseous combustion products, lbm/sec

V_g = velocity of gaseous phase, ft/sec

V_s = velocity of condensed phase, ft/sec

Writing eq. 1 and 2 in terms of two conditions and combining yields

$$(F^0_{1000})^2_2 = \frac{(1-x\Delta)_2}{(1-x\Delta)_1} \left[(F^0_{1000})^2_1 + \frac{2J\eta q}{g_o} \left(\frac{tA}{m}\right)_1 \right] - \frac{2J\eta q}{g_o} \left(\frac{tA}{m}\right)_2 \qquad (3)$$

Eq. 3 can be used to predict large motor specific impulse from the micro-motor specific impulse if condition (1) is for the micro-motor and condition (2) is for the large motor.

The quantities t, A, and m should be known for both conditions. The thermal efficiency term, η, may be calculated using the theoretical Tc and Te from thermochemical calculations. The weight fraction of condensable products, x, will also be available from thermochemical calculations. The terms Δ and q will generally not be known and must be estimated.

The effective heat flux, q, should be dependent upon such things as flame temperature, emissivities of the flame and surrounding exposed motor hardware, type of gas flow (laminar or turbulent), etc., and can be expected to vary somewhat with the type of propellant being tested. The velocity lag term, Δ, is dependent upon nozzle geometry, density and particle diameter of the condensed phase. Since the nozzle geometry and density of the condensed phase will be known, Δ will depend upon the assumed particle diameter.

Results from tests of a series of plastisol propellants having aluminum concentrations from 5 to 22% by weight and theoretical flame temperatures from 3010°K to 3460°K have been correlated by Eq 3 to determine values for effective heat flux and effective particle diameter of the condensed phase. It was found that for all compositions tested an effective heat flux of 1100-1500 Btu/sec-ft^2 and an effective particle diameter of 1.3-1.8 microns would cause Eq. 3 to accurately describe the actual specific impule variations from micro-motors to larger motors.

Specific procedures to follow for determination of large motor specific impulse from small motor firings depends upon how much propellant is available for testing. Based upon small motors presently available, several recommended procedures for various propellant quantities are outlined below.

If 30-150 grams of propellant is available, fire as many .75C.50-1.5 motors as can be cast and determine F^0_{1000} for all rounds. Scrutinize the data carefully and accept those rounds which give every indication of having burned normally, and which were subjected to no unusual perturbations. Calculate an estimated effective heat flux (q) from Eq. 4. Estimate effective particle diameter (N) to be 1.5 microns, and calculate the resulting Δ for the .75C.50-1.5 motors and the large motor. Calculate the predicted large motor specific impulse from Eq. 3, using the average F^0_{1000} from acceptable .75C.50-1.5 rounds.

If 160-350 grams of propellant is available, fire at least 3 each micro-motors in lengths of 1.5, 2.5, and 3.5 inches, and as many additional motors of each length as can be cast. Assume any N and determine the resulting Δ values for the three lengths of micro-motors. (See Ref. 11 and 12). Using the actual F^0_{1000} values for two of the micro-motor lengths, solve Eq. 3 for q. The q obtained, in conjunction with the assumed N, causes Eq. 3 to correlate the two F^0_{1000} values. Repeat the procedure to obtain q for the two other combinations of motor lengths. Average the three q values obtained, and plot the average q versus the assumed N. Repeat the entire procedure for a different assumed N, again plotting average q versus N. Repeat until an extensive curve of q versus N has been generated. Any point on the resulting curve of q versus N represents values which will cause Eq. 3 to correlate F^0_{1000} values for the three lengths of micro-motors. Calculate q from Eq. 4. Enter the curve of q versus N and determine the corresponding N. Use these values and the .75C.50-1.5 motor conditions to calculate predicted large motor specific impulse from Eq. 3.

If more than 360 grams of propellant is available, fire at least 3 each .75C.50-1.5, 75C.50-2.5, and .75C.50-3.5 micro-motors, and at least two 2C1.5-4 motors. Treat the micro-motor data as outlined above, generating a curve of q versus N from micro-motor data. In addition, generate another curve of q versus N obtained by correlating .75C.50-1.5 and 2C1.5-4 specific

impulse data. This second curve should intersect the q versus N curve generated by correlating micro-motor data. Use the q and N at the point of intersection to calculate predicted large motor specific impulse from Eq. 3.

CURRENT APPLICATIONS

The micro-motor has been used to evaluate the specific impulses of a series of high-energy NF-propellants of current interest to this Division. Results of these evaluations are given in Table III, along with predicted values of specific impulse for the Rohm & Haas 6C5-11.4 impulse test motor. Predicted specific impulse values were calculated from Eq. 3, assuming an effective condensed phase particle diameter of 1.5 microns. Effective heat flux values used varied with theoretical flame temperatures (Tc) and were calculated from the empirical equation

$$q = 6.382\,(Tc/1000)^4 + 156.4\,(Tc/1000) \qquad (4)$$

The empirical constants in Eq. 4 were determined using an empirically-determined heat flux of 1300 Btu/sec-ft^2 for 112cb propellant (Tc = 3325°K), and assuming that the heat flux was 60% radiative (proportional to T_c^4) and 40% convective (proportional to T_c).

Two 100-gram charges of Composition NF-5 have been fired in the Rohm & Haas 2C1.5-4 motor, yielding an F^0_{1000} of 248.0. An F^0_{1000} of 248.3 was predicted for NF-5 in the 2C1.5-4 motor, using Eq. 3 and the actual micro-motor F^0_{1000}. The close agreement between measured and predicted values serves to verify the validity of the method used to predict large motor specific impulses from micro-motor firings of novel, high energy propellants. This same method has been used to predict values of F^0_{1000} for the Aerojet 10KS2500 motor (100-lb charge) from values of I^0_{1000} obtained in 6C5-11.4 motors with excellent success (15). Other current efforts include the scale-up of NF-5 and other compositions to further validate this prediction technique.

TABLE III

Specific Impulse for NFPA Propellants

Composition[1]	Wt-% of Al	I_{calc}	Measured F^0_{1000} for .75C.50-1.5 Micro-motor	No. of Rounds	Predicted I^0_{1000}[2] for 6C5-11.4
NF-2	8.8	262.2	240.0	3	248.5
NF-5	11.9	266.1	244.6	10	251.1
NF-8	18.0	266.8	243.4	5	253.0
NF-9	1.0	257.1	238.6	5	240.3
NF-10	14.0	266.3	244.5	5	251.6
NF-23	22.2	266.0	239.8	4	251.8
NF-26	1.1	257.1	239.7	1	241.3
NF-31	5.0	262.1	241.0	2	245.2
NF-32	10.0	266.1	244.0	4	249.5
NF-33	15.0	266.4	241.5	3	249.8
NF-34	20.0	266.0	237.3	4	248.9
NF-39	15.0	264.5	243.8	1	251.9
NF-40	15.0	270.5	249.5	2	257.4

[1]Compositions 2 through 39 have 2,3-bis-(difluoroamino)propyl acrylate binder. Composition NF-40 is a plastisol propellant having 1,2 bis-(difluoroamino) -3-cyano propane as the plasticizer (9, 16).

[2]I^0_{1000} is identical to F^0_{1000} if (1) the static test motor is the 6C5-11.4 motor, (2) the actual action time averaged pressure is between 900-1100 psig, and (3) the actual expansion ratio is between 7-10.

FUTURE APPLICATIONS

Micro-motors presently in use as described above are limited to case bondable propellants of low casting viscosity and require manual manipulation during casting and firing. These drawbacks make it highly desirable to redesign the metal parts and associated equipment so that both viscous and highly hazardous propellants can be evaluated. The result of this redesign which is now underway will be called ARPA Motors. These will be a set of motors which will have maximum utility to all facilities interested in evaluation of high-energy propellants and will have associated with them the experimental techniques and methods of data interpretation as presented above.

The ARPA motors, as being developed, will allow this Division to expand its high energy propellant evaluation as new ingredients become increasingly available.

SUMMARY AND CONCLUSIONS

The work presented here is the result of several years of experience and extensive efforts in the area of propellant evaluation and particularly two years of work with the micro-motors described above. All of our experience indicates that no aspect of the evaluation techniques can be taken lightly, but that significant results can be obtained from very small motors.

As shown by work of other facilities, small end burning charges have certain inherent desirable advantages. These include ease of manufacture of useable charges (cast, pressed, slurry), and longer burning times.

Consideration has been given to end-burning charges by this Division, but no evaluation of specific impulse is made with this configuration due to the inherently larger corrections, and difficulty of data interpretation. The only possible value of the end burning charge is for the evaluation of "mixtures" of ingredients which cannot be cast in an internal burning charge. Even then the data must be treated with suspicion.

The data presented above show that the micro-motors as described give precise, reproducible data when proper care is taken and that these results are meaningful in that predictions of impulses for larger motors can be made on a rational basis. It should be added, however, that the predicted values of specific impulse are highly sensitive to the measured results, and therefore multiple firings of a small motor are necessary. It is desirable to have multiple firings of different lengths of micro-motors coupled with one length of a two-inch motor for best results.

The method described has been used in the evaluation of a large number of novel propellants having binders containing NF-materials giving predicted values of I^{0}_{1000} up to 257.4 lbf-sec/lbm for NF-40, a plastisol propellant having 2,3 bis(difluoramino)-3 cyano propane as the plasticizer.

Work is underway to make this evaluation system more valuable by the development of ARPA motors.

REFERENCES

1. Thiokol Chemical Corp., Elkton Division, Midpoint Summary Report "Advanced Solid Propellant Research and Development Program" No. E173-61, Dec. 4, 1961.

2. American Cynamid Co., "Integrated Research and Development Program on Solid Rocket Propellants," Progress Report No. 8, Nov. 1, 1961.

3. Dow Chemical Co., "Advanced Research on Solid Rocket Propellants," Report No. AR-3Q-61, Oct. 1, 1961.

4. Minnesota Mining and Manufacturing Co., "Chemical Research as Related to Advanced Solid Propellants," Report No. 10, Nov. 1, 1961.

5. Esso Research and Engineering Co., "Quarterly Progress Report on Research on Advanced Solid Propellants," Rept. No. 61-4, Dec. 10, 1961.

6. Aerojet General Corporation, Chemical Division, "Research and Development on High Performance Solid Composite Propellants," Report No. 0223-01-9, May 15, 1961.

7. Ibid, Report No. 0223-01-10, August 18, 1961.

8. R. M. Lowrey and L. M. Brown, "Ballistic Evaluation of Solid Propellants," Bulletin of the 17th Meeting of JANAF Solid Propellant Group, May, 1961.

9. Rohm & Haas Quarterly Progress Report on ARPA Projects, No. P-61-21, October 25, 1961.

10. Cockrell, B. L., "Ballistic Scaling of Specific Impulse," Bulletin of the 10th Meeting of the JANAF Solid Propellant Rocket Static Test Panel, October, 1961.

11. Rohm & Haas Company "Quarterly Progress Report on Interior Ballistics," No. P-60-7, November 21, 1960.

12. Rohm & Haas Company "Quarterly Progress Report on Interior Ballistics," No. P-61-1, June 22, 1961.

13. Rohm & Haas Company "Quarterly Progress Report on Interior Ballistics," No. P-61-7, October 3, 1961.

14. Rohm & Haas Company "Quarterly Progress Report on Interior Ballistics," No. P-61-13, December 15, 1961.

15. Rohm & Haas Company "Quarterly Progress Report on Interior Ballistics," No. P-62-1, (in publication).

16. Rohm & Haas Company "Quarterly Progress Report on ARPA Projects", No. P-61-27, January 15, 1962.

LASER INITIATION OF SOLID PROPELLANT ROCKET IGNITION

by

Dean A. Rains*
Associate Branch Manager
Solid Propellant Rocket Branch

UNITED TECHNOLOGY CORPORATION
A Subsidiary of United Aircraft Corporation
Sunnyvale, California

ABSTRACT

Safe and smooth ignition of large solid propellant motors has been demonstrated in many static tests utilizing head-end mounted, electrically initiated, rocket-type igniters. However, probable use of large motors in clusters imposes requirements of safety, assurance of no misfires, reliability, reproducibility, and simultaneity that may be difficult to achieve with conventional electrical initiation systems. A promising approach to satisfying these requirements is the use of Laser-beam initiation of head-end mounted rocket-type igniters. A Laser produces a high-energy, short duration light pulse by exciting a ruby crystal. Laser initiation has the advantage of stand-mounted ignition control independent of the airborn system.

Two types of ignition experiments have been conducted at United Technology Corporation to explore Laser initiation: (1) open-air ignition experiments with small propellant samples were used to determine which initiation materials were suitable for triggering propellant combustion by Laser initiation; and (2) firings with a full-scale, large motor igniter were initiated by a Laser beam. Ignition time delay measurements from these tests are presented and discussed. Possible designs of complete Laser initiation schemes are described. Problem areas are pointed out and areas of future investigations are recommended.

INTRODUCTION

Safe and smooth ignition of large solid propellant motors has been demonstrated in many static tests, utilizing head-end mounted rocket-type igniters. However, probable use of large solid propellant motors in clusters imposes new problems and requirements upon ignition systems.

The desired characteristics of an ignition system for large solid propellant motor clusters include:

1. The igniter system, including the arming device, must be safe to install and arm with the missile in place on the pad.

* The author wishes to express his appreciation to Herbert Berman, Richard Serviss, and Howard Williams of Applied Systems Corporation, Palo Alto, California and William Gladden, Joseph Priapi, George Ratslaff and Clarence Carlton of United Technology Corporation.

2. It must be possible to arm the igniter with no possibility of premature firing.

3. The ignition system must be as nearly 100 percent reliable as possible.

4. The system should be designed to assure simultaneous ignition of all motors within the cluster.

5. The system must provide reproducible ignition without significant pressure peaks and without damage to motor components.

6. The ignition system (at least the initiator) should be mounted on the launch stand and not be connected either electrically or mechanically to the airborne system.

A unique and promising approach is proposed by United Technology Corporation to satisfy these requirements in the use of Laser beam initiation of forward head mounted rocket-type igniters. Laser produces a high-energy, short-duration light pulse by exciting a ruby crystal. Laser initiation has the advantage of stand-mounted ignition control, independent of the airborne system. No actual arming of the igniter is required, eliminating this hazardous operation and precluding the possibility of premature firings.

TECHNICAL DISCUSSION

Preliminary Ignition Tests An exploratory program was conducted by United Technology Corporation and Applied Systems Corporation to determine the feasibility of utilizing the short duration, intense radiation emitted by a Laser to ignite solid propellant. The experimental Laser, consisting of a power supply and optical head shown in Figures 1, 2 and 3, was used for these tests. The optical head contains a ruby crystal, helical excitor tube, and reflecting housing. Ruby Laser crystals are normally doped with 0.05 percent chromium and emit in a narrow spectral band centered at 6934°A. The peak output energy and pulse duration of the unit employed are estimated to be one joule and one millisecond. The angular spread of the beam is approximately 10 milliradians.

Propellant samples were located about eight feet from the Laser head. A 133 mm focal length f/2.8 lens was used as the target on the first tests. A 95 mm f/1.5 double convex lens replaced this lens for the final tests. Figure 4 shows an overall picture of the test setup. Figure 5 shows a close-up of the lens and propellant sample setup.

A number of propellant samples were tested. The results of all of these tests are summarized in Table I. All of the tests were run at the full output of the power supply of 2,500 volts. Figure 6 shows one of the several ignitions accomplished by a Laser pulse.

TABLE I. LASER IGNITION EXPERIMENTS

Materials	Results
Propellant	No Reaction
Match Head + Propellant	Ignite Match - No Propagation
Igniter Material (Boron + KNO_3) + Propellant	Point Ignition - No Propagation
Black Powder + Propellant	Black Powder Ignition - No Propagation
Black Powder + Igniter Material + Propellant	Reproducible Ignition

The conclusions based on these experiments were:

1. A Laser would not ignite PBAN propellant without some additional material to start the ignition process.

2. The temperature of burning match material ignited by the Laser was insufficient to ignite propellant.

3. Propellant was not ignited by igniter material directly, but point ignition of the igniter material was achieved with a Laser.

4. Black powder in a small cavity on the propellant could be ignited repeatedly by Laser, but the propellant would not ignite.

5. In each instance that both black powder and igniter material were used, the propellant was ignited. Only one or two grains of black powder were required to fire the igniter material and it is likely that much lower light intensities would have fired the black powder.

6. The results of these final tests indicate that, with appropriate optics, the Laser would be effective at distances required for ignition of large rocket motors and that the beam could be split to ignite several motors simultaneously.

7. Future efforts should be devoted to a demonstration of complete motor ignition with a Laser. Motor ignition could be initiated by a Laser with actual ignition being accomplished with a conventional pyrogen igniter.

Motor Tests At the conclusion of these preliminary experiments, application of these results to solid propellant rocket ignition was possible. The plan conceived was to: (1) ignite an initiator from a large igniter motor by a Laser; and (2) if this test were successful, attempt to ignite a large igniter motor with an initiator ignited by a Laser pulse. Success in these two tests demonstrated the utility and feasibility of Laser initiation of large motor ignition.

The small motor test bay at the United Technology Corporation Development Center was used for the two Laser-initiated igniter tests. The Laser

head, power supply, and other auxiliary equipment were installed in a test bay adjacent to the motor bay. The Laser beam was directed at 90 degrees to the motor axis and reflected into the motor nozzle opening by an adjustable mirror located directly in front of the nozzle opening (see Figures 7 and 8). The distance from the Laser to the target focusing lens mounted on the initiator was approximately 180 inches.

The test motor for the first test consisted of a modified initiator mounted with a lens located in a steel motor simulating the free volume of an igniter motor. The motor used for the final demonstration test was the standard RP-1 igniter motor (see Figure 9 for a detailed description), using a modified initiator and lens.

The Laser equipment consisted of an experimental head and power supply. The power supply consisted of a capacitor bank (225 mfd, 4000 volts) with an energy storage of 1800 joules. The operating threshold of the Laser is approximately 2000 volts (450 joules), with a light output of one-half joule for one millisecond at an efficiency of 0.1 percent.

The Laser beam has a divergence of approximately one-half degree, so that it has a one-inch diameter at eight feet. The Laser beam was focused on a small black-powder charge mounted on the nose of the initiator basket by a high resolution, three-inch focal length camera lens. The lens was mounted on the modified initiator basket by a tubular lens mount. Figure 10 is a photograph of the modified initiator which contained boron potassium nitrate and the powder charge capsule located on the tip of the initiator. The front of the powder charge, to be coincident with the focal plane of the lens, was placed one-half inch in front of the original basket tip. During the course of the motor experiments, it was found necessary to add paper powder caps to the front of the black powder charge to insure initiation of the igniter train.

After initial checkout tests of black powder samples, two successful igniter tests were conducted, using a Laser pulse, triggered remotely, to initiate the ignition motors.

Test No. 1: The first test, conducted 3 November 1961, was the initiator test only. The ignition pressure trace for this firing is shown in Figure 11.

Test No. 2: The second test, also conducted 3 November 1961, was a complete igniter motor firing, and the ignition was successful. The ignition pressure trace for this firing is shown in Figure 12.

The ignition delay was almost 0.20 second, compared to 0.035 second for a conventional squib-initiated igniter motor firing. Figure 13 shows the pressure trace for a conventional RP-1 igniter firing for comparative purposes. The problem is not ignition delay itself, but reproducibility of the ignition trace. More testing will be required to define the reproducibility of the Laser ignition system.

The eventual application of Laser initiation will be in clusters of large solid propellant rocket motors. Figure 14 is an illustration of how a Laser beam initiation scheme could be applied to a large solid propellant

rocket booster. A cluster motor arrangement can be initiated by a single Laser beam split optically by prisms or beam splitters or by a set of Laser heads triggered and powered by a single power source. Misfire protection can be afforded by shades, mirror covers, or optical blocking equipment, which can be removed just before firing.

The conclusions of the motor test program are:

1. Laser initiation of large solid propellant motors is a feasible and attractive solution to the problem of initiation of motor clusters.

2. Alignment and prefocus are the critical problems of Laser initiation. Schemes will be required to accurately align and focus an optical system on the launch stand. Visual sighting of some type is required.

3. The failure of black powder to ignite in these tests indicates that the energy output of the Laser equipment used in this test was less than the unit used in the previous laboratory tests. Further tests of igniter materials are required to determine ignition energy requirements of black powder and other materials and to pick the materials most suitable for the Laser initiation train.

FIG. 1 LASER HEAD

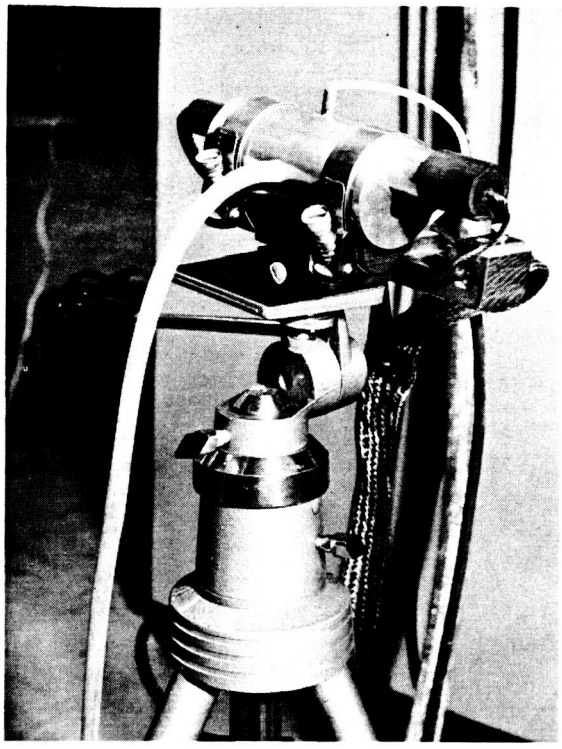

FIG. 2 LASER HEAD CLOSEUP

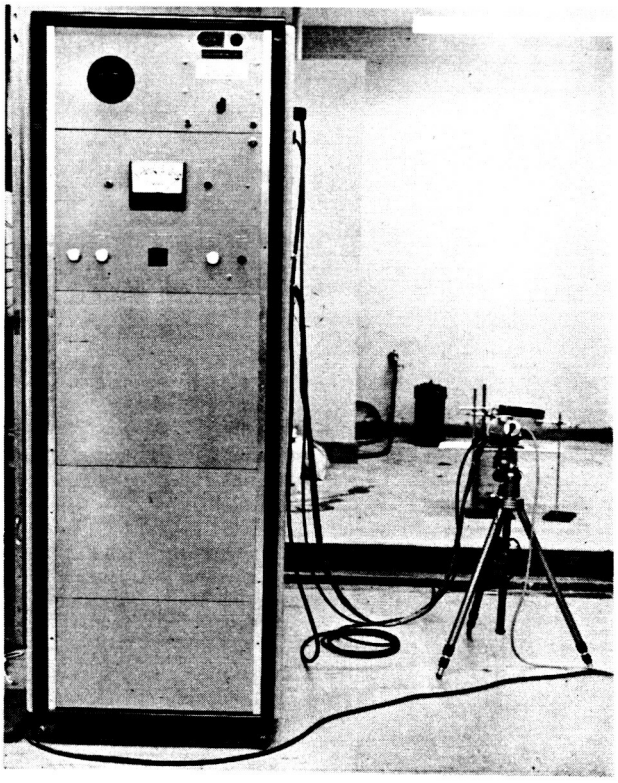

FIG. 3 LASER POWER SUPPLY

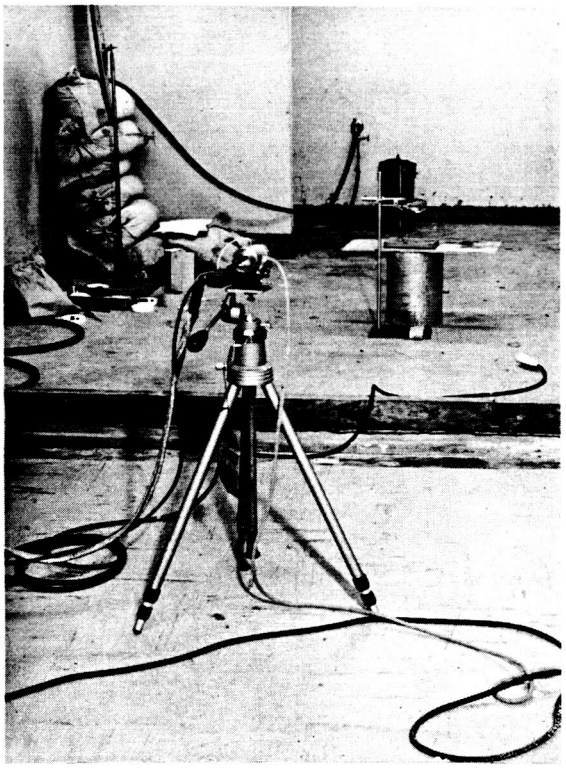

FIG. 4 OVERALL EXPERIMENTAL SETUP FOR LASER EXPERIMENTS

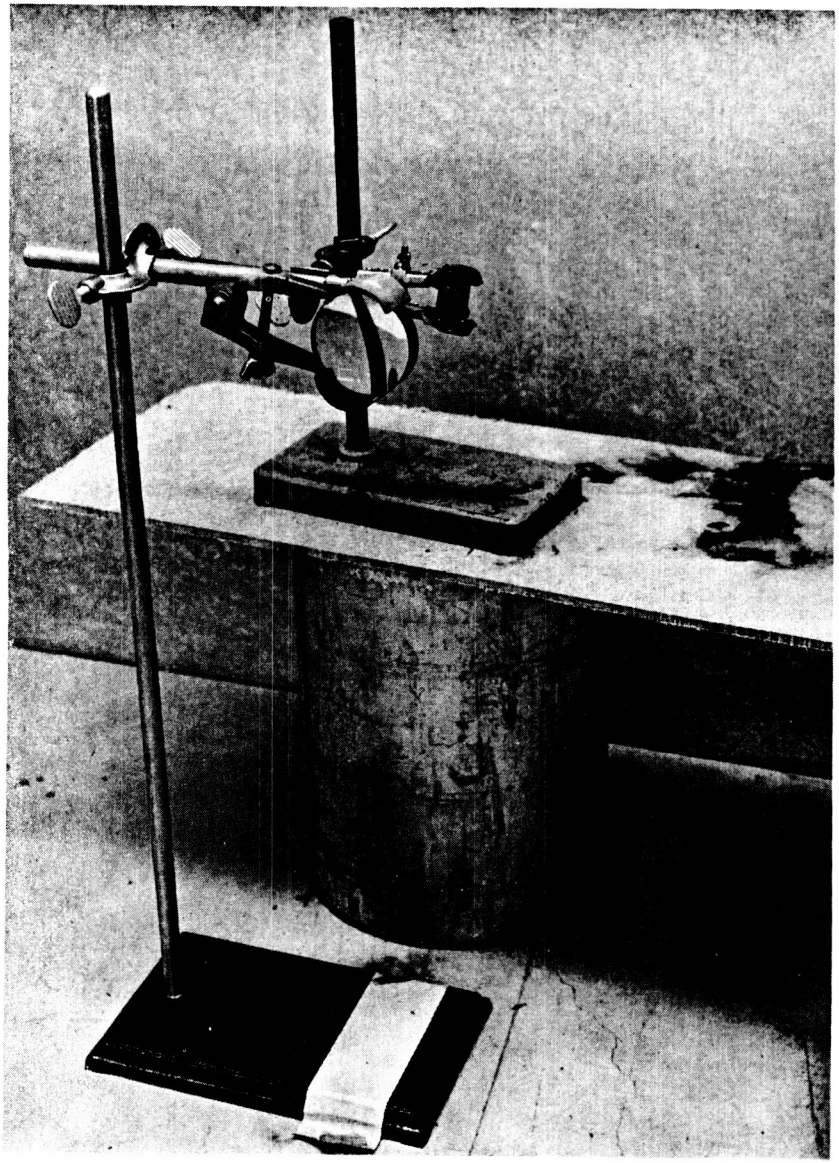

FIG. 5 PROPELLANT SAMPLE FOR LASER EXPERIMENTS

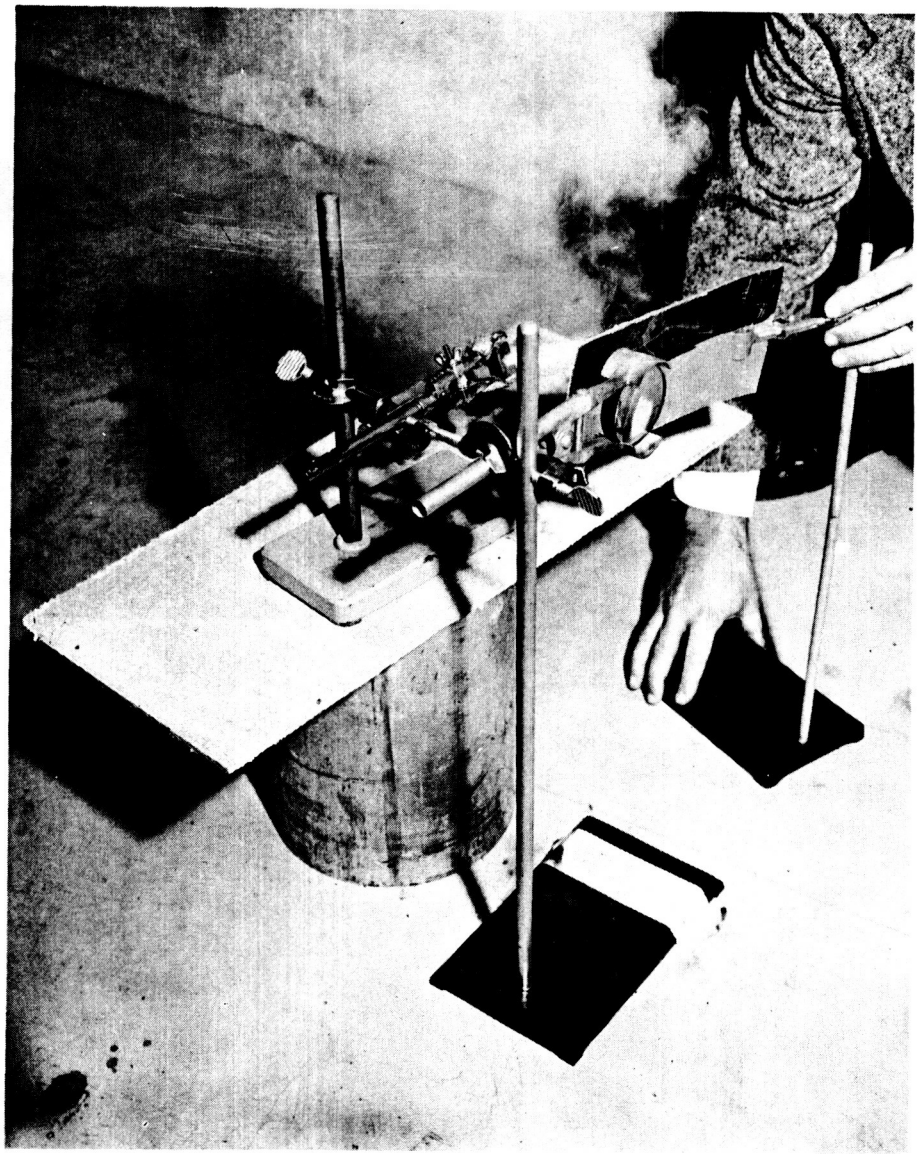

FIG. 6 PROPELLANT COMBUSTION FOLLOWING IGNITION BY LASER

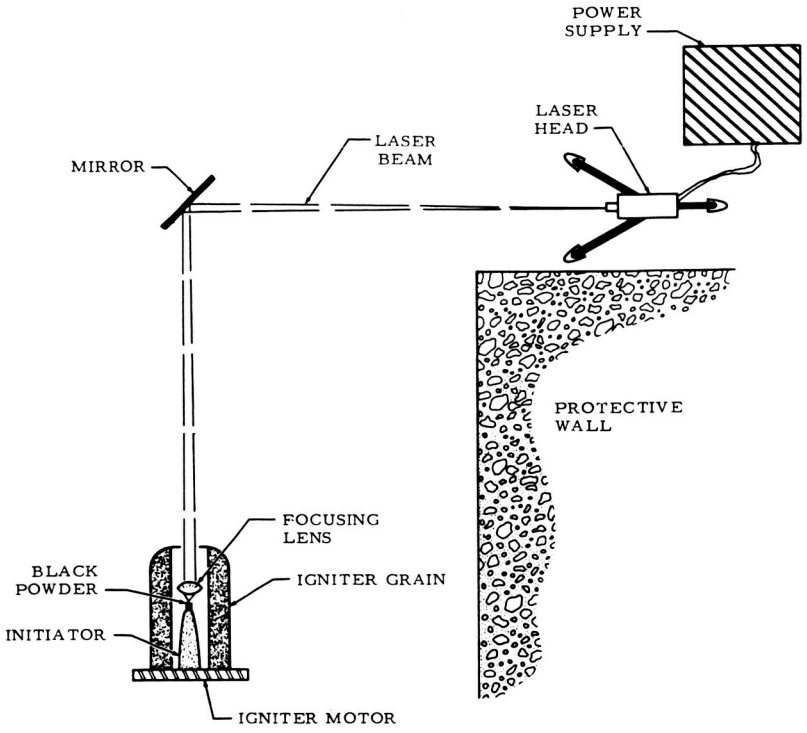

FIG. 7 DIAGRAM OF LASER IGNITION TEST SETUP FOR DEMONSTRATION TEST

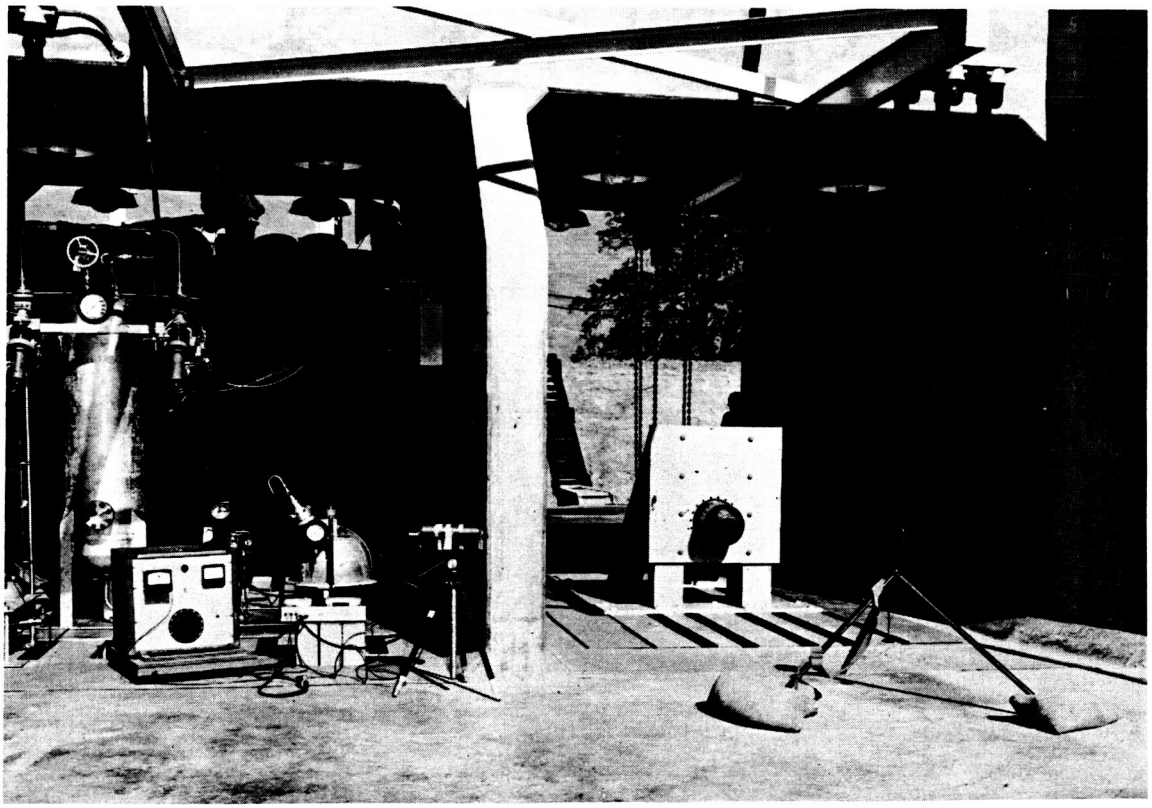

FIG. 8 LASER IGNITION TEST SETUP

IGNITION DATA

TYPE	Rocket-Type Igniter System
MAX OPERATING PRESSURE, PSI	1000
ACTION TIME, SEC	0.700
THRUST, LB	5000
PROPELLANT WEIGHT, LB	26.5
INITIATOR	Boron Potassium Nitrate (Pellet Charge)
GRAIN	24 point star configuration (cartridge loaded)

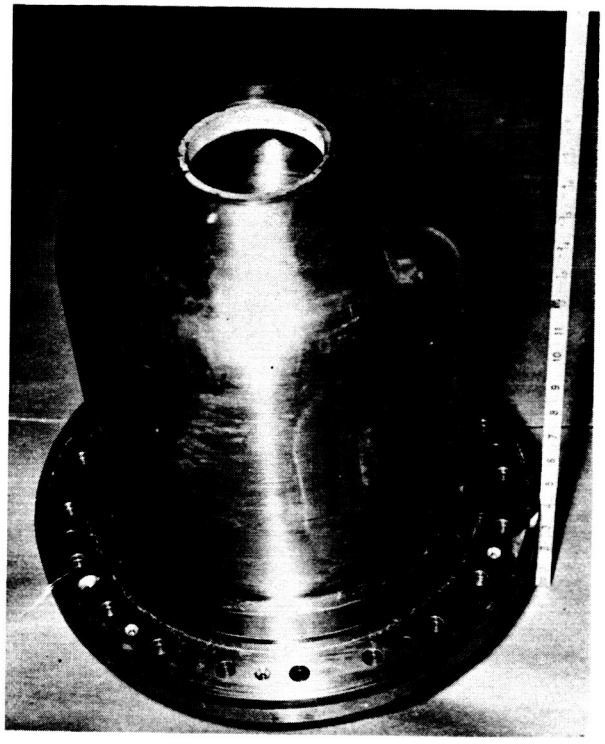

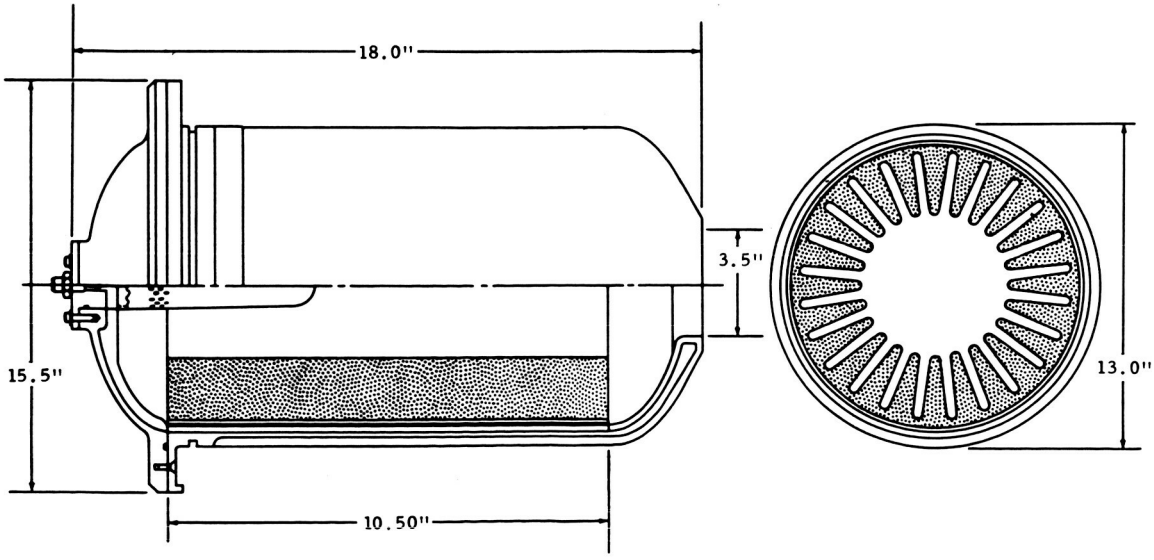

FIG. 9 RP-1 ROCKET IGNITER DATA SHEET

FIG. 10 MODIFIED INITIATOR BASKET USED IN RP-1 IGNITER MOTOR FOR LASER DEMONSTRATION TEST

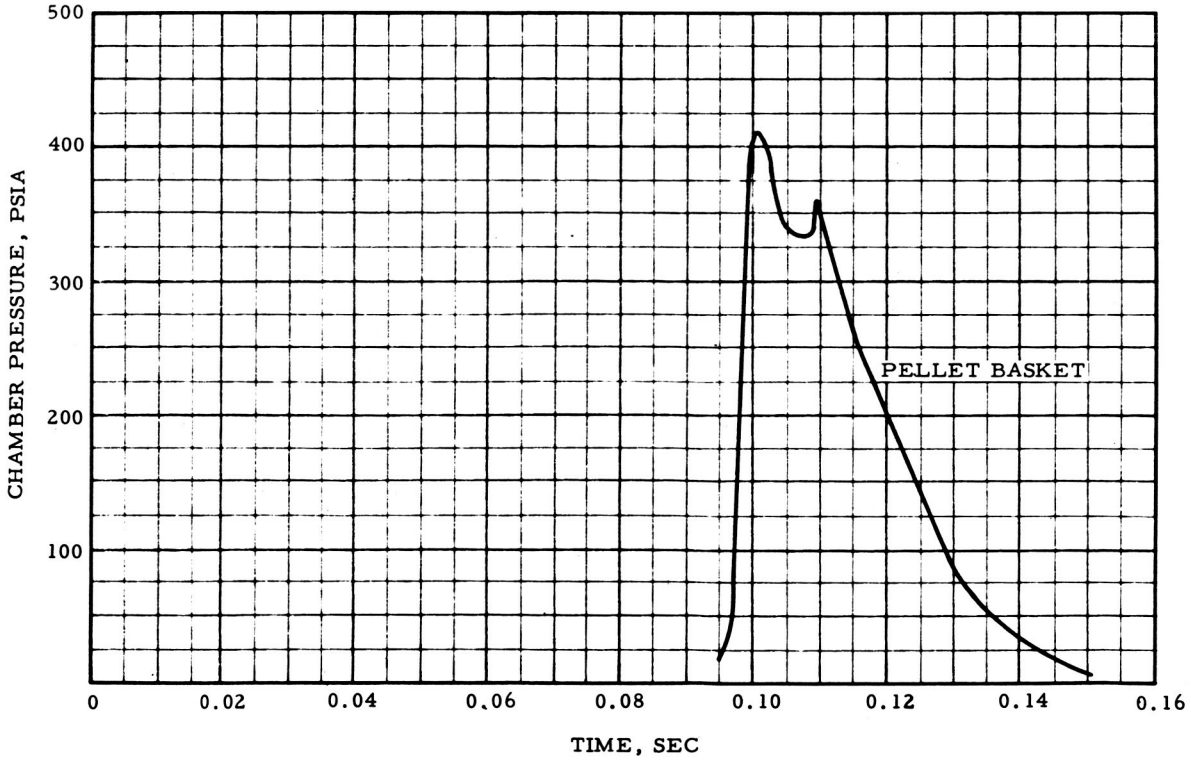

FIG. 11 IGNITION PRESSURE: TRACE FIRST TEST FIRING.

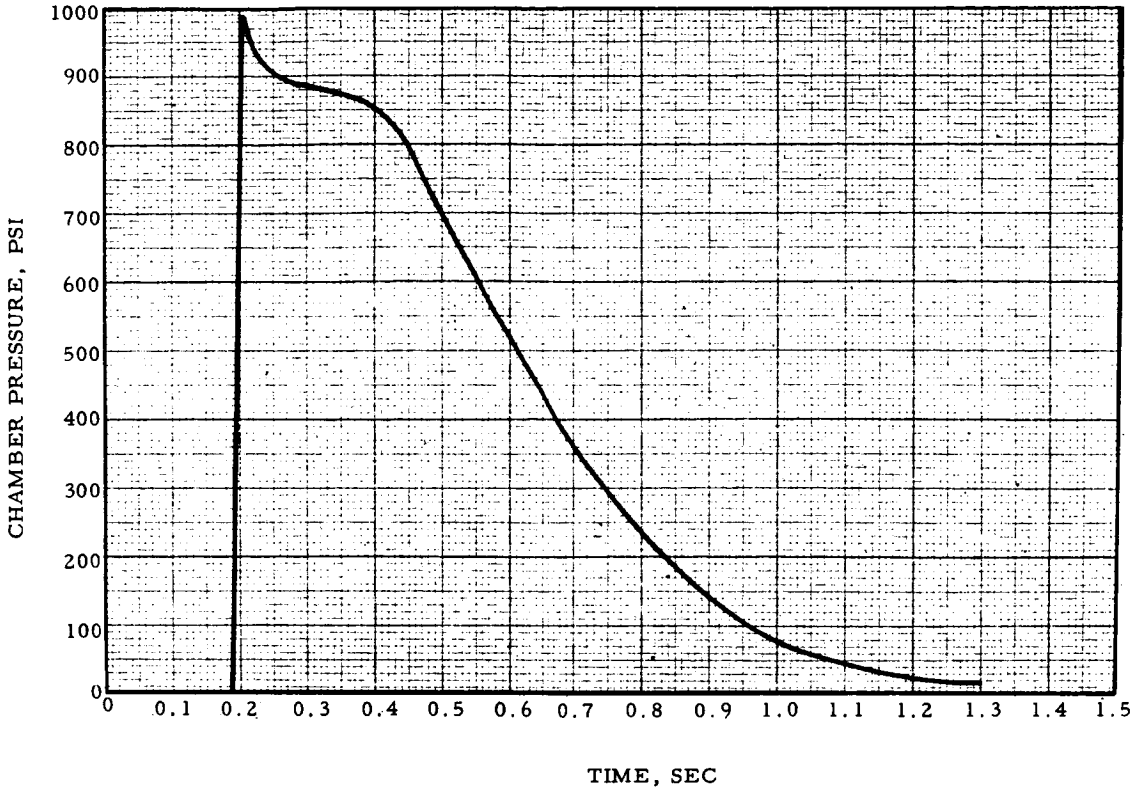

FIG. 12 IGNITION PRESSURE TRACE: LASER-INITIATED IGNITER MOTOR

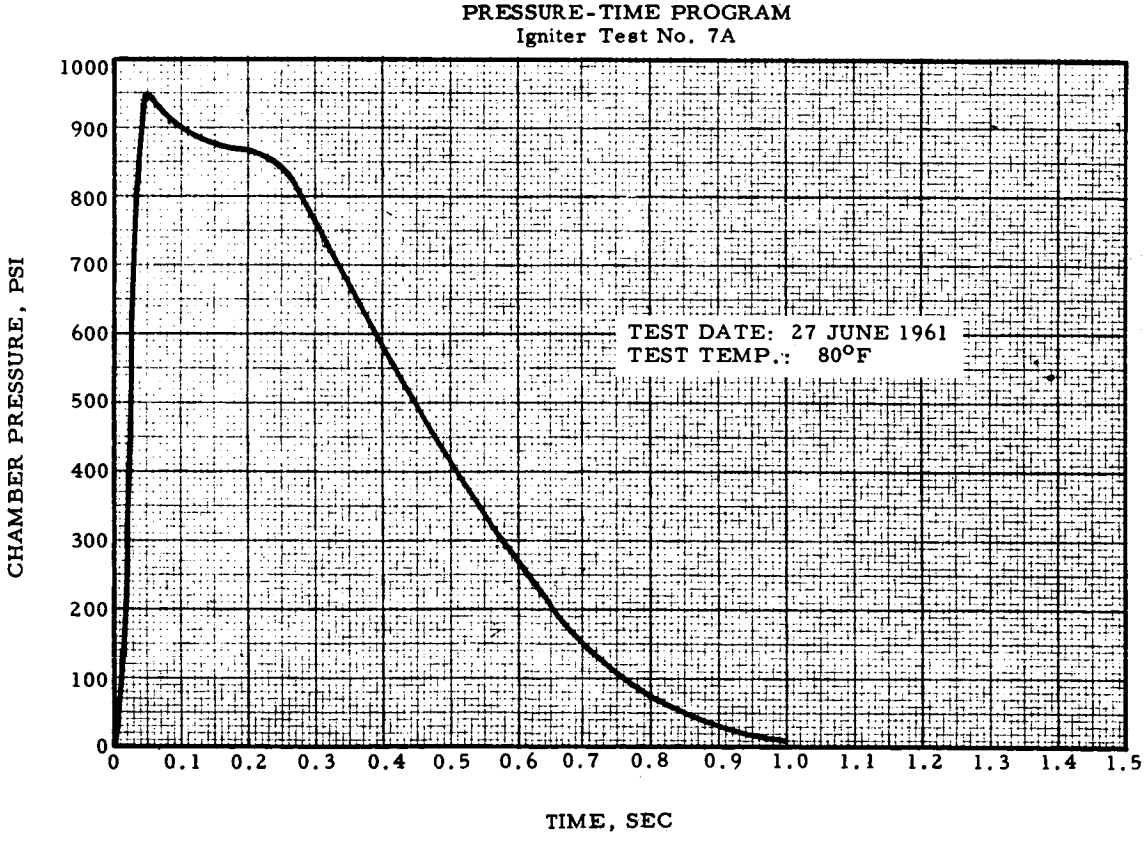

FIG. 13 IGNITION PRESSURE TRACE: ELECTRICALLY INITIATED IGNITER MOTOR

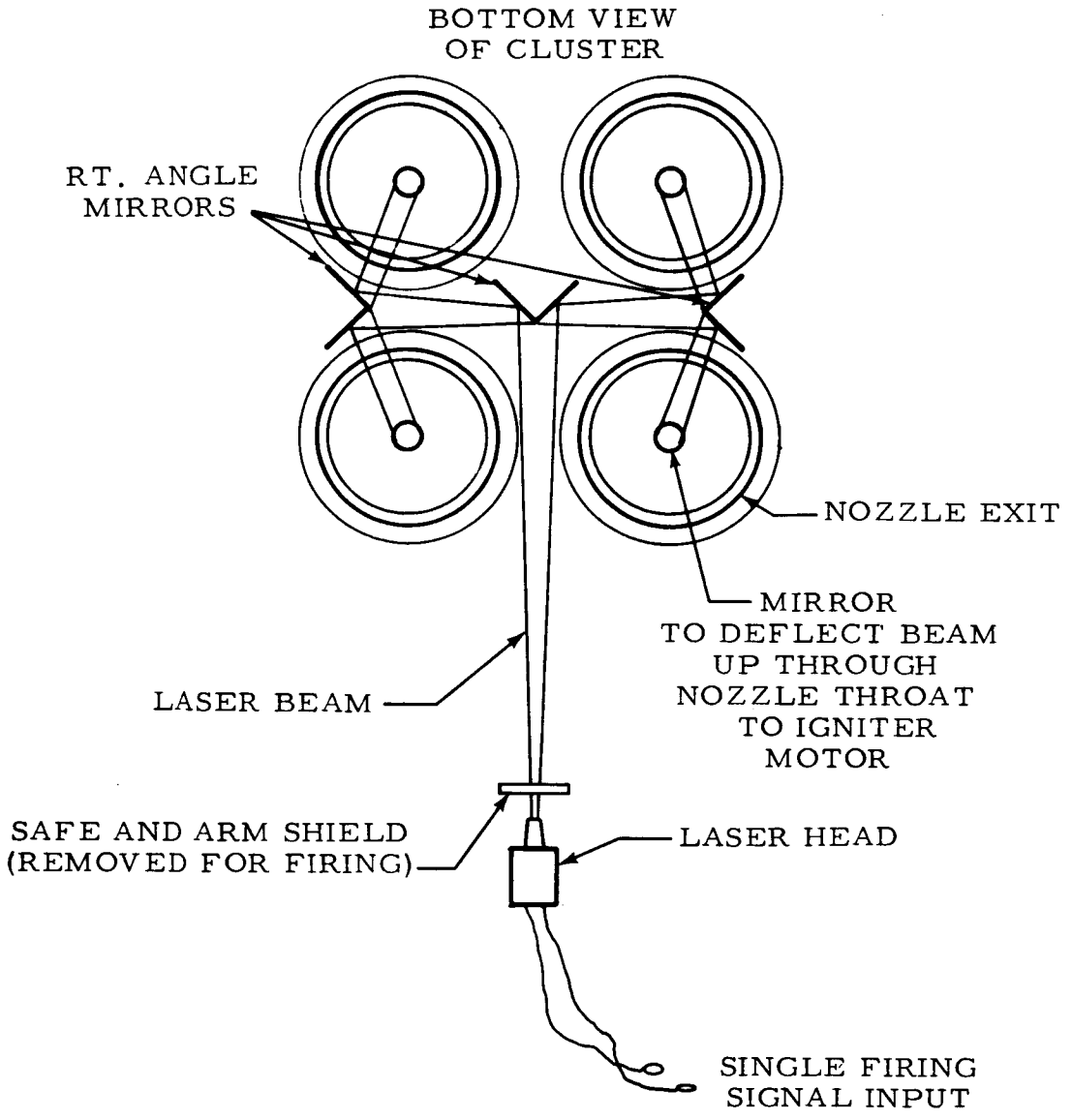

FIG. 14 LASER INITIATION OF A CLUSTER OF SOLID-PROPELLANT MOTORS

[redacted]

INVESTIGATIONS OF PLASTIC AND FOAMED MANDRELS

Ray A. Miller and Ronald Vetter
U. S. Naval Ordnance Test Station
China Lake, California

ABSTRACT

Two methods of producing plastic and resin mandrels for solid propellant rocket motor casting have been developed. The first method involves casting mandrels of filled plastic. These plastic mandrels offer advantages over machined or otherwise manufactured metal mandrels. For example, the plastic mandrels cost less, and may be prepared in a shorter time. Epoxy plastic filled with aluminum was selected from several possible material candidates. Some of the systems tested included epoxies filled with Teflon, phenolic microballoons, steel, minerals, aluminum, as well as unfilled epoxies and other plastics both filled and unfilled. Some of the criteria used to select the best system included economics, shrinkage comparisons, thermal conductivities, and density. Data for these factors are presented and discussed.

Molding methods employing rigid polyurethane, epoxy, flexible polyurethane, and the final choice—a flexible room-temperature-vulcanizing silicone rubber having self-release properties—are elaborated upon. High mold precision is obtained using master mandrels of various materials; the molds may be re-used to produce desired replicates. Useful lives of particular molds vary with such factors as surface area, design intricacy, and angle of axial taper of the mandrel as well as rubber curing characteristics and mold case design.

Mandrel release from propellant has been effected using waxes, greases, and Teflon-resin formulas; however, data presented show that a silicone rubber applied over suitable primers provides best results and is semi-permanent depending on mandrel design characteristics and handling.

The second method of producing mandrels makes use of certain frangible foams which are not removed from the weapon after the propellant has been cured. These foamed mandrels have the possible advantage of low cost, short procurement time, increased motor performance (since more intricate optimum shapes are feasible), elimination of processing steps since the mandrel remains in the motor to provide support for the propellant, protection for the propellant from weathering, and superior ignition characteristics.

To realize the above advantages light weight, frangible, rigid, chemically inert, unicellular foams have been investigated. Low cost fabrication methods are important since each mandrel may be used only once. Results and techniques are given on work using polystyrene, polyurethane, epoxies, filled and combination foams.

Motor firings were performed with 5-inch diameter rounds using foamed mandrels. The perforation of 5-inch diameter rounds was formed by a mandrel

machined from a block of styrofoam. Ignition delays from these and conventional 5-inch diameter motors appeared to be equal. The rate of pressurization was lower with the rounds containing the styrofoam mandrels.

INTRODUCTION

Cast rocket motor core, or mandrel, fabrication involves expense and requires time due to milling intricate shapes with tapered dimensions and close tolerances. For multiple unit loading, a large number of identical mandrels are required. Efforts to mass produce these parts cheaply have evolved into rigid, filled plastics cast into flexible molds. A variety of polymeric materials have been tested as matrices, using several inorganic and organic fillers.(1)

Since moderately high stresses are applied during extraction from the cured grain, the material must have sufficient tensile strength. Actual needed values vary with unit size and shape. The casting slurry must be of such viscosity (preferably below 50,000 cp and not thixotropic) to flow easily into an intricate mold. Vacuum casting techniques tend to aid flow as well as eliminate voids in the finished products.

This fabrication method does require a master mandrel. This may be made from almost any material if the RTV silicone rubber described herein is utilized.

Preliminary work in fabricating mandrels is described and test data for various parameters presented and discussed herein. A second phase of work investigated is also presented. Foam mandrels present some interesting possibilities as well as problems. Fabrication of various compositions, inert and energetically loaded, as well as other innovations, are introduced with the data so far obtained. These units are bonded into the grain during cure and play a part in grain ignition.

Fabrication techniques of castable foam mandrels are similar to those used for producing plastic mandrels.

EXPERIMENTAL PROCEDURES

Only one pattern is required to fabricate plastic mandrels. This pattern may be made of almost any suitable material, the only requirement being that if a porous material is used, the surface should be sealed with wax or a similar material. In the past, aluminum, steel, epoxy-aluminum, and wooden patterns were used. The aluminum and steel patterns need not be Teflon-coated. The epoxy-aluminum patterns require no release agent.

The chase is designed so that the minimum wall thickness of the silicone rubber is at least 1/4 inch. If very large mandrels are to be produced, the mold should be designed to follow the contours of the mandrel pattern, and thereby, economize on the amount of silicone rubber required.

The mold surface is cleaned thoroughly and dryed. It is then painted with 81822 Primer (G.E.) and allowed to stand overnight. It is then coated with XS-4004 Primer (G.E.) and dried for at least 2 hours at room temperature. After the silicone prepolymer has been cast into the metal tube and cured, the

rubber will be case-bonded to the chase, forming the internal cavity. This is done to keep the mold from constricting or warping as a result of shrinkage of the rubber.

The pattern is positioned in the metal tube by using a suitable alignment fixture. This is required for centering the pattern and regulating the length of the chase.

The proper amount of RTV-60 (G.E.), or equivalent, is weighed out along with the catalyst. After being mixed thoroughly, this catalyzed RTV rubber is cast under vacuum into the chase. The chase is then allowed to cure at room temperature for 72 hours. If the chase is to be used at elevated temperatures, it is post-cured at temperatures that are increased incrementally (50 to 100°F increments above 250°F) until it has been post-cured at a temperature higher than the desired service temperature.

The pattern may be removed from the chase either by hand or by an hydraulic jack.

The epoxy resin and aluminum for the mandrel are weighed and mixed. The proper amount of catalyst is then added. Typical formulations and corresponding physical properties may be found in Table I. After degassing, the mixture is cast into the cavity. A metal stud smaller in diameter than the central hub of the mandrel may be inserted into the plastic to give increased strength, although this is not ordinarily required. The plastic is then cured and post-cured.

TABLE I. EPOXY FORMULATIONS AND THEIR PHYSICAL PROPERTIES

Formulation no.	Ingredients, %							Physical properties	
	Epon 815	Epon 828	Epon 526	Alcoa 123	Hardner 951	Devcon B	Hardener B	Tensile strength, psi	Elongation, %
1	46.5	....	....	50.0	3.3	....	....	5,337	5.9
2	37.4	....	....	60.0	2.6	....	....	4,170	5.3
3	28.0	....	....	70.0	2.0	....	....	4,244	5.4
4	....	36.7	10.0	50.0	3.3	....	....	2,876	3.2
5	....	27.4	10.0	60.0	2.6	....	....	2,975	3.8
6	....	22.7	10.0	65.0	2.3	....	....	5,321	...
7	36.7	....	10.0	50.0	3.3	....	....	4,712	6.5
8	27.4	....	10.0	60.0	2.6	....	....	3,977	6.2
9	18.0	....	10.0	70.0	2.0	....	....	5,263	7.4
10	....	....	....	....	...	90.0	10.0	2,065	3.9

Upon removal of the plastic mandrel from the chase, the mandrel is painted, or sprayed, with primers 81822 and XS-4004 in the same manner as described for the priming of the mold tube walls. This is necessary since the RTV rubber will not bond to the epoxy without a primer coat. The mandrel is then coated with RTV rubber to act as a release agent from propellants.

Most molds for small mandrels will produce at least 20 mandrels before mold damage is evident. Two molds of a mandrel 2.5 inches in diameter and

70 inches long have produced over 30 plastic reproductions each, while at a temperature of 110°F to speed production.

Mandrels cast on RTV-60 molds are smaller in all dimensions than the pattern because of shrinkage of the epoxy-aluminum formulations used. Figure 1 compares the dimensions of an aluminum mandrel pattern with the dimensions of a plastic reproduction.

	A	PATTERN VARIATION, IN.	B	PATTERN VARIATION, IN.
Mandrel Pattern (AL)	0.191	0	4.734	0
Epoxy-AL Cast in RTV-60 Mold	0.179	-0.012	4.722	-0.012

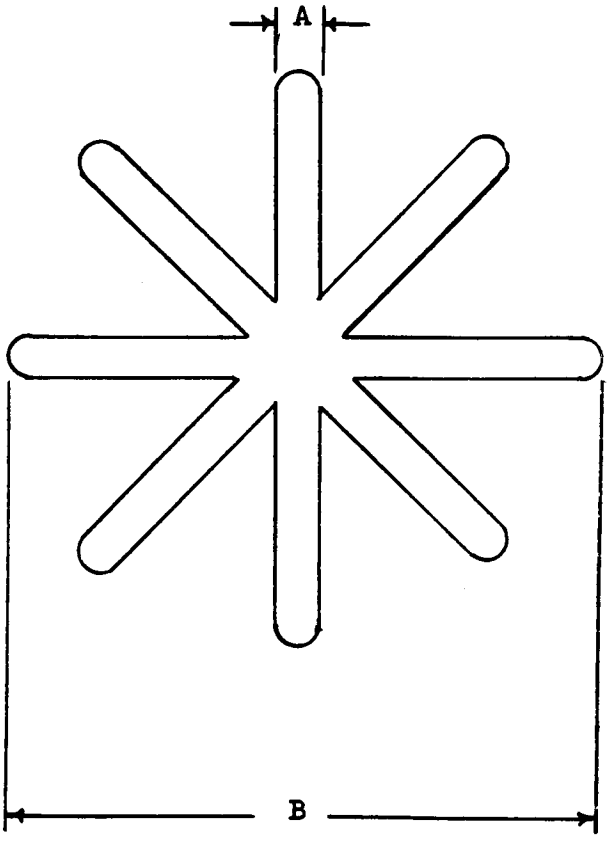

FIGURE 1. DIFFERENCES IN DIMENSIONS BETWEEN PLASTIC AND ALUMINUM MANDREL

Many different formulations of plastic have been used. Some of the resins evaluated were Epon 828, 815, and 562, Devcon, and various polyesters. Aluminum, Teflon, phenolic microballoons, and carbon black were evaluated as fillers. The best formulations appeared to be mixtures of epoxies, since higher elongations were obtained at approximately the same level of tensile strength than with the individual resins. The physical properties desired are from 4,000 to 5,000 psi tensile and 5 to 10% elongation. Fairly high concentrations of aluminum are used to hold shrinkage to a minimum, as well as to reduce costs and increase the thermal conductivity of the plastic mandrels.

Figure 2 shows the effect of varying the aluminum content on the thermal conductivity. Some types of propellant require curing by heating the inside of the mandrel as well as the outside of the motor, in order to shorten the curing time. For these motors, special mandrels are cast with internal heating pipes in place.

The surface roughness of the plastic mandrels is essentially the same as that of the pattern. Measurements of the roughness of various plastic mandrels were, on the average, from 14 to 30 microinches. These data are presented in Table II.

TABLE II. SURFACE ROUGHNESS COMPARISON OF PATTERN AND PLASTIC REPRODUCTION

Mandrel type	Fin No.	Pattern[a]	Plastic[a]
4 1/2-in. coned mandrel	1	20	18
4 1/2-in. coned mandrel	2	17	15
4 1/2-in. coned mandrel	3	17	14
4 1/2-in. coned mandrel	4	18	18
12-in.coned mandrel	1	25	25
12-in.coned mandrel	2	25	25
12-in. unconed mandrel	1	25	30
12-in. unconed mandrel	2	32	25
2 1/2-in. round mandrel	..	30	23

[a] Surface finish in microinches. Measurements made on a Type Q Profilometer manufactured by Physicists Research Company, Ann Arbor, Mich. Tracer head type LA 4-33 was used.

A thin coat of RTV rubber is used as the release agent between the plastic mandrel and the propellant. This type of mold-release agent has several advantages over other types. The surface of the propellant is free of residue that might interfere with ignition. The plastic mandrel may be used several times before recoating is necessary. As high as 40 releases from propellant have been obtained from a single coating. The coating is applied and cured at room temperatures, allowing the coating of mandrels which would deform or degrade at the temperatures required for sintering Teflon coatings.

Release properties of the RTV rubber, when applied to plastic mandrels, compare very well with the corresponding properties of mandrels coated with Teflon. In one case, a Teflon-coated tapered mandrel released at 1.75 psi,

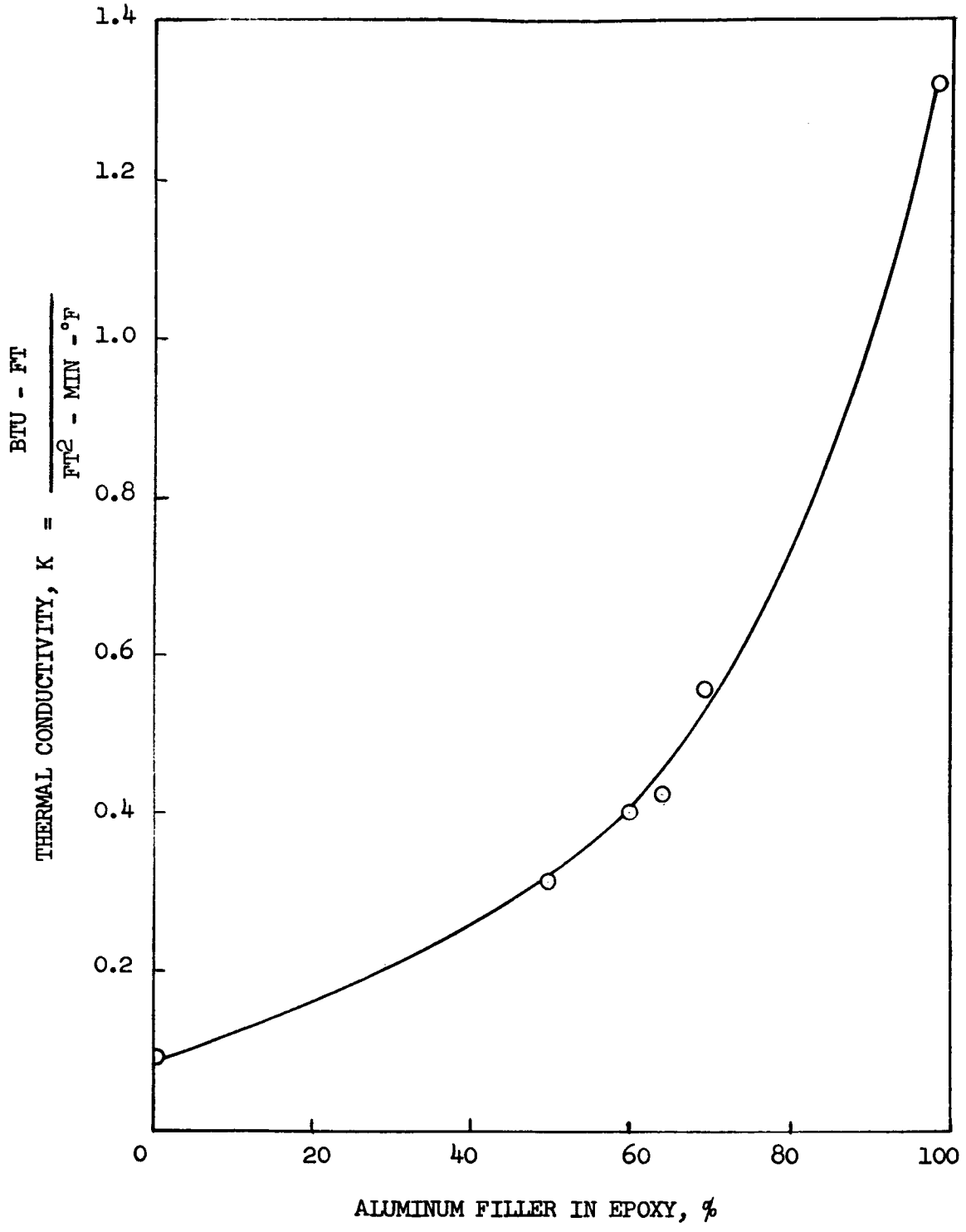

FIG. 2. THERMAL CONDUCTIVITY VERSUS PERCENTAGE OF ALUMINUM FILLER.

and an identical mandrel coated with RTV required 1.95 psi. This difference is small and probably insignificant. These "shear" measurements demonstrate that the RTV rubber does possess very good release properties.(2,3)

Foam Mandrels The first foam mandrels were made from styrofoam block machined to a cylinder. These were coated with oxidizer-rich ignition slurry. After the solvent evaporated, a polyurethane propellant was cast around them in 5-inch motors. Pressure measurements during static firings showed lowered pressurization rates with similar ignition delays.(4,5)

Machining of the foams is difficult and not feasible for complicated shapes. Consequently, other methods of fabrication were investigated.

Koppers Co. Dylite polystyrene beads were used to make the foams also, but without success. Tests were certainly not exhaustive and temperature control, mold design, pre-expanding, and molding techniques were not adequate. Using epoxy resins to generate heat in a hybrid foam with the polystyrene beads yielded materials of too great strength.

A short literature survey did not yield much information on "hot wire" cutting of foams. A "hot-wire" apparatus was designed and built. It consisted of stainless steel shaped to the configuration of a mandrel section perpendicular to the axis of the mandrel with support-conductor sections 180° apart connected to the power source. Several sizes and shapes of metal cross-sections were made. A sharp-edged strip about 0.035 inch thick by 1/8 inch performed best of the unsupported "cutters" tried, but deformed due to nonuniform feed rate of the foam through the unit (hand pushed) and inadequate temperature control.

A supported apparatus was built which is sturdily mounted on micarta and electrically connected in series with a separate metal "cutter" section for each "fin" of the mandrel. The unit requires a round billet as feedstock and functions quite well.

Fabrication techniques have been established for cast foams. Polyurethane foam mandrels are formed in much the same manner as plastic mandrels. A master mandrel is fabricated from aluminum, steel, epoxy-aluminum, wood, or a combination of these. The pattern is placed in a suitable mold, and a silicone rubber compound of the room-temperature-vulcanizing (RTV) type is cast around it. After the silicone rubber is cured, the pattern is removed, leaving a female reproduction of the master mandrel. The mold is then split longitudinally to facilitate removal of the foam mandrels. The cavity is sprayed with a suitable release agent since some bonding of polyurethane foams to the RTV rubber has occurred. Aerosol polyethylene release agent, carnauba wax in toluene, Dow Corning 20 compound mold release, and Injection Molders Supply aerosol silicone release agents were tried with the RTV silicone molds. The IMS silicone spray seemed to function best of these. After coating the mold, the appropriate foam formulation is poured into it. After curing, the mold is split open slightly and air blown around the mandrel to release all surfaces. The mandrel is then removed from the cavity.

In work with small foam mandrels, it has been considered desirable to cast a metal rod into the center of each mandrel. This rod is then used to hold the mandrel in position for the casting operation. After the propellant

is cured, the rod is removed from the mandrel and a small amount of foam is used to fill the cavity. The igniter may be foamed in place during this operation.

Epoxy foam mandrels using water, azo-bis-isobutyronitrile, and ammonium carbonate as blowing agents are fabricated by the procedure described above. High densities in thin sections and the high exotherm temperatures using epoxy foams were considered undesirable.

Motor firings (5 inch) yielded results varying from good quick ignition to complete failure to ignite when the center core (where the centering rod had been) "popped" out with the igniter.[6] Tougher, denser foams yielded longer delays or caused ignition failure. Motor firings, in general, indicate lower pressurization rates using foam mandrels than the control rounds exhibit. Table III summarizes the firings to date. Foams containing 47% NH_4ClO_4 yielded very high pressurization rates. Foams with 8 to 15% NH_4ClO_4, however, give lower peak pressures indicating that the pressurization rate may be controlled by varying the amount of ammonium perchlorate incorporated into the foam. A foam mandrel filled with a 50-50 mixture of magnesium-Teflon gave an initial pressurization rate of 2 psi/millisec. This filler was chosen because of its low gas evolution characteristics. This mandrel also gave the characteristic decline in pressure after an initial igniter peak, indicating that the skin on the foam mandrel is inhibiting the grain surface somewhat.

TABLE III. RESULTS OF FIRING MOTORS CONTAINING FOAM MANDRELS

Type of Mandrel	Pressure Rise Rate, psi/millisecond
Control - no foam	48
Control - no foam	40
Control - no foam	30
Inert foam	No ignition
Inert foam	No ignition
Inert foam	13
Inert foam	8
Inert foam	No ignition
Inert foam	No ignition
Inert foam	No ignition
47% NH_4ClO_4 in foam	140
47% NH_4ClO_4 in foam	90
Styrofoam	6
8.2% NH_4ClO_4 in foam	1
15.2% NH_4ClO_4 in foam	5
47% NH_4ClO_4 in foam with aft-end ignition	3
31% magnesium-Teflon in foam	2

Figure 3 shows a pressure vs time plot typical of the 5-inch EVA motor. Figure 4 represents the same engine containing a 2 lb/ft^3 polyurethane foam. Figure 5 represents a motor fired with a polyurethane foam mandrel containing 47% NH_4ClO_4.

DISCUSSION

Plastic Mandrels The major requirements of uniformity from unit to unit as well as lowered cost are well fulfilled particularly for smaller mandrels.

Properly designed mold alignment spiders reproduce exact alignment of studs when the RTV silicone mold proper is bonded to the rigid mold case (usually steel or aluminum). This is necessary for some mandrels because the stud or aft portion only provides the alignment during cast and cure of the grain.

Master mandrels have been made from wood, aluminum, steel, and epoxy/aluminum. Modifications to mandrels for special test purposes have been made by adding material to or machining material from a plastic reproduction without sacrificing the original.

To illustrate the cost advantage, a master mandrel for a spherical motor cost $3,000. The subsequent cost of 20 identical plastic mandrels was $508. or slightly over $25. each. Shown in Figure 6 are plastic mandrels which were produced for the family of U. S. Naval Ordnance Test Station spherical rocket motors.

Listed below are a few of the advantages and disadvantages of plastic mandrels.

Advantages

a. Mandrel procurement time is short.

b. Reduced cost.

c. Light weight and easier to handle than metal mandrels.

d. Thermocouples may be cast in any desired area in the mandrel.

e. Heating elements can be encapsulated.

f. A single mold can produce 20 or more mandrels before patching is necessary.

g. No mold release agent is required on the RTV portion of the mold, producing excellent surface finishes.

Disadvantages

a. Small shrinkages create plastic mandrels slightly smaller than the pattern. (This can be adjusted by the thickness of the RTV mold-release agent applied.)

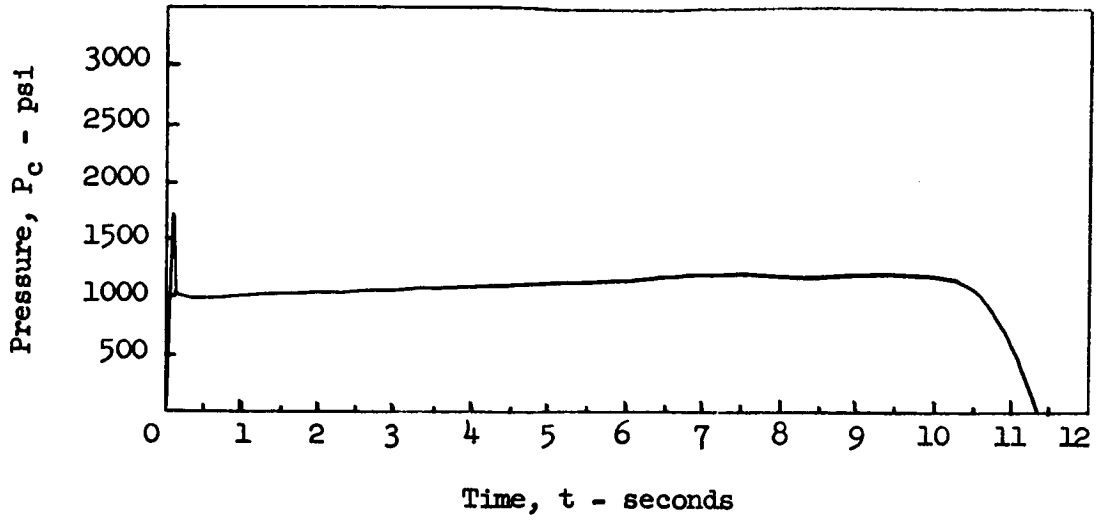

FIG. 3 NORMAL 5-INCH EVA MOTOR FIRING TRACE

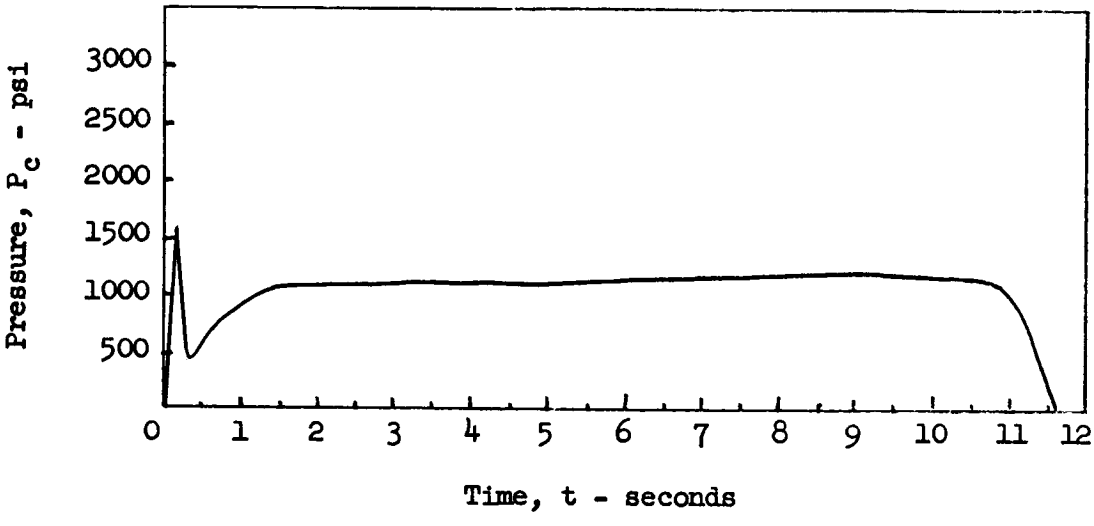

FIG. 4 FIRING TRACE WITH 2 LB/FT^3 POLYURETHANE FOAM

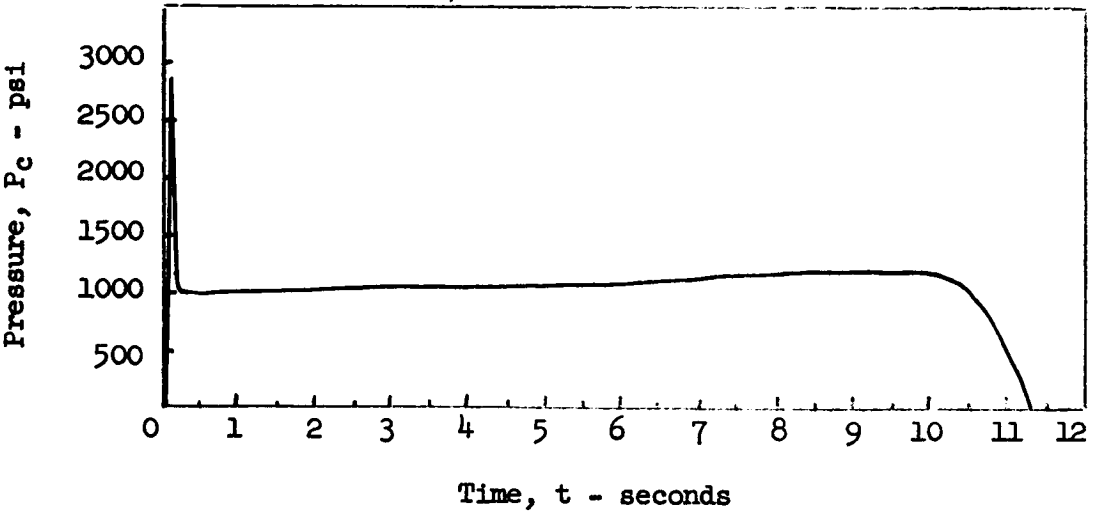

FIG. 5 FIRING TRACE WITH 47% NH_4ClO_4 IN FOAM MANDREL

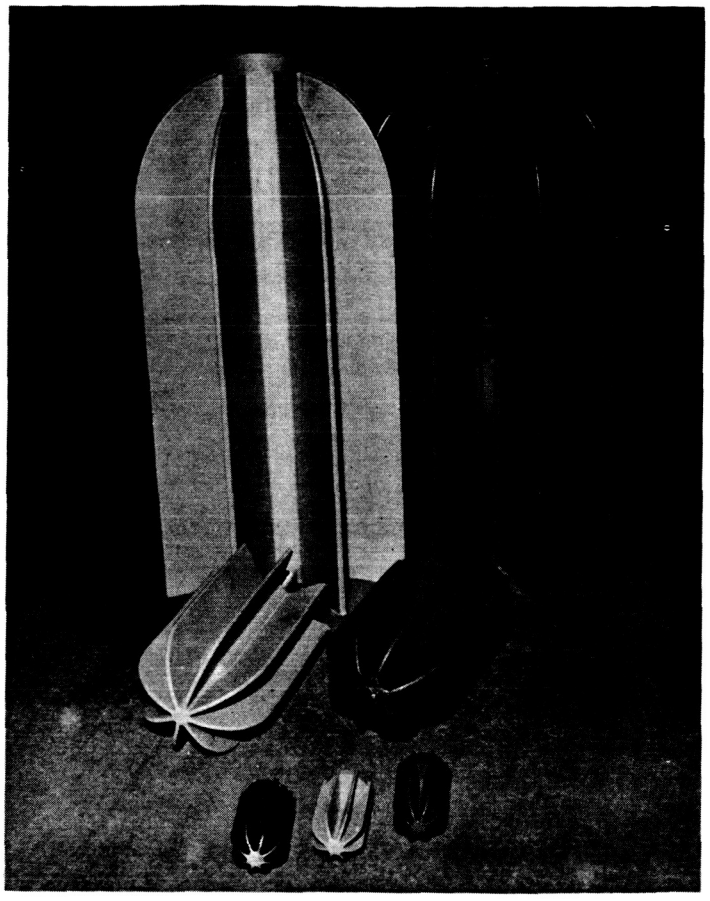

FIGURE 6. PLASTIC MANDRELS FOR 4.5-, 12-, AND 24-INCH SPHERICAL ROCKET MOTORS

b. Epoxy-aluminum formulations have less strength than aluminum, resulting in a higher damage rate.

c. RTV release agent is more susceptible to scratching and peeling than a Teflon coating on aluminum.

Foam Mandrels Previous work involving casting a frangible foam into the exit section of a rocket motor as a weather seal and pressure maintaining device for aiding ignition led to the concept of performing these functions with a foam mandrel.

Fabrication of mandrels from commercial "block" low-density polystyrene using "hot-wire" techniques has been demonstrated, and casting of other polymeric foams to shape has also been accomplished although the frangibility believed necessary for ballistic reasons causes problems in extricating the units from molds.

Motor firings have been inconsistent as can be seen from the data. Inhibiting of the grain surface may be occurring due to the tendency for cast foams to be more dense near interfaces allowing the igniter gases to channel out through the softer, less dense center to exhaust.

Energetic coatings have been applied. These are normally solvent solutions or slurries and the solvents soften some foam materials.

Loading the foam with oxidizer material to aid ignition increases the density and makes mixing hazardous as well as harder to accomplish, and creates new problems of consistent burning rate, pressure and temperature exponents control, and perhaps other unrecognized problems.

Listed below are some of the advantages and disadvantages of foam mandrels:

Advantages

a. Low cost.

b. Short procurement time.

c. Increased motor performance through intricate shapes possible.

d. Support for propellant during storage.

e. Weather seal to prevent propellant degradation due to humidity aging.

f. Improved ignition characteristics possible.

g. Light weight mandrel for handling ease.

Disadvantages

a. Unable to withstand rough handling.

b. Light weight of mandrel necessitates anchoring during casting.

c. One mandrel required for each motor produced.

SUMMARY

A description of the development of a successful technique for producing cores or mandrels for composite rocket motor casting is presented. Economy of time and money is realized through casting the mandrels of epoxy-aluminum in RTV (room temperature vulcanizing) silicone rubber molds formed about a master pattern.

Release from the propellant after curing of the composite cast grain is accomplished most efficiently by utilizing a thin coat of this same RTV silicone rubber over suitable primers on the mandrel. This release system is re-usable for a number of castings and has release properties not much inferior to sintered Teflon coatings.

Initial results indicate that foam mandrels can be fabricated cheaply enough, particularly if some of the design advantages over regular mandrels are utilized. Intricate shapes which prohibit mandrel extraction after curing can be used; a weather seal and pressure cap are automatically

incorporated; grain support is provided; and correct formulation may enhance ignition—perhaps even constitute the major portion of the igniter.

CONCLUSIONS

The plastic mandrels with RTV silicone rubber release coatings are completely satisfactory and are being used regularly at the U. S. Naval Ordnance Test Station in the composite facility.

The RTV silicone molds are optimum since exact detail is reproduced, the material is self-releasing unless primed with special coatings, and the material is flexible, facilitating easy extrication of the cast mandrel from the mold, yet has good "set" and does not sag in the sizes used.

It is feasible to produce foam mandrels and cast motors using them. However, development must continue and concentrated effort is needed in the ignition area. Inert, coated, and pyro-modified foams should be formulated and tested in larger numbers of static and flight motor tests.

REFERENCES

(1) Miller, R. A., and Sampson, H. T.;"A New Approach to Plastic-Mandrel Fabrication (U)." U. S. Naval Ordnance Test Station NavWeps Report 7651, NOTS TP 2674, June 1961. (Unclassified Report).

(2) Vetter, R. F., Technical Memorandum Reg. No. 4552-94, U. S. Naval Ordnance Test Station, 24 March 1960 (Unclassified).

(3) Vetter, R. F., Technical Memorandum Reg. No. 4552-121, U. S. Naval Ordnance Test Station, 9 May 1960 (Unclassified).

(4) Baldwin, J. E., Technical Memorandum Reg. No. 4551-57-61, U. S. Naval Ordnance Test Station, 14 November 1960 (Unclassified).

(5) U. S. Naval Ordnance Test Station TP 2542, Technical Progress Report 252, Quarterly Progress of Process Development Division, 1 November 1959 to 31 January 1960 (Confidential Report).

(6) U. S. Naval Ordnance Test Station TP 2730, Technical Progress Report 262, Quarterly Progress of Process Development Division, 1 February 1961 to 30 April 1961 (Confidential Report).

[redacted]

CONSTANT FLOW-RATE SOLID PROPELLANT GAS GENERATOR UNDER WIDE ENVIRONMENTAL TEMPERATURE RANGE

L. LoFiego, R. Melchione, F. Kluenker

Bermite Powder Company

Saugus, California

ABSTRACT

A mechanical system has been demonstrated that reduces the π_K of the solid propellant of a gas generator to substantially zero. Essential feature of the device is a valve which permits a variable and predetermined nozzle throat area. Valve movement is restricted by a cammed surface which in turn is preset by a bi-metal element. The higher the environmental temperature to which the grain is subjected, the greater is the set-back of the valve, resulting in an increased effective throat area of the gas port. The pressure in the generator provides the energy not only to drive the valve against the cammed surface, but also to drive a detent into the cam, preventing any further action of the bi-metal during the combustion phase of the gas generator.

Work accomplished includes: (1) derivation of experimental data on the propellant, relating burning rates as a function of temperature; (2) correlation of burning rate with throat area and chamber pressure; (3) provision of a manually-operated system which permits varying A_t as desired; (4) testing and proving feasibility of achieving an effective $\pi_K = 0$ with the manual device; (5) evaluation of valve materials for suitability under thermal shock and erosive conditions; (6) design, development and testing of a device which automatically adjusts the throat area to compensate for the effect of temperature on the grain.

INTRODUCTION

The solid propellant gas generator is a conveniently packaged source of energy. When subjected to extremes of temperature, however, it delivers its energy at a variable rate. It was the purpose of this program to provide a device whereby such a generator would produce energy at a constant rate independent of the environmental temperature conditions.

The advantages of a constant mass-flow rate gas generator are apparent. Efforts to accomplish this end have been made by adjusting the ballistic behavior through chemical composition of propellants or by providing a constant temperature environment local to the generator.

Our approach was to develop a mechanical valve, associated with a neutral burning generator and operating as a preset variable orifice, which would provide a general solution to the problem. This approach was proposed, accepted and funded by the Bureau of Naval Weapons under Contract NOw 61-0681-C.

[redacted]

TECHNICAL DISCUSSION

There are two properties of a solid propellant which cause the propellant to function variably at different temperatures. The well-known tendency to burn faster and provide higher pressures as the initial grain temperature increases is expressed by the terms π_K, σ_p, and σ_K.

π_K, the pressure sensitivity coefficient with respect to temperature, accounts for pressure changes with grain temperature when K_n, the ratio of the area of propellant to the area of throat, remains constant.

σ_p is the equivalent expression for change in burning rate with grain temperature at a particular value of chamber pressure. σ_K is the equivalent expression for change in burning rate with temperature at a constant K_n value.

Consideration, then, of simple ballistic theory shows that as we increase K_n both pressure and burning rate will increase, though not necessarily equally. The magnitude of these changes will depend on the pressure-vs-K_n and the pressure-vs-burning-rate characteristics of the particular propellant used; thus, we need only to provide a variable orifice, where effective area is determined by the grain temperature and programmed to the three interrelated parameters of pressure, burning rate, and K_n. We are then able to provide either a constant pressure device, or a constant mass-flow device, or a device of any selected performance combining these two.

For convenience, a typical solid propellant was used. Its characteristics are shown in figures 1 and 2.

To provide a device with a constant mass-flow rate, a line of constant burn rate is drawn through the pressure rate curves of the several temperatures of figure 1. In the example shown, this line intersects at 350, 465 and 680 psi, respectively. Locating these points of pressure on the corresponding K_n-p lines of figure 2, we read off the three values of K_n at these three temperatures which will give us a device operating at the same pressure regardless of temperature. When plotted, we can obtain a curve showing the K_n at any temperature within the selected range, and thus the burning rate will remain constant, giving a constant mass-flow rate for a neutral-burning grain.

Similarly, to provide a device operating at constant pressure, a line of constant pressure is drawn through the curves of figure 2, and the values of K_n read as 156, 184, and 215 at p = 350, for example. When these points are read from figure 1, it can be seen that the burning rates will be .22, .25, and .28 inches per second at the several values of temperature and K_n.

Thus, a constant pressure generator will not usually provide a constant mass-flow rate, nor will a constant mass-flow rate generator provide a constant pressure device.

We now have the required design considerations for providing a variable orifice which will compensate for the effects of temperature on the performance of a solid propellant.

[redacted]

EXPERIMENTAL APPROACH

Consideration of the several problems associated with a variable orifice led us to select a needle valve as the basic approach. The pressure developed by the generator itself was utilized to actuate the valve, since additional energy of sufficient magnitude would not be normally available.

To set the valve in a given position, a cammed surface was provided which was programmed to the calculated set-backs such that the linear displacement provided effective orifice sizes corresponding to the design values of K_n with temperature.

Figure 3 shows the features of the manually-adjustable experimental generator used to prove feasibility and evaluate materials. The features are:

1. An end-burning grain
2. A thermocouple to sense grain temperature
3. A needle valve of precise geometry
4. A valve seat of precise geometry
5. A rotatable cam providing calculated set-back
6. An indexed dial to set the cam surface, manually controlled

The operation is evident. The cam is set such that, on ignition, the gases force the valve against the cam, opening the valve to a predetermined annulus and providing an orifice of a given effective area. The pressure holds the valve in position. It is to be noted that this scheme provides a pre-setting as a function of temperature, and it is not intended that the valve position vary during the firing itself.

To provide a frame of reference, firings were made at three temperatures and at a fixed value of $K_n = 184$. The results are shown in figure 4.

Starting with this basic design, the set-backs required to provide the necessary variation in K_n were calculated. Figure 5 shows the results of these calculations. Four curves are shown. One generates the cam surface by cam rotation for a device of constant pressure. The second is for a device of constant burning rate (or mass-flow), while the other curves reflect cam rotation with grain temperature and change in K_n with linear advance. The values are all large enough to indicate mechanical feasibility. Based on these calculations, cams were provided for both types of compensation.

Figure 6 shows the results of a series of constant pressure firings. Comparison with figure 4 shows that the previous spread at 2.5 seconds for the uncompensated device is 210 psi between +170 and -40°F, whereas figure 6 shows a corresponding spread of 20 psi. Compensation for π_K was thus achieved.

Figure 7 shows the test results for a device designed to give constant mass-flow rate. The values of the burning rate were determined by the time interval from ignition to a built-in pip at a known length of grain, and also at the first indication of tail-off. The concurrence is quite

satisfactory.

The final design, wherein the valve is automatically adjusted with grain temperature, is shown in figure 8. The two special features are:

1. A bimetallic sensor that rotates the cam as a function of grain temperature

2. A lock, actuated by pressure of the generator on ignition, whereby a wedge is driven into a soft metal seat, preventing rotation of the cam by the sensor after ignition

A working model of the final experimental valve was fabricated. Evidence of adequate control of the cam by the temperature sensor is shown in figure 9. The rotation of the cam with temperature was plotted for points both of increasing and decreasing temperature. The resulting envelope shows a hysteresis effect about the theoretical, but the deviations are not excessive for the purpose.

During the course of this investigation, it was assumed that high-temperature materials for the valve and valve seat should be investigated. Among the materials coming under scrutiny were:

SAE Steel 4130 (Valve and Seat): This material was completely unsatisfactory. The conditions of high temperature, high velocity and chemically objectionable gases caused rapid destruction of the valve. It is interesting to note that whereas the valve was destroyed in about 0.5 second, the valve seat survived quite well.

Molybdenum (Valve and Seat): The valve showed a very slight deformation on one firing, and was reuseable without rework for a second firing only. The valve seat, however, showed no significant change after several firings. It may be concluded that this material is satisfactory for a one-shot device.

Zirconia-Coated Molybdenum (Valve Only): A molybdenum valve was flame-sprayed with zirconia and ground to size. This valve operated ballistically in a satisfactory manner, but the coating flaked off on disassembly. Since this spalling could have occurred during the firing, this material is not considered acceptable.

Tantalum Carbide-Coated Molybdenum (Valve Only): Erosion and, possibly, spalling occurred, as deduced from pressure drop and post-firing examination. This valve was unsatisfactory.

Graphite-Tipped Valve: ATJ graphite was machined to a tip and inserted in a 4130 body. Performance was only moderately successful. Because of the unusually severe gas conditions of the test vehicle, it is probable that graphite can be utilized in a valve used on a less erosive, lower flame temperature gas generator.

Tungsten (Valve and Seat): Tungsten was found to be entirely satisfactory and capable of repeated usage. It is the material of choice of those investigated, providing the somewhat high cost is not prohibitive. However, by judicious use in the critical areas only, this objection may be invalidated.

[redacted]

CONCLUSIONS

It appears that a general solution to the problem of variable solid-propellant gas generator performance with temperature has been effected. It is necessary only that the propellant ballistics be sensitive to changes in K_n with respect to burning rate and chamber pressure, and that the sensitivity be of a magnitude amenable to mechanical correction.

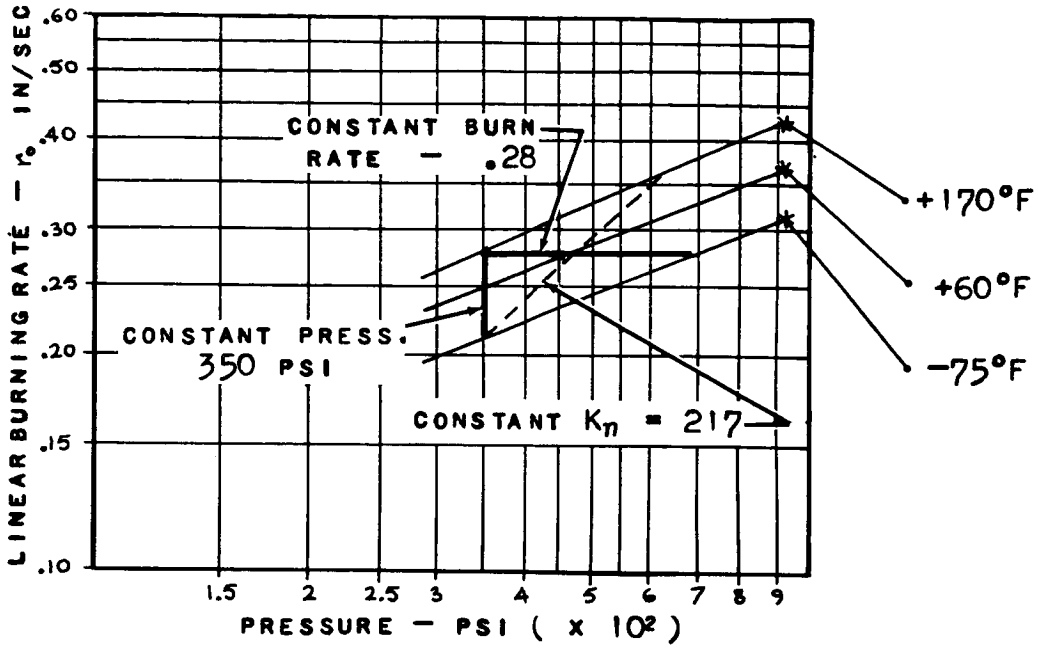

FIGURE 1

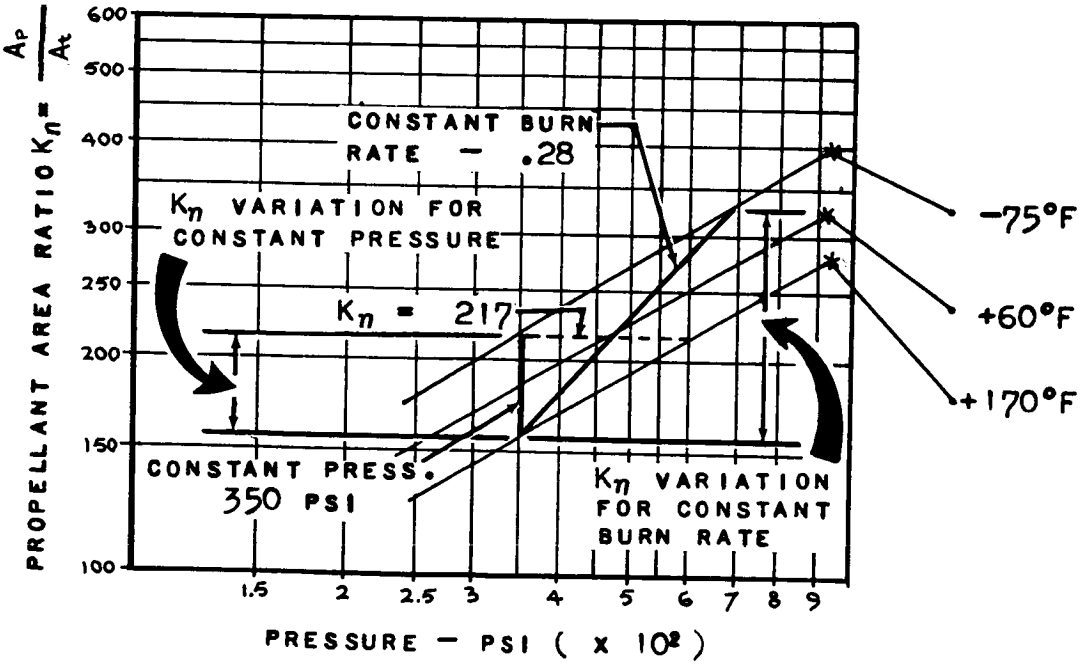

FIGURE 2

[redacted]

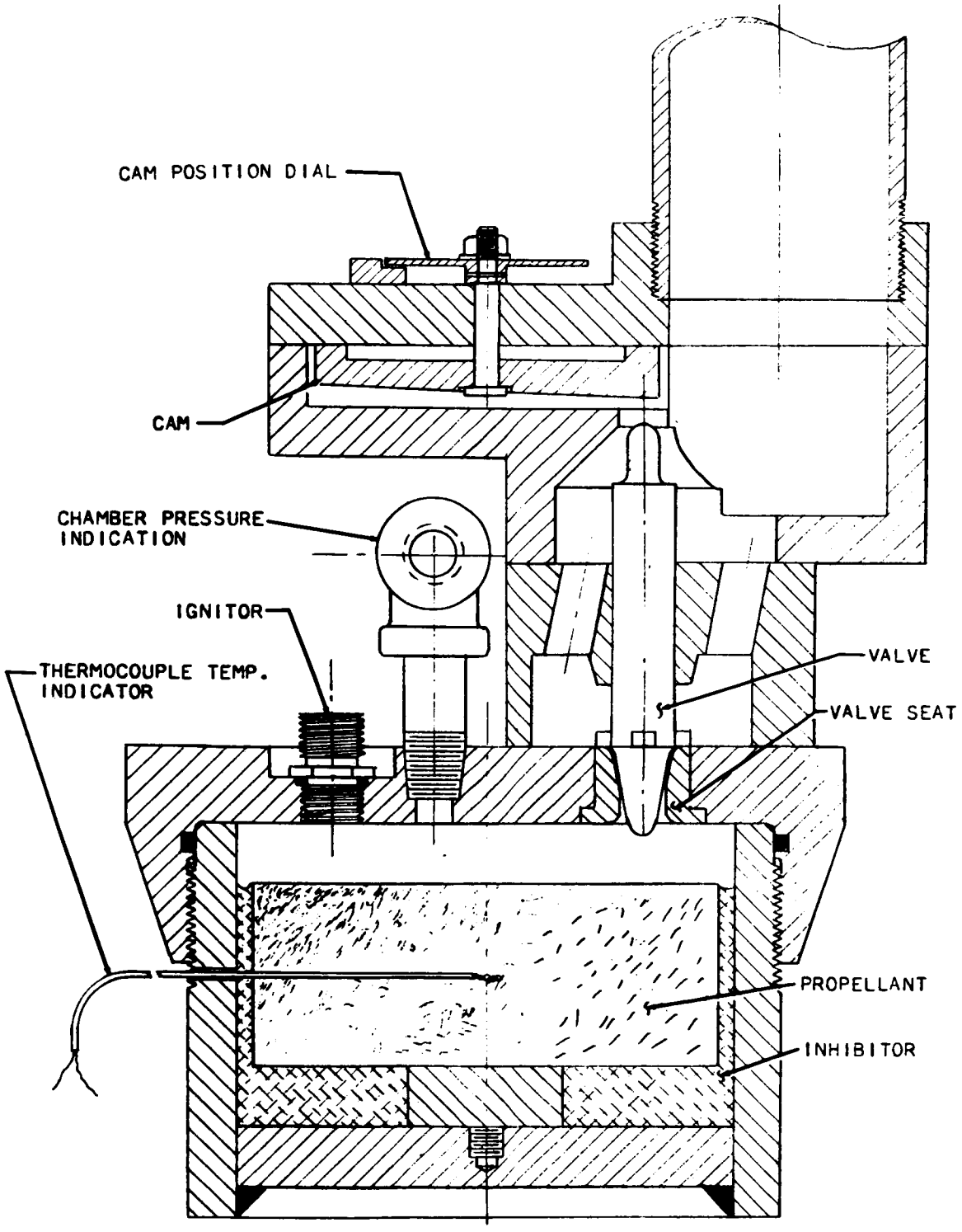

FIG. 3 TEST VEHICLE; MANUAL ADJUSTMENT

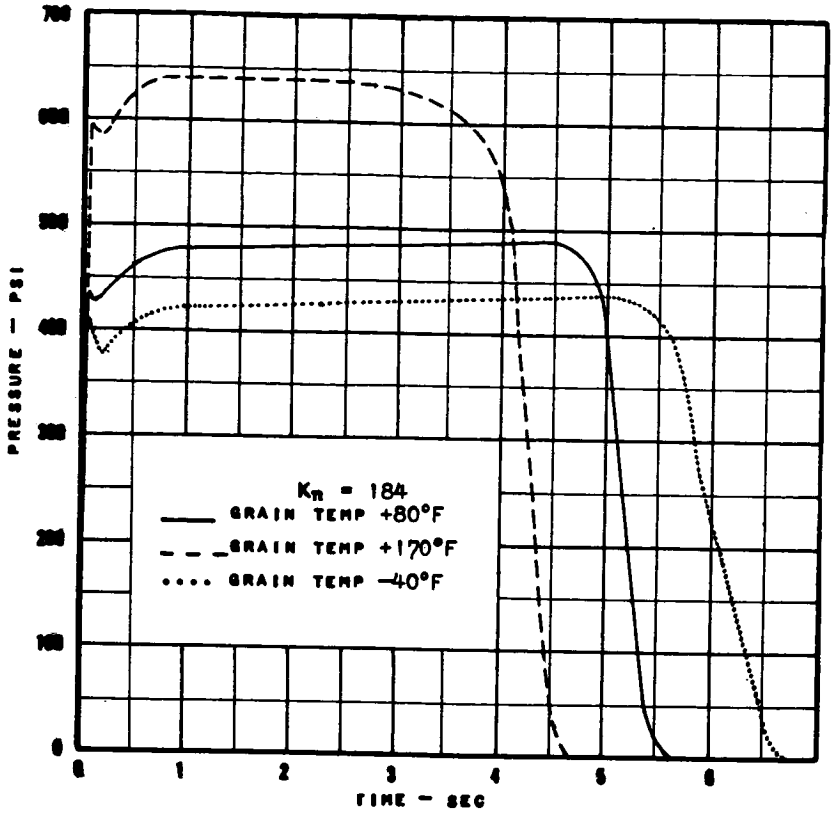

FIG. 4 TEST FIRINGS; K_η = CONSTANT

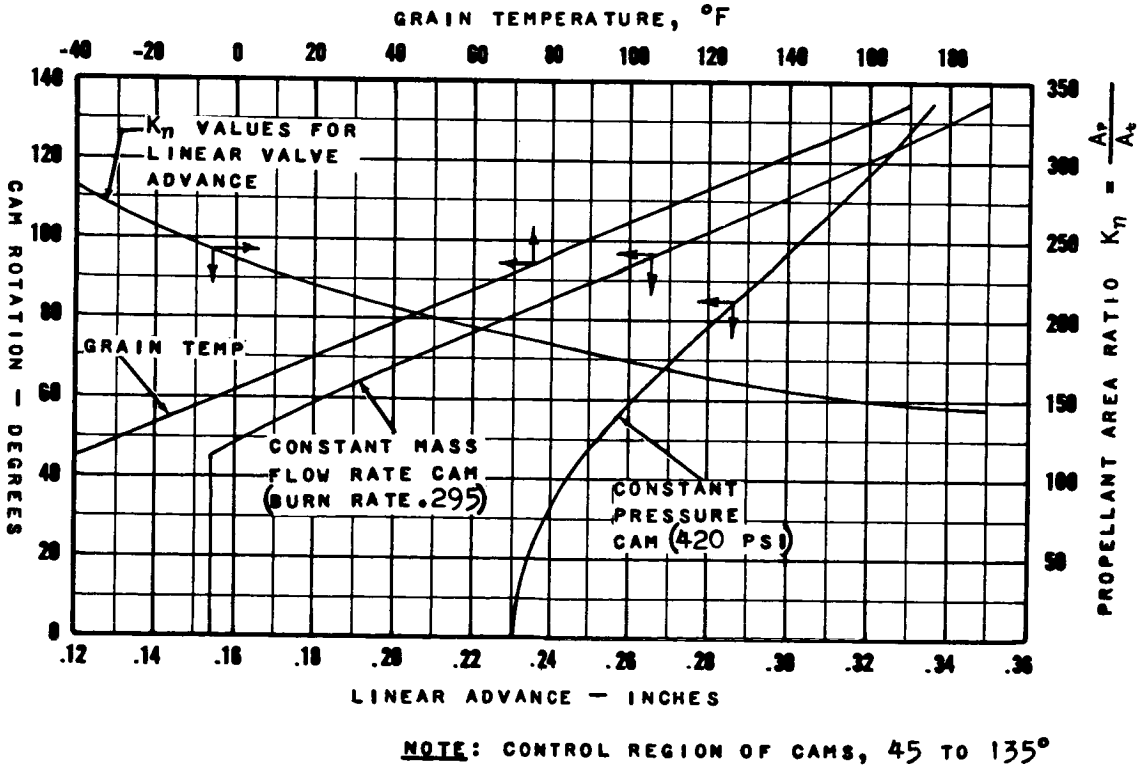

NOTE: CONTROL REGION OF CAMS, 45 TO 135°

FIG. 5 CAM CHARACTERISTIC CURVES

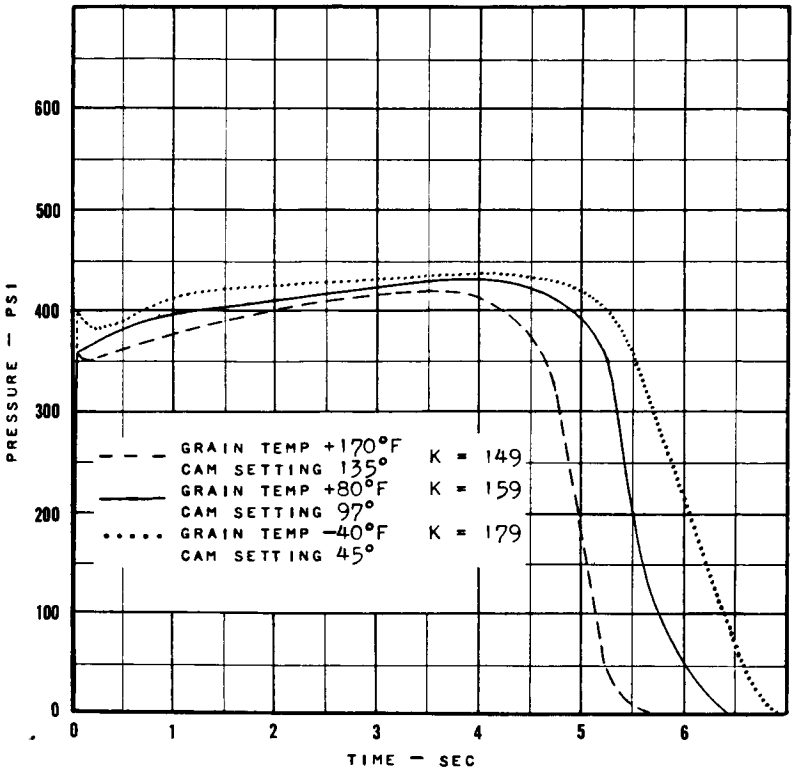

FIG. 6 TEST FIRINGS: CONSTANT CHAMBER PRESSURE

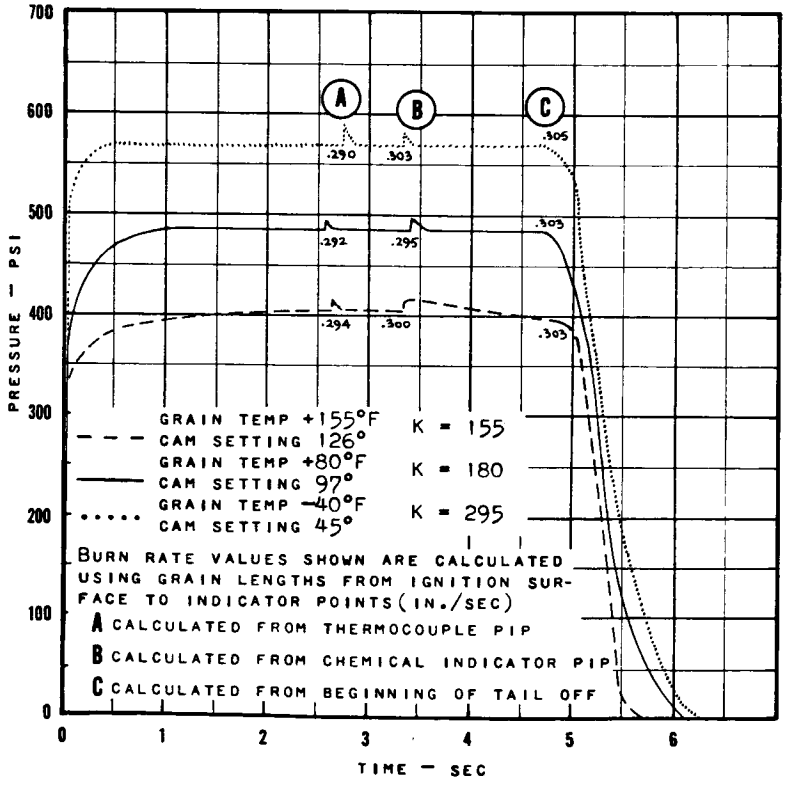

FIG. 7 TEST FIRINGS: CONSTANT MASS FLOW RATE

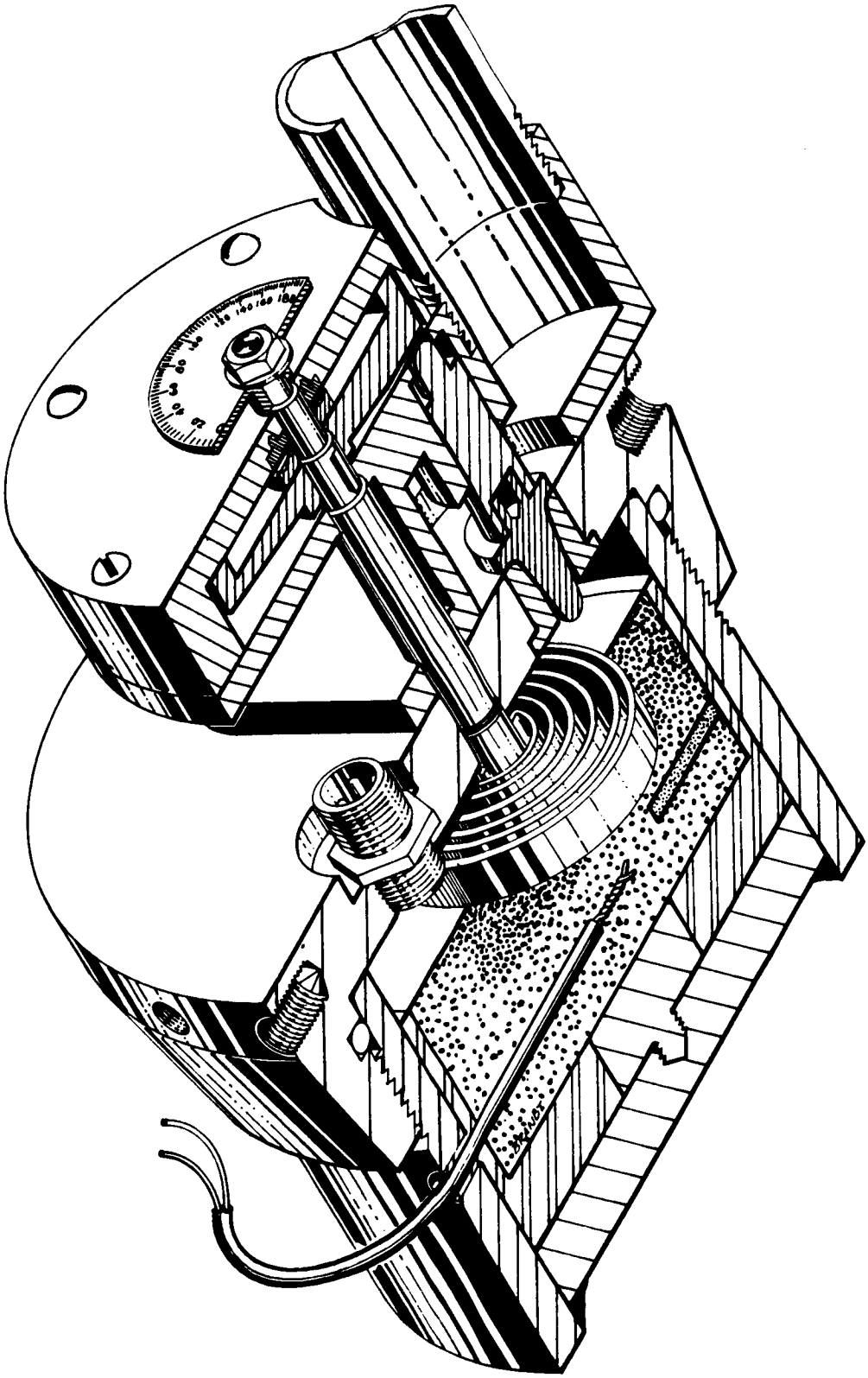

FIG. 8 GAS GENERATOR; AUTOMATIC SYSTEM CONCEPT

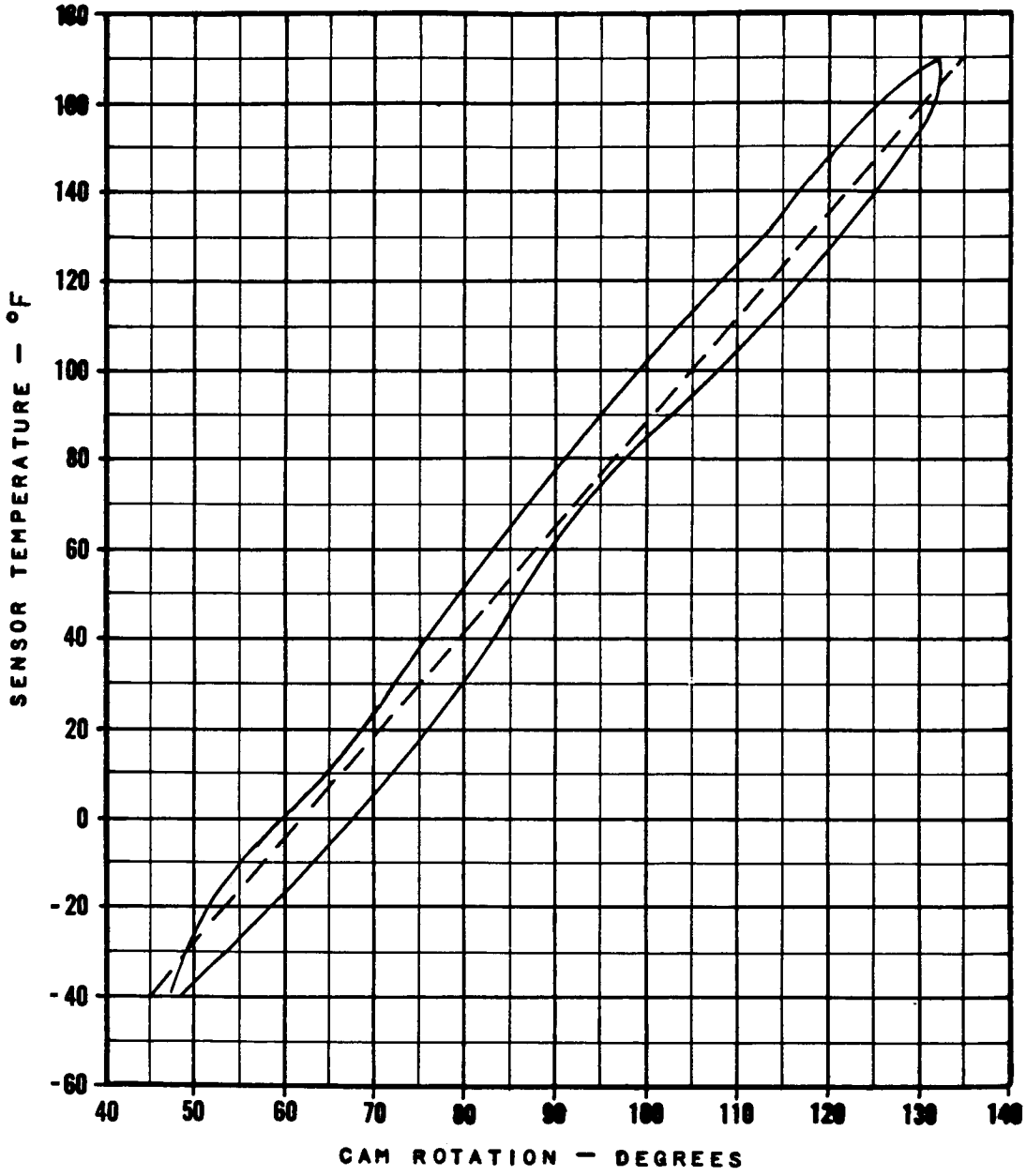

FIG. 9 BIMETALLIC SENSOR HYSTERESIS

SYMPOSIUM ON

NOZZLES AND THRUST VECTOR CONTROL

Chairman

Major W. C. Rice
6593d Test Group(Dev.)DGS

[redacted]

TVC SYSTEM ANALYSIS FOR SOLID SPACE BOOSTER APPLICATION

by

Steven M. Breslau[1]
Manuel Fuentes[2]

THIOKOL CHEMICAL CORPORATION

ABSTRACT

This paper presents a discussion of the method of analysis and results of a study conducted pertaining to potential TVC systems for large space boosters. System reliability, development considerations, system costs, and performance optimization were analyzed.

Limited development programs and high program costs dictate the need for a highly reliable TVC system. The need for simplicity in TVC systems is apparent. Vehicle trajectory, thrust deflection requirements, internal ballistic requirements, and thrust duration are parameters which influence the selection of a TVC system for a space booster.

It is apparent that no specific TVC system can be designed and fabricated for the prototype motor without some development effort. Therefore, one of the major objectives of subsequent studies on a selected system is to analyze potential problem areas, establish methods of investigation, and develop adequate testing techniques.

INTRODUCTION

Numerous types of control devices have been successfully developed for thrust vectoring of vehicle boost stages. The techniques currently used to attain this capability can be broadly classified as follows:

A. Changes in the momentum angle of the gases at the exit plane by the deflection of a heat resistant body in the exhaust jet.

B. Changes in the momentum angle of the gases by movement of the axis of the nozzle relative to the missile axis.

---

1. Project Supervisor, Reaction Motors Division
2. Supervisor, Thermodynamics Section, Wasatch Division

C. Changes in the momentum angle of the exhaust gases by the side force created by the momentum of an injection fluid and the induced static pressure (unbalance) acting over an area of the internal section of the nozzle surface.

D. Changes in angle of direction of the missile by auxiliary jets.

For the first classification, deflection devices, jet vanes and jetevators have proven effective. For the second classification, hinged and rotary nozzles have been developed and used successfully. For the third classification, secondary liquid injection has achieved adequate vectoring and for the fourth classification, small vernier motors have been successfully used.

For large space vehicle application, limited development programs and large program costs dictate the need for a highly reliable TVC system. The need for simplicity in a TVC system is apparent.

Vehicle trajectory, thrust deflection requirements, internal ballistic requirements, and thrust duration are parameters which influence the selection of a TVC system for a space booster.

Other factors which are also considered in evaluation TVC systems are:

A. Usefulness and effectiveness over a broad thrust range.

B. Minimum degradation effect on the performance of the propulsion system.

C. Reliability and simplicity from performance and control aspects.

D. Ability to achieve high response rates (to be specifically determined by the vehicle or mission requirements).

E. Consumption of small amounts of energy, either from the main propulsion system or auxiliary power sources.

F. Capability of operating in a space environment (low pressure, temperature cycling, incident radiation).

Future TVC problems will be aggravated by the development of higher energy propellants containing more metallic compounds and hotter gas temperatures. Also burning time of large space boosters is being extended to approximately 100-120 seconds. As a result, design materials will be exposed to severe environmental conditions for time periods in excess of current demonstrated materials capabilities.

[redacted]

SYSTEM REQUIREMENTS

A. Design Criteria

The nature of the large booster program presents the necessity for consideration of not only performance requirements but also other criteria which affect the selection of a method of vector control. These criteria are associated with the length of development time available and the desire to keep the control system as independent of the main motor as possible. The latter consideration permits a minimum of TVC system development using the full scale motor, thereby contributing to the probability of obtaining a ballistically successful firing in the first full scale motor test. As a result, criteria were established for evaluation of the TVC systems.

1. Reliability - The most important factor considered in the system selection has been inherent system reliability. The design of each system compared was developed with system reliability in mind and the inherent reliability was predicted for each system.

2. Development Considerations - The factor next in importance was the proposed development program. Two development areas were considered as primary. They were:

   a. The necessity for keeping the vector control system as independent from the main motor as possible, thereby allowing it to be separately developed, as a system, and assuring minimum risk during the first full scale motor firing.

   b. Consideration of the state-of-the-art of the components which make up the system. A major development problem for a component may well pace the entire program.

3. System Cost - The resultant system cost, aside from development costs, was the next factor in importance.

4. Performance - Another element of concern was system performance. This parameter has been incorporated as equivalent system weight, in which considerations such as system weight reduction during flight (dumping) and main motor performance changes due to a particular method of vector control are taken into account.

Although it is not thought of as a requirement, each motor having its own vector control system was considered an advantage. This would allow the potential use of the motor as a single unit or in varied clusters, keeping it flexible for future applications.

[redacted]

B. Motor Requirements

The motor characteristics and ballistic requirements used for this study are presented in Table I. The motor weighs 1,347,500 lb; this includes the weight of a fixed nozzle without the TVC system. The motor weight was used as the baseline for comparing the weight penalty on the missile by the TVC systems evaluated.

Figure 1 shows the general arrangement of the first stage cluster and over-all missile system configuration used for the study.

TABLE I

LARGE BOOSTER MOTOR CHARACTERISTICS
(EACH OF EIGHT MOTORS)

Motor Diameter (in.)	160
Tangent to Tangent Case Length (in.)	1,066.6
Average Chamber Pressure, psia (sea level and at 70°F)	850
Average Thrust, lb (sea level and at 70°F)	2.427×10^6
Duration (sec)	120
Specific Impulse, lb-sec/lb (sea level) (Reference)	247
Propellant Weight (lb)	1,205,500
Motor Weight (lb)	1,347,500
Total Motor Impulse (lb-sec)	291,240,000
Nozzle Type	Contoured
Throat Diameter (in.)	48.7
Exit Diameter (in.)	158

C. Control Requirements

The control requirements for the TVC system were based on a duty cycle established from the two-dimensional trajectory analysis conducted for the missile system. The duty cycle is the required thrust-deflection time history of the missile. The following factors were included in the

analysis of the duty cycle:

1. Basic control for unperturbed vehicle in flight.

2. Control requirements for basic vehicle plus wind loads.

3. Control requirements for basic vehicle plus moments induced by uneven motor thrust characteristics.

4. Control requirements in cutoff flight regime for vehicle with 3σ limits for tailoff characteristics.

5. Control requirements for missile with nonmovable aerodynamic surfaces.

6. Control requirements for nonsimultaneous ignition.

Included in the data are missile attitude turning rates and thrust deflection requirements.

Figure 2 presents the predicted duty cycle for the missile system. The basic control requirements are presented in Table II. The control or side impulse (integrated from the duty cycle) was estimated as 1.115 percent of the total motor impulse and maximum angle of deflection of 2.5 degrees.

TABLE II

LARGE BOOSTER THRUST VECTOR CONTROL SYSTEM PERFORMANCE REQUIREMENTS (EACH FOR EIGHT MOTORS)

Total Control Impulse per Motor (lb-sec)	1.625×10^6
Maximum Deflection Angle	2.5 deg
Maximum Side Force for 2.5 deg (lb)	106,100
TVC System Maximum Response Time (sec)	0.25
Minimum TVC Design Frequency (cps)	3

STUDY OF TVC METHODS

It became evident early in the evaluation study that the development requirements for this program indicate the use of a system which is presently in an advanced state-of-the-art. This would apply to both the principle of vector control selected

and the component elements which make up the system. The use of such a system would ensure maximum confidence and a minimum development schedule, since the primary concern would be in scaling present components to the required size, which is a major program in itself.

To further assure early development success, the system selected should be preferably one in which development would not be effected by the extended duration and high main motor flow rates encountered in a large booster vehicle. For instance, systems which incorporate elements present in the main motor gas stream would probably necessitate the development of materials beyond the present state-of-the-art, or considerable design and test work to prove out presently available test materials. Even then, survival would not be proven until tested using a full scale motor.

To summarize, the ideal system would be one in which:

A. Components would not be effected by the extended booster motor ballistic environment and could be confidently scaled.

B. The full scale system would be separately developed in parallel with main motor development.

C. Malfunction or failure of the system during a full scale firing would not abort the main motor test.

With these points in mind, the following potential vector control approaches were compared:

A. Inert liquid injection

B. Reactive liquid injection

C. Hot gas injection

1. Chamber gas

2. Gas generation

D. Aerodynamic surfaces

E. Swivel nozzles

F. Rotating main motors

G. Jet vanes

H. Jetevators

I. Separate control motors

1. Solid propellant

2. Liquid propellant

J. Mechanical protuberance

K. Combinations of above

As can be seen, initial evaluations eliminated many concepts after very little consideration. A group of eleven system approaches was then selected for more detailed design investigations and, based upon established criteria, the recommended system was chosen.

A. Impractical Systems

A cursory evaluation of the potential TVC systems indicated that the following control methods were either impractical or could not meet the basic design criteria:

1. Chamber Bleed System - In a chamber bleed system, gas is bled from the main motors and injected through a hot gas valve. This type of gas system is considered the most efficient since no additional tankage or gas generating equipment is required and the injectant is at the same temperature as the main stream gas. The main problems in the development of a chamber bleed system are the necessity for development on the main motor, and the need to advance the state-of-the-art of hot gas valves and components. While considerable work is being done in the rocket industry on hot gas valves for secondary injection, most of this work is in the early development stages and on a much smaller scale than that which would be required for a motor of the required size. The high cost of large booster vehicles and the development effort which would be required in view of the current state-of-the-art of hot gas valves impose a serious question on the advisability of selecting a chamber bleed system.

2. Mechanical Protuberance - The idea of using a mechanical protuberance to deflect the jet in a nozzle instead of using a secondary injectant has been advanced for thrust vector control. In this system a mechanical device (probably a pintle or a jet tab) would be inserted through the side of the exit cone of the nozzle and moved in and out as required to deflect the main stream in a manner similar to the effect of injecting a fluid or gas into the stream. This type of device could be made relatively simple, provided the pintle or jet tab could be made to withstand the erosion effects of the main stream.

Since this approach to thrust vector control is new to the state-of-the-art and since considerable testing would be required on the full scale system to develop this device and associated materials problems, the mechanical protuberance was not considered feasible for the large booster TVC and was, therefore, eliminated from further study.

3. Jet Vanes - The use of jet vanes for thrust vector control was discarded early in the TVC methods study. It was considered that the state-of-the-art of materials is such that jet vanes could not be made to last for the motor duration of 115 seconds. In addition, a jet vane system, if it could be developed, would be extremely inefficient since the vanes are carried for the full flight inside the nozzles causing continuous drag. Development would have to be pursued on a full scale basis, and would probably require additional motor firings.

4. Jetevators - The use of jetevators was also discarded early in the TVC evaluation program. Although jetevators have been successfully used in the Polaris program, it was considered that the higher gas temperature and longer duration, in addition to the much higher thrust, flow rate, and back flow problems, would preclude scaling of this type of system for large boosters. Full scale development would probably necessitate additional motor firings.

5. Rotating Motors - Rotation of the main motor with the main nozzle canted five degrees to the centerline of the motor was also considered for thrust vector control. In the case of an eight motor cluster, it would only be necessary to rotate the four outer motors. This type of system would result in only a slight loss in total system impulse, but would incur a weight penalty due to the structure, actuation system, and bearings which would be required. Because of the proposed motor's size, and due to the necessity for developing the system on the main motor, rotating motors were eliminated from consideration.

6. Air Vanes - The use of air vanes (aerodynamic fins) for vector control was also discarded because of its weight disadvantage and because of the ineffectiveness of this system at launch and high altitude.

7. Combination of Systems - A hybrid system which would employ jet vanes for the early portion of the flight and then drop the vanes and use secondary injection was also considered and discarded as being impractical since a trade-off study indicated higher weight penalties and disadvantages of both systems would be inherent.

A hybrid system in which a secondary injection system would be used in conjunction with air vanes to provide thrust vector control at launch and tail-off was also considered. However, due to the added complexity of the control system which would be required, and since no appreciable weight saving over a straight secondary injection system could be foreseen, this combination system was also discarded.

B. Candidate System

As a result of the initial evaluations previously discussed, a group of candidate systems was chosen for detailed comparisons and rigorous trade-off studies leading to the selection of a recommended TVC approach. The systems were:

1. Freon 113 injection with nitrogen pressurization
2. Freon 114I2 injection with nitrogen pressurization
3. N_2O_4 injection with nitrogen pressurization
4. N_2H_4 injection with nitrogen pressurization
5. $(CH_2)_2O$ injection with nitrogen pressurization
6. H_2O_2 injection with nitrogen pressurization
7. Freon 113 injection with solid propellant pressurization
8. Hypergolic (N_2O_4/UDMH + N_2H_2) hot gas injection
9. Swivel nozzle system
10. Auxiliary solid propellant motors
11. Auxiliary liquid propellant motors

C. Secondary Injection Vector Control Systems

The principle of secondary injection for thrust vector control has been receiving considerable interest recently for use in solid propellant motor systems. This is understandable since the dramatic increase in the sizes and operating durations of propulsion units required for new missile systems stretches the state-of-the-art of nozzle materials and design. Secondary injection allows the use of a fixed nozzle and a separate system unaffected by motor environment.

Secondary injection thrust vector control systems are generally categorized as either inert liquid, reactive liquid, or hot gas systems.

1. Inert Liquid Injection - Most of the secondary injection work which has been performed on both small scale and large motors has been conducted using inert liquids as injectants. Freon has been the most common injectant used. This injectant was selected since it possesses low boiling point, low specific heat, high density, and low heat of vaporization, most of the characteristics considered desirable for an inert injection. An inert liquid system has the advantages of using simple components, is simple to operate, and is the most advanced system from the state-of-the-art point of view. For these reasons, this system received very serious consideration for the space booster.

The main problems encountered in the design and development of a Freon inert liquid system are associated with the relatively low performance of this liquid. In general, amplification factors for inert liquid systems range between 0.4 and 0.7. As a result, considerably more injectant must be carried with an inert liquid system than with a reactive liquid system which has a higher amplification factor, and the weight of an inert liquid system would be higher.

In considering a Freon system for study, a review of test data shows that tests have been conducted with Freon 12, 113 and 114. Early secondary injection testing was conducted with Freon 12. Subsequently, Freon 113 which is of higher density but approximately the same cost as Freon 12 was used. The Freon 113 yielded slightly higher performance than Freon 12. More recent tests have been performed using a still higher density fluid, Freon 114I2. This fluid, however, costs considerably more than Freon 113, approximately ten times as much, and while a slight increase in amplification is obtained, this increase must be weighted against the increase in cost and the gain in injectant density (tankage considerations).

The maximum required thrust deflection of 2.5 deg for the space booster (an average deflection of 0.32 degrees for full duration) is well within the proven capabilities of liquid secondary injection. Testing has indicated that, beyond 4 deg deflection, the efficiency (k value) of most injectants tends to fall off rapidly, and leads to the decision to use all motors for vector control (2.5 deg maximum) instead of using the outer motors only (5 deg maximum).

The following specifications were established for developing the design of the Freon control systems:

	Freon 113	Freon 114I2
Density, lb/cu ft	100	175
Amplification factor	0.50	0.50
Maximum force ratio, F_s/F_a	0.0437	0.0437

	Freon 113	Freon 114I2
Injection location, ϵ_i/ϵ	0.35	0.35
Angle of injection, deg	25	25
Injection pressure, P_i, psia	850	850
Number of orifices at each injection point	3	3

An amplification design value of 0.50 was selected for the Freon injection system. This value is considered somewhat conservative on the basis that the average deflection angle is considerably less than 2.5 deg, but since a great deal of data were not available on scale effects, it was deemed advisable to provide an allowance for possible performance losses which may be incurred when scaling existing state-of-the-art Freon secondary injection systems to the size required for the vehicle. The effects on amplification factor of injection location, injection pressure, angle of injection, injection orifice pattern and injection assignment, i.e., number of main motors required for control, were also considered in arriving at the design value of 0.50.

Although the injection pressure does effect the amplification factor, the initial performance advantage of a high pressure is more than offset by the added inert weights of the tankage necessary to contain the higher pressure fluids. For this comparison, an injection pressure equal to the chamber pressure of the main motor was selected.

A three-hole orifice injection was selected primarily because of mechanical design and main gas flow considerations. In addition, higher performance is realized with multihole injection.

The method of pressurizing the injectant must also be considered when selecting secondary injection systems especially for large booster systems. Both cold gas and hot gas pressurization were considered. Hot gas pressurization offers an appreciable weight saving over cold gas, provided the pressurization system can be designed to match the thrust vector demand curve of the motor.

The resulting system design is shown in Figure 3 and Figure 4. Figure 3 illustrates a typical tankage installation for the vehicle cluster. Each tank has been oversized 14 percent to allow for malfunctioning of one system without effecting the required mission. The liquid injection system consists of a separate fluid system for each of the eight clustered motors. Liquid and pressurizing gas (nitrogen) are contained in spherical tanks which are located between

the main motor nozzles. Because of the reliability considerations, there is no manifolding between systems. The systems are tied together electronically be means of the TVC signals supplied to the injector valves. A sufficient excess of injectant and pressurant has been included in each system to allow for successful thrust vector control with one of the eight independent systems completely inoperative.

A schematic of the fluid system is shown in Figure 4 and is typical for each of the eight clustered systems. As shown in the schematic, both the pressurant and injectant tanks have fill and drain capability. Liquid is contained within its tank by means of burst discs on both sides of the tank.

All components used in the system are considered to be state-of-the-art hardware. The gas pressure regulator and injector valves are larger than existing similar components, but no serious development problems are anticipated as a result of this increase in physical size and capacity. Using this method of vector control, the components will not be subjected to very high temperature extremes, eliminating many design and development problems.

The third Freon system consisted of a pressurizing system with solid propellant grain. The pressurization technique consists of a single package of five separate grains, ignited upon demand and designed to burn in such a manner as to match the demands of the TVC duty cycle and generate sufficient pressurizing gas to displace the entire supply of liquid.

The grains burn at a chamber pressure of 900 psia to provide the required Freon tank pressure. A solid diluent (ammonium oxalate monohydrate) is included to reduce the gas temperature to 1000°F prior to entering the injectant tanks. In this system, the injectant tanks contain bladders to separate the hot gas from the liquid Freon.

The five separate grains and their operation, as related to duty cycle, are shown in Figure 5. The five separate grains perform the following functions:

Grain No. 1: The sustainer grain which is ignited upon launch. It burns continuously to provide pressurizing gas to adjust for nozzle misalignment and main chamber pressure differences.

Grain No. 2: They are ignited upon launch and provide pressurizing gas for the initial control.

[redacted]

Grains No. 3 and 4: They are ignited on demand signal, providing the bulk of the pressurant required during the mid-portion of the duty cycle for high altitude wind-load correction.

Grain No. 5: They are ignited on demand signal for the final tail-off requirements.

The injection system components are identical to the components used in the cold gas pressurized systems. The hot gas pressurizing system would require no pressure regulators since the rate of liquid displacement in combination with the matched rate of gas generator from the solid grains serves to provide a constant Freon tank pressure. A relief valve in the pressurizing system is necessary to vent off any excess gas.

The design and weights summaries are presented later.

2. Reactive Liquid Injection - The use of reactive liquids as secondary injectants is receiving considerable attention as the state-of-the-art of secondary injection advances. Reactive liquids offer higher amplification factors than inert liquids and the corresponding reduction in total system weight. While not as much testing has been performed using reactive liquids as has been done with inert liquids, a review of the data obtained shows a gain in amplification factors depending upon the test conditions and the reactive liquid used. Amplification factors ranging from 0.7 to 1.0 have been obtained.

The following reactive injectants were evaluated for SITVC application:

a. N_2O_4 (nitrogen tetroxide) was selected because it possesses a high bulk density as well as a high amplification factor. In addition, it can be stored in standard steel tanks. It has the disadvantage of delivering an oxygen rich mixture which could effect the erosion rate and reliability of the main nozzle, particularly since plastic materials are used in the nozzle construction.

b. H_2O_2 (hydrogen peroxide) test data obtained from H_2O_2 tests have indicated that this injectant yields higher amplification factors than N_2O_4. It also possesses a high bulk density. It is felt that since H_2O_2 will decompose with temperature, performance improvements can be obtained by designing the injection system to take advantage of this characteristic. If partial decomposition of the H_2O_2 is initiated prior to injection, it may be possible to increase performance. The disadvantage of this injectant is the

[redacted]

requirement for use of aluminum tankage and the fact that, as with N_2O_4, it will deliver oxygen rich mixtures to the nozzle.

c. N_2H_4 (hydrazine) was considered for further study for large booster because it is a monopropellant which would deliver fuel rich mixtures to the nozzle and thus should not effect nozzle reliability. Although hydrazine has a lower bulk density than N_2O_4 and H_2O_2, this factor must be weighed against the performance and reliability of hydrazine versus N_2O_4 and H_2O_2.

d. $(CH_2)_2O$ (ethylene oxide). Although there are very limited test data available on the use of $(CH_2)_2O$ as a secondary injectant, it was felt that this reactive liquid should be considered for large booster since it has the performance advantages of H_2O_2 and delivers fuel rich mixtures to the nozzle. $(CH_2)_2O$ will decompose with temperature as does H_2O_2 and since its products would be fuel rich, it would appear to be worth further study and consideration as a secondary injectant. The main disadvantage of $(CH_2)_2O$ is its low bulk density. However, this factor could be compensated for by other characteristics.

The following fluid properties and injection parameter values were established to develop the design of reactive liquid control systems:

	N_2O_4	N_2H_4	$(CH_2)_2O$	H_2O_2
Density (lb/cu-ft)	87.4	62.0	52.8	89
Amplification factor, $(I_{sp})_i/(I_{sp})_a$	0.8	0.95	1.0	1.0
Maximum force ratio, F_s/F_a	0.0437	0.0437	0.0437	0.0437
Injection location, ϵ_i/ϵ	0.35	0.35	0.35	0.35
Angle of injection (deg)	25	25	25	25
Injection pressure, P_i, psia	850	850	850	850
Multiorifice injection, No. of orifices	3	3	3	3

The amplification values are based on the following facts, the average angle through the flight is 0.32 deg and the maximum angle is only 2.5 deg. Sufficient test data have been obtained on N_2O_4, N_2H_4, and H_2O_2 to have a good basis for the selection of the performance factor values. Sufficient test data are not available on ethylene oxide to determine its amplification factor; it is believed this liquid will behave similar to hydrogen peroxide.

Consistent with the design of the inert and reactive liquid systems, a design of the hypergolic liquid was prepared to develop tankage and component size and weight, determine relative system and component complexity and state-of-the-art, and develop the weight penalty on the missile because of the TVC system.

In developing a preliminary design and calculating the performance of the hypergolic liquid system, an amplification factor of 1.5 was used. This assumption is based on data and information from hot gas secondary injection tests. The design specifications used for the hypergolic liquid system are the same as those previously discussed for other systems with the following addition.

A. Amplification Factor = 1.5

B. Fuel = 50/50 mix UDMH/N_2H_4

C. Oxidizer = N_2O_4

D. O/F Ratio = 2.2

E. Injection Chamber C* = 5560 fps

F. Injection Chamber L* = 15

G. Maximum Injection Chamber Pressure = 600 psi

For the purpose of analysis and comparison with other TVC systems, a demand type system was selected for design; i.e., a system which would operate only when thrust vector control was required and not on a continuing basis. While more development effort would be required for the demand system, this system was selected on the basis of the weight savings it afforded over a continuously operating system. In addition, the effect of dumping in hot gases through four secondary injection chambers into the main motor nozzle was not known, but it was felt that this effect would be detrimental to motor performance. The use of auxiliary gas generating systems employing liquid propellants offers several advantages over solid gas generating systems primarily because control of liquid motors to meet the thrust vector system demand curve is possible. A gas generator using hypergolic liquid propellants was, therefore, considered for TVC. With a hypergolic liquid system the need for a hot gas valve is eliminated since hot gases can be generated directly on combustion chambers mounted on the main motor nozzle. Control of the hot gas injection is obtained by controlling the flow rate of the liquid propellants. In addition, since it is possible to shut down the restart liquid gas generators, only the propellants necessary to generate gases to meet the TVC demand

The effects on amplification factors for injection location, injection orifice pattern, and injection assignment (number of main motors required for control) were considered in arriving at the values assigned to the amplification factors.

The maximum required thrust deflection of 2.5 deg for the space booster is well within the proven capabilities of reactive liquid secondary injection. Testing has indicated that, beyond 5 deg deflection, the efficiency (k value) of most reactive injectants tends to fall off and led to the decision to use all motors for vector control (2.5 deg maximum) instead of using the outer motors only (5 deg maximum).

The design requirements and pressurizing techniques were similar to the Freon injection systems. The resulting design is partially shown in Figure 6 which shows the typical tankage installation for the system in the motor cluster.

The component arrangement, installation and operation are similar to the Freon systems.

All components used in the system are considered to be state-of-the-art hardware. The gas pressure regulator and injector valves are larger than existing similar components, but no serious development problems are anticipated as a result of this increase in physical size and capacity. Using this method of vector control the components will not be subjected to very high temperature extremes, eliminating many design and development problems.

3. Hot Gas Injection - The hot gas secondary injection system selected for more detailed analysis was one which used hypergolic liquid propellants to generate hot gas for injection. This system allows metering of liquid propellants to achieve gas throttling, having the advantages of a hot gas system without the necessity for a hot gas valve. Accordingly, a preliminary design was prepared to permit evaluation and comparison of the hypergolic liquid system with the other thrust vector systems selected for analysis.

Studies and test data obtained on secondary injection thrust vector control have shown that hot gas injection systems are superior in performance to inert and reactive liquid systems. Amplification factors of 1.5 to 2.0 have been obtained with hot gas injection in comparison with factors generally less than 1.0 for other systems. Because of their performance superiority, it was considered extremely desirable to study hot gas systems for the space booster.

curve need be carried, thus affording a weight reduction over solid gas generators.

A layout of the system design is shown in Figure 7.

In sizing the hypergolic liquid system, consideration was given to several tankage arrangements. An arrangement consisting of a complete set (i.e., pressurant and injectant) of tankage for each motor similar to that used in the inert and reactive liquid system designs was not considered feasible for the hypergolic system. This arrangement would result in a total of 24 tanks for the hypergolic system and involve considerable piping and manifolding. The arrangement finally selected for the hypergolic liquid system was one which used a total of 12 tanks--four pressurizing, four fuel, and four oxidizer tanks. While this system did not afford protection against a propellant throttle valve malfunction in the open position, it was the best arrangement from the standpoint of the preliminary system comparison. Should the hypergolic system be selected, further study could be devoted to malfunction protection. Based on the tankage arrangement selected, tank sizes and weights were developed.

In general, the components previously described for the inert and reactive liquid systems are identical to those required for the hypergolic liquid system except for small size differences. The major new components required for the hypergolic liquid system are the quad check valve assembly and throttle valve.

Since it was not considered feasible to throttle the secondary injection chambers over a thrust range equivalent to a control range of +2.5 degrees, a thrust range of one-third maximum to maximum thrust was assumed. This thrust range would be equivalent to a control range of 0.5 to 2.5 degrees. To obtain control over ranges less than 0.5 degrees, modification of the control system to provide selection as well as proportional control of the individual secondary injection chambers was required. The control system would be modified to operate as an incremental system; i.e., a system in which individual chambers would be operated in their low-thrust level to provide incremental control for angles less than 0.5 degrees. This type of system would provide control in increments of 0.06 degrees. Chambers would be selected in symmetrical patterns about the pitch and yaw axis so as not to induce roll moments when pitch and yaw are required.

4. Swivel Nozzles - The largest solid propellant motors in use today employ swivel nozzles, and the feasibility of using the swivel nozzle for thrust vector control has been demonstrated. Swivel

nozzles should provide the lightest weight system for the booster thrust vector control with very little loss in thrust. Although a large amount of testing has been performed and considerable knowledge accumulated on swivel nozzle design, this information has been accumulated on nozzles considerably smaller in size than that required for a large space booster; however, its advanced state-of-the-art has prompted further study within the section of detailed comparisons.

The single plane hinged or swivel nozzle is presently the method of vector control used in the largest developed solid propellant motors. This approach is feasible when a multiplicity of nozzles (or motors) is used, since control can be accomplished in two perpendicular planes by hinging nozzles in planes perpendicular to each other. Roll control can also be provided in this manner.

For the eight motor cluster described, a system of eight swivel nozzles has been selected. Four nozzles will vector in each of two perpendicular directions:

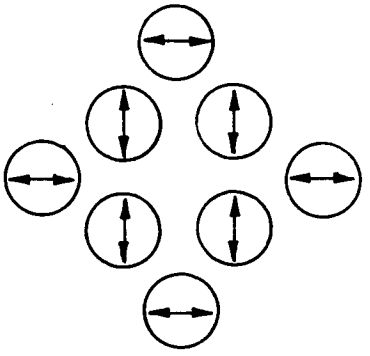

Since four operate in a single direction, each must be capable of $\pm$ 5 degrees, to produce an over-all vector effect of $\pm$ 2-1/2 degrees for all eight motors.

Concerning the actual swivel nozzle design, it was decided to use the simple single O-ring seal approach which has proven successful at Thiokol Chemical Corporation. A design layout showing this approach, as applied to a large booster motor, is shown as Figure 8. Discussions of the nozzle materials, as such, will not be covered here, since this would pertain to any nozzle, whether fixed or swivel. Discussion will be limited to vectoring considerations.

The nozzle has been designed to swivel in one plane, using a pair of diametrally opposite trunnions or pivot points for the ball and socket. A single O-ring seal is used, with a silicone rubber filler upstream in the split line. This approach is based upon development results obtained in a large motor program. In addition, a positive grease protection is shown at the split line.

To increase the confidence level of this TVC nozzle design, a continuous silicone grease injection system has been provided for the split line. Silicone grease will be injected just upstream of the O-ring, keeping the split line full of grease, cooling and protecting the seal.

After considering several systems for supplying power to actuate the nozzles, it was concluded that a gas pressurized hydraulic oil system would be most economical and most reliable. This system consists of a bottle filled with a high pressure gas at ambient temperature which feeds through a shut-off valve and a pressure regulator to a second bottle containing hydraulic oil. The hydraulic system operates at lower pressure than the stored nitrogen, and would be pressurized only a short time before firing. The pressurized oil would operate through the control system to ordinary hydraulic actuators from which it would be dumped overboard. A design of a large motor system is included as Figure 8.

A specific system as described above was established for eight single axis vector control nozzles. A hydraulic system pressure of 3000 psia was chosen, and the actuators were thus sized at 5 in. bore, 2 in. shaft, and 14 in. stroke. Such a unit, including mounting hardware, weighs 160 pounds each or 1280 pounds for the eight actuators required.

Based on the design duty cycle, the total oil required is 21.15 gallons. Allowing a 20 percent reserve, the oil tank was sized at 25 gallons. Nitrogen is used to pressurize the hydraulic fluid. Helium also was considered, but it was rejected since the weight saving was nominal, the initial pressurization required was higher, and the expanded gas temperature was considerably lower.

In the proposed system, the nitrogen is allowed to expand down from 9000 psi to 3000 psi. This gives an expanded gas temperature of 330°R (-130°F). An analysis was made to determine the effect of this cold gas on the hydraulic oil using very conservative assumptions. It was concluded that the expanding nitrogen presents no problems.

Some consideration was given to heating the pressurizing gas as it expanded. This might be accomplished by using a coil in the inlet section of one of the nozzles. If the nitrogen were heated to 500°F then the amount of N_2 required would be only about one-third of the nitrogen indicated. This approach was not selected, however, since additional plumbing and controls would be required. Thus, the possible weight reduction would have to be balanced against the increased system complexity and decrease in reliability.

When determining the additional weight contributed by a swivel nozzle system over and above the main motor system, weights must be calculated and the weight of a fixed nozzle system subtracted. The weights are discussed later.

5. Separate Motor Control - One of the primary considerations in the selection of a thrust vector control system for the space booster is the requirement for development of the TVC system separate from the main motor, if possible.

In this respect, separate control motors constitute the only TVC system which can fulfill this requirement. Thrust vector control using a separate motor is obtained by rotating the motors for pitch, yaw and roll control. In their zero position, the separate motors provide positive impulse to assist the main motor and offset their own weight. However, the advantage is offset by the size of the control motors. For the solid propellant motor, at least, the control thrust level is constant, dictated by the maximum (2.5 deg) control requirement. Liquid propellant control motors could be throttled to some extent, thereby decreasing their size.

Because of efficiency and envelope considerations, the control system becomes one for the entire cluster, eliminating the convenience and flexibility of having a separate system for each booster motor.

Keeping these points in mind, separate solid and liquid motors were considered for vector control

Solid propellant control was investigated using a group of eight motors, mounted in a plane perpendicular to the thrust axis of the cluster and utilizing nozzles at right angles to the control motors. Rotation of the control motors about their own axis would produce the required side loads for vector control. Thrust of these motors not used for control would add to the thrust of the main cluster.

Figure 9 shows a packaging layout prepared for standard cylindrical or spherical motors. Both extend beyond the cluster envelope, and, because of the clustering arrangement, come dangerously close to burning each other, or the main nozzle shrouding, when vectored.

Because of obvious packaging considerations, and the major rotation and support problems associated with the cylindrical motors, it was decided to consider spherical solid propellant control motors for the space booster. Each motor's thrust is 220,000 pounds with a nozzle expansion ratio of 10:1. These motors would use the same

propellant as the main motor, and produce the same specific impulse.

The control motor specific impulse is equal to the main motor impulse of 247 lb-sec/lb at sea level. The average specific impulse is 255 using a 10:1 nozzle expansion ratio.

Control dynamics are predictable since there is no delay in rocket thrust for TVC and the actuator must only overcome rocket inertia. Two basic types of actuation systems have been considered for use with this attitude control system; they are either an hydraulic or a hot gas system. The desired actuation system could be used for this application while drawing on known experience and design. The high dynamic response of the control rocket required for this application (170 degrees in one second) dictates a high torque requirement to rotate the relatively large mass of the vector motors.

The main problems associated with separate motors are in relation to the positioning mechanisms which are required. The size of the motor actuation system is dependent upon the system power requirements which are determined by the required response of the TVC system. For instance, if the response time of the TVC system is doubled, the power required for actuation of the separate TVC motor will increase by a factor of 8.

Control forces are provided by rotating the control rockets, in sets, for pitch, yaw, and/or roll control. In the zero position they provide propulsive impulse for the main booster to offset their weight. The control rockets are rotated as a complete unit to eliminate the necessity for hot gas seals.

It can be seen from Figure 9 that the spherical motor for this application meets the space envelope more readily than the longer cylindrical motor. The improved mounting which reduces structural weight and shielding requirements as well as the factor of improved mass fraction for the spherical motor shows its use to be the better of the two for the motor cluster. Actuation of these motors is controlled by a reversible geared turbine drive using hydrogen peroxide decomposed through a catalyst bed as a power source. To actuate each of the solid vector motors through 170 degrees in one second's time, 7600 horsepower is required. Turbine gear systems of this horsepower and configuration are well within the state-of-the-art and give a high reliability factor.

For a lower response rate requirement of the over-all TVC system, such as allowing twice the time to rotate through 170 degrees, a power requirement 1/8 of that stated above would be needed. Such a change, which is reasonable, could result in an entirely different selection of actuator systems and supplies.

The separate liquid vector motors are similar to the solid motors previously discussed. The liquid motors do have several advantages over the solid motor. The main advantages include the versatility of the motors, which can be throttled over a thrust range, thus reducing the total weight required to be carried by the main motor for the TVC system. Much lower power is required to actuate these motors. Placement of the motor is at the option of the design with less shielding requirements necessary. However, the separate liquid motors do have the disadvantage of requiring more parts and thus a more complicated system to accomplish this same control mission.

The separate liquid motor TVC system is shown in Figure 10. Two cylindrical tanks, positioned in the center of the eight motor cluster, are used to supply propellant for four of the TVC motors. Four spherical oxidizer tanks and four spherical fuel tanks are provided between throats of the main motors to supply propellants for the other four TVC motors. The four helium spherical tanks are positioned between the nozzle throats of the four center booster motors.

The TVC motor has a specific impulse of 252 lb-sec/lb for maximum throat and 193 lb-sec/lb for minimum thrust at sea level. The average impulse for minimum thrust is 252 using a 10:1 nozzle expansion ratio.

The control dynamics are predictable since there is little inertia to be overcome by the actuators and many liquid rocket motors have been throttled at a higher rate of response rate than that required for this application. The actuation system for rotating the thrust chamber would be a standard hydraulic piston operated by a servo valve using the pressurized fuel as an actuating medium. The 4 in. diameter piston with an 8 in. stroke will give the response rate required for the vehicle. The TVC electrical control with position feedback for chamber position will rotate and throttle the motor to give the vehicle correction in proportion to the guidance command signal.

Using four liquid motors in pitch and four in yaw, the thrust for the TVC chamber is 220,000 lb to provide 2-1/2 deg maximum deflection angle for the large booster vehicle. The liquid motors would be throttled to 1/3 flow rate when high thrust is not required for the high deflection angle requirement. The maximum propellant flow rate for each motor is 841 lb/sec with the minimum flow rate reduced to 1/3 its value. Storable liquid propellants used for this application are nitrogen tetroxide as an oxidizer and a 50 percent mix of unsymmetrical dimethylhydrazine and 50 percent hydrazine as the fuel. The liquid motors are mounted near the aft skirt of the main solid motors and rotated through 170 degrees to provide for the thrust vector requirements. Fuel from the main tankage supply is used for the servo actuator in order to provide the torque required through the rack and

the pinion to rotate the thrust chamber.

The separate liquid motor TVC is a pressurized bipropellant feed system with the pressure being obtained from four high pressure (5000 psi) helium tanks. Squib valves are actuated to start the helium flow through the heating coils around the chamber exhaust back through the helium tank to heat the source supply of helium. The helium gas is heated to 250°F before it flows through the parallel regulators, over pressure shutoff valves, and through check valves and burst discs to the main propellant tanks. This prestart sequence brings pressurized propellants to the combined pilot shutoff valves. Just prior to firing the main booster motor the TVC liquid engines are started at 1/3 flow rate and checked before activation of the main booster igniters.

The liquid control motors are rotated as required to provide attitude control for the large booster vehicle. Thrust of these motors is held at 1/3 value until the motor is rotated to its extreme for correction control at which point it is throttled up if additional force is needed to correct the vehicle attitude. These TVC motors can be operated during the tail-off and slightly beyond the main motor duration to provide for vernier trim of final velocity.

RELIABILITY

The studies performed in the preceding section led to the determination of sizes and types of components and tankage required, weights involved, and the general design arrangements for each vector system. This information will lead to a direct comparison of the performance and efficiency expected from each system. However, in selection of the most suitable system for the space booster application, there are additional factors of major importance which must be considered of which reliability is one of the most important.

The nature of the large space program has dictated reliability as the most important consideration for system selection. The philosophy behind the solid propellant large space booster stresses the inherent reliability of solid propellant motors, which, to remain effective, must be reflected in auxiliary systems which are part of the propulsion package.

In evaluating the expected comparative reliability of each system it became necessary to determine the degree of reliability which could be realistically attained within the development time allotted. Certain systems contain components which, because of the state-of-the-art and the extension of sizes involved, would require major development programs to achieve high reliability. In these cases, it became necessary to estimate the degree of reliability which could be attained during the defined development period.

Comparative reliability ratings were assigned to each system, based upon the complexity, i.e., number of components present in each system; and the degree of reliability believed attainable for these components during the prescribed development time.

In each system considered, the most reliable selection, quantity, and arrangement of components were chosen, as discussed previously within the preliminary design evaluations. Table V shows the development of the comparative reliability factors for each system, based upon the number of components involved and their relative reliability merit.

DEVELOPMENT CONSIDERATIONS

The second consideration in the trade-off comparison conducted concerned system development. The applicability of each system to be largely developed separately from the main motor, in order to keep the number of full scale motor firings to a minimum, is considered of major importance, since it would reduce the cost and development time to a minimum and produce an efficient program.

The comparative ratings were determined based upon:

A. The state-of-the-art of the components used.

B. The state-of-the-art of the method of vector control itself.

C. The system's ability to be separately developed.

D. The effect of the main motor environment upon the system, since it would affect development.

E. The magnitude of the development program, considering complexity of testing, time involved, and relative development costs, and including the practicality of completing a successful program within the time allotted.

SYSTEM COST

The third weighted parameter for system selection is cost. The cost is based on the expense of injectant fluids and associated hardware and relative costs of the candidate systems.

SYSTEM PERFORMANCE

The last major comparison consideration selected is system performance. This has been obtained from the design and weight data developed in the previous portion of this section, using "equivalent" system weights calculated.

To put all potential TVC systems on a common basis for performance comparison, a weighing factor has been developed based on the relationship between specific impulse, inert weight, and axial thrust for the predicted boost stage trajectory and ballistic parameters. The weighing factor is obtained by reducing specific impulse and axial thrust to equivalent inert weight. The total equivalent inert weight of the TVC systems is derived from the following system sources:

A. Inert weight of the system hardware and components.

B. Equivalent inert weight of expending material such as gases or liquids.

C. Inert weight equivalent of the axial thrust degradation or thrust gain experienced with a particular TVC device.

The inert weight of the TVC system hardware is simply the weight of all additional hardware carried when compared to the booster dry weight with no TVC system. This includes weight of tankage, piping, structure, components, and in the case of the swivel nozzle system and secondary injection systems, the increase in nozzle weight due to added nozzle structure required over a fixed nozzle with no secondary injection.

To establish the equivalent inert weight of an expending fluid, a trajectory computer program was modified to include this parameter. When a boost stage employs a material which is consumed or expended during the operation of the stage, such material is not all accelerated to the terminal velocity; thus, its effect is less than for an equal weight which stays aboard throughout the flight. The equivalent inert weight is defined as the fixed weight which will produce the same reduction in terminal velocity as experienced by the expending material during flight. To determine this fixed weight it is useful to use an equivalent inert weight ratio. Multiplying the weight of the expending material by this ratio gives a chargeable inert weight which is valid for comparative purposes. The equivalent inert weight ratio is essentially a function of three basic parameters:

A. Vehicle mass ratio.

B. Ratio of expenditure rate to the main propellant burning rate as a function of time.

C. Ratio of the axial specific impulse (if any) of the expended material to the specific impulse of the main propellant.

Since the vehicle mass ratio and specific impulses are normally established by ballistic requirements, the only parameter that affects the inert weight ratio is the duty cycle, i.e., the flow rate of the expending material with flight time. From the duty cycle the fluid flow rate history can be established and the inert weight ratio determined.

A typical large space booster with different first stage inert weights and no expending material was flown on a two-dimensional trajectory and optimized for maximum burnout equivalent velocity at each inert weight to establish a burnout velocity and weight curve. The vehicle was then reflown with:

A. Material expending at constant rate, progressive rate, and regressive rate throughout the flight.

B. Material expending at the rates specified for a typical large booster duty cycle.

The results are shown in general form in Figure 11. The inert weight can be used to determine the equivalent inert weight of the various fluids used in the secondary injection TVC systems or any application where fluid is expending.

EFFECT ON THRUST

The thrust decrement or increment induced by the TVC systems can be converted to equivalent inert weight by relating the inert weight and specific impulse of the missile system to ΔF_a, axial thrust degradation or increase by the following approaches:

A. Establishment of specific impulse versus equivalent velocity and inert weight versus equivalent velocity curves.

B. Cross plotting to obtain a specific impulse versus inert weight curve.

C. From the cross plot the inert weight equivalent to one second of I_{sp} for a cluster of any number of motors can be determined.

D. A relationship to relate thrust, ΔF_a, to equivalent inert weight can be established by using the following ballistic equation:

$$I_{sp} = F_a \frac{C^*}{(g)\ (P_c)\ (A_t)} \qquad (1)$$

$$\pm\ \Delta I_{sp} = \frac{\Delta F_a\ C^*}{(g)\ (P_c)\ (A_t)} \qquad (2)$$

The ΔF_a, thrust change (gain or loss), for specific TVC is determined from correlation curves, F_s/F_a versus $\Delta F_a/F_a$, shown in Figure 12. This figure shows the relationship between the thrust loss or gain as a function of the side force requirements for different TVC methods. The curves, for the most part, are based on test data and performance of existing TVC systems. It can be noted that for mechanical TVC type systems the rotating nozzle gives the least thrust loss to a motor system while the jetevators and jet vanes cause the greatest thrust degradation.

Secondary fluid systems, whether cold or hot injection, add thrust to the main motor.

Conversion of ΔF_a to inert weight can be accomplished as follows: From equation (2) above, the loss of gain in motor thrust caused by TVC is converted to ΔI_{sp}. The equivalent inert weight is determined from trade-off ratios. For the first stage cluster 25,370 lb inert weight is equivalent to one second of I_{sp}. Over-all equivalent inert weight (weight penalty) of the TVC systems is the summation of:

A. Weight of the dry system;

B. Equivalent inert weight of expending material;

C. Liquid requirements, if any, for tail-off transients; and

D. Equivalent weight reduction or increase due to thrust degradation or increase.

The results can be presented in parametric form by relating the equivalent inert weight of the various TVC systems to the side impulse requirements. With this type of correlation, the systems can be readily analyzed and compared for performance. (Figure 13) The analysis will show that the system which has the lowest equivalent inert weight will have the least effect on total booster performance.

COMPARISON OF SYSTEMS

A. Secondary Injection - Liquid Systems

The nitrogen pressurized liquid injection systems are identical except for minor differences in the sizing of the injectants. There are no major problems pertaining to the operational function or state-of-the-art, but there are difficulties in relation to scaling up the available components. These difficulties, of course, would be applicable to any space booster system. Components are not effected by the main motor environment and the entire liquid system could be separately developed as a working package.

The performance during firing would be a concern after system development. Its scaling effect would be investigated in a subscale development program. The worst that could be expected from a liquid secondary injection system would be insufficient control deflection or total impulse, which could possibly be improved by changing injectants, increasing flow rates, and/or tankage sizes. A malfunction in the system would not effect an unsuccessful main motor firing.

Separate SITVC systems for each motor would provide enough injectant to afford mission completion even if one system fails. This is not possible with all vector control systems. A separate system also allows a flexibility

in clustering, or using motors separately for other missions if desired.

These points have resulted in a high reliability and development factor for liquid secondary injection systems.

The differences in reliability and development ratings between liquid SITVC systems became dependent upon injectants. Performance ratings are a direct comparison of their equivalent weights. Cost considerations were developed based upon a survey of expected injectant prices in the large quantities necessary. The cost of the injectant is the major budgetary consideration in relation to the total system. Basic injectant comparisons, aside from the already discussed performance differences, are:

1. Freon 113 - This inert injectant has been the most widely used and, therefore, affords the greatest amount of test data. Thiokol firings, using a 40,000 pound thrust motor, showed no compatibility problems with the system of nozzle materials. Freon 113 is relatively inexpensive, and it is readily available.

2. Freon 114I2 - Differences between this and Freon 113 concern performance and density. The cost is approximately ten times that of Freon 113. Development considerations would be identical, except for a possible problem in the availability of the quantities necessary. Presently, Freon 114I2 is not being produced in large production lots.

3. N_2O_4 (Nitrogen Tetroxide) - This injectant is reactive in nature. Combustion products are oxidizing. They react well with the fuel rich solid propellant gases, but could affect the nozzle materials being considered. Small quantities of water presently in N_2O_4 may cause a tankage corrosion problem, which, although slight, could contaminate the system and possibly cause jamming or sticking of the valves. These points have been considered in the selection of reliability and development ratings in Tables V and VI. N_2O_4 is very inexpensive.

Generally, reactive liquids would cause some increase in potential development problems; however, N_2O_4 has been tested in large scale motors sufficiently to be considered state-of-the-art.

4. N_2H_4 (Hydrazine) - Hydrazine, as an injectant, autodecomposes producing fuel rich gases in the main motor nozzle. It is relatively expensive, but would present less development problems than would be expected using N_2O_4.

5. $(CH_2)_2O$ (Ethylene Oxide) - Ethylene oxide was considered as an injectant since the decomposition products developed would be fuel rich and should exhibit high performance because of its autodecom-

position characteristic. There are limited available test data for this injectant. It is available and inexpensive.

6. H_2O_2 (Hydrogen Peroxide) - Peroxide has been used as an injectant and has an excellent performance record. It decomposes with temperature, producing oxygen rich gases, as does N_2O_4, and therefore would probably exhibit the same development problems. Aluminum tankage would be necessary and corrosion problems could be considerable. H_2O_2 is available and relatively inexpensive.

The possibility of using a solid propellant pressurizing source instead of pressurized gas was investigated by applying it to a Freon 113 system. The system which resulted would be lighter and, therefore, exhibit better performance, but would be more complicated due to the use of a pressurizing bladder to separate the gas and injectant and a multiple grain system. The multiple grain approach is necessary in order to approximately match the vector control duty cycle, and to make the solid grain pressurizing system competitive.

Both reliability and development factors were considered to be lower than for a cold gas system, due to the multiple grain ignition necessary and the requirements for a positive expulsion bladder.

B. Secondary Injection, Hypergolic Liquid Gas Generation

A system for injecting gases from a hypergolic gas generator into the main nozzle would present a much more complex problem than the liquid systems. This would affect both the reliability and development factors.

The components required to provide three to one throttling of the generator flow, plus shutoff of the bipropellant system, are more numerous and sophisticated than those for liquid injection. Also, the effects of incorporating a larger single injection hole (about 10 in. diameter) in the main nozzle exhaust cone may be detrimental to the main nozzle.

The reliability of this system has been decreased even more since it is impractical, from a packaging standpoint, to have a separate system for each motor.

The resultant cost of this system would be low, when developed, and the comparative performance would be high.

C. Swivel Nozzles

Presently, the largest solid propellant vector control systems in use employ swivel nozzles. Performance studies indicate that a swivel nozzle developed for a large space booster would undoubtedly provide the lightest system.

[redacted]

However, these performance advantages must be weighted against possible disadvantages which would be critical in a large space booster program. Subscale nozzle development testing would not be very fruitful, since such technology is already in existence. Development required would have to be carried out on a full scale motor, which could create a tremendous expense and a lengthy program in which a major development problem would cripple the entire main motor effort. A failure of a swivel nozzle would abort the main motor firing and important and expensive test information not relating to the vector control effects would not be obtained.

Reliability and reproducibility of the actuation torque required are problems in present large swivel nozzle programs. This has affected the reliability factor assigned to swivel nozzles for large booster application.

The flexibility of using a motor as a separate entity or in a different cluster arrangement is hampered when swivel nozzles are used, since control is in one plane only, the development of gimbaled nozzles for such an application is in a questionable state-of-the-art.

D. Separate Motor Control

Separate motor control has the advantage of being completely independent of the main motor system, which, as has been stated previously, is a major consideration.

E. Solid Propellant Motors

Solid motors offer the simplest approach, from a system standpoint, to separate motor control. The main problems associated with the system concern rotating (inertia) and positioning the 220,000 pound thrust motors within the required response rates and the associated power requirements and structure.

It is also expected that the development of so large a control motor with a 90 deg gas turn in the aft closure would present a major development problem within the time allotted. The contouring of aft closure insulation is a major consideration in previous large motor programs and probably would be in this program also.

Two additional minor considerations are the fact that the vector control system is designed for a specific cluster and is not directly related to each main motor, limiting motor use flexibility, and that mission reliability is effected greatly when the possibility of one control component malfunctioning is considered.

F. Liquid Propellant Motors

The liquid motor control approach produces a higher performing system than the similar solid approach. However, the development and

reliability factors are not as good because of the greater number of components involved and the general development problems which would be associated with a large throttleable swivelled liquid thrust chamber.

Development of a liquid motor system would be based upon reusability of the control motor components, which results in a relatively inexpensive and short duration program.

Comments regarding motor use flexibility are similar to those made for the solid control motor. The control system is development for the particular cluster concerned.

Consideration of the comparison factors discussed above led to the development of Table VIII, in which systems have been ranked relatively for each of these factors. Also, relative weight emphasis between these factors has been assumed and a total over-all rating established. This has been the basis for selecting the system best suited for the large booster vehicle under study.

The studies analyses are presented in Tables III through VII and summarized in Table VIII. A brief description of each table follows:

Table III - Design Summary. The table presents the pressurization levels, volumes and tankage sizes. Freon 114I2 requires the least tankage and Freon 113 the greatest tankage of the SITVC systems. Hydrogen peroxide requires the least tankage of the reactive liquid systems.

Table IV - Systems Weight Summary. The table shows a weight breakdown of the system and components. The lightest (inert weight) system is the nozzle system which weighs 7,980 lb. This value represents the weight required in addition to the weight of the fixed nozzles (reference system).

Table V - Reliability Rating Summary. The table shows the number of components considered for the various subsystems of each TVC system. The Freon systems have the highest reliability and the hot gas system the least reliability.

Table VI - Development Rating Summary. The table presents the various development considerations considered in rating the TVC systems. The factors considered were development costs, practicality and compatibility. Freon 113 system appears to be more compatible with the development program scope and philosophy.

Table VII - Equivalent Weight Comparison. The table presents the equivalent weight breakdown for each TVC system. The breakdown

includes the system dry weight, expending liquid weight, pressurant weight, and reduction in weight equivalent to gain in impulse.

CONCLUSIONS

Based on the ballistic and control requirements outlined in this study, Freon 113 secondary injection system is the recommended method of vector control for the eight-cluster vehicle.

ACKNOWLEDGEMENT

The authors wish to thank the personnel of the Preliminary Design and Analysis Department, Wasatch Division, and Project Engineering, Reaction Motors Division, Thiokol Chemical Corporation, for their support on trajectory and trade-off studies, reliability analysis, and detailed analysis of selection systems.

TABLE III
DESIGN SUMMARY - SECONDARY INJECTION AND SEPARATE MOTOR APPROACHES

	Method of Pressurization	Maximum Injectant per Injector lb/sec	Maximum Injector Area sq in.	K	Inj Density lb/ft^3	Inj Press. psi	Total Injectant Volume cu ft	Total Pressurant Volume cu ft	Dimensions (8 Tanks Each)	
									Injectant Tank Diameter in.	Pressurant Tank Diameter in.
Freon 113	Stored Nitrogen at 5000 psi	862	7.55	0.5	95.8	850	1304	456	81	58
Freon 114I2		716	4.75	0.6	166.4	850	624	219	61.4	44.8
N_2O_4		536	4.91	0.8	87.36	850	875	297	72.0	49.6
N_2H_4		452	4.96	0.95	62.0	850	1034	350	75.7	53.4
$(CH_2)_2O$		430	5.07	1.0	52.7	850	1155	410	78.6	56.3
H_2O_2		430	3.92	1.0	88.9	850	685	244	66.1	47.3
Freon 113	Solid Propellant	862	7.55	0.5	95.8	850	1304	38	81	-
Hypergolic N_2O_4/UDMH+N_2H_4		287	86.5 throat area	1.5	72.3 avg	600	488	176	62.18x 56.36F	53.36

Separate Control Motor	Method of Pressurization	Isp	Propellant Density lb/cu ft	Total Propellant Volume cu ft	Total Pressurant Volume cu ft	Motor Dimensions
Solid Propellant Motors	-	255	112	-	-	149 Dia Spherical
Liquid Propellant Motors	Turbopump	270	87.7 ox. 55.1 fuel	11,465	189	8 tanks, 86 inch dia x 1106 inches long

TABLE IV

SYSTEM WEIGHTS SUMMARY

Secondary Injection Systems	COMPONENT WEIGHTS (LB) Total Injectant Weight	Total Pressurant Weight	Injectant Tankage Weight	Pressurant Tankage Weight	Piping & Components Weight	SYSTEM WEIGHTS (LB) Support Structure Weight	Dry Weight	Initial System Weight
Freon 113	124,000	9800	5750	11,600	5,800	3450	26,600	160,400
Freon 114I2	102,800	4704	2500	5,470	5,800	2705	16,475	123,979
N_2O_4	76,408	5985	3750	7,425	5,800	2185	19,160	101,553
N_2H_4	64,132	7028	5500	8,825	5,800	2185	22,310	93,470
$(CH_2)_2O$	61,200	8050	5088	10,080	5,800	1900	22,868	92,118
H_2O_2	61,200	4900	3910	6,080	5,800	1810	17,600	83,700
Freon 113 Solid Grain Press.	124,000	3517	5750	600	3,800	3210	13,360	140,877
Hypergolic N_2O_4/UDMH+N_2H_4	35,120	3535	2160	4,328	14,521	1190	22,199	60,854

	Basic Swivelled Nozzle Weight	Actuation System Weight	8 Swivel Nozzle systems	8 fixed nozzles (ref)
Swivel Nozzle System	83,760	1783	85,503	71,520

Separate Control Motors	Total Propellant Weight	Total Pressurant Weight	Motor Inert Parts Weight	Components Weights	Support Structure Weight	Total System Weight
Solid Propellant Motors	823,968	-	62,016	10,000	55,600	951,584
Liquid Propellant Motors	841,100	4050	25,640	17,790	20,000	908,580

TABLE V

RELIABILITY RATING SUMMARY

		Pressurization System		Propellant or Injectant System		Combustion or Injection System		Electrical Control System		Total Merit Rating	Rank
	SITVC SYSTEMS	No. Comp	Merit	No. Comp	Merit	No. Comp	Merit	No. Comp	Merit	No. Comp Merit	No. Comp Merit
LIQUID	Freon 113	44	1	20	1	64	2	10	1	5.0	1.0
	Freon 114I2	44	1	20	1	64	2	10	1	5.0	1.0
	N_2O_4	44	1	20	1.5	64	2.5	10	1	6.0	1.2
	N_2H_4	44	1	20	1.5	64	2.3	10	1	5.6	1.1
	$(CH_2)_2O$	44	1	20	1	64	2	10	1	5.0	1.0
	H_2O_2	44	1	20	1.5	64	2.5	10	1	6.	1.2
	Freon 113 Solid Grain Press.	11	1.5	24	2	64	2	15	1.5	6.7	1.4
Hot Gas	Hypergolic N_2O_4/UDMH+N_2H_4	44	1	56	3	128	12	30	3	19	3.8
Separate Motor Control System	Solid Propellant Motors	11	0.8	5	0.5	24	6	10	1	8.3	1.7
	Liquid Propellant Motors	36	1.2	44	2	24	6	10	1	9.2	1.9
	Swivel Nozzles	Press. 4	System 1.5	Hydraulic 27	1.	Nozzle Sys 2	6.5	10	1	10	2.0

TABLE VI

DEVELOPMENT CONSIDERATIONS RATING SUMMARY

	SITVC SYSTEMS	Development Cost Rating	Practicality Rating (1)	Compatibility Rating (2)	Over-all Rating	Over-all Rank
LIQUID	Freon 113	1.0	1.0	1.2	1.2	1.0
	Freon 114I2	1.5	1.0	1.2	1.82	1.52
	N_2O_4	1.4	1.75	1.3	3.18	2.65
	N_2H_4	1.3	1.5	1.2	2.34	1.95
	$(CH_2)_2O$	1.3	1.5	1.2	2.34	1.95
	H_2O_2	1.4	1.75	1.3	3.18	2.65
	F113, Solid Grain Press.	1.7	2.0	1.2	4.08	3.4
Hot Gas	Hypergolic N_2O_4/UDMH + N_2H_4	7.0	2.5	2.5	43.8	36.4
Separate Motor Control Systems	Swivel Nozzles	4.0	1.4	3.0	16.8	14.0
	Solid Propellant Motors	5.0	2.0	1.0	10.0	8.33
	Liquid Propellant Motors	7.0	2.0	1.0	14.0	11.7

(1) Practicality of Achieving Development within Program Scope

(2) Compatibility with the Large Booster Program Philosophy

TABLE VII

EQUIVALENT WEIGHT COMPARISON

System	Pressurization Method	K	Dry Weight	Effective Wt of Expended Propellant	Pressurant Weight	Unexpended Injectant Weight	Weight Reduction due to Liquid Impulse	Equiv Inert Weight
F113		0.5	26,600	(19,600 + 10,640)	9800	16400	10640	72400
F114I2	Nitrogen	0.6	16,475	(16,230 + 8820)	4704	13600	10640	49189
N_2O_4	At	0.8	19,160	(12,188 + 6619)	5985	10216	10640	43528
N_2H_4	5000 psi	0.95	22,310	(10,231 + 5556)	7028	8572	10640	43057
$(CH_2)_2O$		1.0	22,868	(9700 + 5264)	8050	8160	10640	43402
H_2O_2		1.0	17,600	(9700 + 5264)	4900	8160	10640	34984
F113	Solid Grain Press.	0.5	13,360	(19,600 + 10,640)	3517	16400	10640	52877
Hypergolic $N_2O_4/^{UDMH}_{N_2H_4}$	N_2 @ 5000 psi	1.5	22,199	(6470 + 3512)	3535	351	10640	25427
Swivel Nozzle	-	-	13,983*		-	-	2580**	16563
Solid Prop. Motor	-	-	127,616	823,968	-	-	916598	34986
Liq Prop. Motor	Turbopump	-	63,430	-	4050	8500	103260	-27280

*Includes additional nozzle weight over fixed nozzle with no secondary injection
**Increased weight due to slight thrust loss

TABLE VIII

THRUST VECTOR CONTROL SYSTEMS RATING SUMMARY

	Injectant	Method of Pressurization	Reliability (X 3)		Development (X 2.5)		Cost (X 2)		Performance (X 1)		Over-all	
			Rank	Merit	Rank	Merit	Rank	Merit	Rank	Merit	Rating	Rank
Liquid	Freon 113	N_2 at 5000 psi	1.0	3.0	1.0	2.5	1.64	3.28	4.37	4.37	13.15	1
Liquid	Freon 114I2	N_2 at 5000 psi	1.0	3.0	1.52	3.77	2.13	4.26	2.97	2.97	14.00	4
Liquid	N_2O_4	N_2 at 5000 psi	1.2	3.6	2.65	6.63	1.24	2.48	2.63	2.63	15.34	6
Liquid	N_2H_4	N_2 at 5000 psi	1.1	3.3	1.95	4.87	1.42	2.84	2.60	2.60	13.61	3
Liquid	$(CH_2)_2O$	N_2 at 5000 psi	1.0	3.0	1.95	4.87	1.44	2.88	2.62	2.62	13.37	2
Liquid	H_2O_2	N_2 at 5000 psi	1.2	3.6	2.65	6.63	1.18	2.36	2.11	2.11	14.70	5
Liquid	Freon 113	Solid Gas Generator	1.4	4.2	3.40	8.5	1.0	2.0	3.19	3.19	17.89	7
	Hypergolic N_2O_4/UDMH + N_2H_4	N_2 at 5000 psi	3.8	11.5	36.4	91.0	1.39	2.78	1.54	1.54	106.82	11
Hot Gas	Solid Propellant Motors		1.7	5.1	8.33	20.8	4.6	9.2	2.11	2.11	37.21	9
Hot Gas	Liquid Propellant Motors		1.9	5.7	11.7	28.2	1.73	3.46	-1.66	-1.66	35.70	8
	Swivel Nozzle		2.0	6.0	14.0	35.0	1.72	3.44	1.0	1.0	45.44	10

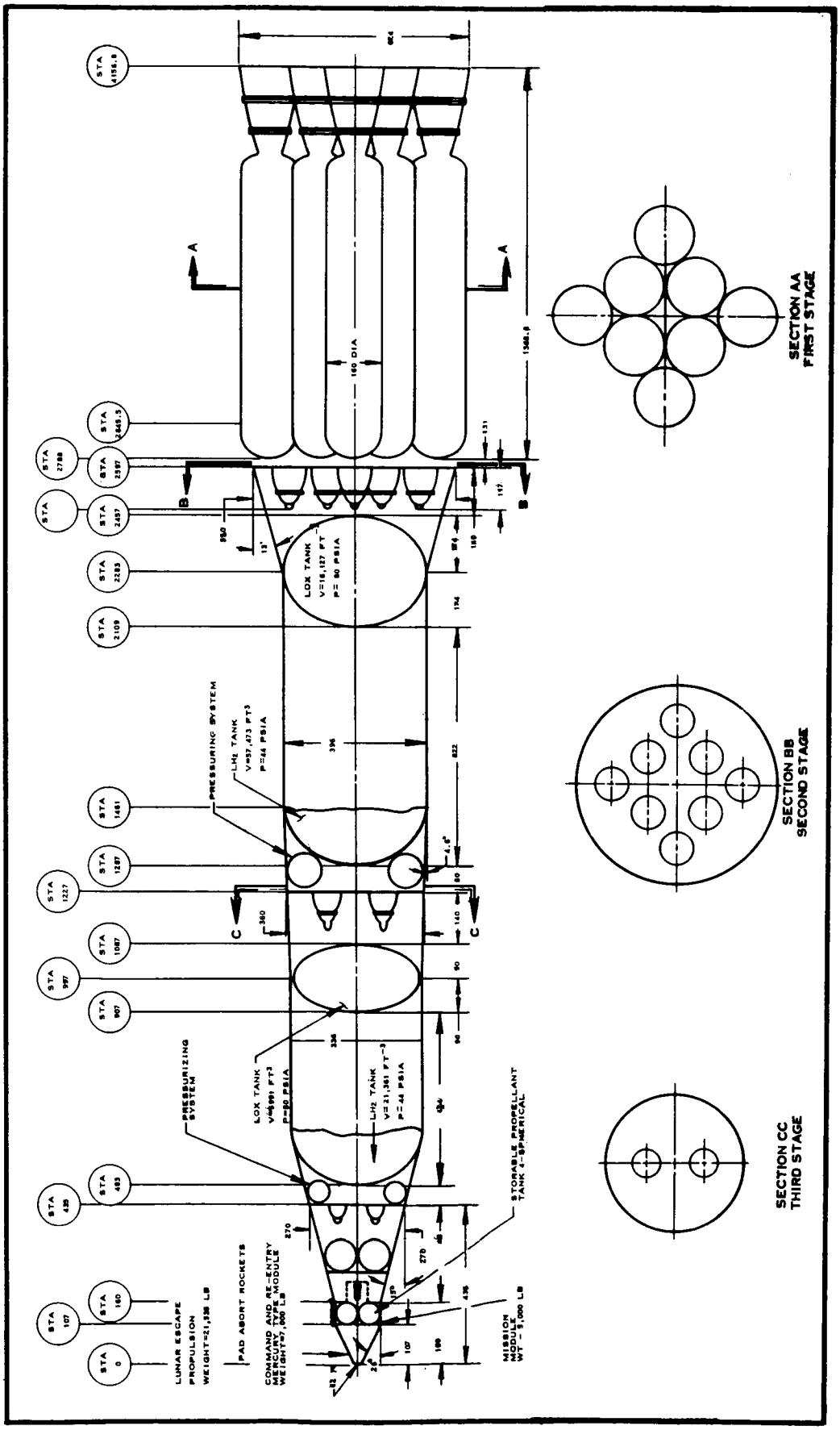

FIG. 1 THE GENERAL ARRANGEMENT OF THE FIRST STAGE CLUSTER AND OVER-ALL MISSILE SYSTEM CONFIGURATION

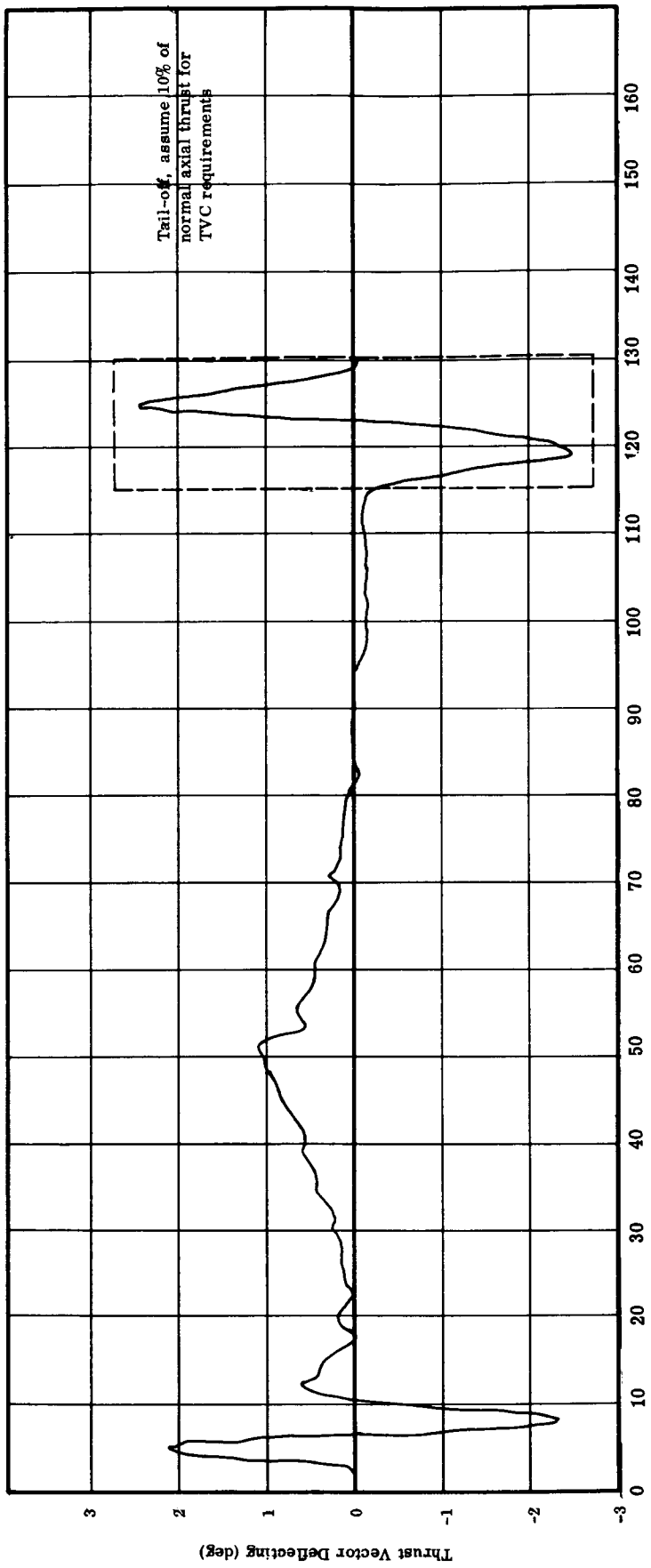

FIG. 2 ESTIMATED TVC DUTY CYCLE FOR SOLID BOOSTER

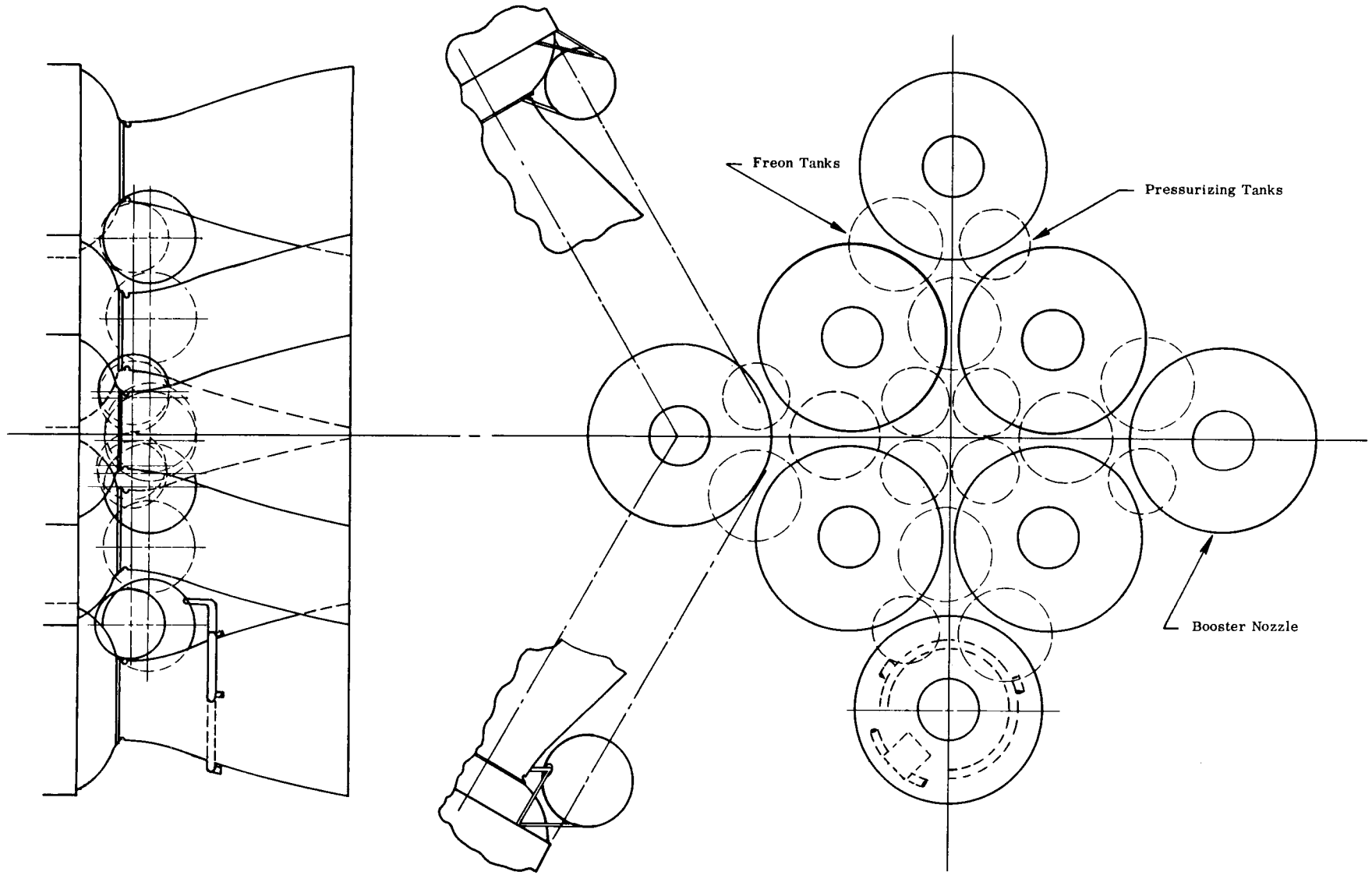

FIG. 3 FREON 113 INJECTION TVC SYSTEM TANKAGE LAYOUT

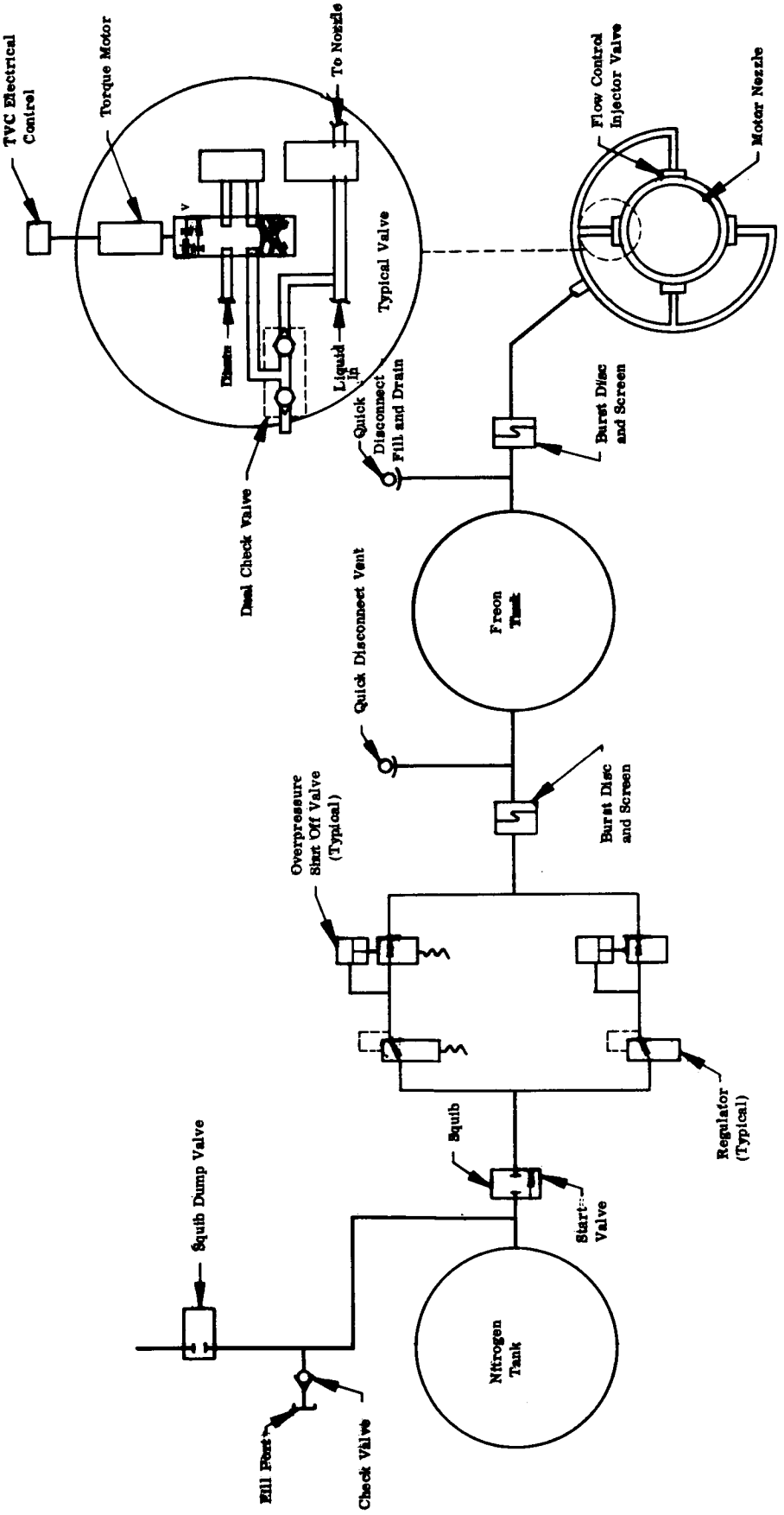

FIG. 4 SCHEMATIC DIAGRAM FREON 113 INJECTION TVC (TYPICAL)

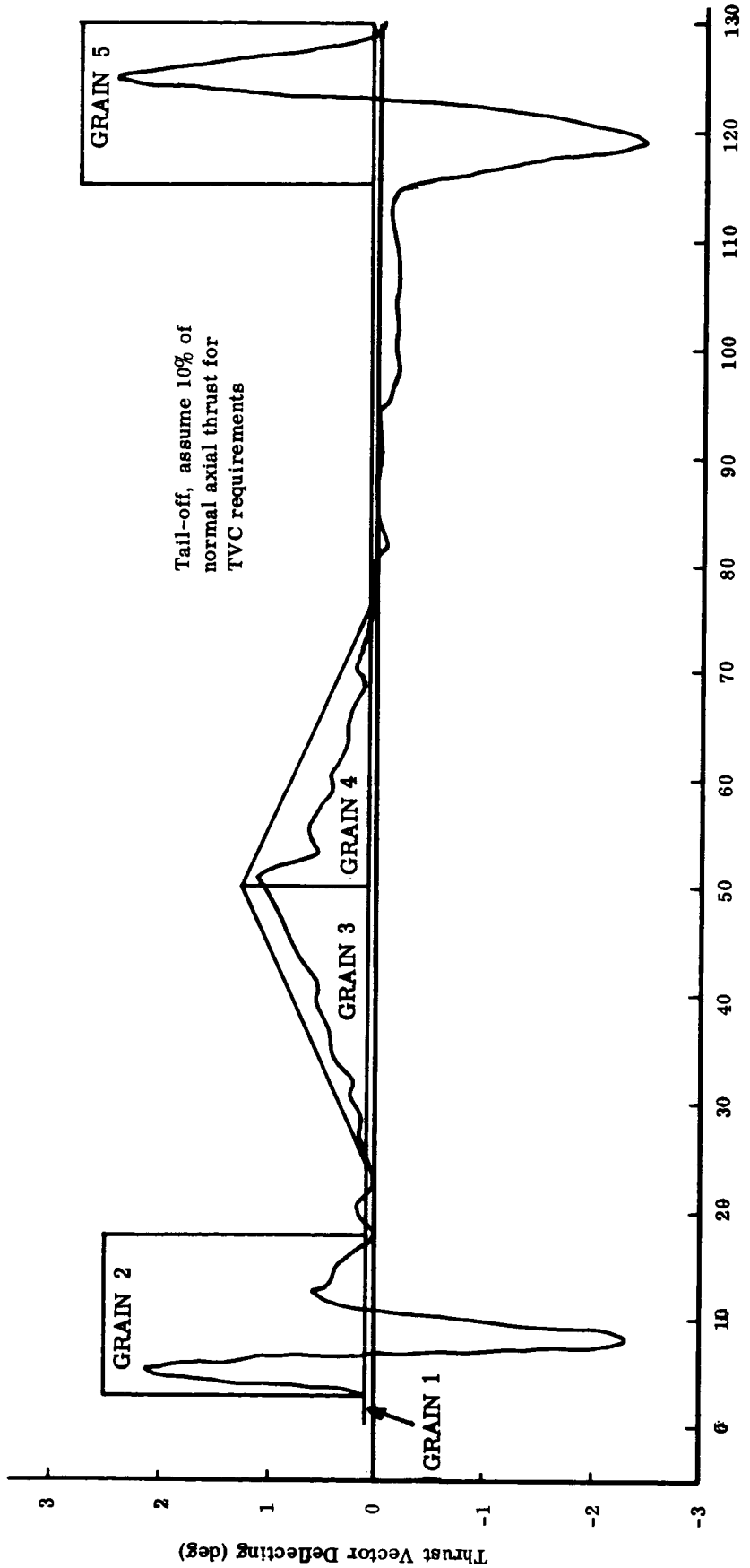

FIG. 5 ESTIMATED TVC DUTY CYCLE FOR SOLID BOOSTER

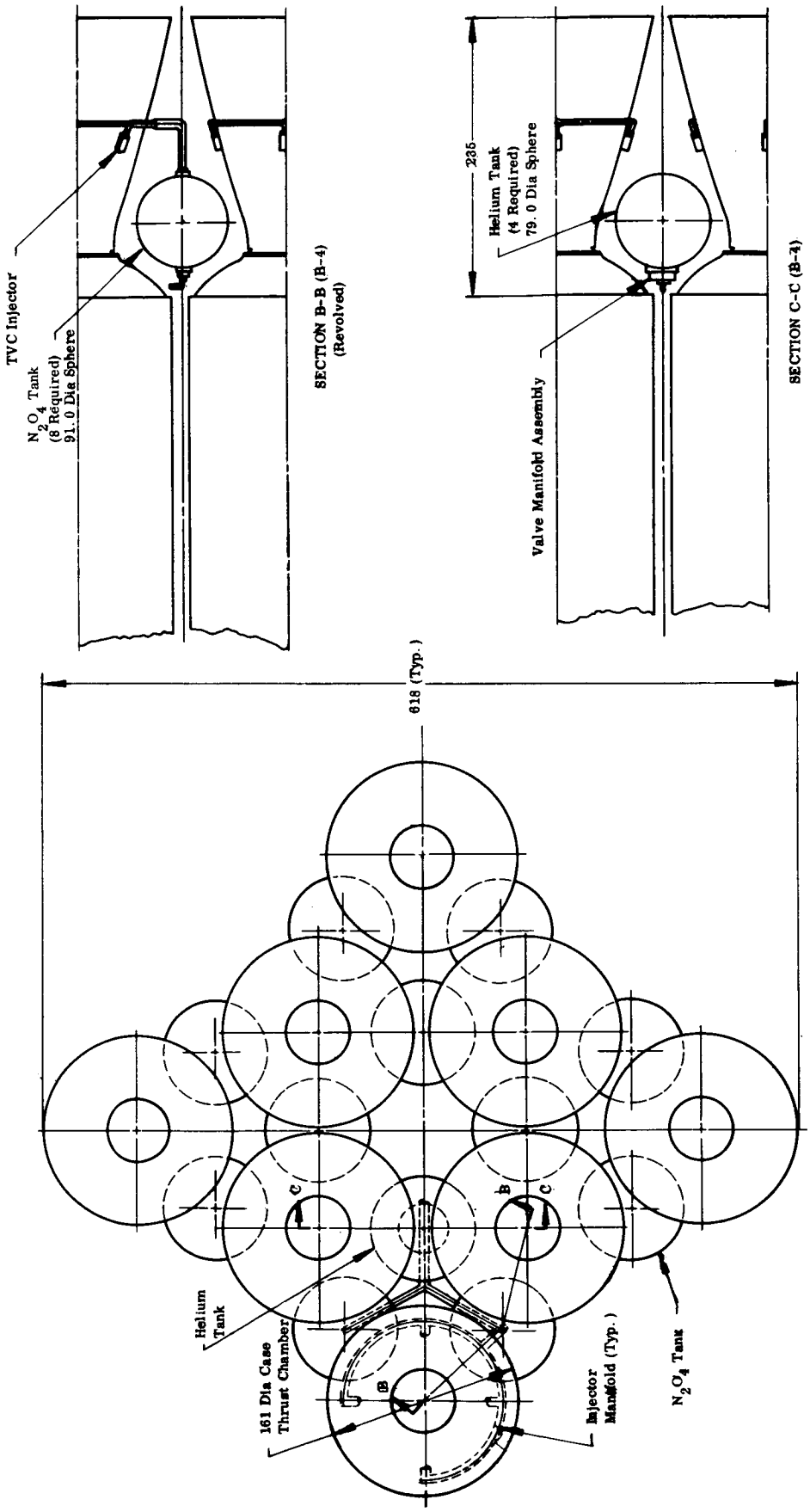

FIG. 6 TANKAGE INSTALLATION REACTIVE SYSTEM LIQUID (N_2O_4)

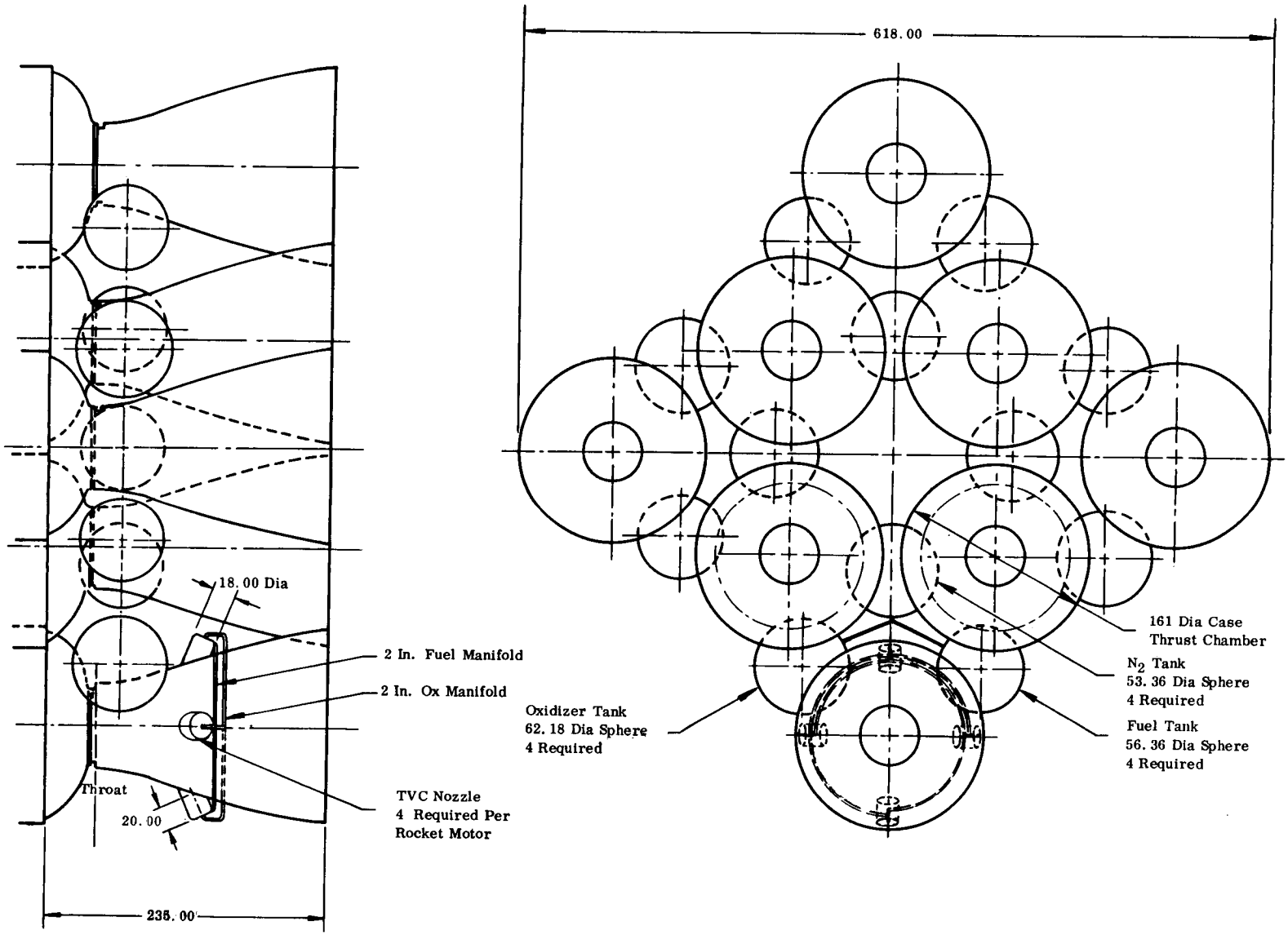

FIG. 7 TVC SYSTEM HYPERGOLIC LIQUID

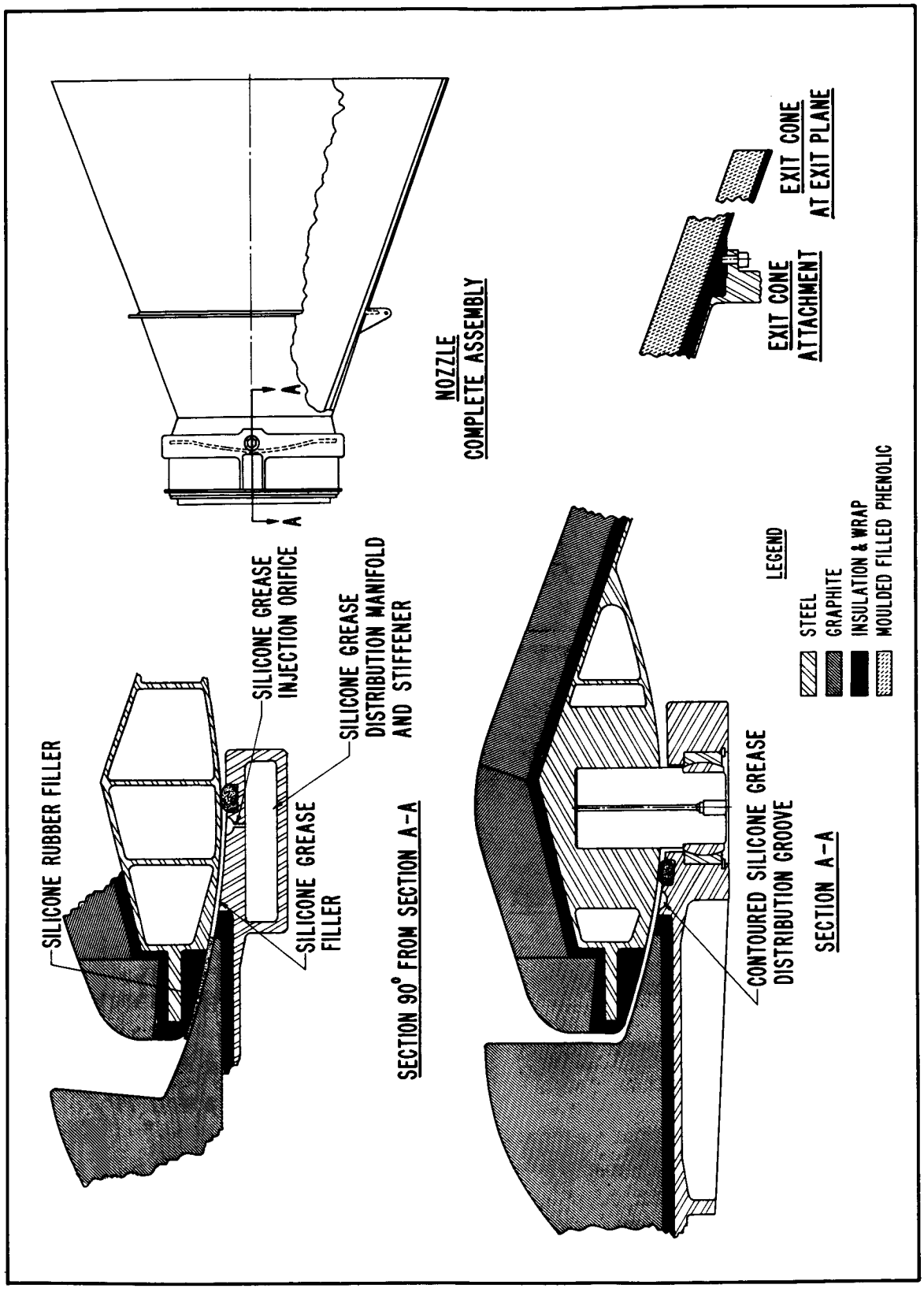

FIG. 8 TYPICAL LARGE SINGLE AXIS SWIVEL NOZZLE

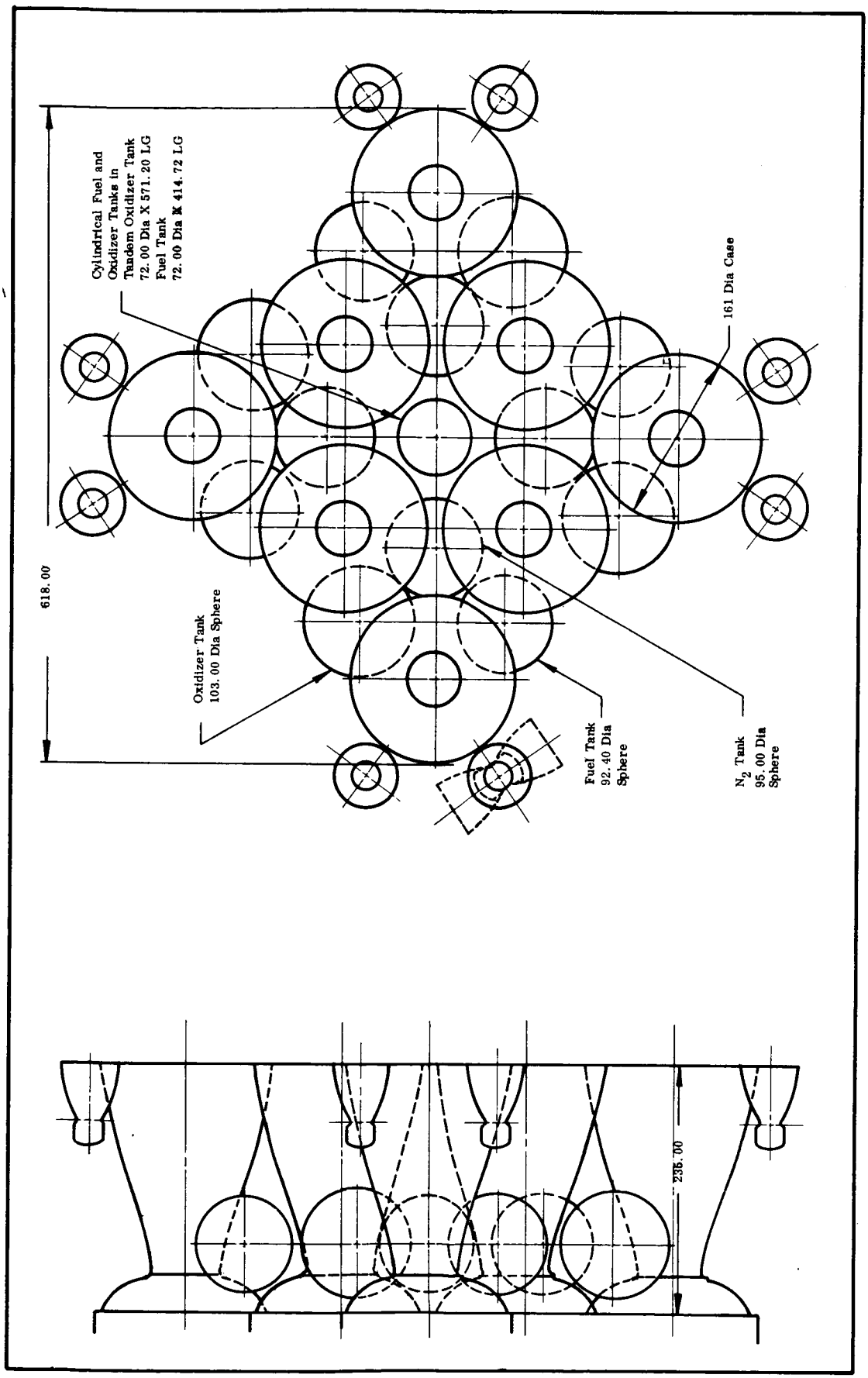

FIG. 10 TVC SYSTEM SEPARATE MOTORS LIQUID

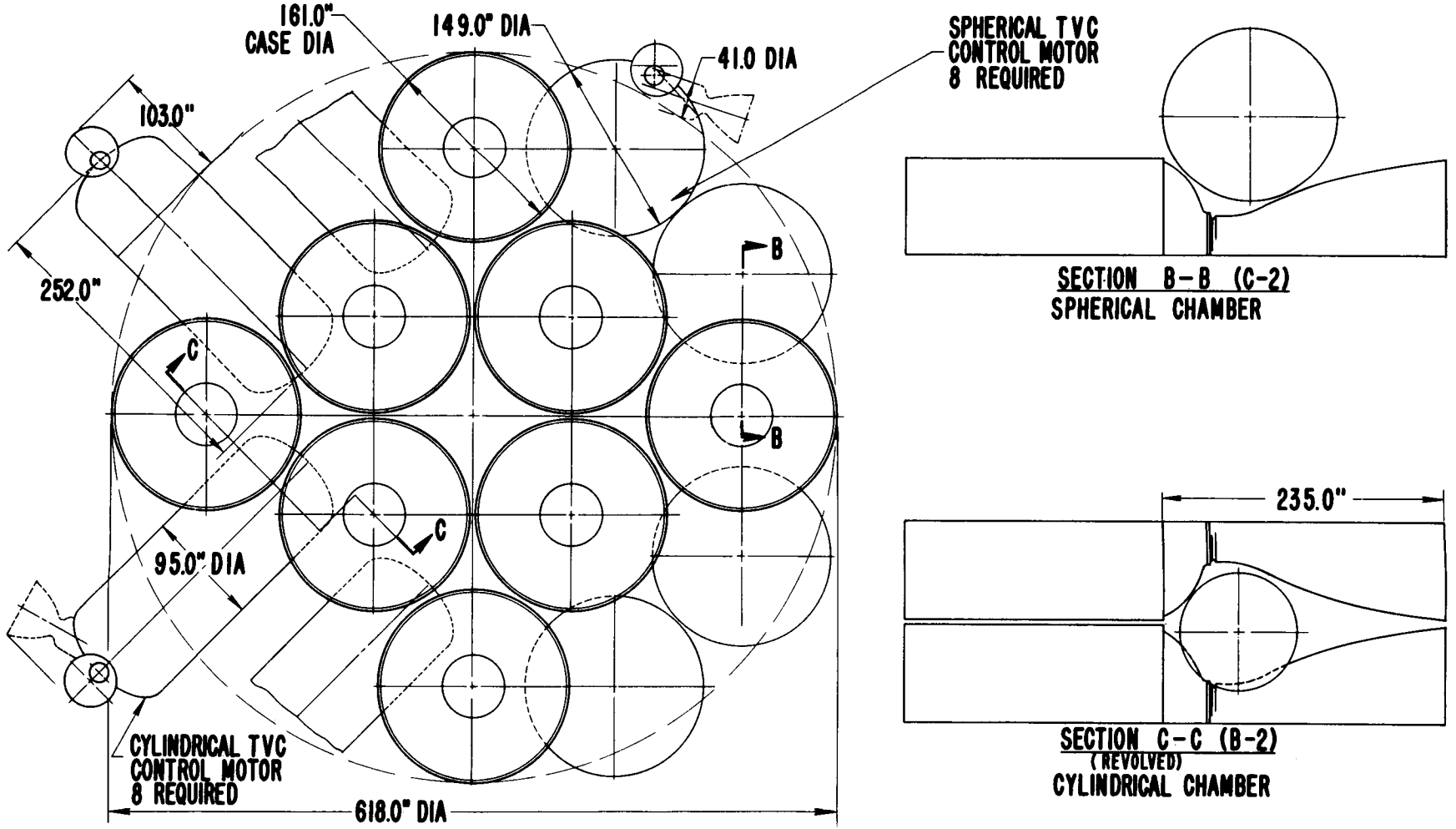

FIG. 9 TVC SYSTEM SEPARATE MOTORS SOLID

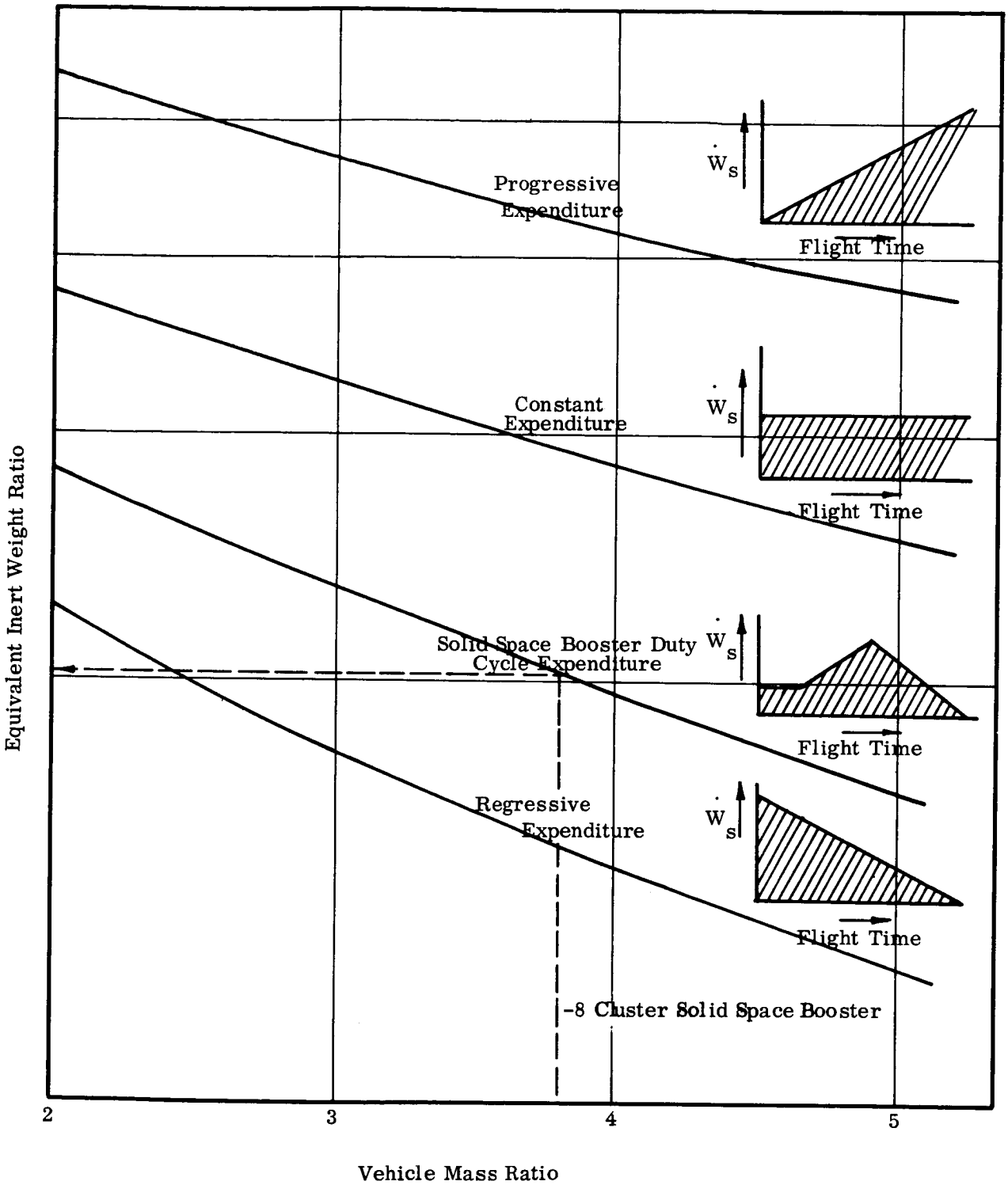

FIG. 11 EQUIVALENT INERT WEIGHT RATIOS OF EXPENDING MATERIALS (FLUID INJECTION) VS VEHICLE MASS RATIO WITH PARAMETER OF EXPENDITURE RATE

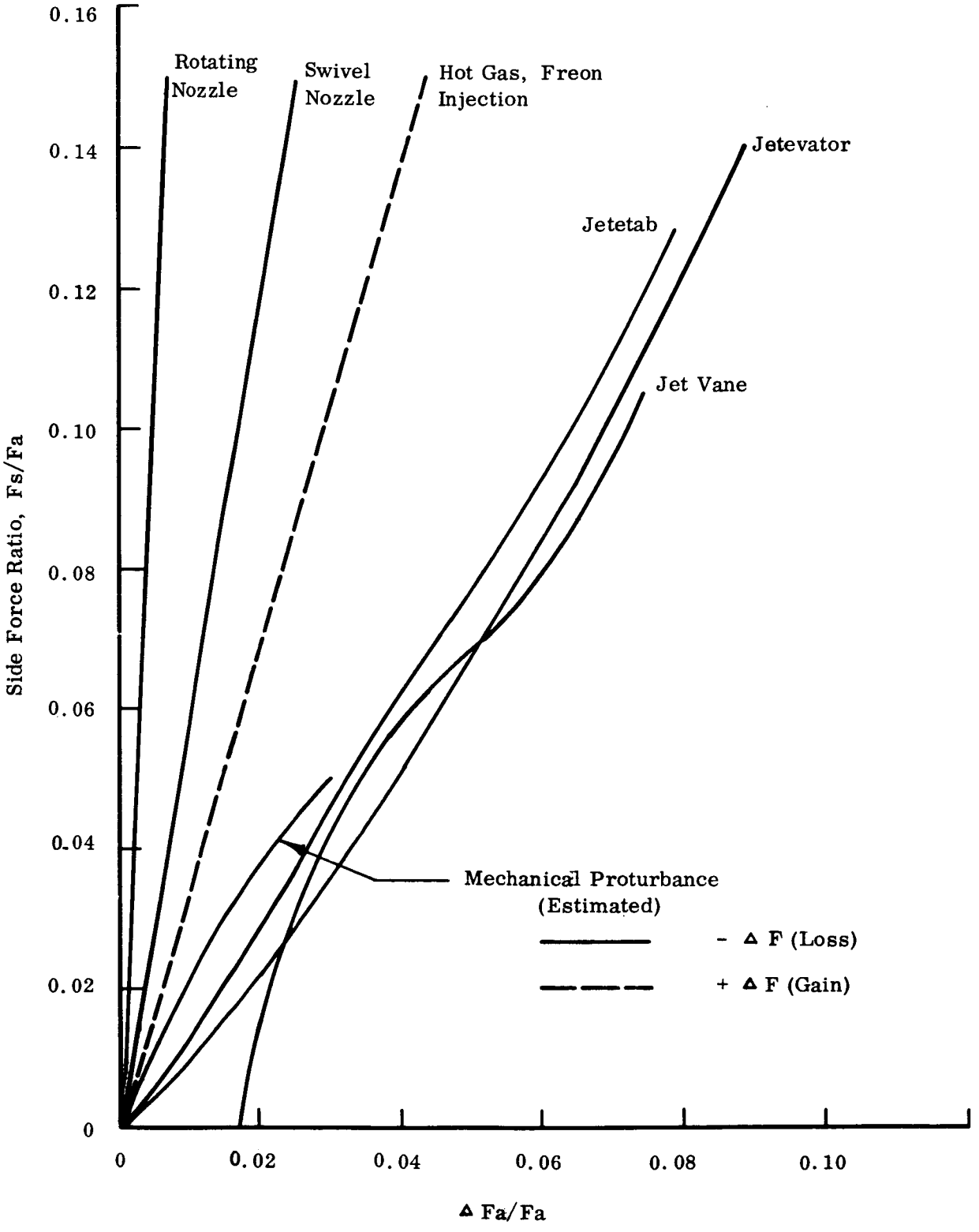

FIG. 12 EFFECT OF TVC SYSTEMS SPACE BOOSTER THRUST

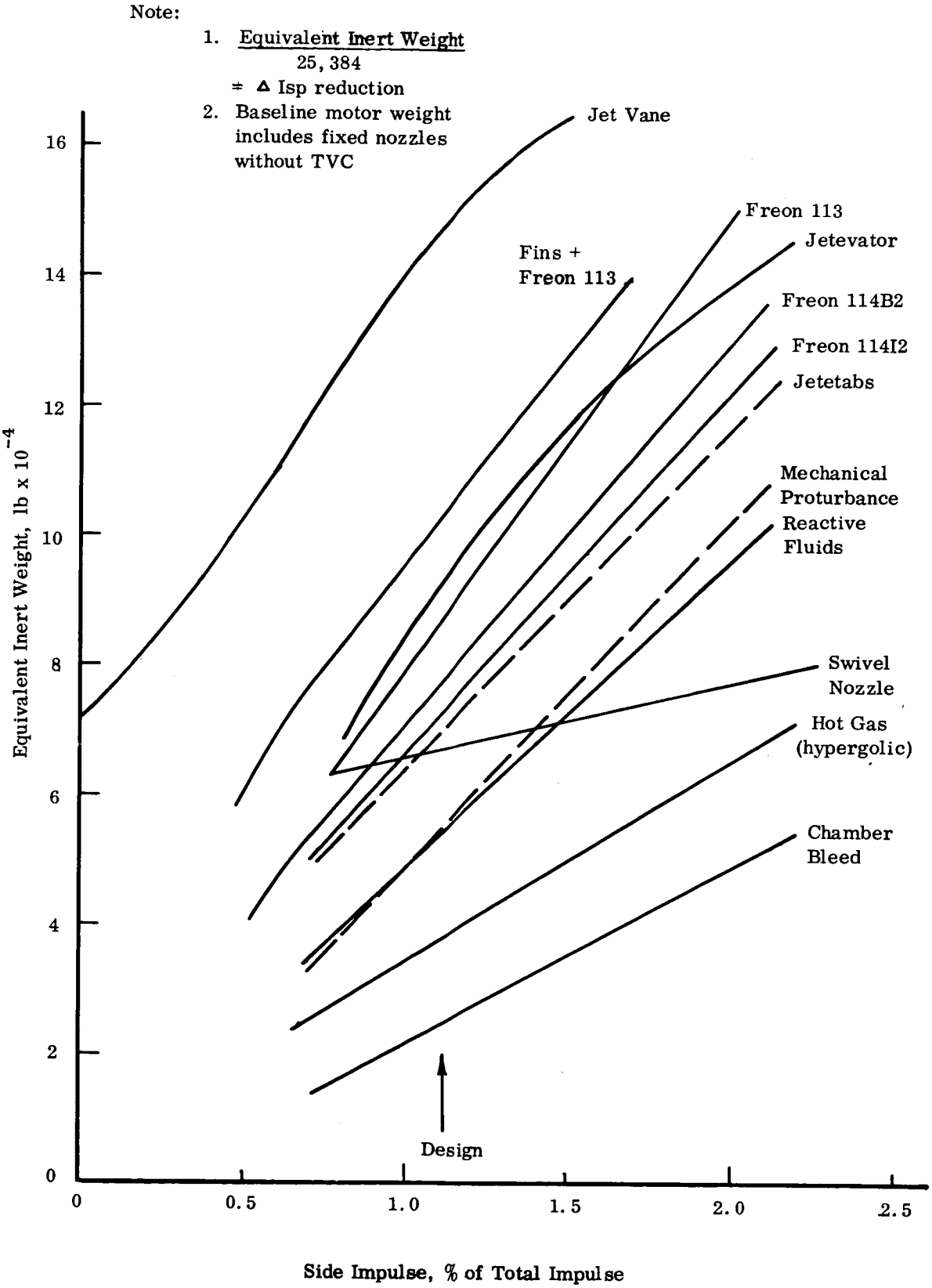

FIG. 13 EQUIVALENT INERT WEIGHT OF TVC SYSTEMS

THRUST VECTOR CONTROL BY REACTIVE LIQUID SECONDARY INJECTION

by
J. J. Fox, A. Fukumoto and D. W. Sedgley
Power Systems Division, The Marquardt Corporation

SUMMARY

During the past one and one-half years The Marquardt Corporation has been active in the field of secondary injection for thrust vector control. Much of the analytical work performed during this time was devoted to the investigation of control system problems and over-all system aspects. In the latter area early theoretical performance analysis of various injection fluids indicated potential performance gains were possible with reactive fluids. Since available data on the performance of reactive fluids were meager, an experimental program was initiated to explore the performance capabilities of reacting liquids as secondary injection fluids. The objective of this investigation was to determine the feasibility of a secondary injection system using a reacting (exothermic) liquid which would not have the high temperature structural problems of a hot gas injection system, but which would be capable of generating larger side forces per pound of secondary fluid than comparable non-reacting liquid injection systems. The data obtained at The Marquardt Corporation has indicated that under proper injector conditions the available stay time in a primary propulsion nozzle is sufficient to achieve an exothermic chemical decomposition. Reacting liquid performance at small deflection angles appears to be far superior to other presently considered injection systems and offers the missile designer a highly efficient and simple control system. This work has been largely carried on under a company sponsored independent research program, and recently additional work in this area is being sponsored by the United States Air Force.

INTRODUCTION

Reactive fluids as used herein refer to such fluids as exhibit exothermic decomposition when injected into the expansion nozzle of a primary propulsion engine. Inert fluids such as the more stable Freons are typified by endothermic decomposition in a nozzle and are considered non-reacting. The degree of reactivity of a reactive liquid injectant is determined by the chemical kinetics occurring in a complex flow field. While the complexity of this thermo-chemical reaction is such that rigid quantitative analysis is virtually impossible, certain physical and chemical properties which are readily obtainable will allow qualitative analysis. Results of this type of inductive analysis must be verified by testing. This approach is useful, however, in that the field of candidate injectants can be justifiably narrowed to a few selected fluids.

Several theoretical models have been formulated to synthesize secondary injection performance. The most notable of these are presented as References 1 and 2. Although the concept of rocket guidance by means of injection of a fluid into the primary exhaust gas stream

dates back to 1952, a rigid theoretical analysis is not available because of the complexity of flow interactions in three dimensions. Existing analyses are severely limited because of the necessary simplifying assumptions required to allow solution. These analyses, particularly in regard to reacting liquids, are only useful in a qualitative form whereby trends can be anticipated.

The test program was conducted using an uncooled, liquid bipropellant work-horse type motor. Test propellants were 50-50 UDMH and hydrazine, with nitrogen tetroxide as the oxidizer. The test motor was rated at 1200 pounds nominal thrust and operated near stoichiometric propellant mixtures. Most of the test effort was devoted to the exploration of the performance characteristics of reactive liquid injectants. Results indicate that reacting liquid secondary injection performance is dependent upon injection techniques. Injection of Freon 113 was investigated only briefly to provide a valid basis of comparison. Additional tests with a bipropellant rocket motor as an auxiliary gas generator were conducted to establish a performance level for hot gas injection.

DISCUSSION

Injectant Considerations. Droplet burning time and energy release by the injectant are important criteria for the selection of a reactive liquid for secondary injection thrust vector control. Energy release is available from the heat of reaction of a propellant type injectant which is invariably exothermic, whereas the typical oxidizer with endothermic decomposition depends upon chemical reaction with the main exhaust stream to produce a net positive energy contribution.

Physical properties which influence the selection of a secondary fluid are:

1. Low boiling point and low heat of vaporization which minimize ignition delay and increase the fraction of fluid decomposed within the nozzle.

2. Low heat capacity which minimizes heat transfer and energy loss in the main stream.

3. High reactivity which produces high energy release and rapid chemical reaction.

4. Low gas density which causes maximum perturbation of the main stream due to maximum gas evolution.

Hydrazine or UDMH are among the most attractive fluids in the monopropellant category because of their high exothermic heat release. The mixture, 50-50 UDMH - hydrazine, was selected for experimental evaluation in order to take advantage of the desirable properties of each constituent plus the additional property of storability of the mixture. Additional energy release is possible by association of the carbon and hydrogen content of the products of

decomposition with unburned oxidizer existing in the main gas stream. The important values for each liquid are listed in Table I.

TABLE I

CANDIDATE FUELS FOR LIQUID INJECTION

Fuel/Propellant	Density	C_p	ΔH_v	B.P.	ΔH_f
	#/ft^3	BTU/#°R	BTU/#	°F	Kcal/mole
N_2H_4	62.5	.74	539	230	12
UDMH	49.7	.65	241	146	12.74
50-50 UDMH-N_2H_4	56.1	.69	426	158	12.25

Decomposition of oxidizers used as injectant fluids requires transfer of heat from the primary gas stream since this process is invariably endothermic. In addition, it is preferred that decomposition products of the oxidizer chemically react with a fuel-rich exhaust stream to offset the energy initially absorbed from the main stream. Therefore, selection of an oxidizer for secondary injection is dependent on the composition of the primary engine exhaust products. For example, the probability for chemical reaction of fluorine containing oxidizers such as chlorine trifluoride, tetrafluorohydrazine and the Freon compounds is increased when they are injected into gas streams containing boron, lithium and aluminum to form high energy products such as BF_3, LiF and AlF_3. It might appear that oxidizer type injectants would represent the optimum fluid for use in conjunction with solid propellant motors; however, the endothermic decomposition of most oxidizers represents a liability which may or may not be entirely compensated by the high energy metal/oxidizer reactions. Typical oxidizers considered as candidate injection fluids are listed in Table II.

TABLE II

OXIDIZERS FOR LIQUID INJECTION

Oxidizer	Density	C_p	ΔH_v	B.P.	ΔH_f
	#/ft^3	BTU/#°R	BTU/#	°F	Kcal/mole
ClF_3	106	.31	106	53	- 44.4
N_2F_4	89.2	.25	55	-99	- 5
Freon 114I2	168	.10	84	235	-160
N_2O_4	92	.37	178	70	- 5.4

Since typical main engine performance usually involves a fuel-rich combustion process, oxidizer-rich monopropellants should be considered as injectant fluids. The high energy monopropellant Cavea B is shock sensitive at its optimum (O/F = 2) mixture. However, it is completely insensitive to hydrodynamic shock using the standard liquid propellant test method (Reference 3) at O/F = 4.6 (Reference 4). An oxidizer-rich monopropellant therefore appears to have the advantages of both fuel and oxidizer type injectant fluids, however, additional analysis and investigation will be required to verify the possibility.

The time required to burn a propellant droplet is an important criterion in system design for thrust vectoring by reactive liquid injection. A formula for the burning time of a monopropellant droplet suspended in its own decomposition products was derived by Spalding and Jain (Reference 5) with the result that

$$\frac{t_b \dot{m}_{f''}}{(\lambda/r_d)\rho r_{do}^2} = f\left(\frac{1}{\lambda_o}\right) \qquad (1)$$

where t_b is the time during which the droplet changes from r_{do}, its initial radius, to zero radius; λ_o is the value of λ when droplet radius is r_{do}; $\dot{m}_f''$ is the mass burning rate in the flame; and ρ is the liquid density.

The symbol λ represents the ratio of the mass burning rate of propellant in a plane laminar flame, to the mass rate of vaporization at the droplet surface if chemical reaction is absent. The mass burning rate and λ_o are directly influenced by λ, therefore, propellants displaying large values of λ are desirable. Reference 5 shows that hydrazine has a distinct advantage in this respect over other monopropellants such as ethyl nitrate and propyl nitrate burning in low pressures (1 to 10 atm) which are experienced in nozzle divergent sections.

Initial conditions (Reference 6) which increase the fraction of propellant vaporized in a given time are high main stream pressure, high initial droplet temperature, small droplet size, and low droplet velocity in the exit direction. These parameters can be satisfied by injecting the secondary liquid in an upstream direction at a high pressure drop into the divergent section of the nozzle, close to the throat. Study and analysis in this area are required to define the optimum injection configuration.

Injection Considerations. A simplified one-dimensional model of secondary injection for thrust vector control was developed to assist in explaining some of the phenomena that were expected to occur during the tests. The basic assumption used in the development of the model is that the injected liquid stream shatters into droplets immediately upon leaving the orifice. Thus, the development is simply determining the trajectory of the droplet in a supersonic stream. The derivation of the equations of the droplet penetration into the supersonic stream and of the stay-time is presented below.

Referring to Figure 1, the summation of the forces acting on the droplet in the x-direction is

$$\Sigma F_x = D_x + W_{d_x} - m_d a_x = 0 \qquad (2)$$

and in the y-direction

$$\Sigma F_y = m_d a_y - D_y - W_{d_y} = 0 \qquad (3)$$

where D is the drag of the droplet (the subscript denoting the direction), W_d is the weight of the droplet, m_d is the mass of the droplet, and a the acceleration of the droplet.

The drag of the droplet is defined as

$$D = .5\rho_o A_d C_d V^2 = \xi V^2$$

where ρ_o is the density of the primary stream, A_d is the area of the droplet, C_d is the drag coefficient of the droplet, and V is the velocity of the droplet with respect to the primary stream.

From this definition of the velocity, the component in the x-direction is $(V_o - V_x)$ and the component in the y-direction is V_y. Equations (2) and (3) can then be written as

$$\xi (V_o - V_x)^2 + W_{d_x} - m_d a_x = 0 \qquad (2a)$$

and

$$m_d a_y - \xi V_y^2 - W_{d_y} = 0 \qquad (3a)$$

or

$$m_d \frac{d^2x}{dt^2} - \xi (V_o - \frac{dx}{dt})^2 - W_{d_x} = 0 \qquad (2b)$$

and

$$m_d \frac{d^2y}{dt^2} - \xi (\frac{dy}{dt})^2 - W_{d_y} = 0 \qquad (3b)$$

Solving Equations (2b) and (3b) for x and y, respectively, yields

$$x = V_o t - \frac{m_d}{\xi} \log_\epsilon \left[\cos \sqrt{\frac{\xi W_{d_x}}{m_d}}\, t + (V_o - V_i \sin\beta) \sin \sqrt{\frac{\xi W_{d_x}}{m_d}}\, t \right] \qquad (4)$$

and

$$y = - \frac{m_d}{\xi} \log_\epsilon \left[\cos \sqrt{\frac{\xi W_{d_y}}{m_d}}\, t - (V_i \cos\beta) \sqrt{\frac{\xi}{W_{d_y}}} \sin \sqrt{\frac{\xi W_{d_y}}{m_d}}\, t \right] \qquad (5)$$

where V_i is the injection velocity, t is the time, and β the injection angle.

The significance of these equations is quite apparent. For reactive liquid injection the most important parameters are the stay-time and rate of reaction of the droplet. Equation (4) shows "stay-time" can be prolonged by (1) injecting the liquid as close to the throat as possible (low stream velocity V_o), (2) injecting the liquid upstream (large negative injection angle β, Figure 1) at a high velocity (V_i), (3) injecting the liquid where the primary stream density is low, (4) utilizing heavy (high density) liquids, and (5) large droplets. If the conditions of Item 1 are satisfied, the conditions of Item 3 cannot be satisfied. However, since the drag of the droplet is directly proportional to the square of the velocity, Item 1 may be the controlling factor.

Intuitively, it would appear that larger side forces can be obtained if the reaction of the secondary fluid occurs in the proximity of the nozzle wall. Consequently, the depth of penetration should be minimized. For this reason, some "trade-off" must be made for optimum performance. Equation (5) shows that the depth of penetration is dependent upon the mass of the droplet, injection velocity, and injection angle. By reducing the mass of the droplet, the penetration is reduced but the "stay-time" is also reduced. However, the reaction time (Equation 1) of a small droplet is less, and this factor appears to control the choice of droplet size. A compromise may be made here by reducing the size of the droplets while employing a high density liquid. The high injection velocity (V_i) is desirable for long "stay-time" but undesirable for minimum penetration. This can be remedied by employing high injection velocities with large negative injection angles.

It would appear therefore, that the optimum injection location for reacting liquid secondary injection thrust vector control would be as near the throat as possible. Experience has shown that this is not necessarily the case. Two boundary conditions apparently exist which limit the optimum injection location. Both these boundaries exist for exhaust nozzles of practical size, and do not exist for diminutive test nozzles. The first limit is reached when the gas evolved from the vaporized liquid (or injected gases for that matter) overexpands within the nozzle (Figure 2A). Since the induced lateral force (amplification) is caused by a generated overpressure acting on the nozzle wall, an underpressure condition due to overexpansion of injected or evolved gases will reduce the resultant lateral force. Therefore, the most upstream injector location and pattern should be such as to preclude overexpansion of the injection gases within the primary nozzle.

A second limitation dictates that the high pressure (overpressure) zone does not act upon more than 180° of the nozzle surface (Figure 2B). As the high pressure area approaches nozzle center line height, the pressure area forces begin to cancel each other since lateral components are acting in opposing directions. This region of overpressure therefore produces no net side force and only results in increasing nozzle stress levels. The nature of the overpressure distribution within the primary nozzle is not exactly known. Static pressure surveys taken at JPL indicate that the overpressure

resulting from liquid secondary injection is not axi-symmetrical. A three-dimensional contour map shown in Figure 3 illustrates the unsymmetrical pressure distribution documented by JPL (Reference 7). A means to positively assess these boundary conditions has not yet been determined by the writers. It is felt, however, that evaluation of these boundaries will hold the key to scaling problems for secondary injection systems in various size rocket motors.

The analyses presented thus far for reacting liquid injection are strictly qualitative in nature, however, considerable insight is obtained as to the effect of selected variables. This has proven to be a valuable aid in planning and in correlating our test program. Published data from sources such as represented by References 1 and 2 have also been extremely helpful.

Published data from the Naval Ordnance Test Station at China Lake indicate a relationship exists between the rate of change of momentum of the injected fluid to the side thrust developed. Reference 8 presented a logarithmic graph of the normalized ratio F_s/F_m as a function of $(\dot{W}_s/\dot{W}_m)^2/g\rho A$, where the latter term is essentially a rate of change of momentum ratio. The latter term reduces to $(\dot{m}_s V_i)$ divided by $(\dot{W}_m^2)$, which is essentially a secondary-to-primary momentum ratio, since momentum of the exhaust gases is proportional to $\dot{W}_m^2$. This plot can be represented by an empirical equation as follows.

$$\frac{F_s}{F_m} = C_1\left(\frac{\dot{W}_s^2}{\dot{W}_m^2 g \rho A}\right)^{1/2} \tag{6}$$

where C_1 is an empirically derived constant. Equation (6) can be rearranged to give:

$$I_{sp_s} = \frac{C_1^2 I_{sp}}{g\dot{W}_m} \frac{V_i}{\tan\delta} \tag{7}$$

When the engine parameters are held constant (for a given engine), Equation (7) reduced to:

$$I_{sp_s} = \frac{C_2 V_i}{g\tan\delta} \tag{8}$$

where

$$C_2 = C_1^2 \frac{F_m}{\dot{W}_m^2}$$

Additional relationships between pertinent parameters may be obtained and are presented for further analysis.

$$\tan\delta = \sqrt{\frac{C_2}{F_m}} \sqrt{\frac{\dot{W}_s}{g}} V_i \tag{9}$$

$$I_{sp_s} = F_m \frac{\tan\delta}{\dot{W}_s} \tag{10}$$

$$I_{sp_s} = \sqrt{\frac{C_2 F_m}{g\rho}} \sqrt{\frac{1}{A}} \qquad (11)$$

A generalized graph based on these relationships is presented in Figure 4. For a constant set of main engine and secondary liquid injection characteristics, that is the values of the constants C_1 or C_2 are known or can be evaluated, the performance of any liquid secondary injection system may be predicted.

Experience gained in this program indicates that the constant C_2 is affected by factors such as physical and chemical properties of the injectant, and of the main engine propellants, as well as engine and injection geometry. The empirical constant C_2 may be mathematically represented as

$$\prod_{i=1}^{n} K_i$$

where K is an influence coefficient representing each controlling factor.

Liquid injectant properties which tend to maximize performance, or C_2, have already been discussed under the heading of Injectant Considerations, and factors relating to injection geometry have been discussed under Injection Considerations.

Other geometric influences not previously discussed, such as orifice shape (other than circular) and orifice number and distribution, can also be expected to influence the value C_2 in a particular installation.

Results of this investigation show, for example, that the value of K representing the effect of injection location would be a major influence on the value of C_2. Each of the important injectant properties such as heat of formation and density, and each engine parameter such as injection angle and injector orifice configuration would have a K value whose magnitude would be proportional to the effect of the parameter upon secondary injection performance.

Since C_2 is an empirically derived constant and a method for calculation of this constant was not at hand, the objective of our test program was to determine the value of C_2 for a reacting liquid secondary injection system. For a system where the injection velocity is held constant (i.e. constant injector pressure drop), Equation (8) indicates a hyperbolic relationship exists between lateral $I_{sp_s}(F_s/\dot{W}_s)$ and deflection angle ($\tan^{-1} F_s/F_m$). The actual performance level (absolute values) of a system can be said to be proportional to the value of the constant C_2. Optimization of injection parameters such as injection location, injection angle and injected fluid properties will produce the maximum C_2 and therefore the maximum lateral I_{sp_s}.

Test Results. The preceding discussion of theoretical secondary injection considerations can serve as the basic framework within which the test results can be evaluated. As outlined in the

Introduction, the test program was conducted using an uncooled liquid bipropellant motor for the primary propulsion system. Primary propellants were 50-50 UDMH and hydrazine with nitrogen tetroxide as the oxidizer. The reacting secondary injection fluid selected for evaluation was the 50-50 mixture of UDMH and hydrazine. A two-component force device was used to measure lateral and axial forces on the test motor. Standard pressure transducers and flow meters were used to record test parameters. All data were recorded on a standard recording oscillograph. A photograph of the test installation for reacting liquid secondary injection is shown in Figure 5.

Reacting liquid secondary injection performance data shown in Figure 6 was obtained at constant injection velocities. Flow rate was varied by changing injection area while maintaining a constant injection pressure. Performance characteristics were thus evaluated at two injection velocities by testing at two injection pressures of 155 psig and 480 psig. The curves drawn through the data points of this figure actually represent the empirical equation presented as Equation (8). The constant C_2 for these data was determined to be 1.21. Actual side forces and secondary flows may be calculated from the definitions of the abscissa and ordinate of this plot since the axial thrust was 1200 pounds.

A study of Equation (8) and the data of Figure 6 shows that the classification of injection liquids by the secondary specific impulse parameter alone is misleading, since high I_{sp_s} values can be obtained with most fluids at very small deflection angles. A more factual representation is obtained when both secondary specific impulse and the corresponding deflection angle are quoted.

Secondary injection performance with a reacting liquid shown in Figure 6 represents a culmination of testing wherein the effects of various parameters were evaluated. For the particular reacting liquid chosen for evaluation, the most important parameters appear to be injector location and injection velocity. Injection location appears to be an especially sensitive parameter. It was found during the program, for example, that moving the injection station from an area ratio of 1.65 in a 4:1 expansion nozzle to an injection area ratio of 1.61 resulted in an increase in C_2 of almost 200%. Injection of the hydrazine mixture at a downstream location, which closely approximates the optimum injection location for a non-reacting type injectant, resulted in low values of lateral impulse corresponding to levels of performance exhibited by non-reacting fluids such as Freon.

As injection location was moved in an upstream position, reacting liquid secondary injection performance increased. This increase in performance was attributed to the decomposition of the secondary fluid and to a possible chemical reaction with the main engine combustion products within the primary nozzle. Color motion pictures were taken of the exhaust patterns during one series of tests. Inspection of these films revealed not only a change in the shock pattern of the exhaust system but a definite change in color of the exhaust system downstream of the injection location. This change in exhaust color and the high performance level are taken to indicate that thermal

decomposition and chemical reaction were occurring within the primary nozzle.

Secondary injection tests were performed with Freon 113 to establish the performance level of typical non-reacting secondary injectants and to provide a correlation with the reacting liquid data obtained. Since the performance of Freon 113 has been documented by several experimenters, it was felt that the Freon tests would essentially calibrate the test equipment and procedures used in the reacting liquid study. Freon 113 test procedures differed from the reacting liquid tests in one respect; the Freon 113 was injected through a constant area injection port and the flow rate was varied by varying injection pressure. Results of these Freon tests are also shown on Figure 6 for comparison purposes. Injection pressures for these tests varied from 500 psig to 1000 psig. A horizontal line is drawn through the Freon data points in accordance with Equation (11). This equation indicates that constant lateral I_{sp} is to be expected at constant injection area. The C_2 value determined for Freon 113 from these tests was calculated to be .12. It should be noted, however, that no attempt was made to optimize injection parameters for a Freon injection system. The Freon was injected at the location and angle which was found to be optimum for reacting liquid secondary injection. It is anticipated that a somewhat higher C_2 value for Freon may be obtained at the optimum injection location for Freon type injectants. The major point of interest is that the level of Freon performance documented is approximately that which is commonly agreed upon by other investigators as typical performance values for Freon type injectants. Thus, this approximate correlation is taken as an indication of the validity of the reacting liquid data and does serve the useful function of providing an index of performance.

Hot gas test firings were conducted in which a micro rocket combustion chamber with a sonic nozzle was used as an auxiliary secondary gas generator. Secondary injection mass flow was varied by operating the micro rocket at various chamber pressures. The same propellant combination (50-50 UDMH - N_2H_4 and N_2O_4) was used in both the primary and secondary engines. Exhaust gases from the secondary micro rocket were injected through a sonic nozzle at an area ratio of 2.25 on the primary engine exhaust nozzle. A photograph of the test installation is shown in Figure 7. Motion picture coverage was also obtained for this test series. Hot gas injection data are shown in Figure 8. At this writing theoretical analysis of hot gas injection is not complete and therefore a dashed line is drawn through the data points of this figure. These tests were somewhat similar to the Freon injection tests in that injection area was constant and flows were varied by variations in injection pressure (i.e. secondary combustion chamber pressure). A major difference is that the injected fluid in this case was a compressible fluid and injected at high temperatures. As can be seen from Figure 8, the hot gas performance level was quite high especially at the larger deflection angles. Apparently a system of this type would be advantageous where large deflection angle capability and/or large average vector deflection angle is required. While such a system as was tested may be preferred in a vehicle where one or both of the fuels are already available, this system may have merit for solid propellant applications. The auxiliary rocket is a source

of hot injection gases and as such can be considered comparable to chamber bleed injection systems. The auxiliary rocket injection system has one major advantage over the chamber bleed systems in that control is obtained by valving the flow of liquid instead of valving hot, erosive combustion chamber gases.

SYSTEM DESIGN CRITERIA

A qualitative understanding of injector characteristics can be inferred from Equations (8) and (11) and from the generalized performance plot (Figure 4). It can be seen from Equation (8) that I_{sp_s} is a direct function of injection velocity. Also, it is seen that the relationship between I_{sp_s} and deflection angle is hyperbolic at a constant injection velocity.

For a given deflection angle then, I_{sp_s} can be improved by increasing injection velocity (Equation 8) and by decreasing injection area (Equation 11). Equation (8) shows however that secondary specific impulse increases to an infinite value as the thrust deflection angle diminishes and injection velocity is held constant. This is an empirical relationship and, as is often the case, must be applied within certain physical limitations. Since secondary stream momentum $(\dot{W}_s/g)V_i$ decreases with decreasing thrust deflection angle (Equation 9), a discontinuity in Equation (8) is expected at a small angle where the secondary stream momentum is not sufficient to penetrate the boundary layer. Therefore, high I_{sp_s} values are not anticipated below the discontinuity at very low thrust deflection angles. Equation (9) indicates that this critical value of secondary stream momentum corresponds to a unique deflection angle for fixed engine conditions and, through changes in $\sqrt{C_2/F_m}$, will have different absolute values for other engine configurations. It is anticipated that secondary injection thrust vector control will be possible for the complete range of small deflection angle requirements although the I_{sp_s} performance at very small deflection angles may be low.

Since the density of a liquid injectant is practically constant, Equation (11) shows that $I_{sp_s} = f(1/\sqrt{A})$. Therefore, from a theoretical basis, I_{sp_s} is independent of deflection angle at a constant area, which is a trend observed in this company's experiments and in the experiments of others.

Certain characteristics of secondary injectant fluids merit discussion when the complete thrust vector control system is considered. Performance capability of the fluid is perhaps of foremost importance, and the value of C_2 (defined in Equation 8) is the most comprehensive index of performance. It appears that reacting liquids offer very definite performance increases (larger values of C_2) over non-reacting liquids. Large C_2 values imply high secondary specific impulse and, consequently, minimum injectant weight at vehicle takeoff. Secondary fluid density must also be considered because of space limitations aboard a vehicle. It appears then that initial injectant selection is a function of C_2 and density of the stored secondary fluid.

Vehicle requirements may also impose other system considerations. The thrust vector control duty cycle must be known in order to calculate secondary injection flow and tankage. System trade-off studies based upon lateral impulse "guesstimates" are frequently analogous to the comparison of apples and oranges. Analysis based upon "rule of thumb" lateral impulse requirements are useful only in that they do establish trends and approximations, provided that consistent ground rules are adhered to.

Thrust vector control duty cycle may also dictate the choice between liquid and hot gas secondary injection systems. If the required duty cycle indicates a large average thrust vector deflection angle ($\bar{\delta} = \frac{1}{T}\int^{T} \delta dt = > 3°$) will be representative of the system, a comparison of the data shown in Figures 6 and 8 will indicate that a hot gas secondary injection system would be desirable, at least from a performance standpoint.

Other system considerations would include items such as system operating pressures, material compatibility and storability of the loaded system. The 50-50 UDMH/hydrazine blend is unique among secondary injectant liquids in that its high value for C_2 (see Equation 8) provides outstanding I_{sp_s} performance at low system operating pressures. Material compatibility and storability characteristics of this storable fluid are well known and do not present undue limitations or unknowns to the system designer.

Comparison of various secondary injection systems with other methods for obtaining thrust vector control is a subject which is sufficiently complex such that separate treatment is justified. A review of secondary injection performance has been presented which provides additional information to be included in individual system evaluations.

CONCLUSIONS

1. The feasibility of a secondary injection system using a reacting liquid capable of generating larger side forces per pound of secondary fluid than comparable non-reacting liquids has been demonstrated. Results of testing have indicated that exothermic chemical decomposition of the selected reacting liquid is possible within the available "stay-time" in a primary nozzle.

2. At constant liquid injection velocity, a hyperbolic relationship between secondary specific impulse and thrust deflection angle has been defined. The relationship is such that secondary specific impulse increases as thrust deflection angle decreases.

3. Classification of secondary injection fluids by secondary specific impulse alone is misleading. The corresponding thrust vector deflection angle for the quoted secondary specific impulse should also be given. A parameter C_2, which is a function of the factors influencing thrust vectoring performance, is defined, and is a more appropriate means of classification.

4. The reactive liquid 50-50 UDMH - N_2H_4 is superior to a non-reactive liquid (Freon 113) on the basis of both C_2 value and

secondary specific impulse, and the performance improvement is sufficient to offset the density advantage of the non-reactive liquid. As an example, optimized Freon 113 performance at thrust deflection angles of 1.5 degrees has been accepted as approximately 100 seconds I_{sp_s}, while the demonstrated reacting liquid performance at the same thrust deflection angle (1.5°) was 400 seconds I_{sp_s}.

5. The performance level for secondary hot gas injection was documented. Combustion products from a secondary chamber were exhausted directly into the primary nozzle. Secondary specific impulse of 250 seconds was obtained at a thrust deflection angle of 5.75 degrees. A hot gas secondary injection system appears to have particular advantages in applications where large deflection angle capability is required.

NOMENCLATURE

A	Injector Orifice Area, ft^2
A_d	Projected Droplet Area
a	Droplet Acceleration
B.P.	Boiling Point, °F
C_d	Coefficient of Drag for Droplet
C_p	Specific Heat, BTU/lb°R
C_1	Constant; Function of Engine and Injection Geometry, and Physical and Chemical Properties of Injectant and Propellants, $(lb/sec^2)^{1/2}$
C_2	Constant, $C_1^2 F_m/\dot{W}_m^2$, dimensionless
D	Drag of a Droplet
F	Force or Thrust, lb
g	Constant, 32.2 ft/sec^2
I_{sp}	Specific Impulse $F_m/\dot{W}_m$, seconds
I_{sp_s}	Secondary Specific Impulse $F_s/\dot{W}_s$, seconds
K	Influence Coefficient, dimensionless
m	Mass, slugs
$\dot{m}$	Mass Flow Rate, slugs/second
n	Total Number of Influence Coefficients, K

P_{c_s}	Secondary Chamber Pressure, psia
P_i	Injection Pressure, psi
P_s	Secondary Stream Static Pressure on Nozzle Wall, psi
r	Radius
r_{do}	Initial Droplet Radius
t	Time
T	Total Time for Thrust Vector Control
V	Velocity, ft/sec
V_i	Secondary Injection Velocity, ft/sec
V_o	Main Gas Stream Velocity, ft/sec
W	Weight, lb
$\dot{W}$	Weight Flow, lb/sec
X	Axial Location in Nozzle
β	Secondary Injection Angle
δ	Thrust Deflection Angle, degrees
ΔH_f	Heat of Formation, Kcal/mole
ΔH_v	Heat of Vaporization, BTU/lb
λ	Burning Rate to Evaporation Rate Ratio
λ_o	Value of λ when $r_d = r_{do}$
ξ	$1/2\ C_d \rho_o A_d$
ρ	Density, lb/ft^3
ρ_o	Density of Primary Stream

SUBSCRIPTS

b	Burning
d	Droplet
f"	Burning in Flame Front
m	Main or Axial
s	Secondary or Lateral

x Direction Parallel to Nozzle Wall

y Direction Normal to Nozzle Wall

REFERENCES

1. Wu, Jain-Ming, Chapkis, R.L., and Mager, A., "An Approximate Analysis of Thrust Vector Control by Fluid Injection", (National Engineering Science Co.), ARS Solid Propellant Rocket Conference February 1 - 3, 1961, Salt Lake City, Utah

2. Benham, C.B., and Green, C.J., "Parameters Controlling the Performance of Secondary Injection", (NOTS), Bulletin of the 17th Meeting JANAF-ARPA-NASA SP Group, May 1961 (Confidential)

3. "Liquid Propellants Test Methods Recommended by the JANAF Panel on Liquid Propellants Test Methods", Johns Hopkins University, March 1960

4. Cuddy, W.A., "Synthesis and Evaluation of High Energy Liquid Monopropellants", Wyandotte Chemicals Corporation, December 20, 1960 (Confidential)

5. Spalding, D.B., and Jain, V.K., "Theory of the Burning of Monopropellant Droplets", (Imperial College, London), Combustion and Fuels Subcommittee - Aeronautical Research Council, ARC 20,176, May 19, 1958

6. Priem, Richard J., "Propellant Vaporization as a Criterion for Rocket Engine Design, Calculations of Chamber Length to Vaporize a Single n-Heptane Drop", July 1957

7. Newton, J., "Secondary Injection for Thrust Vector Control", Research Summary No. 36-9, Vol. 1, April 1 to June 1, 1961, Jet Propulsion Laboratory, Pasadena, California

8. Green, C.J., and McCullough, Foy Jr., "Secondary Injection Thrust Vector Control with Storable Liquids as Injectants", (NOTS) Bulletin of the JANAF-LPG, November 1960 (Confidential)

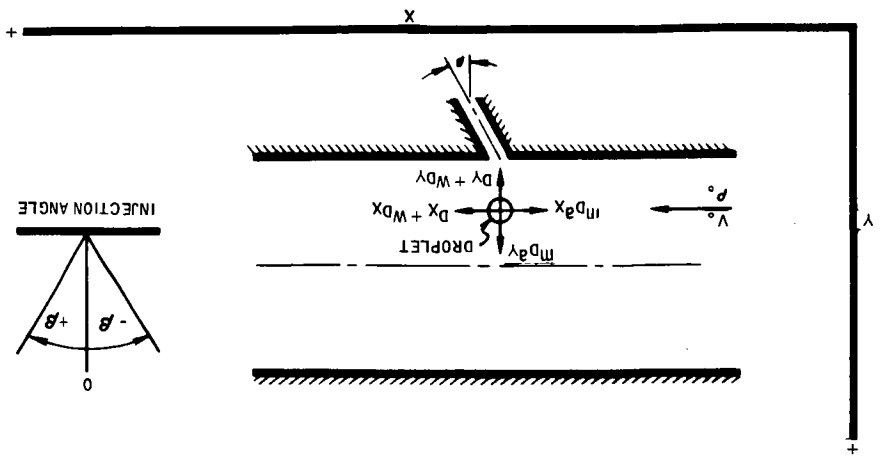

FIG. 1 ONE-DIMENSIONAL MODEL OF SECONDARY LIQUID INJECTION FOR THRUST VECTOR CONTROL

BOUNDARY CONDITIONS CONTROLLING OPTIMUM INJECTION LOCATION

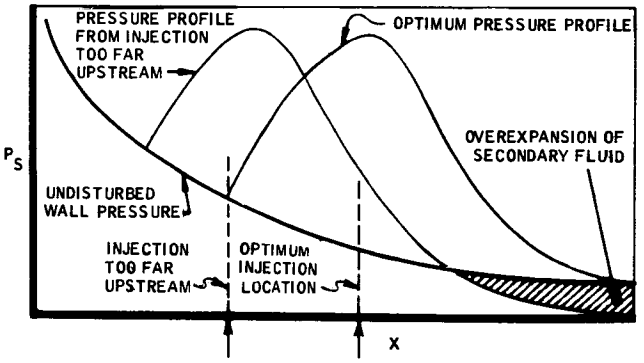

FIG. 2A STREAM STATIC PRESSURE VS. NOZZLE LOCATION

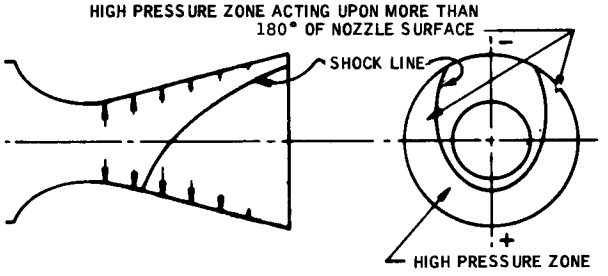

FIG. 2B NEGATIVE HIGH PRESSURE ZONE CAUSED BY EXCESSIVE SHOCK VERTEX ANGLE

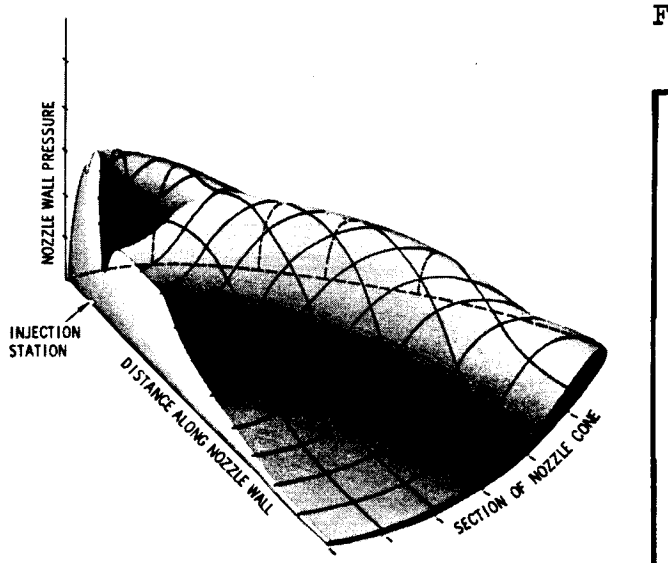

FIG. 3 NOZZLE PRESSURE MAP FOR FREON LIQUID SECONDARY INJECTION

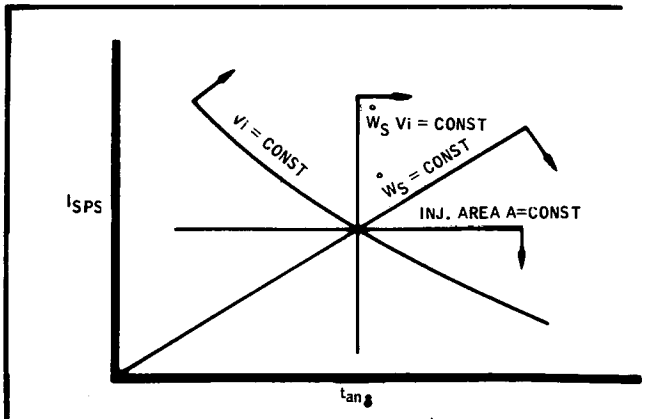

FIG. 4 SECONDARY INJECTION THRUST VECTOR CONTROL GENERALIZED PERFORMANCE

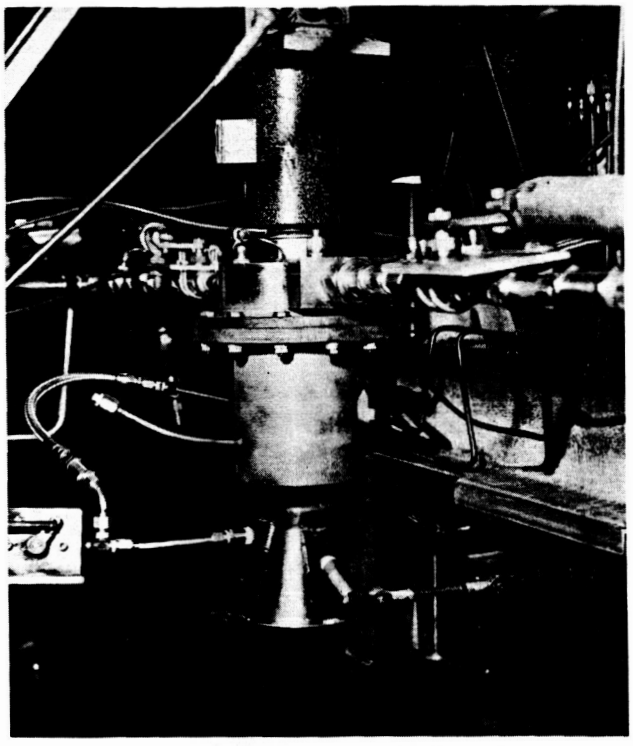

FIG. 5 1200 LB. THRUST ENGINE LIQUID SECONDARY INJECTION THRUST VECTOR CONTROL

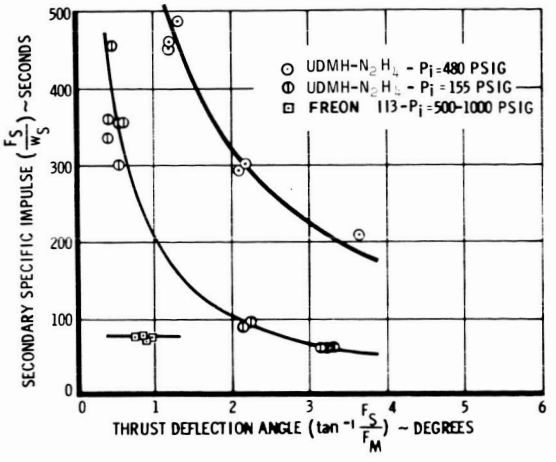

FIG. 6 SECONDARY SPECIFIC IMPULSE VS. THRUST DEFLECTION ANGLE FOR SELECTED FLUIDS

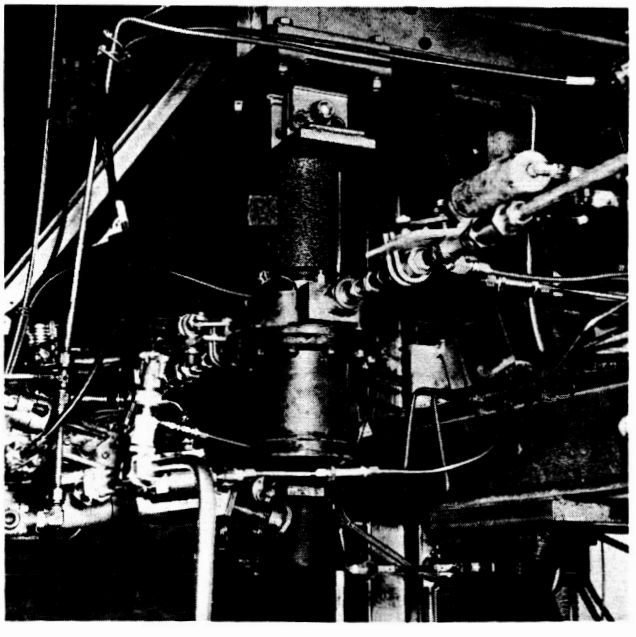

FIG. 7 1200 LB. THRUST ENGINE HOT GAS SECONDARY INJECTION THRUST VECTOR CONTROL

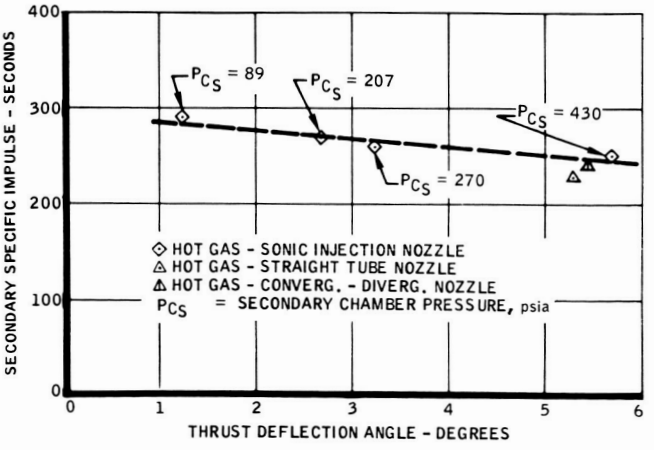

FIG. 8 SECONDARY SPECIFIC IMPULSE VS. THRUST DEFLECTION ANGLE FOR SECONDARY HOT GAS INJECTION

CURRENT NOZZLE DESIGNS AND ADVANCED CONCEPTS FOR SOLID ROCKET MOTORS

H. A. Krayenbuhl and T. O'Callaghan
Aerojet-General Corporation

ABSTRACT

Since the inception of solid rocket motor development, scientists and engineers have made rapid strides in propellant technology, principally increasing specific impulse, a basic parameter of propellant performance. The nozzle designer has had to keep pace with these advances through the development of nozzles capable of withstanding high flame temperatures, chemical attack and erosive environments from metal oxides. This paper concerns the development of nozzles which represent advances in the state-of-the-art, one through an increase in motor size and the other through resistance to an extreme flame temperature. The first part of the paper concerns the design, analysis, fabrication and successful testing of nozzles for motors containing approximately 100 tons of propellant producing 500,000 lb. of thrust for 90 seconds duration. These are the 100 in. diameter giants of the Large Solid Rocket Program. The second part of the paper concerns the new ways for the design of nozzle inserts to withstand flame temperatures from 6150-6600°F, through the use of the slotted washer concept.* This development originated within the Polaris R & D project with the purpose of minimizing thermal stresses.

PART I: DESIGN OF LARGE ROCKET NOZZLES

Introduction The designer of nozzles for large solid rockets was faced with a problem of selecting a system of materials which would withstand the aforementioned severe firing conditions, incorporating throughout a simplicity of design which would render fabrication of the nozzle feasible and relatively inexpensive. The original intent of AGC was to fire several motors in excess of 100 in. in diameter to demonstrate feasibility of the concept. A nozzle configuration was to be selected to give the best possible flow pattern from a standpoint of maximum thrust coefficient and minimum erosion of materials. Materials were to be selected on the basis of past performance, reliability, and ease of fabrication. The design redundance was to be used whenever possible to ensure successful firing. TVC was not a requirement on the first feasibility demonstration motors. (The valuable assistance of S. J. Williams and A. F. Oberta in the preparation of this paper is gratefully acknowledged).

General Description of Nozzle Design In view of the above design criteria a single nozzle configuration with a "conventional" approach to component design was chosen. By conventional it is meant that the throat assembly, from inside to outside, consists of a heat sink, insulation material and structural support. The exit cone consists of an ablating liner and a structural support.

Aerojet's vast experience in other past and current solid rocket program was invaluable, a careful study of which basically determined the final design and materials selection. In the throat section the heat sink is

* A Patent Application is in process in connection with the slotted washer concept disclosed in this paper
(F. J. Climent as assignor to the Aerojet-General Corporation)

graphite, protected from initial thermal shock on the inside by a coating of zirconium oxide. The graphite is in two sections, an entrance cap extending far down into the closure, and the throat insert. The insulator between heat sink and structural material is an overwrap of asbestos tape-phenolic resin. The structural material initially was heat treated 4130 steel.

In the exit cone the ablative material is high silica cloth tape pre-impregnated with phenolic resin wrapped so that the layers are parallel to the motor centerline. The structural material is normalized 4130 steel.

The throat section and exit cone assembly are fabricated separately from each other, the final assemblies being bolted together at a joint just aft of the graphite throat.

Gas Flow Considerations For optimum flow characteristics the single nozzle configuration was the obvious choice. An important factor in efficient flow is the selection of the radius of curvature of the throat section. This determines the rate at which the gases converge and is definitely dependent on throat diameter. A "low rate" or gentle convergence reduces turbulence, thereby increasing nozzle efficiency and permitting boundary layer buildup to reduce erosion. For small nozzles with throat diameters of eg., 1 - 6 in., by a coefficient, is generally 1.5 - 2.0 times the throat radius. As the diameters increase, the coefficient will decrease. For example, for a diameter of 25 in. radius of curvature of .75 times throat radius allows a slower rate of conversion than a 4 in. nozzle with a 2 R_t radius of curvature. Therefore, the design of larger nozzles (diameters upwards of 20 in.) a radius of curvature of .5 to .75 R_t was used.

In light of the design criteria established, a contoured exit cone, although necessary for optimum flow conditions, was not considered feasible for the first firings because of the additional expense in fabrication. A conical exit cone with a half angle of 20° was selected as a compromise between fabrication cost and performance. The smaller the half angle (to about 15°) the higher the nozzle coefficient, the larger the half angle (to about 28°) the shorter the length and therefore, the less expensive it becomes.

Test results indicated that flow conditions in the nozzle were excellent. Nozzle efficiency (percent theoretical nozzle coefficient) varied between 98 and 99%.

COMPONENT DESCRIPTION

We shall now turn to a detailed discussion of the design of each component.

Entrance Cap and Throat Assembly The basic consideration in selecting a graphite for the heat sink was availability. There was a very small choice of graphites available in the diameters required. Most of the graphites made in large sizes were used in electrodes and bearings. The procedure was to obtain the pertinent properties of the candidate graphites and determine which grade would best meet the requirements of the thermal stress analysis and a predicted erosion study.

In the final analysis the grade selected was shown to be acceptable for

durations up to 60 seconds; the longest firing time of the first five motors to be fired. Past experience with the particular graphite on smaller throats indicated that it had fair erosion resistance.

Test results of the graphite when fired in the large scale units were gratifying; there was little or no deterioration of the entrance cap and the slight erosion in the throat amounted to no more than 1% increase in total area of the throat, with a maximum flame temperature of 5450°F, and durations of 40 to 60 seconds.

In selecting the material for the entrance cap, it was quite apparent that in the lower mach number regions, where heat input was rather low, it was not necessary to provide as high a grade of graphite as for the throat insert. Although at first it appeared that size would be a problem, once the graphites were evaluated on the basis of acceptable thermal stresses, it was found that available sizes and grades were adequate to do the job. As durations were increased, the strength levels of the graphite had to be improved which meant planning ahead and ordering the highest quality of graphite available in the sizes necessary to ensure structural adequacy in the entrance cap and throat insert. Even though the entrance cap does not encounter the thermal stress problems that the insert does and may therefore be of lower quality graphite, all the necessary precautions are taken in the design of this part as well. The design of both entrance cap and throat insert are interconnected from fabrication and thermal expansion standpoints. The throat insert and entrance cap are intentionally made in separate pieces; the joint between the two pieces (Figure 1 showing detail) is precut to precise dimensions to ensure that, as the throat insert expands axially forward in the motor due to thermal expansion, it will not break or cause the entrance cap to fail due to excessive loads. The gap between the two faces is filled with a material which deteriorates with increasing temperature, thus giving the insert room to expand. Fabrication of the insert assembly begins with the machining of the joint between the entrance cap and insert. The two pieces are mated and the O. D. is final machined.

The outer cylindrical portion of the entrance cap graphite is now overwrapped with a high silica cloth impregnated with phenolic resin to increase the effective diameter and to afford mechanical retention to the outside diameter of the graphite. The entire assembly is overwrapped with .25 - .4 asbestos tape preimpregnated with phenolic resin. This overwrap provides the insulation between the heat sink and structural material and also ensures a tight bond on the graphite insulator interface, preventing gas leak paths thru the assembly to the exit cone. To further guard against gas leakage, the entire insert assembly is bonded into a tapered steel case. The bonding agent used is a somewhat flexible epoxy resin. The graphite is then coated with .040 in. of flame sprayed zirconium oxide. Ejection loads, which are quite severe due to the large forward area of the graphite exposed to the high pressures within the chamber, are borne by the tapered steel shell and by a steel stop extending up over the aft end of the graphite. To date, five motors have been successfully test fired using this concept in sizes ranging from throat diameters of 17 to 28 inches. Two of these were sub-scale 65 inch diameter motors and the remainder were full-scale 100 inch flight-weight hardware. In only 1 instance was cracking observed in the insert, this was in the aft end and was determined to be due to water quenching on shut-down.

The graphite insert acts as a heat sink to abosrb the heat transferred

from the exhaust gas, and in so doing undergoes a severe temperature change throughout the firing. Through the combined effect of this heat sink and the excellent insulative properties of the asbestos tape wrap, the temperature of the steel structure does not rise significantly during the firing. The first indication of heat penetration occurs several minutes after firing when the paint on the steel shell begins to discolor.

Heat Transfer Heat transfer has not been a severe a problem as in smaller motors, due to the large diameter which reduces film coefficients. There are no protuberances or discontinuities within the nozzle, and the heat transfer problem may be analyzed using basic pipe flow techniques. Film coefficients range in the neighborhood of 300 - 800 BTU/hr.ft^2°F, depending on the surface temperature, chamber pressure and location in the nozzle, and the effective increase in the driving temperature. The temperature distributions through the nozzle are determined with the aid of the IBM 7090 computer, which permits rapid solution of the transient heating problem, taking into account the change in thermal properties with temperature (graphite thermal conductivity decreases by a factor of five over its operating range while its heat capacity triples), the material loss due to ablation and erosion and variance in heat input throughout the firing. The results of such an analysis are shown in Figure 2 and 3, one showing the temperatures at the end of firing for a typical nozzle design, and the other showing the temperature as a function of time for the inner and outer surfaces of the graphite and asbestos tape. Note the lower curve rises but slightly, indicating the superb insulating qualities of the asbestos wrap. Note also the slight drop in surface temperature toward the end of the run, due to a regressive pressure curve which reduces heat input toward the end of firing.

One of the "gray areas" of the thermal analysis is the prediction of the behavior of the ZrO refractory coating. This material has a melting temperature of 4500°F; however, it is undoubtedly true that mechanical effects have a great deal to do with its removal. Erosion by solid particles and degeneration of the bond between the graphite and the ZrO both tend to remove the coating much sooner than the time predicated on pure ablation. The determination of these mechanical effects is currently under study at AGC.

While design of insert assembly was relatively straight forward from a thermal analysis standpoint, the thermal stress problem in the graphite throat insert proved to be more complicated, particularly with the advent of 90 and 120 second firing durations and higher flame temperatures, which was increased to 5890°F from 5450°F. Thermal stresses in the graphite insert are due to three causes: gradient, restraint, and internal pressurization. Let us examine each in detail.

Gradient stress is due to the temperature differential between the inner and outer surface, where the inner (hotter) material wants to expand and is restrained by the outer (colder) graphite, thereby producing a compressive stress on the inside of the piece, and a tensile stress on the outside. The magnitude of this gradient stress is sufficient to crack the graphite per se in some cases.

If the insert is restrained as it is in this case by the asbestos tape and steel, an additional compressive stress will be set up throughout the graphite. It attempts to expand overall due to the increased mass mean temperature, but the movement is retarded by the backup.

The pressurization stress is due to the gas pressure within the nozzle and produces a tensile stress throughout the wall. The stress is minor in relation to the other two.

The above three stresses add algebraically to give the net stress through the graphite structure. These stress values are obtained by means of a computer program which solves for the stresses by matching displacements at the interfaces, treating the structure as a set of semi-infinite concentric cylinders. A typical curve of hoop stress vs temperature is shown on Figure 4, along with the allowable stress-temperature curve for the candidate type of graphite. One should realize that the data for the allowables at the upper end of the curve represents an approximation of a wide spread of data and failure may depend upon where a particular piece of graphite falls. Note the increase in compressive stress caused by the extended duration and increased flame temperature. Note also the slopes of the allowable curves and predicted stress curves in the region in question. A slight increase in surface temperature widens the margin between the two curves considerably. In order to bring the stresses back within range of the allowables, design changes must be made to reduce the gradient and/or the restraint. Unfortunately, assuming a relatively rigid backup, reducing thickness of graphite to relieve gradient stress increases restraint stress, as a smaller piece of graphite must absorb the same amount of heat, thereby increasing the mass mean temperature and expansion. This also increases the initial tensile loads on the outer surface. The situation is aided to some extent by the fact that tensile stresses reach their maxima early in the run, while compressive stresses are minimized somewhat later. The present design approach therefore, is to provide initial restraint to the graphite to reduce initial outer tensile stress by either a steel band or by a wrap which then allows expansion at a precalculated time, when the inside compression approaches the allowable compressive stress later in the run. This expansion may also be controlled by the introduction of a light crushable material or structure. It should be remembered that in no case do any of the backup materials receive enough heat to cause structural problems, this being blocked by the asbestos wrap. A similar design was successfully tested on one motor where a gap was machined in the end of the insert allowed controlled expansion and kept inner compressive and outer tensile stresses within allowable limits.

As firing durations and flame temperatures increase, the utility of graphite for inserts reaches its limit due principally to gradient stress. A way must therefore be found to either reduce the surface temperature or to increase the conductivity of heat through the insert through a design innovation or improved material properties, principally conductivity and allowable stress.

Exit Cone Assembly The material chosen for the ablating portion of the exit cone assembly was a silica cloth-phenolic resin system. There was considerable experience at Aerojet with this system, in both molded and tape wrapped forms, with results indicating, in general, excellent reliability and very good erosion resistance.

The mechanized tape wrap method, then recently developed, was used for fabrication since matched die molding was economically unfeasible for such large, one-of-a-kind items. Furthermore, erosion resistance of a tape wrapped part is equal to or greater than a high pressure molded part.

[redacted]

onjecture in tape wrapped parts is the angle at which the tape is . It is generally conceded that as the angle formed by the tape and the .. line of the cone increased more toward 45°, the erosion resistance also increases, as doesthe cost (due to the necessity of using the more expensive bias cut tape) and the strength of the part decreases. We chose the 0° angle or parallel to centerline wrap because of the increased strength and minimum cost.

Fabrication of the part involves the mechanized wrapping of the tape on a steel mandrel and curing at approximately 300°F in an autoclave. It is significant to note that the erosion resistance is very much dependent on the density of the part. The density in turn is dependent on the manner in which the tape is wrapped and the fabricator's know-how in the staging and curing of the phenolic resin.

Thickness of the ablating liner was determined by a study of erosion results of other firings which used a single nozzle configuration, being careful to allow for differences in mass flow, flame temperature, and percentage of aluminum content. On this basis a predicted erosion contour for our case was calculated and a safety factor added to arrive at the final thickness of the cone.

The finished liner is bonded into the structural shell of the exit cone with an epoxy adhesive. Redundant O-ring seals are utilized between the liner and steel to prevent gas leakage between the two parts. Further redundancy is added by bolting a retaining ring to the aft end of the cone to prevent ejection of the cone should there ever by gas leakage between the liner and steel.

Four of the five motors test fired in the program embodied this method of fabrication and were completely successful. The removal of the liner material is very even around the nozzle and appears to follow an orderly procedure. The surface rapidly rises to the ablation temperature, the resin evaporates, the silica fibers are melted and swept away by the gases and solid particles. Immediately below the ablating surface a char layer, some .2 in. thick, is formed and moves outward with the receding surface.

Due to the excellent reproducibility on the successful firings, it would appear that increased durations might be withstood by increases in thickness; however, mass ratio requirements have spurred the search for materials with better erosion resistance such as graphite cloth or carbon cloth, to be used as inserts in the high erosion areas. These materials have seen use in the industry, but due to the additional expense of the cost of the basic material plus fabrication techniques, their application has been limited to the most necessary of cases. Increased conductivity of these materials raises interface temperature, thus compounding bonding problems. However, for long firing durations on the order of 120 seconds, the decrease in erosion rate may mean a weight saving of 3 to 4 times over using only high silica cloth and phenolic resin for this part.

[redacted]

PART II: THE SLOTTED WASHER THROAT CONCEPT FOR SOLID ROCKET NOZZLES *

Introduction and Problem Statement. In the preceding part of this paper a presentation was made of the developmental steps necessary for the reliable design of a single graphite nozzle for application to a large solid rocket motor where thrust vector control was not a requirement and propellant flame temperature was not in excess of 5890°F. In the remainder of the paper we will confine our attention to nozzles whose throat diameters are by comparison smaller; individual small nozzles are used for example on the POLARIS missile where the thrust vector control requirements are met by using one pair of nozzles to control pitch, the other pair to control yaw. These smaller nozzles will, of course, on their inner periphery, be subjected to a hot environment similar to that in the nozzles of a large rocket motor; however the severity of exposure, as measured by erosion or plastic flow, and the actual heat transferred will vary from one motor type to another depending on the flame temperature of the propellant used, on the chamber pressure and on the relative dimensions and physical properties of the nozzles. When a given material, such as graphite, is employed for a throat insert of a small nozzle, the erosion characteristics are much more detrimental in altering the ballistically significant throat area than when the same material is used for a large nozzle. This is a consequence of the fact that for equivalent exposures the depths of erosion will be the same in both instances but the percentage increase in throat area will be more marked in the case of the smaller nozzle. Ballistic design trade-offs and grain configuration requirements in the case of the POLARIS motors cannot tolerate any substantially large change in throat area. The use of more massive nozzle throat inserts in an attempt to keep the graphite cool and thus assist in reducing erosion is also not feasible because of space limitations.

It should be stressed that while the new concepts presented here have been developed in connection with small high temperature nozzles they are also fully applicable to large nozzle designs although cost considerations may not warrant this application.

In the POLARIS program initial effort on the A-1 missile was directed toward graphite nozzles, later endeavors to the development of molybdenum nozzles, which were then used exclusively on the A-1 and A-2 flight designs. The concurrent development of high specific impulse propellants for use with the A3 missile meant that higher flame temperatures would have to be practicable if the greatest benefit of the increased specific impulse of these propellants was to be obtained. This meant, in turn, that rocket parts exposed to the gas would be subjected to higher temperatures and that thermal stresses could be extremely critical in accommodating a reliable operating transient temperature range.

Among the refractory metals, tungsten is at present the only proven material capable of withstanding these temperatures while at the same time

* A patent application is in process in connection with this concept (F. J. Climent as assignor to the Aerojet General Corporation). Contributors to this section are F. J. Climent and T. O'Callaghan.

providing a suitable aerodynamic throat contour. The refractory metals have, of course, the disadvantage, in one sense, of having a high specific gravity so that in selecting them as against graphite and its concomitant large erosion a trade-off study in missile range must be made to assure a proper application. The high specific gravity does of course help to increase the heat sink effect of the insert and in this sense it acts beneficially.

Even with solid tungsten throat inserts structural failures have occurred as a result of the very severe firing conditions; the number of these failures has however been decreasing with constant improvements in tungsten material properties. Post-firing inspections of some insert designs used on the POLARIS missile have shown cracking in directions perpendicular to those of the principal stresses, particularly on the outer surface of the throat insert (Fig. 6). Thus the longitudinal stresses initiate circumferential cracks and the hoop stresses cause cracks in the meridional planes. On occasion, when the cracks are sufficiently severe, such a nozzle throat insert may be ejected, especially when the cracks extend all the way from the outer to the inner surface.

Advantages of the Split Washer Design Concept. In view of the difficulties mentioned above, the idea was conceived of "pre-cracking" the tungsten throat inserts by assembling them from:

Suitably machined tungsten washers (Figs. 7b and c), or from

Split washers, i.e. open rings (Fig. 7d).

Advantages envisaged for these design concepts were as follows:

(a) By splitting the throat inserts into a series of narrow full-ring type washers with longitudinally contoured internal surfaces (Fig. 7b) the longitudinal stresses can, for all practical purposes, be eliminated. This has the subsidiary advantage in the tensile region of raising the level of hoop stress necessary to cause meridional cracks. The full ring washer concept theoretically reduces both the hoop and radial thermal stresses also and therefore, a priori, reduces the chances of further cracking due to high hoop loads. If the mechanical properties of the insert (Young's Modulus, E, and the coefficient of expansion, α) were independent of temperature then the radial and the hoop stresses in a radially unrestrained insert would, for example, be reduced by 100ν %, where ν is the Poisson's ratio of the material (for tungsten about 0.3). Mathematically this may be seen from the fact that when a thermal stress problem has been solved for "plane strain" conditions the solution for "plane stress" conditions will be found by multiplying the radial and hoop stresses of the "plane strain" solution by $1-\nu$. In this context the "plane strain" solution is applicable to a long insert, the "plane stress" solution to an axially short insert of washer type. Even with practical material properties, which vary with temperature, this benefit is still to be expected with washers since some mechanical constraints have, in effect, been removed from the system. This is borne out by the stress calculations, the results of which are presented graphically in Fig. 8; in practice the stress distribution will not be as severe as that depicted since plasticity effects on the inner portion of the insert will change the overall stress distribution.

(b) Pre-splitting the throat insert into an assembly of circular washers has the advantage that under the partially reduced stresses the parts can remain locked in position, a feature which is not necessarily present when thermal stress is allowed to take its course and crack the solid insert more randomly during the firing. The chances of portions of washer type inserts being ejected during firing are very much less, provided the washers are not severely overstressed, since the "packing" restraint of the immediately adjacent uncracked washers prevents this. In the designs evaluated to date on full-size POLARIS nozzles all washers used have been encased by ZTA type graphite for axial support.

(c) The benefits to be gained by the use of washer type throat inserts can be considerably enhanced by splitting the circular washers themselves, e.g. by giving them the appearance of radially thick piston rings (Fig. 7d). Whilst in going from a solid throat insert to a full washer type insert a stress reduction of about some 30% can be attained for the hoop and radial stresses, an even greater and very significant reduction of the absolute stress values can be accomplished by splitting the washers radially. This is indeed the major breakthrough in nozzle insert design since it allows all the stresses to be reduced to a very low level. To prevent any axial flow of gases which would interfere with the aerodynamic efficiency of the nozzle the radial split in one washer is arranged to face a solid portion of the two neighboring washers.

The 30% stress reduction which can theoretically be effected by using unrestrained circular type washers can in practice only be realized if the isotherms at any given time in a solid insert all lie parallel to the nozzle axis. Splitting a solid insert into washers means that, unless special measures are taken to facilitate axial heat flow, local hot spots and excessive plasticity may occur at the internal surface where previously the presence of some axial heat flow assisted to alleviate overheating. In the designs under investigation at Aerojet General Corporation thin copper spacer-washers have been placed between the tungsten washers for the express purpose of facilitating axial heat flow so that full benefit can be gained from the "plane-stress" design.

A comparison of hoop stresses in the various types of inserts is shown in Fig. 9 assuming for ease of analysis in this instance that the insert mechanical properties do not vary with temperature. This superposition of results brings out clearly the superiority of the split washer design.

Methods of Stress Analysis. To calculate the stresses in the various types of inserts it was assumed that elastic conditions prevailed throughout and that no plastic deformation occurred. This assumption was rendered necessary, in part, by the dearth of meaningful data on tungsten at high temperatures and at high strain rates. The particular mechanical data used to represent E and α as a function of temperature are shown graphically on Fig. 10. Another assumption made in deriving the results is that the inserts were radially unconstrained. The following stress analysis techniques were employed.

(1) In the plane strain solution for solid inserts the insert was considered as a very long cylinder and allowance was made for the variation

both of Young's Modulus, E , and of the coefficient of thermal expansion, α , with temperature. A computer program was written to determine hoop, axial and radial stresses and strains based on the stress function type of solution presented by Stansic and McKinley[1]; the differential equation of the stress function was solved by a general FORTRAN computer technique developed by R. D. Glauz for second-order differential equations[2]. In the stress program polynomial functions of temperature were used to represent E and α and the temperature variation through the thickness of the insert was programmed to be input as data in either of two ways: a) as a logarithmic or other differentiable function of the radius, or b) as temperature data at discrete, equally spaced, radial points. The latter technique will be used in conjunction with temperature outputs from the Lockheed Thermal Analyzer Program[3].

Another computer program was written to allow for the additional variation of the Poisson's ratio, ν , with temperature. This program was based on the concept of splitting up a solid insert into a series of several concentric isothermal cylinders, allowing these cylinders to expand freely to their final temperature and then introducing axial forces and radial pressures on each cylinder to so alter their shapes that they could be re-assembled without radial interferences or mutual axial overhang.

These computer programs were checked out with numerical solutions presented in the literature inter alia by Geckler[4] and by Stansic [1] for Poisson's ratio values of 0.5 and 0.25, respectively; excellent agreement was obtained.

The influence of small Poisson's ratio variations on the stress levels was found to be insignificant so the stress function technique of Stansic was used in computing final results. Some other work on the stress analysis of tungsten inserts allowing for variable mechanical properties has been presented by Vigness[5,6]. At time of writing an additional computer program is being written to estimate the effects of possible radial restraints on the stresses generated in solid inserts with variable mechanical properties.

(2) Stress analysis of washers was accomplished by means of the isothermal concentric cylinder concept, touched on above, with the difference that no axial forces were introduced, i.e. a plane stress solution was used. It was thus possible to allow for the temperature variability of mechanical properties (E, α , ν) in the program. Possible buckling of the washers under a radial temperature gradient, a subject treated by Queinec[7], was not taken into account in these calculations; this phenomenon was however observed in one of the full scale firings.

(3) Stress analysis of split washers was, in the case of the original concept, based on constancy of mechanical properties with temperature since the boundary conditions and the conditions for the ready application of St. Venant's principle impose mathematically rather stringent requirements. The stress equations of Boley[8] were programed for linear temperature gradients in the split washers and excellent agreement was found with the dimensionless results presented by him.

One other factor was not allowed for in preparing these computer programs and that is the fact that energy is necessary to make the inserts

deform under the thermal gradients. Since this energy must be supplied by the original heat input at the inner surface of the insert it means that the temperatures actually occurring in an ideal insert would in fact be less than those derived from the Lockheed Thermal Analyzer Program and resultant stresses would also be less. The magnitude of this effect has not been estimated; however, it should ultimately be possible to include it in a combined heat transfer and thermal stress analysis computer program.

Synopsis of Firing Results. Eight nozzles incorporating some of the design features enumerated above have been evaluated on three full-scale second stage POLARIS A3 firings. Seven of these nozzles had only one fully circular tungsten washer, the thickness of which ranged from 0.170" to 0.500". The eighth nozzle used had a throat insert consisting of two fully circular tungsten washers, each 0.170" thick, separated by a copper washer 0.003" thick. Tungsten densities ranged from 95 to 99% of theoretical. In all instances the washers were embedded in either ATJ or ZTA graphite. Although the theoretical flame temperature of the propellant used was 6180°F, the erosion, as measured by the percentage increase in throat area, lay in the 2.5 to 6.5% range, i.e. only about 1/5 of the minimum erosion that might be experienced with a graphite nozzle of the same size at a similar temperature.

Whilst an evaluation of the split washer concept was not originally planned in connection with these initial subscale firings, one of the inserts in a single insert throat design was observed to be partially cracked in the meridional direction in at least three places on the outer surface before the firing. A companion nozzle, also with one washer type insert, cracked during the firing. Post-firing examination of these washers indicated that they remained topologically intact throughout the firing.

In no instance was a washer type insert ejected during a firing. Plastic flow was evident at the inside surface. Partial recrystallization and some grain growth was also observed at this flame surface. Erosion of graphite used to retain the washers was severe in some instances, up to 70% by area upstream of a washer and 40% by area downstream. Firing durations exceeded 75 seconds and chamber pressures were about 275 psia. Figure 11 is a schematic of one of the full-scale nozzle designs evaluated.

To date, only one subscale nozzle has been fired to specifically evaluate the split washer concept. A cross-section of the nozzle is shown in Fig. 12. In this instance seventeen tungsten washers, each 0.100 in. thick were stacked together with interspersed washers made of .002 in. copper strip. In the firing propellant flame temperature was about 6540°F, chamber pressure about 500 psia, and firing duration 8 sec. Erosion, as measured by increase in throat area after the firing, was found to be negative. The original throat diameter of 1.900" increased near the location of the split to 1.902" but it was 1.876" in other locations. Splitting of the washers occurred on disassembly as evidenced by the fresh nature of the exposed surfaces.

These test results confirm our belief in and bear out the great potential for the split washer concept in the POLARIS program. The concept is significant not only for new designs but also as a remedial measure for upgrading existing hardware with but minor modifications.

REFERENCES

(1) Stansic, M. M. and McKinley, R. M. "A Note on Thermal Stresses in Hollow Cylinders," Ingenieur-Archiv, XXVII (1959), pp. 227-241.

(2) Glauz, R. D. and Bender, E. "DIFF 2 - Second Order Differential Equation Solver Using Sixth Differences," Computing Services Division, Aerojet General Corporation, Sacramento, California.

(3) Fick, J. L. and Abrahams, R., Lockheed Missile Systems. "Lockheed Missile Systems Version of Thermal Network Analyzer Program," (Dept. 59-12, Building 102B, Lockheed, Sunnyvale).

(4) Geckler, R. D. "Thermal Stresses in Solid Propellant Grains," Jet Propulsion, February 1956, pp. 93-97.

(5) Vigness, I. "Thermal Stress Transients in Nozzles," NRL Project 62R05-19B, Technical Memo No. 157, Shock and Vibration Folder No. 908 (S.P. Task Assignment 71402, Project Order 970, 30 June 1961).

(6) Vigness, I. and Clements, E. W. "Thermal Stress Transients in a Flat Slab," NRL Project 62R05-19B, Technical Memo No. 179, Shock and Vibration Folder No. 908 (S.P. Task Assignment 71402, Project Order 970, 30 November 1961).

(7) Queinec, Alain. "Thermal Buckling of Centrally Heated Circular Plates," Stanford University, June 1961, Contract AF49(638)-223.

(8) Boley, G. A. and Weiner, J. H. "Theory of Thermal Stresses." John Wiley and Sons, Inc., New York 1960. Library of Congress Catalog Card Number 60-6446.

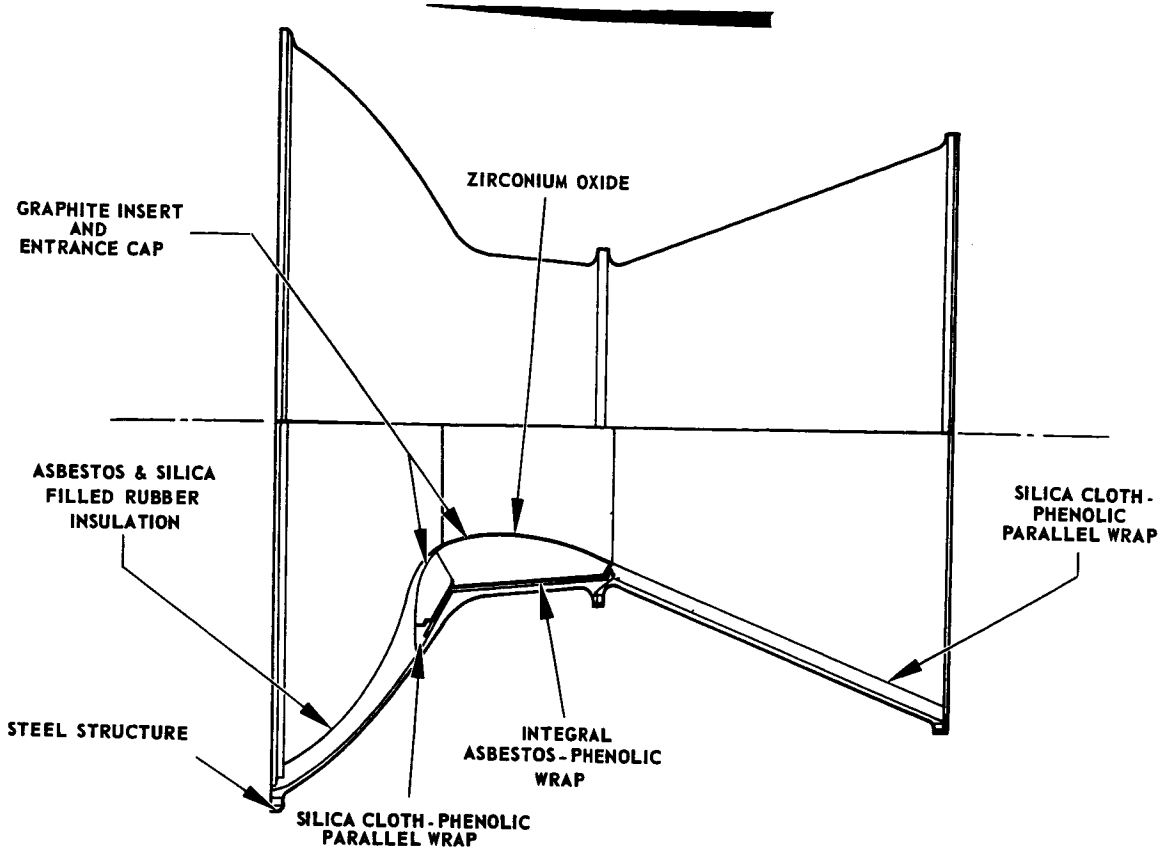

FIG. 1 TYPICAL 100 IN. DIAMETER MOTOR NOZZLE

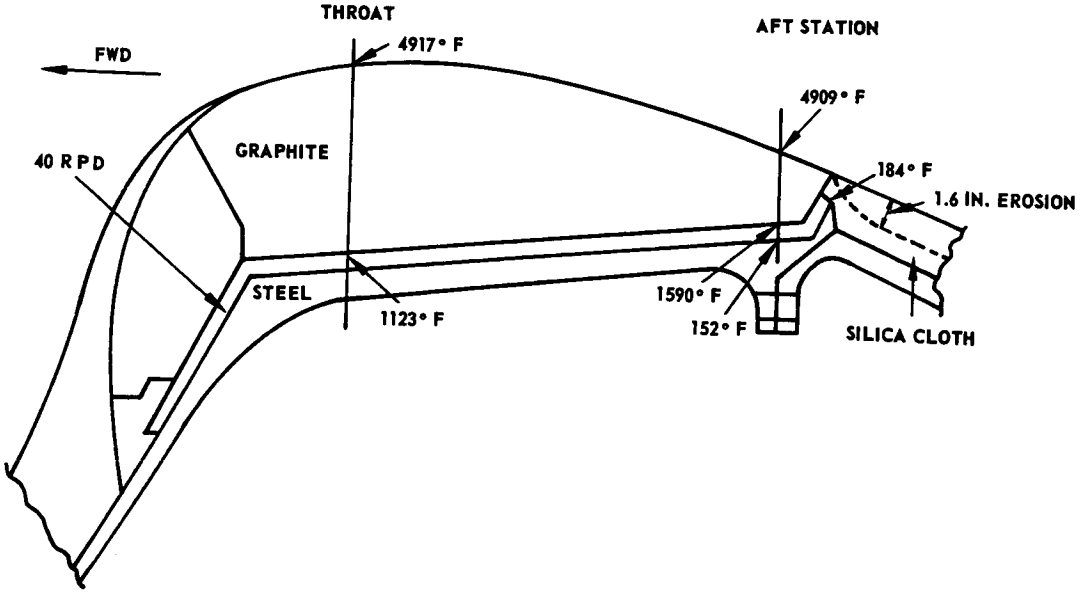

FIG. 2 TEMPERATURES AFTER 93 SEC. OF FIRING

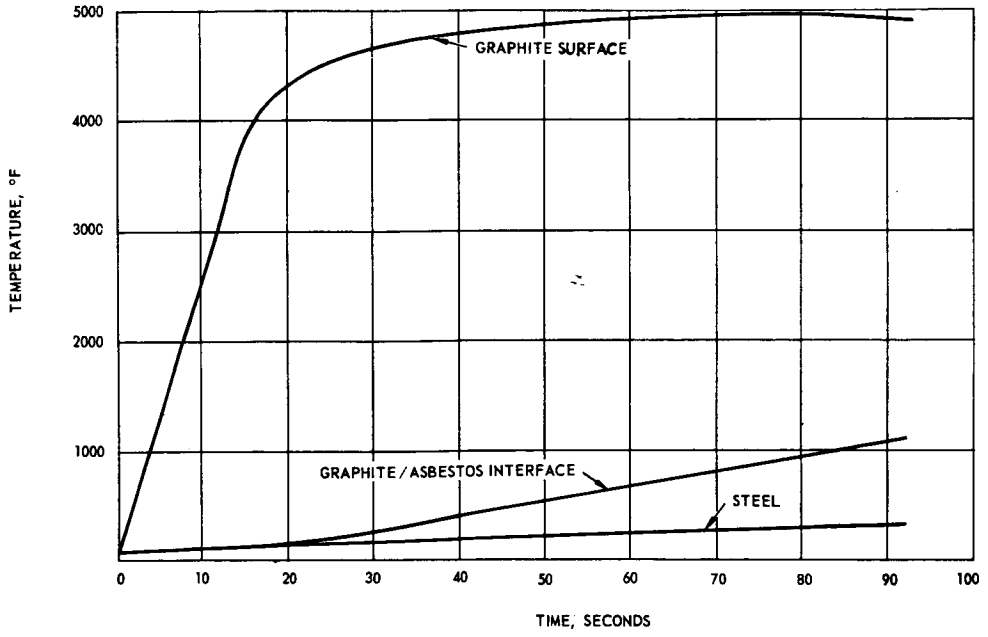

FIG. 3 TEMPERATURE VS TIME FOR THROAT STATION

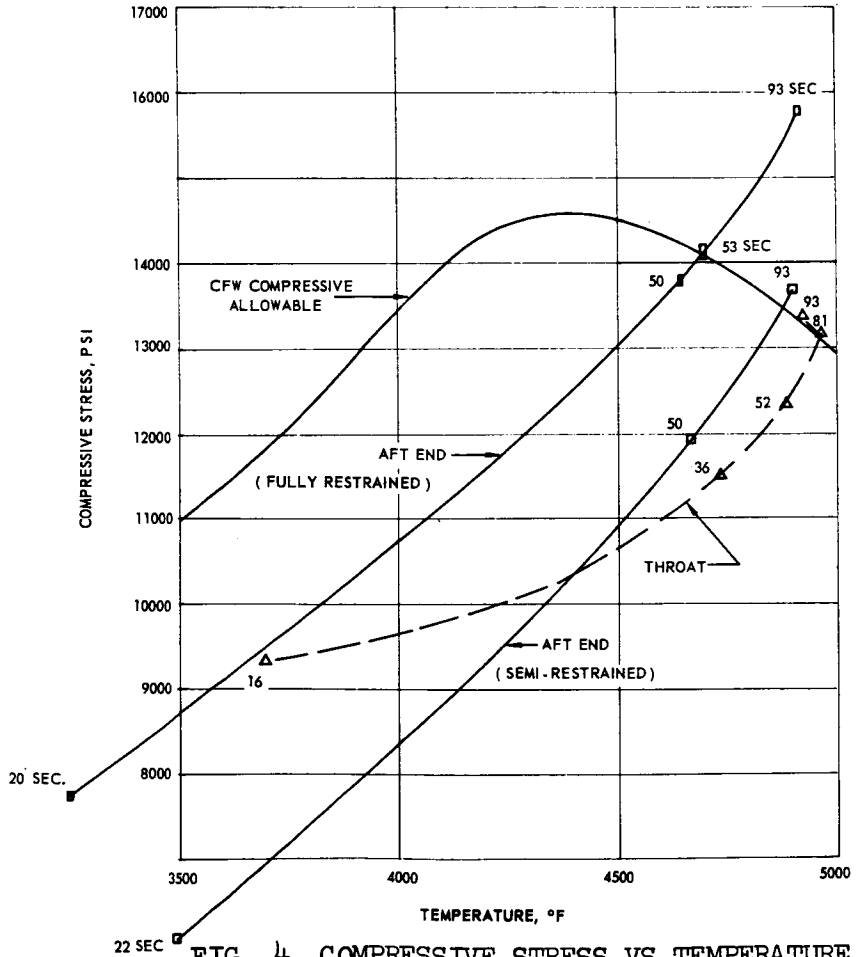

FIG. 4 COMPRESSIVE STRESS VS TEMPERATURE
(Inner Surface of Graphite)

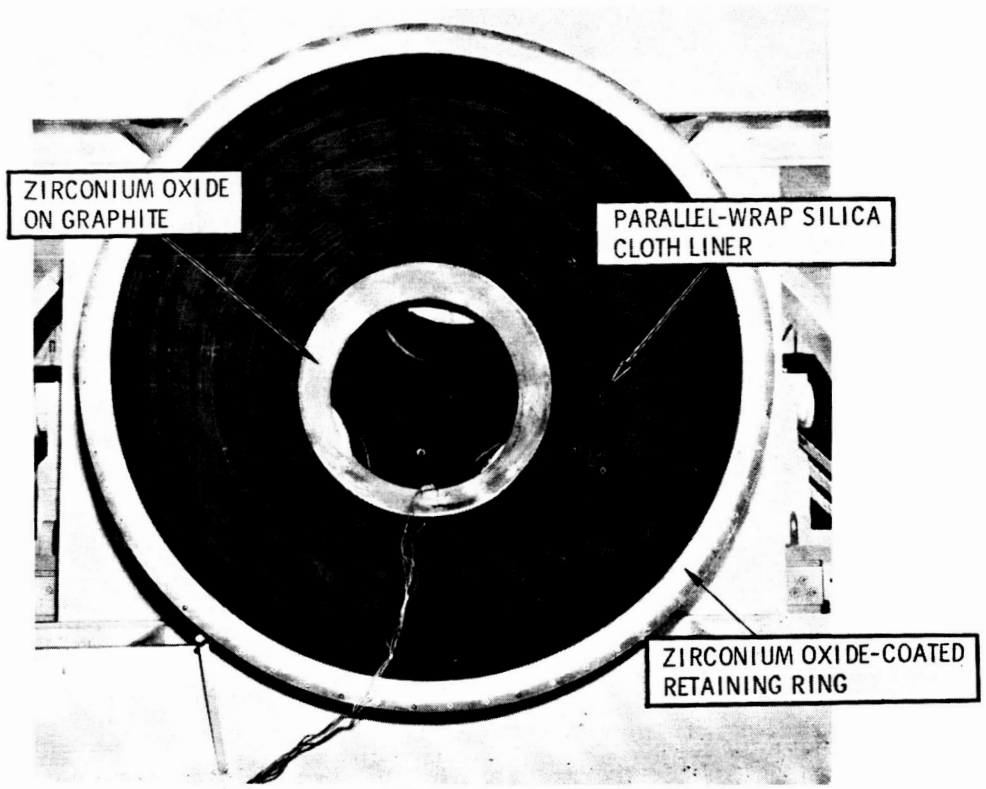

BEFORE FIRING

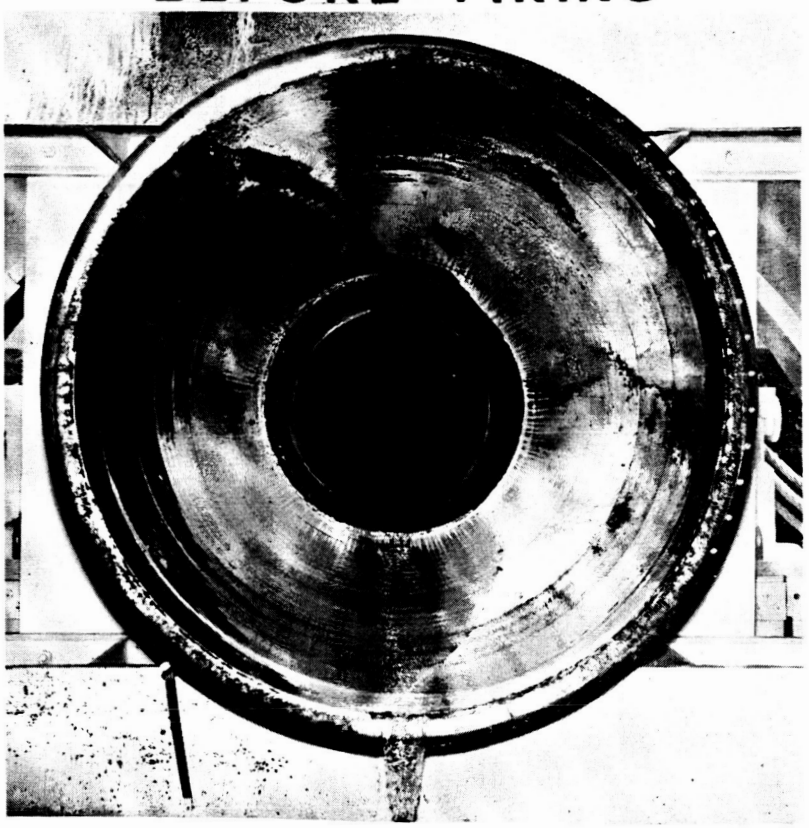

AFTER FIRING

FIG. 5 VIEW FROM AFT END OF CONE, BEFORE AND AFTER FIRING

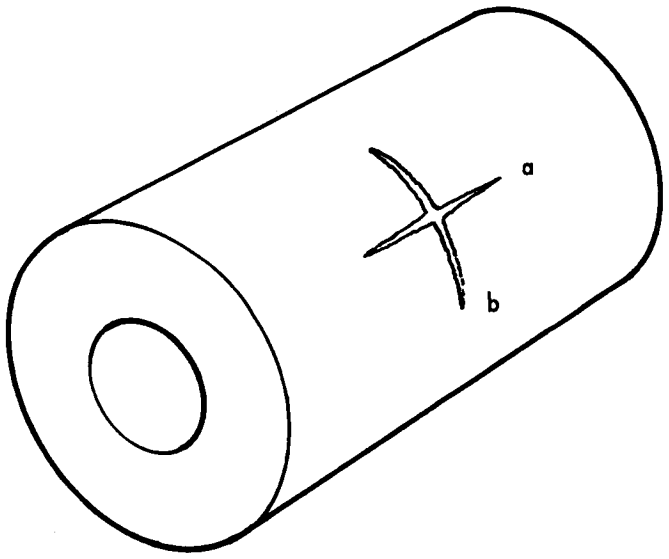

FIG. 6 TYPICAL CRACK STRUCTURES ON SOLID THROAT INSERTS
a) Longitudinal Cracks Caused by Excessive Hoop Stresses
b) Circumferential Cracks Caused by Excessive Axial Stresses Associated with the "Plane-Strain" Condition

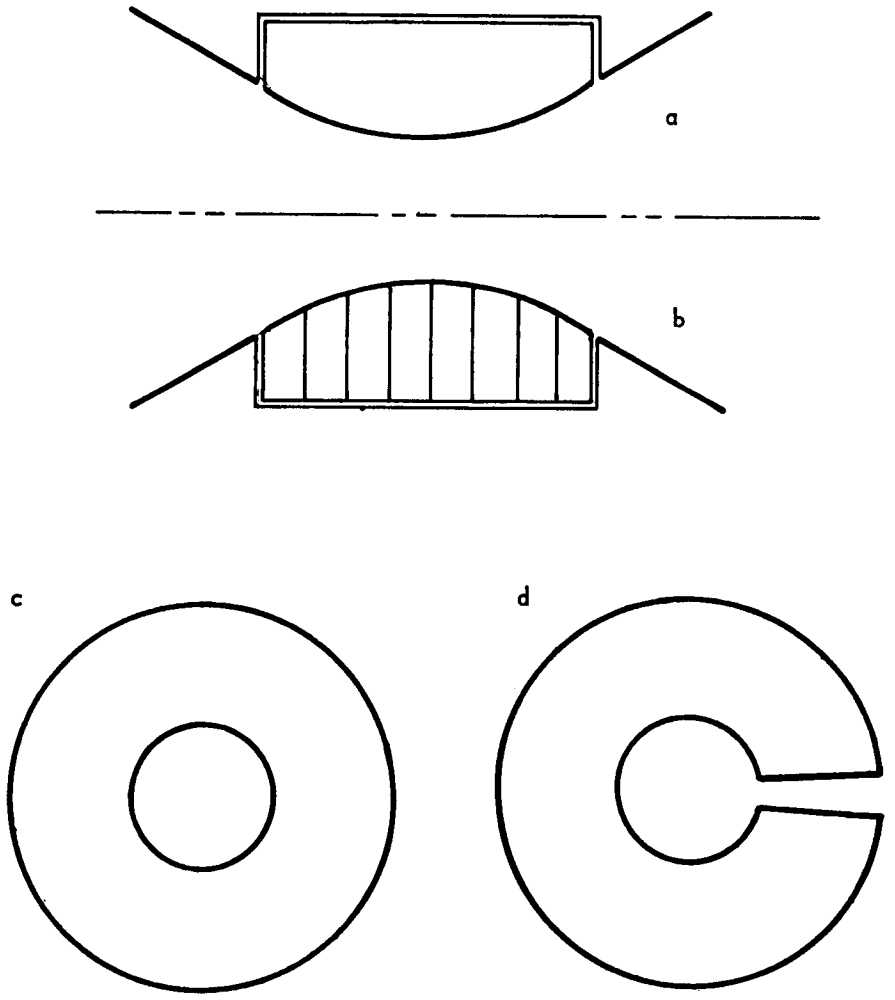

FIG. 7 a) Conventional Solid Throat Insert (Schematic)
b) Full Washer Type Insert
c) Elevation of Typical Washer
d) Elevation of Typical Split Washer

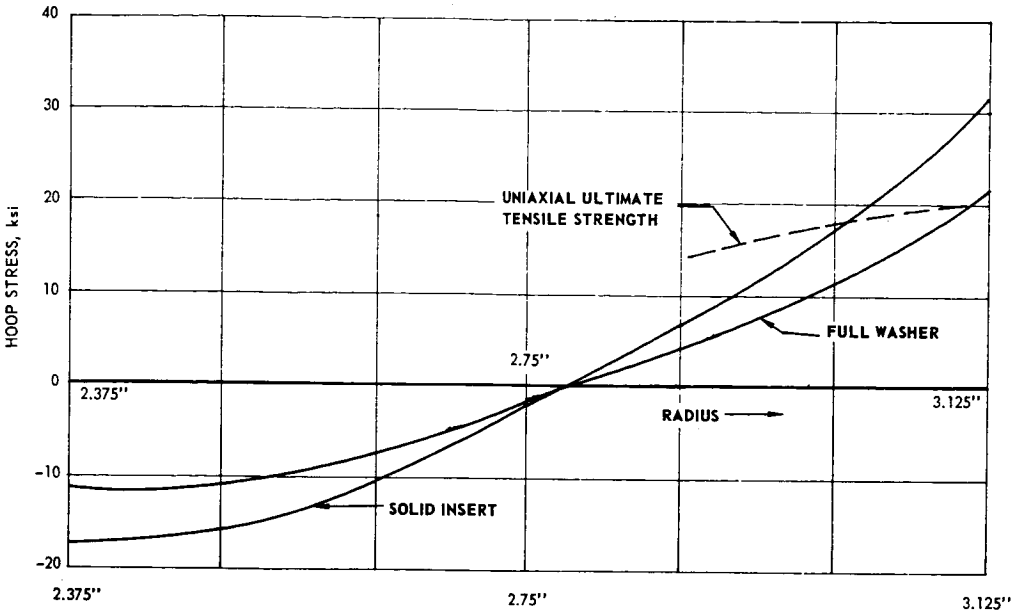

FIG. 8 COMPARISON OF HOOP STRESSES IN SOLID AND WASHER TYPE INSERTS. R_i = 2.375", R_o = 3.125"; T_i = 5000°F, T_o = 3000°F; Mechanical Properties E, α, ν Temperature Dependent; Logarithmic Type Temperature Distribution.

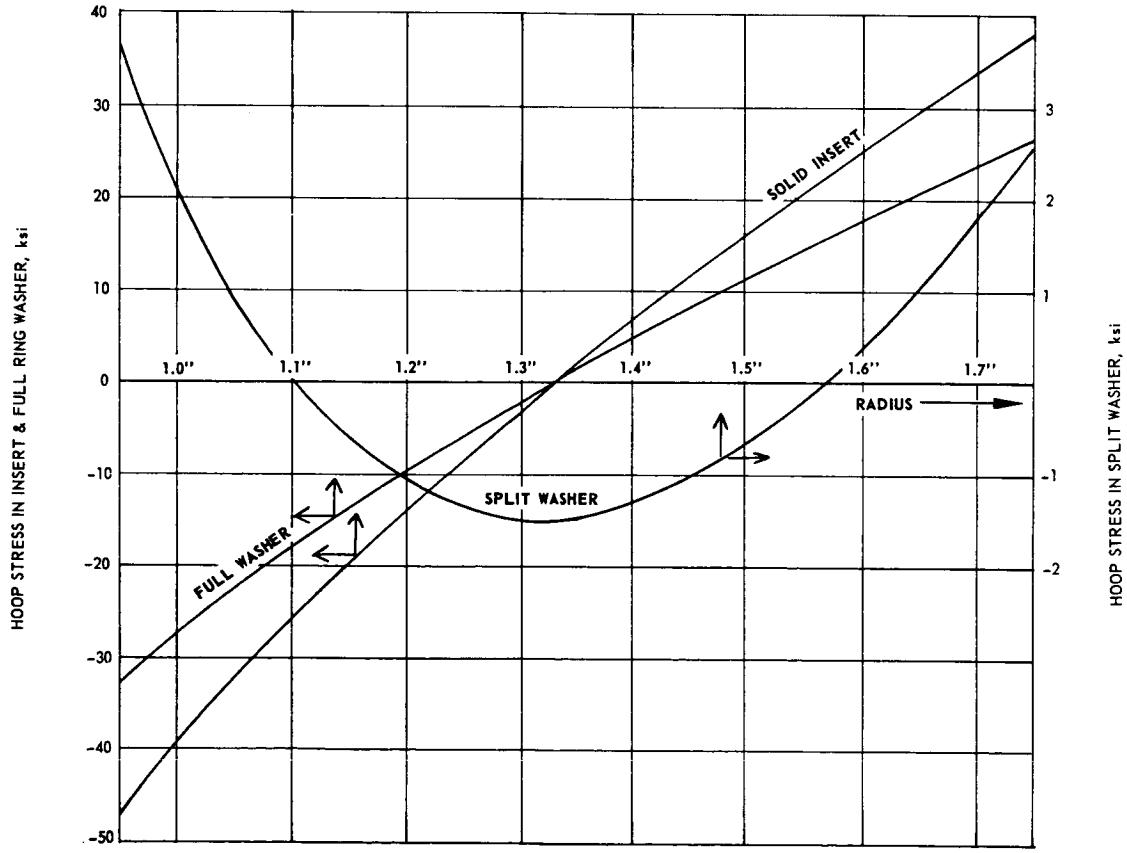

FIG. 9 COMPARISON OF HOOP STRESSES IN A SOLID INSERT, A WASHER TYPE INSERT AND A SPLIT WASHER TYPE INSERT FOR $(E)(\alpha)(\Delta T)$ = 60 ksi AND A LINEAR TEMPERATURE GRADIENT. Note Expanded Scale for Split Washer.

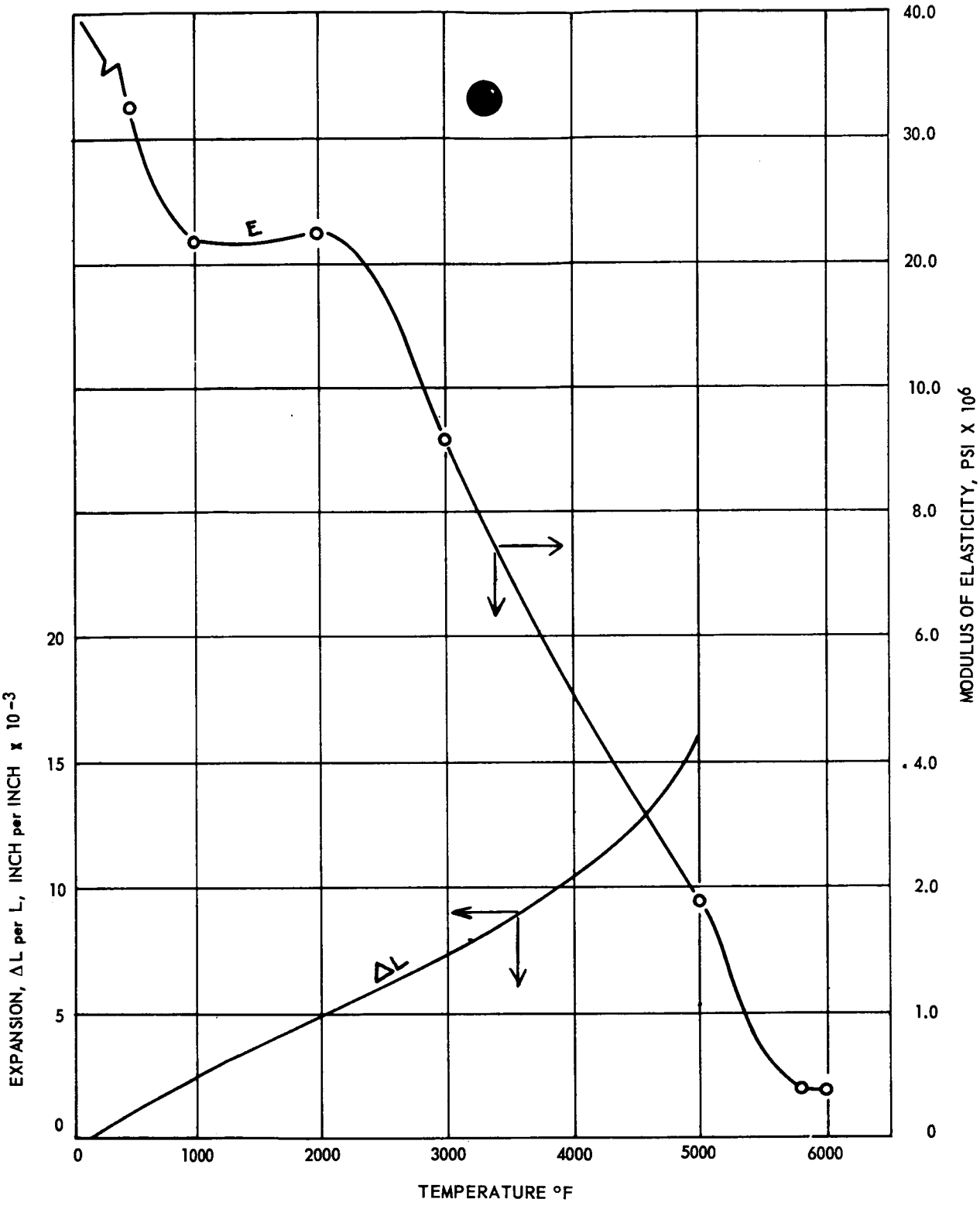

FIG. 10 VARIATION OF YOUNG'S MODULUS AND THERMAL EXPANSION OF PRESSED AND SINTERED TUNGSTEN, 95% THEORETICAL DENSITY, WITH TEMPERATURE

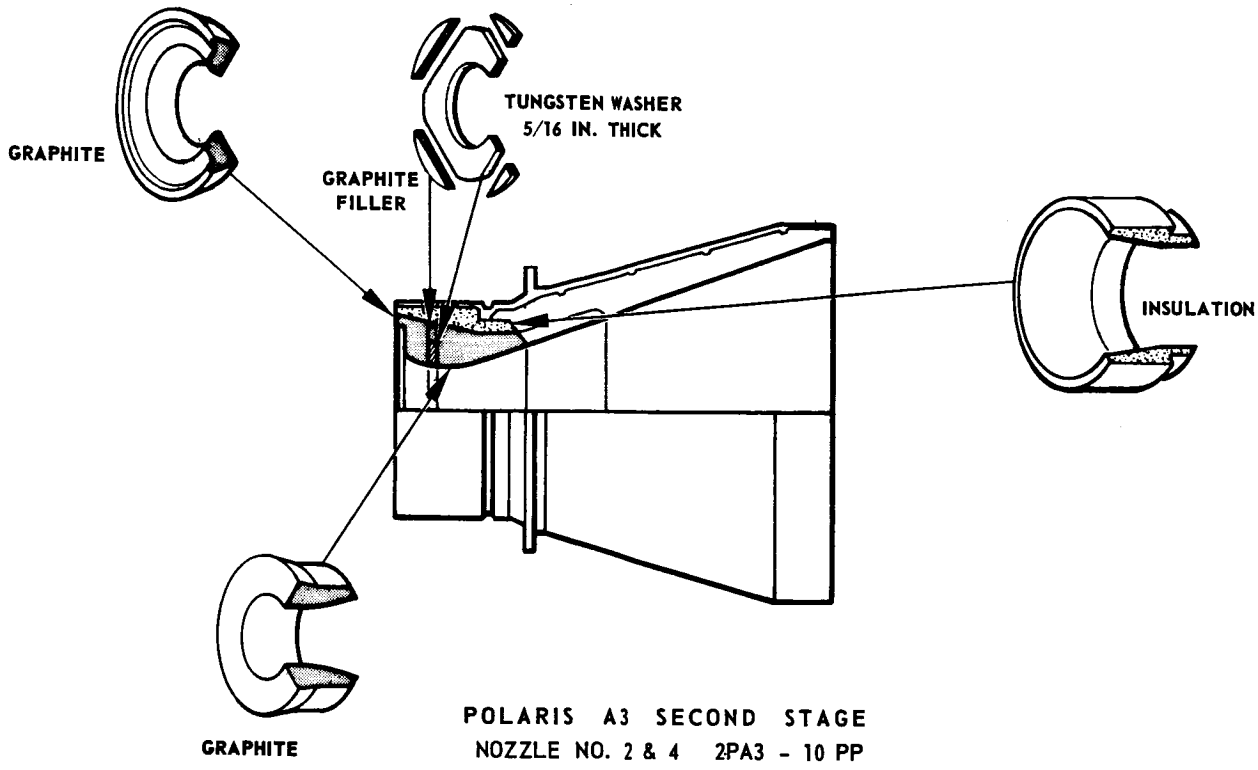

FIG. 11 SCHEMATIC VIEW OF NOZZLE OF SINGLE WASHER INSERT TYPE

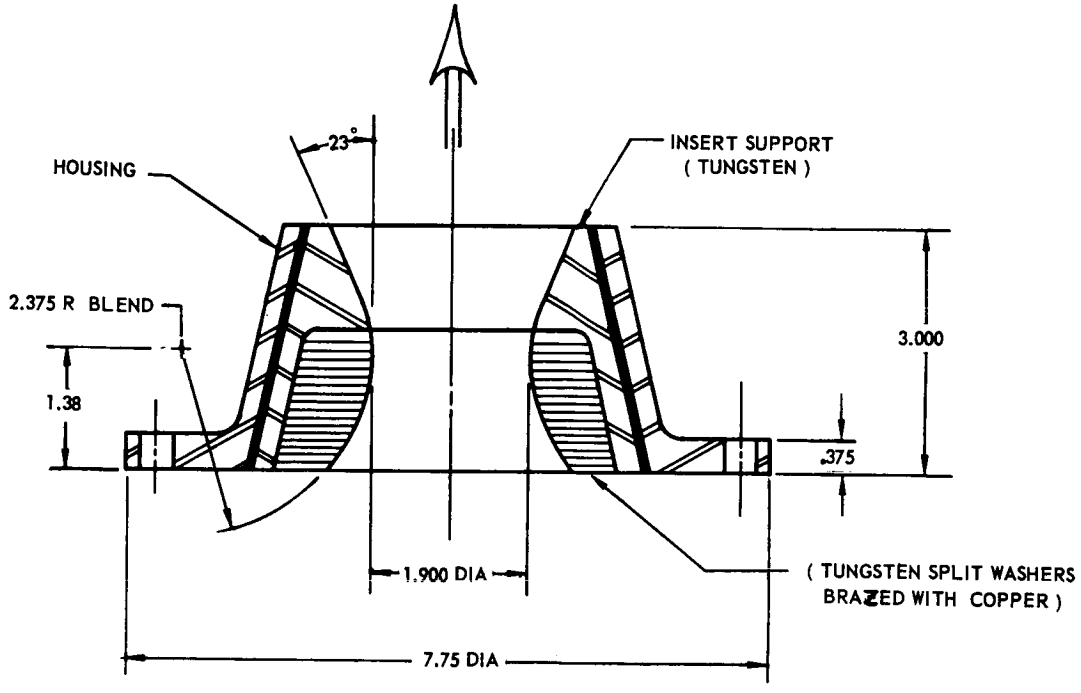

FIG. 12 CROSS SECTION OF SUBSCALE NOZZLE THROAT
USED TO EVALUATE THE SPLIT WASHER CONCEPT

X62-10280

AN ABLATING NOZZLE CONCEPT FOR SOLID-PROPELLANT ROCKET MOTORS

M. A. Schwartz and C. M. Frey
Materials Branch, Research Division
United Technology Corporation
Sunnyvale, California

ABSTRACT

A concept is described for solid-propellant rocket motor nozzles involving the use of lightweight ablating materials formed into tubular throats. The theoretical and experimental investigations of this concept have included heat-transfer studies, rocket-motor materials evaluation studies, two-phase flow studies, and design considerations. A model is proposed for the behavior of tubular ablating nozzles, and experimental results indicate the validity of considering the tubular ablating concept for very large nozzles.

INTRODUCTION

Under sponsorship of the U. S. Air Force,* an exploratory study was conducted to investigate the potential of employing ablatable materials in a tubular nozzle configuration for aluminized solid-propellant rocket motors. This nozzle concept, based on the successful results obtained in liquid-propellant motor firings at United Technology Corporation and on theoretical heat-transfer analyses, offers potential benefits through use of easily fabricated reinforced plastic materials for nozzle throats -- especially for large motors.

Generally speaking, the principal problem areas for solid-propellant nozzles relate to their erosion and corrosion susceptibility, weight, fabricability, reliability, and cost. The design approach to be discussed herein offers a means of circumventing, or learning to live with, these problem areas.

This paper is divided into essentially four phases of the program relating to the tubular ablating nozzle-design concept, namely: heat-transfer studies, rocket-motor materials evaluation studies, two-phase flow studies, and design concept discussion. There is no attempt made to delve deeply into the theoretical analyses and experimental programs conducted in the more specialized areas; these will be subjects of future papers by those individuals directly concerned.**

The results of this study to date are still considered preliminary and some aspects of the study are not yet fully understood. However, sufficient work has been accomplished to define a model of the fundamental behavior of tubular ablating throats.

---

* Contract AF 04(611)-7436 with Edwards Air Force Base.

** Heat Transfer - W. S. Kennedy. Two-phase Flow - J. J. Allport and R. Dunlap. Motor Performance - D. Talaska and H. Wolff. Materials - B. D. Matin.

HEAT-TRANSFER STUDIES

The object of these studies is to determine the heat-flux distribution in a tubular throat in order to understand and indicate the degree of ablation based on heat transfer. Figure 1 presents the theoretical model for indicating heat transfer in the tubular configuration.

The boundary layer is thinnest at the forward end of an extended throat and grows in thickness as a function of throat length. The smallest effective flow area is thus at the aft end of a tubular throat where the sonic plane probably exists. It would appear, then, that there are potentially two areas of high heat transfer: one where the boundary layer is thinnest, the other where the sonic plane is located as indicated in Figure 1. At all other axial stations, the heat transfer should be lower, producing a saddle-shaped curve for the heat-transfer coefficients as a function of distance.

In order to verify this analysis, experiments were conducted to measure both the pressure and heat-transfer distribution along a tubular throat. The pressure distribution was determined by firing a copper nozzle containing five pressure-tap holes located axially along the tubular throat. The results of this test indicated a throat entrance Mach number of 0.83 and a pressure drop down the length of the tube, culminating in the Mach one aerodynamic or sonic plane at the exit end of the tubular throat.

The heat-transfer distribution was measured by means of a calorimetric nozzle as shown in Figure 2. This nozzle consists essentially of a stack of copper wafers separated by asbestos-phenolic spacers. Each copper wafer contains a thermocouple located 0.028-inch below the heated surface. Figure 3 shows the nozzle as viewed from the exit cone end.

A PBAN* propellant containing two percent aluminum was employed for the two-second, 300 psi chamber-pressure firing. In Figure 4, the heat-transfer coefficient as a function of axial nozzle position, at one second after ignition, is presented. It may be concluded from this test that the greatest heat transfer occurred at the forward end of the tubular throat, reaching a minimum toward the downstream end and increasing slightly at the throat exit.

The entire heat-transfer curve falls below the maximum predicted by the Bartz equation for a conventional nozzle of the same throat diameter. This can be qualitatively explained by noting that, at the upstream entrance to the tube throat, the boundary layer is as thick as or thicker than (because of a less severe pressure gradient) the conventional nozzle boundary layer at the throat. But free-stream conditions are less severe (M = 0.83), resulting in a lower peak heat transfer. At the downstream end, Mach one is achieved but the boundary layer has thickened considerably and the result is a lower heat transfer than at the entrance.

* Polybutadiene acrylonitrile

ROCKET MOTOR MATERIALS EVALUATION STUDIES

In order to determine the general behavior of materials in a tubular nozzle configuration, five materials were selected for evaluation in rocket motor firings. These include two solid graphites, ATJ and CFZ, and three phenolic resins reinforced with Refrasil, graphite, and carbon cloths.

Tests were conducted in an end-burner motor designed primarily for small-scale nozzle evaluation (see Figure 5). When fully loaded, this test motor holds a grain 12 inches in diameter and 15 inches in length. With PBAN propellant containing 17 percent aluminum and having a 0.25-inch per second burning rate at 600 psia, firing durations of 60 seconds are achieved. The shorter firing durations are obtained by using a shorter grain and filling the forward end of the motor with an inert, encased plaster block.

All test nozzles were measured before and after test to determine their respective ablation profiles. The results of the tests are shown in the following figures. Figure 6 represents the ablation profiles for three ATJ nozzle firings. On all nozzles, throat diameters are 0.75 inch while the length of the tubular section is 2.25 inches (L/D = 3.0). With both the ATJ and CFZ graphites, the ablation rates were low. Of particular interest in the ablation profiles is the relative straightness of the surfaces. Figure 7 presents photographs of these nozzles after cross-sectioning. Expansion cones were lost on a number of the test nozzles because of the nozzle design (changed later in the program).

Figure 8 indicates the ablation profiles for two Refrasil-phenolic firings. The much greater rate of ablation is apparent as is the relative straightness of the throat. Figure 9 shows the cross-sectioned nozzles of Refrasil-phenolic. Figure 10 indicates the ablation profiles for three graphite cloth - phenolics. These materials ablated the least of the three reinforced phenolics. Figure 11 indicates a cross-sectioned graphite-phenolic nozzle with a superimposed grid to show the original contour. There is an observable lengthening of the nozzle because of the delaminating tendency of the 90°-oriented materials used. The carbon cloth - phenolics, as observed in Figure 12, behaved highly erratically with large pieces of the nozzle breaking away continuously during firing. This is believed to be due to the high thermal expansion of the material.

Two conventionally contoured nozzles, one of Refrasil-phenolic and the other of ATJ graphite, were also tested in order to obtain a preliminary basis for comparison with tubular nozzles. Figure 13 shows the ablation of both nozzle configurations with the Refrasil-phenolic material.

The ablation rates of all the nozzles are presented in Table I. These rates are based on the total duration of each firing and can only be considered relatively valid for tests not resulting in large chamber pressure drops. The reduced chamber pressure causes decreased burning rates and longer burning durations, and therefore misleading lower ablation values. Because of this, ablation-rate values for the 20-second firings listed in the first column are considered more reliable than the others.

The graphites are shown to have the lowest ablation rates, with the higher density CFZ material ablating the least. A comparison of tubular

and conventional ATJ nozzles did not indicate any significant difference in ablation rates. In the case of the Refrasil-phenolic nozzles, the conventionally contoured nozzle ablated at a surprisingly lower rate than did the tubular. However, the degree of possible scatter in material behavior has not been established and the results presented must be considered truly preliminary.

A comparison of chamber pressure and thrust curves for the two Refrasil-phenolic nozzles is shown in Figure 14. Surprisingly, the tubular-nozzle firing obtained a specific impulse of 227 seconds, compared to only 208 seconds for the conventional nozzle. Both nozzles produced similar maximum chamber pressures although the pressure with the tubular nozzle remained considerably higher throughout the entire firing duration. (It is to be noted that the chamber pressure is generally found to be about 10 percent higher for the tubular geometry, a phenomenon which is attributed to the thickening of the boundary layer down through the tubular section and consequent reduction of effective throat area.) The higher maximum thrust also associated with the tubular nozzle can be attributed to an increasing throat area or possibly an increased burning surface. The under expansion of both nozzles can only affect the C_F by two to three percent, to the detriment of the conventional type but not nearly enough to reflect the nine-percent difference in specific impulse. There are still unanswered questions in the analysis of these results, such as the part played by the rapidly decreasing chamber pressure, and the apparent low values of specific impulse as compared to the theoretical value. This one comparison test can only be viewed as an early attempt in drawing any pertinent conclusions. However, the comparison does suggest the need for further investigation.

TWO-PHASE FLOW STUDIES*

The objective of these studies is to analyze the performance aspects of tubular-throat rocket motors as regards two-phase flow effects. It was originally postulated that the tubular throat would permit a decrease in the solid-particle velocity lag with an attendant performance increase. The longer time that the particles remain in the gas stream before being discharged from the nozzle enables them to approach more closely the velocity of the gas stream.

A theoretical analysis and subsequent experiments involving differential cold-flow nozzle tests have essentially agreed with the original postulation. The basic measurement was the c* difference between two nozzles having identical inlet and exit geometries but one having a tubular throat and the other a conventional one, such as shown in Figure 15. Two different inlet geometries were tested, one with a 0.25-inch-radius inlet (shown in Figure 15) and the other with a 4.0-inch-radius inlet.

The results of the cold-flow tests are shown in Figure 16 as the increase in c* as a function of the particle-weight fraction. The upper and lower sets of data refer to nozzle pairs having a radius of curvature at the throat inlet of 1/4 and 4 inches, respectively. All nozzles had 1/4-inch diameter throats and the tubular throats had an L/D of 4.0. Nitrogen at a chamber pressure of 265 psia and temperature of 294° K, and glass spheres of 7.2 μ weighted-mean radius were used as the gas-particle mixture.

* The equipment and techniques involved have been developed on Contract NOw 61-0760-c with the Bureau of Weapons in support of their research program on "Dynamics of Two-Phase Flow in Rocket Nozzles." Its use for this program is appreciated.

The experiments show that the two-phase performance gains obtained with the tubular throat increase with particle weight fraction, and are higher for the more abrupt entrance geometry, as expected. As a matter of interest, the calculated increase in particle-to-gas velocity ratio from the entrance to the exit of the tubular throat was about 55 percent for the nozzle with a 1/4-inch-radius inlet and 20 percent for the 4-inch-radius inlet, nearly independent of particle-weight fraction.

Also shown in Figure 16 are corresponding theoretical curves based on a single particle size equal to the weighted-mean particle radius of 7.2 microns. The agreement with experiment appears quite good. The theoretical trend with particle-weight fraction and nozzle geometry, as well as the predicted level of the c* increase, are substantiated by the data. The fact that the theoretical predictions are somewhat higher than the measured performance increase is not surprising since the theory neglects friction, heat transfer, particle-size distribution, and two-dimensional effects.

It should be pointed out that the magnitude of the c* increase will be less in nozzles of large size because of the natural decrease of particle lag resulting from a reduction of axial gradients in larger nozzles.

DISCUSSION OF DESIGN CONCEPT

Results from the calorimetry nozzle firing substantiate the initial postulation that, with a tubular throat, the maximum heat transfer occurs at the entrance, a minimum occurs within the tubular section, and a second maximum occurs at the exit.

However, in attempting to translate these results to practicality, the nozzle cannot be considered tubular in configuration once preferential ablation commences. If ablation is less rapid at any distance down the throat, the transverse plane at that location then becomes a new throat entrance with the attendant increase in heat transfer. The heat-transfer peak at the "throat entrance" can thus be considered to be continuously moving, acting to smooth out any narrow sections of the tubular section. Depending on the rapidity with which this sweeping action moves, the tubular throat would tend to retain a tubular configuration, but increasing in diameter.

Although still to be verified, it is assumed that peak heat transfer in a conventionally contoured throat will be higher than the peak heat transfer in the tubular throat. This assumption is based on the lower Mach number occurring at the entrance to the tubular throat where heat transfer is determined to be at a maximum, as well as on the higher theoretical total heat transfer determined from the Bartz coefficient as compared to experimental tubular data. The boundary layer can also be considered to be thinner in the conventional than the tubular throat. The higher rate of heat transfer and the resultant ablation in the conventional throat could indicate the reason for the more rapid ablation occurring at the downstream end of the tubular throat. The sweeping action means that the moving throat caused by higher entrance heat transfer moves within the initial tubular throat towards the downstream end. At the downstream end, the tubular throat has become a conventionally contoured throat with the attendant Mach one conditions in addition to the high heat transfer attributed to throat entrance conditions.

Because the condition of severer heat transfer and ablation only occurs cyclically, its average rate should be only slightly greater than at the entrance and center sections of the tubular throat. Depending on the duration of test, the nozzles should essentially retain their tubular shape, although there may be a tendency toward coning.

In viewing an actual rocket-motor firing in the light of the foregoing discussion, it is established that the tubular shape is retained and that the ablation profile appears essentially as a straight line.

In considering the applicability of ablating throat materials such as graphite cloth - phenolic to very large rocket motors, scaling-up of the data presented herein to an arbitrarily selected 30-inch diameter throat indicates only a four percent total throat-area increase after 120 seconds of firing. This is well within the realm of practicability and is comparable to a ten-second firing on the scale (0.75-inch diameter throat) of the tests reported in this paper.

Consideration of the fabricability of reinforced plastics for very large motors is also in its favor. The molding or lay-up techniques required for their fabrication are much less size-dependent than are the techniques required for high-temperature fabrication of refractory-type materials and even solid graphite. Generally speaking, fabrication costs of these molded or laminated materials do not increase with increasing size at as rapid a rate.

Another consideration for the tubular-throat concept is the insurance factor built into it as regards the possibility of defects in the construction materials. A defect in the throat of a conventional nozzle could be catastrophic as compared to the much larger defect required to produce the same damaging effect in the tubular nozzle - approximately in proportion to their respective throat surface areas.

CONCLUSIONS

1. The tubular-throat concept for solid-propellant rocket motor nozzles has been shown to possess sufficient merit to warrant its consideration for truly large motors.

2. Based on heat-transfer studies and subscale rocket-motor firings, a model has been postulated for the behavior of tubular ablating nozzles.

3. Based on cold-flow experiments, the validity of a c* performance increase attributable to decreasing solid-particle velocity lag has been determined.

4. The relative merits of two solid graphite and three reinforced phenolic resin materials in terms of their ablation behavior and rates has been determined.

5. Indication of performance improvement of tubular-throat nozzles over that obtainable with conventional nozzles has been established.

[redacted]

TABLE I

ABLATION RATES*

Material	Nominal Firing Durations		
	20-sec	40-sec	60-sec
CFZ Graphite	$\frac{0.015}{20.4}$ = 0.0007 in./sec*	$\frac{0.036}{36.8}$ = 0.00098 in./sec*	---
	667 to 547 psi **	631 to 530 psi	
ATJ Graphite	$\frac{0.027}{21.1}$ = 0.0013 in./sec	$\frac{0.064}{38.34}$ = 0.0017 in./sec	$\frac{0.056}{57.0}$ = 0.00098 in./sec*
	679 to 541 psi	609 to 456 psi	630 to 494 psi
	$\frac{0.025}{20.3}$ = 0.0012 in./sec***		
	620 to 502 psi		
Graphite Cloth Phenolic	$\frac{0.099}{21.01}$ = 0.0047 in./sec	$\frac{0.126}{39.3}$ = 0.0032 in./sec	$\frac{0.185}{65}$ = 0.0028 in./sec
	670 to 409 psi	656 to 334 psi	634 to 208 psi
		$\frac{0.123}{38.6}$ = 0.0032 in./sec	
		615 to 345 psi	
Refrasil Cloth Phenolic	$\frac{0.191}{22.37}$ = 0.0085 in./sec	$\frac{0.319}{45.38}$ = 0.0066 in./sec	
	610 to 234 psi	632 to 123 psi	
	$\frac{0.150}{22.3}$ = 0.0067 in./sec***		
	620 to 212 psi		

* $\frac{\text{Total radial ablation (inches)}}{\text{Total duration (seconds)}}$ = Ablation rate (inches/second)

** $P_{c_{start}}$ and $P_{c_{finish}}$

*** Conventionally contoured throat

[redacted]

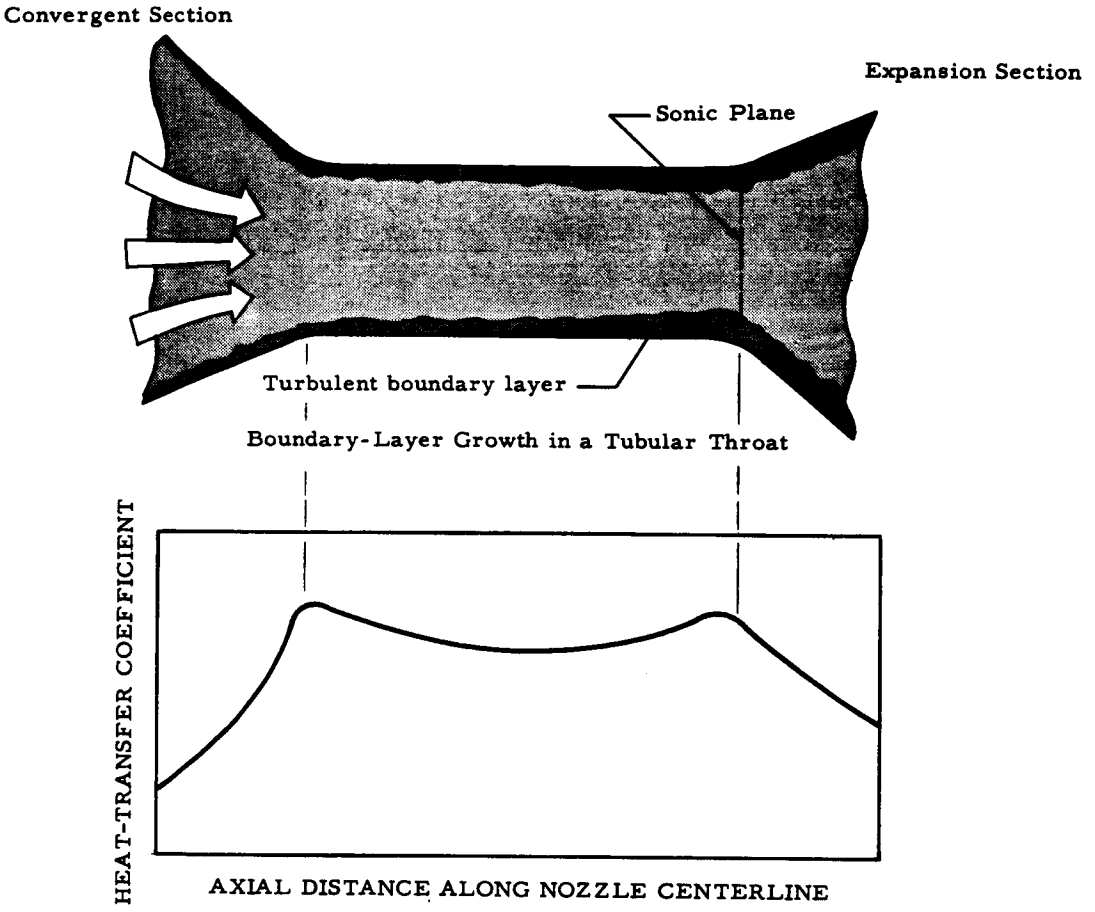

FIG. 1 HEAT TRANSFER AND BOUNDARY-LAYER GROWTH

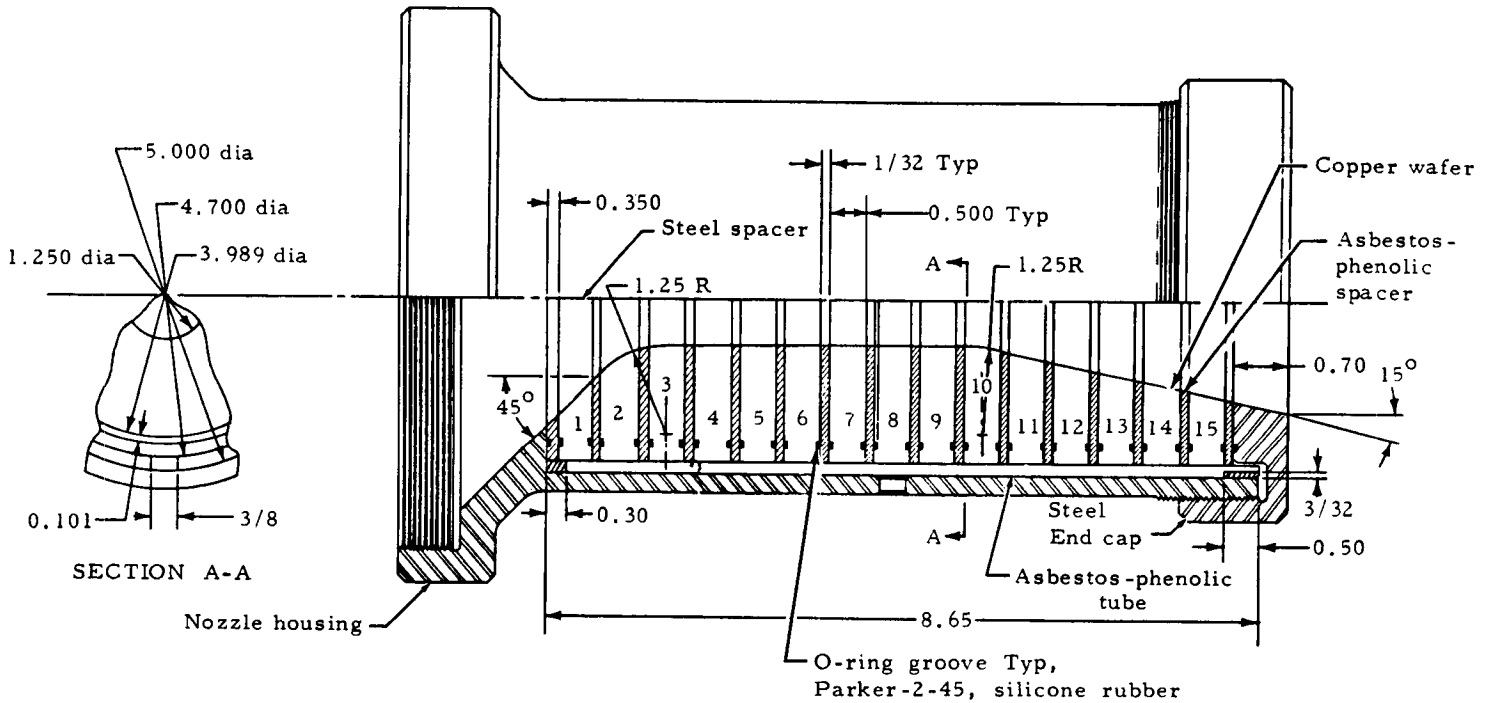

NOTE: All linear dimensions are given in inches.

FIG. 2 CALORIMETER-NOZZLE LAYOUT

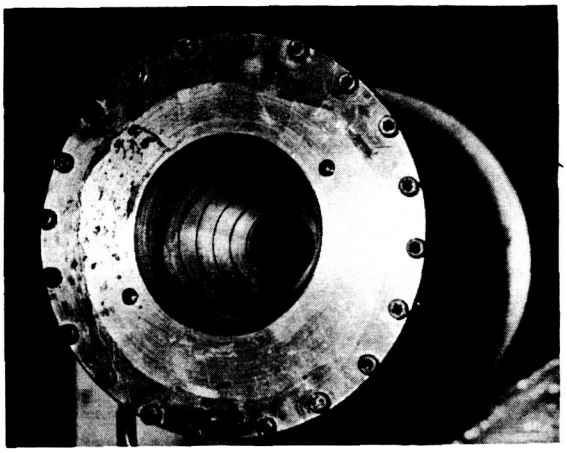

FIG. 3 PRE-FIRED CONDITION,
VIEWED FROM EXIT-CONE END

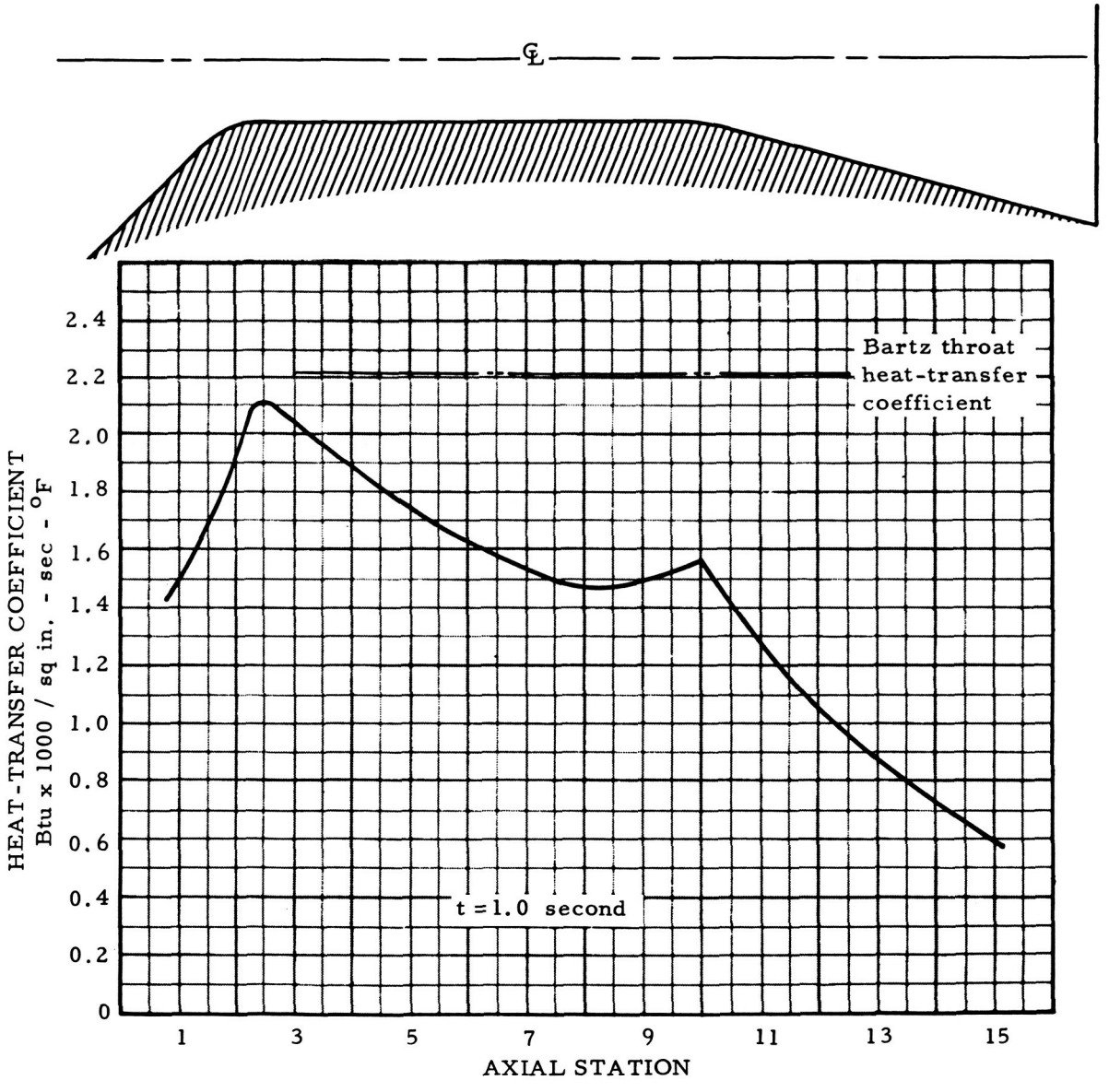

FIG. 4 HEAT-TRANSFER COEFFICIENT VERSUS AXIAL STATION
IN TUBULAR NOZZLE (EXPERIMENTAL VALUES)

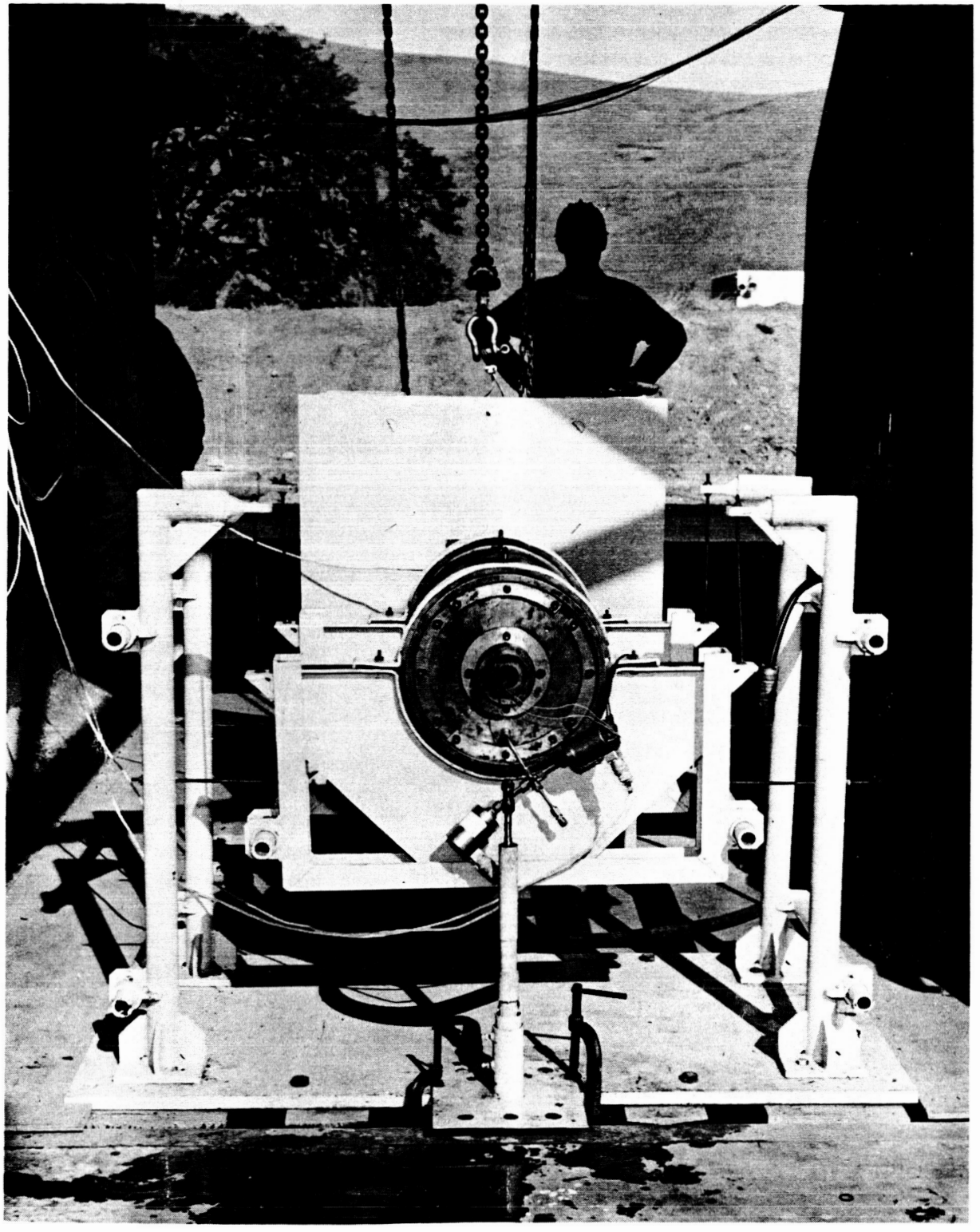

FIG. 5 NOZZLE EVALUATION MOTOR IN POSITION FOR STATIC FIRING

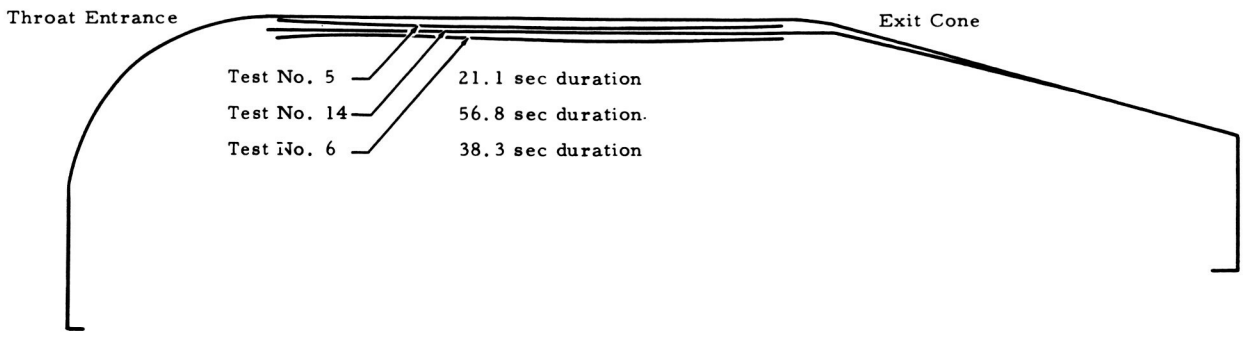

FIG. 6 POSTFIRING ABLATION PROFILES FOR ATJ GRAPHITE TUBULAR NOZZLES

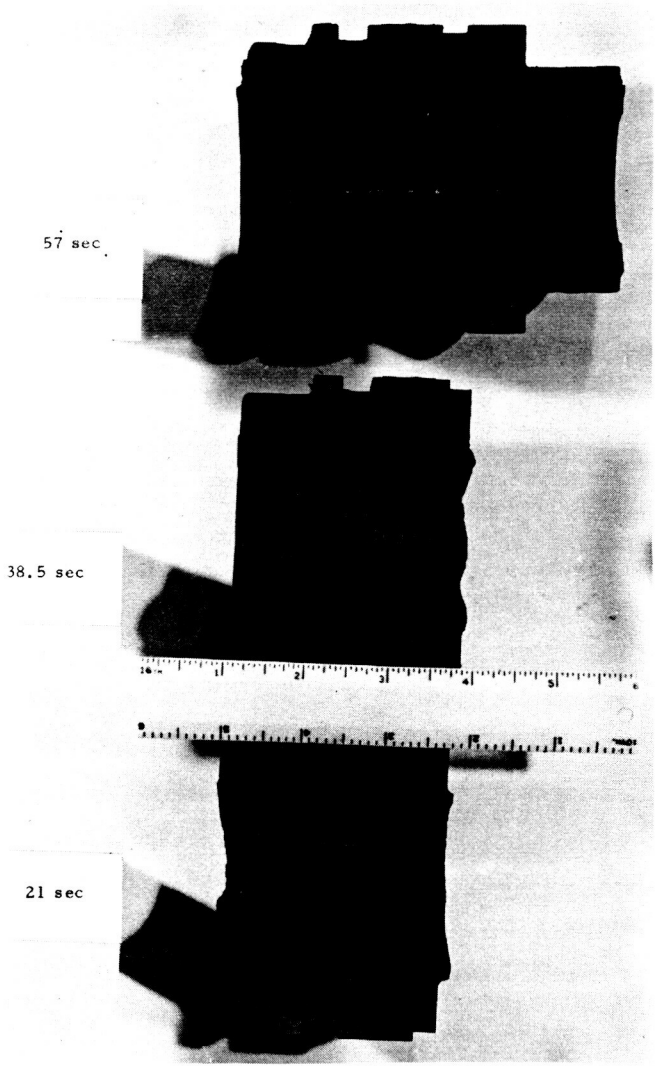

FIG. 7

CROSS-SECTIONAL VIEW OF TUBULAR NOZZLES INCORPORATING ATJ GRAPHITE MATERIAL

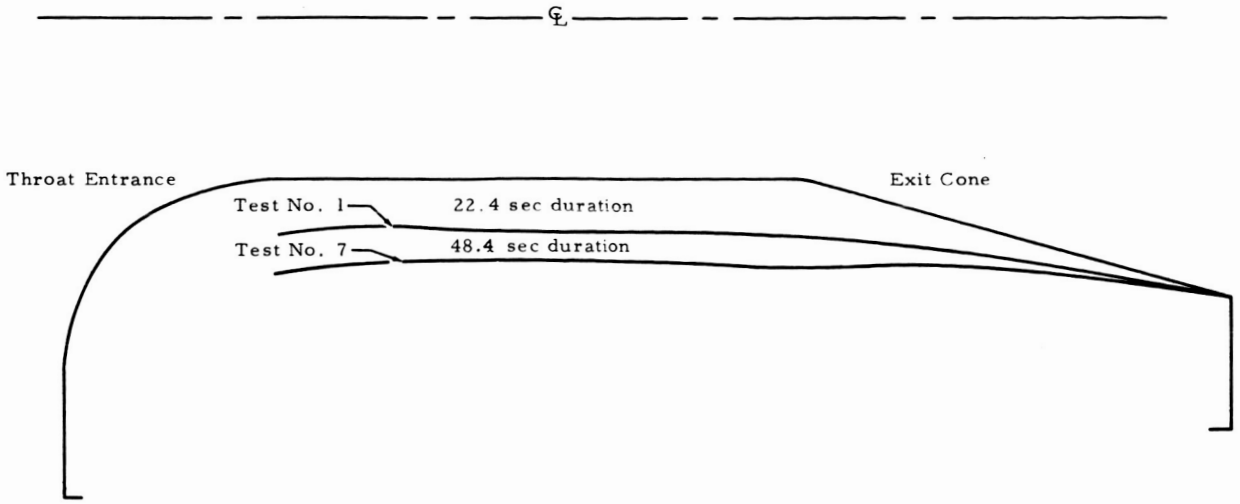

FIG. 8 POSTFIRING ABLATION PROFILES FOR REFRASIL CLOTH - PHENOLIC TUBULAR NOZZLES

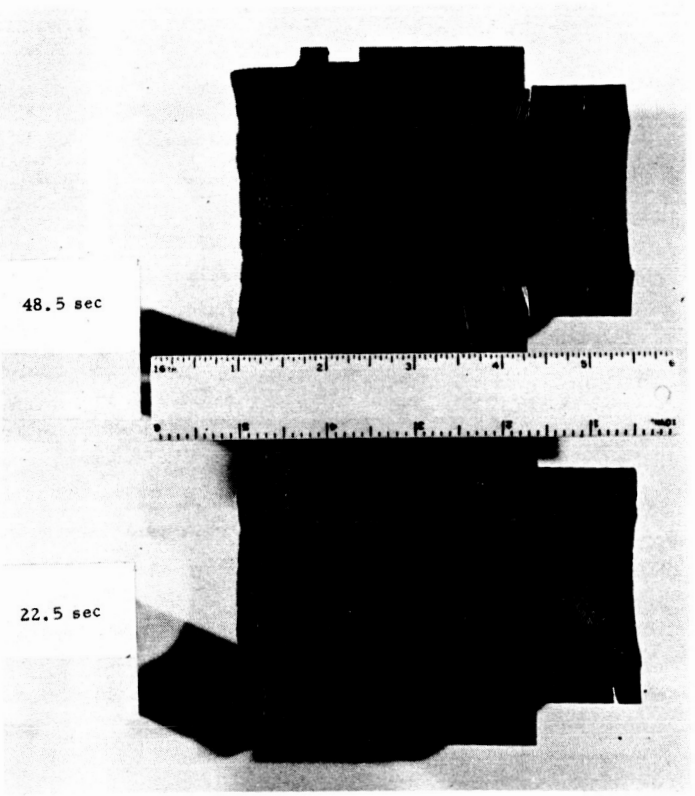

FIG. 9 CROSS-SECTIONAL VIEW OF TUBULAR NOZZLES OF REFRASIL - PHENOLIC MATERIAL

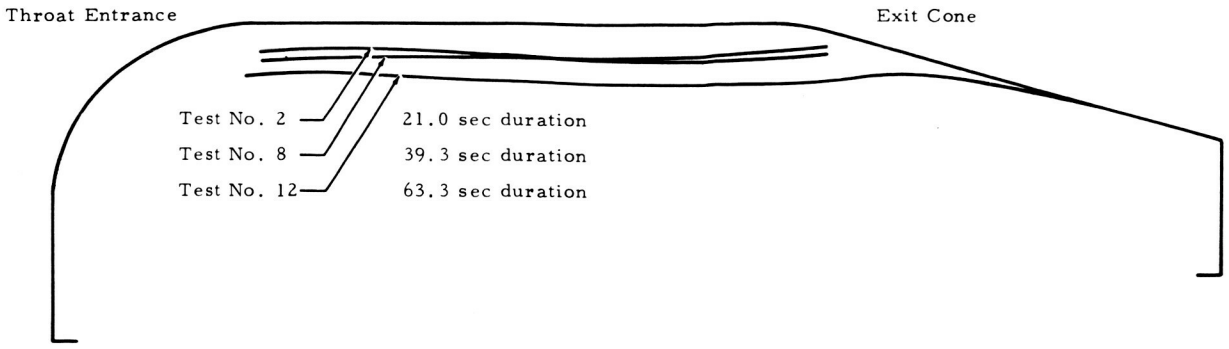

FIG. 10 POSTFIRING ABLATION PROFILES FOR GRAPHITE CLOTH - PHENOLIC TUBULAR NOZZLES

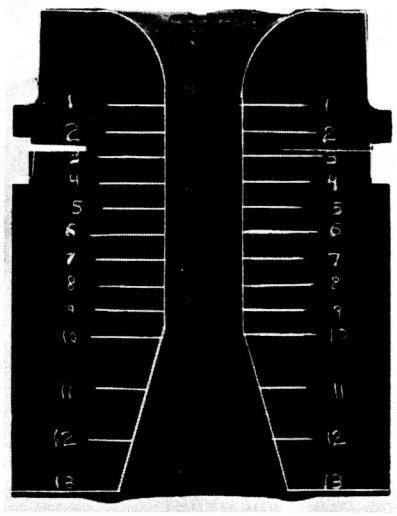

38.5 sec

FIG. 11 CROSS-SECTIONAL VIEW OF TUBULAR NOZZLE OF GRAPHITE CLOTH - PHENOLIC MATERIAL WITH PREFIRING CONFIGURATION DELINEATED

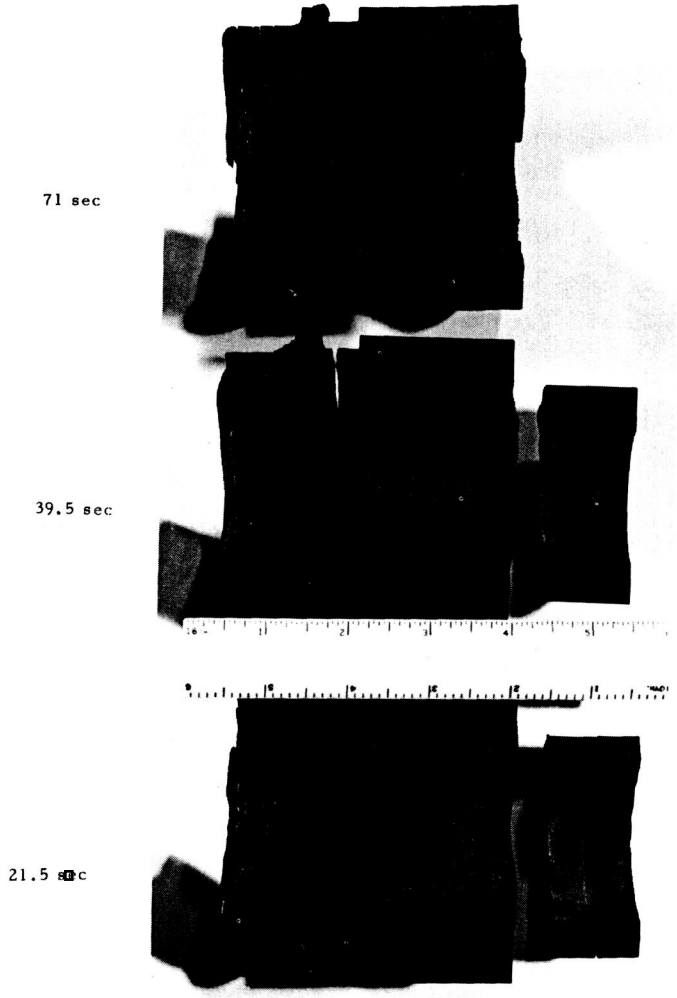

FIG. 12 CROSS-SECTIONAL VIEW OF TUBULAR NOZZLES OF CARBON CLOTH - PHENOLIC MATERIAL

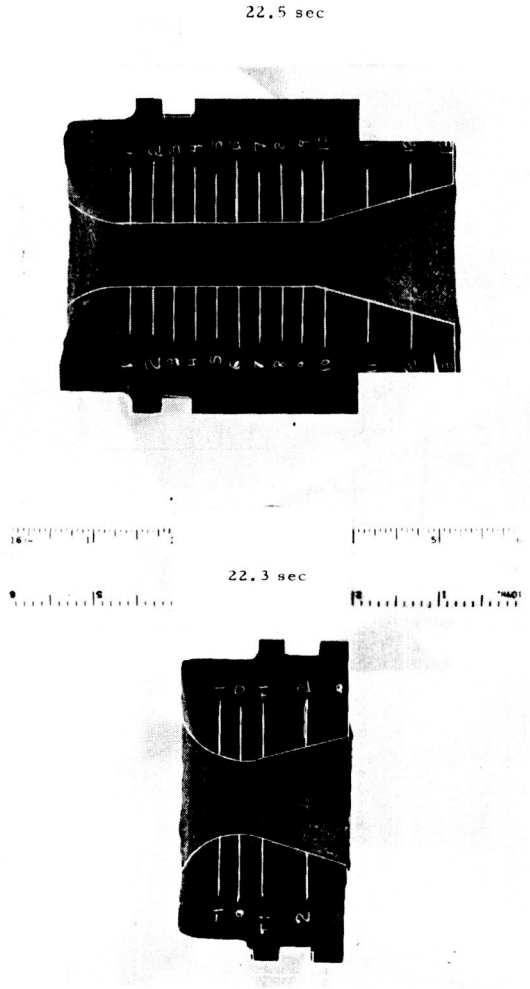

FIG. 13 CROSS-SECTIONAL VIEW OF TUBULAR AND CONVENTIONAL NOZZLES OF REFRASIL - PHENOLIC MATERIAL WITH PREFIRING CONFIGURATION DELINEATED

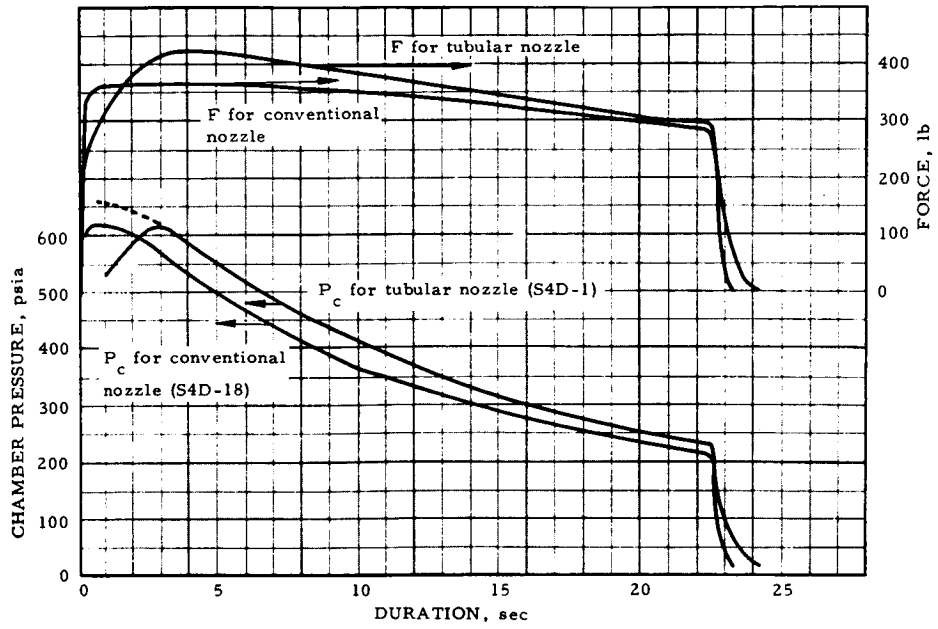

FIG. 14 COMPARISON OF PERFORMANCE WITH TUBULAR AND CONVENTIONAL NOZZLES OF REFRASIL CLOTH - PHENOLICS

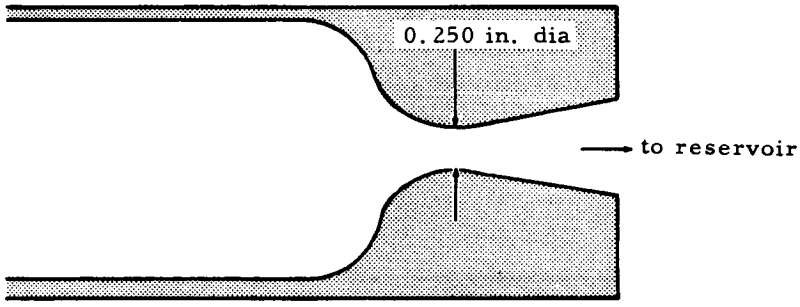

Conventional Nozzle Configuration

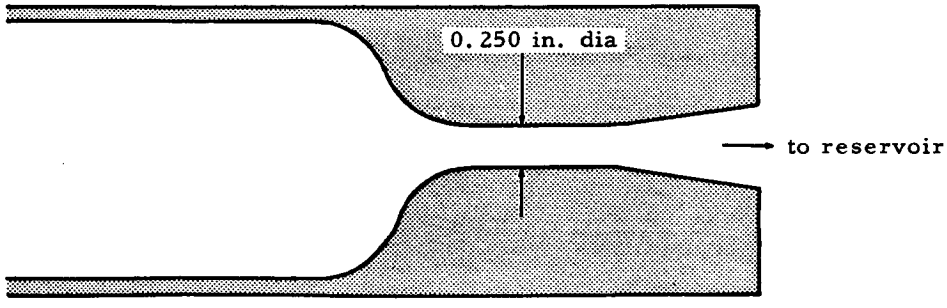

Tubular Nozzle Configuration

FIG. 15 TYPICAL NOZZLE CONFIGURATIONS FOR STUDY OF TWO-PHASE FLOW IN THE DIFFERENTIAL NOZZLE APPARATUS

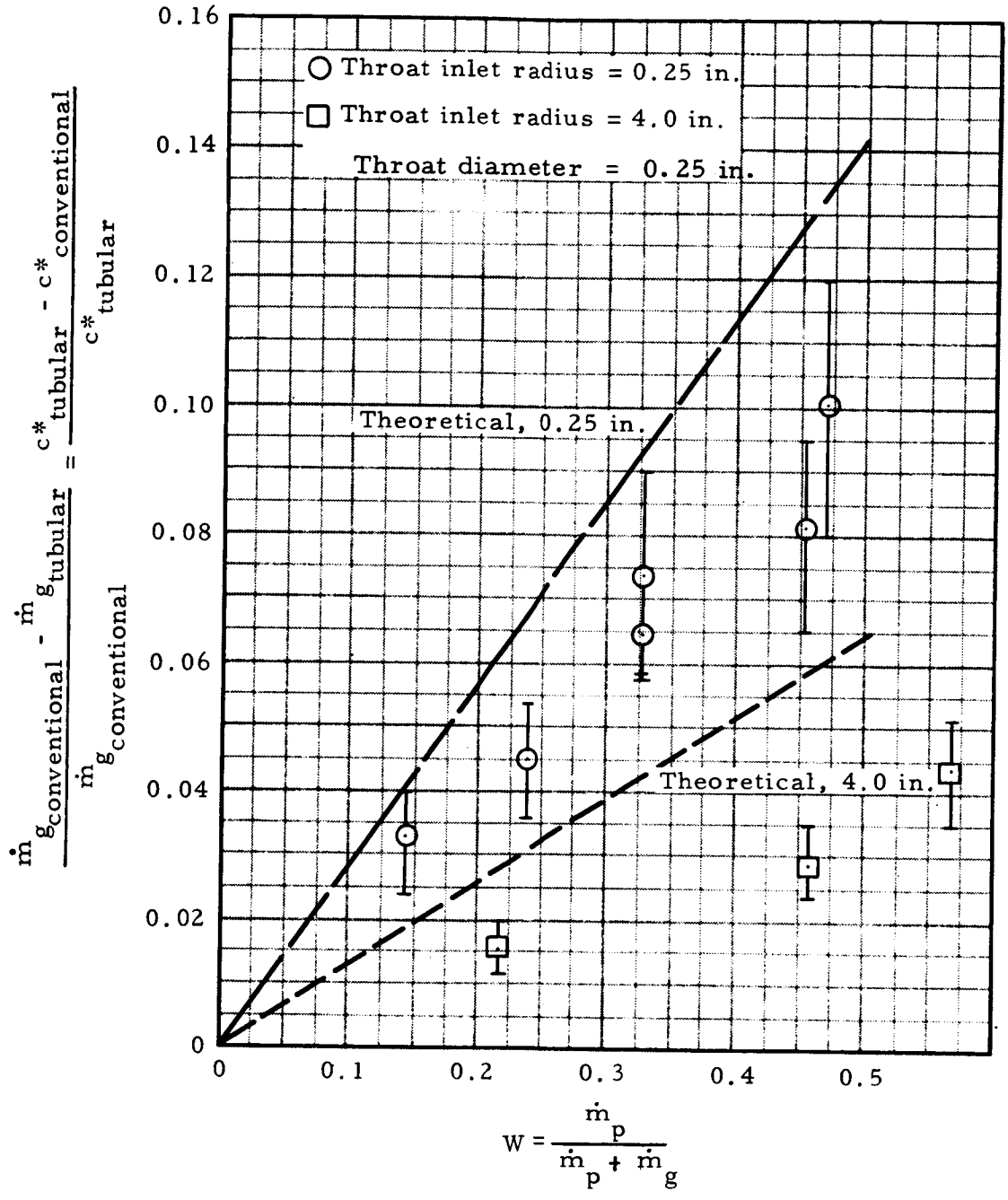

FIG. 16 PROPORTIONAL INCREASE IN c* FOR TUBULAR-THROAT NOZZLE COMPARED TO CONVENTIONAL NOZZLE VERSUS PARTICLE WEIGHT FRACTION

[redacted]

THE HISTORY AND DESIGN OF A SUCCESSFUL PROPELLANT GAS VALVE FOR THRUST VECTOR CONTROL

D. G. Drewry and H. D. Harmoning
Hercules Powder Company
Allegany Ballistics Laboratory
Rocket Center, W. Va.

ABSTRACT

Research during the past several years has shown that propellant gas injection provides a thrust vector control method which is more efficient, more reliable, and lighterweight than current methods. The major obstacle has been the design of a valve capable of controlling the flow of high temperature aluminized propellant gas. This report describes the design and demonstration of a valve that successfully controlled these hot particulate gases.

A straight-through type valve with a single strut-supported centerbody was designed and successfully test fired with an aluminized composite modified double base propellant with a flame temperature of 6300°F. The materials of construction were phenolic body, graphite seat and nozzle, and rubber plug. The test firing lasted for 34 seconds with a maximum chamber pressure of 285 psia. The valve was cycled on-off 10 times during the firing without any leakage. Examination of the valve after the firing indicated that the maximum life would have been about 50 seconds.

Experimental work with actuated valves and dummy valves leading to the design of a successful propellant gas valve is described. Work is continuing to further optimize the valve design.

INTRODUCTION

To be considered advancements, new methods of thrust vector control should improve the reliability and the performance of a rocket system. The use of propellant gas as a secondary injectant for thrust vector control can do both. The key to a successful propellant gas injection system is a lightweight valve capable of controlling the flow of the extremely hot propellant gases of present and future. Recent advances in use of lightweight materials (reinforced plastics, graphite, and thin refractory metal shells) to produce structures which will withstand the extreme temperatures for short times has assured the development of such a valve. The vectoring effectiveness of propellant gas injection has been demonstrated at other facilities[1,2,3,4] and at Allegany Ballistics Laboratory (ABL)[5,6].

Currently ABL is engaged in the development of on-off valves for application in propellant gas injection systems. Efforts in this area have been funded by the Bureau of Naval Weapons, Special Projects Office of the Bureau of Naval Weapons, and the National Aeronautics and Space Administration. Late in 1959, ABL began to investigate the feasibility of valves for use with aluminized Composite Modified Double Base (CMDB) propellant gas. The industry was surveyed to determine if there was any experience in building hot gas valves for gas temperature in excess of 4000°F. None was found, although several companies expressed interest in working on such valves. At this time it was decided that the design of on-off type

valves would be attempted first, as it was thought these would be easier to build while proportional control valves would be eventually more desirable.

A successful propellant gas valve was evolved from a series of preliminary valve tests and dummy valve tests. Several valve flow passage configurations were evaluated by test firings with dummy valves before a suitable design was found. After the successful valve firing, dummy valves were again utilized for further optimization.

PERFORMANCE TESTS OF PROPELLANT GAS INJECTION

The effectiveness of propellant gas injection has been demonstrated at other facilities and at ABL. Also, cold gas tests have been made at this laboratory to determine performance when the injection system is used with both the conventional conical nozzle and the isentropic spike nozzle.

There is almost a direct correlation between the results of cold gas tests and the results of tests with both clean propellant and aluminized CMDB propellant. A summary of these test results is shown in Figure 1.

The side thrust produced by propellant gas injection in the usual operating range (4 degrees thrust deflection, $F_s/F_a = 0.07$) is approximately twice that attained by a nozzle similarly located but exhausting radially overboard, and about 5 times as effective as Freon injection. Cold flow tests at ABL have shown that degradation of the total thrust may be minimized by proper location of the injection port with only nominal loss of thrust deflection efficiency.

PRELIMINARY PROPELLANT GAS VALVES

The first valves were designed and fabricated by vendors with ABL supplying technical data and design suggestions. The initial valve requirement was for an on-off valve to handle 0.5 lb./sec. of aluminized CMDB propellant gas at 300 psi. Thermionic Controls (now a part of Moog ServoControls, Incorporated) manufactured a straight-through, Y-type valve which operated successfully for 44 seconds before leakage. A description of this valve and firing is reported in the 16th JANAF Bulletin (5).

Late in 1960, a need developed for rapid design of on-off valves suitable for installation in a truncated spike nozzle. The design parameters for these valves were as follows:

1. A flight-weight version of the valve tested must weigh no more than 30 pounds.

2. Flow rate should be 7.5 lb./sec. at 300 psi.

3. Propellant for application and test was to be aluminized CMDB.

Four different valves were built at the same time and tested. Each of these valves incorporated certain unique features. The first of these valves tested, a straight-through type with a centerbody, was reported in the 17th JANAF Bulletin (6). The remainder of these valve firings are described in this section.

90° Angle Valve with Rubber Plug and Tungsten Seat

The valve shown in Figure 2a and 3, was designed and fabricated by Moog ServoControls, Inc. The valve was a 90° angle valve with a rubber plug and tungsten nozzle for a seat, and was hydraulically actuated to open and to close by 3,000 psi. pressure.

The valve operated for five cycles and 13 seconds before leakage occurred (Figure 2b). Valve leakage was caused by severe erosion of the rubber plug both from contact with the hot tungsten seat and by gas flow impingement when the valve was open. The dam around the rubber plug, which was supposed to protect the plug when the valve was open, eroded severely early in the firing, thus exposing the side of the plug to the impingement of particle-laden gas flow.

90° Angle Valve with Tungsten Plug and Graphite Seat

The valve shown in Figure 4a was designed and fabricated by the Chandler-Evans Corporation. This was a hydraulically actuated 90° angle valve with a tungsten plug seating against a graphite nozzle.

The valve failed to close during the firing because of an inadequate actuation system. An after-firing inspection indicated that the servo-valve was not functioning properly and thermal expansion caused the valve stem to bind. The tungsten stem supporting the plug failed when erosion of the protective dam allowed the stem to be exposed to the propellant gas flow. The tungsten plug was severely eroded (Figure 4b).

90° Angle Valve with Shrouded Rubber Plug and Graphite Seat

The valve shown in Figure 5a was designed and fabricated by the Kidde Aero-Space Division, Walter Kidde and Company, Incorporated. This was a pneumatically actuated 90° angle valve with a graphite-shrouded rubber plug and a graphite nozzle for the plug to seat on.

The valve failed to close after opening the second time (Figure 5b). The valve body and nozzle did not suffer severe erosion. The lip on the graphite nozzle was almost completely removed, possibly by fracture instead of erosion. Although the valve failed early in the test, the valve would have worked much longer if there had not been a structural failure of steel at the joint of the stem to the plug and a breakup of the graphite shield over the stem.

EVALUATION OF NEW VALVE DESIGNS

In the previous valve tests it was evident that the gas flow pattern in the valve determines the life of a valve. The use of dummy valves was conceived at this time in order to evaluate new valve design concepts and to improve potential designs quickly and at low cost.

Five propellant gas valve configurations were tested as dummy valves in static firings. The valves were made of phenolic to permit determination of high erosion areas with short firing times. Rubber simulated the valve plug in the open position. The firing times were approximately three seconds at 300 psia. with 6300°F. aluminized CMDB propellant. Two valves were of straight-through design and three were of streamline angle design.

Straight-Through Valves with Single Strut Supported Centerbody

Two straight-through dummy propellant gas valve designs with a single strut-supported centerbody have been tested. The valves were made of asbestos-filled phenolic with a simulated plug of asbestos-filled buna-S rubber.

Total firing time of the first valve design was approximately six seconds. Figure 6 shows a cross section of the internal configuration after the two firings and photographs of the valve. Erosion within the dummy valve was not severe except at one point in the nozzle, directly behind the plug support. This erosion area was located at the intersection of two flows of aluminum oxide particles. The valve withstood the two firings very well, and test results indicated there would be no major problems for the design of an actuating valve of this type.

The second straight-through valve (Figure 7) was a modification of the first design to improve the flow in the region where the plug seats. A subsonic duct was added downstream of the valve to simulate an actual application. The test results were very good, in that the erosion rate in the areas of importance was low and uniform, and there was no excessive erosion on any other parts of the valve. The high-erosion point on the valve seat of the original design had been eliminated.

Streamline Angle Valves

The complex duct geometry of the streamline angle valves prevented successful direction of the particles within the valves. Fig. 8 shows two of the three valves tested. The injection ports and seats were badly eroded in the areas of particle impingement, while other areas showed low erosion rates. Gas circulation caused severe and uneven erosion of the rubber plug which was withdrawn from the gas stream. These specific valve designs do not appear feasible. The tests did show that particles in particle-laden gas streams can be successfully directed to prevent severe erosion in certain areas.

SUCCESSFUL STRAIGHT-THROUGH VALVE WITH SINGLE STRUT SUPPORTED CENTERBODY

The next phase of the valve design program was to build a prototype (actuated) valve. Utilizing the dummy valve tests, described in the previous section, a straight-through valve design with a single strut-supported centerbody was found to be satisfactory from the standpoint of erosion on the critical seating area as well as the valve internal flow passages. The valve was scaled from the second straight-through valve design.

Description of Valve

The straight-through propellant gas valve was designed by ABL and Moog ServoControls, Inc., and fabricated by Moog ServoControls. A cross-sectional view of the valve is shown in Figure 9. The valve assembly includes the valve itself, subsonic ducting from the valve to the injection port, and the injection port. The valve was designed for a mass flow rate of 6.5 lbs./sec. at 300 psi. An asbestos filled buna-S rubber plug was hydraulically actuated to close against an ATJ graphite seat. The valve body was constructed of asbestos-filled phenolic with steel used for the actuation system hardware and casing. The total weight of the valve, less casing, was 75 pounds. The

phenolic body was over-designed to guard against failure in the event of erosion. The steel case was used to simplify construction and was not considered as part of the valve.

Description of Test Firing

The test firing of the valve took place November 21, 1961, utilizing an aluminized CMDB propellant (calculated flame temperature of 6300°F. at a chamber pressure of 300 psia.). Figure 10 shows the motor and valve before and after firing. The chamber pressure varied from 285 psia. when the valve was closed to 185 psia. when the valve was open. The decrease in chamber pressure resulted from increased throat area and consequential lower propellant burning rate when the valve was open. The valve was programmed to remain closed the first 2.8 seconds of firing, then begin cycling one second open--one second closed for the remainder of the firing. Due to a drift in the signal generator, the cycle time was greater than two seconds except for one manual cycle toward the end of firing. The valve actuation program for the 34 seconds of firing is shown in Figure 11.

Test Results

The valve was cycled ten times during the 34-second firing without leakage. The valve was then cycled two times and held in the closed position. Pressure measurement in the duct between the valve seat and the injection port (P_2 in Figure 11) increased from atmospheric pressure when the valve was closed to slightly less than chamber pressure (P_1 in Figure 11) when the valve was open, and returned to atmospheric pressure each time the valve closed, thus indicating that the valve did not leak. This was confirmed by motion pictures of the test firing.

A linear potentiometer attached to the plug recorded the position of the plug throughout firing (Figure 11). When the valve opened and closed, the plug returned each time to the previous final closed position, indicating that there was negligible erosion on the plug during actuation or while the valve was open. While the valve was closed, the plug slowly moved toward the seat. This movement is attributed to ablation of the rubber (branding) from contact with the hot graphite seat. The average rubber plug ablation rate was 0.085 in./sec. while the plug was in the closed position. During the firing, 1.50 inches of the usable 2.0 inches of rubber, were consumed. During the cool-down period after the firing, 0.39 inch of rubber was lost, leaving 0.11 inch of rubber remaining upon disassembly of the valve. The ATJ graphite seat showed no erosion or cracks at post-firing examination.

A plot of chamber pressure (P_1), plug position, hydraulic actuation pressures (P_3 and P_4), and signal to actuate versus time for a typical cycle (first cycle) is shown in Figure 12. The following is a summary of the actuation times based on the first cycle.

Time Period	To open (seconds)	To close (seconds)
Actuation signal to plug motion	0.038	0.037
Plug motion	0.047	0.045
Actuation signal to completion of plug motion	0.085	0.082

As the plug eroded, the time period of plug motion increased to 0.064 second at the end of firing because of the longer stroke, while the other time periods remained constant. The work requirement to cycle the valve from closed to open to closed was 1590 ft.-lb. initially and increased to 2590 at the end of the firing.

The internal erosion of the valve surfaces and char from the flow of propellant gas is shown in the cross-section view of Figure 9b. As predicted from the firing of a slightly smaller dummy valve, there were no severe or unsymmetrical areas of erosion. In fact, the flow patterns were identical on both valves, even though they were different in size. Below is a tabulation of the erosion rates in several areas of the valve and the comparative rates measured on the dummy valve:

Location	Velocity (Mach Number)	Conditions	Erosion Rates (in./sec.) Dummy Valve	Prototype
Duct	0.10	Straight Flow	0.018	0.005
Leading edge of Plug Support	0.04	Wedge in Flow	0.040	0.015
Seating Area	0.10	Turning Flow	0.019	0.0063
Duct Downstream of Seat	0.30	Straight Flow	0.020	0.011

VALVE DESIGN OPTIMIZATION

After successfully testing a straight-through type valve, efforts were directed toward improving the valve design. The specific objectives were to reduce valve size, weight, and power requirement, and to improve the supporting structure for the centerbody. Unfortunately, there is little information available on subsonic flow which would be applicable to valve design when using a particle-laden gas. Consequently, dummy valves were used to reduce development time.

Straight-Through Valve with Three Strut-Supported Centerbody

The distance between the plug and seat was shortened from the previous valve to reduce the length of the stroke and subsequently reduce the power requirement, centerbody size, and overall valve weight. Three struts were used in place of the previously tested one-strut configurations, as three struts facilitate lightweight structures. The following three-strut designs were incorporated into the valve for simultaneous evaluation.

1. Short strut with round leading edge and blunt trailing edge located further upstream from the seat than in previously tested valves (Figure 13, Section C-C).

2. Long strut with round leading edge and blunt trailing edge to locate the stagnant area occurring behind the blunt trailing edge so that it protects the rubber plug (Figure 13, Section D-D).

3. Streamlined strut to resemble a subsonic airfoil (thickness/length ratio = 0.3) to reduce the turbulent wake behind the trailing edge (Figure 13, Section E-E).

The dummy valve was test fired twice at approximately 360 psia. chamber pressure for durations of three seconds each. Both blunt trailing edge struts, when employed in the three-strut configuration, produced turbulence where the converging flow around the struts combined and hence caused severe erosion on the simulated rubber plug. If this occurred on an actuated valve, there probably would have been leakage between the plug and seat. Streamlining the strut reduced the turbulent wake. There was no unsymmetrical or high erosion behind the streamlined strut.

Straight-Through Valve with Two Strut-Supported Centerbody

Based on the results of the previous dummy valve test, another straight-through dummy valve was designed and tested. Two airfoil-shaped struts were used to support the centerbody of the valve (Figure 14). The valve was designed for a mass flow rate of 6.5 lbs./sec. at 450 psia. chamber pressure.

The valve was test fired twice for a total firing time of 5.4 seconds at an average pressure of 450 psia. This was the first valve test firing in this higher pressure range. There was no unsymmetrical erosion on the plug or seat, nor any other part of the valve.

SUMMARY AND CONCLUSIONS

The straight-through valve with the single strut-supported centerbody was the first lightweight propellant gas valve which operated successfully for its design life of 34 seconds. The mass flow rate was more than ten times greater than that of the first, and most successful, valve previously tested. The post firing analysis of the data and examination of the valve indicated that the valve would have been capable of operating without leakage for at least 16 more seconds, making a total valve life of 50 seconds.

It appears that the valve life in this particular design is not dependent upon the number of cycles but upon the time the plug is in contact with the hot graphite seat. Since ablation of the rubber plug was the limiting factor in the valve life, methods of reducing plug ablation should be investigated. If this ablation can be reduced, the valve life can be increased several times. The use of the single strut in this valve produced no detrimental erosion effects, but did create some structural design problems. An optimization study of this design indicated that by removing excess phenolic, graphite, and structural members a 40 pound valve could be built.

The objective of the next phase of the design program, to produce a still lighter and more reliable valve, was verified through the use of dummy valves. These objectives were met by employing two improved airfoil-shaped struts to support the centerbody and by reducing the plug stroke.

Following is a summary of the conclusions drawn from the design of on-off type valves for use with high temperature aluminized CMDB propellants at chamber pressures below 500 psi.:

1. The straight-through valve represents the best chance for short-term successful propellant gas valve development. The plenum-type angle valves are also feasible, but the seating surfaces and the plug are subject to severer erosion conditions than in the straight-through design. The streamlined angle valve designs are the most difficult.

2. The best seating combination for good sealing and high actuation speeds is a soft plug (filled elastomer) against a hard seat of graphite (or phenolic, if erosion of the phenolic can be minimized). A material with properties between graphite and phenolic, such as a graphite filled phenolic, may meet the low surface temperature and low erosion requirements.

3. Because of the difficulty of predicting aerodynamic and heat transfer effects in particulate gases, the effects of the internal design on erosion can be evaluated economically with the propellant gas and a dummy-scaled model. The design parameters concluded from one valve configuration may not be valid for another configuration.

4. Currently, hydraulic fluid appears to be the best actuation medium, since a more positive response can be attained with it than with a gas. The weight of power packages for valves such as those tested, with the actuation fluid producing the entire force to actuate the valve, appears to be within usable limits. Future refinements in the actuation system, such as a balanced actuator and shortened stroke, should reduce the actuation power requirements, thereby reducing the power package weight. Although the actuation system is not a critical-problem area, it plays an important role in the design of a successful valve.

REFERENCES

(1) M. Schulmeister, "Static Evaluation Tests of an Oblique Shock Wave System for Rocket Exhaust Deflection," (CONFIDENTIAL), U. S. Naval Rocket Test Station, NARTS 77, TED-SI-5519, December 1955.

(2) G. F. Hausmann and J. T. Corso, United Aircraft Corporation, "Thrust Axis Control of Supersonic Nozzles by Airjet Shock Interference," (CONFIDENTIAL), NAVORD 3146, Proceedings of U. S. Navy Symposium on Aeroballistics, NOTS, Pasadena, California, May 13-15, 1952.

(3) C. B. Benham and C. J. Green, Propulsion Development Department, "Parameters Controlling the Performance of Secondary Injection," U. S. Naval Ordnance Test Station, China Lake, California, (CONFIDENTIAL), Bulletin of the Seventeenth Meeting of JANAF-ARPA-NASA Solid Propellant Group, May 23-25, 1961, Page 367.

(4) V. H. Ransom, S. A. Lorenc, J. J. Williams, T. L. DeYoung, "Results of a Program for Theoretical and Experimental Evaluation of the Plug Nozzle Concept," (CONFIDENTIAL), Aerojet-General Corporation, Bulletin of the Seventeenth Meeting of the JANAF-ARPA-NASA Solid Propellant Group, May 23-25, 1961, Page 325.

REFERENCES (cont'd.)

(5) D. G. Drewry and R. M. Newman, Jr., "Methods for Thrust Vector Control of Solid Propellant Rockets," (CONFIDENTIAL), Bulletin of the Sixteenth Meeting of Joint Army-Navy-Air Force Solid Propellant Group, June 14-16, 1960, Page 227.

(6) D. G. Drewry, B. T. Hnatiuk, T. E. Kallmeyer, H. D. Harmoning, D. P. Hanley, and D. P. Hug, "Propellant Gas Injection for Thrust Vector Control of Solid Propellant Rockets," (CONFIDENTIAL), Bulletin of the Seventeenth Meeting of JANAF-ARPA-NASA Solid Propellant Group, May 23-25, 1961, Page 385.

Conical Nozzles

Symbol	X/L	α	ϕ	Injection Orifice	I_{sp}	By
△	0.755	12.5°	12.5	Super Sonic	208	NARTS
⊙	0.500	15.0°	0	Super Sonic	263	ABL
⊡	0.500	15.0°	0	Sonic	211	ABL
◇	0.750	15.0°	0	Sonic	211	ABL

Spike Nozzle

Symbol	X/L	l/L	ϕ	Injection Orifice	I_{sp}	By
▽	0.15	0.30	0	Sonic	263	ABL

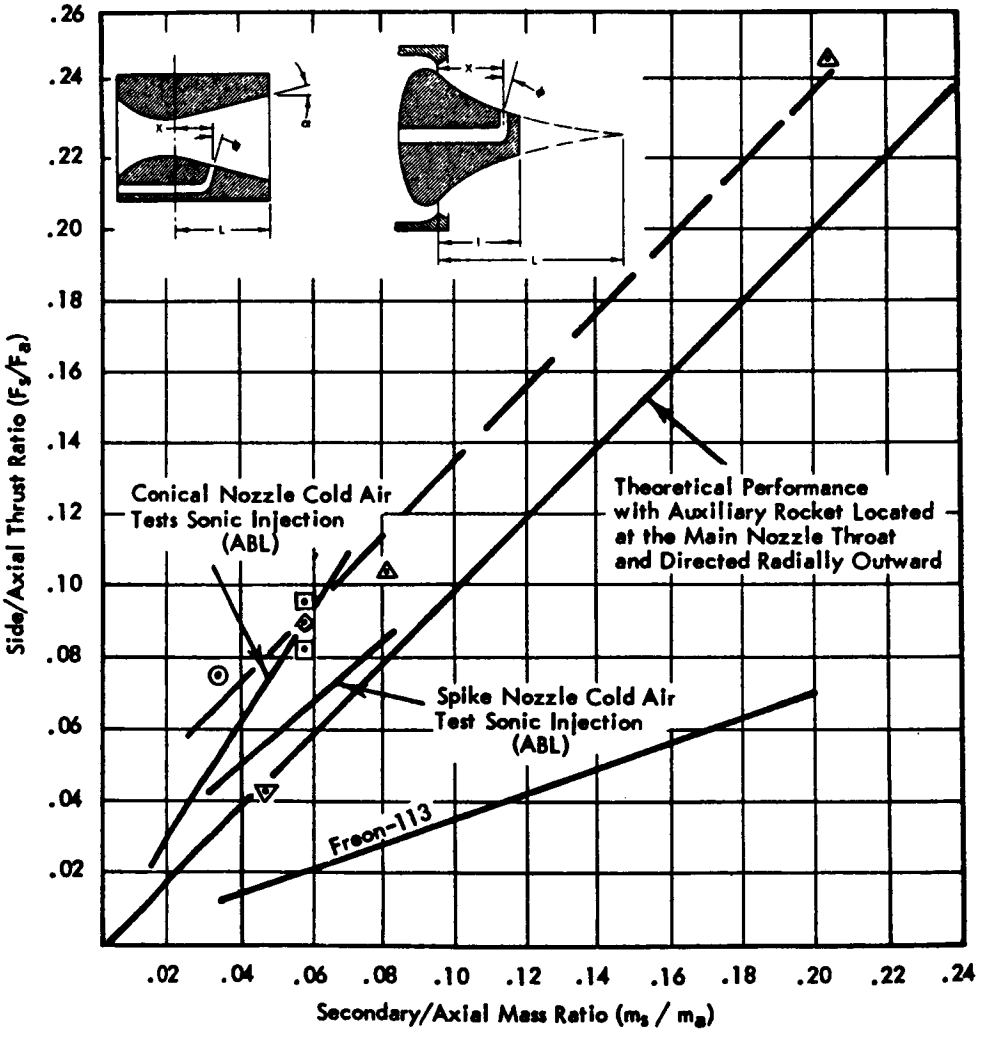

FIG. 1 THRUST VECTOR CONTROL BY SECONDARY INJECTION

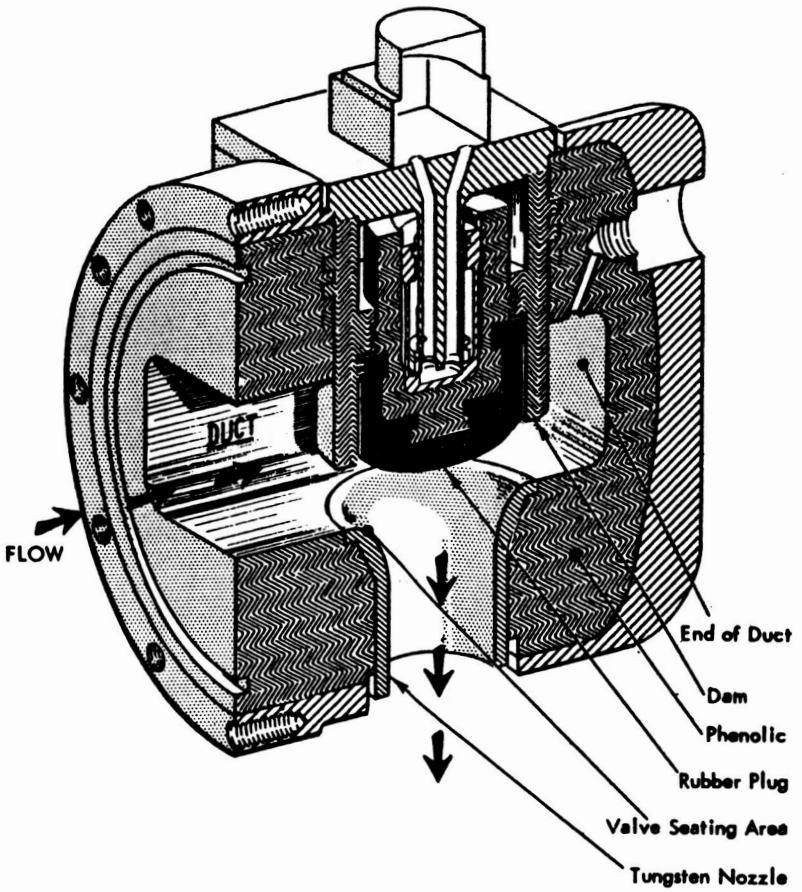

(a) SCHEMATIC HALF SECTION OF THE VALVE

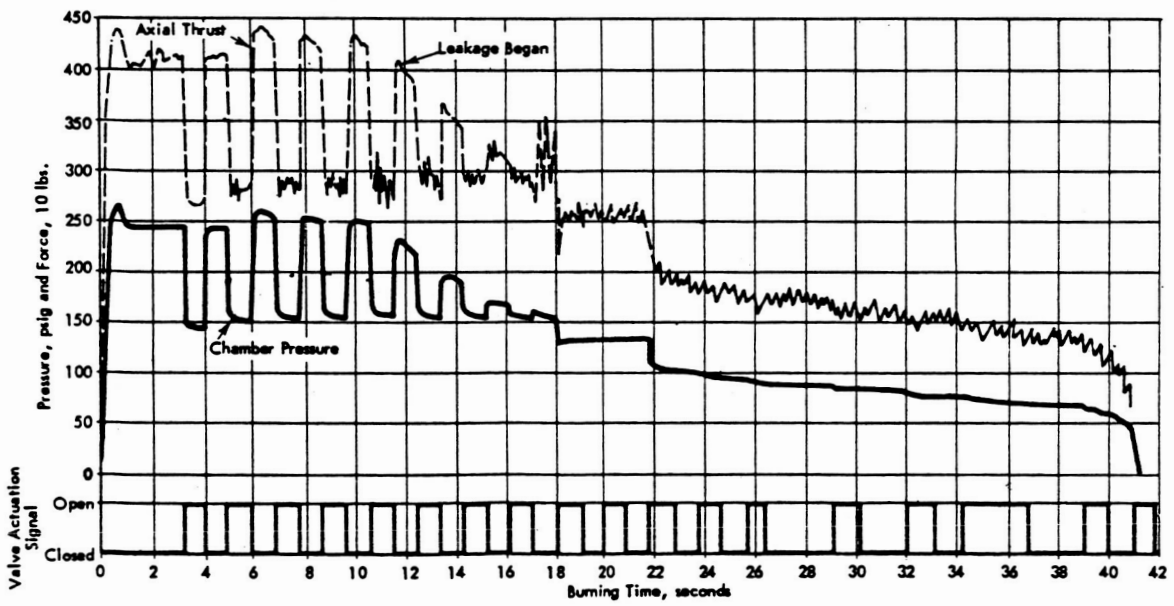

(b) FIRING RECORD

FIG. 2 90° ANGLE VALVE WITH RUBBER PLUG AND TUNGSTEN SEAT

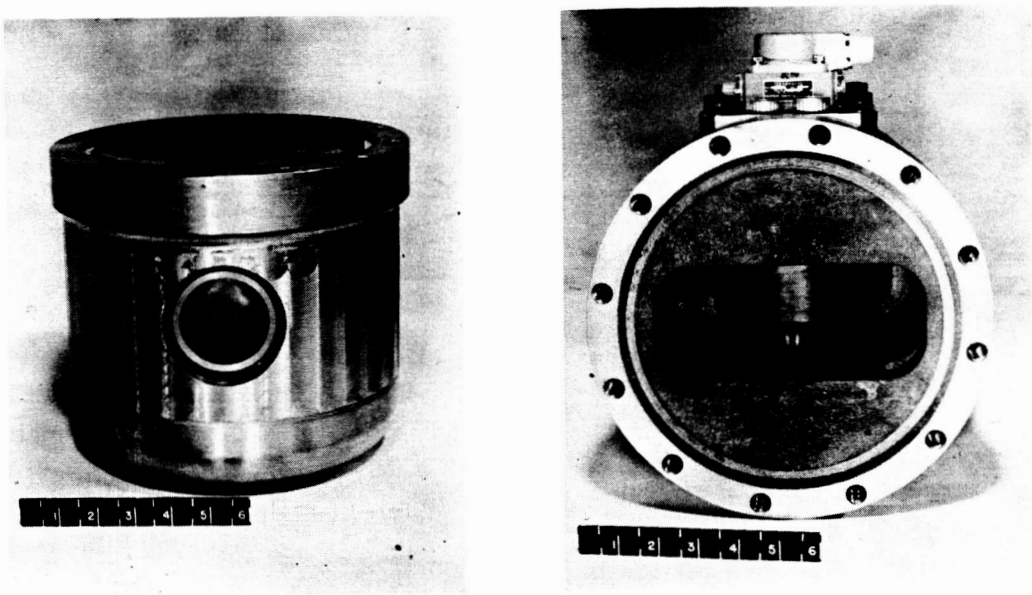

(a) BEFORE FIRING

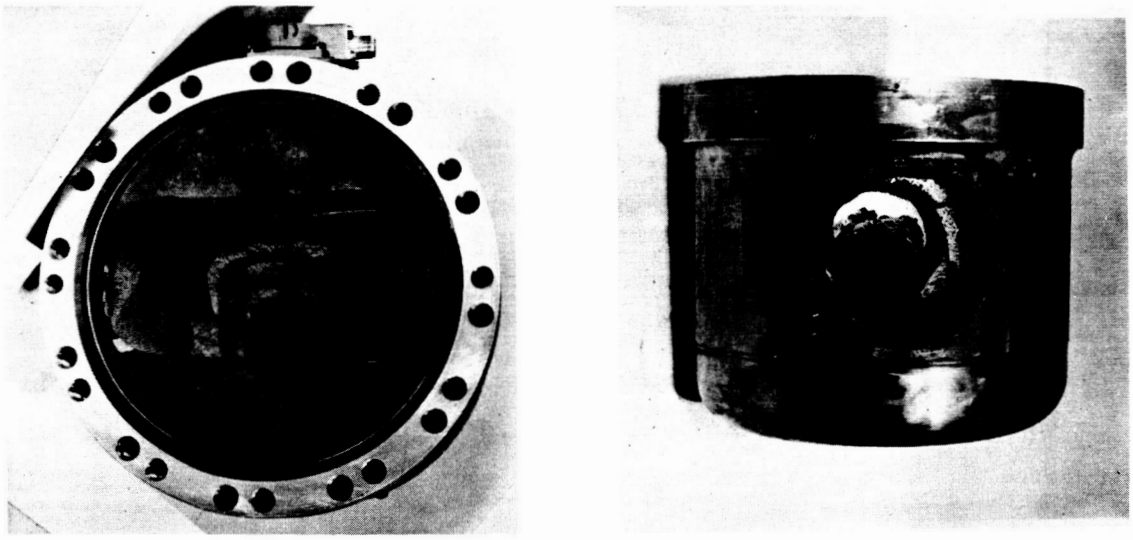

(b) AFTER FIRING

FIG. 3 VIEWS OF 90° ANGLE VALVE WITH RUBBER PLUG AND TUNGSTEN SEAT

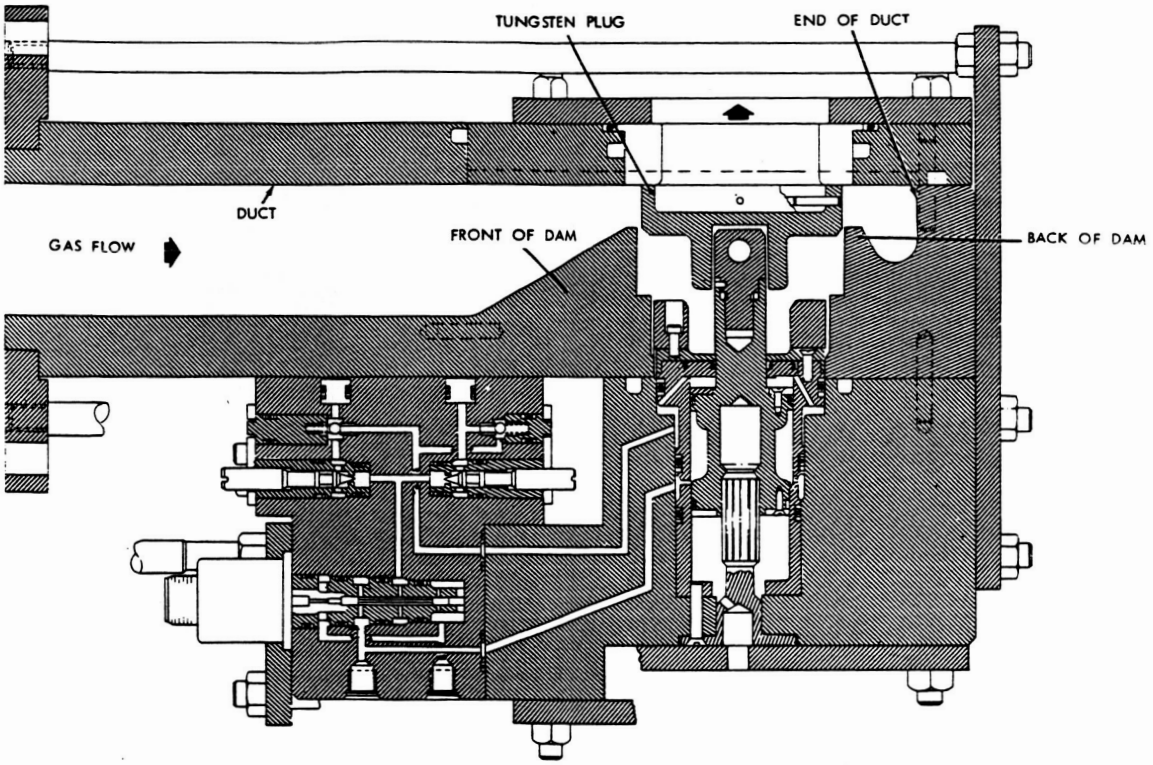

(a) HALF SECTION OF THE VALVE

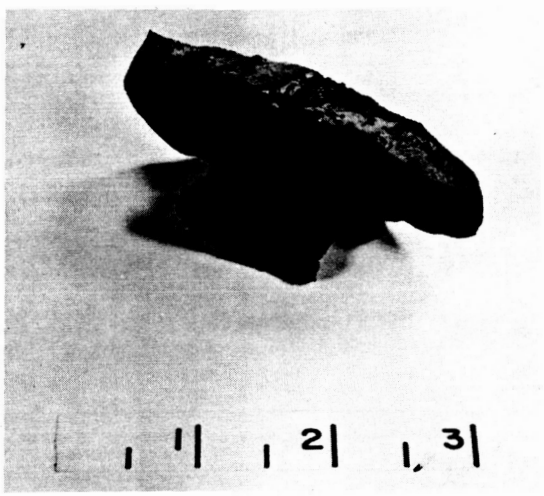

(b) TUNGSTEN PLUG AFTER FIRING

FIG. 4 90° ANGLE VALVE WITH TUNGSTEN PLUG AND GRAPHITE SEAT

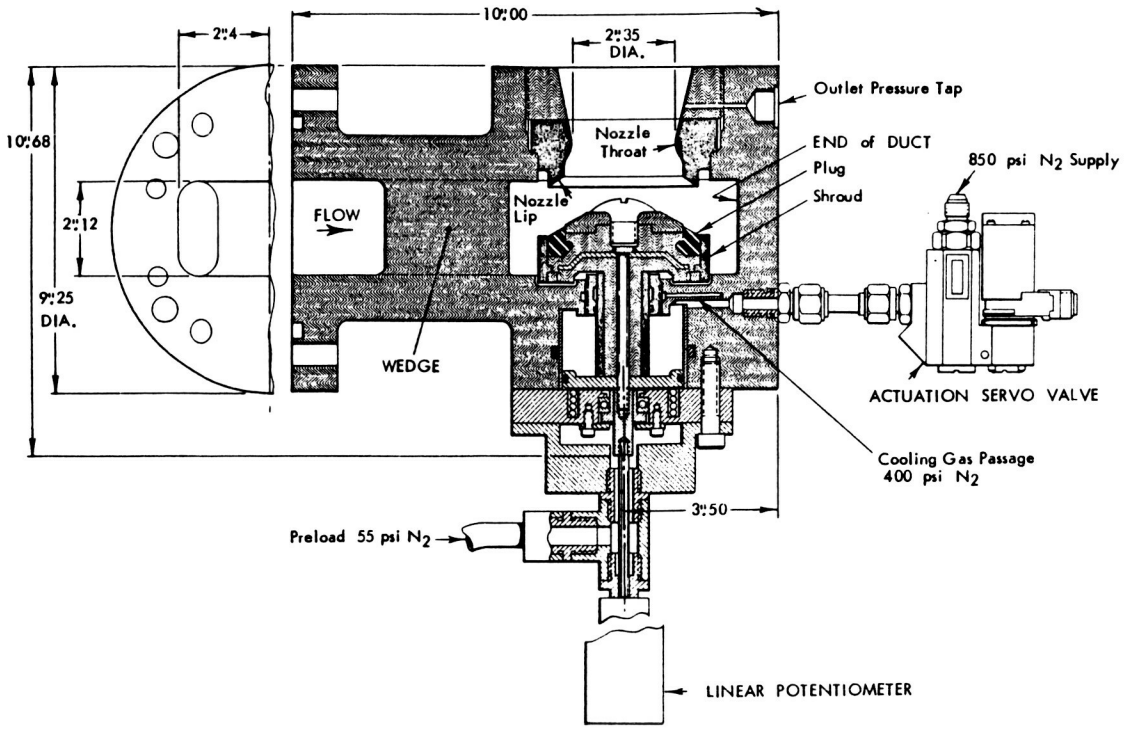

(a) HALF SECTION OF THE VALVE

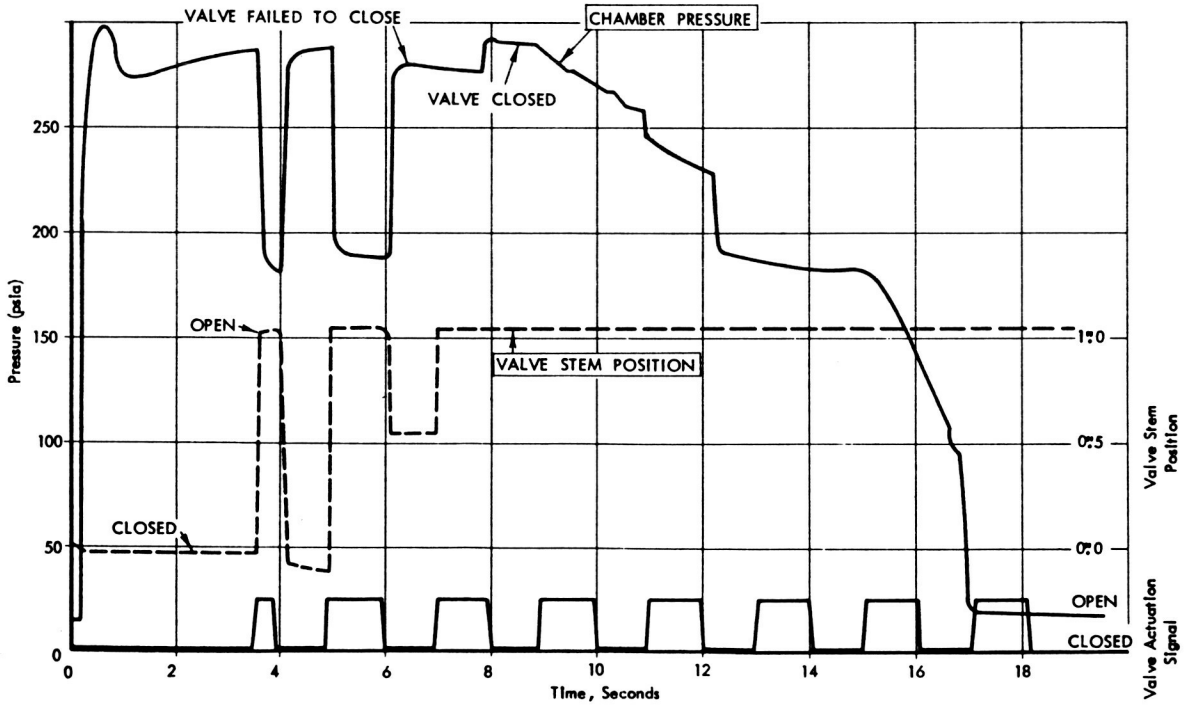

(b) FIRING RECORD

FIG. 5 90° ANGLE VALVE WITH SHROUDED RUBBER PLUG AND GRAPHITE SEAT

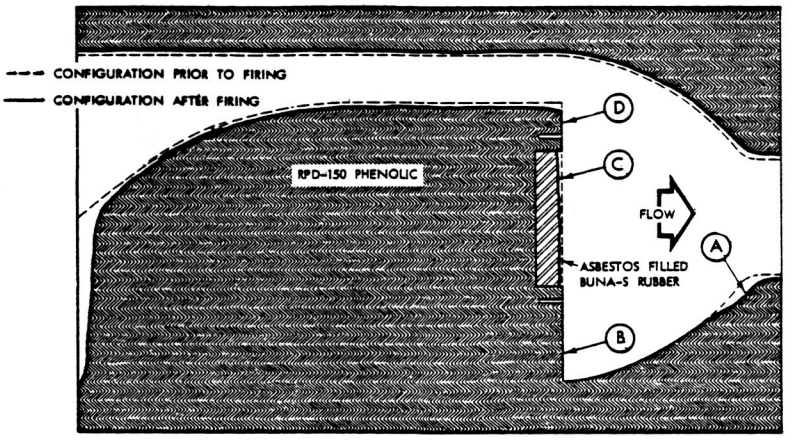

(a) HALF SECTION

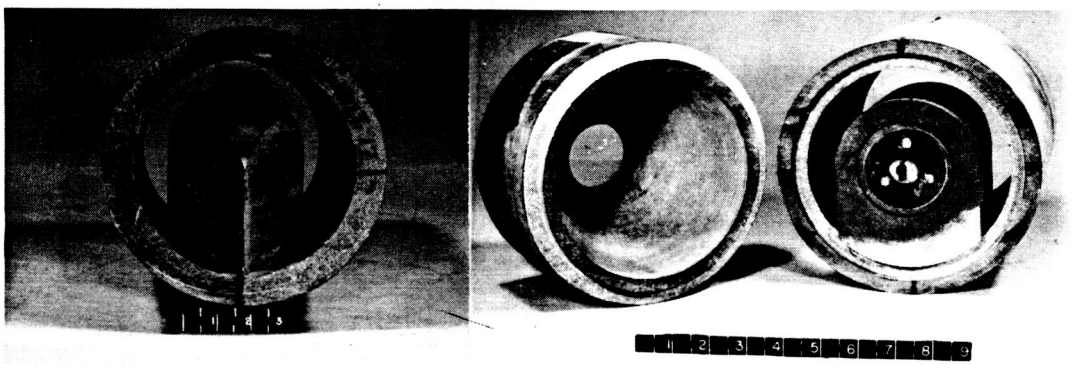

(b) BEFORE FIRING VIEWS

FIG. 6 FIRST STRAIGHT-THROUGH VALVE WITH SINGLE STRUT-SUPPORTED CENTERBODY

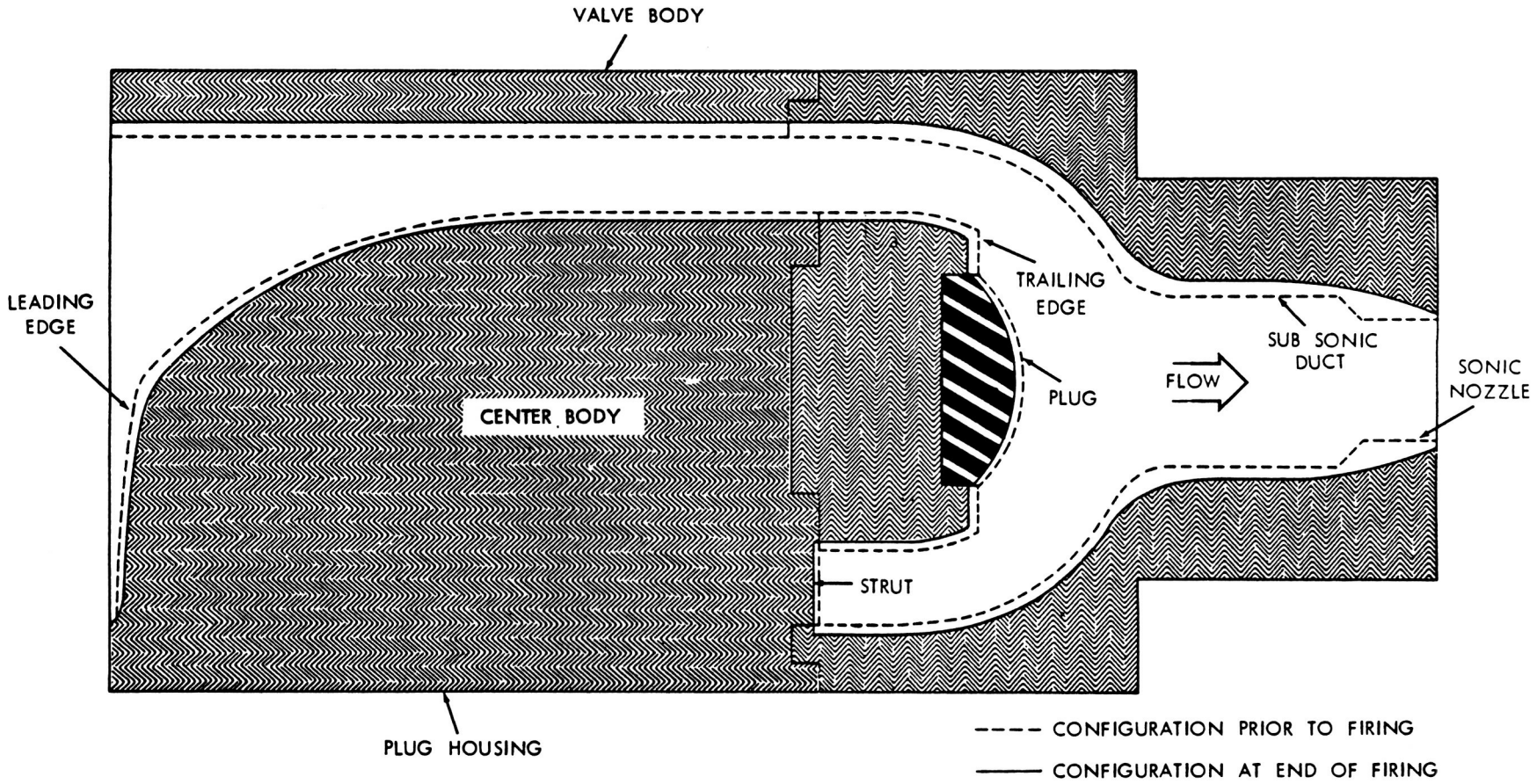

FIG. 7 SECOND STRAIGHT-THROUGH VALVE WITH SINGLE STRUT-SUPPORTED CENTERBODY

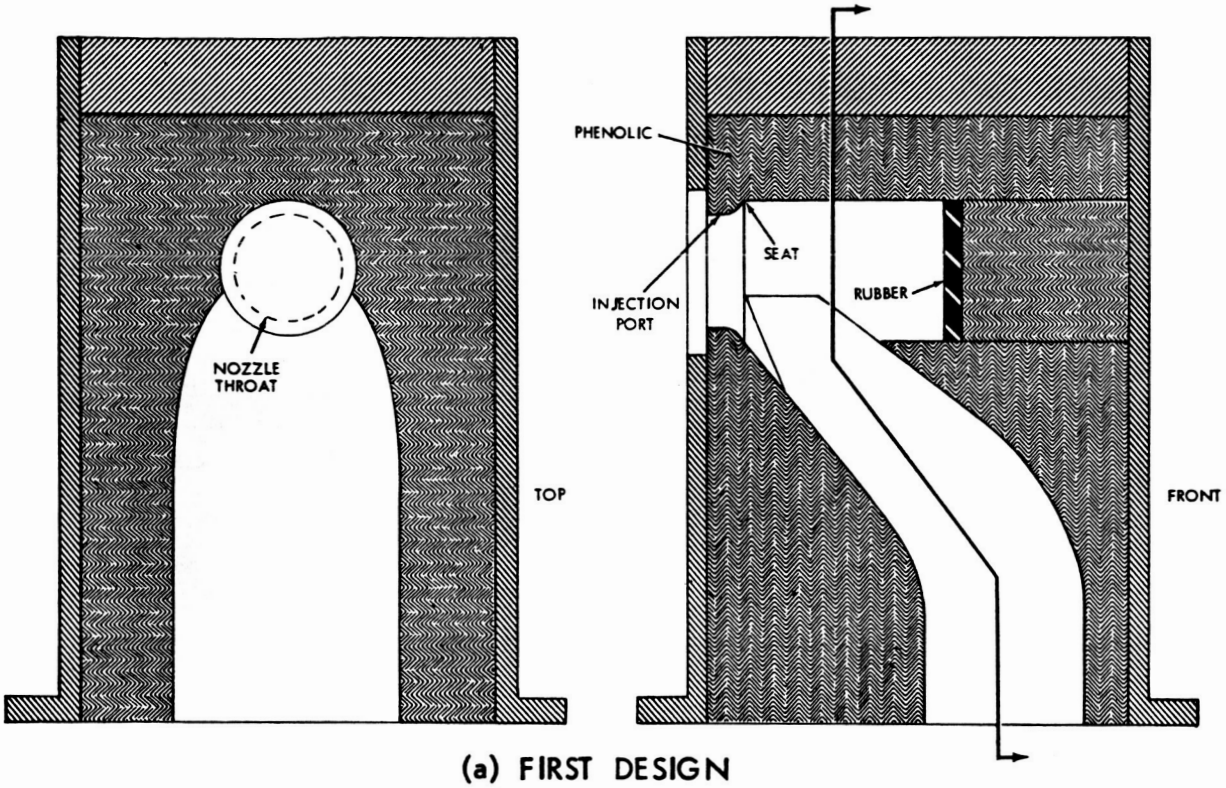

(a) FIRST DESIGN

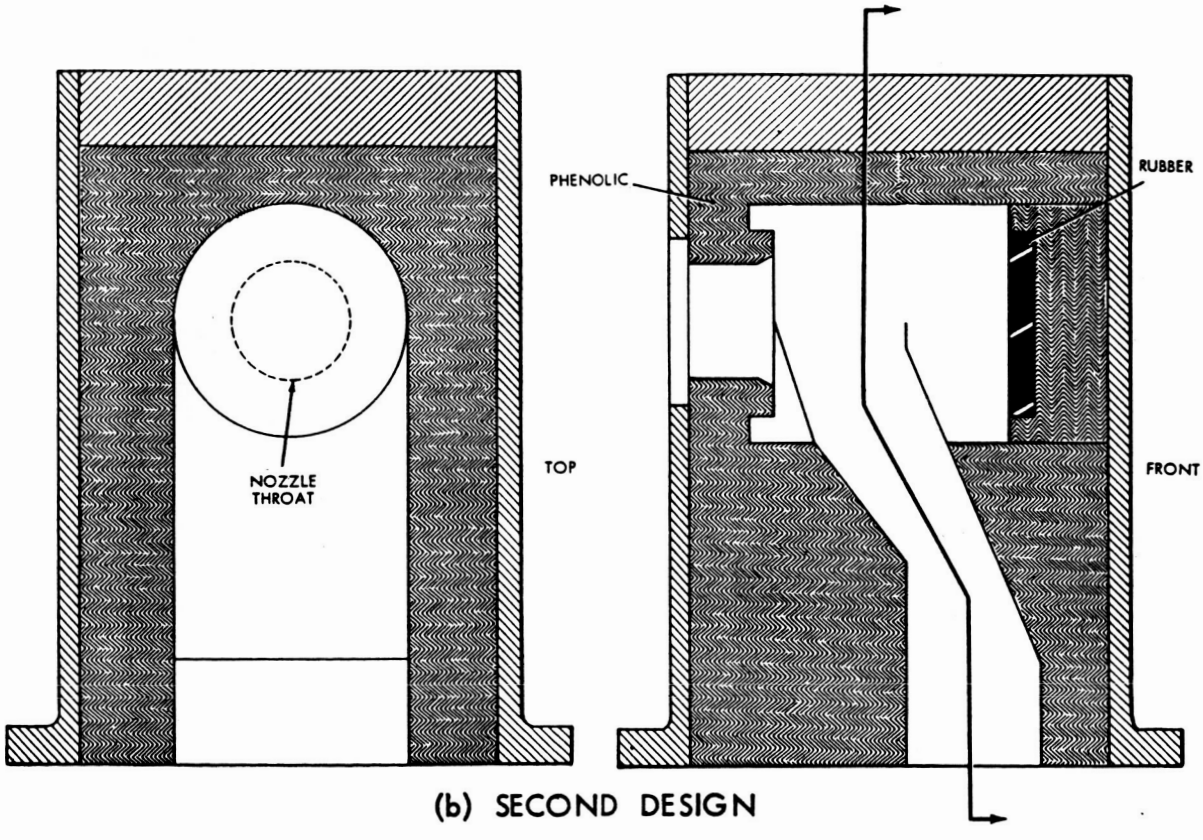

(b) SECOND DESIGN

FIG. 8 SECTIONED VIEWS OF STREAMLINE ANGLE VALVES

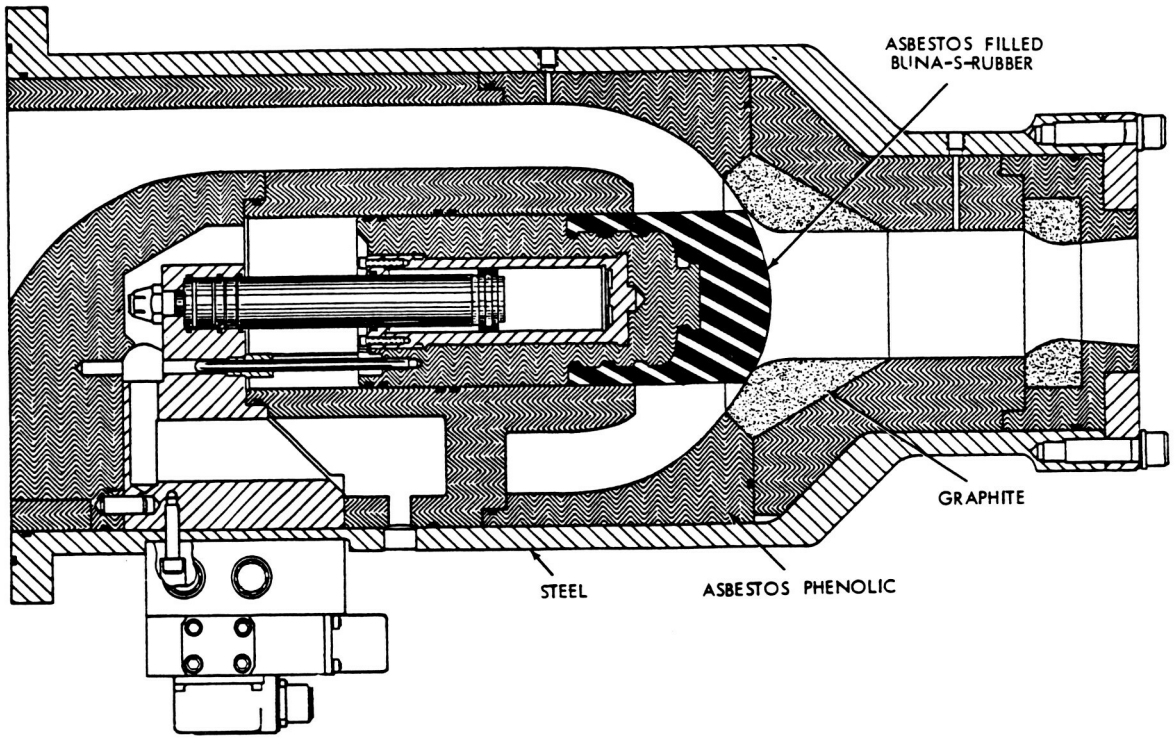

(a) CROSS SECTION OF THE VALVE

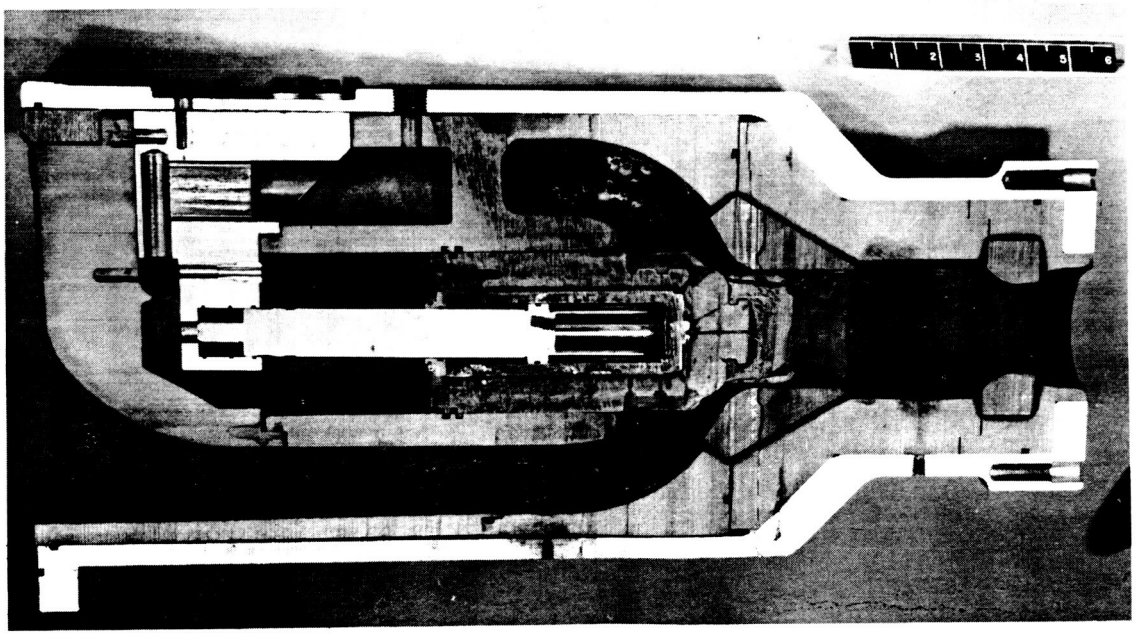

(b) SECTION VIEW OF VALVE AFTER FIRING

FIG. 9 STRAIGHT-THROUGH VALVE WITH SINGLE STRUT-SUPPORTED CENTERBODY

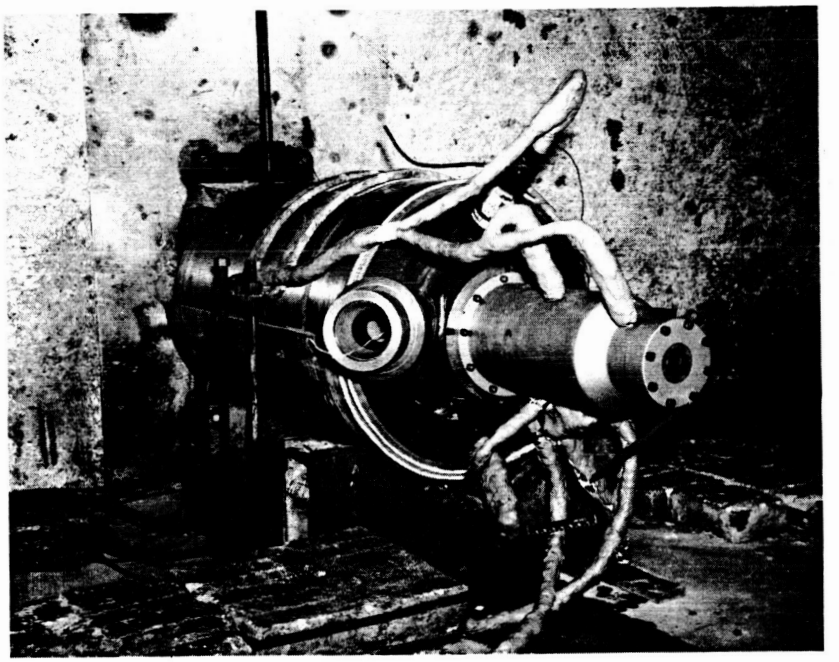

BEFORE FIRING

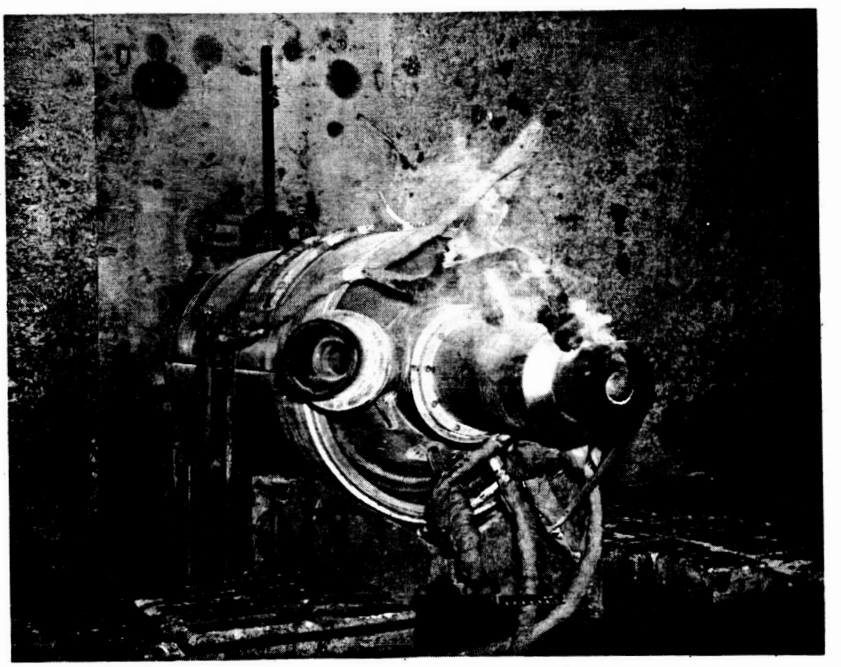

AFTER FIRING

FIG. 10 STRAIGHT-THROUGH VALVE MOUNTED ON 29" D MOTOR IN FIRING BAY

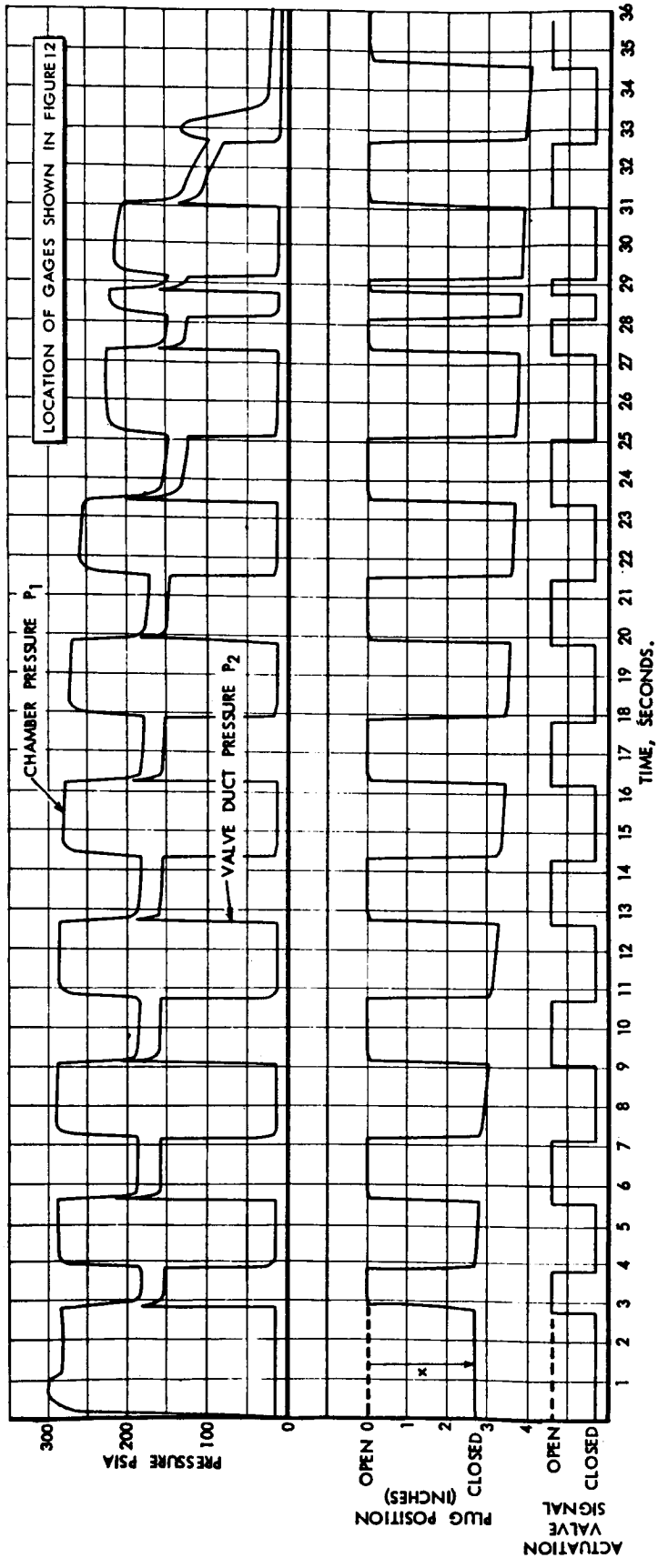

FIG. 11 FIRING DATA

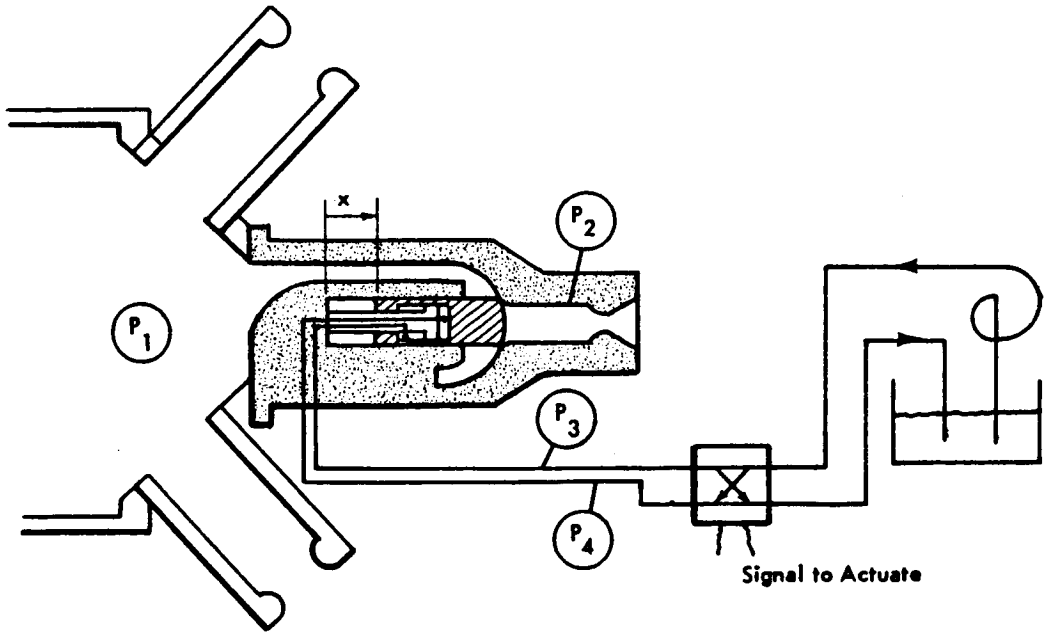

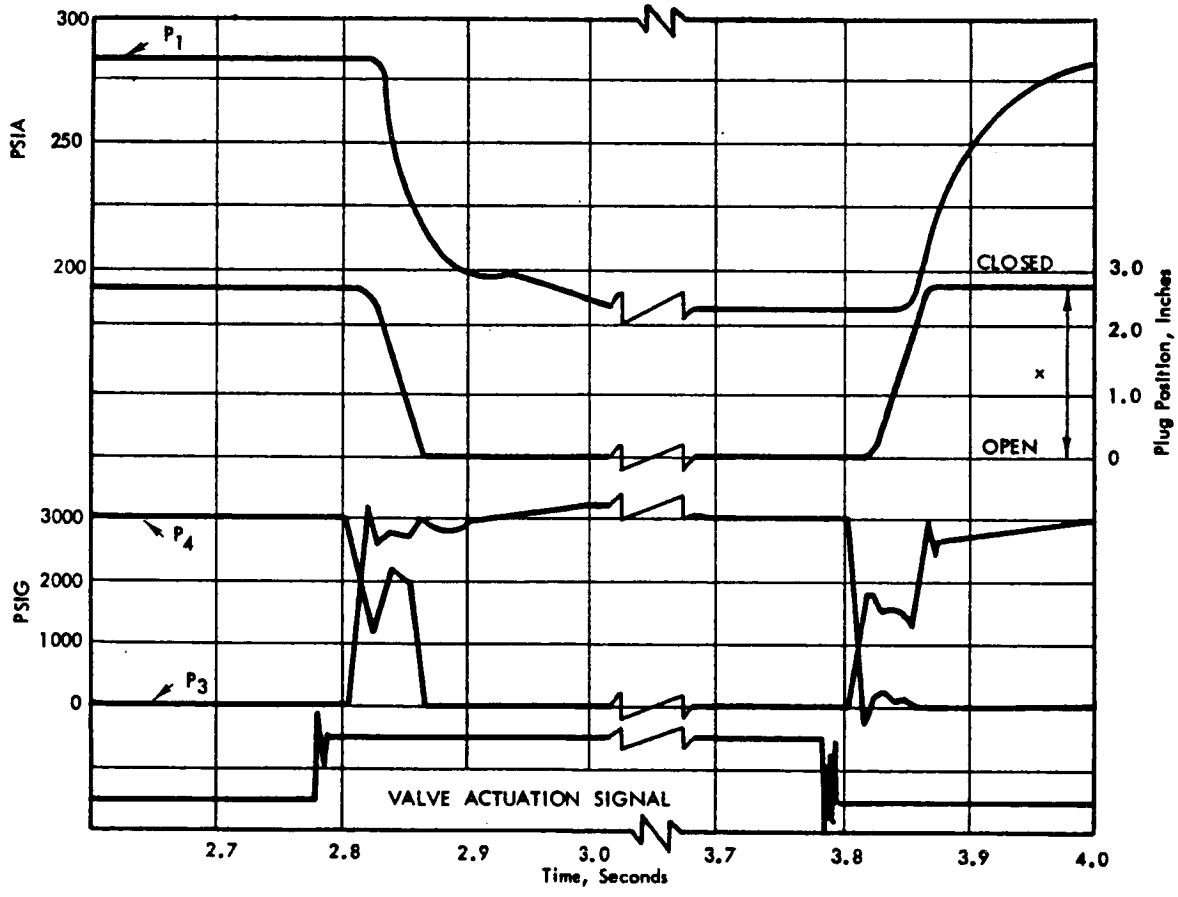

FIG. 12 TYPICAL OPENING AND CLOSING CYCLE

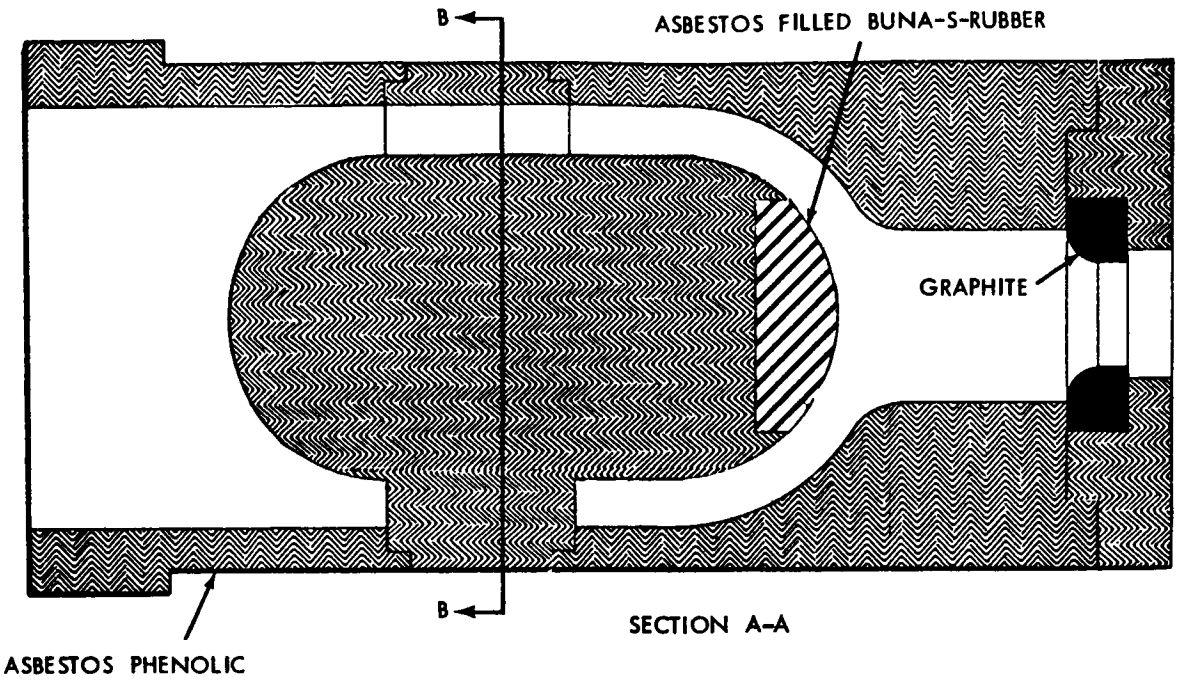

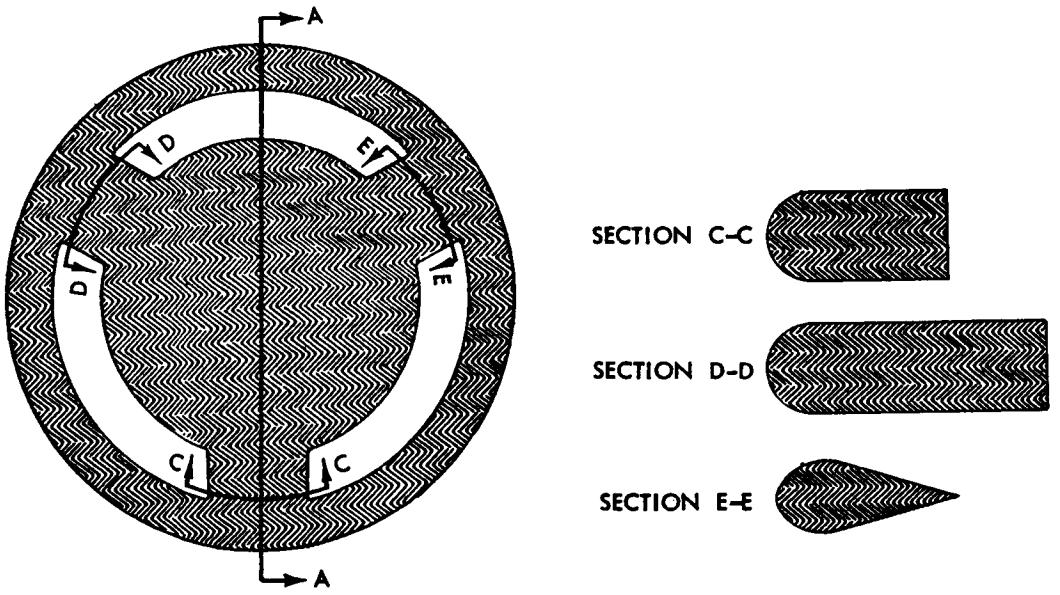

FIG. 13 STRAIGHT THROUGH WITH THREE STRUT-SUPPORTED CENTERBODY

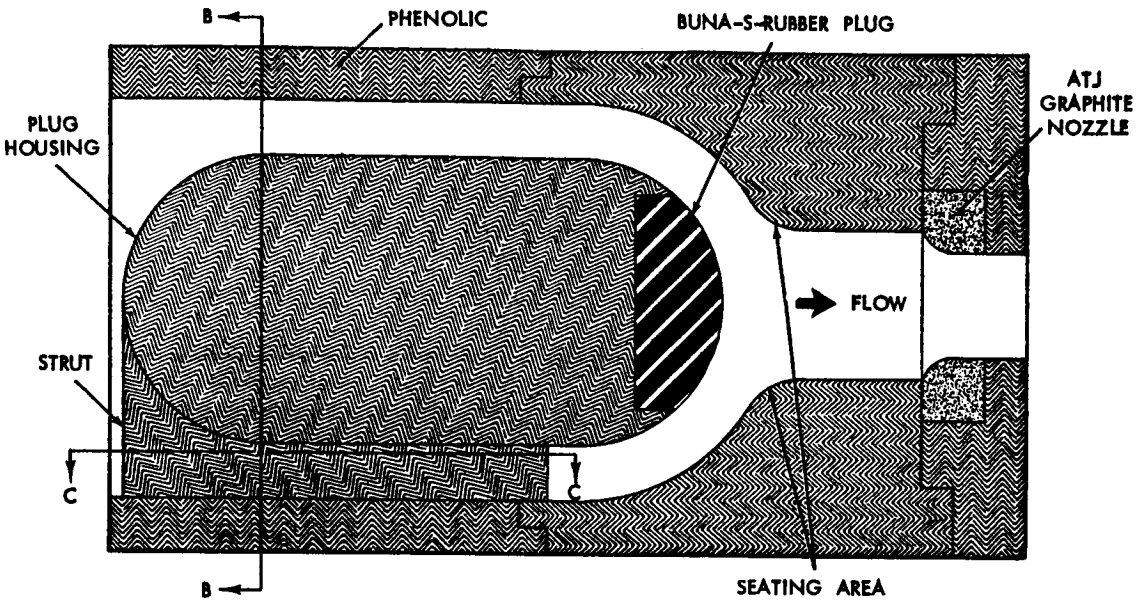

SECTION A-A

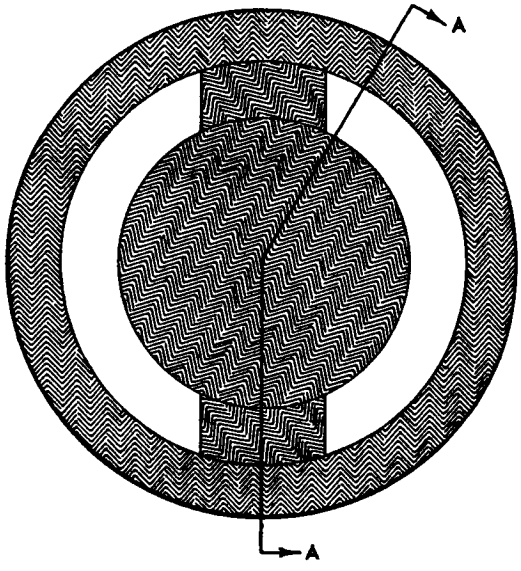

SECTION B-B

SECTION C-C

FIG. 14 STRAIGHT-THROUGH VALVE WITH TWO STRUT-SUPPORTED CENTERBODY

SYMPOSIUM ON

ROCKET MOTOR MATERIALS

Chairman

Mr. E. Olcott
Atlantic Research Corporation

THE EFFECT OF SURFACE DECARBURIZATION ON SPECIFIC STEELS

Lowell E. Hershey
Ingersoll Kalamazoo Division
Borg-Warner Corporation
Kalamazoo, Michigan

ABSTRACT

The purpose of this study was to determine the effect of varying depths of surface decarburization on the strength and notch toughness of three steels. The steels tested were MBMC #1, Super Tricent and AISI 9262 which are of similar composition except for increased carbon content.

The materials were evaluated in three thicknesses, .050", .100" and .150", for notch toughness using sharp center notched specimens and standard tensile specimens. Surface decarburization was obtained using an endothermic gas generator and the decarb depth was determined by a microhardness survey.

It was concluded that surface decarburization increased notch toughness and decreased the yield strength for all three materials, in all thicknesses and in a regular and predictable manner dependent upon the percentage of the total thickness that is decarburized.

INTRODUCTION

Surface decarburization has been shown to be beneficial in obtaining high strength results in missile cases and experimentally to increase the notch toughness of test specimens by a number of contributors to missile industry knowledge. I have no idea who first noted this phenomena but it may have been inadvertently discovered in a manner similar to our experience. Several years ago we fabricated a number of prototype cases of MBMC #1 steel for the purpose of demonstrating its applicability for high strength case applications as indicated by uniaxial tensile specimen tests. The first group were fabricated from .100" thickness sheet and 8 out of 10 burst below the tensile strength of the test specimens. Then a series of .050" thickness cases of the same design were hydrotested and 12 out of 17 burst above the tensile specimen results with many bursting above 290,000 psi.

In 1960 another group of prototype cases were begun in an effort to produce consistent high strength burst results. Decarburization and welding were completely eliminated in this group to eliminate variables. Lower burst strengths resulted indicating that decarburization was a factor. About this time the USS Seminar on the Evaluation of Missile Steels held June 9, 1960 in Pittsburgh was attended and upon noting their relatively good results on MBMC #1 steel that had been severely decarburized we became convinced that decarburization was the variable we were seeking. The remaining prototype cases were heat treated with varying depths of decarburization. The results were relatively consistent high burst strengths on power spun seamless cases but no pattern or optimum depth of decarburization was indicated from the few cases tried. A study of decarburization using sharp notched specimens to quantitatively define the effect of varying amounts of decarburization was then undertaken and this study is the subject of my paper.

This work was conducted under BuWeps Contract NOrd 15719.

Acknowledgements

Mr. S. J. Matesky, Bureau of Naval Weapons, Technical Director Contract NOrd 15719.
Prof. W. R. Weeks, Western Michigan University
Mr. E. S. Mills, Project Engineer, Ingersoll Kalamazoo Division
Mr. D. Thomason, Engineer, Ingersoll Kalamazoo Division
Mr. L. Castle, Technician, Ingersoll Kalamazoo Division

MATERIAL

Three materials in three thicknesses each were tested, MBMC #1, Super Tricent and AISI 9262 steels. The analysis of each is shown in Table 1.

TABLE I. CHEMICAL ANALYSIS OF MBMC #1, AISI 9262 AND SUPER TRICENT

Chemical Composition	MBMC #1	Super Tricent	AISI 9262
Carbon	0.42	0.49	0.615
Manganese	0.80	0.92	0.90
Silicon	1.65	1.65	1.85
Chromium	0.76	0.86	0.35
Vanadium	0.07	0.11	-
Nickel	-	2.00	-
Molybdenum	-	0.40	-
Phosphorus	0.015	0.010	0.008
Sulphur	0.007	0.006	0.010

The major emphasis was on the evaluation of MBMC #1 steel and the additional materials were chosen from available analysis close to that of MBMC #1 but with additional carbon. It can be seen that each material is a high carbon - high silica steel. The major departure was the nickel and molybdenum content in the Super Tricent. It was believed that these materials would indicate the effect of increased carbon content with surface decarburization on MBMC #1 steel.

The MBMC #1 and Super Tricent were obtained as forged cylinders and processed into sheets of .050", .100" and .150" thickness by power spinning the cylindrical blank to the appropriate thickness and then slitting and unrolling the tube to form sheet. The AISI 9262 was procured as cross rolled sheet from warehouse stock.

All materials were from electric furnace air melt heats. Air melt materials were used in the interest of economy since the MBMC #1 was on hand and because of the long lead time to obtain vacuum arc remelt material. It was our opinion that the results should indicate the minimum values and greatest variations to be expected from the materials tried.

PROCEDURE

The basis for the evaluation of the effect of surface decarburization was fracture toughness testing of the materials in general accordance with the Special ASTM Committee Report on Fracture Testing of High Strength Sheet Materials taken from the January and February 1960 ASTM Bulletin.

Center notched specimens having a .001" maximum notch root radius obtained by machining were used for all testing. The exact design of specimen is shown in Figure 1. This design conforms with the ASTM recommendation except for the .150" thickness specimen where the W/B ratio is smaller than recommended. This was done to utilize the same testing fixtures for all thicknesses. This could result in lower notch toughness values for the .150" thickness specimens but was apparently not a noticeable factor in the results obtained.

The tensile specimens were standard 10" x 1" specimens having a 1/2" wide x 2" long gage length.

The surface finish of the materials was maintained in the "as processed" condition to simulate the material finish that would occur on a fabricated case. The MBMC #1 and Super Tricent specimens were cut from the hoop direction of the spun tube and, therefore, represent the most severe stress condition existing in the case tube.

Both the notched and tensile specimens were completely machined prior to heat treat so that the notched specimens simulated a crack prior to heat treat, thereby receiving the decarburization in the notch root.

The specimens were cleaned of all scale by means of mechanical brushing and/or acid pickle prior to heat treat.

The AISI 9262 steel as received contained a layer of decarburization approximately .005" deep on each side. The carbon was restored to the surface by heat treat before proceeding with the final heat treat.

The specimens were heat treated in an 8 cubic foot Lindberg electric atmosphere controlled furnace. The atmosphere generator was of the endothermic type with atmosphere input at the rate of 300 cubic feet per hour. The atmosphere dew point and time in the furnace were varied to obtain various depths of decarburization. The specimens were suspended in a vertical position on a fixture during heat treat. Quenching was in oil at 100 to 130°F. Tempering was accomplished in a small Hump electric furnace.

The austenitizing and tempering temperatures for each material were determined by tensile specimen results and were selected as shown in Table II.

TABLE II. HEAT TREATMENT CONDITIONS SELECTED FOR DECARBURIZATION STUDY

Material	Austenitizing Temperature °F	Tempering Temperature °F
MBMC #1	1600	400-<u>500</u>-600
Super Tricent	1575	500-<u>600</u>
AISI 9262	1625	500-<u>600</u>-700

In this report we will show data on only the tempering temperature underlined for each material. These tempering temperatures are representative of the best overall results obtained for each material except for AISI 9262 at 700°F tempering temperature where the notch toughness was high at shallow decarb depth and the yield strength remained relatively high. The 600°F tempering temperature provided a more comparable condition for evaluation.

One of the most important and most difficult items encountered in evaluating decarburization was the method of determining the decarb depth of the various specimens. The method used for this study was a microhardness survey using a Kentron microhardness tester with the Tukon indentor.

The depths of decarb shown in this report were taken with a 200-gram load and represent a minimum of three surveys. The surveys were taken on both sides of the specimen near each end and the center. In instances where the side to side variation was considerable, additional surveys were made to obtain the average. The decarburization depth was considered to be that depth up to a hardness equal to the core hardness less 5%. Figure 2 illustrates graphically the method of decarb depth determination used throughout this study.

A microhardness survey from both the tensile specimen and the notch specimen was used to plot the respective curves. In most instances one specimen of a group of three processed together is used to determine the depth of decarb for the average value of the notch toughness or yield strength of that group.

The method of calculation of the K_c was the ink stain method for the majority of specimens. In cases where there was doubt of the ink stain due to spatter or drying the shear lip method was used. The majority of the .150" thickness specimens were calculated using the shear lip method.

The G_c values were calculated from the relationship $G_c = \frac{K_c^2}{E}$ with E considered constant at 30 million.

All tests were conducted at room temperature.

RESULTS

The results of varying depths of decarburization on the notch toughness measured by G_c and on the yield strength for MBMC #1 steel are illustrated in Figure 3. Although the plotted points do not follow the curves exactly a very definite trend is shown. The variations can be readily explained by the difficulty in determining an exact depth of decarb for a specific specimen, the method of calculation permits some error and variations in thickness from specimen to specimen would introduce additional error. On the basis of percentage variation from the curve shown the yield strength curves vary by less than 2%. The G_c shows variations as high as 10%.

The curves indicate a straight line relationship of the notch toughness and yield strength with the depth of decarburization. This infers that a similar pattern of decarburization occurred each time and this agrees with our observations. As a matter of fact attempts were made to vary the gradient of decarburization but this was not successful as long as the austenitizing temperature was held. Longer periods of time gave a greater depth of decarb but little change in the gradient.

One point on the .050" thickness curve labelled "1" was obtained on a center notched specimen heat treated in our regular production furnace, which is a much larger version of the small furnace used for this work. Its adherence to the established curve was gratifying.

The crossover of the .100" and .150" thicknesses G_c curves at .006" depth did not seem feasible and cannot be explained except that at the very shallow depths of decarb the values are more difficult to determine accurately and slight variations in the procedure of heat treat may have occurred. For example, it was found that exposure time to the air of the specimens when quenching will change the notch toughness value. This is particularly noticeable at the shallow depth of decarburization.

From the curves of Figure 3 the importance of depth of decarb is evident for MBMC #1 material. The notch toughness as measured by G_c can be increased from very low values to relatively high values, depending upon thickness and decarb depth. A corresponding decrease in yield strength occurs as the toughness increases but the percentage of loss in strength is less than the percentage of gain in toughness. It is evident that if decarb is to be used to increase toughness then the thickness is a major factor and changes in thickness must be evaluated. End rings on a case represent changes in thickness for attachment purposes and for absorbing bending stresses. If decarb is to be used to promote notch toughness then designs of transitions to end attachments must consider this effect.

By converting the depth of decarburization for a given level of notch toughness to a percentage of the thickness it can be seen that for the same percentage of thickness the notch toughness is about the same regardless of thickness. This is more clearly illustrated by Figure 4. The percentage relationship appears to hold quite well, although at the larger percentages the spread in this study increased. The many points shown represent all three materials and all three thicknesses. The straight line relationship holds for all three materials. From this curve it would appear feasible to determine the decarb depth in per cent for a given toughness value desired and apply this to any thickness of the materials tested up to at least .150" thickness.

The curves of decarb depth versus G_c and yield strength for Super Tricent are shown in Figure 5 and for AISI 9262 in Figure 6. The Super Tricent at 600°F tempering temperature is almost identical to MBMC #1 steel at 500°F tempering temperature. The AISI 9262 shows a similar pattern to the other materials but with a lower G_c and higher yield strength at a specific decarb depth.

Another measure of relative toughness is the ratio of the notched strength to the yield strength. This ratio versus the depth of decarburization for the MBMC #1 steel is shown in Figure 7. Similar data for Super Tricent and AISI 9262 are tabulated in Table III. The AISI 9262 was somewhat erratic at the .050" thickness with ratios well above and below the MBMC #1 values, and it would be necessary to assume the lower values as typical. The AISI 9262 ratio values for the .100" and .150" thicknesses were less erratic and definitely indicate values lower than MBMC #1 at equivalent decarb depths. The ratio values are all less than unity indicating notch sensitive materials.

In order to obtain some idea of the relationship of the results for MBMC #1 steel from these tests and the situation existing in actual cases a comparison with some prototype case work accomplished in early 1960 using MBMC #1 steel and reported in IKD Report SPDIR-25 issued July 14, 1960 was

made. The depth of decarburization was determined by the microhardness method outlined previously in this study from a section from each of the spun cases burst by hydrotest. The yield strength and ultimate strength for each case was taken from the uniaxial tensile specimens heat treated with each case. Since the cases were fabricated from .050" spun stock processed the same as the specimens in this study they should follow the .050" curves taken from the present study. Figure 8 shows the values of the case results compared to the present decarburization study results. The yield and tensile strengths compare closely. The burst strengths range up to 1.15 times the uniaxial tensile strength in a manner indicating conformance to the decarb depth-strength relationship developed in the current study. Prototype cases fabricated by the roll and weld method are in process which may indicate a relationship to depth of decarburization to obtain high strength burst results similar to those obtained on the spun cases.

CONCLUSIONS

The conclusions drawn from this study that apply to the materials tested using an endothermic gas generator for atmosphere control were:

1. Surface decarburization increases notch toughness significantly and in direct relationship to the depth.

2. Surface decarburization decreases the yield strength in direct relationship to the depth.

3. Surface decarburization increases the notch strength-yield strength ratio in direct relationship to the depth.

4. The effects of surface decarburization apply to varying thicknesses equally from .050" to .150" thickness on a percentage of the thickness basis for MBMC #1, Super Tricent and AISI 9262 steels.

5. The values of notch toughness and yield strength obtained using decarburization were highly predictable and repeatable for the materials tested.

6. Increasing the carbon content from .42% to .60% resulted in no marked changes in the strength level or notch toughness effect of surface decarburization in the tempering temperatures range from 500 to 600°F.

TABLE III. NOTCH STRENGTH TO YIELD STRENGTH RATIO DATA FOR SUPER TRICENT AND AISI 9262 STEELS

Material	Avg. Number of Specimens	Nominal Thickness	Decarb Depth	Ratio σ_{NS}/σ_{YS}
Super Tricent	3	.05	.002	.44
	3	.05	.003	.46
	2	.05	.004	.51
	3	.05	.005	.48
	2	.05	.008	.64
	3	.05	.010	.81
AISI 9262	3	.05	.000	.155
	3	.05	.004	.328
	3	.05	.006	.79
	2	.05	.007	.71
	3	.05	.008	.844
	3	.05	.010	.64
Super Tricent	3	.10	.002	.33
	3	.10	.005	.44
	2	.10	.007	.50
	2	.10	.008	.47
	2	.10	.010	.60
	2	.10	.010	.48
AISI 9262	3	.10	.000	.157
	3	.10	.001	.281
	3	.10	.006	.474
	2	.10	.007	.434
	3	.10	.008	.391
	6	.10	.012	.46
Super Tricent	3	.15	.003	.34
	6	.15	.005	.39
	5	.15	.007	.44
	2	.15	.008	.52
	2	.15	.011	.60
AISI 9262	3	.15	.000	.12
	9	.15	.006	.28
	3	.15	.007	.28
	3	.15	.012	.40
	3	.15	.015	.48

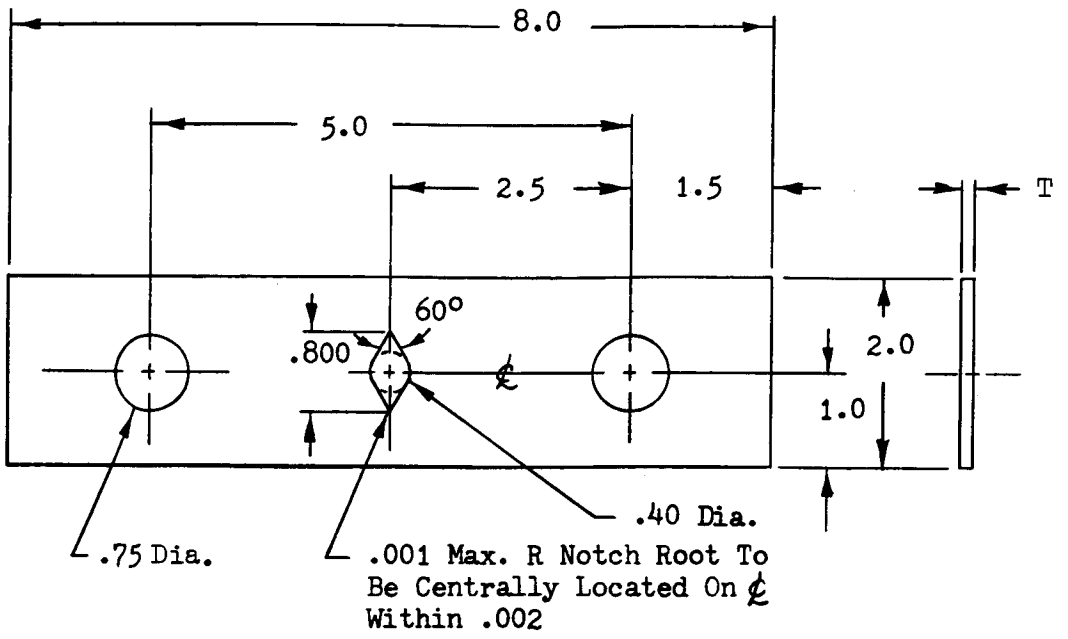

FIGURE 1. DIMENSIONAL SPECIFICATION OF CENTER NOTCHED SPECIMEN

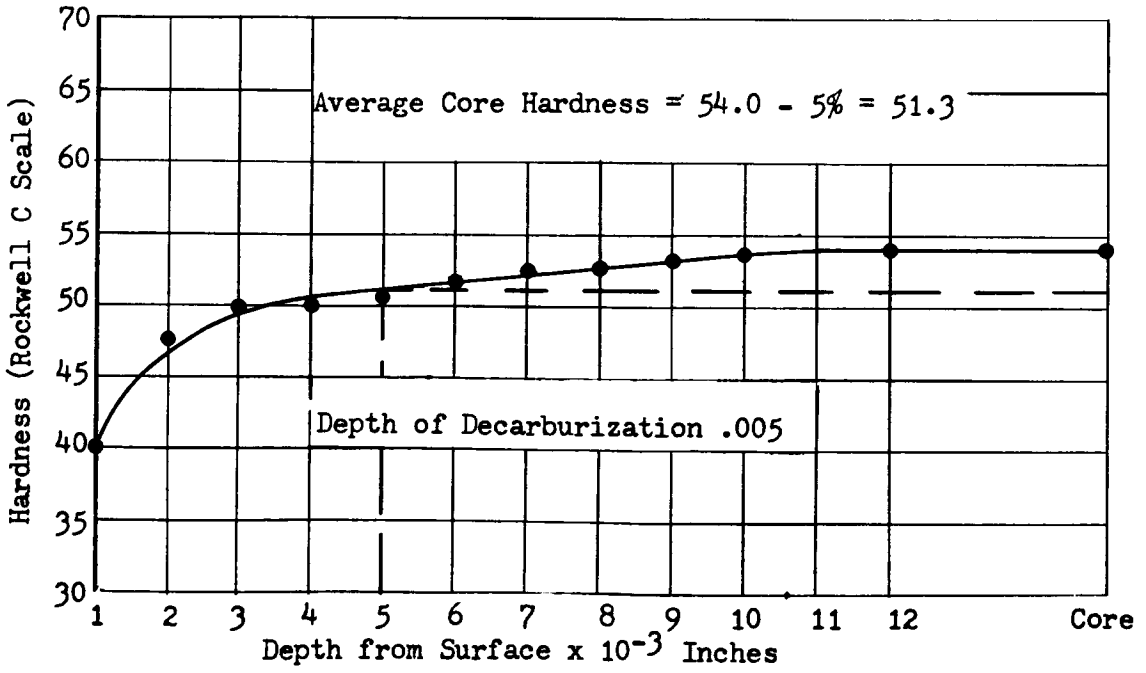

FIGURE 2. PLOT OF MICROHARDNESS SURVEY & DEPTH OF DECARBURIZATION DETERMINATION

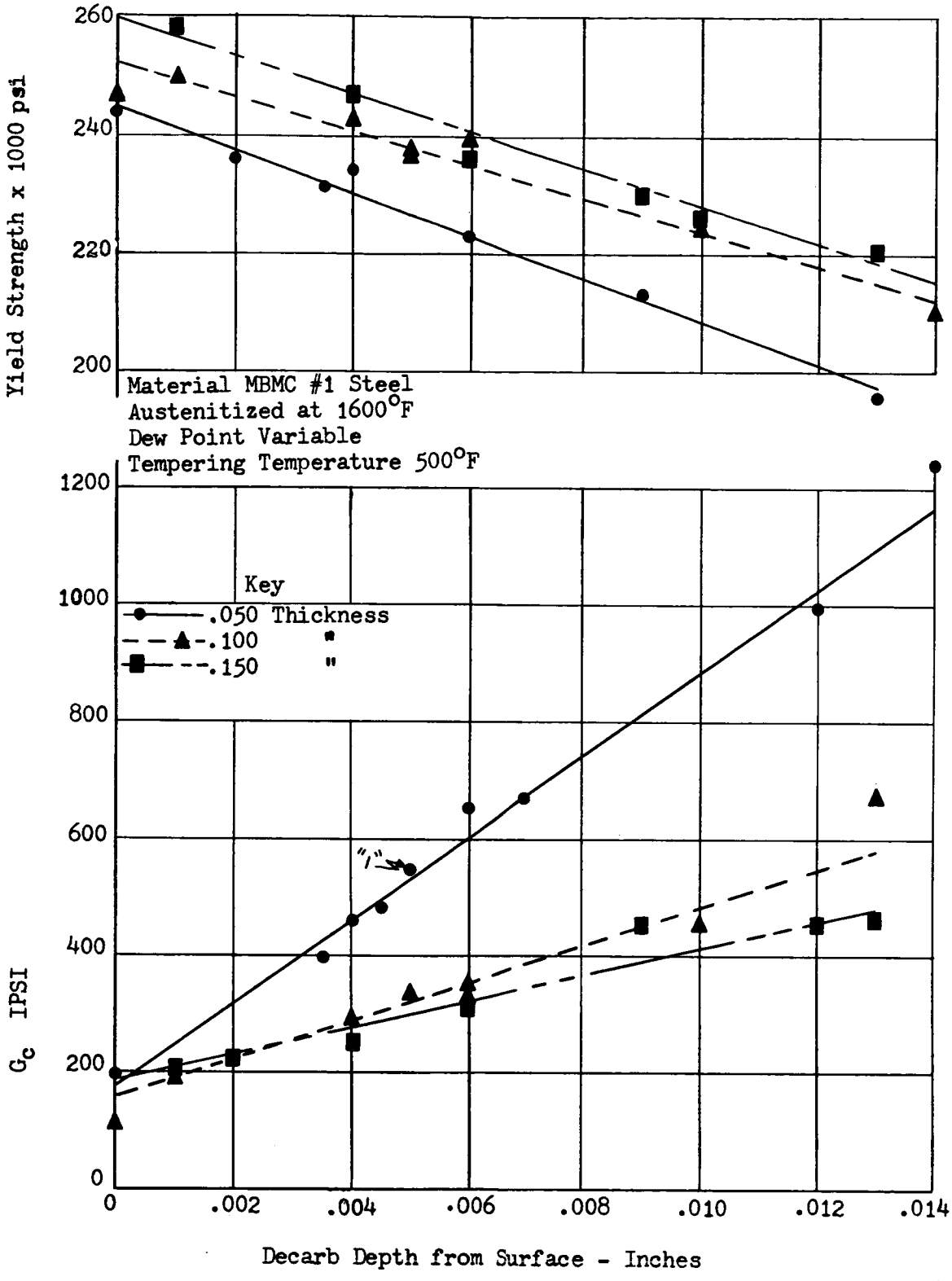

FIGURE 3. G_c & Y.S. RELATIONSHIP TO DECARB DEPTH - MBMC #1 STEEL

KEY

● .050 thickness
▲ .100 "
■ .150 "

Data include all three steels
Figures 3, 5 and 6.

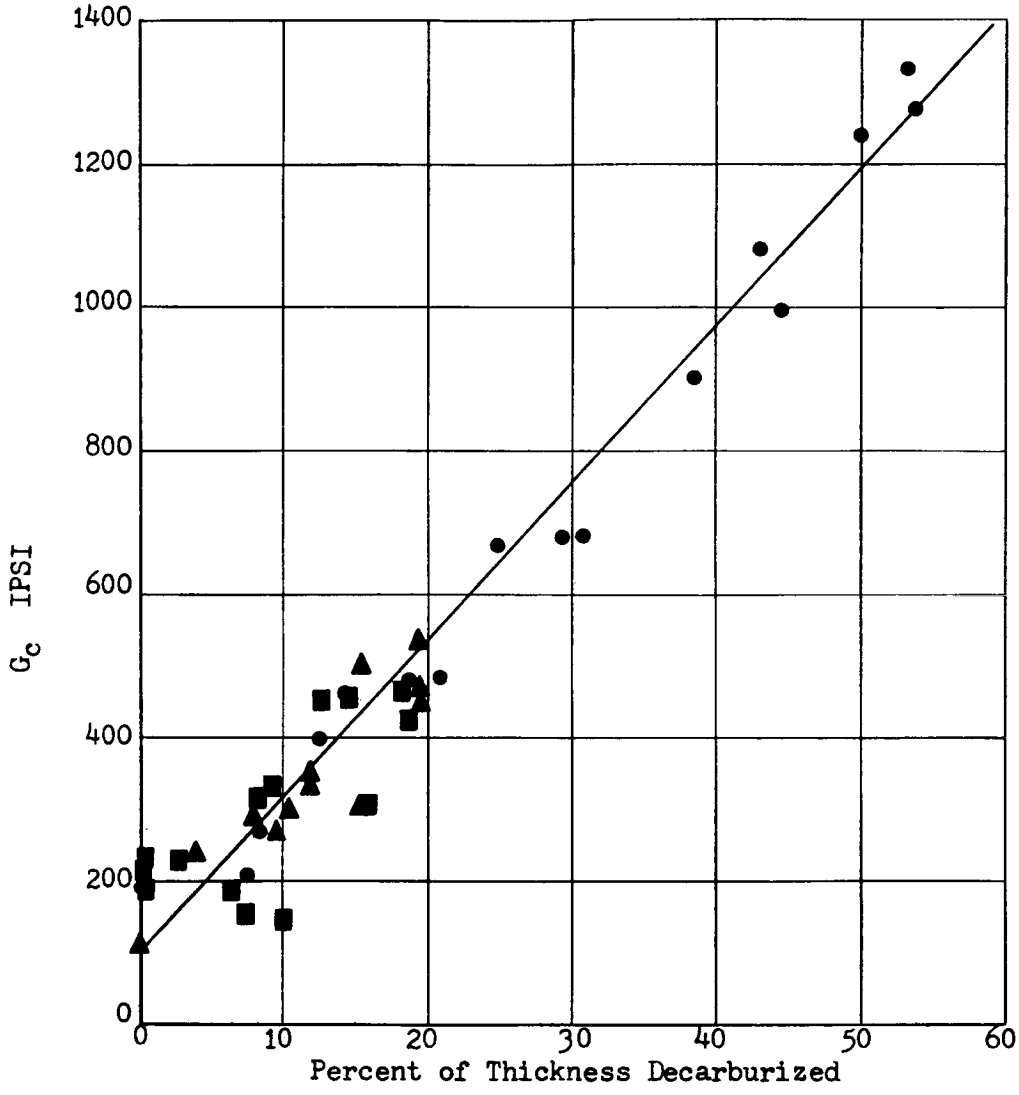

FIGURE 4. RELATIONSHIP OF G_c TO PERCENT OF THICKNESS DECARBURIZED

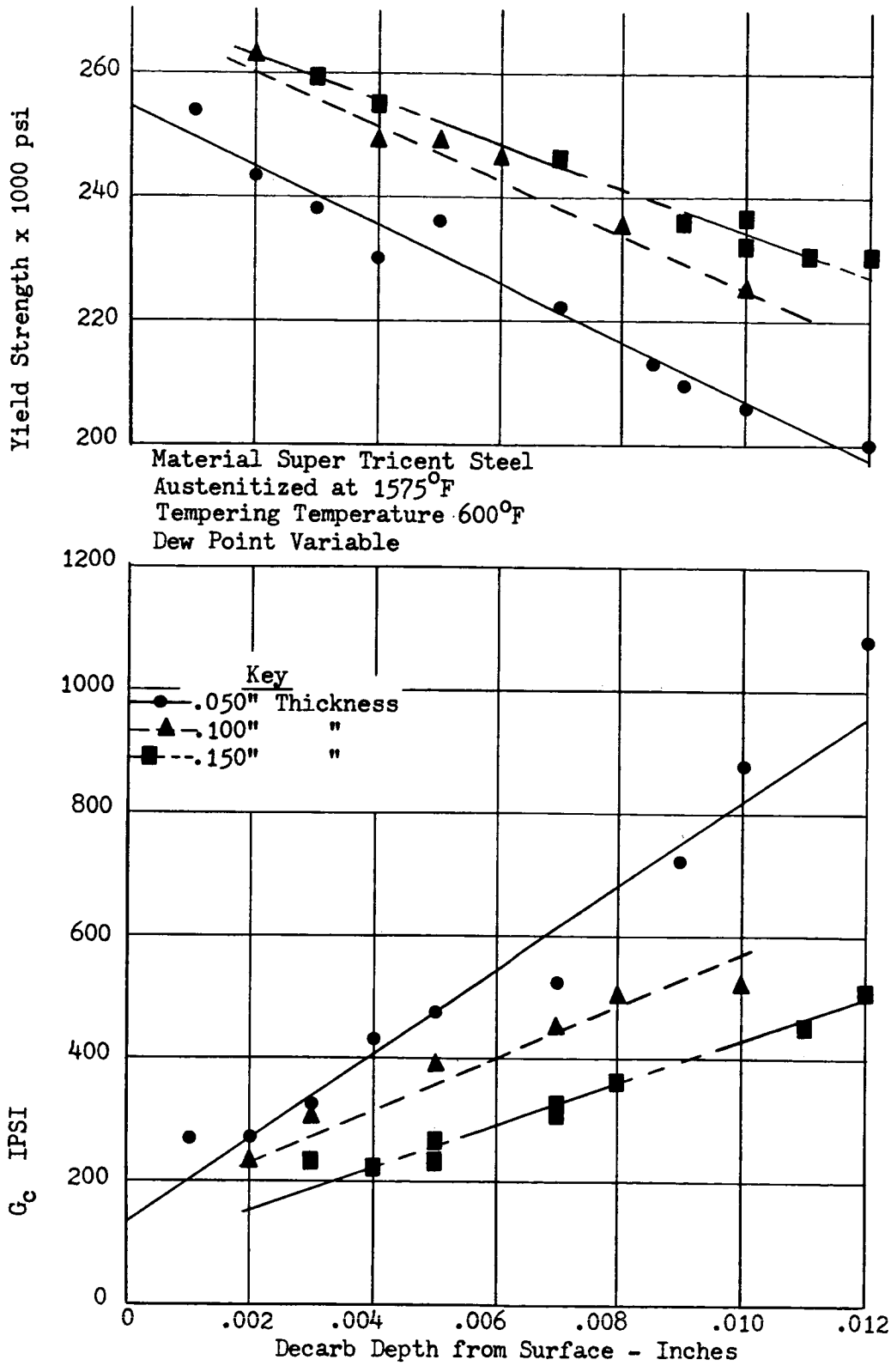

FIGURE 5. G_c & Y.S. RELATIONSHIP TO DECARB DEPTH - SUPER TRICENT STEEL

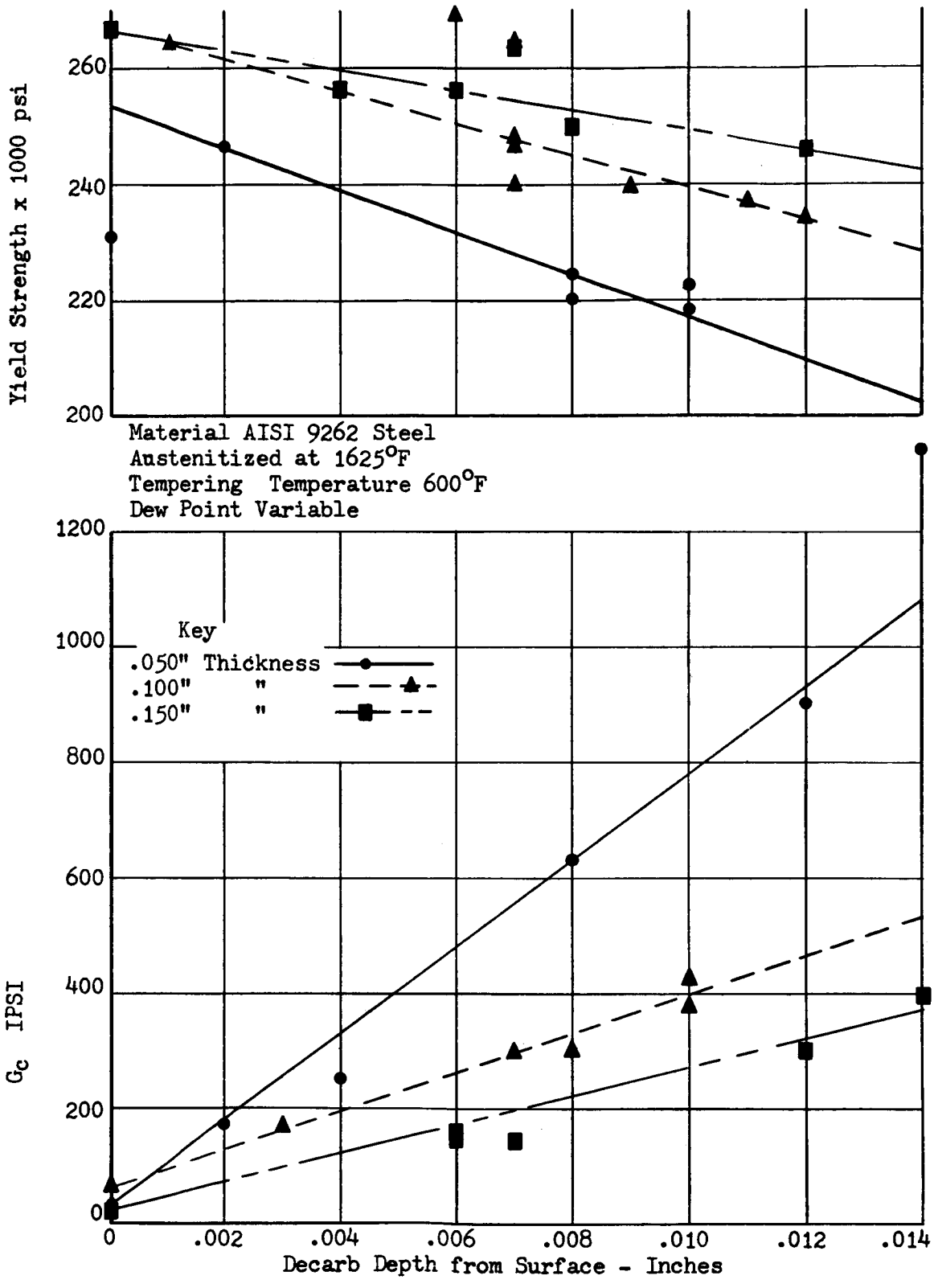

FIGURE 6. G_c& Y.S. RELATIONSHIP TO DECARB DEPTH - AISI 9262 STEEL

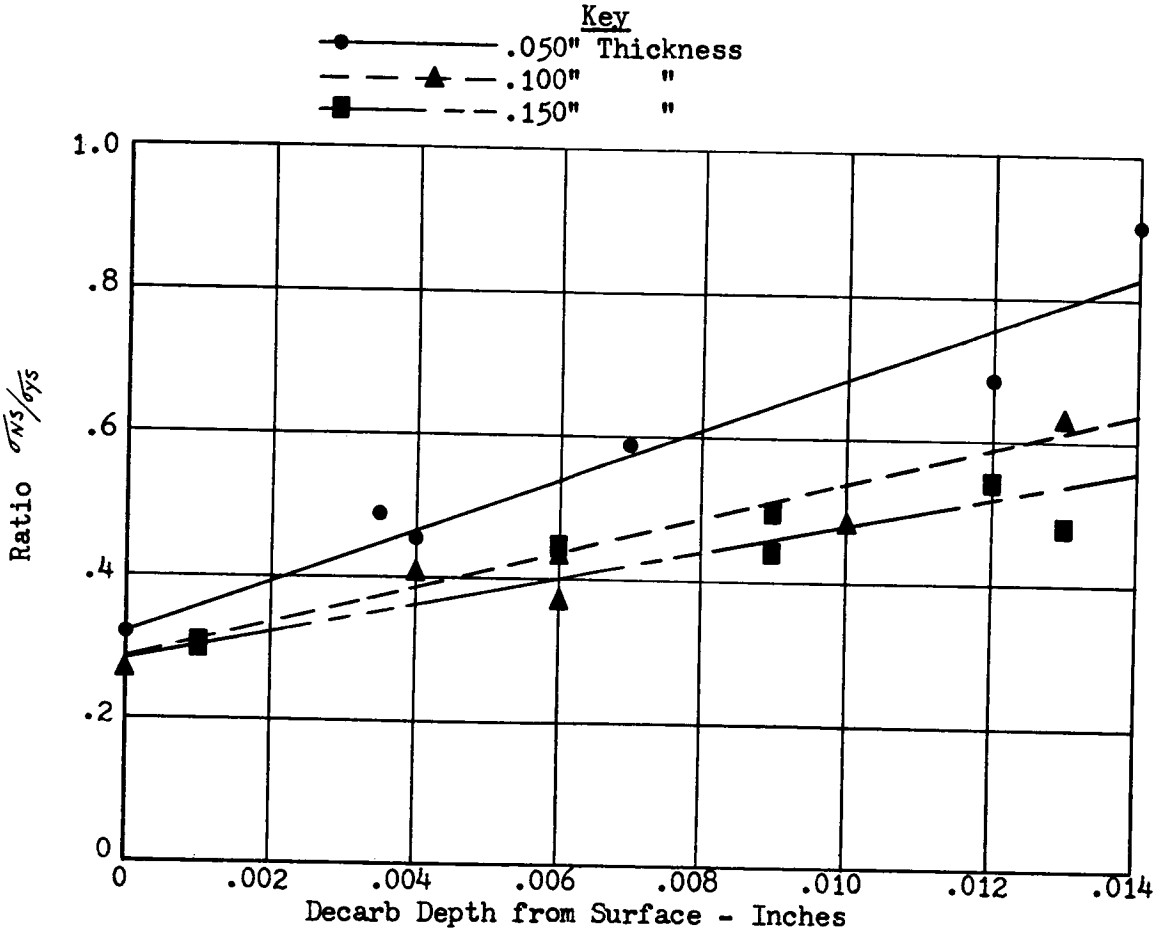

FIGURE 7. RELATIONSHIP OF NOTCH STRENGTH - YIELD STRENGTH RATIO WITH DECARB DEPTH - MBMC #1 STEEL

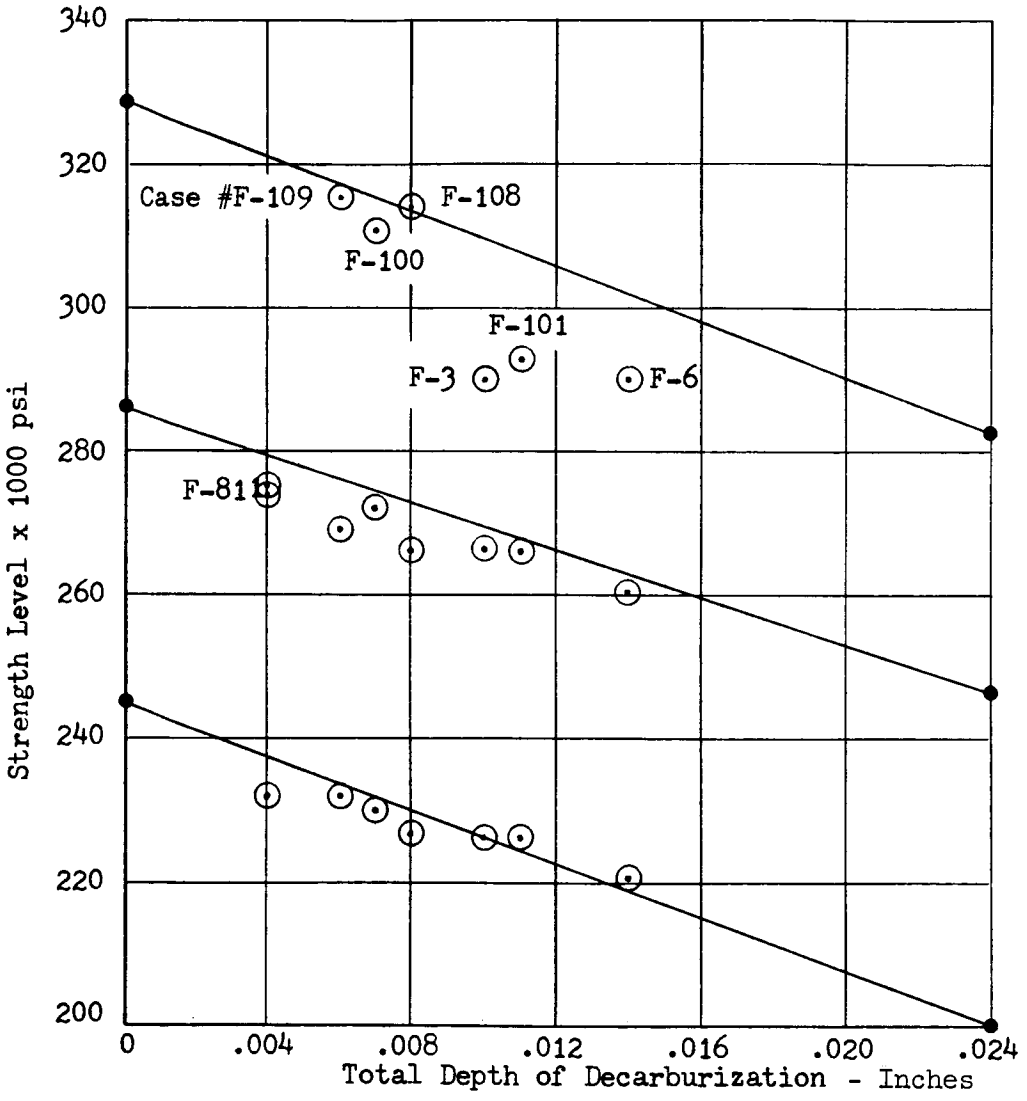

FIGURE 8. PROTOTYPE CASE RESULTS FROM 1960 WORK COMPARED TO CURRENT DECARB RESULTS

DESIGN AND FABRICATION OF TUNGSTEN FOR ROCKET NOZZLE COMPONENTS

L F Glasier, Jr., P P Crimmins and D R Collis
Aerojet-General Corporation
Solid Rocket Plant
Sacramento, California

ABSTRACT

The environmental conditions, design, material properties and thermal analysis are discussed for solid propellant rocket motor nozzles of the heat sink or uncooled type utilizing tungsten throat liners.

The fabrication, properties, and performance of pressed, sintered and metal infiltrated tungsten; spun tungsten sheet metal; and pressed, sintered and forged tungsten are presented and discussed.

INTRODUCTION

The design considerations, experience, and materials fabrication described in this paper are limited to nozzle flame barriers or throat liners for solid propellant rocket motors of the uncooled or heat sink type designs. The environmental conditions, especially gas flame temperatures greater than 5000°F, rather simply dictated the choice of the material for nozzle throat liners. Tungsten was the material selected in spite of high density, a paucity of high temperature properties data, a minimum of experience in the fabrication of the sizes (throat diameters up to 5 inches) and possibly complex shapes required, and a variety of fabrication methods that existed approximately 2 to 3 years ago.

Tungsten still remains the material choice for throat liners, now possessing a good firing performance record and an even greater potential for continued and expanded use as material and fabrication knowledge and experience continue to increase.

The environmental conditions that are considered in designing a nozzle throat liner, the basic configuration of a typical and a specific successful design, some results of analysis and testing, and certain material fabrication techniques and results are discussed in the following sections of this paper.

DESIGN

Environment. In general, the design experience described in this paper is limited to solid propellant gas flame temperatures between 5000°F and 6000°F, and to motor operating pressures of about 500 psi.

The following is a tabulation of several parameters that influence the design and performance of throat liners:

Propellant Flame Temperature	5500°F
Mass Flow Rate	40 lbs/sec
Pressure at Nozzle Throat	300 psi

Gas Velocity	3500 ft per sec
Duration	60 sec
Gas Temperature @ Throat	5100°F
Heat Flux @ Throat	950 BTU/Sq.ft-sec

The values shown are for a typical rocket nozzle, and are the foundation of the thermal analysis discussed in a subsequent section. Unless a neutral pressure-time relationship exists, these parameters will be time dependent, and should be considered in the thermal analysis.

Once the basic environmental conditions of the nozzle are defined, a detailed thermal analysis is performed in order to fully define the thermal gradients and stresses in the nozzle throat liner. Before the thermal analysis is discussed, a typical throat assembly configuration will be described and some properties of tungsten presented.

Nozzle Throat Configuration. One of the most essential aspects of designing a successful tungsten nozzle throat is the manner in which the liner is supported in the nozzle. Tungsten has a high thermal conductivity, therefore the material supporting the liner must be capable of withstanding high temperatures, e.g. approaching 5000°F. In addition, the stresses that are induced by thermal expansion require that structural support be provided over the entire length of the throat liner. The ejection forces applied to the nozzle throat assembly are then transmitted to the structural housing of the nozzle.

An efficient throat system that has been developed for supporting tungsten liners in a movable nozzle is illustrated in Figure 1. In this design, a tungsten liner approximately 0.25" thick is supported in a graphite ring. The tungsten and the graphite are not bonded but are very carefully lapped together (a) to insure uniform support to the tungsten, (b) to prevent gas flow or leakage behind the throat, and (c) to insure a high coefficient of heat transfer across the interface. A requirement for 95% surface contact has proven adequate. To prevent cracking of the graphite due to thermal expansion of the tungsten, a molybdenum ring is used to provide hoop support. The molybdenum ring is shrink fitted onto the graphite, prior to assembly, and produces an initial compressive stress in the graphite. To avoid overheating of the molybdenum ring during firing, a coating of zirconium oxide is applied to the outside diameter of the graphite. The molybdenum ring transmits nozzle throat loads directly into the structural housing. All interfaces between tungsten and graphite and between graphite and molybdenum are slightly tapered. This taper is a practical method for insuring proper assembly tolerances and prevents concentric parts from slipping aft, or being ejected, under loading.

Material Properties. In order to predict the thermal gradients and stresses in a tungsten nozzle liner, as a precursor to satisfactory performance, certain material properties of tungsten must be available.

While it is possible to obtain 100% of theoretical density in tungsten, it is not essential in some design applications. It is therefore desirable to know the mechanical and physical properties of tungsten over a range of densities (75% to 90% TD). Figure 2 shows the effect of density on the relationship of tensile strength vs temperature and Table

1 lists some physical properties of tungsten at 95% of theoretical density at various temperatures. Space does not permit a description of all the material properties developed but from the foregoing data a requirement of 95% of theoretical density was found to be practical for the specific throat liner design considered.

Thermal Analysis. Figure 1 is a cross sectional sketch of a nozzle using a tungsten throat liner, and will be used to illustrate the results of thermal analysis. Figure 3 shows the predicted temperatures at 32 different locations in this nozzle throat assembly at the end of 60 seconds of motor operation. A discussion of the method of analysis will not be made, but it is pointed out that temperature dependent properties must be considered, in order to obtain meaningful predictions.

No thermal resistance has been assumed for the various interfaces. This is an assumption that is being investigated further, although a fair correlation of predicted temperatures to actual temperatures has been established. Tests are being conducted to determine heat transfer across an interface as a function of surface finish and contact pressure. Analyses of the metal and plastic components in the fired nozzle tend to confirm the thermal predictions previously described in Figure 3. The highlights in confirming the temperatures at various locations are as follows:

(a) Melting of the leading edge of the molybdenum ring confirms the analysis temperature of 4970°F at the tungsten molybdenum interface, location T4. The melting temperature of molybdenum is about 4750°F.

(b) The charring of the plastic sealing compound near location T32 indicates a temperature of 700°F, and approximately confirms the analysis temperature of 850°F in the titanium structure.

(c) The temperature predictions in the molybdenum-titanium joint area are between 800 and 900°F. Since the plastic material used here did char (indicating approximately 800°F) and the "O" rings have not started to melt, (estimated melt temperature of 1000°F), the analysis appears valid in this area. Locations T30, T31 and T32 are in this zone, and temperatures of 850° to 900°F were predicted.

MATERIALS FABRICATION

The material fabrication development of tungsten at the Aerojet-General Corporation has been varied and wide, but for this presentation only the following fabrication methods and results will be briefly presented:

1. cold pressed, sintered and metal infiltrated,
2. sheet metal spinning and
3. cold pressed, sintered and forged.

All three of the fabrication methods originate with cold pressed and sintered tungsten which will not be discussed because of the thorough coverage currently available in the literature. The infiltration concept deals with the fabrication and performance evaluation of a deliberately produced low density, pressed and sintered matrix and the utilization

of the porous structure as metal coolant reservoir. The second approach involves the fabrication, by spinning techniques, of sheet metal (produced from hot worked, pressed and sintered material). The forging is concerned with the hot working of high density (ca. 90% TD), pressed and sintered tungsten into a desired configuration and microstructure.

Cold Pressed, Sintered and Metal Infiltrated. The concept of infiltrating a porous, pressed and sintered tungsten matrix or skeleton with a sacrificial coolant-type material is extremely attractive for rocket nozzle throat applications. The possible advantages include evaporative cooling, reduced thermal gradient stresses, increased strength and ductility over a non-infiltrated high density matrix, and a possible slight weight saving. Many problems were posed initially however; such as, optimum infiltrant and quantity; optimum matrix structure, density and strength; scale-up problems for large nozzle shapes; and so forth. All of these problems and more are under investigation at the Aerojet-General Corporation, but from a practical engineering standpoint silver has been successful in a nominally 80% dense tungsten matrix. Motor firings with silver infiltrated tungsten throat liners have been successful with propellant gas temperatures as high as 6600°F at 900 psi and for durations of 60 seconds and longer. Silver loss in throat liners is difficult to measure quantitatively but has been high (50 to 70%), erosion has been low to negligible and the incidence and severity of cracking appears reduced compared to copper infiltrated material and non-infiltrated, high density tungsten (in some designs).

Testing and evaluation to date have been chiefly confined to silver and copper as infiltrants with tungsten matrix densities in the range of 75% to 85% of theoretical; thereby capitalizing on the powder metallurgy experience available in the making of electrical switch gears. The density range is based on the problems encountered in infiltration above 85% density, due to the reduction in interconnected porosity, and the considerably reduced mechanical strength of tungsten below 75% of theoretical density. Both infiltrants possess good thermal conductivity, reasonable heat sink qualities (heat capacity, heat of fusion and heat of vaporization), adequate boiling points at atmospheric pressure, practicable melting points for infiltration, and are non-reactive with tungsten.

All producers consider at least part of their processing details proprietory but some information can be reported in generalities. Hydrogen reduced tungsten powder in about the 4 micron particle size range is generally utilized. The powders are hydrostatically pressed and sintered (3100 to 4200°F) to nominally 80% of theoretical density. The tungsten powder is "conditioned" or "doped" to promote infiltration, which is performed at 2200°F to 2400°F in a hydrogen atmosphere or in a vacuum through capillary action only. With good control, producing the tungsten matrix with a high degree of interconnected porosity and maximum infiltration, it is possible to obtain infiltrated billets 10 inches in dia. by 5-1/2 inches high by 4 inches I.D. with composite densities of 96% of theoretical as illustrated in Figure 4. A density of 100% is not possible with capillary flow alone because of the liquid to solid contraction in both silver and copper. The pressing, sintering and infiltration of small billets, up to about 2 inches in diameter, is considerably easier than the large sizes required for rocket nozzle inserts. It has likewise

been found that hydrostatic pressing produces a more "infiltratable" matrix than explosive compaction or hot pressing.

The strength of the 80% dense tungsten matrix is considerably increased by the infiltrant but this benefit decreases rapidly until the strength of the matrix is assumed at around 2000°F. Tensile ductility is imparted by the infiltrant, with measurable elongations appearing as low as 500°F, but more consistently at 1000°F. The strengthening effect appears related to the annealed or cast strength of the infiltrant and possibly its ability to "wet" tungsten. Silver infiltrated tungsten is stronger as measured by tensile tests. (Figure 5)

The mechanism of cooling and evaporation and the resultant microstructure of the tungsten matrix are affected by the vapor pressure and boiling point of the infiltrant. The vapor pressure of silver is higher than copper at all temperatures as illustrated in Figure 6; therefore free boiling can occur at lower temperatures than copper at equal system pressures, thus the liner temperature is limited by the boiling of silver. The higher the infiltrant boiling point, under the pressure conditions in the nozzle, the higher the liner temperature can rise and the weaker the tungsten and therefore the greater the erosion.

Experience to date has indicated that the increased liner temperature, that occurs when copper is used as the infiltrant, results in voids in the weakened tungsten matrix due to the thermal expansion and vapor pressure of the liquid coolant. This surface structure is very susceptible to erosion. The use of copper also promotes the formation of subsurface layers of densified tungsten which seal of the infiltrant from the flame surface further reducing the coolant effectiveness and increasing temperature. Figure 7 illustrates these microstructural effects that lead to degraded performance (erosion) in a motor firing.

Optimum performance is obtained when the infiltrant boils, at the system pressure level, at some temperature less than normal operation and when the infiltrant feeds the flame surface as it is depleted by boiling away. Silver has demonstrated this capability better than copper with gas temperatures of 6000°F to 6600°F and over a pressure range of 150 to 900 psi. Silver losses have ranged from 50% to 70% throughout the insert thickness as illustrated by the uniform silver loss in Figure 8.

Sheet Metal Spinning. The shear and/or conventional spinning processes are ideally suited to the fabrication of relatively thin walled tungsten nozzle components. This results from the fact that in addition to producing the required part configuration in a minimum processing time, both processes, if controlled within specified operating parameters, result in a tungsten component possessing an unrecrystallized, fine grained, fibrous microstructure. The desirability of such a microstructure in comparison to a recrystallized large grained, relatively unworked material is reflected in the following general characteristics:

a. higher strength at temperatures up to approximately 3000°F,

b. lower ductile-to-brittle transition temperatures,

c. improved thermal shock resistance,

d. improved fabrication characteristics during subsequent processing operations such as welding and machining and

e. improved resistance to damage and/or cracking during handling.

In shear spinning, a flat blank or conical preform is formed over a rotating mandrel of the desired configuration by two diametrically opposed forming tools. A thickness reduction is produced during this operation which is a function of the included angle of the conical mandrel being employed. This relationship is shown in Figure 9 for both 60° and 30° included angle mandrels. During conventional spinning operations the preform is also formed to a rotating mandrel of the desired configuration, however, unlike shear spinning only one forming tool is employed and a thickness reduction is not normally produced. Consequently, conventional spinning operations do not produce a significant degree of warm working in the microstructure.

Although both processes can be employed individually to produce various part configurations, they are normally employed in conjunction with each other; the shear spinning process being utilized to initially reduce the flat starting blank to a conical preform followed by conventional spinning to produce the required final component configuration. Such a processing sequence is shown schematically in Figure 10 for a typical convergent-divergent nozzle throat liner.

As indicated in Figure 10, the starting tungsten blank is initially reduced by shear spinning to a conical configuration. Thickness reduction in excess of 50% is not recommended during any one shear spinning operation; consequently this initial reduction is normally performed to produce a 60° included angle conical preform. Prior to forming, the spinning mandrel is preheated to approximately 900°F, and the preform to approximately 1800-2100°F. No atmosphere protection is employed and heating is accomplished utilizing oxygen-acetylene torches. During the preheating and forming operations, care must be exercised to prevent heating of the part above 2100°F since recrystallization of the tungsten component may be encountered if this temperature is exceeded. Molydisulphide base or graphite-water suspension lubricants are applied to the preform and mandrel to prevent scoring of the part surfaces as the tungsten is formed back over the mandrel surface. The remaining forming parameters such as mandrel speed, forming tool feed rate and contact radius are a function of the configuration of the part being formed. Representative parameters for shear spinning (50% Thickness Reduction) a 10 inches diameter blank would be a Mandrel Speed of 250 RPM, and a forming tool feed rate and contact radius of 8 inches per minute and 1/2" respectively.

Following this initial shear spinning operation the 60° included angle preform is further reduced to a 30° included angle conical shape utilizing shear spinning techniques. During this operation an additional 50% thickness reduction is produced resulting in a total thickness reduction from the starting blank of 75%. The processing parameters are normally consistent with those noted previously for the initial shear

spinning operation. The resultant 30° included angle preform is then trimmed, hydrohoned to remove any excessive surface oxidation, and stress relieved at 1750°F for 1 hour in a dry hydrogen atmosphere. During this operation no recrystallization of the shear spun component is produced.

The final part configuration determines whether a third preforming operation by conventional spinning is necessary. If the angle between a line connecting the ends of the completed convergent-divergent component, and the center line of the part, is approximately 9-15 degrees, the component can be conventionally spun directly from the shear spun preform. If this angle is less than 8°, it becomes necessary to add a third preforming operation. As indicated in Figure 10 this additional preforming operation is conducted by conventional spinning and further reduces the included angle of the cone without an appreciable change in wall thickness. Following this third preforming operation, the convergent-divergent configuration is formed utilizing conventional spinning techniques. During both conventional spinning operations, the forming temperatures, lubrication and heating method indicated previously for the shear spinning operations are employed. Again the forming tool contact radius and mandrel speed are a function of the part configuration being formed. Typical values for a 5" minor diameter part of the configuration illustrated in Figure 10 would be a mandrel speed of 306 RPM and a forming tool contact radius of 1".

Following these operations the completed part is hydrohoned, stress relieved at 1750°F for 1 hour in a dry hydrogen atmosphere and trimmed to the required dimensions.

Many different thin walled tungsten nozzle components have been successfully formed at the Aerojet-General Corporation, utilizing the shear and/or conventional spinning approach outlined above. The formed components have ranged from 0.030" to 0.250" in thickness and up to 14" in diameter. During these programs extensive metallurgical investigations have been conducted to establish the starting material requirements and the effects of the process on the metallurgical properties of unalloyed tungsten.

In regard to the sheet or plate starting material requirements, for shear and/or conventional spinning applications, it has been determined that a relatively fine grained (ASTM 5-9), uniformly wrought material, containing approximately 50-75% warm work produces the most acceptable spinning results. The material should be stress relieved and no evidence or recrystallization should be present prior to spinning. The microstructure of typical starting material is illustrated in Figure 11. The surface finish of the starting blanks should be approximately 64 rms and contain no surface nicks, laps, seams, or other defects which could act as stress risers or fracture origins during spinning.

The results of metallurgical investigations conducted on shear spun tungsten, show that this process imparts a high degree of working (dependent on the degree of reduction employed) to the microstructure. This work is more pronounced at the spun (forming tool contact) surface than at the unspun surface and in the axial direction (parallel to the material

flow) than in the hoop direction. These effects are illustrated in Figure 12. Conventional spinning operations do not impart a significant degree of working to the microstructure of the formed component.

Through extensive metallographic examination studies it was determined that recrystallization of the unspun tungsten blanks varied between 2425° and 2575°F (depending on the degree of prior warm working). Recrystallization of the shear spun material occurred between 2350° and 2425°F. Recrystallization first occurred in the unspun samples in the more highly-worked areas of the cross section. Recrystallization of the shear spun samples occurred initially at the spun (forming tool contact) surface and progressed inward toward the unspun surface as the annealing temperature was raised as was expected. The initial recrystallized grain size near the spun surface of the shear spun specimens (both 50 and 75% reduction) was finer and more uniform in comparison to that present near the unspun surface or in the unspun specimens. These effects are illustrated in Figures 13 through 16.

The results of limited bend testing, conducted to determine the ductile-to-brittle transition temperature of shear spun (75% reduction) tungsten, indicate that the working resulted in a lower transition temperature (350-475°F) in comparison to that (600°F) of unspun tungsten of the same approximate thickness (.060"). These results also indicate that in addition to superior spinning results, a higher degree of warm working (50-75%) in the starting blank prior to shear spinning is desirable in that a noticeable difference is produced in the bend, ductile-to-brittle transition temperature of the final spun component.

Pressed, Sintered and Forged. The forging of tungsten nozzle components up to 2 inches in wall thickness has been extensively investigated by AGC through a number of research and development programs conducted in conjunction with commercial forging vendors. The main objective of these programs has been to develop forging parameters and techniques for pressed and sintered tungsten which will result in a nozzle component possessing a fine grain, uniform, wrought microstructure. Because of the difficulty in obtaining a suitable starting preform from arc-cast tungsten, pressed and sintered tungsten billets were used in these programs and subsequent production efforts. Considerable progress has been made in the processing of thin walled (.5" thick) components, as illustrated in Figure 17. Large numbers of these parts have been successfully produced which met both dimensional and metallurgical requirements. Recently, success has been attained in producing components possessing wall thicknesses in excess of 2 inches.

Although forging processing techniques and parameters vary considerably, forged components are generally produced utilizing the basic upsetting, recrystallization, and back extrusion approach shown schematically in Figure 18. Hammer forging equipment has been used almost exclusively, although techniques and parameters for mechanical press forging operations are currently being developed and show considerable promise.

For either type of forging operation (hammer or press), unalloyed, pressed and sintered tungsten starting billets were employed. The

dimensions of the billet depend on the required finished part configuration; however, billet height to diameter ratios between 1.5:1 and 2.2:1 are normally employed, with starting billet densities between 90 to 95% of theoretical. The initial upsetting operation reduces the billet height approximately 40 to 50% and results in a density of approximately 98% of theoretical. A series of 4 to 10 hammer blows may be required to produce the finished upset height depending on the capacity of the hammer being employed and the size of the billet. During upset forging, the part temperature is deliberately reduced from a starting temperature of 2800 to 2900°F to a finishing temperature between 2400 to 2600°F in order to prevent localized recrystallization or grain growth in the more highly worked areas of the upset.

Following the upsetting operations the part is subjected to a recrystallization treatment. The actual cycle employed varies depending on the forging source. Typical cycles range from 3050°F for 15 minutes of 2400°F for 1 hour. The main objective of this treatment is to produce a uniform fine grained (ASTM 5 and finer) material amenable to the high degree of working to be applied during subsequent back extrusion operations.

After the recrystallization treatment, the upset or pancake is back extruded to produce the final part configuration. The forging techniques and parameters employed during these operations vary between forging vendors and with the final part configuration. Normally, at least one additional reheat is required and depending on the height, thickness and diameter of the part being processed, the component may be reversed during back extrusion. This latter approach is employed mainly for heavy walled (excess of 1.5" thickness) inserts of relatively large diameter (8"). By reversing the part following the initial back extrusion operation, the degree of metal movement is reduced and the possibility of excessive temperature rise during forging through adiabatic heating is lessened. Such a temperature rise is undesirable due to the possibility of recrystallization and/or grain growth in the more heavily worked or possibly die locked areas of the part. However, in forging thinner walled inserts such as those illustrated in Figure 17, the finished configuration is produced by back extrusion in one direction. Back extrusion starting temperatures of 2400 to 2800°F are normally employed and the part temperature is reduced as forging progresses. Depending on the degree of metal movement required to produce the final part configuration, 1 to 3 reheats are employed. The reheat temperature is controlled by the temperature employed in the previous forging strike and is not permitted to exceed the previous forging strike temperature by more than 100°F, in order to prevent recrystallization of the more heavily worked areas of the component. Using this general processing sequence the final part is back extruded from the recrystallized upset previously produced. Depending on the size of the component being forged and the capacity of the hammer being employed, 4 to 10 back extrusion strikes are normally required to produce the final part. Finishing temperatures approximate 2100 to 2300°F and the final component density is in excess of 99% of theoretical. The degree of warm working present in the finished part varies as a function of the component thickness, design and the forging technique employed; however, it approximates 50-60% for the thinner walled components illustrated in Figure 17. Following forging each part

is stress relieved at 1800 to 2100°F and subject to dye penetrant and ultrasonic inspection.

Considerable variation exists between forging vendors in regard to process controls and associated forging equipment. Optical pyrometers are used by most sources to control part temperature during forging. Some sources employ proprietary coatings to prevent excessive oxidation of the component during processing although no detrimental effects have been noted in the properties of these parts when coatings are not utilized. In the absence of coatings it is necessary to allow excess billet material for oxidation losses. In regard to heating facilities gas fired furnaces are normally employed, the gas mixture being adjusted to control oxidation losses to a minimum.

Considerable work remains to be accomplished in evaluating the mechanical properties of unalloyed tungsten forgings. However, the results of metallurgical investigations have indicated that if the components are forged within specified parameters a fine grain, wrought, fibrous microstructure results which possesses desirable properties similar to those noted in the discussion of spun sheet metal. The microstructure obtained in the forged nozzle insert illustrated in Figure 17 is presented in Figure 19. As indicated, the structure is fine grained and worked (50 to 60% warm work), with no evidence of recrystallization. It is interesting to note that while the mechanical property evaluations have not yet been completed, the results of full scale motor test firings indicate that the microstructure presented in Figure 19 is superior to a less severely worked and/or recrystallized material shown in Figure 20. Cracking has been observed, after firing, in nozzle inserts possessing the less severely worked microstructure, and no cracking has been found in the inserts possessing the more severely worked structure. These results indicate the superior thermal gradient stress resistance for the more highly worked material.

From the foregoing it is obvious that the technology of tungsten forging has advanced to the point where it should be considered a prime method for the fabrication of nozzle components. This is particularly true for the processing of parts possessing wall thickness in excess of .5". Additional work remains to be accomplished in fully defining the mechanical properties attainable in these components. However, the basic processing know-how and facilities for producing such components are presently available at a number of commercial forging sources.

TABLE I

PHYSICAL PROPERTIES OF FORGED TUNGSTEN

(95% Maximum Density)

Mean Coefficient of Expansion

Temperature, Range, °F	Coefficient (10^{-6} in./in./°F)
85 - 4000	4.19
85 - 4400	4.30
85 - 4800	4.47
85 - 5200	4.65
85 - 5600	4.93
85 - 6000	5.24
85 - 6100	5.35

Specific Heat

Temperature, °F	Btu/lb - °F
68	0.032
1832	0.036
2925	0.0445
3625	0.0475

Emissivity

Temperature, °F	
3860	0.277
4225	0.289
4585	0.300
4940	0.312
5300	0.323
5670	0.335
6025	0.347

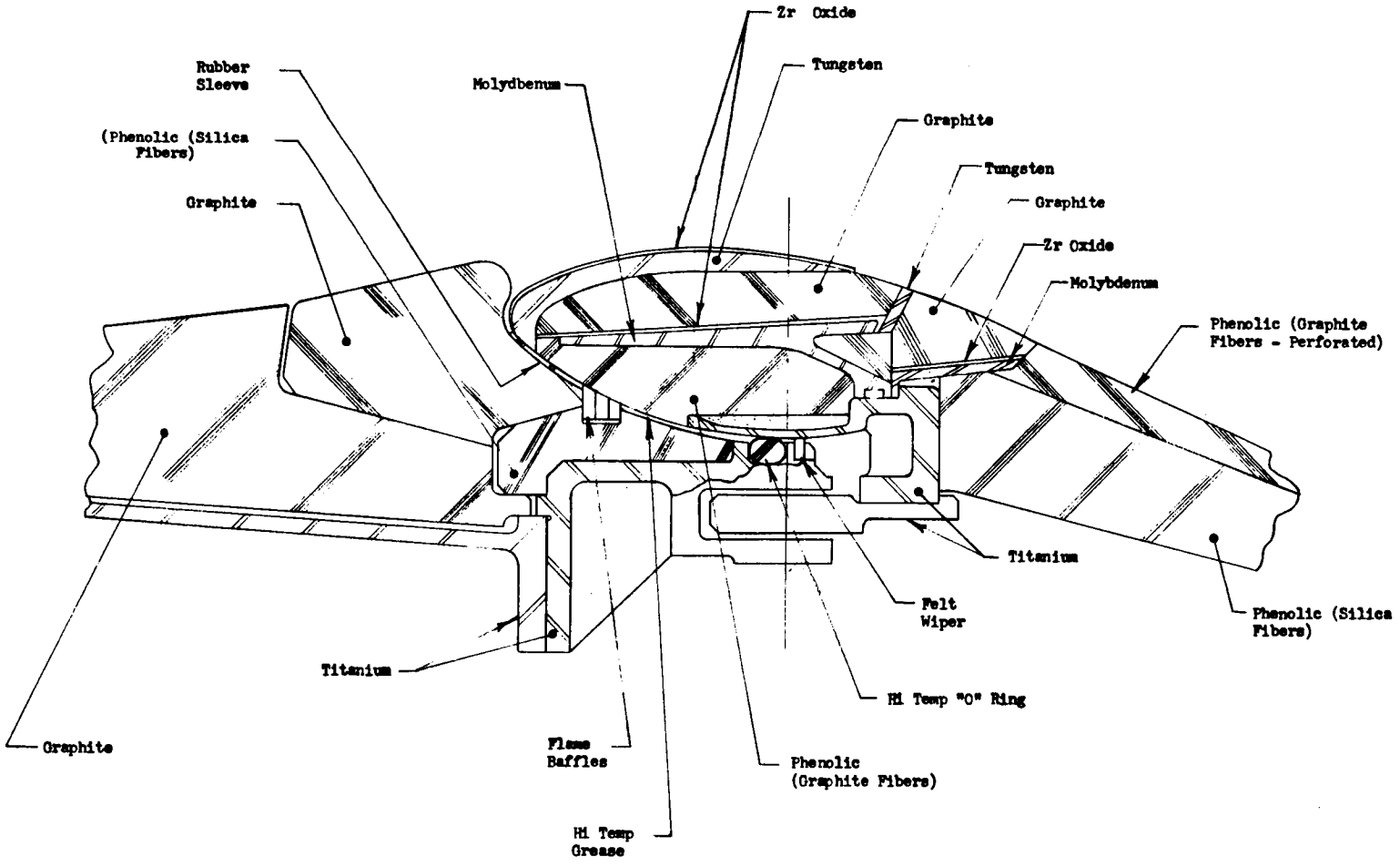

FIG. 1 SKETCH OF A TYPICAL NOZZLE THROAT ASSEMBLY WITH A TUNGSTEN THROAT LINER

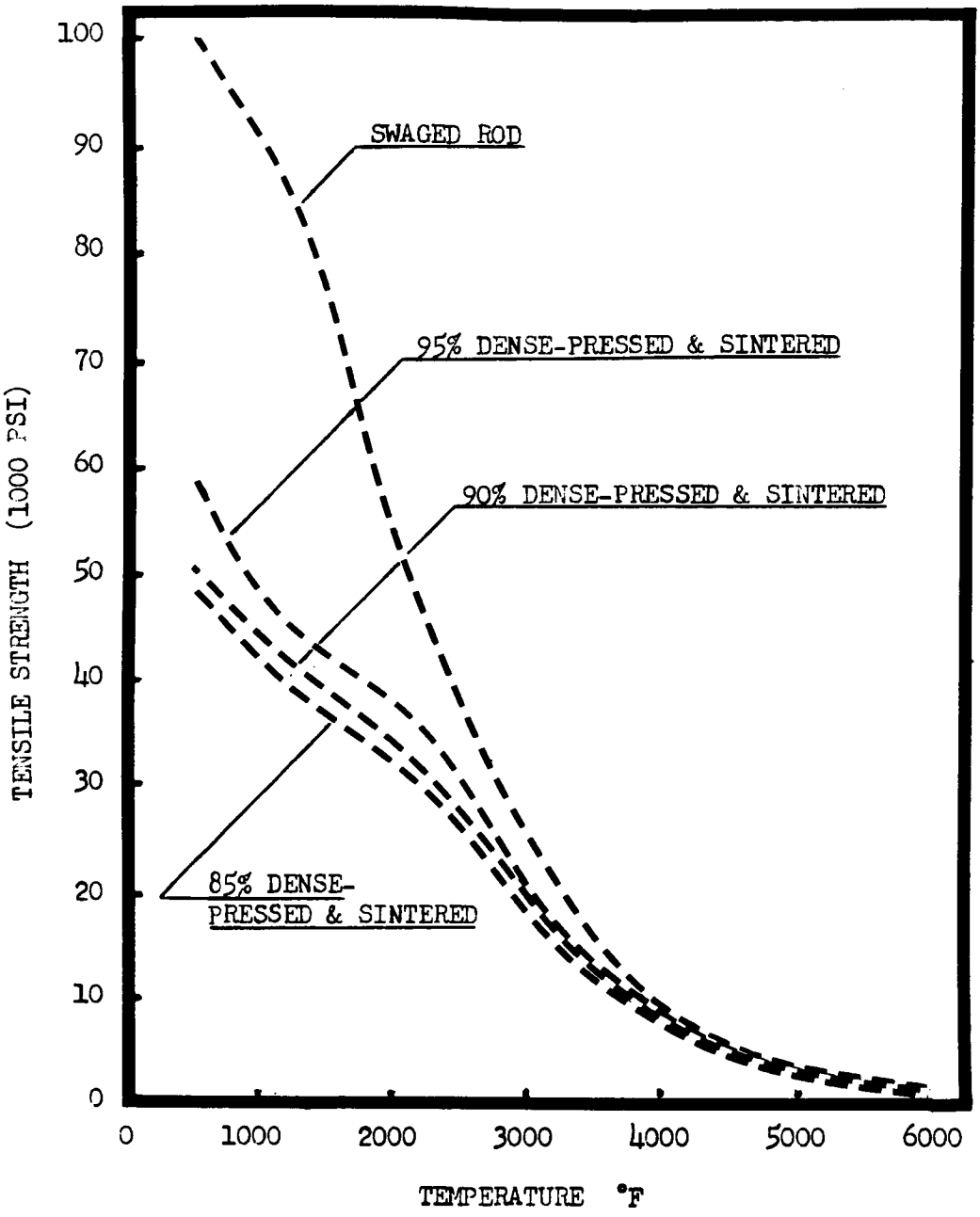

FIG. 2 TENSILE STRENGTH VS TEMPERATURE AND DENSITY FOR TUNGSTEN

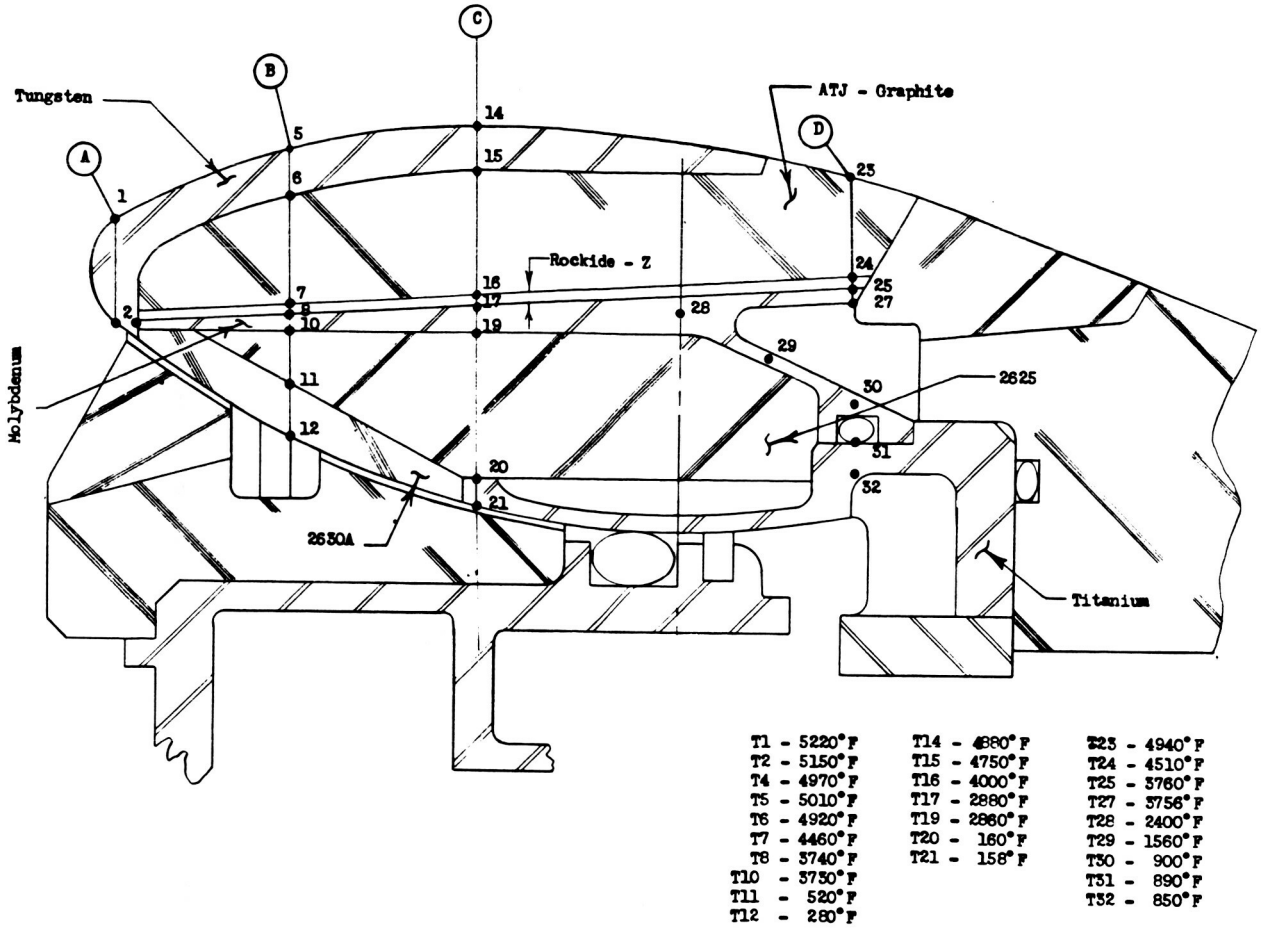

FIG. 3
PREDICTED TEMPERATURES IN A NOZZLE THROAT ASSEMBLY AFTER 60 SECONDS OF FIRING

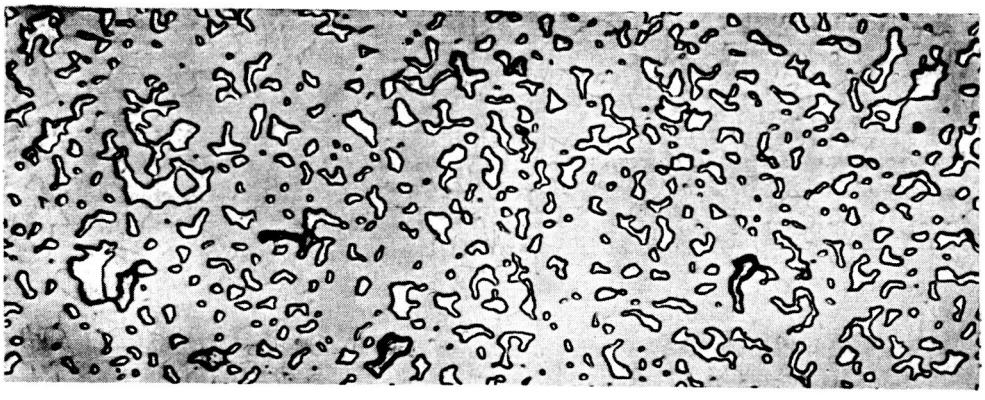

Unetched Mag: 500X

FIG. 4 MICROSTRUCTURE OF SILVER INFILTRATED TUNGSTEN PRIOR TO FIRING

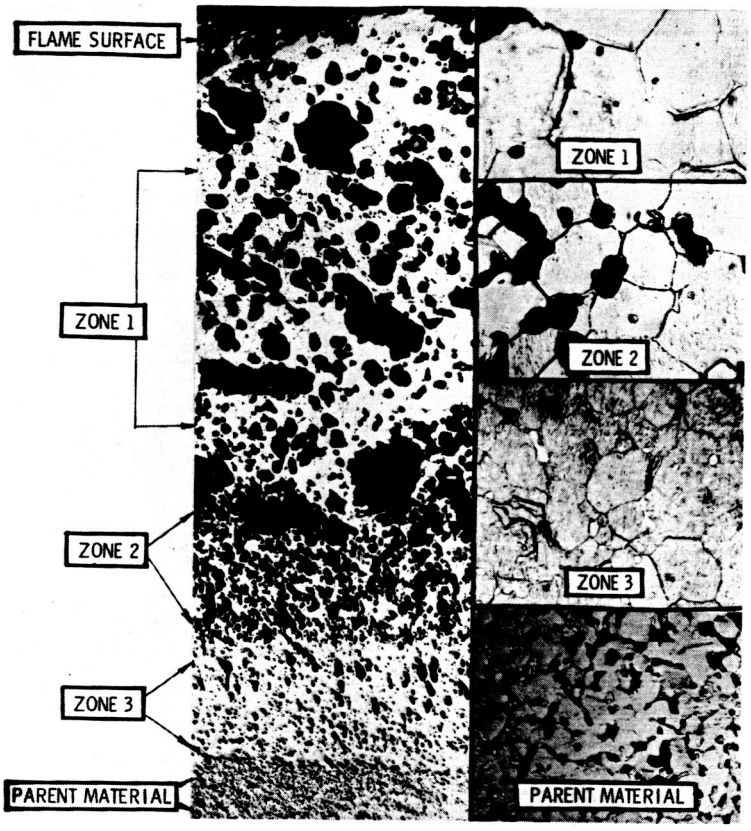

FIG. 7
MICROSTRUCTURE OF FLAME SURFACE OF COPPER INFILTRATED TUNGSTEN THROAT LINER IN POST-FIRED CONDITION

Etch: Murakami's Mag: 30X unetched
300X etched

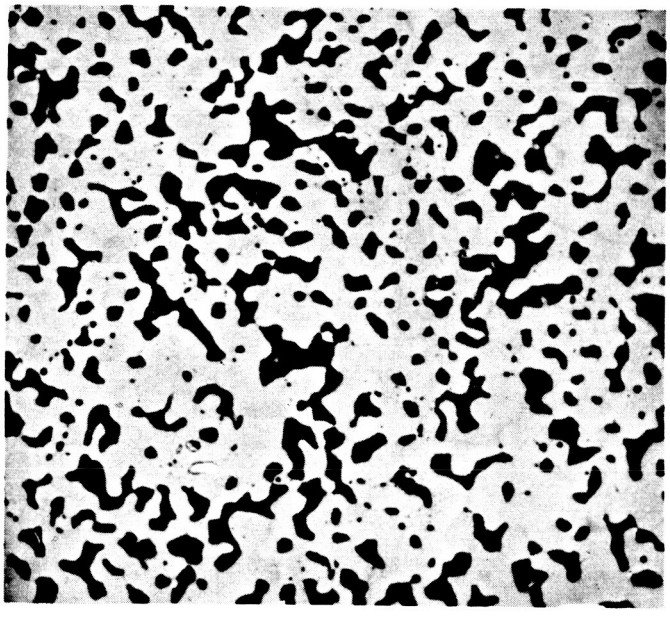

FIG. 8
MICROSTRUCTURE OF FIRED SILVER INFILTRATED TUNGSTEN SHOWING HIGH SILVER LOSS

Unetched Mag: 500X

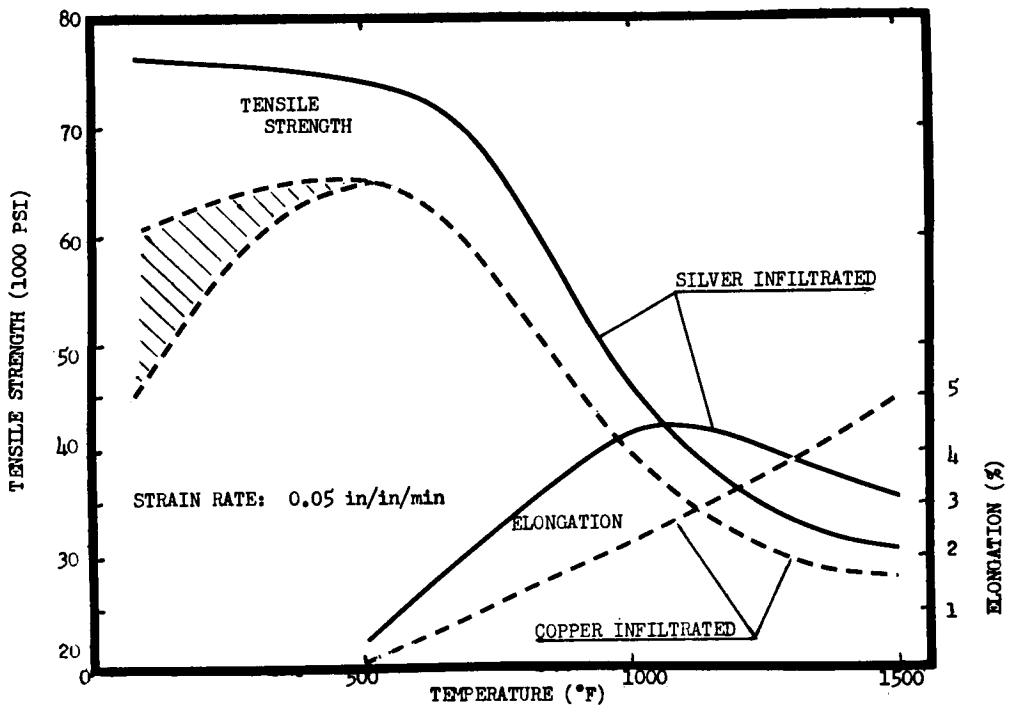

FIG. 5
TENSILE STRENGTH AND ELONGATION OF SILVER AND COPPER INFILTRATED TUNGSTEN VERSUS TEMPERATURE. PRE-INFILTRATED MATRIX DENSITY 80% OF THEORETICAL

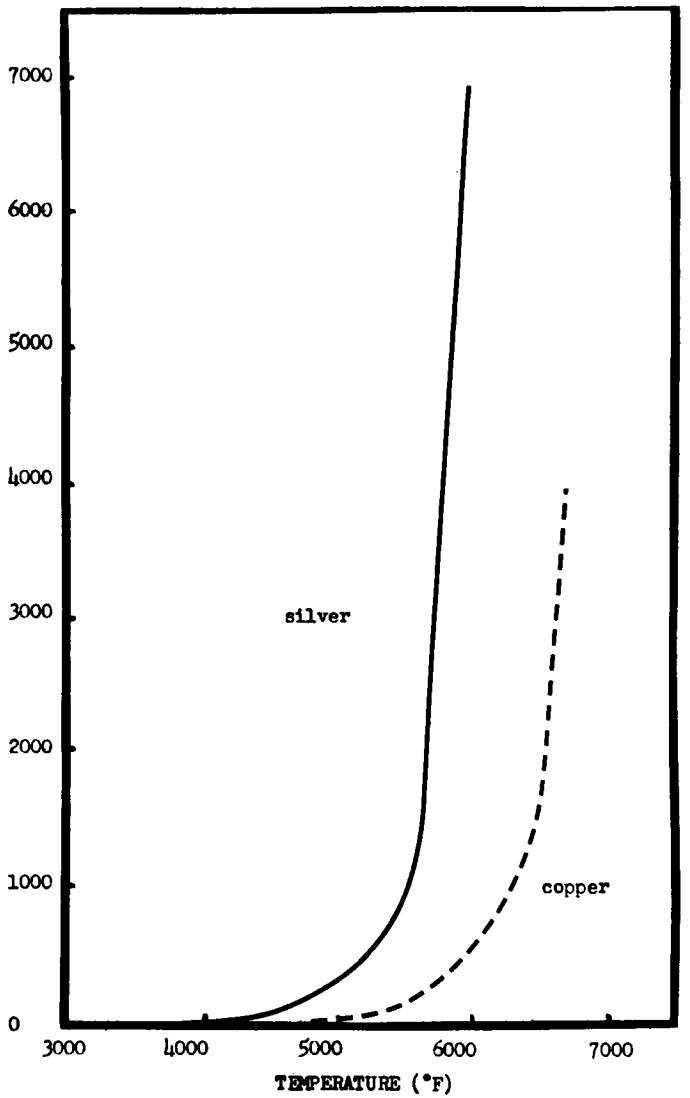

FIG. 6
BOILING POINT OF COPPER AND SILVER AS A FUNCTION OF PRESSURE AND TEMPERATURE

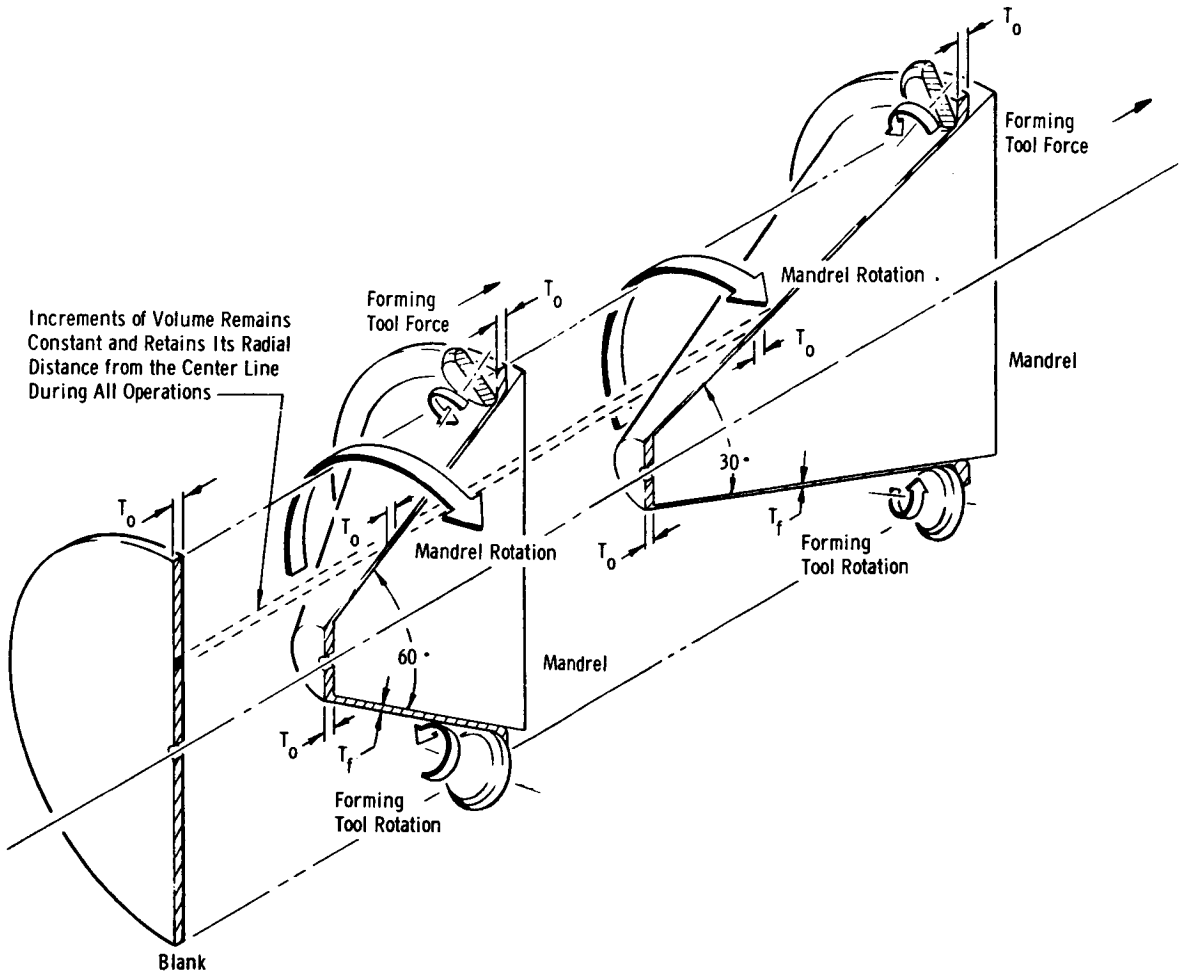

60° Included Angle Mandrel

Sample Calculation

Starting Thickness (T_o) .250"
Mandrel Included Angle(α) 60°
Equation: $T_f = T_o$ Sine 1/2 α

OR $T_f = .250" \times .5$

$T_f = .125"$

50 percent Wall Reduction

30° Included Angle Mandrel

Sample Calculation

Starting Thickness (T_o) .250"
Mandrel Included Angle(α) 30°
Equations: $T_f = T_o$ Sine 1/2 α

OR $T_f = .250" \times .2588$

$T_f = .064"$

75 Percent Wall Reduction

FIG. 9
SCHEMATIC DIAGRAM ILLUSTRATING THE SHEAR SPINNING PROCESS AS APPLIED TO THE PROCESSING OF CONICAL CONFIGURATIONS AND SAMPLE CALCULATIONS SHOWING THE RELATIONSHIP BETWEEN THE STARTING BLANK THICKNESS (T_o), THE SHEAR SPUN COMPONENT THICKNESS (T_f) AND THE INCLUDED ANGLE (α) OF THE SPINNING MANDREL EMPLOYED

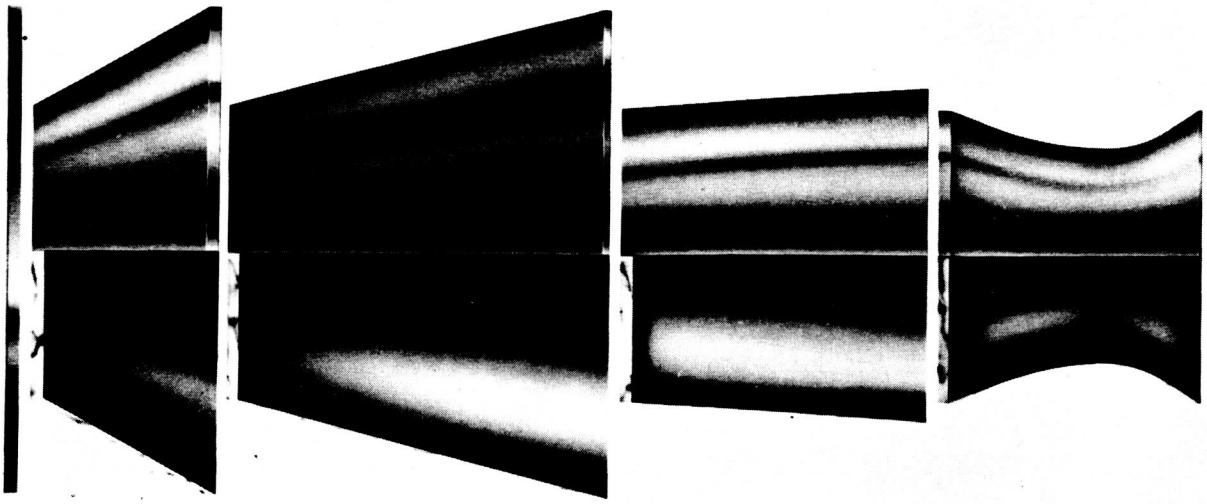

1st Forming Operation (Shear Spinning)

2nd Forming Operation (Shear Spinning)

3rd Forming Operation (If required) (Convential Spinning)

4th Forming Operation Finished Configuration (Convential Spinning)

FIG. 10
SCHEMATIC DIAGRAM ILLUSTRATING THE FORMING SEQUENCE USED IN THE FABRICATION OF TUNGSTEN CONVERGENT-DIVERGENT THROAT LINERS

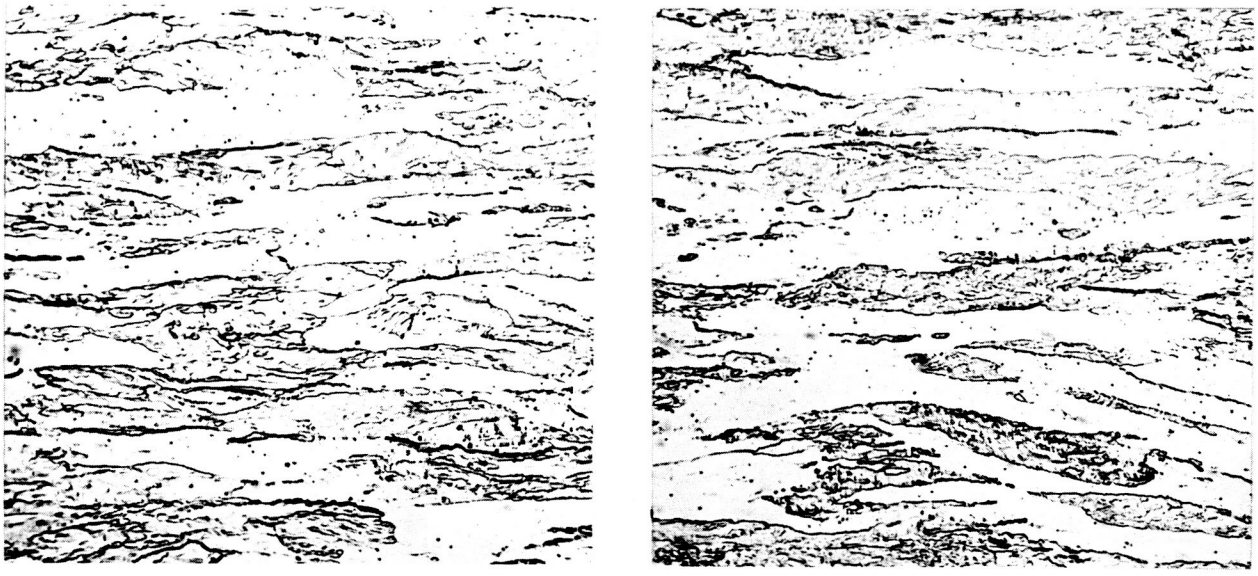

Etch: Murakami's

Mag: 250X

FIG. 11
REPRESENTATIVE DESIRABLE MICROSTRUCTURE
FOR "SPINNING QUALITY" UNALLOYED TUNGSTEN

Parallel

Transverse

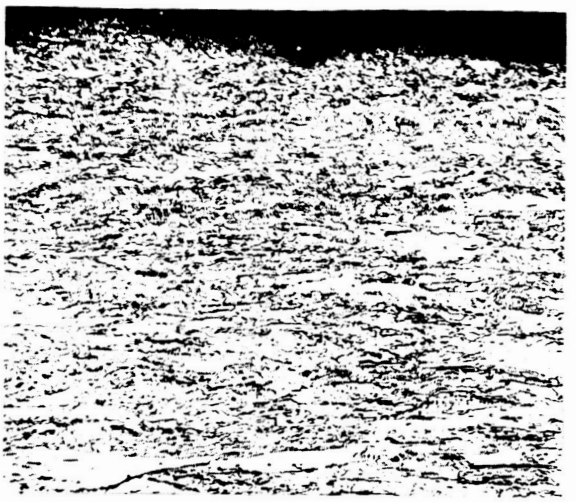

Spun Surface

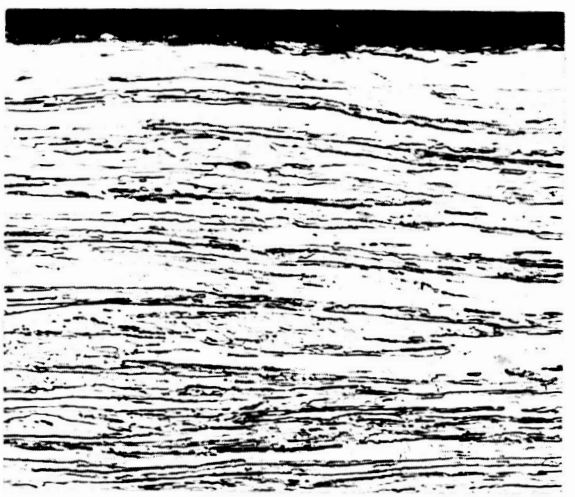

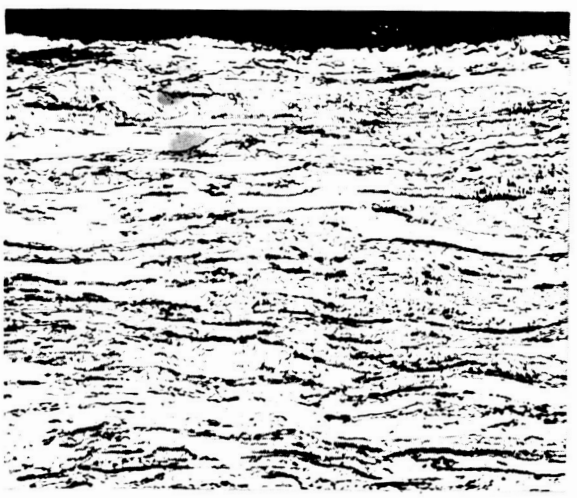

Unspun Surface

Etch: Murakami's

Mag: 250X

FIG. 12
TYPICAL MICROSTRUCTURE OF SHEAR SPUN (75% REDUCTION) UNALLOYED TUNGSTEN - AS SPUN CONDITION - PARALLEL AND TRANSVERSE REFERS TO ORIENTATION IN RESPECT TO THE SURFACE SPINNING MARKS WHICH RUN IN THE HOOP DIRECTION

Unspun

Spun (75% Reduction)

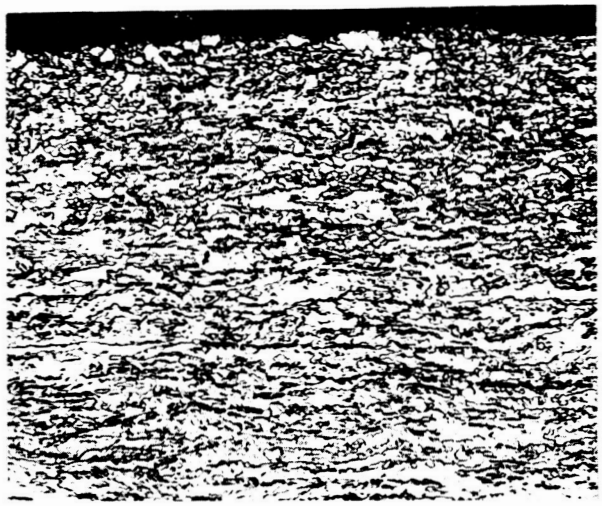

Spun Surface

Unspun Surface

Etch: Murakami's

Mag: 250X

FIG. 13
TYPICAL MICROSTRUCTURE OF UNSPUN AND SHEAR SPUN (75% REDUCTION) UNALLOYED TUNGSTEN AFTER ANNEALING AT 2350°F FOR 30 MINUTES

Unspun

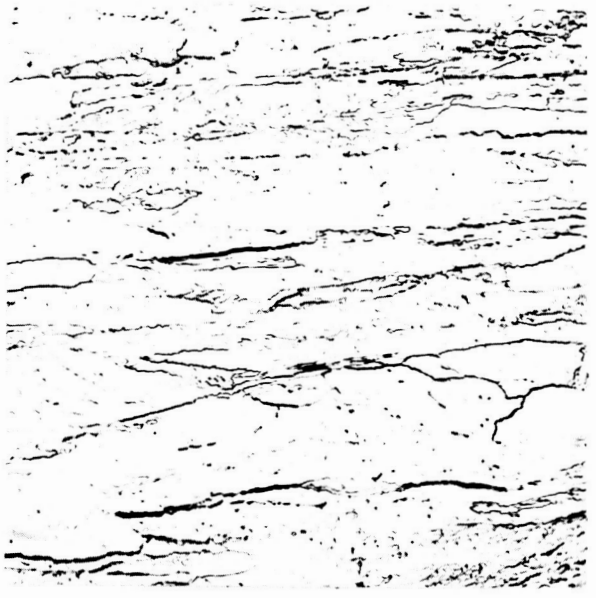

Spun (75% Reduction)

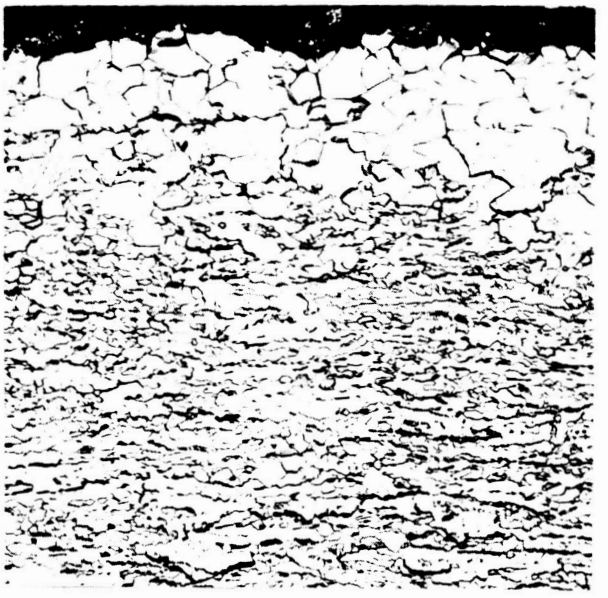

Spun Surface

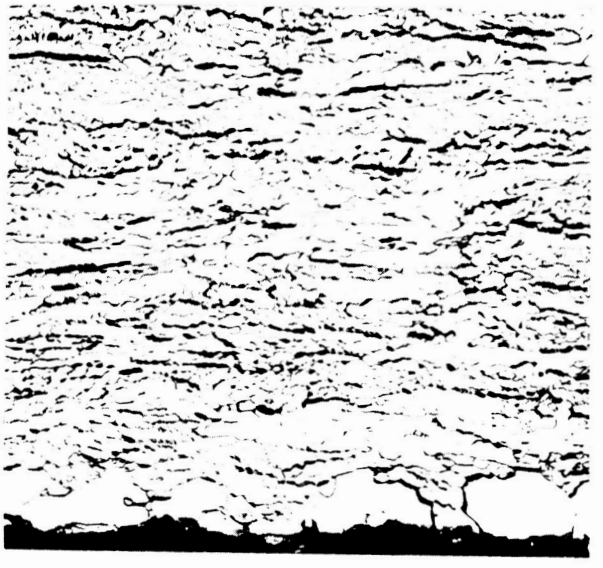

Unspun Surface

Etch: Murakami's

Mag: 250X

FIG. 14
TYPICAL MICROSTRUCTURE OF UNSPUN AND SHEAR SPUN (75% REDUCTION) UNALLOYED TUNGSTEN AFTER ANNEALING AT 2500°F FOR 30 MINUTES

Unspun

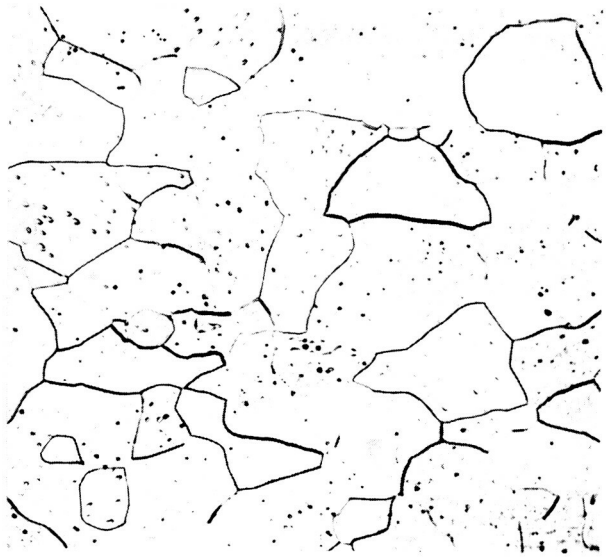

Spun (75% Reduction)

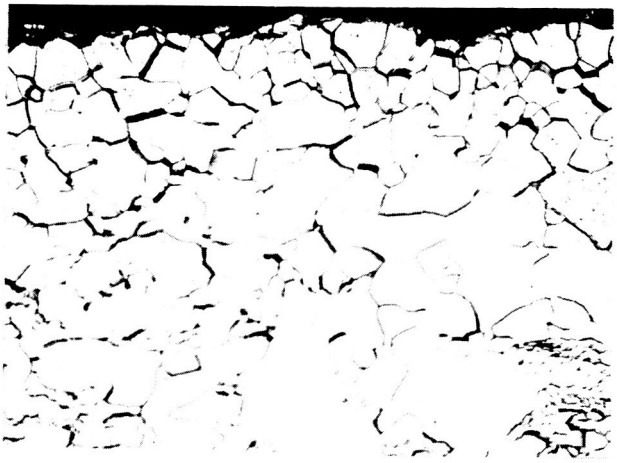

Spun Surface

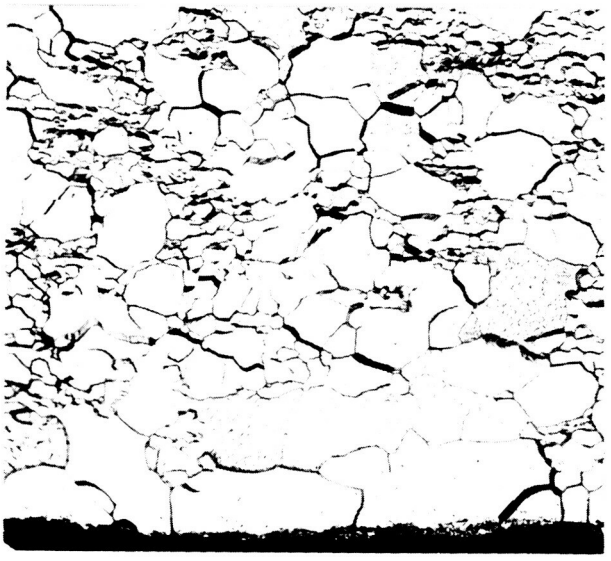

Unspun Surface

Etch: Murakami's

Mag: 250X

FIG. 15
TYPICAL MICROSTRUCTURE OF UNSPUN AND SHEAR SPUN (75% REDUCTION)
UNALLOYED TUNGSTEN AFTER ANNEALING AT 2575°F FOR 30 MINUTES

Unspun

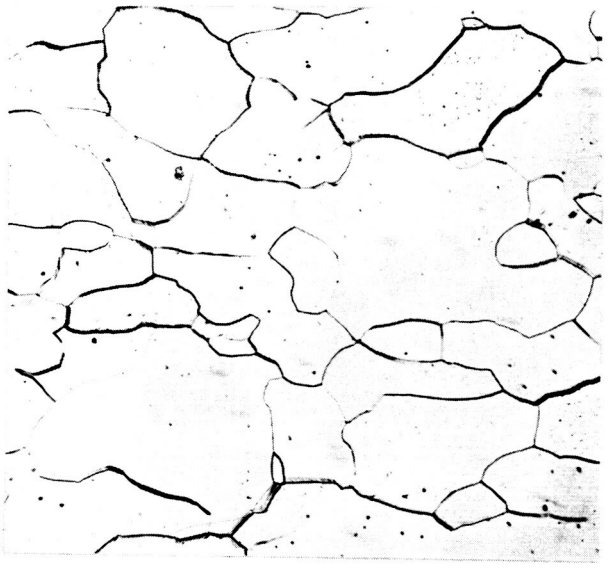

Spun (75% Reduction)

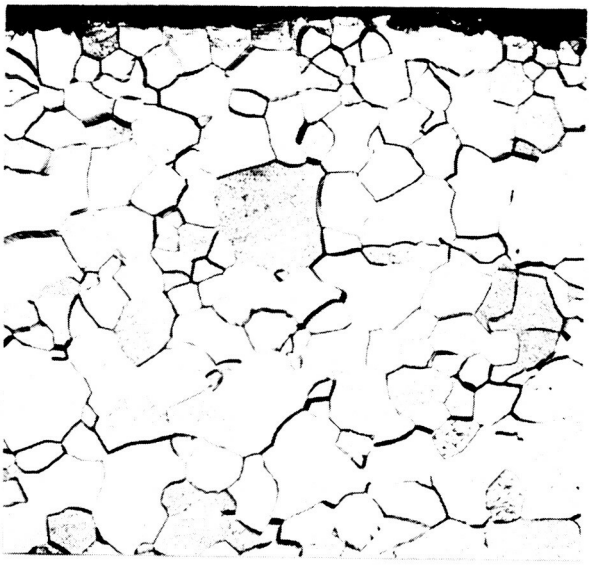

Spun Surface

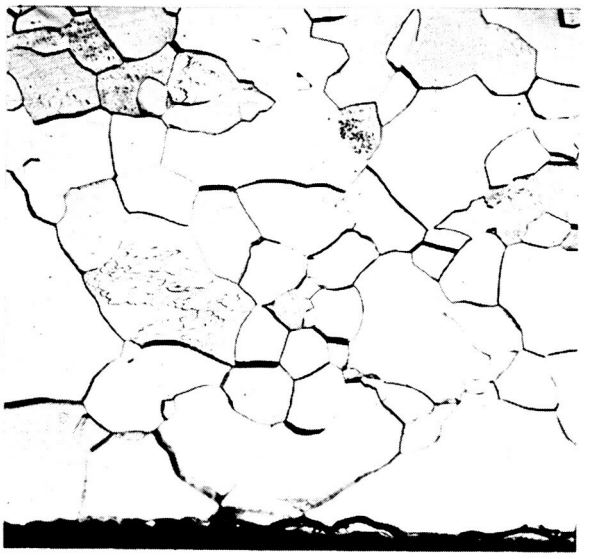

Unspun Surface

Etch: Murakami's

Mag: 250X

FIG. 16
TYPICAL MICROSTRUCTURE OF UNSPUN AND SHEAR SPUN (75% REDUCTION) UNALLOYED TUNGSTEN AFTER ANNEALING AT 2800°F FOR 30 MINUTES

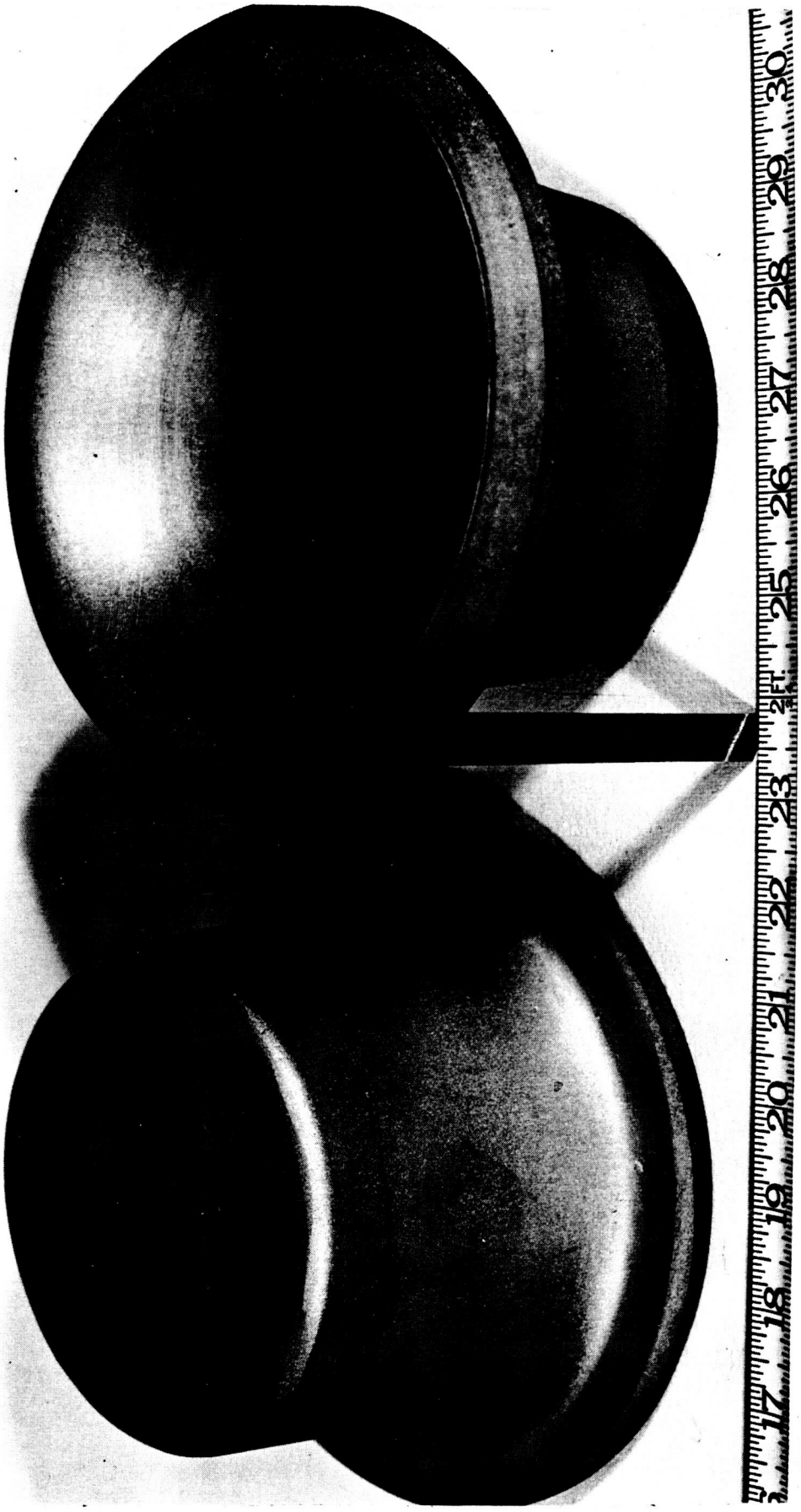

FIG. 17 FORGED UNALLOYED TUNGSTEN NOZZLE INSERTS

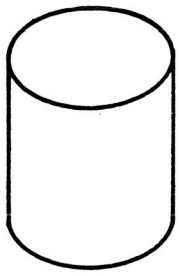

Starting Billet (Pressed and Sintered)

Height/Diameter Ratio - 1.5-2.2
Density - 92-95%

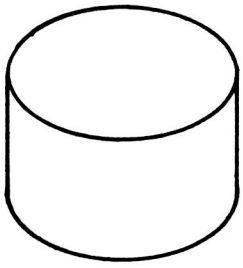

Upset

40-50% Reduction
Start - 2800-2900°F
Finish - 2400-2600°F
Density - Approximately 98%

Recrystallize

Temperature - 2400-3050°F
Time - 15-60 minutes

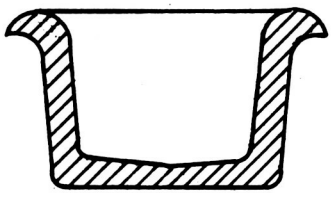

Back Extrusion (Finish Configuration)

Start - 2400-2800°F
Finish - 2100-2300°F
Density - 99% Plus
Reduction - Webb - 60-80%
Wall - 50-70%

FIG. 18
SCHEMATIC DIAGRAM ILLUSTRATING THE BACK EXTRUSION FORGING SEQUENCE GENERALLY EMPLOYED IN PRODUCING UNALLOYED TUNGSTEN NOZZLE INSERTS

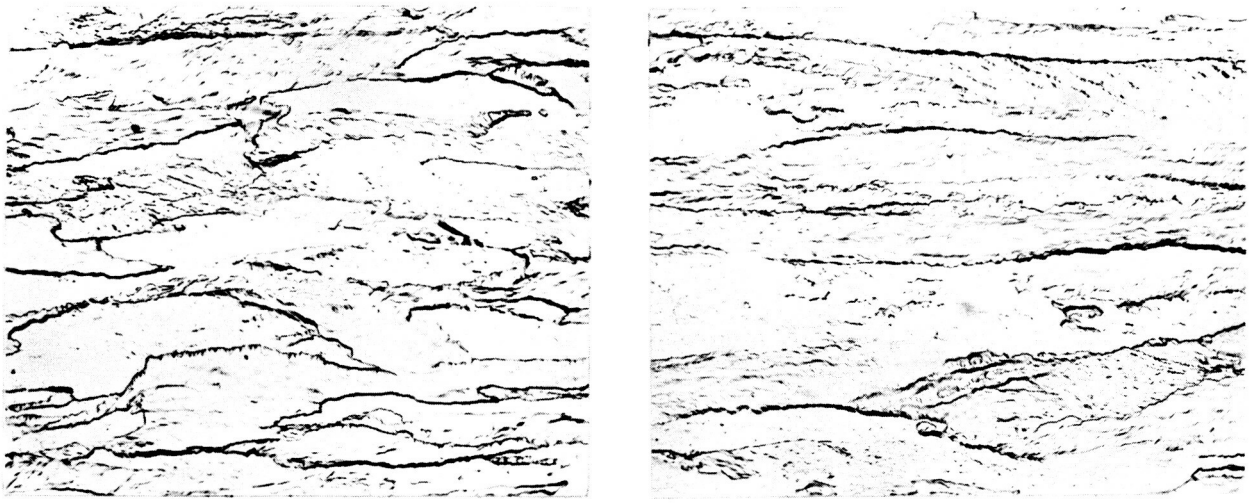

Etch: Murakami's Mag: 250X

FIG. 19
TYPICAL MICROSTRUCTURES OF FORGED PRESSED AND SINTERED, UNALLOYED TUNGSTEN NOZZLE INSERTS FROM THE COMPONENTS ILLUSTRATED IN FIG. 17

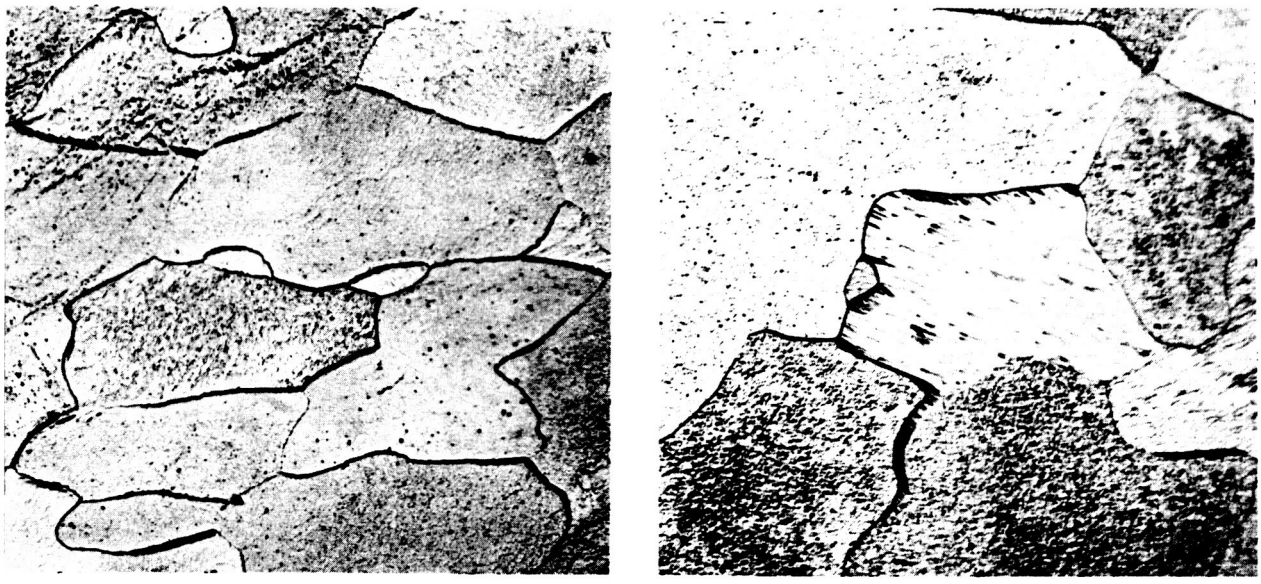

Longitudinal Transverse

Etch: Murakami's Mag: 250X

FIG. 20
MICROSTRUCTURE OF FORGED, PRESSED AND SINTERED TUNGSTEN ILLUSTRATING UNDESIRABLE GRAIN SIZE AND SHAPE

ELASTOMERIC INSULATION FOR SOLID PROPELLANT ROCKET MOTOR CASES

by

C. R. Burnett and W. J. McLaughlin

Structural Materials Division
Aerojet-General Corporation
Azusa, California

ABSTRACT

Elastomeric insulation for solid propellant rocket motor cases were developed and tested in laboratory facilities and subscale rocket motors.

The effect of fillers and additives on the thermal and ablative properties of elastomers were evaluated and the significance of the filler type, and amount were determined.

Fiber-reinforced silicone elastomers demonstrated high effective heats of ablation and improved internal insulation properties. This material represents a considerable improvement over the commonly used organic elastomers. Problems such as bonding of the silicone to the solid rocket propellant and case materials were solved by polymeric compounding.

INTRODUCTION

The insulation in rocket motor cases represents parasitic weight. When insulation weight is reduced, greater range and pay loads are possible. Several hundred pounds of insulation are required in today's intercontinental and intermediate range ballistic missile solid propellant rocket motor cases. Tomorrow's higher thrust solid propellant rockets may well require insulation weights measured in tons, unless significant advances are made in insulation technology. Furthermore,

Acknowledgements

The authors wish to express their appreciation to D. R. Collis and R. G. Knauer of Aerojet-Sacramento, R. R. Lasorsa and D. M. Monroe of the Dow-Corning Corp. who helped guide this work. Dr. S. Brelant, E. J. Gunter and J. F. Creedon of Aerojet-Azusa were especially helpful because of their interest, suggestions, and encouragement. This project was supported in part by the United States Air Force as part of Contract AF 33 (600)-36610.

recent advancements in rocket motor case technology has reduced the inert weight of the case and have resulted in increased demand for lightweight, elastomeric insulation.

Polyisobutadiene acrylonitrile reinforced with silica or asbestos, is the most commonly used solid propellant rocket motor case insulation in current use. Significant weight reduction has recently been achieved by utilizing reinforced siloxane elastomers. The development and evaluation of improved, lighter-weight internal insulations will be described in this paper.

DISCUSSION

The properties required for insulation material for solid rocket motor cases are moderate elongation, high specific heat, low thermal conductivity, good ablation characteristics, and high erosion resistance. Elastomers display the physical, thermal, and ablative properties that make them useful for insulating both internal and external areas of rocket motors.

Internal Insulation Studies

Aerojet-General Corporation at Azusa, California has conducted studies on the thermal and ablative properties of elastomers and elastomeric composites for use as internal insulation in rocket motors during the past two years.

Seven elastomers were evaluated. These materials were: polyisoprene (natural rubber), polyisobutadiene-styrene (GRS), polyisochloroprene (Neoprene), polyisobutylene-isoprene (butyl), poly-1-1-dehydroperfluorobutylacrylate (FBA (1F4)), polyisobutadiene acrylonitrile (low acrylonitrile content), polyisobutadiene acrylonitrile (high acrylonitrile content), and siloxane elastomer.

The elastomers exhibiting the best ablation resistance were incorporated into a filler study. Four fibrous fillers (glass, wool, chrysotile asbestos, and acrylic fiber) and four particulate fillers (silica, carbon black, precipitated clay and microballoons) were evaluated.

The ablative properties of the samples were determined by the use of a Giannini P-140 Plasmatron. Argon was used as the working fluid in all tests. Thermal conductivities of the specimens were determined using an Alundum Guarded Hot Plate. The specific heats of the materials were determined by the use of a change-of-phase calorimeter. The brittle point of the elastomeric materials was determined by the temperature at which a sample broke when bent through an arc of 180°.

Elastomer Evaluation

All elastomers were mixed with the essential curatives prior to evaluation. Semi-reinforcing furnace-black was added to each of the elastomers (except silicone) to obtain increased stability. Iron-oxide was added to the silicone elastomer. The ablative properties of each

elastomer were determined and are presented in Table I. Thermal conductivity of each elastomeric material is presented in Figure 1, and the specific heat of each elastomer is shown in Figure 2.

The silicone elastomer that was evaluated had the lowest mass ablation rate and lowest surface regression rate (the rate that the heated surface erodes in an ablative environment) of all the elastomers examined. Butyl and high acrylonitrile content Buna-N elastomers also displayed good ablative properties. Natural rubber was eliminated from further consideration because of its poor aging properties, and because it starts to revert to the unpolymerized form at the temperature and time required to cure epoxy resin-glass filament composite cases.

The effective heats of ablation of the three elastomers displaying the best ablation characteristics were determined and are presented in Figure 3.

Filler Evaluation

Four fibrous fillers (chrysotile asbestos, glass, acrylic fiber and wool) and four particulate fillers (carbon black, precipitated clay, silica, and clay beads) were selected for study.

Five elastomers were selected for the filler evaluation. These included the silicone, butyl and high acrylonitrile content Buna-N elastomers that exhibited the best mass ablation rates in the elastomer study. Chlorobutyl and Viton elastomers that had not been previously evaluated, were also included in this study.

Table II shows the mass ablation rates of these materials.

Results of Preliminary Evaluation

The effects of each variable was considered independently of the others by averaging the results obtained from the data. The following generalizations were obtained from the analysis:

1. The mass ablation rate of the insulation material is influenced by the composition of the elastomeric binder. The elastomers evaluated are listed in order of decreasing performance:

(a) Silicone
(b) Chloro-Butyl
(c) Butyl 035
(d) Buna-N
(e) Viton

2. The mass ablation rate of the insulation material is influenced by the shape and composition of the reinforcing filler. The filler materials evaluated are listed in order of decreasing performance:

(a) Chrysotile Asbestos Fiber
(b) Wool Fiber
(c) Glass Fiber

(d) Acrylic Fiber
(e) Silica Particles
(f) Carbon Black Particles
(g) Clay Particles

3. The mass ablation rate of the insulation material is decreased by an increase in the amount of fibrous-filler loading for all filler-to-elastomer ratios up to 45 parts filler per 100 parts elastomer. Higher loadings of fibrous fillers show an increase in mass ablation rate.

4. The filler-to-elastomer ratio of particulate type fillers does not appreciably affect the ablative properties of the composite insulation.

Composite Formulation

Buna-N and silicone elastomers were selected for further study in composite formulations. The effective heats of ablation of these elastomers are shown at heat fluxes from 100 to 1500 Btu/ft^{2}sec in Figure 3.

The high effective heat of ablation of the silicone elastomer suggested that further weight savings could be gained by optimization of the reinforcement content of this material. Fillers selected for this study were chrysotile asbestos, silica, and glass.

It was noted that silicone elastomers from different manufacturers displayed a wide variance in ablative properties. Infrared spectrographic analysis of these elastomers indicated that the silicones containing phenyl side groups showed a thicker, more tenacious char, and performed better in the Plasmatron tests. Therefore, silicones with 0, 7.5 and 30 mole percent of phenyl groups were evaluated. The mass ablation rate (shown in Figure 4) indicated that higher phenyl content resulted in lower mass ablation rates at higher heat fluxes.

Composite samples were prepared using a silicone elastomer containing 7.5 mole percent phenyl groups, because silicones containing higher phenyl content were not available in sufficient quantity. These samples contained varying concentrations of silica and chrysotile asbestos. The mass ablation rates were determined for these formulations and are shown in Figure 5.

The silicone elastomer that demonstrated the greatest resistance to ablation had a tensile strength of 550 psi and 350 percent elongation. It was calculated that the material would provide a 30 to 35% reduction in the insulation weight as compared to the best Buna-N base insulation available.

The silicone base insulation material was therefore tested in a subscale rocket motor burning an aluminized unpolymerized solid propellant. Results of this test were compared to the performance of an unfilled silicone and to the Buna-N/asbestos insulation fired under similar conditions using the same motor. The results are shown in Table III.

[redacted]

Silicone-to-Propellant Adhesive Development

Glass-fiber-reinforced silicone elastomeric insulation displayed great potential as an improved internal insulation rocket motor material. However, an adhesive to bond the material to the cast propellant was necessary before the material could be used as an internal insulation material. Several good adhesives are available commercially for bonding silicone to metals, but no adhesive was available for bonding silicones to the polymers that are used in the solid propellants.

Previous work[1] in obtaining room temperature curing agents for fluorocarbon elastomers indicated that secondary amines with reactive-chemical groups could be attached to polymer chains containing fluorine. Crosslinking could then occur across the reactive sites thus attached to the chain.

Fluorinated silicone and diethynol amine were selected in the Aerojet program because of the reactivity of hydroxyl groups with the polyurethane in the propellant. Attempts to obtain adhesion of the silicone to the propellant through a tie-gum of this material were encouraging, although the results were unpredictable. Adhesion in 90° peel of tie-gum-propellant samples ranged from 0 to 11 lb/in. It was observed that curing of the tie-gum varied widely between samples. It is postulated that the balance of magnesium oxide, used as an acid acceptor, to the amine is extremely critical, since the peroxide curatives utilized in silicones are susceptible to organic material and acetic conditions and thereby affected the state of cure. No improvement in the predictability of the adhesive bond was detected when a solvent solution of the gum was made and applied to the silicone and cured, or when the material was applied as gum stock. However, when the material cured satisfactorily, adhesion to both the silicone and to the propellant was obtained. The inability in obtaining consistent results lead to the abandonment of this approach. The method of mixing the tie-gum is described in Appendix A for those interested in pursuing this method.

The second attempt to bond the silicone to the propellant was through the use of a blend of silicone and gum urethane. Both of these materials can be cured with peroxides. When this tie-gum was placed against a silicone elastomeric material that had been pre-cured, adequate adhesion was obtained between the silicone and the polyurethane-silicone blend when the resultant laminate was cured under heat and pressure.

Initial attempts to obtain adhesion between the silicone-urethane tie-gum and the propellant resulted in low adhesive values. Later experiments indicated that the tie-gum must be cured to the silicone and the resultant laminate post-cured to volatilize the products of the peroxide reaction before bonding to the propellant. The table below

(1) A Room Temperature Vulcanization System for Selected Fluorine-Containing Polymers, W. G. Griffin, Materials Lab., WADC, WADC-TR-59-42.

[redacted]

shows the adhesion obtained between the urethane-silicone tie-gum (pre-coated with a thin coat of di-isocyanate) and a polyurethane base solid propellant.

Peel Strength	9.5 lb/in.
Lap Shear Strength	172 lb/in.
Flatwise Tensile Strength	149 lb/in.

MATERIALS SCREENING

The exorbitant cost of test firing full-scale rocket motors makes it necessary to adapt a screening program for evaluating materials. At Aerojet a series of tests have been developed for the evaluation of internal insulation materials. In all tests the performance of candidate materials is compared to that of a "standard" material. The "standard" material was chosen on the basis of full-scale firing performance data as the best available insulation material used in solid propellant rocket motors. Materials that perform in a manner superior to the "standard" material are further evaluated. Initial testing is performed in a subsonic, alumina-containing, plasma jet. The results of this test have been correlated to the results of full-scale firings for several missiles. The results of the evaluation of many elastomeric compounds are presented in Tables I and II, and Figure 5.

Subsequent ablation tests are performed in a subscale end-burning solid rocket motor. The chamber wall and aft-closure of the motor are insulated with the experimental insulation material. This motor utilizes an aluminized, polyurethane propellant which burns for approximately 20 seconds at 5600°R and 650 psig chamber pressure. A schematic of this motor is presented as Figure 6. The ablation rates of the experimental insulation are determined at several points on the aft-closure and at the point of maximum erosion on the chamber wall. A typical set of data taken from the chamber wall is presented in Table III.

The thermal and physical properties are determined for these materials which appear to offer the greatest improvement in erosion resistance. The properties determined include thermal conductivity, specific heat, effective heat of ablation, density, tensile properties, hardness, bonding characteristics, etc.

Patches of experimental materials selected on the basis of minimum erosion rates in the subscale motor are bonded on the internal insulation of full-scale motors for static firing. The performance of the patches are compared with the performance of the surrounding material. An entire full-scale motor is insulated with a new material and test fired when an experimental material appears to be significantly superior to the "standard" material. At the time of writing the first full-scale motor insulated with an experimental silicone material was about to be fired. The anticipated ablation velocities are presented in Figure 7.

CONCLUSIONS

1. Insulations fabricated using silicone elastomers that contain phenyl groups can provide significant weight-savings and improved performance in solid propellant rocket motors.

2. Elastomeric internal insulation materials usually require fibrous reinforcing filler materials to prevent rapid erosion of the char layer.

3. A satisfactory bond between silicone-base insulation materials and urethane-base solid propellants can be obtained.

TABLE I. THE ABLATION PROPERTIES OF VARIOUS ELASTOMERS*

Elastomeric Compound	Average Mass Rate ($lb/ft^2 sec$)	Average Ablation Velocity ($in./ft^2 sec$)
Natural Rubber	0.412	0.0589
Neoprene	0.655	0.0810
Butyl	0.422	0.0615
GRS	0.595	0.0828
Buna-N(1)	0.660	0.0913
Buna-N(2)	0.442	0.0627
Silicone	0.357	0.0556

(1) Low Acrylonitrile
(2) High Acrylonitrile

* Determined at a heat flux of 1119 $Btu/ft^2 sec$ using an argon plasma.

TABLE II. AVERAGE MASS ABLATION RATE OF THE FILLER-LOADED ELASTOMERIC COMPOUNDS*

Filler Loading PPHR	Type	Elastomer	Average Mass Rate ($lb/ft^2 sec$)
A.	Fibrous Fillers		
25	Acrylic	Buna-N	0.542
35		Butyl 035	0.428
55		Silicone	Could not mold sample
65		Chloro-Butyl	0.425
45		Viton AHV	0.263
35	Asbestos	Buna-N	0.259
65		Buna-N	0.196
25		Butyl 035	0.314
45		Butyl 035	0.199
45		Silicone	0.189
65		Silicone	0.343
25		Chloro-Butyl	0.197
55		Chloro-Butyl	0.165
35		Viton AHV	Could not mold sample
55		Viton AHV	0.330
45	Glass	Buna-N	0.489
55		Butyl 035	0.443
25		Silicone	0.138
35		Chloro-Butyl	0.522
65		Viton AHV	0.727
55	Wool	Buna-N	0.550
65		Butyl 035	0.434
35		Silicone	0.247
45		Chloro-Butyl	0.413
25		Viton AHV	0.415
B.	Particulate Fillers		
35	Clay Microballoons	Buna-N	0.792
45		Butyl 035	0.715
65		Silicone	0.131
55		Chloro-Butyl	0.563
45	Ground Clay	Buna-N	0.694
35		Butyl 035	0.467
55		Silicone	Could not mold sample
65		Chloro-Butyl	0.461
55	Silica	Buna-N	0.414
65		Butyl 035	Could not mold sample
35		Silicone	Could not mold sample
45		Chloro-Butyl	0.478
65	SAF Black	Buna-N	0.653
55		Butyl 035	0.490
45		Silicone	Carbon Black cannot be used as filler
35		Chloro-Butyl	0.394

* Determined at a heat flux of 1360 $Btu/ft^2 sec$ using an argon plasma.

TABLE III. SUBSCALE MOTOR CHAMBER LINER FIRING DATA*

Chamber No.	Chamber Liner	Maximum Erosion-Char Depth (mils)	Maximum Ablation Velocity (mils/sec)	Average Maximum Ablation Velocity (mils/sec)
1	Buna-N + Asbestos	130	3.14	2.94
2	Buna-N + Asbestos	164	2.73	
3	Silicone + Glass	81	1.72	1.70
4	Silicone + Glass	94	1.68	
5	Silicone Elastomer	160	2.86	2.86

* Motor operated at average chamber pressure of 650 psig, using a 16% aluminum unpolymerized propellant, burning at 5600°F.

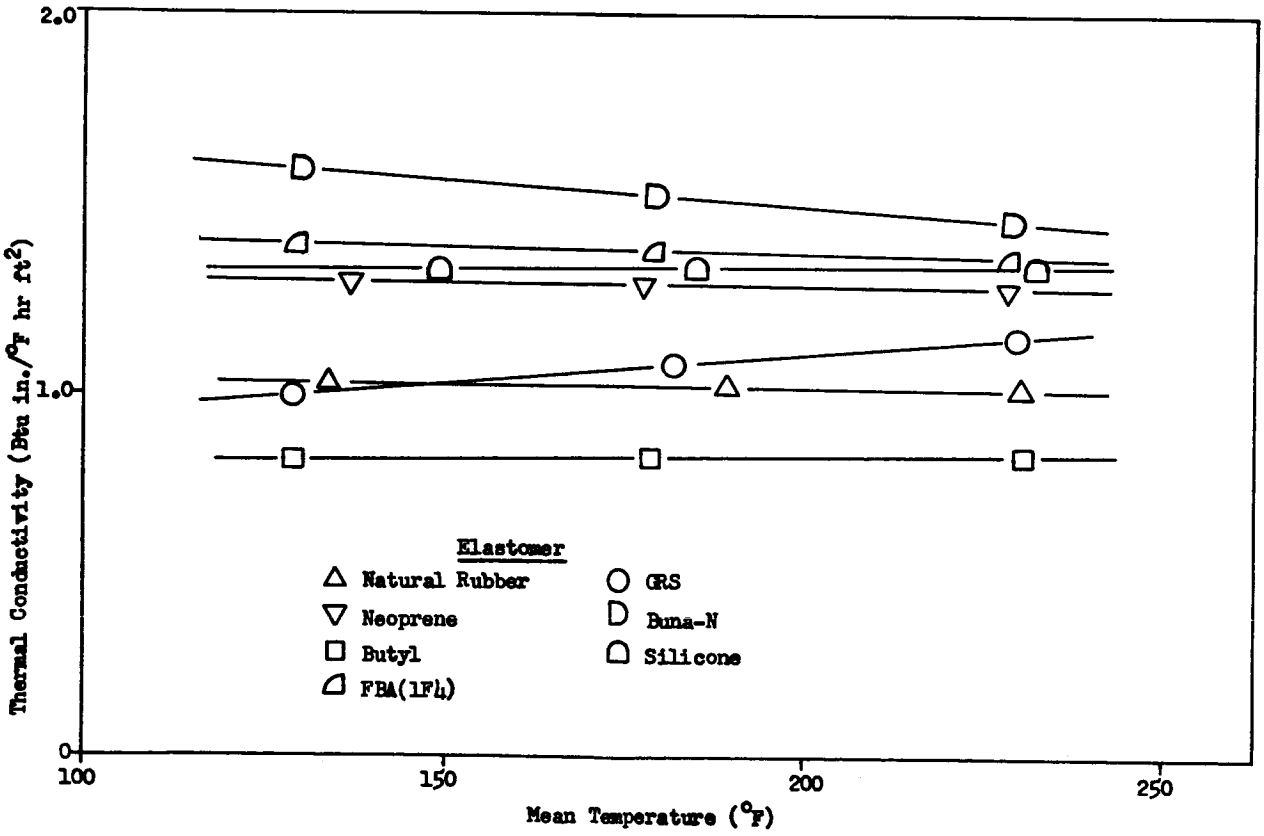

FIGURE 1. THERMAL CONDUCTIVITIES OF ELASTOMERS

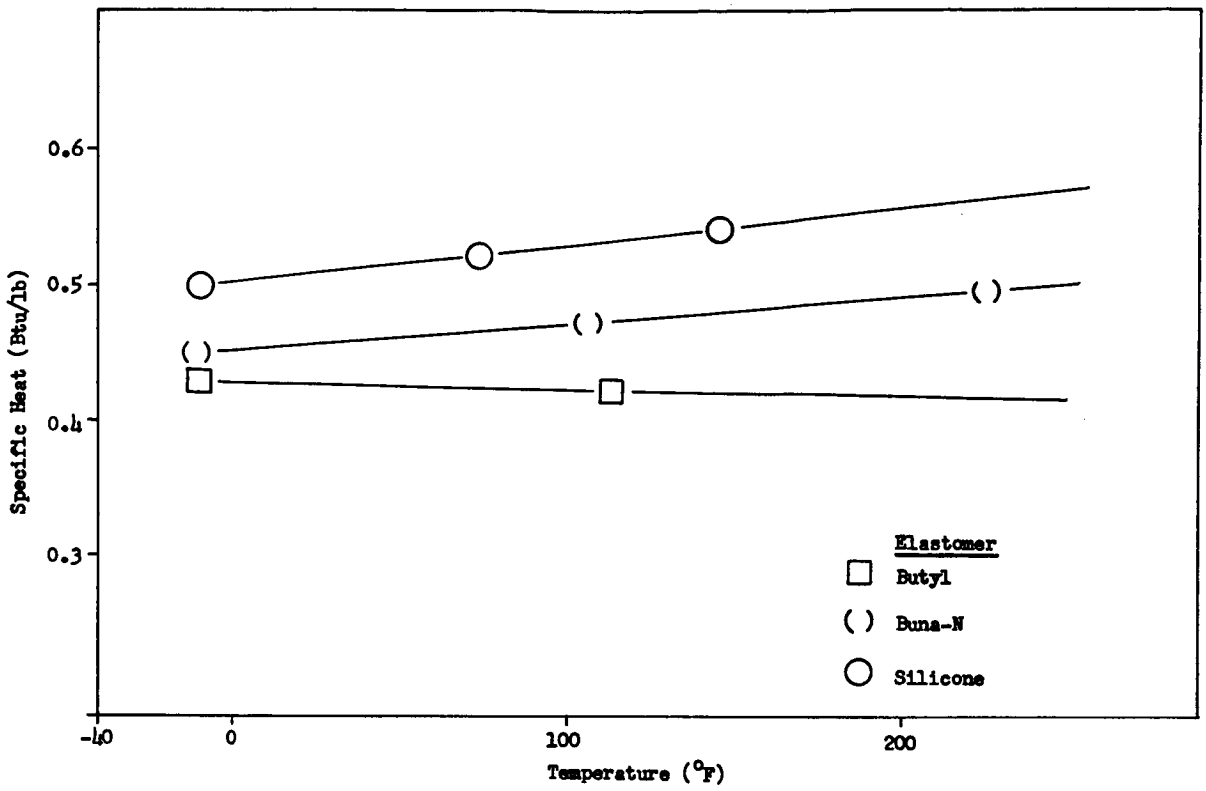

FIGURE 2. SPECIFIC HEAT OF SILICONE, BUTYL AND BUNA-N COMPOUNDS

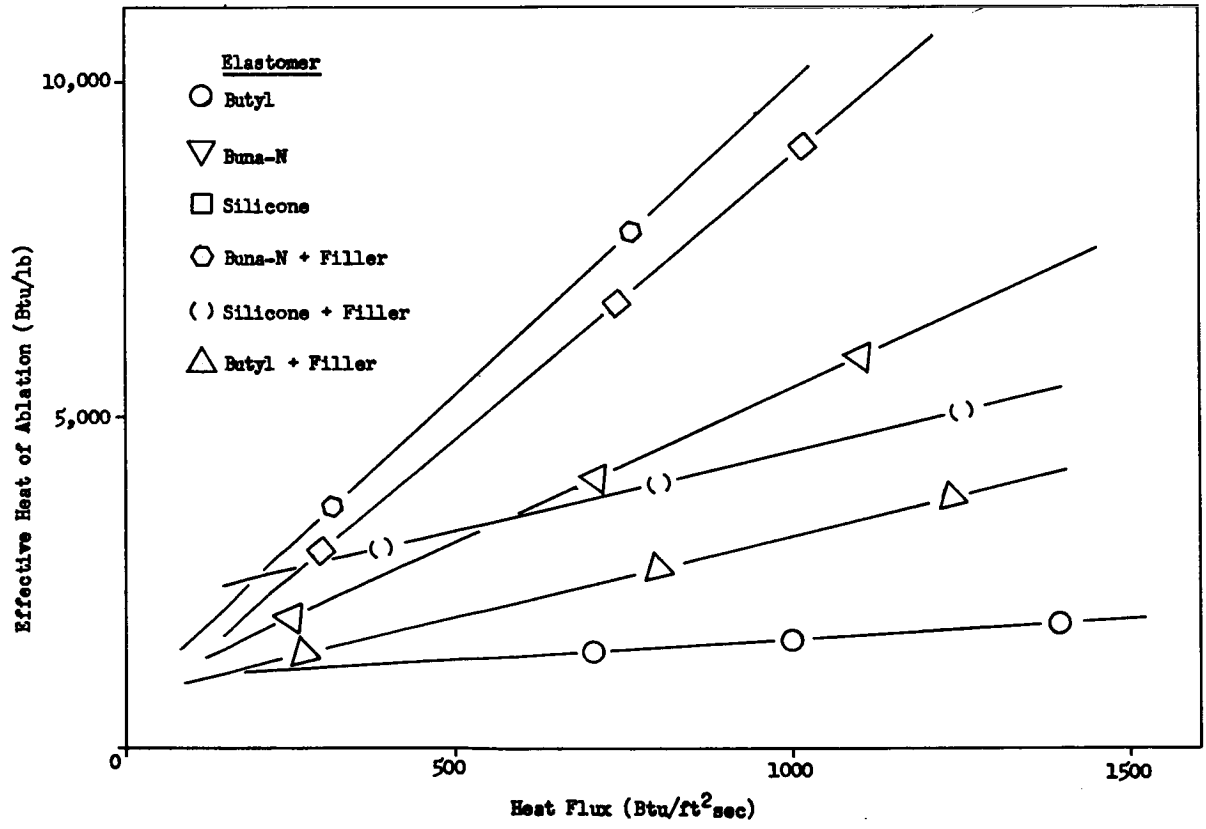

FIGURE 3. THE EFFECT OF FIBROUS FILLER ON THE EFFECTIVE HEATS OF ABLATION OF BUTYL, BUNA-N AND SILICONE

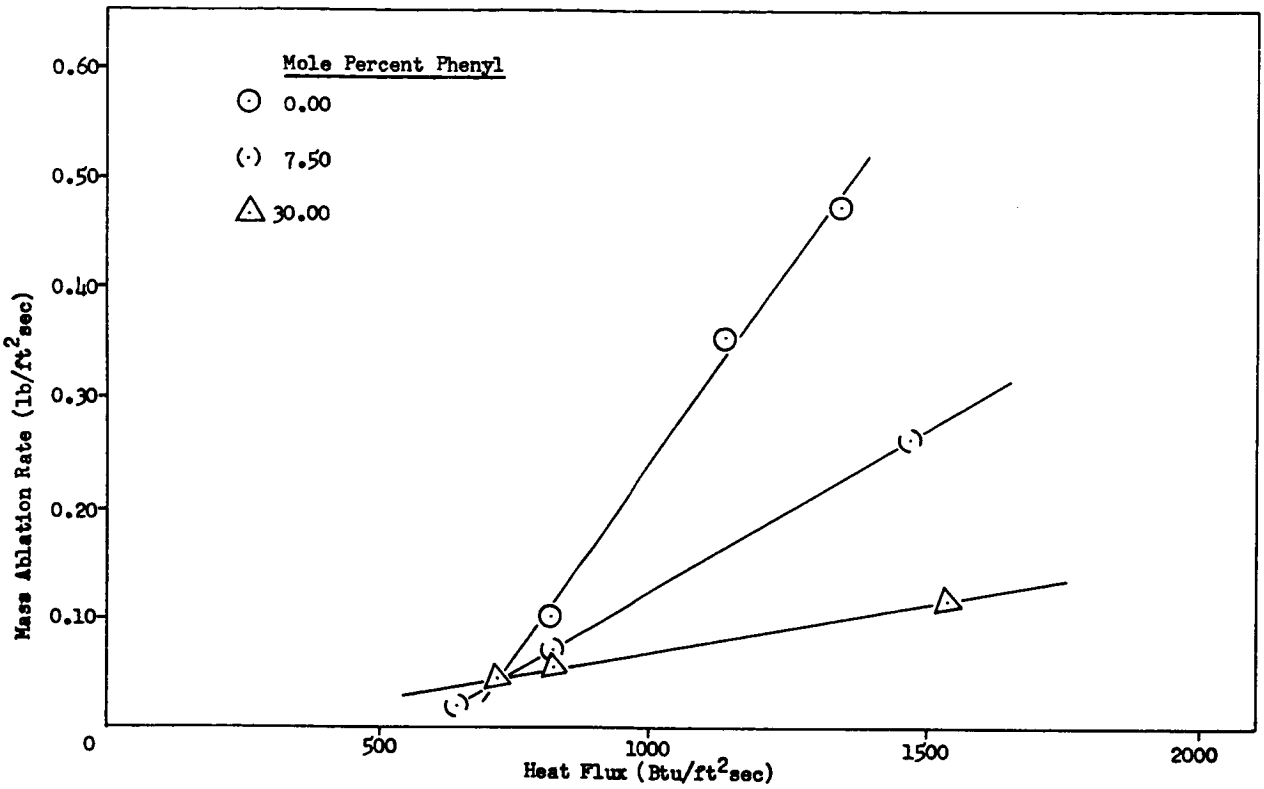

FIGURE 4. THE EFFECT OF PHENYL CONTENT ON THE MASS ABLATION RATE OF SILICONE ELASTOMERS IN THE SUBSONIC PLASMA JET

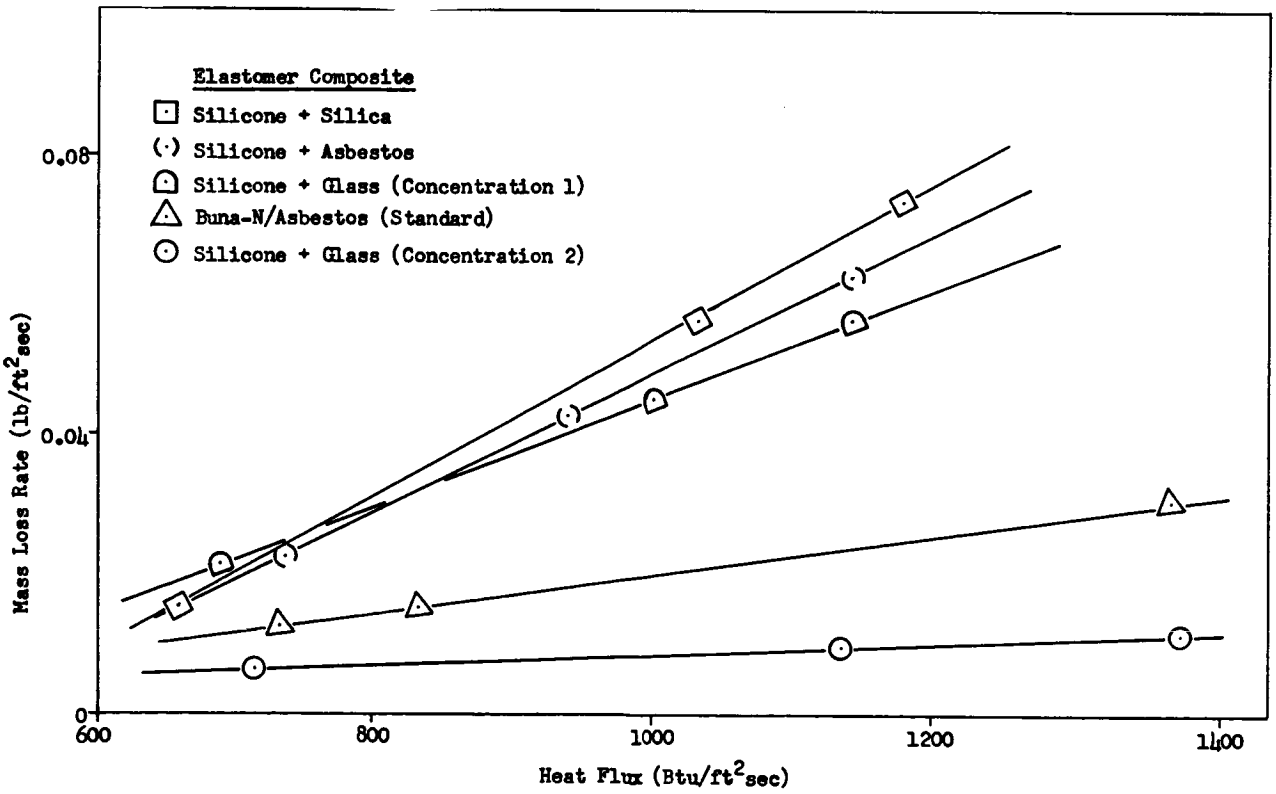

FIGURE 5. THE EFFECT OF FILLERS ON THE MASS LOSS RATE OF SILICONE ELASTOMERS IN THE SUBSONIC PLASMA JET

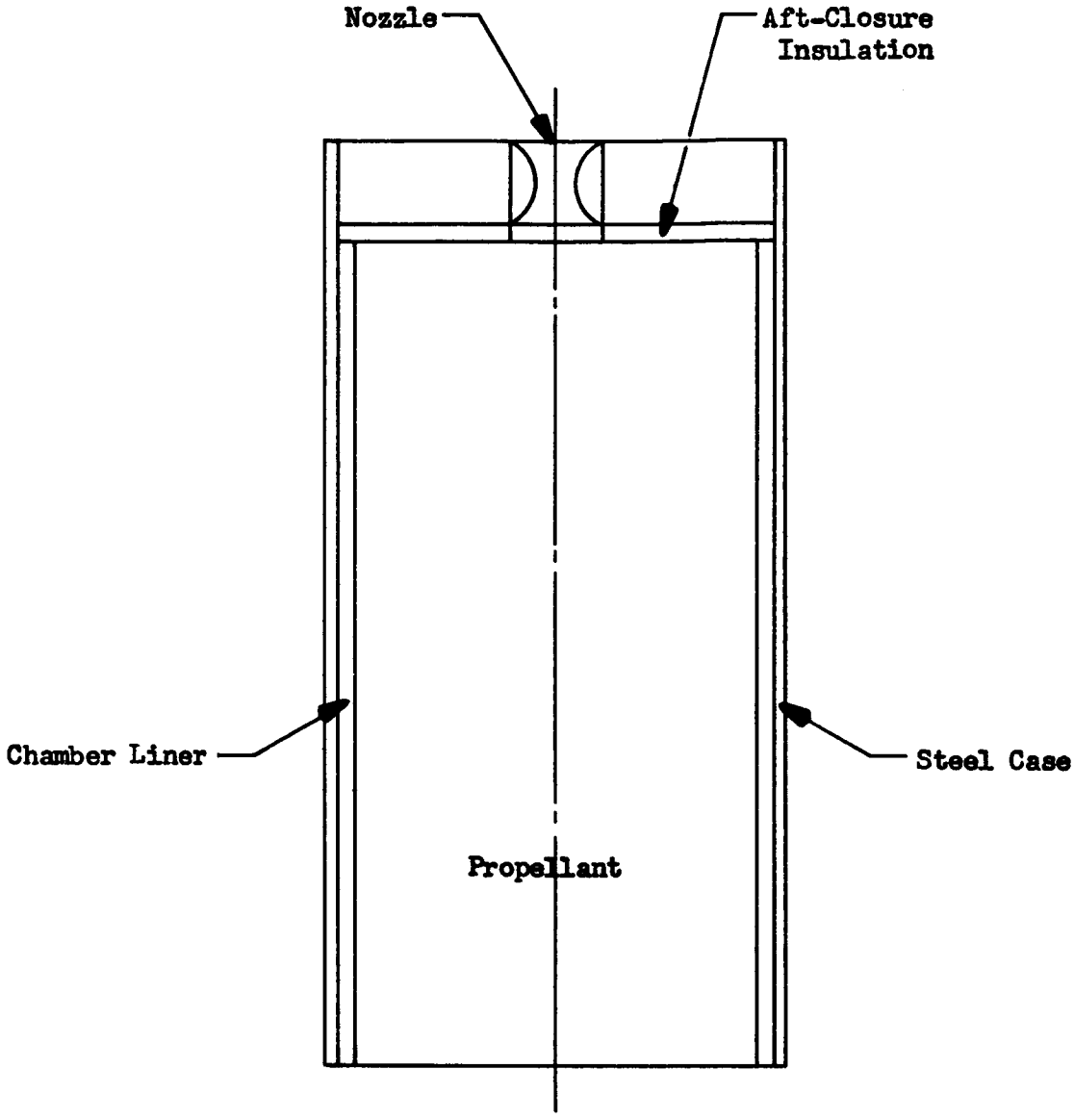

Chamber diameter = 5.1-in.
Firing duration ≐ 20 sec
Chamber pressure ≐ 650 psi
Initial insulation thickness ≐ 300 mils
Initial nozzle throat diameter ≐ 0.5-in.

FIGURE 6. SCHEMATIC OF SUBSCALE SOLID ROCKET MOTOR PRIOR TO IGNITION

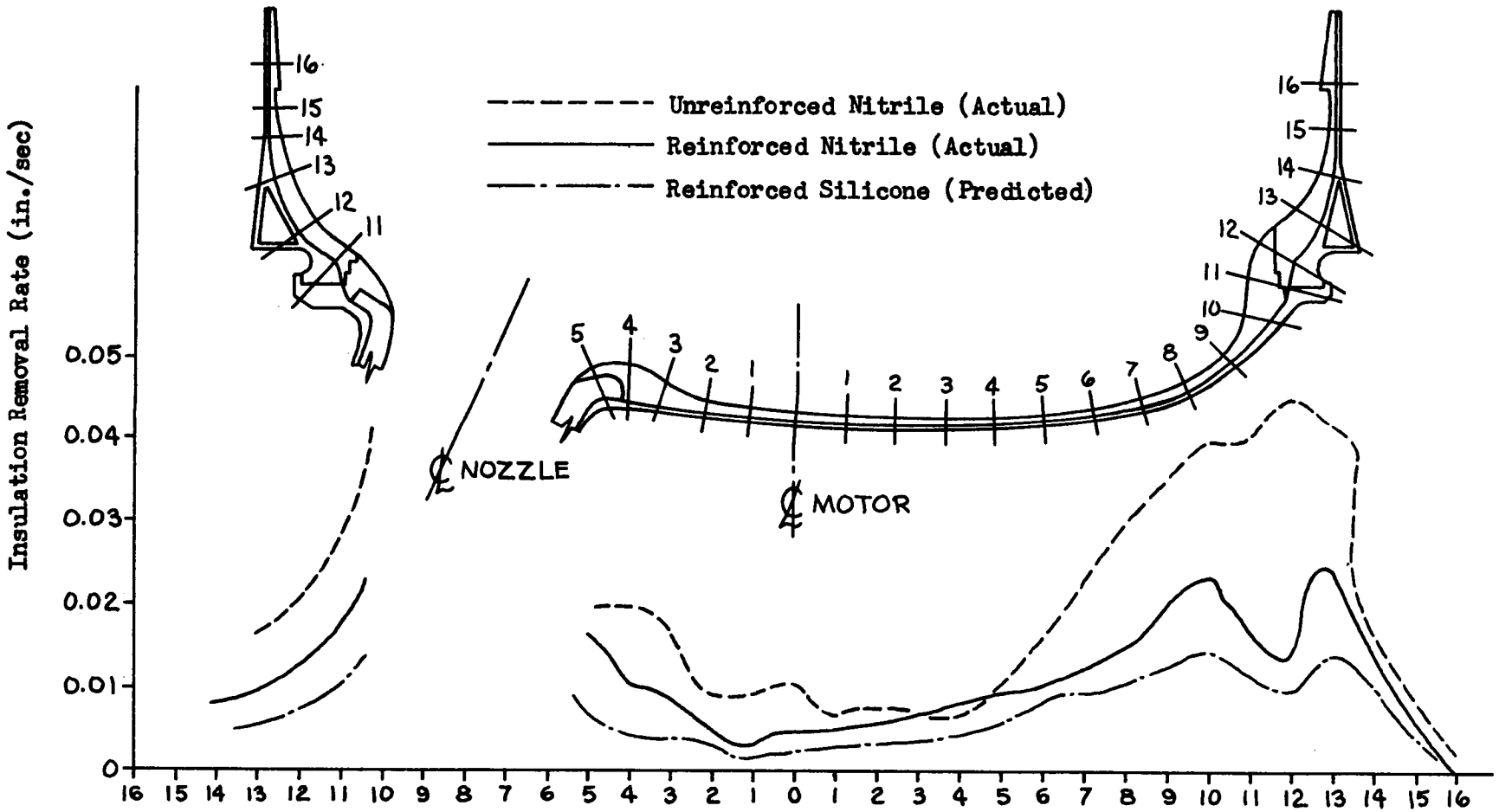

FIGURE 7. TYPICAL INTERNAL INSULATION PERFORMANCE PROFILE FROM A SOLID ROCKET

[redacted]

APPENDIX A

METHOD OF MIXING TIE-GUM

1. The silicone, the secondary amine, and magnesium dioxide were mixed on a cold rubber mill.

2. The temperature of the mill rolls was raised to 325°F and the batch was added to the mill and left for 30 minutes to react the amine with the fluoro-silicone. (No chemical tests were conducted to determine the amount of amine that was reacted with the polymer.)

3. The peroxide was mixed into the batch on a cold rubber mill and the batch was sheeted.

[redacted]

GRAPHITE AND CARBON CLOTH PHENOLICS-- THEIR USE AND APPLICATIONS IN SOLID PROPELLANT MOTORS

by Robert V. Fox

THIOKOL CHEMICAL CORPORATION
Wasatch Division
Brigham City, Utah

ABSTRACT

Since 1959, two types of cloth phenolics were developed for use in the missile industry. These phenolics, graphite and carbon cloth, exhibit high temperature properties which give them the necessary characteristics required for use in laminates and molding compounds for solid propellant motors.

The two materials have been used in areas of high velocity gas flow, high temperature, and severe particle impingement. The first major use of graphite cloth phenolic at Thiokol Chemical Corporation was as an erosion shield in the aft closure of a subscale Air Force MINUTEMAN research and development motor. The aft closure of a four port motor with a six point grain configuration was exposed to severe particle impingement and turbulent gas flow. Glass and silica cloth phenolics were satisfactory, but graphite cloth phenolic gave a weight saving of 30 percent. Additional work was done on the use of these materials for case and closure insulation, blast tubes, nozzle throats, and exit cones. Erosion data from full scale firings indicate that the use of this family of materials is very practical and in some cases may almost be a necessity to produce lightweight reliable parts.

Graphite cloth is made from fabric, woven from organic fibers, by graphitizing at temperatures up to 5000°F. In a typical cloth, these fibers have tensile strengths of 50,000 to 100,000 psi. The cloth will assay over 99.96 percent graphitic carbon. Carbon cloth also is made from organic fiber fabric, but is processed at 1300-1500°F and assays more than 99 percent carbon. The fiber diameter for both materials is approximately 0.00033 in. The cloths, when coated with a high temperature phenolic resin, such as those conforming to MIL-R-9299, Class II, Type Two, may be chopped into squares, and macerated or slit into tapes of different widths.

Now that more data and fabrication experience have been attained, the current applications of these materials are achieving the results originally expected from their use.

[redacted]

INTRODUCTION

Graphite cloth as a reinforcing material for phenolic plastics was first introduced into the missile industry in 1959. Graphite cloth was proposed as a reinforcement that would provide much greater ablation resistance for plastics than other reinforcements in use extensively at that time, such as glass, silica, and asbestos.

Another new reinforcement, carbon cloth, was introduced into the missile industry in 1961. Carbon cloth was suggested as a reinforcement to provide plastics with approximately the same ablation resistance as graphite cloth, but with increased tensile and compressive strength and lower thermal conductivity.

Since their introduction, various applications have been found for utilizing graphite and carbon cloth for solid propellant motors developed by Thiokol Chemical Corporation. The value of these materials has increased as our working knowledge increased.

Composition

Graphite cloth is made from selected organic fibers that are woven into a cloth and heated to approximately 5000°F. The woven, high purity graphite fibers are the only constituents of the cloth, which assays over 99.96 percent graphitic carbon. Produced by the National Carbon Company, the cloth is available in either a square weave (WCA) or a twill weave (WCH), in widths up to 45 in. and lengths up to 170 yd. Other type weaves, lengths, and widths are available upon request.

The carbon cloth is also made from selected organic fibers that are woven into a cloth and heated to approximately 1300-1500°F. The fibers of the carbon cloth assay over 99 percent carbon. Because of the amorphous structure of the carbon fiber, it has approximately 50 times greater effective surface area than the graphite fiber. The carbon cloth is available in the same weaves, widths and lengths as the graphite cloth. Both the carbon and graphite are available in the bulk fiber form. For the bulk fiber, the yarn is cut into 1/4 in. fibers and then heated to the necessary temperature. For the carbon and graphite, the yarn is either woven into a fabric or cut into the bulk form before heating to prevent loss of material because of powdering during the heat-treating. Fibers of other lengths are available upon request.

Carbon and graphite cloths can be used either in a wet or prepreg system. In general, the prepreg material has been the most adaptable for missile hardware. To prepare the prepreg, the fabric is passed through a resin bath and the excess resin is metered off. After the resin bath, the fabric is fed through a hot oven where the solvent is evaporated and the resin staged. The broadgoods can then be slit to any width tape or chopped into 1/2 in. squares for molding compound. In general, phenolic resins conforming to MIL-R-9299 Type 2, Class II have been the most satisfactory for the plastic insulation in solid propellant motors. Other

[redacted]

[redacted]

resins, such as phenyl silane and nylon, have been evaluated; but, since their performance was inferior to phenolics, they will not be discussed in this paper.

Tables I and II list some of the properties of carbon and graphite cloth in both uncoated and coated fabrics.

Table III compares some of the physical properties of graphite and carbon cloth phenolics to silica cloth phenolics and high density graphite.

Evaluation Motors

Thiokol received contracts for research and development on the Air Force MINUTEMAN first stage motor in 1958. In support of the MINUTEMAN program, Thiokol's Wasatch Division developed a number of subscale motors for use in evaluating design configurations and materials to meet the work statement requirements for the MINUTEMAN motor, prior to their use in the full scale first stage. For material evaluation, Thiokol utilizes five motors: TU-132, TU-152, TU-143, TU-190 and TU-222. A brief description of each of these motors, and why they are used for particular evaluations, follows:

TU-132. This is a single, center port motor with an uncured end burning grain. This motor is used as the initial screening motor for all insulation and erosion resistant materials because of its relatively low cost. The average throat diameter for this motor is 0.87 in. The mass flow is 2.78 lb/sec for a 60 sec duration test at an average chamber pressure of 640 psia.

TU-152. The TU-152 motor is similar in design to the TU-132 motor -- a single center port and end burning uncured propellant grain -- but contains approximately 20 times as much propellant as the TU-132. The TU-152 is used primarily to evaluate nozzle, throat, and exit cone materials after they have been successfully tested in the TU-132. This motor has a throat diameter of approximately 4.5 in. The mass flow is approximately 55 lb/sec for a 60 sec test at 500 psia chamber pressure.

TU-190. This is a single, offset port motor which is used primarily to test nozzle design and materials for use on the MINUTEMAN first stage motor. This motor has a six pointed core configuration similar to the MINUTEMAN first stage. The throat diameter for this nozzle is approximately 7.5 in. with an approximate 200 lb/sec flow for a 65 sec test at an average chamber pressure of 670 psia.

TU-143. The TU-143 is a four port motor that was designed as a half scale of the MINUTEMAN first stage. It can be adapted for investigation of propellant, charge configuration, insulation, or nozzle design. Because of the design of the aft-closure metal parts, this motor is very adaptable for evaluating materials and design of the blast tube, and the flow area for the gases from the chamber to the nozzle throat. The firing time for this motor is approximately 30 sec. The throat diameter is approximately four in. with a flow rate of approximately 80 lb/sec/port at an average chamber pressure of 650 psia.

[redacted]

TU-222. The TU-222 is a four port motor used to evaluate designs and materials for the MINUTEMAN first stage. In a four port motor, the aft closure is subjected to very turbulent gas flow and nonuniform erosion patterns. This motor has been used extensively for evaluation of aft-closure insulation materials and designs for use in the MINUTEMAN first stage. The design of the aft-closure metal parts does not permit evaluation of materials in the blast tube, because the maximum allowable wall thickness of insulation and erosion resistant material was only 1.2 in. The motor fires for approximately 55 sec, with an average chamber pressure of 500 psia, and a mass flow rate of 50 lb/sec/port at approximately a 4.5 in. throat diameter.

One other motor, the TU-235, will be mentioned in this report. This motor is the same as the TU-190 except that the aft closure is modified by a center-port nozzle instead of the offset port.

Graphite and carbon cloth phenolics were tested and evaluated in these motors. From these test results, the materials are programmed into the MINUTEMAN first stage and other Thiokol motors.

Evaluation Testing

As we mentioned earlier, the TU-132 is the first motor in which any new material is evaluated. This motor provides data on materials in the blast tube (subsonic gas velocity), throat section (sonic velocity), and exit cone (supersonic gas velocity) areas. (See Figure 1 for cross section of TU-132.)

Materials in the blast tube are subjected to gas velocities of approximately Mach 0.4, and gas temperatures and pressures which are very near chamber temperatures and pressures. If a material exhibits satisfactory erosion and temperature resistance in the blast tube, further evaluation is conducted in the aft-closure areas of larger solid propellant motors. The initial screening of materials for large nozzles is conducted in the exit cone of the TU-132.

The first evaluation of graphite cloth phenolics was conducted with this material in both the blast tube and the exit cone. These tests were performed with the chopped (1/2 in. x 1/2 in. squares) molding compound impregnated with MIL-R-9299 phenolic resins (91LD and SC-1008).

The blast tube test showed that graphite cloth phenolic had the highest erosion resistance of any plastic material yet evaluated. The depth of char was considerably greater than silica cloth phenolics, indicating the necessity of an insulating material as a backup for the graphite cloth. The performance of the graphite cloth phenolic in the exit cone was slightly superior to silica cloth phenolic. Figure 2 shows an erosion profile of this blast tube and exit cone. Localized spalling or chunking out of material was noted in the exit cone. This spalling proved to be a problem with graphite cloth phenolics for some time.

After the successful initial testing of the graphite cloth phenolics, a test program was conducted to investigate modifications of the original material. The aim of these modifications was to substitute various inexpensive filler materials in the system and reduce the percentage of graphite cloth while maintaining or improving the erosion and temperature resistance. Graphite cloth cost approximately $20 per yard; by reducing the percentage from 65 to 50 percent, a cost savings of 23 percent could be realized. Some of the fillers used were magnesium oxide, zinc oxide, potassium titanate, perlite, and graphite powder. The test results from the TU-132 motor indicated that a material with 35 percent modified phenolic resin, approximately 15 percent of any one of the filler materials listed above, and 50 percent graphite cloth, was close to being an optimum system.

From these test results the decision was made to conduct further evaluation of the graphite cloth phenolic in larger motors. The first major application was in the aft closure of the TU-222 motor. Prior to this time, glass fiber, quartz, and silica cloth phenolics had been used as the aft-closure insulation. New parts were designed, using the chopped graphite phenolic molding compound backed up with silica cloth phenolic as an insulator to maintain a low surface temperature (300°F) of the steel aft closure. Figure 3 shows a cross section of the insulated aft closure.

The molding material used for these parts contained approximately 53 percent chopped graphite cloth, 13 percent graphite powder, and 34 percent 91LD phenolic resin. These composite moldings were formed in matched metal dies in a two stage operation. The performance of the graphite cloth phenolic in this application was only partially satisfactory. The total loss of material through erosion was less than with silica cloth phenolics, but the erosion was not uniform. Spalling or chunking out of material occurred in various areas of the closure. The cause of this condition is believed to be the high thermal conductivity of the graphite cloth which caused increased subsurface formation and entrapment of volatile decomposition products. With the expansion of these entrapped volatiles, layers of the chopped graphite cloth were blown out. This spalling was localized, and the amount of spalling did not preclude the use of the material in this overdesigned part. With the graphite cloth phenolic, the design thickness in this motor was decreased 3/8 in., so that an inert weight savings of 40 percent was effected as compared to the silica cloth phenolic design.

From the satisfactory test results of the chopped graphite cloth phenolic in the TU-132 blast tube, a program was also initiated to fabricate blast tubes for a four port motor with this material. At that time, Thiokol was using high density type graphite (1.80 g/cc) in the blast tubes of the first and second stage MINUTEMAN development motors and in other four port subscale motors. Graphite was used in this area primarily because of its erosion resistance. The drawback in the use of graphite was its tendency to crack from thermal and mechanical stresses.

In this particular test, three blast tubes for the TU-143 motor were made from the chopped graphite cloth phenolic. The fourth blast tube was of the standard graphite design. The three graphite cloth phenolic blast tubes were fabricated in matched metal dies and molded at approximately 4000 psi. They were insulated

with a fiberglass phenolic wrap. Figure 4 shows a cutaway view of the aft closure with the blast tube in place.

Postfiring examination of the three graphite cloth phenolic blast tubes showed a very uneven erosion pattern. There were a number of areas in these blast tubes where the material had spalled out, particularly where the blast tube abutted the graphite entrance area of the nozzle. The maximum amount of material lost in the graphite cloth phenolic blast tube was 0.99 in., which is an erosion rate of 33 mils/sec. The blast tube of the standard graphite design had a maximum material loss of 0.48 in. for an erosion rate of 16 mils/sec. It is to be noted that this approximate factor of 2:1 erosion rate of graphite cloth phenolic to graphite was similar to the test results of the TU-132 motor, where the graphite has an erosion rate of 1.8 mils/sec and the graphite cloth phenolic 3.5 mils/sec. Figure 5 is an erosion profile of the blast tubes and aft closure.

No further tests were conducted with the graphite cloth phenolic in the blast tubes of four port motors because of the nonuniform erosion, relatively high erosion rate, and the availability of new improved graphites and improved blast tube designs. These improved graphites and designs eliminated the need for plastic blast tubes.

In conjunction with the tests of the graphite cloth phenolic in the aft closure and blast tubes, the material also was evaluated in the exit cone area of the TU-152 motor. Five tests were conducted using the chopped graphite cloth impregnated with five different resin systems. These exit cones were high compression molded in matched metal dies. After static testing of these cones, one condition was found common to all; the erosion was very uneven with a high degree of material spalling. The spalling was so severe that further testing of the chopped graphite cloth phenolic as an exit cone material was not recommended.

In late 1960, the future of graphite cloth phenolic for Thiokol motors did not appear to be very encouraging. Limited use was being made of the material. Because of the tendency to spall and the resultant unpredictable erosion patterns, the use was not extensive.

In early 1961, a new manufacturing system reduced the spalling of the chopped material. The solution to the spalling problem was accomplished by drilling very small diameter holes through the graphite cloth phenolic to allow the escape of the entrapped volatiles.

Exit cones for the TU-190 nozzle configuration were fabricated of the chopped graphite cloth phenolic. After the molding operation, holes 1/16 in. diameter, 1/2 in. deep, and with 1/2 in. center lines were drilled over the entire interior surface of the chopped graphite cloth phenolic exit cones. The test results, as shown in the erosion profile in Figure 6, were very satisfactory. The erosion was uniform with no evidence whatever of spalling or gouging. These test results were further substantiated from tests in the exit cones of the MINUTEMAN first stage motor. Further testing was performed on exit cones with only the forward half of the cone

drilled and the aft half left undrilled. The results were as predicted. The drilled half had uniform erosion and the undrilled half experienced spalling and gouging. A program currently is being conducted to determine the minimum number of holes required to obtain uniform erosion.

At approximately the same time as the hole drilling program was in progress, another test program using graphite cloth phenolic in the tape wrap form was conducted in nozzles for the TU-152 Motor. Carbon cloth reinforcement 2/50 was introduced for testing at this time. One of the objections to graphite cloth phenolic had been its high thermal conductivity, requiring a backup layer of insulating material, such as asbestos, glass or silica phenolic. The initial laboratory test results on carbon cloth phenolic reported that the thermal conductivity of the carbon cloth phenolic was anywhere from 25 to 65 percent less than the graphite cloth phenolic.

Two static tests were conducted in the TU-152 motor to evaluate the use of graphite cloth phenolic tape and carbon cloth phenolic tape as a throat material and as exit cone material. The objective of these tests was twofold. The objective was first to determine the feasibility of using these materials in the throat and exit cones, with the aim of using them in large solid propellant booster motors. The second was to obtain a comparison of erosion rate and char depth of the two materials in similar tests. Both a throat insert and exit cone were tested in each motor. The throat insert was similar in design to the previously tested graphite inserts with the cloth layup on a 30 degree shingle. The exit cones were wrapped parallel to the nozzle center line. Both the throat inserts and the exit cones were hydroclave cured. The resin content on the carbon cloth was 42 percent and on the graphite cloth, 34 percent.

Table IV lists specific data concerning each test. The general appearance of both nozzles was very good as is seen in Figure 7. Both nozzles were cut in half longitudinally and erosion profiles were taken (see Figure 8). There was no evidence in either the throat or exit cone of either nozzle of spalling or gouging of the materials

One notable difference in the two nozzles was the circumferential delamination in the carbon cloth phenolic. This delamination occurred not only on the aft exit surface of the exit cone that is normal to the nozzle centerline, but throughout the gas exposed area. When the nozzle with the carbon cloth phenolic material was cut in half, it was seen that delamination went forward along the cloth layup surface. This delamination caused no apparent harm during the test, but the fact that it did occur and the possibility of these layers being ejected during test were causes for concern. This application of carbon cloth was relatively new, and this problem was similar to those inherent in any new material application. The apparent cause of this delamination was the high laminar conductivity of the cloth. The material suppliers have since solved this high conductivity problem.

The depth of material charring in the two nozzles was quite uniform. The average depth of char in the carbon cloth phenolic parts was about 20 percent less than in the graphite cloth phenolic (Figure 8). These two tests were very

valuable in obtaining a comparison of the two materials and an evaluation of the materials for large booster motor applications.

Following the TU-152 test program, exit cones for the MINUTEMAN first stage motor were fabricated from both graphite cloth phenolic tape and carbon cloth phenolic tape. These cones were mandrel wrapped with a cloth layup parallel to the center line. In static tests both types of exit cones were successful. Table V lists erosion measurements for these two types of cones and comparative data for a cone of the chopped graphite cloth phenolic with the holes drilled.

One other interesting program has been conducted by Thiokol on graphite and carbon cloth phenolics. This program evaluated these materials in nozzles that fire for 100 seconds or more, as might be required for large solid propellant booster motors. These tests were conducted in the TU-235 motor. In the first test, graphite cloth phenolic tape was used in the convergent entrance section of the nozzle forward of the graphite throat insert and in the divergent exit cone from a point immediately aft of the throat insert to the 3.58:1 expansion area. From this expansion area to the 7.75:1 expansion area, the exit cone was wrapped with carbon cloth phenolic tape. The remainder of the nozzle was wrapped with silica and glass cloth phenolic tape.

The second test nozzle was identical to the first in contour, except that in place of the HLM-85 graphite throat insert, a graphite cloth phenolic tape material was used. Table VI gives some of the data concerning these two tests. The performance of the graphite cloth and carbon cloth phenolics in both tests was very satisfactory.

In the first test of the nozzle with the HLM-85 graphite throat insert, the maximum amount of graphite cloth phenolic was lost just forward and just aft of the throat insert. The erosion rate in these two areas was 2.7 mils/sec. In the area with the carbon cloth phenolic, there was no measurable loss of material. Figure 9 is an erosion profile of the TU-235-2.

In the second nozzle test that had the graphite cloth phenolic throat insert, the maximum erosion rate in the throat section was 6.0 mils/sec. In the convergent entrance section and the divergent exit cone, the maximum erosion rate of the graphite cloth phenolic was 2.5 mils/sec. As in the preceding nozzle, there was no measurable erosion in the carbon cloth phenolic area.

The information obtained from these two tests was very valuable for the design problems envisioned in the nozzles required for large solid propellant booster motors that are to have firing times in excess of 100 seconds. It is apparent that if a slightly regressive pressure and thrust trace are required for a large booster motor, graphite cloth phenolic is an excellent candidate material. The smooth erosion contour and the inherent reproducibility available with these materials will increase their usefulness in large nozzles.

[redacted]

CONCLUSION

The various uses and applications of graphite cloth and carbon cloth phenolic at Thiokol during the last three years have been reviewed. These materials are not the engineer's dream of the perfect erosion resistant and insulating material, but they are filling a vital slot in the state-of-the-art improvement program. The continued and expanded use of these materials is now a reality, particularly in the large booster motor nozzles currently being designed.

New and different applications of these two materials will be made. The use of elastomeric filler in carbon cloth and graphite cloth phenolic systems is now opening up many new possible applications. Carbon cloth and graphite cloth as reinforcements in plastic systems now join silica, quartz, asbestos, glass, and the other dependable reinforcements being used in the insulation materials needed for solid propellant motors.

[redacted]

TABLE I
PHYSICAL PROPERTIES OF UNCOATED CARBON AND GRAPHITE CLOTH

Property	Carbon Cloth*	Graphite Cloth*
Density (gm/cc)	1.40	1.50
Surface area (sq m/gm)	1.50	3
Yarn count/in., warp and fill	26 x 23	27 x 24
Thermal Conductivity of fibers at 70°F (BTU/hr) (sq ft) (°F/ft)	0.2-1.0	22
Specific heat, mean to 400°F (BTU/lb) (°F)	0.22	0.22
Tensile strength at 70°F (psi)	75	24
Fiber Diameter (microns)	8	8
Cloth Weight (oz/sq yd)	7	7.6

*These values are typical of a graphite cloth and carbon cloth as supplied by National Carbon Company.

TABLE II
PHYSICAL PROPERTIES OF COATED CARBON AND GRAPHITE CLOTH

Property	Carbon Cloth Phenolic*	Graphite Cloth Phenolic*
Density (gm/cc)	1.45	1.50
Tensile Strength (psi)	7,500	5,000
Compressive Strength (psi)	25,000	14,000
Flexural Strength (psi)	16,000	9,500
Modulus in Flexure (psi x 10^{-6})	2.2	1.65
Thermal Conductivity ($BTU/ft^2/hr/°F/in.$ @ 100°C)	4.5	5.7
Resin (percent)	34	42
Resin Type	Modified Phenolic	

*These values are typical for a carbon and graphite cloth phenolic, i.e., Fiberite MX-4926 and MX-4551.

[redacted]

TABLE III
PHYSICAL PROPERTIES OF VARIOUS ABLATION MATERIALS

Property	Car. Cloth Phenolic*	Graph. Cloth Phenolic*	Sil. Cloth Phenolic*	Graphite*
Density (gm/cc)	1.45	1.50	1.78	1.84
Tensile Strength (psi)	7,500	5,000	13,000	2,100
Compressive Strength (psi)	25,000	14,000	35,000	7,000
Flexural Modulus (psi x 10^6)	2.2	1.65	2.5	1.7
Thermal Conductivity	4.5	5.7	2.4	7.7

*Typical values

Carbon cloth phenolic - Fiberite MX-4925
Graphite cloth phenolic - Fiberite MX-4551
Silica cloth phenolic - Fiberite MX-2646
Graphite - Great Lakes Carbon HLM-85

TABLE IV
TEST DATA FROM TU-152-57 (CARBON CLOTH PHENOLIC TAPE) AND TU-152-58 (GRAPHITE CLOTH PHENOLIC TAPE)

Data	TU-152-57	TU-152-58
Propellant Weight (lb)	3,159	3,126
Initial Throat Diameter (in.)	4.388	4.392
Final Throat Diameter (in.)	5.142	5.298
Throat Erosion Rate on a Radius (mils/sec)	5.14	6.25
Area Increase in Throat (percent)	37.32	45.51
Initial Exit Diameter (in.)	10.98	10.98
Final Exit Diameter (in.)	10.90	10.91
Exit Plane Erosion Rate	Nil	Nil
Pressure Maximum (psi)	451	498
Pressure Average (psi)	373	373
Web Burning Time (sec)	72.3	68.06

[redacted]

[redacted]

TABLE V
EROSION DATA ON MINUTEMAN FIRST STAGE EXIT CONES

Material	Depth of Erosion (in.) Average	Maximum	Minimum
Graphite Cloth Phenolic Tape	0.25	0.41	0.12
Carbon Cloth Phenolic Tape	0.18	0.28	0.10
Chopped Graphite Cloth Phenolic with Holes Drilled in Cone	0.21	0.35	0.11

TABLE VI
TEST DATA FROM TU-235-2 AND TU-235-3 MOTOR FIRINGS

Data	TU-235-2 (HLM-85 Graphite Throat)	TU-235-3 (Graphite Cloth Throat)
Propellant Weight (lb)	8,600	7,880
Initial Throat Diameter (in.)	5.498	5.277
Final Throat Diameter (in.)	6.136	6.512
Average Throat Diameter Increase (in.)	0.638	1.235
Area Increase in Throat (percent)	24.71	52.28
Throat Erosion Rate on a Radius (mils/sec)	2.92	5.37
Pressure Maximum (psi)	575	650
Pressure Average (psi)	463	428
Web Burning Time (sec)	109.8	114.9

[redacted]

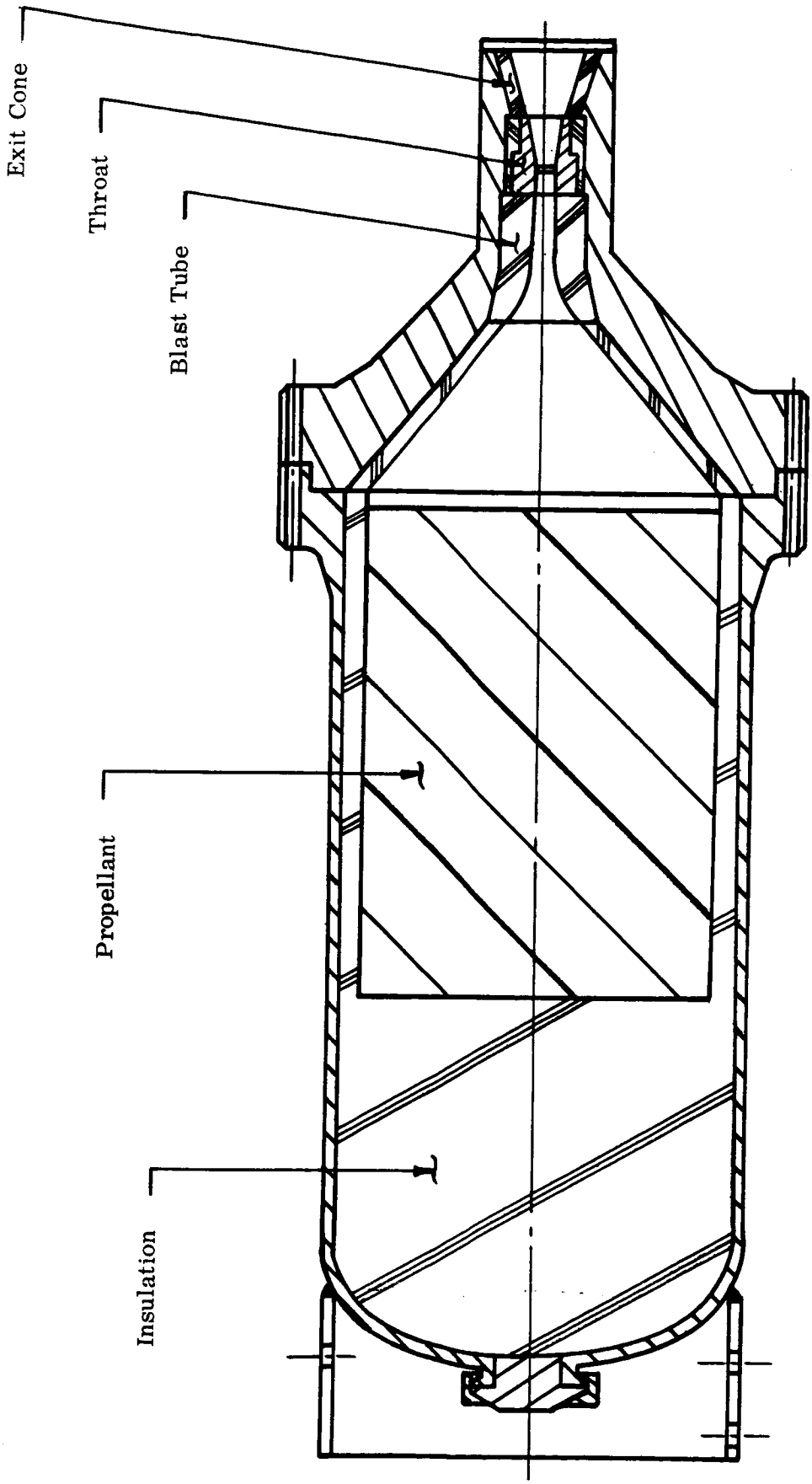

FIG. 1 TU-132 MOTOR ASSEMBLY

STATION (in.)	THICKNESS (in.)	UNCHARRED THICKNESS (in.)
.0.0	0.40	0.12
1.0	0.71	0.43
2.0	0.62	0.41
3.0	0.62	0.36
4.0	0.64	0.30

STATION (in.)	THICKNESS (in.)	UNCHARRED THICKNESS (in.)
0.0	0.43	0.00
0.5	0.43	0.00
1.0	0.46	0.00
1.5	0.49	0.00
2.0	0.52	0.00

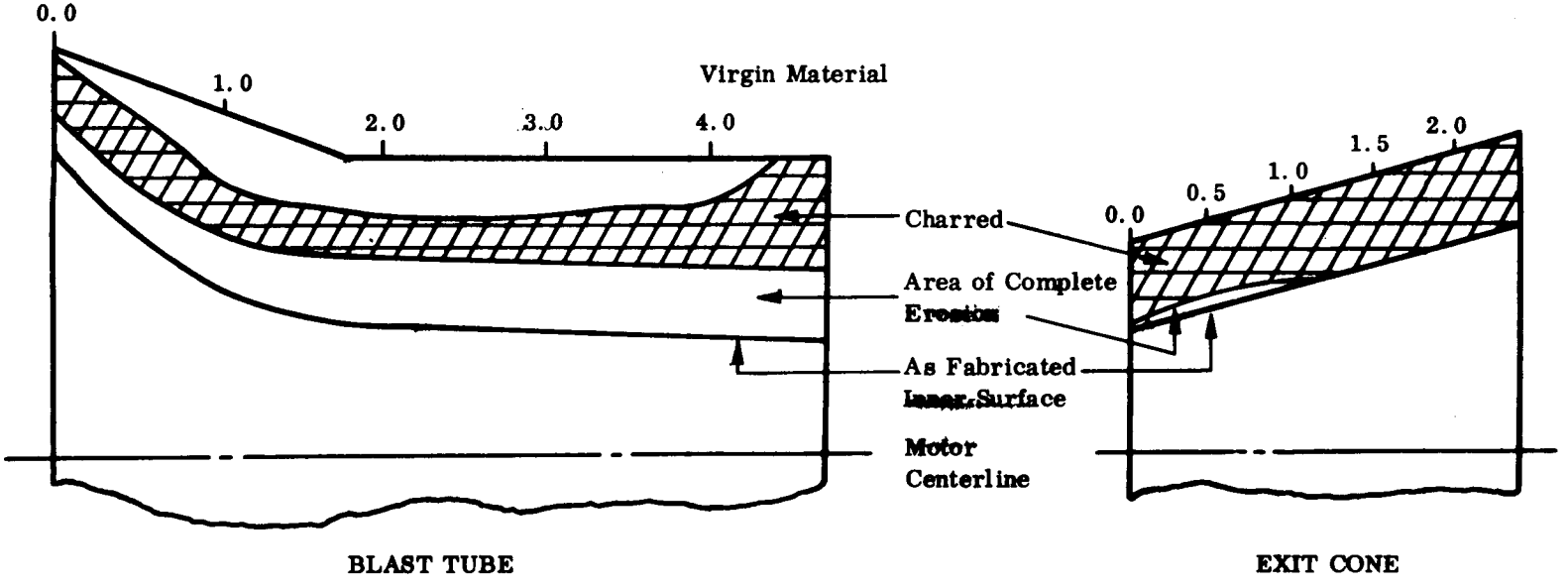

FIG. 2 TU-132 EROSION PROFILE GRAPHITE/CLOTH PHENOLIC (IN.)

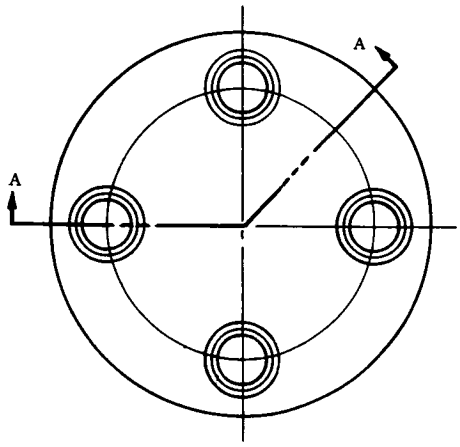

View Looking Forward

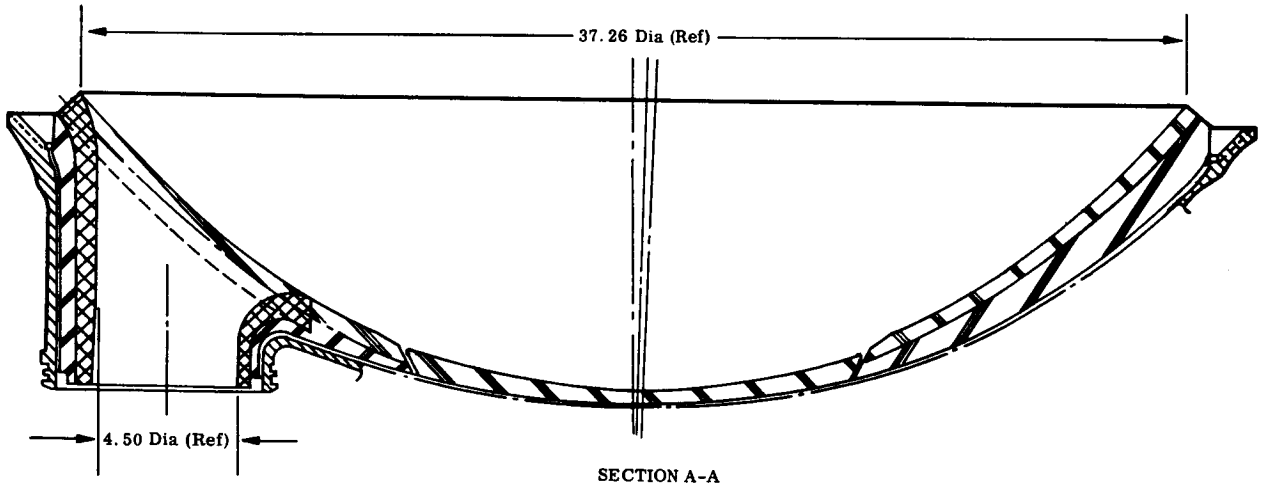

SECTION A-A

FIG. 3 AFT CLOSURE ASSEMBLY, TU-222 MOTOR

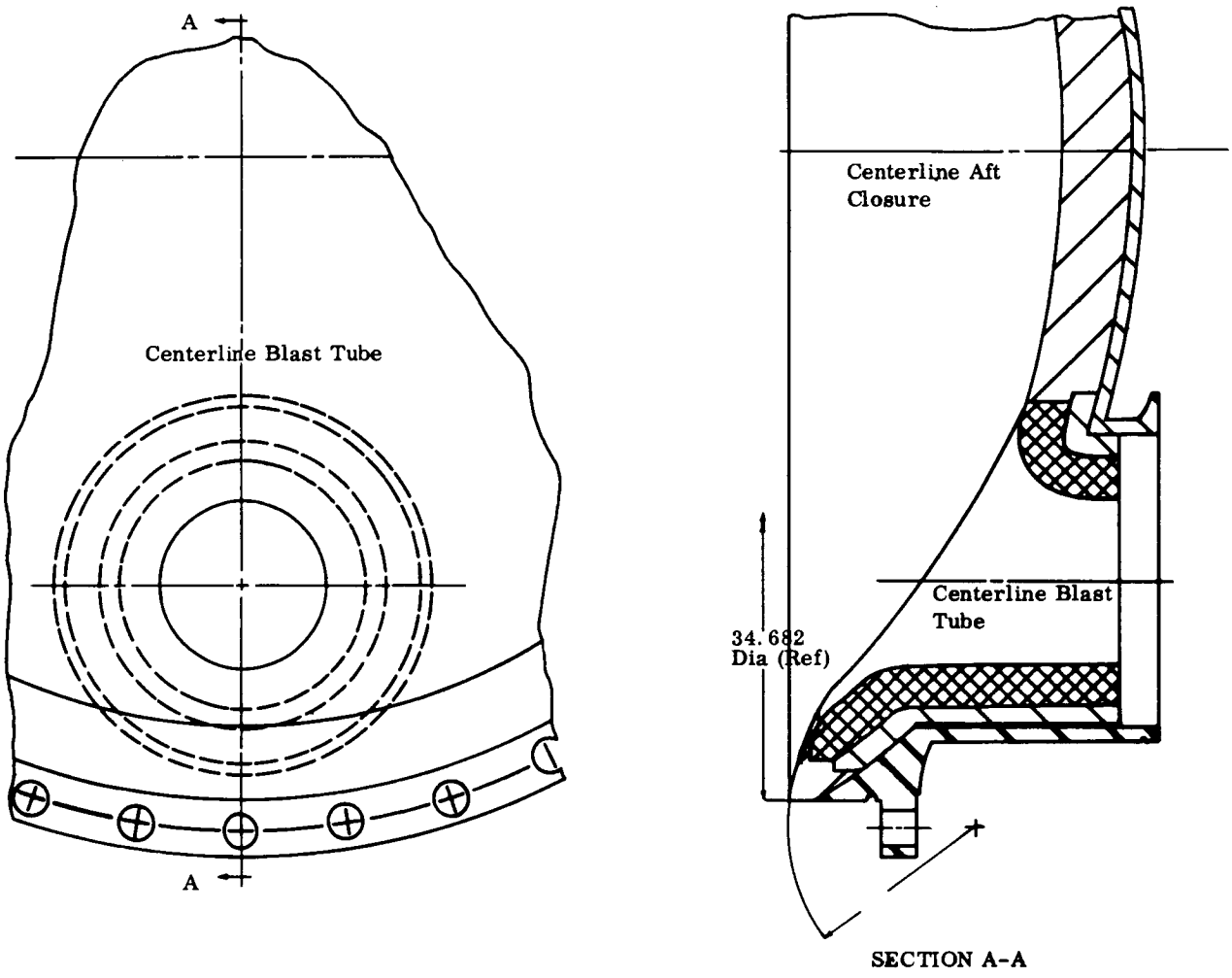

FIG. 4 INSULATED AFT CLOSURE

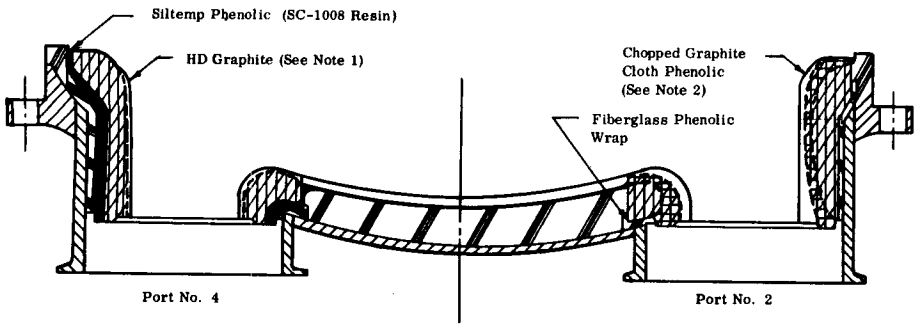

SECTION A-A

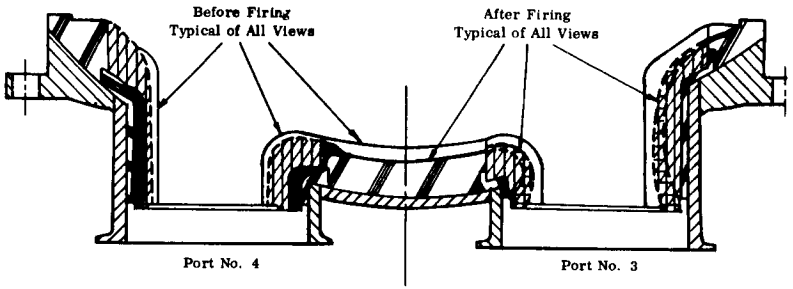

SECTION C-C

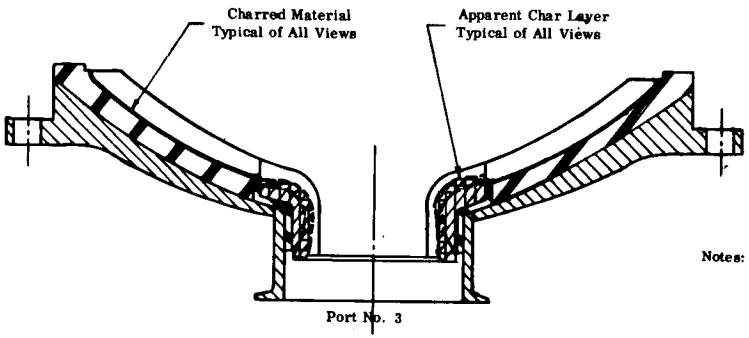

SECTION B-B

Notes:

1. Port No. 4 is HD Graphite
2. Ports No. 1, No. 2, and No. 3 are Chopped Graphite Cloth Phenolic

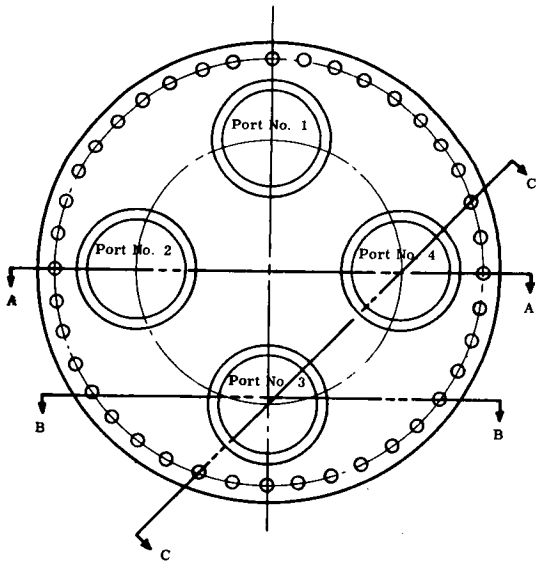

SECTION OF TU-143 AFT CLOSURE

FIG. 5 AFT CLOSURE EROSION PROFILE TU-143

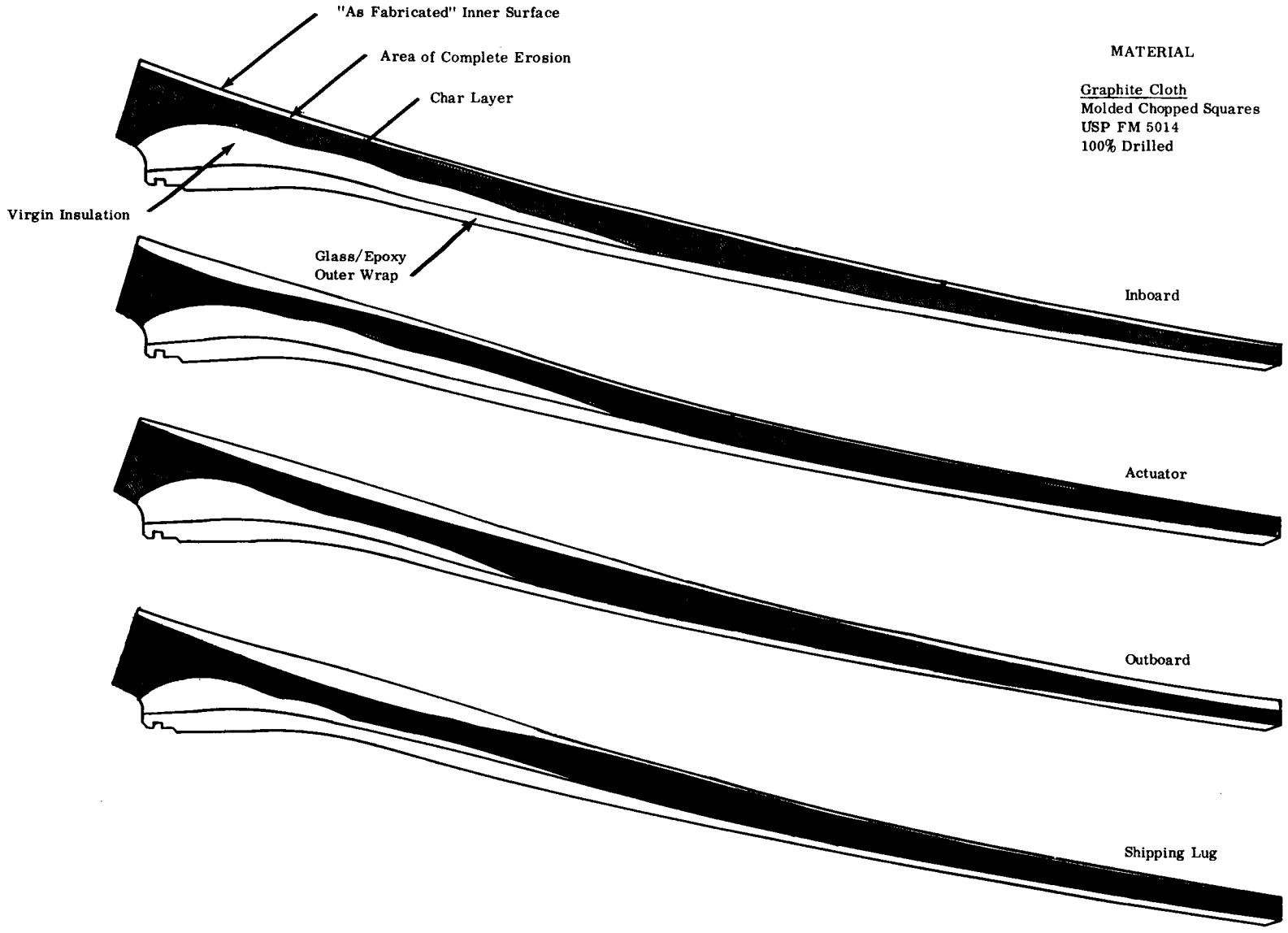

FIG. 6 EXIT CONE EROSION PROFILE

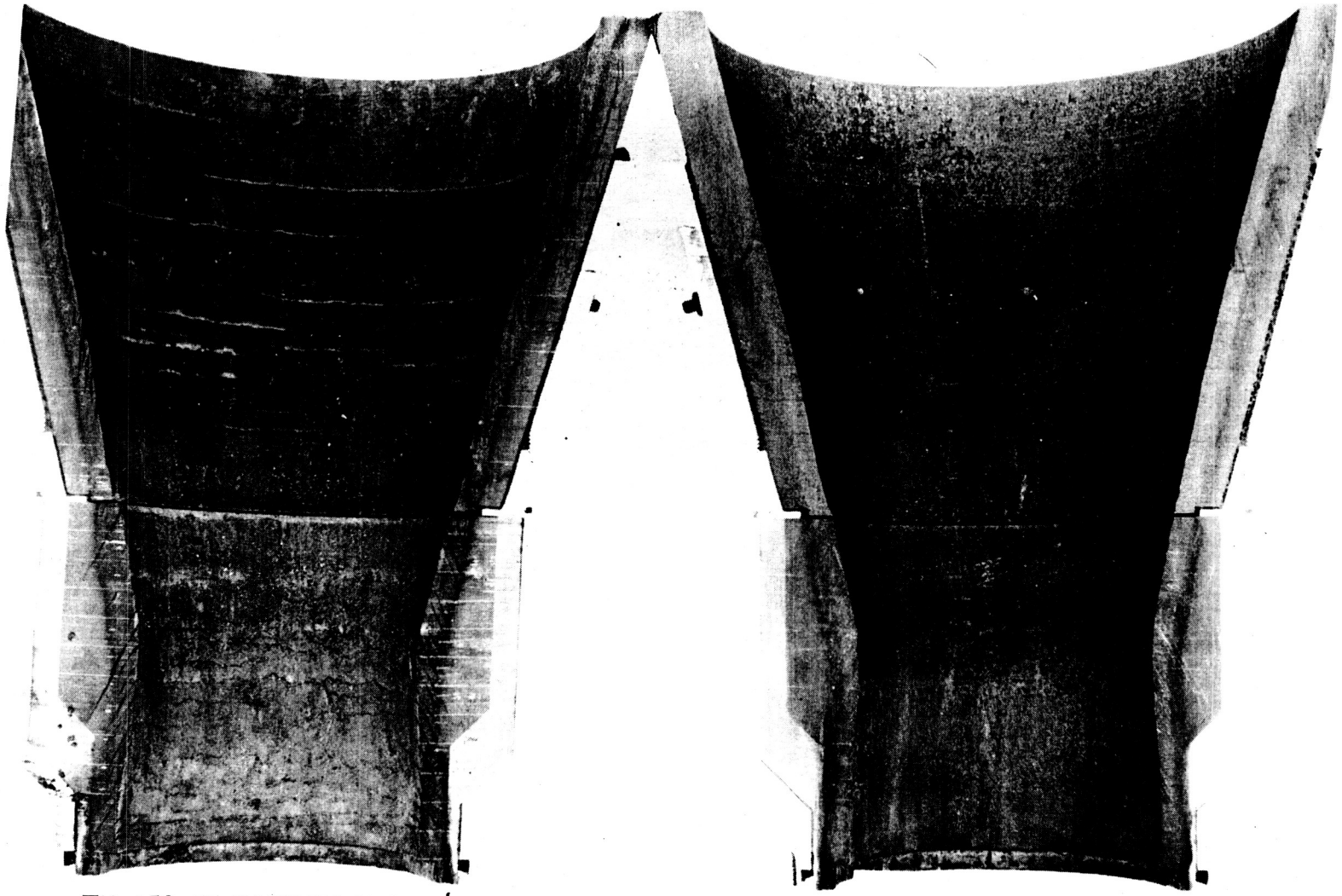

TU–152–57 CARBON CLOTH

TU–152–58 GRAPHITE CLOTH

FIG. 7 EROSION PROFILE

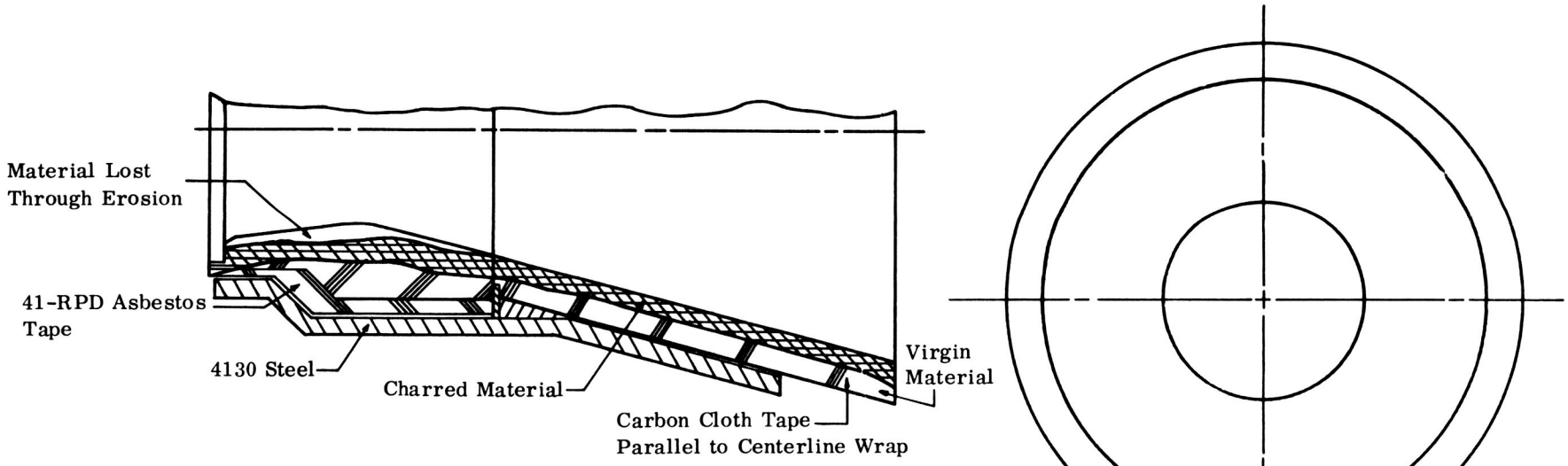

TU-152-57 CARBON CLOTH

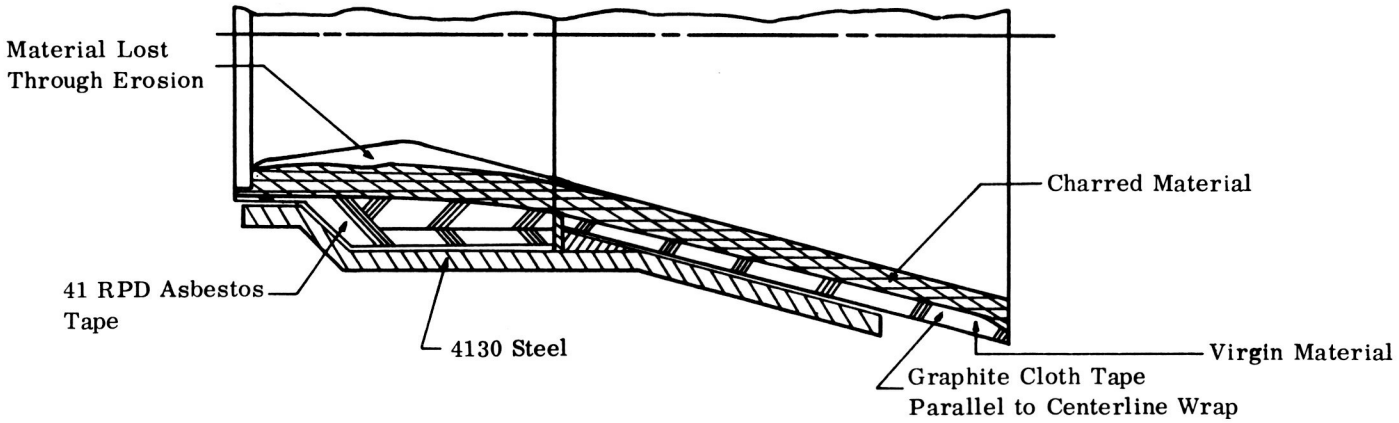

TU-152-58 GRAPHITE CLOTH

FIG. 8 EROSION PROFILE

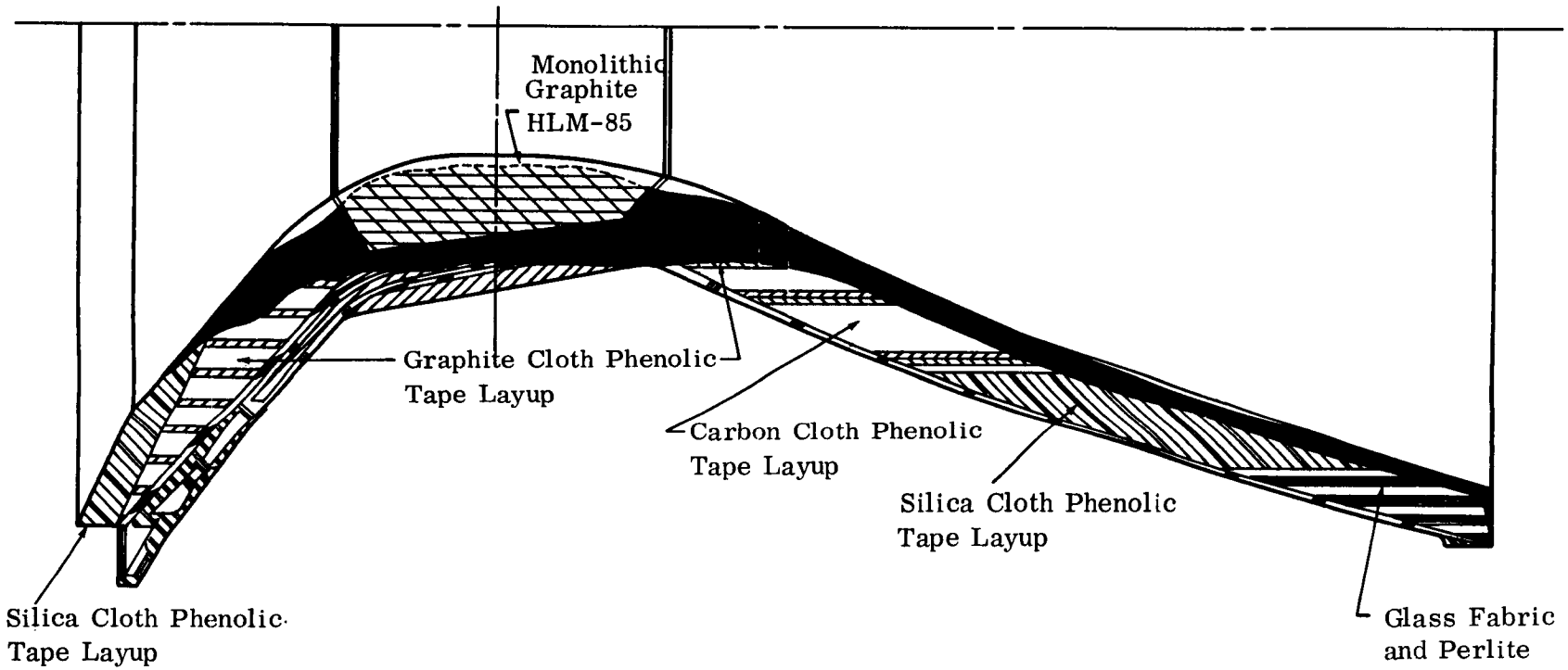

FIG. 9 TU-235 NOZZLE EROSION PROFILE